ZBORNIK RADOVA
PROCEEDINGS

MATRIB 2008

VELA LUKA
OTOK / ISLAND KORČULA, HRVATSKA
26-28. lipnja / June 2008.

ORGANIZATORI / ORGANIZED BY:

HRVATSKO DRUŠTVO ZA MATERIJALE I TRIBOLOGIJU
CROATIAN SOCIETY FOR MATERIALS AND TRIBOLOGY
INSTITUTE OF MATERIALS AND MACHINE MECHANICS
(SLOVAK ACADEMY OF SCIENCES)
DUBLIN INSTITUTE OF TECHNOLOGY

SUORGANIZATORI / CO-ORGANIZERS:

FAKULTET STROJARSTVA I BRODOGRADNJE, ZAGREB
FACULTY OF MECHANICAL ENGINEERING AND NAVAL ARCHITECTURE

GENERALNI SPONZOR / MAIN SPONSOR:

PROPLIN d.o.o. - ZAGREB

SPONZORI / SPONSORS:

MINISTARSTVO ZNANOSTI OBRAZOVANJA I ŠPORTA
INA INDUSTRIJA NAFTE – ZAGREB

IZDAVAČ / PUBLISHER: Hrvatsko društvo za materijale i tribologiju
Croatian Society for Materials and Tribology
c/o FSB, Ivana Lučića 5, 10000 Zagreb
tel.: +385 1 61 68 389; fax: +385 1 61 57 126
e-mail: hdmt@fsb.hr, http://www.fsb.hr/hdmt

UREDNICI / EDITORS: Krešimir Grilec, Gojko Marić, Suzana Jakovljević

CIP zapis dostupan u računalnom katalogu Nacionalne i sveučilišne knjižnice u Zagrebu pod brojem 670844

ISBN 978-953-7040-14-7

NAKLADA / ISSUE: 150

TISAK / PRINT: Vizual media d.o.o., Zagreb

ORGANIZATOR / ORGANIZED BY: HRVATSKO DRUŠTVO ZA MATERIJALE I TRIBOLOGIJU
CROATIAN SOCIETY FOR MATERIALS AND TRIBOLOGY
c/o FSB, Ivana Lučića 5, 10000 Zagreb
tel.: +385 1 61 68 581; fax: +385 1 61 57 126
e-mail: hdmt@fsb.hr, http://www.fsb.hr/hdmt
DUBLIN INSTITUTE OF TECHNOLOGY
INSTITUTE OF MATERIALS AND MACHINE MECHANICS

GENERALNI SPONZOR / MAIN SPONSOR: PROPLIN d.o.o. – ZAGREB

SPONZORI / SPONSORS: MINISTARSTVO ZNANOSTI OBRAZOVANJA I ŠPORTA
INA INDUSTRIJA NAFTE – ZAGREB

ORGANIZACIJSKI ODBOR / ORGANIZING COMMITTEE:

Krešimir Grilec (Zagreb) – predsjednik / president
Darko Andreis (Vela Luka)
Denis Andreis (Vela Luka)
Suzana Jakovljević (Zagreb)
Dario Karlovčan (Zagreb)
Ivan Kramer (Zagreb)
Josip Lovričević (Vela Luka)
Željko Maričić (Vela Luka)
Gojko Marić (Zagreb)
Gorki Miletić (Vela Luka)
Želimir Oršanić (Zagreb)
Dinko Prižmić (Vela Luka)
Danko Žuvela (Vela Luka)
Krešo Žuvela (Vela Luka)

PROGRAMSKI ODBOR / PROGRAMME COMMITTEE:

Vinko Ivušić (Zagreb) – predsjednik / president
Lidija Ćurković (Zagreb)
Tomislav Filetin (Zagreb)
Mladen Franz (Zagreb)
Maurice Grech (Msida, Malta)
Krešimir Grilec (Zagreb)
Jaroslav Jerz (Bratislava, Slovak Republic)
David Kennedy (Dublin, Ireland)
Slobodan Kralj (Zagreb)
Gojko Marić (Zagreb)
Jan Meneve (Mol, Belgium)
Ljiljana Pedišić (Zagreb)
Zdravko Schauperl (Zagreb)
František Simančik (Bratislava, Slovak Republic)
Toma Udiljak (Zagreb)
Dražen Živković (Split)

SADRŽAJ

T. Aleksandrov, D. Ćorić…… 1
ANALYSIS OF MEASURING DEVICE INFLUENCE ON VICKERS HARDNESS VALUES
B. Andričić, T. Kovačić, M. Čagalj……..….. 8
TRANSESTERIFIKACIJA OTPADNIH JESTIVIH ULJA U SVRHU PROIZVODNJE BIODIZELA
M. Balog, P. Krizik, F. Simančik..... 13
STRUCTURAL DAMPING OF HEAT RESISTANT ULTRA-FINE GRAINED PROFILES PREPARED VIA CONSOLIDATION OF FINE AL POWDERS
S. Brkić……. 14
UTVRĐIVANJE PASIVNOG STANJA POVRŠINE NEHRĐAJUĆEG ČELIKA
S. Butković, O. Pašić.…….. 17
DEFINIRANJE PARAMETARA PROCESA NAVARIVANJA SEGMENATA PAPUČA ROTORNOG BAGERA
P. Ćosić, S. Dolinšek, V. Gečevska…… 27
ODABIR PRIMARNOG PROCESA KAO DIO PLANIRANJA TEHNOLOŠKIH PROCESA
D. Ćurčija……. 35
MODELIRANJE MAZIVOGA SLOJA KOD VALJANJA BEŠAVNIH CIJEVI
L. Ćurković, M. Lalić, S. Šolić…… 51
ANALIZA UTJECAJA OPTEREĆENJA NA MIKROTVRDOĆU ALUMINIJ OKSIDNE KERAMIKE UPORABOM RAZLIČITIH MODELA
L. Ćurković, V. Rede, P. Panjan, M. Fudurić Jelača, M. Lalić……... 59
ANALIZA MIKROSTRUKTURE ALUMINIJ OKSIDNE KERAMIKE
N. Dolić, A. Markotić, F. Unkić …….. 67
STRUKTURNA I FIZIKALNA HOMOGENOST BLOKOVA SLITINE EN AW-5083 PROIZVEDENIH POSTUPKOM IZRAVNOG HLAĐENJA
R. Florek, F. Simančík, M. Nosko, R. Uhrík, P. Mihálka ……...…… 79
COOLING AND HEATING PANELS USING ALUMINIUM FOAMS
Z. Glavaš, F. Unkić, K. Terzić…… 83
PROCJENA UDARNE ŽILAVOSTI NODULARNOG LIJEVA U LIJEVANOM STANJU UMJETNOM NEURONSKOM MREŽOM NA OSNOVI KEMIJSKOG SASTAVA
M. Gojić, S. Kožuh, D. Laćman…….. 90
FRAKTOGRAFSKA ANALIZA AUSTENITNOG NEHRĐAJUĆEG ČELIKA AISI 321 NAKON ZAVARIVANJA
K. Grilec, S. Jakovljević, B. Maslać……... 98
EROZIJSKO TROŠENJE NODULARNOG LIJEVA ČELIČNIM KUGLICAMA
K. Grilec, P. Previšić, G. Marić…….…… 104
ISPITIVANJE APSORPCIJE ENERGIJE UDARA ALUMINIJSKE PJENE
L. Haznadarević, J. Kevelj …….……... 111
PRELIMAINARNA ISTRAŽIVANJA TEMPERATURNIH POLJA LEGURA TITANA
M. Jakopčić, K. Grilec…….……... 115
INFLUENCE OF ARTILLERY WEAPON BARREL SUPERHEAT ON EROSION WEAR RESISTANCE OF MATERIAL

J. Jerz, F. Simančík, R. Florek, M. Nosko…… **122**
ADVANCED TECHNIQUES FOR UTILISATION OF ALUMINIUM FOAMS
D. Kennedy, R. Good……... **127**
MECHANICAL ENGINEERING EDUCATION IN IRISH CONTEXT ON ROUTE TO BECOMING A CHARTERED ENGINEER
D Kennedy, K. Scholten…….. **135**
RESEARCH AND EXPLOITATION OF SURFACE ENGINEERING TECHNOLOGY
J. Korab, T. Dvorak, P. Štefanik, Š. Kavecky……... **144**
METAL MATRIX COMPOSITES FOR FUSION REACTOR APPLICATIONS
S. Kurajica, E. Tkalčec, J. Šipušić, G. Matijašić, V. Mandić…….. **152**
SOL-GEL SINTEZA I KARAKTERIZACIJA NANOKRISTALINIČNOG GANITA
J. Macan, S. Markuš, H. Ivanković…… **158**
PREPARATION OF ZIRCONIUM TITANATE CERAMICS BY SOL-GEL PROCESS
K. Macháčková, J. Palubjaková…… **166**
EVALUATION OF SPECIFIC FAILURES OF SYSTEMS THIN FILM – SUBSTRATE FROM SCRATCH INDENTATION IN DETAIL
I. Majnarić, H. Tahirović, I. Zjakić, S. Bolanča..... **173**
THE INFLUENCE OF THE STRUCTURE OF THE OFFSET RUBBER ON THE SCREEN REPRODUCTION
V. Martinac, M. Labor, Z. Gadžo, N. Petric…… **183**
UTJECAJ ANIONSKOG 831A FLOKULANSA NA SEDIMENTACIJU MAGNEZIJEVA HIDROKSIDA DOBIVENOG IZ MORSKE VODE
V. Marušić, D. Krumes, S. Marušić …….. **191**
SVA ČETIRI OSNOVNA MEHANIZMA TROŠENJA U JEDNOM TRIBOSUSTAVU
Z. Meczner, G.Marić, N. Degiuli…… **198**
INOX 316L-MATERIJAL ZA SANACIJU DIMNJAKA GRADA ZAGREBA
S. Miloš, T. Cigula, S. Mahović Poljaček, M. Gojo…….. **205**
CONTRIBUTION TO THE PRINTING INK - PRINTING PLATE – RUN LENGHT INTERACTIONS
I. Mišković…… **211**
SINTEZA I KARAKTERIZACIJA SAMOORGANIZIRAJUĆIH MONOSLOJEVA ALKANTIOLA NA ZLATU
M. Nosko, R. Florek, F. Simančik, R. Uhrik…… **223**
EFFECT OF FOAMING PARAMETERS TO MECHANICAL PROPERTIES OF ALUMINIUM FOAM MADE BY P/M ROUTE AND ITS REPRODUCIBILITY
V. Novosel – Radović, N. Radović, K. Dužić, F. Šafar…… **231**
KARAKTERIZACIJA KOVARINE TOPLO VALJANE TRAKE IZVALJANE IZ KONTI SLABA
K. Nožić, H. Đukić……...…… **240**
EKSPERIMENTALNO ODREĐIVANJE SILE TRENJA
K. Paljar, S. Orlić, E. Tkalčec, H. Ivanković..... **247**
PREPARATION OF SILICON DOPED HYDROXYAPATITE
P. Panjan, Đ. Goršćak, L. Ćurković, M. Godec, M. Čekada, D. Kek Merl, M. Panjan, S. Paskvale…….. **255**
INFLUENCE OF CONVENTIONAL AND POWDER METALLURGY COLD WORK TOOL STEEL SUBSTRATES ON MICROSTRUCTURAL AND TRIBOLOGICAL PROPERTIES OF PVD HARD COATINGS
S. Perinović, B. Andričić, T. Kovačić, V. Vučenović…… **262**
UTJECAJ CITRATNIH OMEKŠAVALA NA TOPLINSKA SVOJSTVA KOMPOZITA POLI(L-LAKTID)/MLJEVENE KOŠTICE MASLINE

D. Prusac, K. Grilec ……..…….. 269
OTPORNOST NA ABRAZIJSKO TROŠENJE KERAMIČKIH PREVLAKA NA ALUMINIJSKIM PJENAMA
A. Rađenović, J. Malina, A. Štrkalj……...…… 277
ADSORPCIJA IONA NIKLA NA VISOKOPEĆNOM MULJU
A. Rađenović, J. Malina, A. Štrkalj……...…… 283
DISTRIBUCIJSKI KOEFICIJENT UKLANJANJA NI^{2+} IONA IZ VODENIH OTOPINA POMOĆU VISOKOPEĆNOG MULJA
N. Repčić……... 289
A NARROW DISTRIBUTION PROVIDES MORE UNIFORM PROPERTIES POLYMERS
M. Rogante , G.P. Marconi..... 295
RESIDUAL STRESS DETERMINATION BY NEUTRON DIFFRACTION IN TUNGSTEN CARBIDE COATED AND SHOT PEENED STEEL SAMPLES
J.Selanec, D. Ćorić, Z.Schauperl…… 301
KARAKTERIZACIJA MATERIJALA ZA RAD NA VISOKIM TEMPERATURAMA
W. Sitek ……...…… 309
MODELLING OF HIGH-SPEED STEELS' HARDNESS USING CATALOGUE DATA
S. Slavica Matešić, J. Radošević, N. Krnić…… 315
MEHANIČKA I ELEKTROKEMIJSKA SVOJSTVA SLITINE EN AW 8006
Lj. Slokar, T. Matković, P. Matković…… 325
NIOBIUM AND COBALT INFLUENCE ON THE MICROSTRUCTURE AND HARDNESS OF Ti-Cr ALLOYS
B. Smoljan, S. Smokvina Hanza, D. Iljkić..... 332
PREDICTION OF WORKING STRESS OF COLD-WORK TOOL STEEL
B. Staniša, L. Ćurković, V. Rede..……. 340
ANALIZA OŠTEĆENJA KLIZNOG LEŽAJA AGREGATA VODNE TURBINE SNAGE 1100 kW HE OZALJ 2
I.Štěpánek, K. Macháčková, J. Palubjaková....……... 347
COMPARISON OF MECHANICAL PROPERTIES AND BEHAVIOUR SYSTEMS THIN FILM – SUBSTRATE PREPARED BY DIFFERENT TECHNOLOGY OF DEPOSITION
I.Štěpánek, K. Macháčková…….....……...…….. 354
POSSIBILITY OF EVALUATION OF MECHANICAL PROPERTIES AND BEHAVIOUR OF SYSTEMS THIN FILM – GLASS SUBSTRATE BY INDENTATION TESTS
J. Šubarić, T. Filetin..……..…… 362
STRUCTURE AND PROPERTIES OF MOLLUSC SHELLS
A. Tabak, N. Mrvac, K. Golubović, A. Koren ……..……... 368
INTEGRATION TRENDS IN DEVELOPMENT OF PRINTING SYSTEMS
D. Tiro, J. Kevelj, S. Rahimić…….…… 376
PLUTAJUĆA PLATFORMA ZA PRIKUPLJANJE OTPADA NA AKUMULACIONIM JEZERIMA
N. Ukrainczyk, J. Šipušić, P. Dabić, T. Matusinović..... 382
MICROCALORIMETRIC STUDY ON CALCIUM ALUMINATE CEMENT HYDRATION
Z. Veljačić, Z. Schauperl..... 389
UTJECAJ TEMPERATURE IZOTERMIČKOG POBOLJŠANJA NA SVOJSTVA NODULARNOG LIJEVA

I. Vitez, D. Krumes, B. Kosec, D. Dolovčak……. 397
OZNAČIVANJE ŽELJEZNIH LJEVOVA PO EUROPSKIM STANDARDIMA
N. Vukojević Medvidović, J. Perić, M. Trgo, I. Nuić ……..…. 404
UTJECAJ OMJERA POČETNIH KONCENTRACIJA OLOVA I CINKA U BINARNIM VODENIM OTOPINAMA NA NJIHOVO UKLANJANJE NA PRIRODNOM ZEOLITU
J. Zelić, J. Ninčević, D. Jozić, D. Krpan-Lisica ……...……. 412
PONAŠANJE PORTLAND CEMENTNOG MORTA S DODATKOM LETEĆEG PEPELA U OKOLIŠU SULFATA
D. Živković, T. Ursić, B. Lela…… 421
MIKROSTRUKTURA I SVOJSTVA ODLJEVKA KLIPA OD Al LEGURE
I. Brnardić, M. Ivanković, J. Macan, H. Ivanković …… 431
CHARACTERIZATION OF ORGANIC-INORGANIC HYBRIDS PREPARED FROM POLY(METHYL METHACRYLATE) AND ORGANICALLY MODIFIED Si – ALKOXYDE
F. Cajner, D. Landek, S. Šolić ……...…… 438
OTPORNOST NA TROŠENJE I KOROZIJU POVRŠINSKI MODIFICIRANIH SLOJEVA
D. Živković, D. Bajić…… 450
ENERGY ABSORBING STRUCTURES FOR THE ROADSIDE
SAFETY EQUIPMENT
D.Kolednjak, D.Kamenečki, Z.Schauperl……. 462
RESISTANCE OF WHITE CAST IRON TO ABRASION TEST
M. Rožić, S. Miljanić, J. Hrenović, L. Sekovanić, T. Gracaković, V. Kropar Vančina, S. Kurajica…… 473
ADSORPCIJA TISKARSKOG BOJILA NA ORGANO-ZEOLIT
J. Farrell, M. Rogante……. 481
A FEASIBILITY STUDY FOR A SANS INVESTIGATION OF PHASE CHANGE MATERIAL FOR ENERGY STORAGE APPLICATIONS
J. Šundrica, T. Filetin…….. 487
INFLUENCE OF ARTILLERY WEAPON BARREL SUPERHEAT ON EROSION WEAR RESISTANCE OF MATERIAL

ANALYSIS OF MEASURING DEVICE INFLUENCE ON VICKERS HARDNESS VALUES

Tamara Aleksandrov, Danko Ćorić

University of Zagreb, Faculty of Mechanical Engineering and Naval Architecture, Department of Materials

Ivana Lučića 5, 10000 Zagreb
e-mail: tamara.aleksandrov@fsb.hr

Izvorni znanstveni rad / Original scientific paper

Abstract

In paper hardness measurements on two different hardness testers are carried out. One of the used hardness testers is referent hardness tester. Analysis of indentations is performed on optic microscope which is integral part of referent hardness tester. Afterwards indentations are analysed on scanning electron microscope with the purpose of higher accuracy of indentation measurements. On the basis of carried analysis comparison of measured diagonals and hardness for the purpose of analysis of measuring device influence on Vickers hardness values is carried out.

Keywords: Vickers hardness, indentation, hardness tester, optic microscope, scanning electron microscope

1. INTRODUCTION

Vickers method is standard method for metals hardness determination especially for metals with hard surface. It consists of indenter indentation in material with prescribed force F (N). Indenter is diamond with a shape of square-based pyramid with an angle of 136° between opposite faces of indenter. Load is applied without any external influence e.g. shock or vibration for 10-15 seconds. Physical characteristics of indenter as well as accuracy of applied load must be controlled in order to attain correct values of hardness. Values of hardness are measured after indentation and are proportional to ratio of applied force and the surface area of indentation.

Samples with indentations are usually analyzed on optic microscope which is integral part of hardness tester and is sufficient for magnifications less than 1000x. Samples can be also analyzed on scanning electron microscope if higher accuracy of measurement is needed.

2. HARDNESS MEASUREMENT

Hardness measurements are carried out on two different hardness testers according to EN ISO 6507-1. Sample on which measurements are carried out is referent block with the value of hardness 296 HV and is showed in figure 2.1.

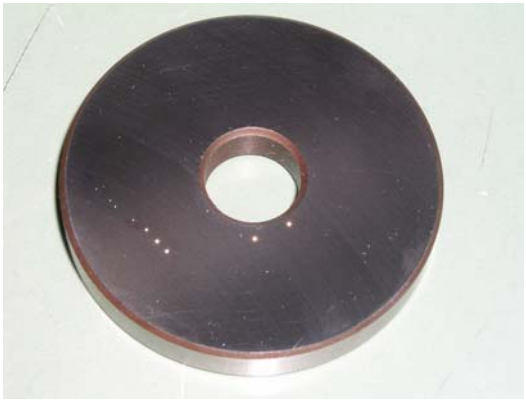


Figure 2.1 – Referent block used for hardness measurements

Hardness testers are located in Laboratory for Testing Mechanical Properties at Faculty of Mechanical Engineering and Naval Architecture and have following characteristics:

Hardness tester 1

- Manufacturer: Zwick, Germany;
- Type: 3212001;
- Serial number: 301011;
- Applied load 49,03 N (HV 5);
- Measurement uncertainty: ± 2 %



Figure 2.2 – Hardness tester 1

Hardness tester 2 – referent hardness tester

- Manufacturer: Indentec, UK;
- Type: 5030 TKV
- Serial number: 05281
- Applied load 49,03 N (HV 5);



Figure 2.3 – Hardness tester 2

Hardness measurements, as mentioned before, consist of diamond indentation in examining sample surface whose results is square-shaped indentation. Indenter and Vickers indentation are showed in figure 2.4

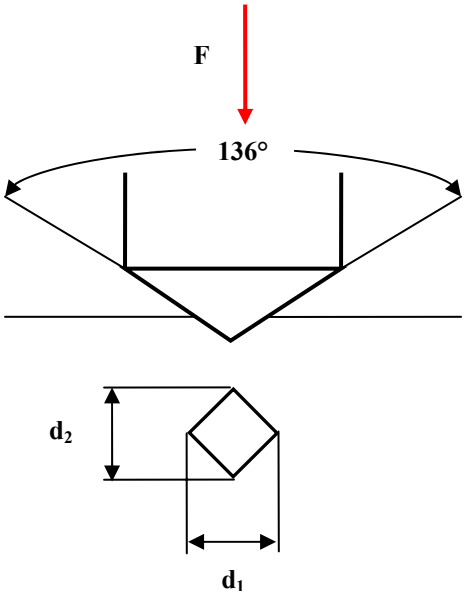


Figure 2.4 – Indenter and Vickers indentation

Sample is placed on hardness tester and surface of sample is observed under optic microscope in order to set height of the test surface and to attain correct illumination of the test surface what is important for accuracy of the resultant measurement.

3. VICKERS INDENTATION ANALYSIS

After hardness measurements Vickers indentation analysis is carried out. Analysis is carried out on optic microscope of referent hardness tester and later on scanning electron microscope in order to attain more precise analysis of Vickers indentations.

Optic microscope of referent hardness tester is fitted with measuring lines. The edge of each line has to be adjusted so that it just touches the corner of indentation what is shown in figure 3.1.

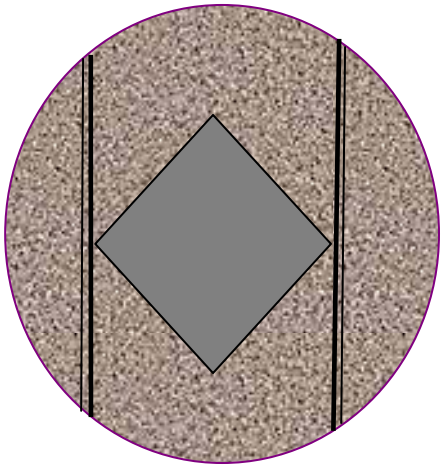


Figure 3.1 – Demonstration of Vickers indentation marking with measuring lines

The distance between measuring lines represents the length of diagonal. The length of diagonal is downloaded into digital display of referent hardness tester. The measuring eyepiece assembly is rotated trough a fixed 90° angle in order to measure another diagonal of Vickers indentation. After the measurement is done values of both diagonal together with hardness value are displayed on the screen of referent hardness tester as shown in figure 3.2.

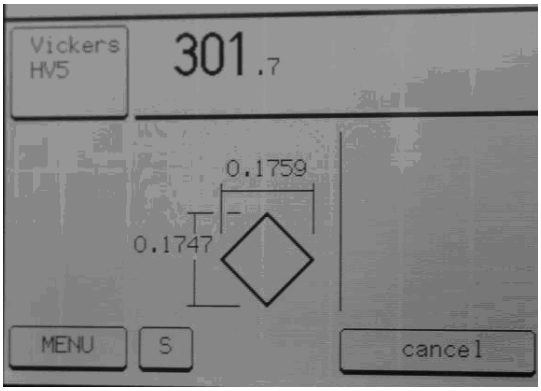


Figure 3.2 – Digital display (screen) of referent hardness tester

The results of hardness measuring are shown in table 3.1. Indentations from both hardness testers are analysed on optic microscope of referent hardness tester in order to achieve higher accuracy of readings as mentioned before.

Table 3.1. – Results of hardness measuring

Number of measuring	Hardness tester 1		Hardness tester 2	
	d,mm	HV5	d, mm	HV5
1	0,1741	305,8	0,1769	296,8
2	0,1738	306,9	0,1760	299,0
3	0,1770	295,9	0,1762	297,6
4	0,1768	296,6	0,1753	301,7
5	0,1738	306,9	0,1766	297,2
	$HV5_{sr}$ = 302,42		$HV5_{sr}$ = 298,46	

From the analysis of Vickers indentations can be seen that the values of measured hardness vary from one hardness tester to another. Hardness values measured on hardness tester 2 (referent hardness tester) poin accuracy error 0,8% while hardness values measured on hardness tester 1 point accuracy error 2,2%. The reason of accuracy error difference can be in physical characteristics of indenter as well as in applied load accuracy.

Hardness indentation are analysed on scanning electron microscope as well. Scanning electron microscope is located in Laboratory for Metallography at Faculty of Mechanical Engineering and Naval architecture and has following characteristics:

Instrument for Vickers indentation analysis – Scanning electron microscope (SEM)

- Manufacturer: TESCAN, Czech Republic;
- Type: VEGA



Figure 3.3 – Scanning electron microscope [1]

Scanning electron microscope located in Laboratory for Mettalography is high quality computer controlled electron microscope and is designed for application in vacuum or at different pressures. Vickers indentations are recorded by placing a sample on which hardness measurements are made in scanning electron microscope chamber. Afterwards analysis of indentations is carried out using software VEGA TC; Manufacturer: TESCAN Digital microscopy imaging. One of the recorded Vickers indentations is shown in figure 3.4.

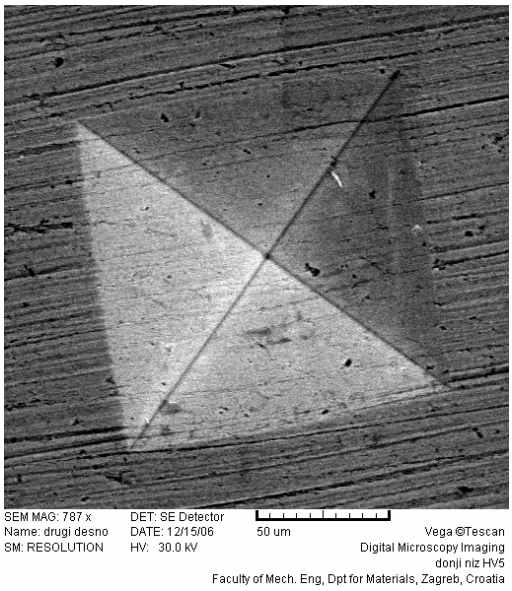


Figure 3.4 – Vickers indentation recorded on SEM

Table 3.2 – Results of Vickers indentation analysis on SEM

Number of measurement	Hardness tester 1		Hardness tester 2	
	d,mm	HV5	d, mm	HV5
1	0,17453	304,25	0,17650	296,32
2	0,17437	305,08	0,17680	297,68
3	0,17493	303,13	0,17662	296,85
4	0,17667	297,19	0,17591	298,25
5	0,17736	294,86	0,17709	295,78
	$HV5_{sr}$ =300,90		$HV5_{sr}$ = 296,97	

On the basis of results can be concluded that values of hardness obtained from recorded indentations and digital analysis differ from values of hardness obtained on optic microscope of referent hardness tester for approximately 2 HV. Hardness values show that accuracy error is smaller comparing with optic microscope of referent hardness tester. Accuracy error decreases for about 0,5% and for hardness tester amounts 1,65% while for hardness tester 2 (reference hardness tester) amounts 0,33%.

4. CONCLUSION

Based on obtained results can be concluded that measuring device has significant influence on measured hardness values. Hardness values measured on hardness tester 2 (reference hardness tester) shows considerably smaller accuracy error comparing with hardness tester 1. The reason for mentioned can be geometry of indenter and accuracy of applied load.

Besides, hardness values obtained from recorded indentations on scanning electron microscope and afterwards digital analysis differ from hardness values from optic microscope for approximately 2 HV. The reason can be in measuring instrument precision and magnification which is higher than 1000x in case of scanning electron microscope.

It is relevant to note that one of the disadvantages of Vickers method is subjectivity of measurement what can cause deviations especially in case of smaller magnifications.

5. LITERATURE

[1] www.tescan.com

TRANSESTERIFIKACIJA OTPADNIH JESTIVIH ULJA U SVRHU PROIZVODNJE BIODIZELA

BIODIESEL PRODUCTION VIA TRANSESTERIFICATION OF WASTE COOKING OILS

Branka Andričić,* Tonka Kovačić, Marijana Čagalj
Zavod za organsku tehnologiju, Kemijsko-tehnološki fakultet Sveučilišta u Splitu, Teslina 10/V, 21000 Split, e-mail: branka@ktf-split.hr

Stručni članak / Professional paper

Sažetak: Sinteza biodizela provedena je transesterifikacijom (alkoholizom) svježih i otpadnih biljnih jestivih ulja metanolom, uz alkalni katalizator, pri 60°C. Iskorištenje na biodizelu iz otpadnih i svježih ulja iznad je 80% i ovisi o vrsti ulja. Gustoća, kinematička viskoznost, plamište i točka smrzavanja svih uzoraka biodizela odgovaraju vrijednostima propisanim standardom ASTM- D6751- 02. Procjena točke smrzavanja biodizela određena je, umjesto klasičnom metodom, primjenom diferencijalne pretražne kalorimetrije (DSC). Rezultati pokazuju da se iz jestivih biljnih ulja prisutnih na lokalnom tržištu nakon uporabe može dobiti biodizel primjerene kvalitete.

Ključne riječi: biodizel, otpadna jestiva ulja.

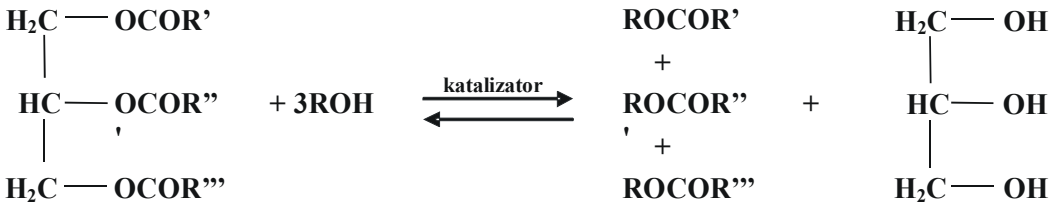
Abstract: Biodiesel synthesis was performed via transesterification (alcoholysis) of fresh and waste cooking vegetable oils with methanol and alkaline catalyst at 60°C. The yield in both cases was above 80% depending on an oil source. Properties of biodesel, i.e. density, kinematic viscosity, flash point and freezing point values satisfy the standard ASTM- D6751-02. The estimation of freezing point was performed by differential scanning calorimetry (DSC) instead by manual freezing point method. Presented results show that waste cooking oils could be successfully convert to biodiesel regarding to fresh vegetable oils on local market.

Key words: biodiesel, waste cooking oils.

Uvod

Zbog različitih utjecaja na cijenu i dostupnost fosilnih goriva, već se dulje vrijeme radi na proizvodnji alternativnih goriva: vodika, alkohola, sintetičkih ugljikovodika te biodizelskog goriva. Međutim, zbog činjenice da se alkohol i biodizel proizvode iz žitarica, odnosno uljarica, cijene tih sirovina na svjetskom tržištu rastu, što je izravno utjecalo i na porast cijene hrane. Stoga se kao neophodna alternativa nameće proizvodnja goriva iz različitih otpadnih sirovina. Prema propisima Europske unije do 2010. godine biodizelsko gorivo trebalo bi supstituirati 10% klasičnog dizelskog goriva, pa se može očekivati porast njegove proizvodnje. Biodizel je moguće proizvesti iz otpadnog jestivog ulja iz kućanstava, restorana, hotela, a da se njegove karakteristike značajnije ne mijenjaju u odnosu na biodizel dobiven iz

svježeg ulja. Zastupljenost otpadnih jestivih ulja u proizvodnji biodizela u Europi manja je od 1 %. Preduvjet za veću zastupljenost je uhodan sustav sakupljanja otpadnih ulja.
Biodizel je smjesa alkilnih monoestera i dobiva se alkoholizom (transesterifikacijom, preesterifikacijom) biljnih ulja (uljane repice, soje, suncokreta) metanolom, etanolom ili drugim alkoholom.
Alkoholiza ili transesterifikacija ulja općenito se odvija prema sljedećoj shemi:



triglicerid **alkohol** **smjesa alkilnih estera** **glicerol**

Reakcija transesterifikacije može se odvijati u prisustvu kiselih ili baznih katalizatora. Najčešće se provodi bazno-katalizirana transesterifikacija jer je oko 4 000 puta brža od kiselo-katalizirane. Reakcija transesterifikacije može se također djelotvorno katalizirati ekstracelularnim i intracelularnim lipazama [1]. Međutim, lipaze su znatno skuplje od alkalnog katalizatora.
Kako je transesterifikacija triglicerida metanolom heterogena reakcija, miješanje reaktanata je od velikog značaja. Utvrđeno je da primjena ultrazvuka može učinkovito zamijeniti klasični sustav s miješanjem i zagrijavanjem [2]. Istovremeno, šaržni proces može postati kontinuiranim [3].
Da bi se smjesa metilnih estera mogla smatrati biodizelom svojstva takve smjese moraju zadovoljavati normirane kriterije (npr. ASTM-D6751-02, DIN V 51606).
U ovom radu prikazani su iskorištenje i svojstva biodizela (kiselinski broj, gustoća, plamište, kinematička viskoznost, točka smrzavanja) proizvedenog iz otpadnog suncokretova i biljnog ulja (smjesa ulja različitih uljarica) te uspoređena s karakteristikama biodizela proizvedenog na isti način iz odgovarajućih svježih ulja. Dobiveni rezultati uspoređeni su s normiranim vrijednostima za biodizel [5].

Eksperimentalni dio

Za sintezu biodizela upotrijebljeno je suncokretovo jestivo ulje (IDK - Tvornica ulja, Čepin) i jestivo biljno ulje (ABN – Tvornica ulja d.o.o., Zagreb). Dio ulja upotrijebljen je za prženje u fritezi i sakupljan nakon uporabe (otpadna ulja). Karakteristike svježih i otpadnih ulja prikazana su u tablici 1. U procesu transesterifikacije katalizator je KOH, alkohol je metanol a sredstvo za sušenje $CaCl_2$ (sve: Kemika, Zagreb).

Tablica 1. Osnovne značajke ulja upotrijebljenih za pripravu biodizela

	Suncokretovo ulje		**Biljno ulje**	
	svježe	**otpadno**	**svježe**	**otpadno**
Gustoća pri 25°C, /kgm^{-3}	915	915	915	917

Kiselinski broj/mg $KOHg^{-1}$	0,163	0,416	0,061	0,305
Peroksidni broj/ $mmolO_2kg^{-1}$	9,8	21,2	8,7	29,0

Kakvoća biodizela izravno je povezana s kakvoćom sirovina. Otpadna ulja stoga se moraju u određenoj mjeri pročistiti prije alkoholize. To podrazumijeva uklanjanje prisutnih čvrstih čestica (filtracija) i uklanjanje vode. Sve sirovine moraju biti bezvodne jer se uz prisustvo vode parcijalno odvija i reakcija saponifikacije (nastajanje sapuna) [5].

Predobrada ulja: Ulje je zagrijano na 50-60 °C, filtrirano, a zatim ponovo grijano na 110-120°C oko 15 minuta da ishlapi eventualno prisutna voda. U ohlađeno ulje dodano je sredstvo za sušenje ($CaCl_2$), ostavljeno preko noći te filtrirano. Ovako pročišćeno ulje spremljeno je u staklene boce s čepom.

Transesterifikacija: U reaktor za transesterifikaciju opremljen miješalom, hladilom i termometrom stavljeno je 200 g predobrađenog ulja i zagrijano do 60°C. Dodana je dvostruka stehiometrijska količina metanola (57,8 mL ili 43,4 g) s otopljenim katalizatorom [6]. Količina katalizatora za svaki uzorak izračunata je na temelju kiselinskog i peroksidnog broja ulja [7], kako slijedi:

$$m\,(KOH) = 0{,}6 / 100 \cdot m_{uk}\,(\text{ulja}) + L_{KB} + L_{PB} \quad (1)$$

$$L_{KB} = 10^3\, K_B \cdot m_u \quad (2)$$

$$L_{PB} = 5{,}6 \cdot 10^{-5}\, P_B \cdot m_u \quad (3)$$

gdje je:
m (KOH) – masa katalizatora KOH/g
m_u – masa ulja (200g)
L_{KB} – masa katalizatora s obzirom na K_B/g
L_{PB} – masa katalizatora s obzirom na P_B/g

Iskorištenje na biodizelu izračunato je na bazi triglicerida (TG) oleina jer su esteri oleinske kiseline najzastupljeniji u jestivim uljima, [8] prema stehiometrijskim omjerima:

1 mol TG (oleina) + 3 mol metanola → 3 mola metil-estera + 1 mol glicerola (4)

Dobivenom biodizelu određeni su kiselinski broj, kinematička viskoznost, plamište i gustoća. Kiselinski broj određen je titracijom s KOH. Gustoća je određena areometrom pri 25°C. Za određivanje plamišta upotrijebljen je aparat po Pensky-Martens-u prema ASTM-u D-93. Kinematička viskoznost određena je Ostwaldovim viskozimetrom pri 40°C. Temperatura smrzavanja biodizela određena je diferencijalnom pretražnom kalorimetrijom (DSC 823^e, Mettler-Toledo) hlađenjem uzorka mase oko 10 mg od 25°C do -50°C brzinom od $10°Cmin^{-1}$. Početna točka smrzavanja određena je kao onset na kristalizacijskoj egzotermi.

Rezultati i rasprava

Transeesterifikacijom svježih i otpadnih ulja, uz iskorištenje veće od 80 %, dobiveni su proizvodi svojstava navedenih u tablici 2. Svojstva dobivenog biodizela zadovoljavaju standard ASTM-D6571-02. Iznimka je BSS, koji ima manju gustoću od one propisane normom. Kinematička viskoznost i plamište biodizela iz otpadnih ulja imaju nešto veće vrijednosti u odnosu na biodizel iz svježih ulja. Vrijednosti plamišta odgovaraju vrijednostima iz literature za upotrijebljena ulja i općenito plamište biodizela iz otpadnih ulja ima više vrijednosti [1, 5].

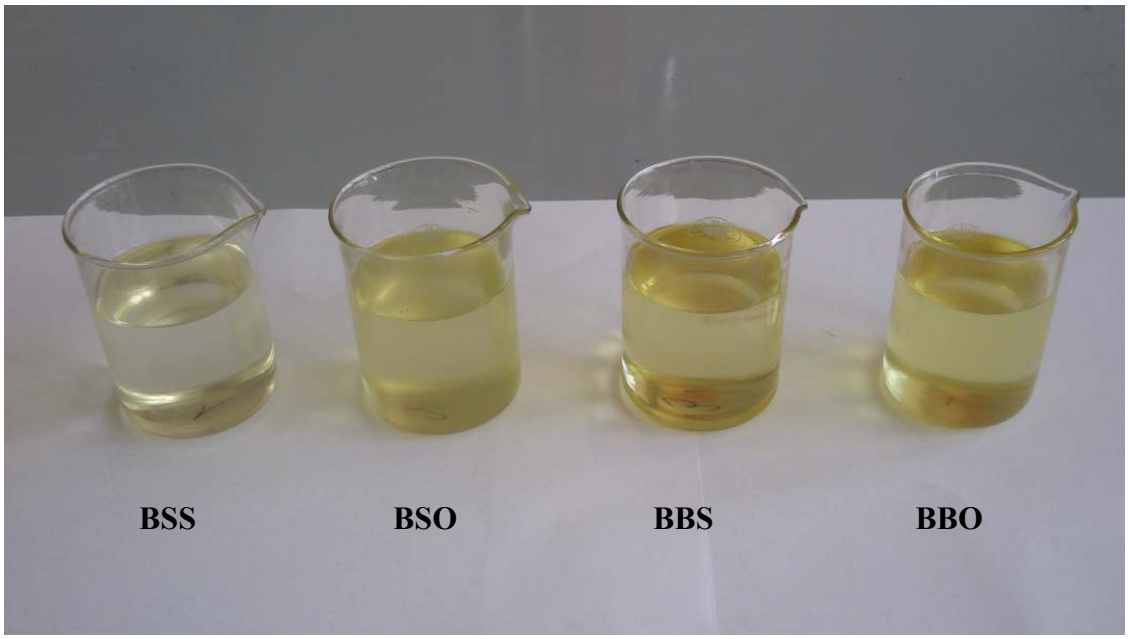
Opaža se da je biodizel proizvedenih iz suncokretova ulja svjetliji od biodizela iz biljnog ulja, slika 1. U praksi, međutim, nije uočena povezanost između obojenosti i kakvoće biodizela. Nijansa obojenosti ovisi o vrsti sirovine i postupcima naknadne obrade, iako nakon duljeg stajanja može biti pokazatelj oksidacije ili kontaminacije drugim tvarima.

Tablica 2. Značajke biodizela dobivenih transesterifikacijom jestivih ulja metanolom

	BSS*	**BSO***	**BBS****	**BBO****	**Ref. vrijednosti (ASTM-D6571-02)**
Gustoća pri 25°C /kgm^{-3}	861	878	875	876	868-880
Kiselinski broj /mg KOHg^{-1}	0,15	0,18	0,17	0,15	max. 0,8
Kinematička viskoznost / mm^{2}s^{-1}	3,96	4,35	4,00	4,11	1,9-6,0
Plamište /°C	182	191	180	200	min. 130
Točka smrzavanja /°C	-5	-4	-5	-4	ovisno o sirovini
Iskorištenje /%	83	81	92	86	

*BSS, BSO: biodizel iz suncokretova svježeg, odnosno otpadnog ulja

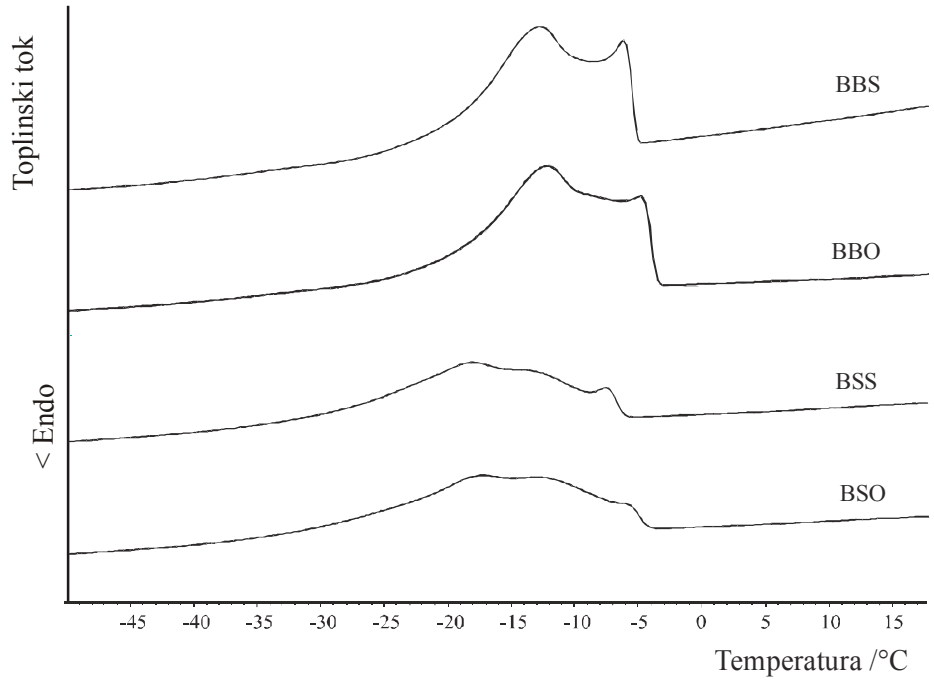
**BBS, BBO: biodizel iz biljnog svježeg, odnosno otpadnog ulja



Slika1. Uzorci biodizela proizvedeni iz svježih i otpadnih ulja

Temperatura smrzavanja biodizela određena je primjenom DSC-a iz razloga što je to jednostavan i pouzdan način određivanja točke smrzavanja biodizelskih [9] i avionskih goriva [10]. Također je ustanovljeno da su podatci pouzdaniji ukoliko se određuju iz krivulje

hlađenja, umjesto iz krivulje zagrijavanja (iz taljenja). DSC krivulje hlađenja uzoraka biodizela prikazane su na slici 2. Iz širine i izgleda krivulje u području kristalizacije vidljivo je da se uzorci biodizela sastoje od najmanje dvije (BBS i BBO) odnosno tri (BSS i BSO) frakcije različite temperature smrzavanja, što je posljedica prisustva metilnih estera različitih masnih kiselina. Tako npr. metil-linoleneat ima najnižu, a metil palmitat najvišu točku smrzavanja (-57°C nasuprot 87°C). Izdvajanjem frakcije ili frakcija više temperature smrzavanja moguće je dobiti frakciju niže temperature smrzavanja [11].



Slika 2. DSC krivulje hlađenja proizvedenog biodizela

Zaključak

Transesterifikacijom otpadnih jestivih biljnih ulja dobije se biodizel čije osnovne značajke zadovoljavaju postojeće norme za biodizel i bitno se ne razlikuju od biodizela dobivenog iz svježih ulja. Na taj način učinkovito se povezuje zbrinjavanje otpadnih ulja i dobivanje goriva.

1. Literatura

[1] H. Fukuda et al. *I. Biosci, Bioeng.* **92** (2001) 405-416
[2] C. Stavarche, M. Vinatoru, Y. Maeda, *Ultrason. Sonochem.* **14** (2006) 380-386
[3] C. Stavarche et al. *Ultrason. Sonochem.* **14** (2007) 413-417
[4] ASTM-D6571-02
[5] J. Van Gerpen, Biodiesel production and fuel quality, www.uidaho.edn/bioenergy/ 21.06.2007.
[6] B. Supple et al. *J. Am. Oil Chem. Soc.* **79** (2002) 175-178
[7] M. P. Dorado et al. *Transactions of ASAE*, **45** (2002) 525-529
[8] D. Swern, Industrijski proizvodi ulja i masti po Baileyu, Nakladni zavod Znanje, Zagreb, 1972, str. 125-162
[9] R. O. Dunn, *J. Am. Oil Chem. Soc.* **7** (1999) 109-115
[10] S. Zabarnick, N. Widmor, *Energy Fuels*, **15** (2001) 1477-1453

Structural damping of heat resistant ultra-fine grained profiles prepared via consolidation of fine Al powders

Balog Martin*, Krizik Peter, Simancik Frantisek

**corresponding author: ummsbama@savba.sk*
Institute of materials and machine mechanics, SAS, Racianska 75, 83102 Bratislava, Slovakia, tel.:+421/249268303, fax: +421/244253301

Izvorni znanstveni rad / Original scientific paper

Abstract

Ultra-fine grained compacts were prepared via consolidation of fine (d_{50} = 1,3 μm) atomized Al 99,7 % powder wherein expensive procedures of powder encapsulating and degassing (i.e. HIP) were avoided. Compact's microstructure featured ultra-fine grains (with grain size down to 0,2 μm) of initial monocrystallic powder particles stabilized with torn powder surface oxide's pinning spots. Such microstructure was found to be structurally stabile even after long term annealings up to 450°C, yielding superior high temperature mechanical properties.

For the studied materials high damping capacity comparing to alike-materials was determined. Average loss factor values (for 1 Hz) gradually increased from very promising values of 0.033 to 0.091 in the temperature range 20°C - 300 °C. Those are superior results which particularly in contrast with wrought polycrystalline Al based alloys showing damping capacity somehow of 10^{-4} – 2.10^{-3}. It is almost unambiguously thought that superior damping of powder compacts was attributed to the high quantity of micropores, stress fields around them and compact's ultra-fine grained character. Alike storage Young modulus no obvious tendency in loss factor evolution referring to compaction temperature was seen.

Very good damping characteristics alongside with properties as low density, good strength, sufficient ductility, thermal stability, good workability and relatively simple processing (affordable price) make herein studied Al powder compacts very promising candidate in applications where conventional high damping materials can not be applied.

Key words

Structural damping, Al, ultra-fine grained, powder, structural stability, mechanical properties

Introduction

The metallic materials commonly used in aircraft and aerospace fields, such as Al and Ti alloys, steels, etc., show low damping capacity (usually of the order of or less than 10^{-3}) [1]. Thus, some problems associated to vibration may emerge and influence the reliability, safety and lifespan of given applications. On the other hand conventional high damping alloys (damping capacity above 10^{-2}) possess densities usually greater than 5 $g.cm^{-3}$, or their strengths are less than 200 MPa (for alloys based on dislocation damping). Those make them impossible to be applied to aircraft and aerospace areas [1, 2, 3]. In recent years, a lot of graphite or ceramic (fibre, whisker or particle) reinforced Al matrix composites with damping capacity above 5.10^{-3} have been developed [68], but they show some drawbacks, such as high cost, poor workability, low ductility etc., retarding them to be widely used [4].

In this study ultra-fine atomized Al powder (d_{50} = 1,3 μm) was compacted into light weigth bulk profiles utilizing PM consolidation route based on applied plastic deformation (i.e. direct extrusion). High amount of introduced grain boundaries were believed to assure enhanced damping characteristics meanwhile with superior mechanical properties of following compacts.

Experimental

1 μm with narrow size distribution (d_{10}=0.66 μm, d_{50}=1.31 μm, d_{90}=2.51 μm) Al powder of technical purity 99.7 %, supplied by company *New materials development G.m.bH*., was prepared by gas atomization in N_2 atmosphere. If not signed differently no special powder handling and thermal pre-treatment were made. Powder green bodies of 89 % of theoretical bulk density were prepared via cold isostatic pressing (CIP) at a pressure of 200 MPa. Compaction was done via conventional direct extrusion (DE) with flat faced die shape (container with diameter of 20 mm) at different extrusion temperatures T_{ext} (350 - 500°C) and at extrusion ratio R = 11:1. CIPed powders were filled into the preheated die and heated up to desired compaction temperatures for 30 min before consolidation. The average ram speed during the consolidation was ~1 $mm.s^{-1}$ (±0.8). Boron nitride spray was used as a lubricant. See complex studies related to consolidation behavior of ultra-fine Al powders elsewhere [5, 6].

Structures of compacts were examined by means of light microscopy, SEM and TEM. To clearly demonstrate presence and distribution of nano-scale oxide dispersions compacts were etched during samples preparation for TEM. Herein, oxide particles tilted and protruded over the etched Al matrix surface helped with their easier localization. On the other hand used preparation misrepresented proper view and seen thickness of dispersions. Relative density of the extrudates was measured via Archimedes route. The mechanical properties at room and at 300 °C were measured on tensile specimens with the gauge of Ø3–30 mm using ZWICK testing machine at the cross ram speed of 1 $mm.min^{-1}$.

3-point bending dynamic mechanical analysis (DMA) experiments were performed on 2980 DMA ver. 1.7B machine at the Technical University of Vienna. Tested PM compacts samples were of 4 x 2 x 50 mm dimension and two samples of each material were tested. Experiments were carried out in one cycle at the heating and cooling rate of 3 $°C.min^{-1}$ within range of room temperature and 350 °C. Frequency of 1 Hz and amplitude of 40 μm were set up. The damping capacity (loss factor) is evaluated in a loss tangent (tan Ø), defined as tan Ø = E´´/E´where E´ (corresponds to Young`s modulus) and E´´ are loss and storage moduli, respectively. E´´ represents the energy dissipated as a heat. When tan Ø is not greater than 0.1, it is interchangeable with the inverse quality factor (Q^{-1}), π^{-1} of the logarithmic decrement (δ), and $(2\pi)^{-1}$ of the specific damping capacity (SDC) [7].

Results

Microstructural observation

Examination of extruded powder compacts showed ultra-fine microstructures, with grains elongated into extrusion direction, stabilized with nanometric broken Al surface oxide dispersions (dark in contrast), (**Fig. 1**). Small powder particles with initial diameter below compact`s transversal grain size remained undeformed within the structure of compacts. Tile-like oxide particles were homogenously redistributed within compacts with predominant position along the grain boundaries (i.e. initial powder surface). Crystallographic form of alumina particles was found to be in α-alumina form (corundum) for whole studied T_{ext} range = 350 °C – 500 °C, (**Fig. 2**). At low T_{ext} = 350 °C (where large deformation energies were introduced) apart of particles shearing, extensive milling of powder particles took place during consolidation. High deformation energies yielded finer microstructures with a number of broken oxides milled into newly formed grains (**Fig. 1**). Compacts extruded at higher T_{ext} showed slightly coarser microstructures with broken oxides found exclusively at grain boundaries (**Fig. 1**). Nanometric dispersions effectively grain pinned microstructure, yielding excellent structural stability with no detected structural changes observed after 20 hours annealing at 350 °C and even after short term 1 hour exposures up to 500 °C. Extreme annealing at 500 °C for 20 hours already accommodated

minor grain growth accompanied with spheroidization (minimization of surface energy) of oxide particles (**Fig. 2**).

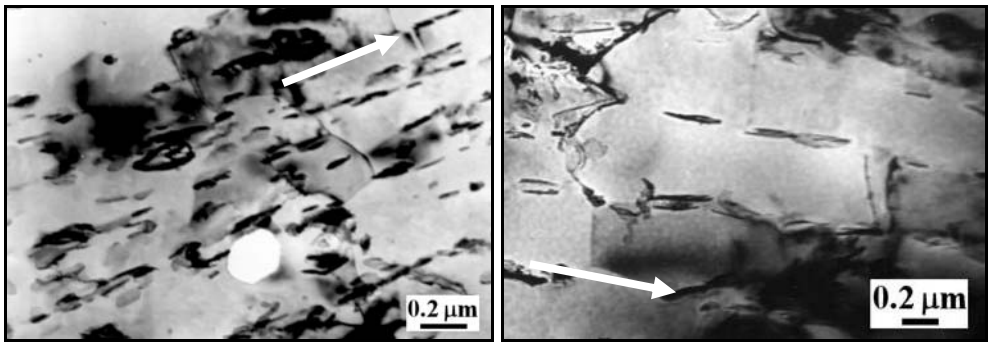


Figure 1 Longitudinal TEM micrographs of 1 μm Al powder compacts prepared via direct extrusion at T_{ext} = 350°C (left) and T_{ext} = 500°C (right). Arrows indicate consolidation directions.

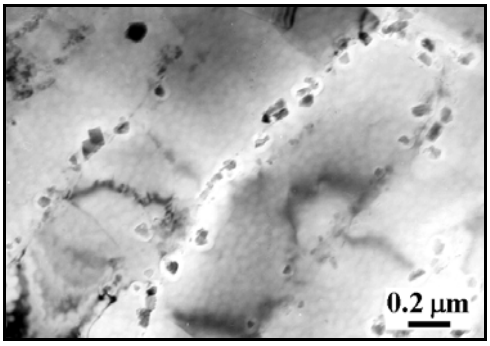


Figure 2 Longitudinal TEM micrographs of 1 μm Al powder compact after 500°C/20hours annealing.

Mechanical properties of compacts

Compacts reached relatively high ultimate tensile strength R_m up to 310 MPa at room temperature, accompanied with good ductility A up to 10 % (**Tab. 1**) and high values of Charpy impact fracture toughness up to 45 J.cm^{-2}. High strength values of sound compacts reflected two major strengthening mechanisms. Fine nature of as-atomized powder resulted in high amount of grain boundaries within compacts, what gave a rise to predominant effect of grain boundaries strengthening. Furthermore, marginal influence Orowan strengthening mechanism was active in case of those compacts where oxide particles were embedded within the grain's areas. The strength decreased with decrease of induced deformation work (i.e. increase of extrusion temperature T_{ext}), where ~10 % decline in R_m from 310 MPa to 280 MPa was determined for compacts prepared at T_{ext} = 350 °C and 500 °C, respectively (**Tab. 1**). The strength difference is partially attributed to oxide particles dispersed within grains and partially to slightly finer microstructure of compacts prepared at low T_{ext} = 350 °C. No significant changes in strength and ductility of extrudates were observed after annealing at 350 °C for 20 hours when compared to as-extruded state. Excellent thermal stability of compacts was supported with relatively high strength at elevated temperatures. For instance at testing temperature of 300 °C extrudants showed high R_m up to 187 MPa. In contrast to contemporary Al alloys based on precipitation strengthening, gradual decrease of R_m with increasing testing temperature without sudden drop due to overaging can be seen for investigated material (**Fig. 3)**. Even at the temperature of 500 °C

compacts still exhibited R_m =70 MPa what is roughly the R_m value for pure Al at room temperature.

T_{ext} [°C]	350	400	450	500
R_m [MPa] / A [%] at RT	310 / 9	305 / 8,7	290 / 10,9	280 / 10,4
R_m [MPa] / A [%] at 300°C	186.7 / 1,7	181.7 / 1,5	168.9 / 2,2	159.9 / 3,3

Table 1 Mechanical properties of extruded compacts at RT and at 300°C (ultimate tensile strength R_m, ductility A) prepared at different extrusion temperatures (T_{ext}).

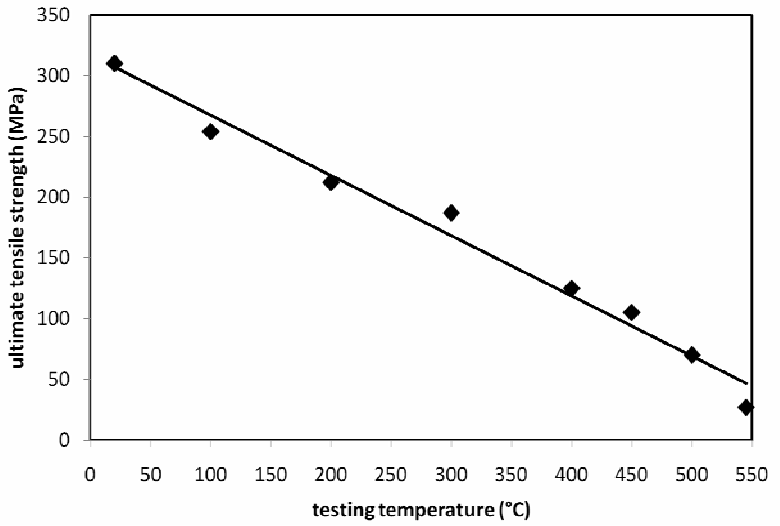


Figure 3 Evolution of ultimate tensile strength of extruded compacts (T_{ext} = 350°C) in hand with testing temperature. All compacts annealed at 350°C for 20 hours before they tested.

Dynamic mechanical analyse

The average damping capacity and Young's storage modulus (E) data at room temperature and 300 °C for 1 µm Al 99.7 % compacts extruded at different T_{ext}, as determined by the DMA, are summarized in **Tab. 2**. For the studied material high damping capacity comparing to alike-materials was determined. Average damping capacity values (for 1 Hz) lie between very promising values of 0.019 – 0.033 at room temperature and 0.065 – 0.091 at 300 °C. This is particularly in contrast with wrought polycrystalline Al based alloys which show damping capacity somehow of 10^{-4} – 2.10^{-3} [10]. Determined values of Young's storage modulus are of those valid for unreinforced Al 99.7 % due to negligible small fraction of α-Al_2O_3 dispersion phase within 1 µm Al 99.7 % compacts (**Fig. 4**, **Tab. 2**).

	at room temperature				at 300 °C			
T_{ext} [°C]	350	400	450	500	350	400	450	500
E [GPa]	67.5	65.1	73.3	72.3	47.5	46.8	52.6	52.4
damping capacity	0.029	0.019	0.038	0.033	0.091	0.068	0.073	0.065

Table 2 Average values of Young's modulus and loss factor at room temperature and at 300 °C of 1 μm Al 99.7 % powder compacts compacted at different T_{ext} obtained from three point bending dynamical analysis

$A1_20_3$ as essentially low damping material shows damping capacity of ~10^{-5}. Therefore, the observed improvement in damping response may be attributed, not only to the intrinsic damping of the particulates, but also to modifications in the microstructure of the matrix derived from the presence of the ceramic particulates. Dissipation of strain energy for this particular case is believed to be governed mainly by thermoelastic and microstructural (i.e. crystallographic defects) effects. Based on [8], thermoelastic contribution (the irreversible thermal flow produced in metallic materials under mechanical vibration) in the present study is negligible since it becomes significant at high frequencies. From crystallographic defects are of main interest line defects (dislocations), surface defects (grain boundaries and inter- faces) and bulk defects (micro-pores and micro-cracks).

Increased dislocation content in studied composite is a result of plastic work induced into the material and thermal mismatch strains at Al / Al_2O_3 interfaces. The presence of strain fields near interface work as frictional barrier to dislocations movement under cyclic loading. On the other hand annihilation of dislocation may retard this mechanism at elevated temperatures.

Polycrystalline metals show viscous-like properties on their grain boundaries. The viscous flow at grain boundaries converts mechanical energy produced under cyclic shear stress into thermal energy, as a result of internal friction. While the average grain size for all compacted is very small this mechanism becomes dominant comparing to conventional coarse grained material. Since the viscosity of grain boundaries is thermally activated it would not be operative until temperature reaches 200 °C [9].

Difference in CTE between particulates and matrix resulted in stress concentration at the incoherent particulate / matrix interfaces, thereby increasing internal friction. As testing temperature increases, the interface effect becomes more profound because the metal matrix softens relative to the ceramic particulate. Reversible movement at the interface is likely to take place. Therefore, the internal friction at the interface is thought to be thermally activated, thereby suggesting that interface damping becomes dominant at high temperatures.

Rather high amount of residual micropores in powder compact structures led to stress concentration in their vicinity (caused by compressed gas) and mode conversion around the pores what significantly enhanced overall damping. Unlike damping based on dislocations movement stress fields around residual micropores retain within compacts after thermal exposures as well. Thus, even high temperature annealing does not reduce structural damping.

It is almost unambiguously believed that superior damping of herein presented compacts was attributed to the high quantity of micropores and their ultra-fine grained character. Evolution of loss factor in hand with increasing temperature for one particular sample made of each compact extruded at different T_{ext} is depicted in **Fig. 5**. Alike storage E curves no obvious tendency in loss factor evolution referring to T_{ext} is seen.

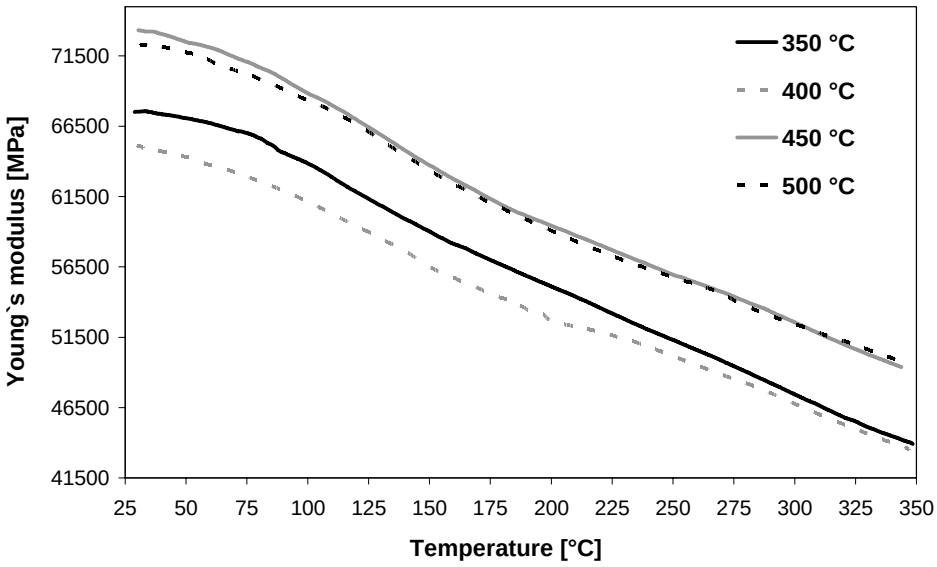


Figure 4 Young's storage modulus course in hand with testing temperature during heating of 1 μm Al 99.7 % powder compacts extruded at different T_{ext} (average values, 3 °C.min^{-1})

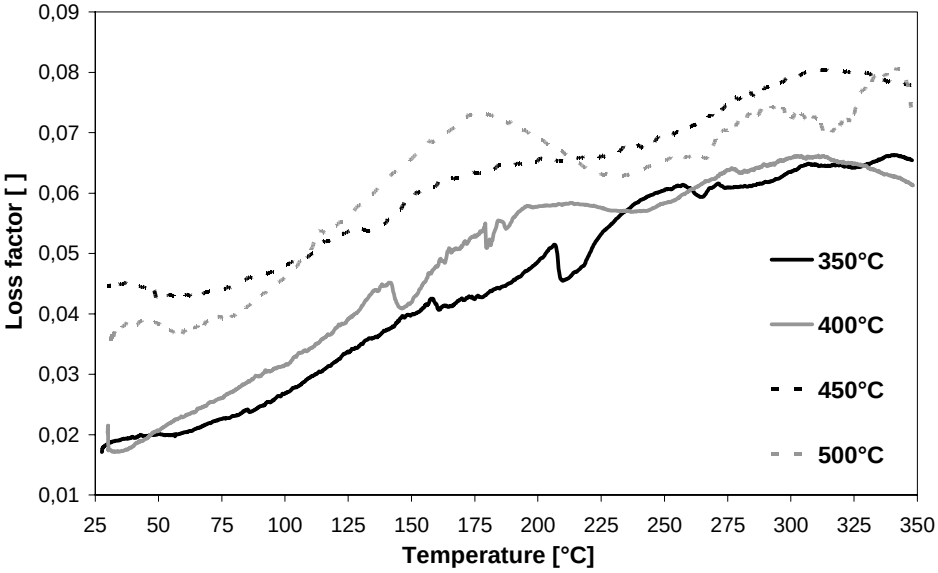


Figure 5 Damping capacity (loss factor) course in hand with testing temperature during heating of 1 μm Al 99.7 % powder compacts extruded at different T_{ext} (3 °C.min^{-1})

Conclusion

Very good damping characteristics alongside with properties as low density, good strength, sufficient ductility, thermal stability, good workability and relatively simple processing make herein studied Al powder compacts very promising candidate in applications where conventional high damping materials can not be applied.

References

[1] Mechanical Engineering Handbook, 2nd edn., Vol. 3, p. 11–138, Mechanical Industries' Press, Beijing (1996)

[2] I.G. Ritchie and Z-L Pan. *Metall. Trans.* 22A, p. 607. (1991)

[3] P. Y. Li, S. L. Dai, D. B. Liu, S. C. Chai, and Y. R. Li, Chin. J. Mater. Eng. August, 44 (1999)

[4] K. S. Ravichandran and E. S. Dwarakadasa, J. Metals. May, 28 (1987).

[5] Balog M., Nagy J., Iždinský K., Simančík F., 2005. Int. J. Mat. & Product Tech., Vol.23, Nos.1/2, 70-78

[6] Nagy J., Simančík F., Balog M., Iždinský K., 2006. Consolidation of rapidly solidified Al-based particles using Equal Channel Angular Extrusion (ECAE). In: Proceedings of ISMANAM 2006,Warsaw, Poland

[7] E. J. Lavernia, R. J. Perez, and J. Zhang, Metall. Mater. Trans. 26A, 2803 (1995).

[8] J. E. Bishop and V. K. Kinra, A Second Law Analysis of Thermoelastic Damping in Elementary Metal-Matrix Composites, Technical Report 91-15, Texas A&M University (1991)

[9] T.S. Ke, Phys. Rev., 71, 533 (1947)

[10] Cambridge Engineering Selector Database

Acknowledgment

The financial support of Slovak Agency for S&T Support under the project APVV 51-031204 is gratefully acknowledged. The authors thank company *New Materials Developement GmbH., St. Pantaleon* for the supply and characterization of fine Al powder, to Slovak Centre of Excellence *NANOSMART* and C.Poletti and G. Requena from *TU Vienna* for DMA and dilatometry analyses.

UTVRĐIVANJE PASIVNOG STANJA POVRŠINE NEHRĐAJUĆEG ČELIKA

CONFIRME THE PASIVE LAYER ON THE STAINLESS STEEL SURFACE

Srećko Brkić
PLIVA HRVATSKA d.o.o., Prilaz baruna Filipovića 25, 10000 Zagreb, Hrvatska

Stručni članak / Professional paper

Sažetak: Mjerenjem otpora na površini nehrđajućeg čelika moguće je utvrditi da li se čelik nalazi u aktivnom ili pasivnom stanju. To je komparativna metoda i uspoređuju se vrijednosti otpora na jednakim duljinama (100 mm) za oba stanja površine na istom uzorku. Dobiveni rezultati mogu se koristiti u primjeni ispitanih uzoraka.

Ključne riječi: nehrđajući čelik, pasivna površina, mjerenje otpora

Abstract: On the stainless steel surface there is possibility to confirm (with resistance measuring method) if the surface is in aktive or in pasive condition. This is comparative method which compare value of resistance on the equal distance (100 mm) for both layer conditions on the same sample. This results could be applied in operation of the treated samples.

Key words: stainless steel, pasive layer, resistance measuring

UTVRĐIVANJE PASIVNOG STANJA POVRŠINE NEHRĐAJUĆEG ČELIKA

UVOD

Prije puštanja u rad mnogih uređaja, spremnika, cjevovoda koji su napravljeni iz nehrđajućeg čelika potrebno je provjeriti da li se površina nalazi u aktivnom ili pasivnom stanju. Ova provjera je obavezna nakon izvođenja postupka pasivacije. U tu svrhu koriste se različite „indirektne“ metode kao što su; feroksilni test, Akimov test, ispitivanje količine slobodnog željeza u otopini, itd. Navedene metode su brze i zadovoljavajuće pouzdane. U ovom radu metodom mjerenja otpora površine, utvrđena je prisutnost pasivnog sloja (filma) na površini nehrđajućeg čelika.

OPIS PASIVNOG STANJA POVRŠINE

Usporenje korozijskog djelovanja na površinske slojeve čelika temelji se na efektu pasivacije. Nakon zavarivanja, rezanja, brušenja, mehaničkog čišćenja, itd. potrebno je izvršiti pasivaciju površine nehrđajućeg čelika. Temperatura tališta kromovog oksida je 1972° C, tako da se zavarivanjem uništava. Ovim obradama došlo je do djelomičnog skidanja pasivnog sloja kojega je potrebno uspostaviti. Pod pasivacijom površine se smatra uspostavljanje vrlo tankog pasivnog sloja kromovog oksida (Cr_2O_3). Taj vrlo tanak anorganski sloj ima debljinu od svega 1 do 3 nm i predstavlja barijeru raznim vrstama korozije.

MJERENJE OTPORA NA POVRŠINI NEHRĐAJUĆEG ČELIKA

Kao uzorak na kojem se je obavilo mjerenje korištena je pločica od nehrđajućeg čelika kvalitete AISI 316L (W.Nr.1.4435) dimenzija 100x100x4 mm. Pločica je brušena, na hrapavost (srednje odstupanje profila) Ra < 0,8 μm. Veličina zrna 320 (UK Grit Ref) koja daje Ra = 0,75 μm. Na dijagonali pločice točkalom su napravljene 4 točke (točkalo i čekić) i to po dvije na duljini od po 100 mm. Pločica je odmašćena u alkoholnoj otopini (10 %), te je pasivirana uz pomoć dušične kiseline (HNO_3 / 30%). Nakon 30 minuta pločica je isprana u pročišćenoj vodi do vrijednosti ulazne vode pH= 5,7 i specifične električne vodljivosti SEP = 0,62 μS/cm. Nakon sušenja površine prirodnim putem dokazano je pasivno stanje površine nehrđajućeg čelika indirektnom metodom (Akimov test). Na prvoj duljini od 100 mm (razmak točaka) izvršena je depasivacija pomoću koncentrirane tehničke kiseline (HCl /36%). U tu svrhu korišten je kist. Mjerenje otpora obavljeno je pomoću instrumenta Multimetar (FLUKE 189), a rezultati su prikazani u tablici I.

Tablica I. – Mjerenje otpora površine nehrđajućeg čelika u aktivnom i pasivnom stanju

Broj mjerenja	Vrijednost otpora za aktivnu površinu (Ω)	Vrijednost otpora za pasivnu površinu (Ω)
1	0,15	0,16
2	0,16	0,16
3	0,15	0,17
4	0,15	0,15
5	0,16	0,17
6	0,16	0,16
7	0,15	0,16
8	0,16	0,16
9	0,16	0,17
10	0,15	0,15
-	Srednja vrijednost = 0,155	Srednja vrijednost = 0,16

ZAKLJUČAK

Mjerenja otpora na aktivnoj i pasivnoj površini nehrđajućeg čelika pokazuju da postoji razlika. Proizvođač instrumenta u svojoj tehničkoj dokumentaciji potvrđuje da njegov instrument ima grešku od ± 0,05 %, ali to nije imalo utjecaja na obavljena mjerenja. Za točnija mjerenja svakako treba koristiti instrument za mjerenje područja u mΩ. Prilikom mjerenja kontakt elektroda sa površinom varira i ovisi o tome da li se elektrode drže okomito ili pod kutom. Sila pritiska elektrode na površinu ima utjecaja na dobivene vrijednosti. Radi toga je za preporuku da mjerenje obavlja jedna osoba. Metoda mjerenjem otpora površine je komparativna i mogla bi se koristiti uz provjeru s nekom od ostalih „indirektnih“ metoda.

LITERATURA

[1] M.Novosel, D.Krumes: Posebni čelici, Strojarski fakultet u Slavonskom Brodu, 1998.
[2] T.Filetin, F.Kovačićek, J.Indof: Svojstva i primjena materijala, FSB Zagreb, 2002.
[3] S.Brkić: Priručnik nehrđajući čelici u farmaceutskoj, prehrambenoj i kemijskoj industriji, HDMT, 2007.

CHARACTERIZATION OF ORGANIC-INORGANIC HYBRIDS PREPARED FROM POLY(METHYL METHACRYLATE) AND ORGANICALLY MODIFIED Si – ALKOXYDE

Ivan Brnardić, Marica Ivanković, Jelena Macan & Hrvoje Ivanković
University of Zagreb, Faculty of Chemical Engineering and Technology, Marulićev trg 19, HR-10000 Zagreb

Izvorni znanstveni rad / Original scientific paper

Organic-inorganic hybrid materials were prepared by the sol-gel process. Simultaneous polymerizations of methyl methacrylate (MMA) and an organically modified silicon alkoxyde, 3-glycidyloxypropyltrimethoxysilane (GLYMO), were performed. Poly(oxypropylene)diamine was used as a curing agent.

Prepared hybrid materials were studied by differential scanning calorimetry (DSC), thermogravimetric analysis (TGA), Fourier transform infrared spectroscopy (FTIR) and by transmission electron microscopy (TEM).

Inorganic phase formed as a result of GLYMO hydrolysis and condensation in the sol-gel process influences the glass transition temperature and improves the heat resistance of hybrid materials.

Key words: organic-inorganic hybrids, sol-gel, PMMA

1. Introduction

In the last decade, organic-inorganic hybrids became a fascinating new field of research in materials science. One of the main reasons for this is the chance of obtaining the desired and sometimes unique end properties, which can be hardly reached if only organic and/or inorganic components are used[1]. In polymer matrices small amounts (several %) of nanometer-sized particles can considerably influence the end properties of these systems. One of the most common ways for nanoparticle preparation is the sol-gel process[2-10]. The inorganic nanostructures can either be formed *in situ* simultaneously with organic polymer or they can be first prepared and then added to polimerizable monomers or to polymer solution.

The presence of covalent bonding between organic and inorganic components reinforces interaction between components and improves the properties of hybrid materials [2].

Hybrid materials based on SiO_2 and acrylic polymers, such as poly(methyl methacrylate), PMMA, were successfully prepared via sol-gel process. Simultaneous polymerizations of organic monomer and hydrolysis and condensation of tetraethoxysylane were peformed[11-13].

In this work organic-inorganic hybrid materials were prepared by the simultaneous polymerizations of methyl methacrylate (MMA) and an organically modified silicon alkoxyde, 3-glycidyloxypropyltrimethoxysilane (GLYMO), with varying MMA/GLYMO molar ratio. Poly(oxypropylene)diamine (D230) was used as epoxy ring-opening reagent.

2. Experimental

2.1. Preparation of organic-inorganic hybrids

Prior to the preparation of the organic-inorganic systems there were a number of preliminary studies which are worth noting[14]. Separately, the polymerization of MMA, the inorganic polymerization of GLYMO by sol-gel process (hydrolysis and condensation reactions), as well as reactions in the systems MMA/D230 and GLYMO/D230 were studied.

Based on the aforementioned preliminary studies[14] the detailed procedure of synthesis of organic-inorganic hybrids can be described as follows: GLYMO was prehydrolyzed with H2O (molar ratio GLYMO:H2O=1:1,5) . Acetic acid was used as a catalyst. This solution was stirred at room temperature for 1h then mixed with D230 (molar ratio Glymo: D230=1:1) and stirred for another 30 min.Various amounts of MMA were then added to the solution. AIBN was used as initiator of MMA polymerization. Numbers in the sample designations (hybrids H3, 5, 7, 9 in Table 1) represent approximate weight percent of inorganic phase calculated as $SiO_{1,5}$. The mixtures were left for 24 h at room temperature and then cured at 65°C for 24 h and post-cured at 140°C for 12 h.

Table 1: *Compositions and labels of investigated systems*

Sample	GLYMO *n*/mol	H_2O *n*/mol	CH_3COOH *n*/mol	D230 *n*/mol	MMA *n*/mol
H3	1	1,5	0,0092	1	15,09
H5	1	1,5	0,0092	1	7,08
H7	1	1,5	0,0092	1	3,64
H9	1	1,5	0,0092	1	1,74

2.2. Characterization

The infrared spectra of investigated systems were recorded by a Fourier transform infrared (FTIR) spectrometer (Bruker Vertex 70) equipped with an attenuated total reflection (ATR) accessory with a diamond crystal. 16 scans were collected for each measurement over the spectral range of 400-4000 cm^{-1} with a resolution of 4 cm^{-1}.

Dynamic differential scanning calorimetry (DSC) measurements were done on a Netzsch thermo analyzer STA 409. To determine the glass transition temperature, *T*g, of hybrids samples were heated from room temperature to 200°C at 10°C/min.

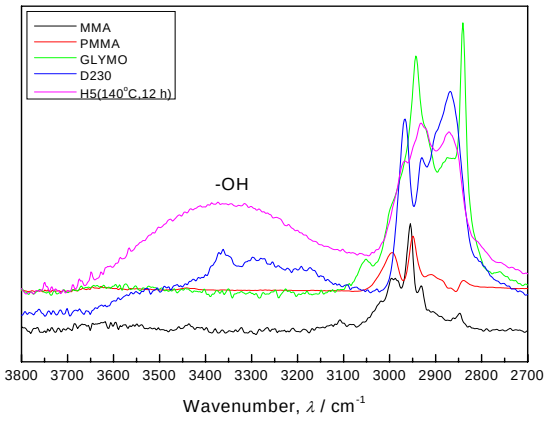
Weight loss of fully cured samples, weighing approximately 15 mg, was measured by thermogravimetric analysis (TGA), using a Perkin Elmer thermobalance TGS-2. The samples were heated from room temperature to 1000°C at a heating rate of 10 ^{o}C/min in the synthetic air atmosphere (gas flow of 150 cm^3/min).

To verify the morphology of the cured samples the materials were investigated by means of transmission electron microscopy (TEM), in JEOL 200 CX microscope with 120 kV acceleration voltage.

Solubility of samples was studied in tetrahydrofurane, THF.

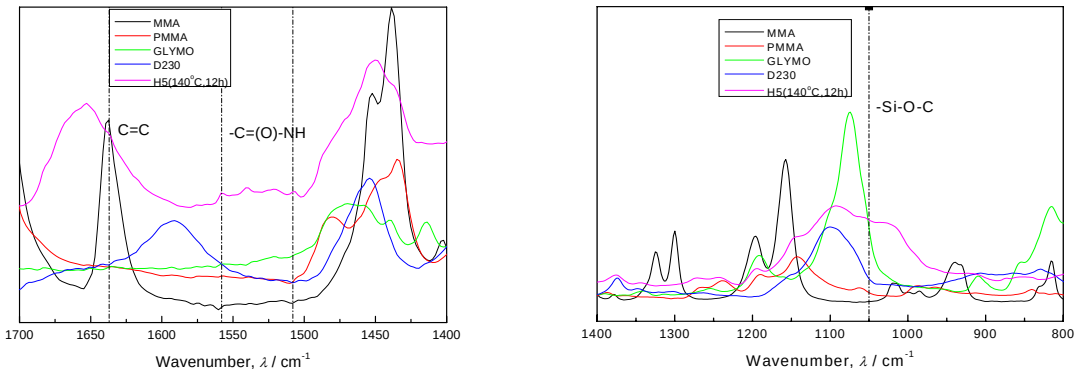
3. Results and Discussion

The results of FTIR analysis of hybrid H5 are given in Figure 1, a-c. Similar results were obtained for other hybrids. For comparison, FTIR spectra of MMA, PMMA, GLYMO and D230 are given as well.



a)

Figure 1. FTIR spectra of hybrid H5. Sample is post-cured at 140^{o}C for 12 h.



b) c)

Figure 1. FTIR spectra of hybrid H5. Sample is post-cured at 140°C for 12 h.

As seen, the sharp band at 1637 cm^{-1}, which is characteristic of C=C bond[15], is disappearing as a result of MMA polymerization. Bands between 1000 and 1200 cm^{-1} are characteristic for Si–O–Si bond and broad peak between 3100 and 3600 cm^{-1} is characteristic for silanol –OH groups. The appearance of new bands, at ~1560 cm^{-1} and 1510 cm^{-1}, which are characteristic for –C=(O)–NH– and band at ~1050 cm^{-1} which is characteristic for –Si–O–C bond[17], is observed.

Figure 2 shows the dynamic DSC thermograms of the PMMA and hybrid materials. As seen, relatively small changes in the glass transition temperature, T_g, were observed. The decrease of T_g in hybrids H3 and H5 in comparison to the PMMA can be caused by remain products of sol-gel process (water and alcohol) which act as plasticizers. In hybrid materials with higher content of inorganic phase (H7 and H9) glass transition was not observed. It could indicate a good interference between organic and inorganic phase. Similar results are reported in the literature[16].

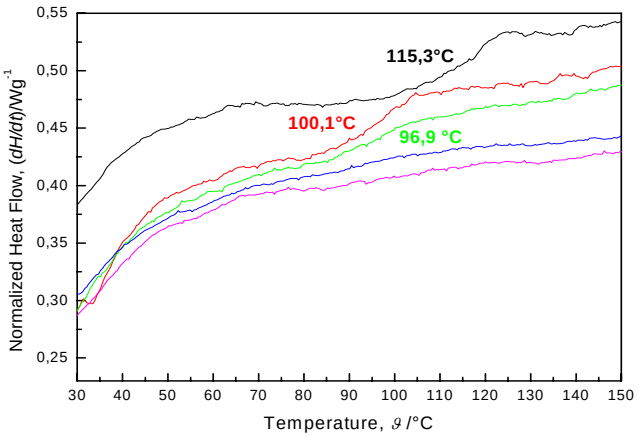
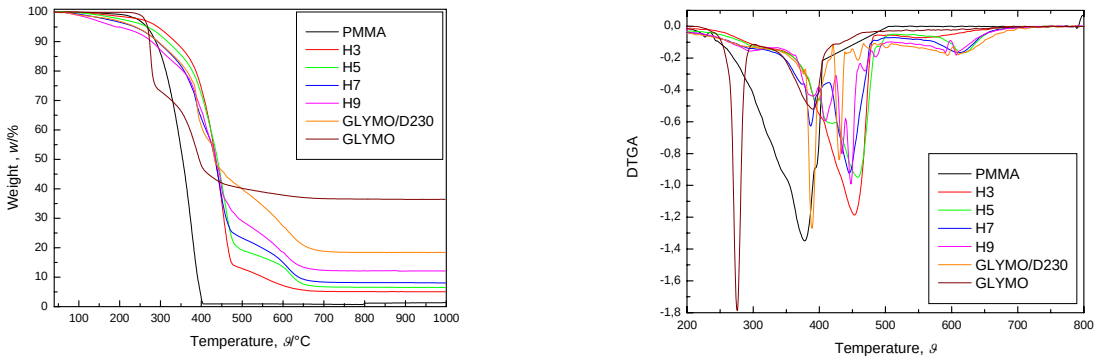


Figure 2. DSC thermograms of PMMA and hybrid systems. The glass transition is seen.

Results of TGA analysis are shown in Figure 3. The temperature at the maximum rate of weight loss was determined from the first derivation of the TGA curves (see Figure 3b) and summarized in Table 2.



a) b)

Figure 3: TGA (a) and DTGA (b) thermograms of investigated systems**.**

As expected, the increase in the GLYMO content in hybrid systems results in the increased weight residue after thermal degradation. Shape of DTGA curves for hybrids (Fig. 3b) imply on complex mechanism of thermal degradation. In hybrid materials H7 and H9, the onset temperature of degradation is shifted toward lower values in comparison with the systems H3 and H5. This could be caused by higher concentration of poly(oxypropylene) chains which are more prone to degradation than inorganic part or PMMA matrix[18]. In hybrid materials the temperature of the maximum degradation rate is higher than the latter for PMMA (Table 2). Presumably, the inorganic part of hybrid material can act as a mass transport barrier for volatile degradation products[3] and can reduce or prevail the negative influence of polymer part on heat resistance of material.

Table 2: *Temperature of maximum degradation rate,* ϑ_{max}

Sample	ϑ_{max} /°C
PMMA	378,1
H3	452,8
H5	458,3
H7	445,2
H9	447,3
GLYMO/D230	429,8
GLYMO	276,2

It should be noted that all hybrid materials were optically transparent indicating no phase separation of the organic and inorganic phases[19,20] at a scale smaller than the wavelength of visible light, that is 400 nm. To verify the morphology of the cured samples hybrid materials H3 and H7 were characterized with TEM (Figure 4 and 5). The TEM images showed quite homogenous distribution of components in the whole volume of material. Rare aggregates of inorganic particles smaller than 400 nm are observed.

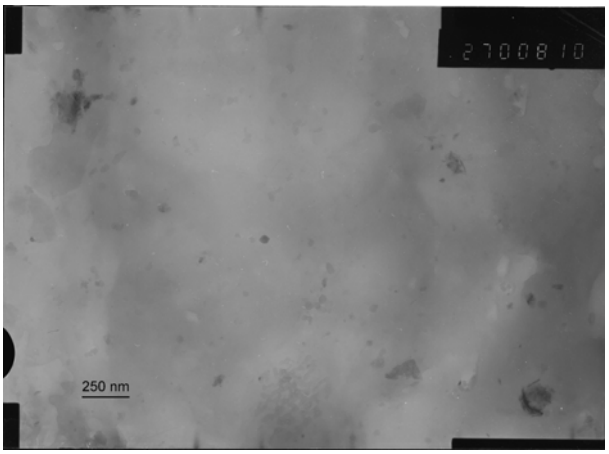


Figure 4. TEM image of hybrid H3.

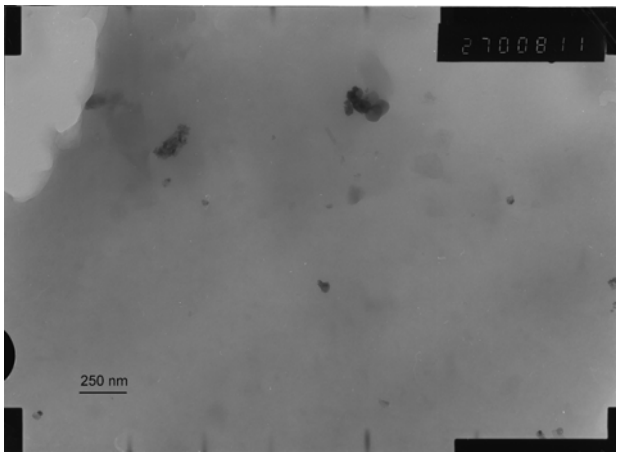


Figure 5. TEM image of hybrid H7.

Prepared samples were held in tetrahydrofurane, THF, for 60 days. PMMA is completely soluble, while inorganic systems (cured GLYMO and the system GLYMO/D230) are almost entirely insoluble. Hybrid materials are partially soluble in THF (between 4 and 20 mass %) what can be attributed to noncrosslinked structures.

Solubility results indicate that prepared hybrid materials are interpenetrating networks, IPN, i.e. combination of soluble linear (PMMA, D230) or grafted polymers (aminolyzed PMMA) and network structures. The latter could be an organic-inorganic network as a result of covalent bonding of PMMA to inorganic structures obtained by sol-gel process or a full IPN of crosslinked PMMA and inorganic network.

4. Conclusion

Poly(methyl methacrylate)-silica hybrids were prepared by a simultaneous polymerization of methyl methacrylate and 3-glycidyloxypropyltrimethoxysilane, using a poly(oxypropylene)diamine as a crosslinking agent. Prepared hybrid materials were studied by FTIR, DSC, TGA, TEM and solubility in tetrahydrofurane.

- FTIR results indicated complete polymerization of MMA in investigated systems.
- Hybrids have lower glass transition temperature than PMMA or the glass transition is not detectable.
- TGA analysis in synthetic air atmosphere showed better thermal stability of hybrid materials compared with PMMA
- The TEM images showed homogenous distribution of components in whole volume of material. Rare aggregates of inorganic particles smaller than 400 nm are observed.
- Solubility results indicated that prepared hybrid materials are interpenetrating networks, IPN, i.e. combination of soluble linear (PMMA, D230) or grafted polymers (aminolyzed PMMA) and network structures. The latter could be an organic-inorganic network as a result of covalent bonding of PMMA to inorganic structures obtained by sol-gel process or a full IPN of crosslinked PMMA and inorganic network.

References

1. U. Schubert, N. Hüsing, A. Lorenz, *Chem. Mater.,* **7** (1995) 2010.
2. L. Matějka, O. Dukh, J. Kolařík, *Polymer,* **41** (2000) 1449.
3. B.M. Novak, *Adv. Mater.* **5** (1993) 422.
4. E. Girardreydet ,T.M. Lam , J.P. Pascault, *Macromol. Chem. Phys.*, **195** (1994) 149.
5. J.E. Mark*, J. Appl. Polym. Sci.,* **58** (1995) 1135.
6. C.L. Jackson, B.J. Bauer , A.I. Nakatani, J.D. Barnes, *Chem. Mater.,* **8** (1996) 727.
7. J.E. Mark, *Polymer* **38** (1997) 4523.
8. D.W. Mccarthy , J.E. Mark , D.W. Schaefer*, J. Polym. Sci. Part B-Polym. Phys.,* **36** (1998) 1167.
9. L. Matejka, O. Dukh, J.Kolarik, *Polymer,* **41** (2000) 1449.
10. W. Zhou, J.E. Mark, M.R. Unroe, F.E. Arnold, *J. Appl. Polym. Sci.,* **79** (2001) 2326.
11. C.A. Avila-Herrera, O. Gomez-Guzman, J.L. Almaral-Sanchez, J.M. Yanez-Limon, J. Munoz-Saldana, R. Ramirez-Bon R*, J. Non-Cryst. Solids,* **352** (2006) 3561.
12. J.M. Yeh,C.J. Weng, W.J. Liao, Y.W. Mau*, Surface & Coatings Techn.,* **201** (2006) 1788.
13. J.M. Yeh, C.F. Hsieh, C.W. Yeh, M.J. Wu, H.C. Yang:*, Polym. Intern.,* **56** (2007) 343.
14. T.Vrabec, *Diploma Thesis*, University of Zagreb, Faculty of Chemical Engineering and Technology, Zagreb, 2007. (Croatian)
15. B. Kaczmarczyk, B. Morejko-Buž., A. Stolarzewicz, *Fresenius' J. Analyt. Chem.,* **370** (2001) 899.
16. J. Habsuda, G.P. Simon, Y.B. Cheng, D.G. Hewitt, D.R. Diggins, H. Toh, F. Cser, *Polymer,* **43** (2002) 4627.
17. C. Wu, T. Xu, W. Yang, *Europ. Polym. J.,* **41** (2005) 1901.
18. J. Pospíšil, S. Nešpurek, *Progress Polym. Sci.,* **25** (2000) 1261.
19. H.K. Schmidt, *J. Sol-Gel Sci. Technol.,* **8** (1997) 557.
20. C.J.T. Landry, B.K. Coltrain, J. A. Wesson, N. Zumbulyadis, J.L. Lippert, *Polymer,* **33** (1992) 1496.

DEFINIRANJE PARAMETARA PROCESA NAVARIVANJA SEGMENATA PAPUČA ROTORNOG BAGERA

DEFINING OF HARDFACING PARAMETERS OF BUCKET-WHEEL EXCAVATOR CRAWLER SHOES

Mr.sc Samir Butković, dipl.ing.maš-Mašinski fakultet Univerziteta u Tuzli
Mail: samir.butkovic@untz.ba
Dr.sc Omer Pašić, dipl.ing.maš- Mašinski fakultet Univerziteta u Sarajevu

Izvorni znanstveni rad / Original scientific paper

Sažetak: Efikasnost rada rotornog bagera u procesu proizvodnje u rudniku u najvećoj mjeri ovisi od frekventnosti i dužine trajanja kvara. Uzimajući u obzir da se kapacitet većine rotornih bagera kreće uglavnom od 1000m^3/h do 6000m^3/h može se zaključiti da bi kvar ovakvog sistema imao veoma negativne posljedice na cjelokupnu efikasnost proizvodnje u rudniku. S tim u vezi, u radu je dat kratak opis rotornog bagera, te problemi i oštećenja koja se najčešće javljaju na njegovom sistemu za horizontalno kretanje.

Bazirajući se na analizi uzroka oštećenja segmenata papuča rotornog bagera, kao jednog od najčešćih uzroka zastoja rotornog bagera, izvršen je odabir dodatnog materijala za proces reparaturnog navarivanja, nakon čega se kroz teoretsku analizu i eksperimentalni rad došlo do modela koji daje ovisnost parametara procesa navarivanja i mehaničkih osobina navarenih slojeva. Rezultati ispitivanja tvrdoće navarenih slojeva kao i metalografska ispitivanja za pojedine uzorake također su predstavljeni u radu.

Ključne riječi: materijal, navarivanje, rotorni bager

Abstract: Bucket wheel excavator efficiency mostly depends on failure time and failure frequency. Taking into account that capacity of the bucket wheel excavators generally vary from 1000m^3/h to 6000m^3/h, their failure would cause very negative consequences on production efficiency on mines. Thus, short description of the bucket wheel excavator, problems and damages which occur on its system for horizontal movement are presented in this work.

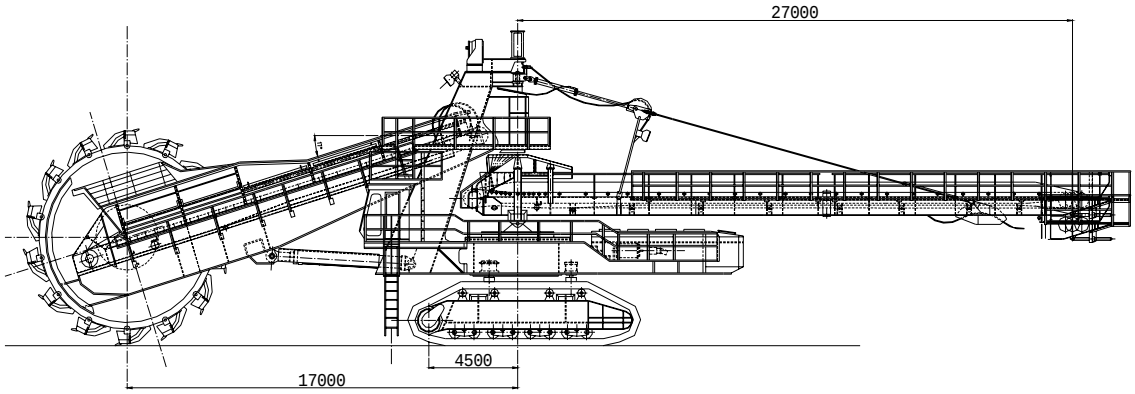
Based on analysis of damage cause of crawler shoe segments, as one of the most frequently occurring causes of bucket wheel excavator failure, selection of filler material for hardfacing process was performed. Then, through the theoretical analysis and experimental work, mathematical model which gives relation between mechanical properties and hardfacing parameters was derived. Hardness measurements results and metallographic examinations of specific samples are presented too.

Key words: material, hardfacing, bucket wheel excavator

1. Uvod

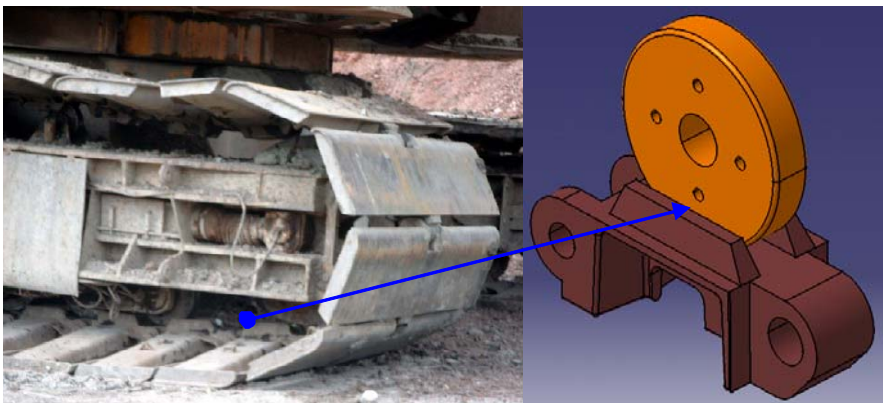
Rotorni bager predstavlja jedan od najvećih uređaja korištenih za kontinuirano otkrivanje i eksploataciju rude na površinskim kopovima, sl.1. Kontinuiranost rada, kao i veoma veliki kapaciteti ovakvih uređaja stvaraju i velike zahtijeve kada je u pitanju njihovo održavanje.

Obzirom da zastoj rotornog bagera izaziva veoma velike troškove, koji su direktno proporcionalni dužini trajanja zastoja, neophodno je sistemski rješavati probleme koji uzrokuju najčešće otkaze rotornog bagera.



Slika 1. Rotorni bager SRs401

Jedan od takvih problema jesu i kontaktni problemi koji se pojavljuju na sistemu za horizontalno kretanje rotornog bagera, sl.2. Velika masa, teški radni uvjeti, nepoznata i vremenski promjenjiva opterećenja, kretanje po neravnom terenu i dr. dovodi do posebno visokih kontaktnih opterećenja koja vode ka postepenom gubitku noseće mase dijelova koji se nalaze u kontaktima, sl. 2. Kao dodatni problem je prisutstvo abrazivnog stijenskog materijala, suho trenje u zoni kontakta kao i bočni pritisci koji su najintenzivniji kod promjene pravca kretanja bagera.



Slika 2. Mehanizam za horizontalno kretanje rotornog bagera [1]

Navedena opterećenja kao i kontaktni pritisci nastali uslijed kretanja bagera prenose se preko kotača i segmenata papuča rotornog bagera na tlo. Ovako visoka kontaktna opterećenja vode ka lokalnom plastičnom deformiranju gazećeg dijela segmenta stvarajući nagomilavanje materijala na krajevima segmenta, što dovodi do ometanog kretanja bagera te pritiskivanja susjednog

segmenta. Nakon određenog vremena zapremina nagomilanog materijala postaje prevelika tako da oštećuje susjedni segment. Nedostatak materijala na gazećem dijelu segmenta postaje toliki da su zazori preveliki i mogu dovesti do prekidanja gusjenice, a dotezanje gusjenice je dalje onemogućeno.
Zamjena oštećenih segmenata, pored troškova zastoja, troškova odvajanja segmenata od ostatka papuče, zavarivanja novog segmenta za ostatak papuče bagera iziskuje i dodatne troškove ljevanja segmenata. Ovdje je također bitno napomenuti da masa jednog segmenta iznosi preko 250kg [1]. Izmjene po pitanju konstrukcije također iziskuju visoke dodatne troškove, prvo zbog troškova konstrukcijske izmjene, a kao drugo, vrijeme potrebno za konstrukcijske izmjene je veoma dugo. Iz tog razloga, kao najadekvatniji način osposobljavanja bagera i njegovo vraćanje u rad u najkraćem vremenu, jeste navarivanje segmenata,sl.3. Pored niza navedenih prednosti, pravilnim odabirom dodatnog materijala, postupka i parametara navarivanja, moguće je postići osobine površinskog sloja segmenata koje će u velikoj mjeri povećati vrijeme između dva zastoja bagera, uzrokovan navedenim problemom.



Slika 3. Segment repariran navarivanjem [1]

2. Eksperimentalni rad

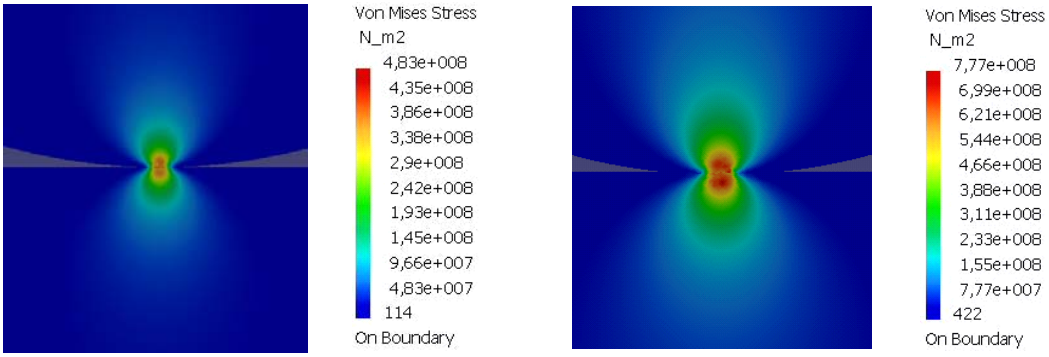
Dobijanje međusobne ovisnosti mehaničkih osobina navarenih slojeva i parametara procesa navarivanja je uvijet koji ima najveću važnost za konkretno izvođenje procesa navarivanja. Iz tog razloga cilj eksperimentalnog rada jeste dobijanje spomenute ovisnosti, sticanje dodatnih informacija o procesu navarivanja kao i donošenje zaključaka koji bi mogli predstavljati određeni doprinos rješavanju problematike navarivanja segmenata papuča rotornog bagera.

➢ *Izbor dodatnog materijala, parametara navarivanja i nivoa variranja*

Proces navarivanja je proces kod kojeg rezultati ovise od veoma velikog broja parametara. U parametre koji imaju određenog utjecaj na tijek i rezultate procesa navarivanja mogu se ubrojiti: dodatni materijal, pogonska energija, broj navarenih slojeva, temperatura između prolaza, promjer elektrode, temperatura predgrijavanja, vrsta struje, dužina luka itd.

S obzirom na uzrok oštećenja odnosno plastičnu deformaciju površinskog sloja segmenata, debljina navarenih slojeva igra veoma važnu ulogu za konačne rezultate procesa navarivanja. Pravu sliku o tome koliko debljina navarenih slojeva utječe na rezultate procesa navarivanja odnosno na ponašanje segmenata u radu, dobit će se ukoliko se izvrši naponska analiza mjesta kontakta segmenta i kotača rotornog bagera, sl.4. Naponska analiza je izvršena prema opterećenjima i dimenzijama rotornog bagera SRs401 čija masa iznosi približno 500t.

Cjelokupna masa zajedno s radnim opterećenjim prenosi se preko 16 kotača koji se kreću po gazećim stazama segmenata papuča [2]. Rezultati naponske analize predstavljeni su na slici 4.



Naponsko stanje na mjestu kontakta za F= 310kN (sopstvena težina bagera)

Naponsko stanje na mjestu kontakta za F=700kN

Slika 4. Naponsko stanje na mjestu kontakta segmenta i kotača bagera [3]

U toku samog izvođenja naponske analize primjećeno je da se maksimalni Von Misesovi naponi pomjeraju prema dubini navara kako se opterećenje na kontaktu povećava. Lako je primijetiti da se maksimalni Von Misesovi naponi kod opterećenja od 300kN nalaze na samoj površini odnosno na samom kontaktu segmenta i kotača bagera. Povećavanjem opterećenja maksimalni naponi se pomjeraju prema dubini segmenta, što znači da kod određenih opterećenja može doći do tečenja materijala ispod navarenog sloja (međusloj) [3].
S tim u vezi, geometrijske karakteristike odnosno debljina navarenih slojeva predstavlja veoma važan faktor za uspješnost procesa navarivanja segmenata papuča rotornog bagera.
Također, u toku procesa navarivanja mora doći do miješanja osnovnog materijala ili materijala međusloja s dodatnim materijalom, samim tim i do razblaženja ili obogaćivanja metala navara legirajućim elementima iz međusloja, što će na kraju imati određeni utjecaj na mehaničke osobine navarenog sloja [4]. Zbog svega navedenog, eksperimentalnim putem se želi ispitati utjecaj broja slojeva na mehaničke osobine navara.
Iz navedenih razloga kao parameter koji je variran u toku izvođenja eksperimenta jeste broj navarenih slojeva. Vrijednosti koje su dodijeljene spomenutom parametru su:

1-prvi nivo: N1 =1 sloj
2-drugi nivo: N3=3 sloja
3-centralni nivo:N2=2 sloja

N-broj slojeva navarivanja
Pogonska energija ili unijeta količina topline u toku navarivanja je parametar koji se direktno veže za proces strukturnih transformacija i termodifuziskih procesa koji se odvijaju u toku navarivanja. Variranjem pomenutog parametra stvaramo različite uvjete u kojima se odvijaju transformacije i očvršćavanje rastopljenog navara, što za posljedicu ima različite mehaničke osobine. Iz tog razloga opravdano je kod izvođenja eksperimenta, navarivanje izvoditi s više nivoa pogonske energije:

1-prvi nivo: Q1≈1 kJ/mm
2-drugi nivo: Q2≈1,8kJ/mm
3-centralni nivo Qsr≈1,4kJ/mm

Q- pogonska energija

Obzirom na uzrok oštećenja, preporuke proizvođača kao i ispitivanja provedena od strane proizvođača, kao dodatni materijal za izvođenje procesa eksperimentalnog navarivanja je odabrana elektroda Wearshield MM 40 s kemijskim sastavom predstavljenim u tablici 1.

Tablica 1. Dodatni materijal za tvrdo navarivanje

WEARSHIELD MM 40				
C [%]	Cr [%]	Mn [%]	Mo [%]	Si [%]
0, 2	3, 5	0, 5	0, 5	1, 5

Kao dodatni materijal za izvođenje navarivanja međusloja je odabrana elektroda EZ-CROM 20 s kemijskim sastavom predstavljenim u tablici 2.

Tablica 2. Dodatni materijal za navarivanje međusloja

EZ-CROM 20				
C[%]	Mn[%]	Si[%]	Cr[%]	Ni[%]
0, 12	6	<1	18, 5	8

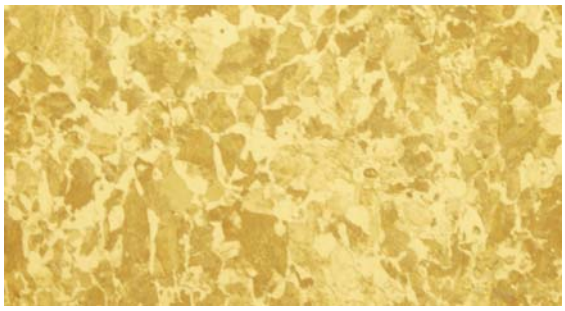
3. Rezultati eksperimentalnog rada

➢ *Osnovni materijal*

Osnovni materijal od koga su ljevani segmenti gusjenica je GS-36Mn5 i po svojoj strukturi odgovara feritno-perlitnim čelicima, sl.5.
Nakon mehaničkih ispitivanja više uzoraka došlo se do granice tečenja i vlačne čvrstoće materijala segmenata koje se kreću u intervalima predstavljenim u tablici 3.

Tablica 3. Mehaničke osobine osnovnog materijala

Granica tečenja [N/mm^2]	470-520
Zatezna čvrstoća[N/mm^2]	600-670
Tvrdoća HV1	250

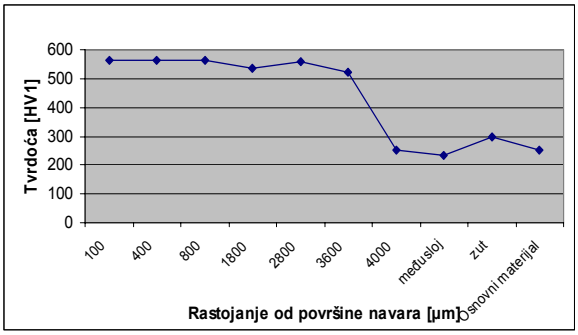


Slika 5. Mikrostruktura osnovnog materijala (3%HNO3, 200x) [1]

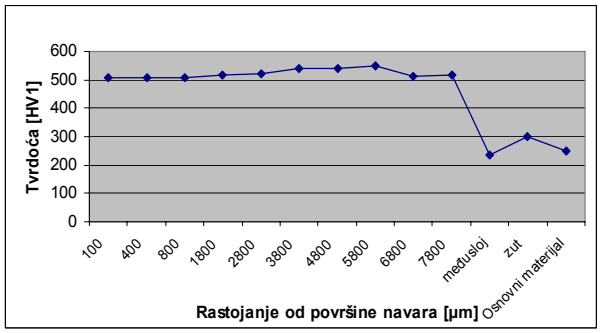
Ukoliko se dobijeni rezultati mehaničkih ispitivanja usporede s naponima dobivenim naponskom analizom kontakta kotača i segmenta bagera, sl.4, vidimo da se granica tečenja materijala segmenata koja je mjerodavna za početak plastične deformacije skoro izjednačila sa naponima koji vladaju na kontaktu. S tim u vezi, može se zaključiti da će i veoma mala prekoračenja opterećenja izazvati tečenje površinskog sloja materijala segmenta.

➢ *Rezultati ispitivanja eksperimentalnih uzoraka*

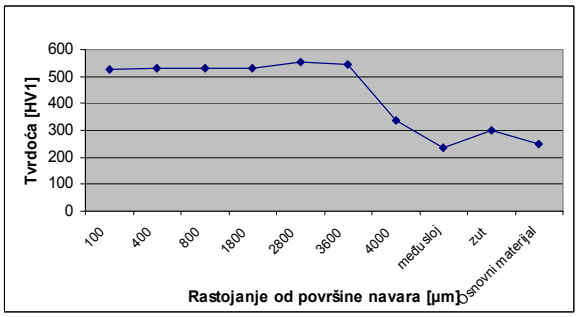
Kao izlazni parametar procesa navarivanja segmenata papuča rotornog bagera odabrana je tvrdoća po dubini poprečnog presjeka navara. Razlog odabira takvog izlaznog parametra leži u samom tipu oštećenja segmenata.
Naime, plastična deformacija površinskih slojeva neće ovisiti samo od površinske tvrdoće nego i od rasporeda tvrdoće i čvrstoće po dubini navara te strukture koja daje izmjerenu tvrdoću. Visoki pritisci koji se javljaju na mjestu kontakta kotača i segmenata papuče se raspoređuju po poprečnom presjeku segmenta i mijenjaju se prema djelujućem opterećenju, sl.4. S tim u vezi na slikama 6 i 7 predstavljeni su rezultati ispitivanja tvrdoće i mikrostrukture eksperimentalnih uzoraka.



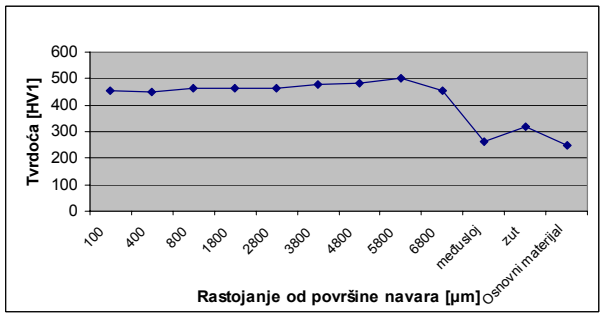
Q1-N1



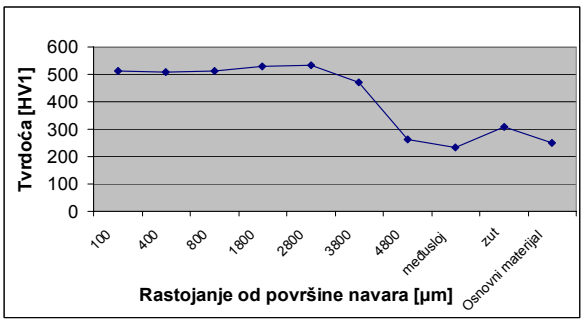
Q1-N3



Q2-N1



Q2-N3



Qsr-N2

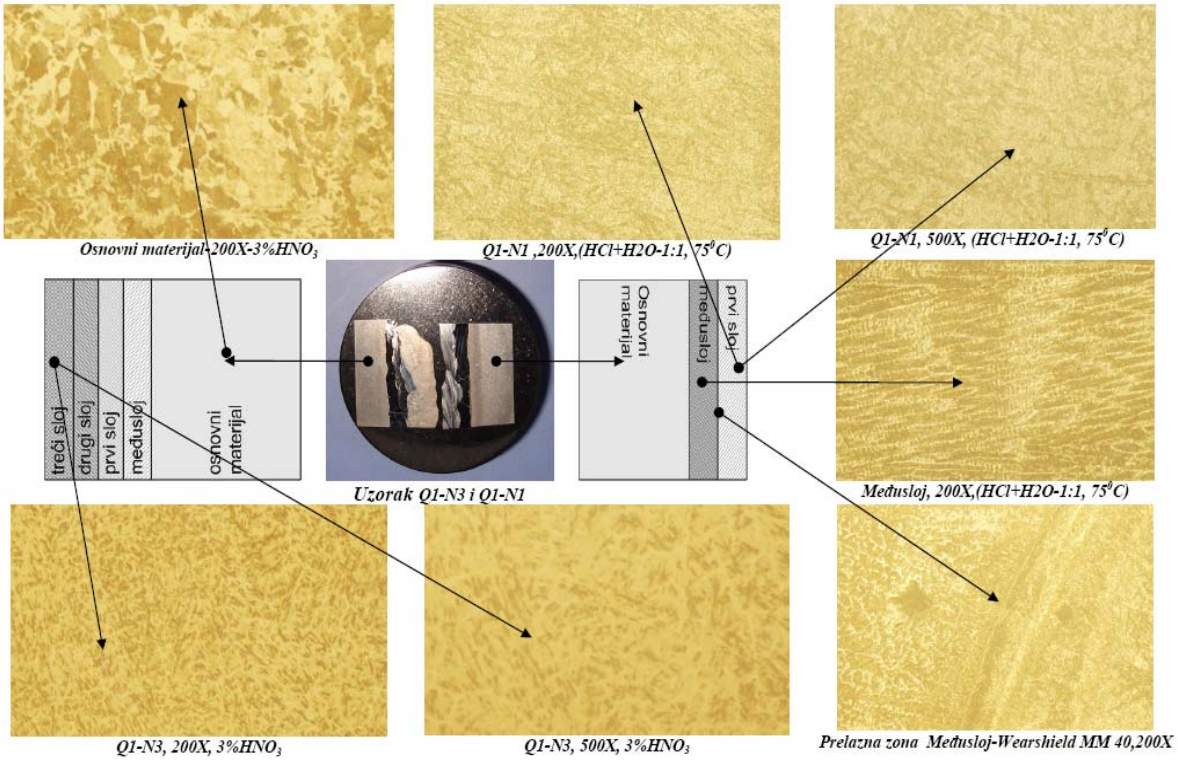
Slika 6. Rezultati ispitivanja tvrdoće eksperimentalnih uzoraka

4. Obrada eksperimentalnih rezultata

Nakon ispitivanja eksperimentalnih uzoraka izvršena je obrada eksperimentalnih rezultata. U tom cilju postoji više statističkih metoda koje omogućavaju donošenje određenih zaključaka uz razumnu mjeru rizika. U radu se koristi metoda najmanjih kvadrata. Suština ove metode je u ocjeni adekvatnosti modela, što se još naziva i regresijskom analizom.
Kao izlazni parametar regresijske analize koristi se prosječna tvrdoća navarenih slojeva na dubini od 2mm. Iz tog razloga u tablici 4 4. predstavljene su prosječne vrijednosti tvrdoće na dubini od dva milimetra za sve ispitivane uzorke

Tablica 4. Srednja vrijednost tvrdoće po dubini navarenog sloja za rastojanje 2mm od površine

Uzorak	Srednja vrijednost tvrdoće [HV1]
Q1-N1	556,25
Q2-N1	532
Q1-N3	510
Q2-N3	440
Qsr-N2	518,5
Qsr-N2	515,75
Qsr-N2	513,5



Slika 7. Rezultati strukturnih ispitivanja na uzorcima Q1-N1 i Q1-N3

Za modeliranje procesa korištena je matrica sa brojem eksperimenata $N=2^k+n_o=2^2+3=7$. Funkcija prosječne tvrdoće se matemetički modelira polinomskom funkcijom koja ima oblik za k=2:

$$Y=b_0+b_1X1+b_2X2+b_{12}X1X2$$

Kodirane vijednosti varijabli Xo,X1 i X2, bez obzira na njihovu fizikalnu mjernu jedinicu, izražene su sa tri vrijednosti 1,0 i -1 koje se dobijaju korištenjem jednadžbi za kodiranje (1), tako da donji nivo poprima vrijednost -1, gornji nivo +1 a srednji nivo 0.

$$Xi = \frac{x_i - x_{io}}{\frac{x_{i\max} - x_{i\min}}{2}} = \frac{x_i - x_{oi}}{\Delta x_i} \quad ...(1)\ [5]$$

S obzirom da je eksperiment planiran i izvođen sa ponavljanjem u centralnoj točki plana, koeficijenti modela $Y=b_0+b_1X1+b_2X2+b_{12}X1X2$ računaju se po sljedećim formulama (2) [5]:

$$b_o=\frac{1}{N}\sum_{j=1}^{N}X_{0j}y_j;b_i=\frac{1}{N-n_o}\sum_{j=1}^{N}X_{ij}y_j,za....i=1,2,..k;b_{im}=\frac{1}{N-n_o}\sum_{j=1}^{N}X_{ij}X_{mj}y_j,za..1\le i\le m\le k, \quad ...(2)$$

Postupak računanja i rezultati predstavljeni su u tablici 5.

Tablica 5. Računanje koeficijenata matematičkog modela

Xo	X1	X2	X1X2	Y	X1Y	X2Y	X1X2Y
1	-1	-1	1	556,25	-556,25	-556,25	556,25
1	1	-1	-1	532	532	-532	-532
1	-1	1	-1	510	-510	510	-510
1	1	1	1	440	440	440	440
1	0	0	0	518,5	0	0	0
1	0	0	0	515,75	0	0	0
1	0	0	0	513,5	0	0	0

b0	b1	b2	b12
512,5714	-23,5625	-34,5625	-11,4375

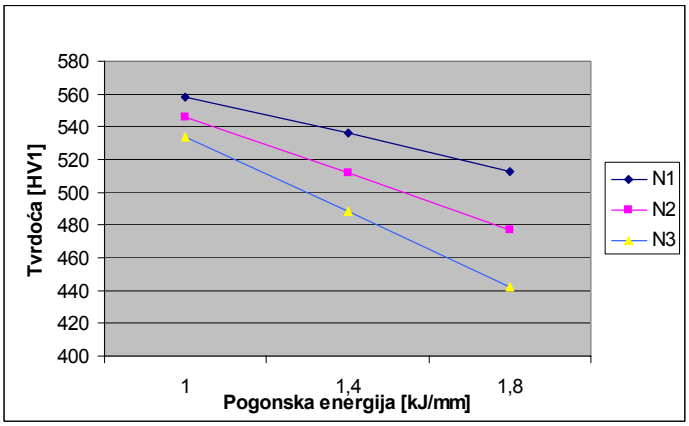
Nakon izračunavanja svih koeficijenata regresijske jednadžbe, možemo predstaviti matematički model:

$$Y=512,5714-23,5625X1-34,5625X2-11,4375X1X2$$

Nakon ispitivanja signifikantnosti koeficijenata i adekvatnosti modela utvrđeno je da su svi koeficijenti signifikantni i da matematički model adekvatno opisuje analizirani proces navarivanja.

Grafički prikaz regresijske jednadžbe ima značajne prednosti u očitavanju rezultata pri promjeni ulaznih parametara, sl.8. Ukoliko izvršimo prijelaz na prirodne koordinate možemo direktnom promjenom ulaznih parametara vidjeti odziv funkcije prosječne tvrdoće. Matematički model u prirodnim koordinatama predstavljen je sljedećim izrazom:

$$Y=583.869-1.71*Q+5.438*N-28.592*Q*N$$



Slika 8. Ovisnost prosječne tvrdoće od pogonske energije i broja navarenih slojeva za elektrodu Wearshield MM40

U rezultatima strukturnih ispitivanja, koji su sprovedeni u okviru eksperimenta, kod svih uzoraka primjećeno je prevladavanje martenzitne strukture, tako da s dovoljnom točnošću možemo primjeniti obrasce koji daju vezu između granice tečenja i tvrdoće materijala [6]. S tim u vezi dobijeni model za tvrdoću možemo transformisati u model za granicu tečenja kao relevantnu za početak plastičnog deformiranja navarenih slojeva:

$$\sigma_Y = 1631{,}3 - 4{,}77*Q + 15{,}193*N - 79{,}886*Q*N$$

5. Zaključak

Predstavljeni eksperimentalni rad i dobijeni matematički model su pokazali da mehaničke osobine navarenih slojeva u značajnoj mjeri ovise o parametru procesa navarivanja. Povećanje vrijednosti pogonske energije ima značajnog utjecaja na povećanje vremena hlađenja točaka u zoni topljenja i zoni utjecaja topline kao i na povećanje maksimalne temperature točaka u zoni utjecaja topline (prethodno nanešeni slojevi). Sve ukupno imalo je rezultat da povećanje pogonske energije uzrokuje smanjenje prosječne tvrdoće navarenih slojeva.

Miješanje dodatnog materijala i materijala međusloja uzrokuje obogaćivanje materijala navara legirajućim elementima iz međusloja uz zanemarljiv gubitak elemenata koji imaju uticaja na tvrdoću navarenih slojeva (ugljik).

S tim u vezi, može se zaključiti da se uticaj materijala međusloja smanjuje s povećavanjem broja slojeva tako da se i prosječna tvrdoća smanjuje povećavajući broj navarenih slojeva.

Analizirajući naponsko stanje na mjestu kontakta segmenta i kotača bagera uočeno je da se povećanjem opterećenja maksimalni Von Misesovi naponi s površine pomiču prema dubini segmenta. S tim u vezi može se reći da konačni rezultati procesa navarivanje neće ovisiti samo od postignutih mehaničkih osobina navarenih slojeva nego i od debljine navarenog sloja. Obzirom da je praktično nemoguće predvidjeti opterećenje koje trpi segment u toku rada bagera može se konstatirati da se povećanjem broja navarenih slojeva direktno utječe na povećanje stupnja sigurnosti od oštećenja segmenata.

Uzimajući u obzir dobijene osobine navarenih slojeva, djelujuća opterećenja i naponsko stanje na mjestu kontakta može se zaključiti da navareni segmenti mogu podnijeti opterećenja znatno veća od nominalnog. Iz tog razloga, kako bi se izbjeglo prerano oštećenje segmenata i zastoj bagera, potrebno je prije same ugradnje novih segmenata izvršiti njihovo navarivanje, što se pokazalo veoma pozitivnim u rudniku Dubrave kod Tuzle,BiH.

6. Literatura

[1]. Samir Butković: Optimizacija procesa navarivanja segmenata papuča rotornog bagera, Magistarski rad, Sarajevo 2007.godine,

[2]. TAKRAF :SRS-401,Upustvo za rukovanje, 1984.

[3]. Samir Butković, E.Šarić,M.Mehmedović:Analiza uzroka oštećenja i izbor dodatnog materijala kod reparature segmenata papuča rotornog bagera, CIMOSov dan raziskav– CRD '07, Koper,Novembar 2007.

[4]. 1999. W. Mayinger, K.J. Metzner: Dissimilar Metal Welds, SMIRT-Conference 2001.

[5]. Milan Jurković:Matematičko modeliranje, Bihać,

[6]. M Umemoto, K. Tsuchiya: Relationship between hardness and tensile properties various single structured steels, Materials Scienc and Technology, April 2001, Vol 17.

OTPORNOST NA TROŠENJE I KOROZIJU POVRŠINSKI MODIFICIRANIH SLOJEVA

WEAR AND CORROSION RESISTANCE OF SURFACE MODIFICATED LAYERS

Franjo Cajner, Darko Landek, Sanja Šolić
Sveučilište u Zagrebu, Fakultet strojarstva i brodogradnje
Ivana Lučića 5, 10000 Zagreb
E-mail: franjo.cajner@fsb.hr, darko.landek@fsb.hr, sanja.solic@fsb.hr

Izvorni znanstveni rad / Original scientific paper

Sažetak:

U radu su prikazani vlastiti rezultati ispitivanja utjecaja na otpornost na adhezijsko trošenje i koroziju ugljičnog čelika C45 nakon postupaka nitrokarburiranja sa i bez naknadne oksidacije u solnoj kupci, boriranja u pasti i vanadiranja u solnoj kupci.. Na uzorcima je ispitana hrapavost površine, mikrostruktura rubnog sloja, te su provedena ispitivanja otpornosti na adhezijsko trošenje i otpornosti na koroziju. Dobiveni rezultati pokazali su dobru otpornost na koroziju i adhezijsko trošenje nitrokarburiranog i naknadno oksidiranog, te boriranog sloja. Vanadirani uzorci pokazali su sklonost pitting koroziji.

Ključne riječi:
nitrokarburiranje, boriranje, vanadiranje, otpornost na trošenje, korozijska otpornost

Abstract:

The paper presents testing results on the influence to adhesion wear and corrosion resistance of carbon steel C45 nitrocarburized with and without salt bath post oxidation, paste boronized and salt bath vanadized. Surface roughness and microstructure analysis were performed on the specimens, and also adhesion wear and corrosion resistance were tested. Results show good corrosion and adhesion wear resistance of nitrocarburized and post oxidized sample and also on boronized sample. Vanadized samples showed tendency to pitting corrosion.

Key words: nitrocarburizing, boriding, vanadizing, wear resistance, corrosion resistance

UVOD

Za površinski oplemenjene dijelove i alate u nizu slučajeva zahtijeva se kombinacija otpornosti na trošenje i otpornosti na koroziju. Stoga je u radu istražena otpornost na koroziju četiri površinska sloja otporna na pojedine karakteristične tipove trošenja. Istražena su svojstva površinskih slojeva nakon modificiranja postupcima nitrokarburiranja sa i bez naknadne oksidacije, boriranja i vanadiranja.

Nitriranje je postupak u kojem u površinu čelika difundira dušik pa se stvaraju Fe-nitridi (npr. Fe_4N i $Fe_{2-3}N$). Ako istovremeno u površinski sloj čelika difundira i ugljik postupak se naziva nitrokarburiranje. Svim postupcima nitriranja i nitrokarburiranja zajedničko je da se odvijaju ispod temperature A_1 tako da mikrostruktura u jezgri obratka ne doživljava nikakvu promjenu (uz nužno prethodno kaljenje i popuštanje na dovoljno visoku temperaturu). Nitriranje se može provoditi u prašku, solnim kupkama (npr. postupak TENIFER), plinu i u plazmi ioniziranih plinova. Nitriranjem (i nitrokarburiranjem) se postižu slijedeća svojstva: povišena površinska tvrdoća, povećana otpornost na (adhezijsko) trošenje, povećana otpornost na koroziju, dobra otpornost trošenju na povišenim temperaturama (500–550 °C), otpornost toplinskom umoru, povećana dinamička izdržljivost, male ili zanemarive deformacije obratka. Dodatno povišenje otpornosti na koroziju postiže se ako se nakon nitrokarburiranja primjeni postupak naknadne oksidacije [1-3].

Boriranje je toplinsko-difuzijski postupak pri kojem u površinske slojeve čelika difundira bor te dolazi do stvaranja Fe- borida (FeB, Fe_2B). Postupak se izvodi na temperaturama 800 do 1100 °C u trajanju od nekoliko sati. Sredstva u kojima se izvodi boriranje mogu biti u obliku praška (granulata), paste (pogodno za lokalno boriranje), plinske atmosfere (vrlo otrovan i rijetko primjenjivan postupak) ili solne kupke. Pri provedbi boriranja čelika s povišenim sadržajem ugljika ispod boridnog sloja nastaje tzv. ugljikov bedem. Do ove pojave dolazi potiskivanjem ugljika uslijed difuzije bora koje dovodi do povećanja koncentracije ugljika ispod zubi boridnog sloja. Pri provedbi boriranja čelika legiranih s povećanim sadržajem Si i Al dolazi do stvaranja tzv. "mekog jarka" ispod boridnog sloja koji loše utječe na eksploatacijska svojstva obratka (tvrdi rub na mekoj podlozi). Stvaranje mekog jarka uvjetovano je povećanjem sklonosti čelika stvaranju ferita potaknute djelovanjem legirajućih elemenata Si i Al. Dubine boridnih slojeva iznose od nekoliko desetaka μm do 0,3 mm ovisno o vrsti čelika, trajanju i temperaturi boriranja, sredstvu za boriranje, brzini grijanja i hlađenja te naknadnoj toplinskoj obradi. Borirani dijelovi imat će, uz nešto nižu žilavost i čvrstoću savijanja, slijedeća svojstva, vrlo visoku tvrdoću, visoku otpornost na trošenje (abraziji, eroziji, kavitaciji i postojanost na visokim temperaturama (do 1050 °C), otpornost prema kiselinama i lužinama. Boriranje se uobičajeno provodi na: ugljičnim i niskolegiranim čelicima, željeznim ljevovima i tvrdim metalima. Najpogodniji čelici za boriranje su niskougljični nelegirani čelici zbog toga jer neće doći do pojave povećane krhkosti zbog malog udjela ugljika [2,3].

Vanadiranje je difuzijski postupak stvaranja vanadijevih karbida koji se provodi u solnoj kupci koja sadrži boraks vanadij u obliku ferolegure i aktivatore pri temperaturama od 850 do 1200°C, u trajanju od nekoliko sati. Po završetku difuzije obradak se sa temperature obrade hladi u vodi, ulju ili slanoj kupki. Mehanizam procesa sastoji se od kemijske reakcije djelomično otopljenog vanadija s ugljikom iz čelika čime nastaje kemijski spoj vanadij-karbid (VC) na površini obratka. Karbidni sloj raste uslijed reakcije ugljika, koji difundira iz čelika ka površini i otopljenog vanadija iz kupke. Nastali sloj sastoji se od vanadija i ugljika, praktično bez željeza. Ispod karbidnog sloja stvara se zona djelomične difuzije vanadija osiromašena ugljikom, koji je difundirao prema površini, stoga su za primjenu vanadiranja prikladni visokougljični čelici ili prethodno pougljičeni niskougljični čelici. Nakon

vanadiranja nastaje tvrdi sloj vanadij karbida debljine do nekoliko μm. Ova sloj otporan je na abrazijsko trošenje, oksidaciju i zadržava visoku tvrdoću do temperatura oko 800°C. Zbog svojih dobrih triboloških i kemijskih svojstva karbidnih slojeva te zbog višestruko povećanog vijeka trajanja vanadiranje nalazi prvenstveno primjenu kod konstrukcijskih dijelova izloženih jakom abrazijskom trošenju i različitih vrsta alata, poput alata za oblikovanje deformacijom, dijelova gravure kalupa za tlačni lijev aluminijskih legura, dijelova alata za oblikovanje polimera i polimernih kompozita [4].

EKSPERIMENTALNI DIO

Ispitni uzorci za analizu korozijske postojanosti izrađeni su od nelegiranog čelika za poboljšavanje, Ck45 u brušenom stanju (kvaliteta površine N5). Kemijski sastav čelika naveden je tablicom I.

TABLICA I. Kemijski sastav čelika Ck45.

%C	%P	%S	%Si	%Mn	%Ni	%Mo	%Cr
0,45	0,012	0,016	0,22	0,64	0,066	0,013	0,09

Za određivanje brzine korozije gravimetrijskom metodom izrađeni su uzorci dimenzija Φ 10x 50 mm, a za određivanje brzine elektrokemijske korozije uzorci su dimenzija Φ 10 x 10 mm. Na ispitnim uzorcima je provedena toplinska obrada sa parametrima prema u tablici II.

TABLICA II. Parametri toplinske obrade, ispitnih uzoraka od čelika Ck45 i postignuta debljina zone spojeva

Postupak toplinsko kemijske obrade	Predgrijavanje	Parametri toplinske obrade	Izmjerena debljina sloja,μm
Tenifer	**350 ^{0}C / 30 min / zrak**	**TF1 / 580 ^{0}C / 120 min / voda**	**~ 18**
Tenifer – Q	**350 ^{0}C / 30 min / zrak**	**TF1 / 580 ^{0}C / 120 min** **AB1 / 380 ^{0}C / 30 min / voda**	**- - - -**
Tenifer – QPQ	**350 ^{0}C / 30 min / zrak**	**TF1 / 580 ^{0}C / 120 min** **AB1 / 380 ^{0}C / 30 min** **Poliranje** **AB1 / 380 ^{0}C / 15 min / voda**	**~ 16**
Boriranje	**900 ^{0}C / 70 min / peć**	**EKABOR 1 /900 ^{0}C /240/min/peć**	**~ 110**
Vanadiranje	**- - - -**	**900 ^{0}C / 240 min / ulje**	**~ 8**

Ispitivanje hrapavosti površine provedeno je na elektromehaničkom uređaju za mjerenje hrapavosti ticalom PERTHOMETER M4Pi. Izmjerena je najveća visina neravnina (R_t, μm) i srednja aritmetička udaljenost profila (R_a, μm).

Tvrdoća je ispitivana na metalografski pripremljenim uzorcima i to na poprečnom presjeku od ruba prema jezgri u Vickersovom metodom HV0,2.

Korozijska postojanost ispitivana je gravimetrijskim i elektrokemijskim metodama [5]. Gravimetrijska metoda određivanja brzine korozije, provodi se u atmosferi zasićenoj kapljicama elektrolita, tzv. slanoj magli. Postupak je normiran prema normi SS DIN 50 021. Slanu maglu čini 5% vodena otopina NaCl na temperaturi 25 ^{0}C, čime se simulira korozija u atmosferi morske vode. Na svim ispitnim uzorcima se prije stavljanja u slanu komoru odredi masa. Nakon dogovorenog broja sati provedenih u slanoj komori s ispitnih uzoraka se skidaju korozijski produkti i određuje se gubitak mase tijekom izlaganja korozijskoj atmosferi, te se također određuje stupanj zaštite prema slijedećoj jednadžbi:

$$z = \frac{v_{KOR\,0} - v_{KOR\,n}}{v_{KOR\,0}} \circ 100\% \qquad (1)$$

$v_{KOR\,0}$ – brzina korozije uzorka u neobrađenom stanju, g / m^{2}h

$v_{KOR\,n}$ – brzina korozije na površinski modificirano ispitnom uzorku, g / m^{2}h

Ispitivanja otpornosti na elektrokemijsku koroziju provedena su pomoću uređaja EG&G PARC Potentiostat/Galvanostat Model 263A, s programskom podrškom Model 352/252 SoftCorr II. Ispitivanja su provedena u klasičnoj elektrokemijskoj ćeliji s tri elektrode volumena 100 cm^3, u 3% NaCl pri 25 ^{0}C. Kao radne elektrode korišteni su prethodno pripremljeni ispitni površinski modificirani uzorci prema tablici II. Svaka elektroda je izolirana lakom po cijeloj svojoj površini osim radne površine, koja je nakon mjerenja odmašćena i pripremljena za ispitivanje. Kao referentna elektroda upotrijebljena je zasićena kalomel elektroda, a kao protuelektroda za zatvaranje strujnog kruga korištena je elektroda od platine. Provedeno je određivanje gustoće korozijske struje metodom Tafelove ekstrapolacije i određivanje polarizacijskog otpora. Mjerenjem potencijala ili razlike potencijala utvrđuje se je li korozija anodno ili katodno upravljana i da li se njen mehanizam vremenom mijenja. Na temelju dobivenih rezultata nije moguće dobiti kvantitativne zaključke o brzini korozije te će se u eksperimentu na temelju dobivenih rezultata mjerenjem izračunati odgovarajući stupanj djelotvornosti zaštite dolje navedenom jednadžbom (2):

$$z = \frac{j_{KOR\,0} - j_{KOR\,n}}{j_{KOR\,0}} \circ 100\% \qquad (2)$$

$j_{KOR\,0}$ – gustoća korozijske struje izmjerena na neobrađenom uzorku, μA / cm^2

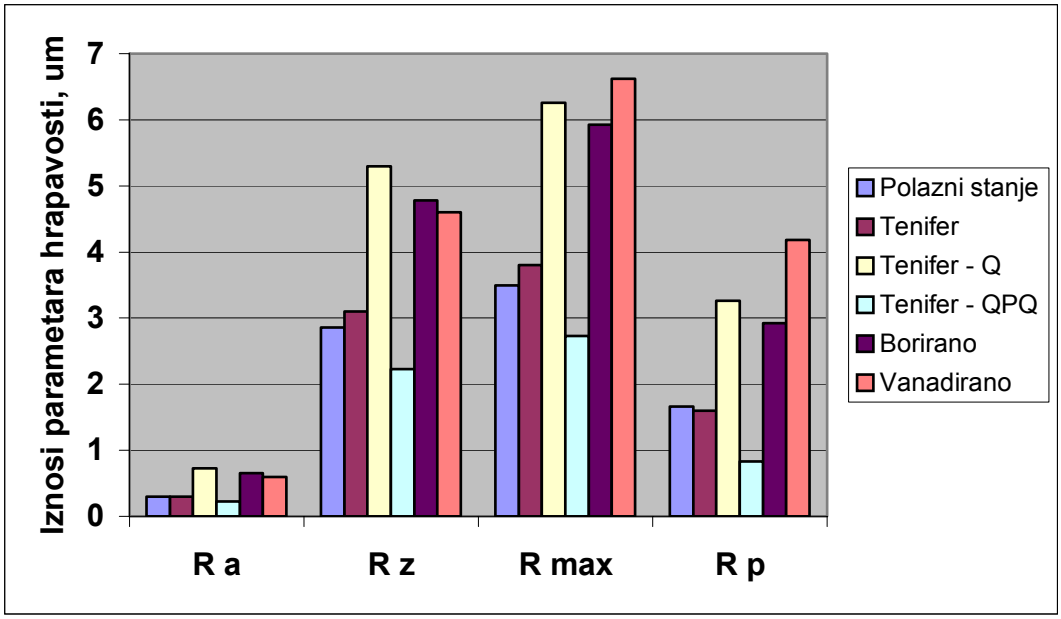
$j_{KOR\,n}$ – gustoća korozijske struje izmjerena na površinski modificirano ispitnom uzorku, μA / cm^2

Ispitivanje otpornosti na adhezijsko trošenje i određivanje faktora trenja provedeno je na uređaju s kliznim kontaktom ispitnog uzorka i tarnog prstena. Klizni kontakt trajao je jednu minutu, što odgovara 30 okretaja tarnog prstena. Polužni sustav baždaren je prije ispitivanja, tj. određena je ovisnost: *progib elastičnog pera* (l, mm) – *sila trenja* (F_t, N). Za svaki pokus korišten je novi tarni prsten od kaljenog čelika. Tijekom pokusa očitavan je progib elastičnog pera, te je pomoću baždarne krivulje izračunata sila trenja. Normalna sila opterećenja kliznog para zadana je težinom utega obješenih na elastično pero. Prije i poslije ispitivanja izmjerena je masa ispitnog uzorka, kao bi se odredio gubitak mase trošenjem [6].

REZULTATI I DISKUSIJA REZULTATA

Rezultati ispitivanja hrapavosti površina prikazani su na slici 1. Uzorak obrađen u oksidacijskoj kupki i nepoliran (Tenifer - Q) pokazao je neznatno višu vrijednost hrapavosti što je čini se posljedica relativno dugog držanja u kupki AB1. Zadržavanje niskih vrijednosti parametara hrapavosti nakon naknadne kratkotrajne oksidacije (Tenifer – QPQ) čini ovaj postupak prikladnim za primjenu kod dijelova i alata koji se toplinski obrađuju nakon

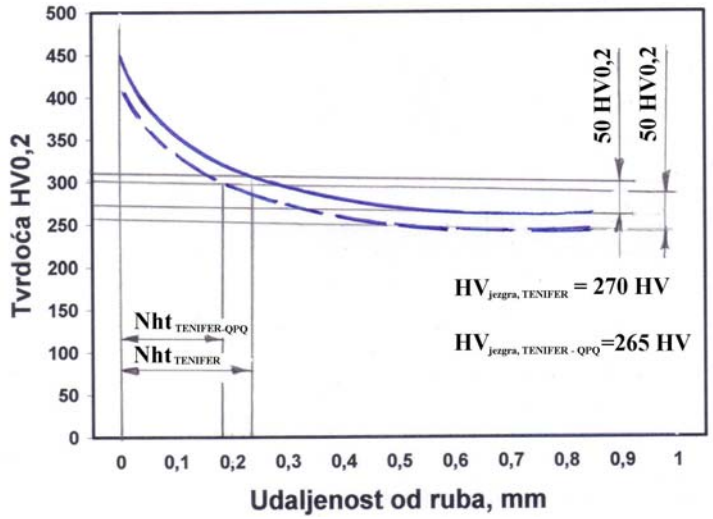
toplinske na konačnu mjeru. Najmanja vrijednost svih parametara površinske hrapavosti postignuta je nakon postupka Tenifer – QPQ što je posljedica poliranja tog uzorka tijekom obrade. Primjenom boriranja vrijednosti površinske hrapavosti se povećavaju u odnosu na toplinski neobrađeno stanje zbog stvaranja boridnog sloja. Postignute vrijednosti parametara hrapavosti slične su parametrima dobivenim postupkom Tenifer – Q. Vanadirani uzorak također pokazuje više vrijednosti parametara hrapavosti u odnosu na polazni stanje pri čemu su vrijednosti parametara slične onima dobivenim postupkom Tenifer – Q i postupkom boriranja. Povećanje parametara hrapavosti je posljedica je stvaranja vanadijevog karbida na površini čelika.



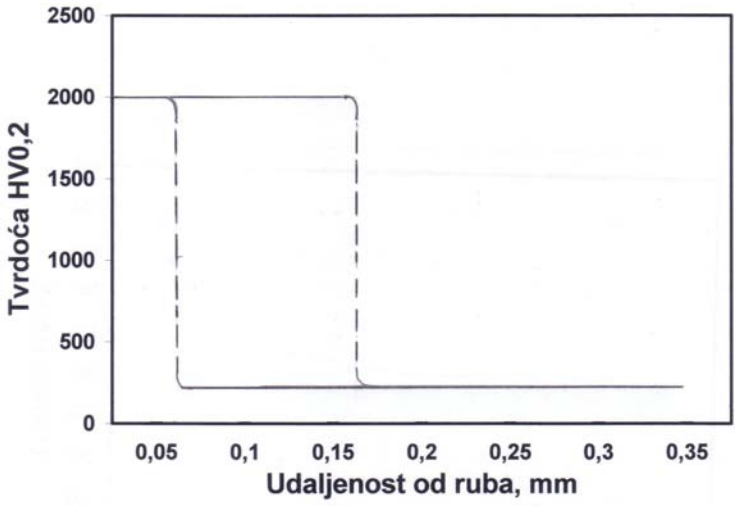
SLIKA 1: Vrijednosti parametara hrapavosti ispitnih uzoraka od čelika Ck45 u polaznom (neobrađenom) stanju, nakon nitrokarburiranja postupcima Tenifer, Tenifer - Q i Tenifer – QPQ te nakon boriranja i vanadiranja.

Rezultati ispitivanje tvrdoće prikazani su na slici 2. Iz ispitane raspodijele tvrdoće u rubnom sloju uočava se da uzorak obrađen postupkom Tenifer pokazuje nešto višu tvrdoću po cijelom presjeku, u odnosu na uzorak obrađen postupkom Tenifer QPQ, što je posljedica izlučivanja Fe – nitrida tijekom naknadne oksidacije. Sloj borida koji je nastao nakon 4 sata pri temperaturi od 900 ^{0}C sastoji se i od Fe_2B i FeB borida, čija je tvrdoća oko 2000 HV dok je tvrdoća jezgre 224 HV. Debljina sloja je oko110 μm. Zbog uzubljenog oblika boridnog sloja debljina sloja varira od 0,07 do 0,17 mm. Raspored tvrdoće na poprečnom presjeku vanadiranog uzorka pokazuje da je ispod sloja vanadijevog karbida nastao neznatan pad tvrdoće, a približavanjem jezgri nakon dubine od 0,2 mm, tvrdoća se ponovo povećava. Razlog smanjenju tvrdoće ispod sloja vanadijevog karbida je osiromašenje ruba uzorka ugljikom koji se s vanadijem vezao vanadij karbid na površini uzorka.

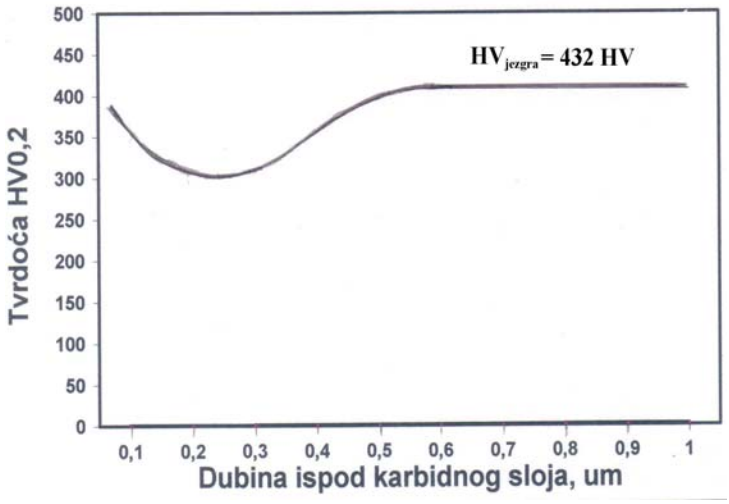
1.



2.



3.



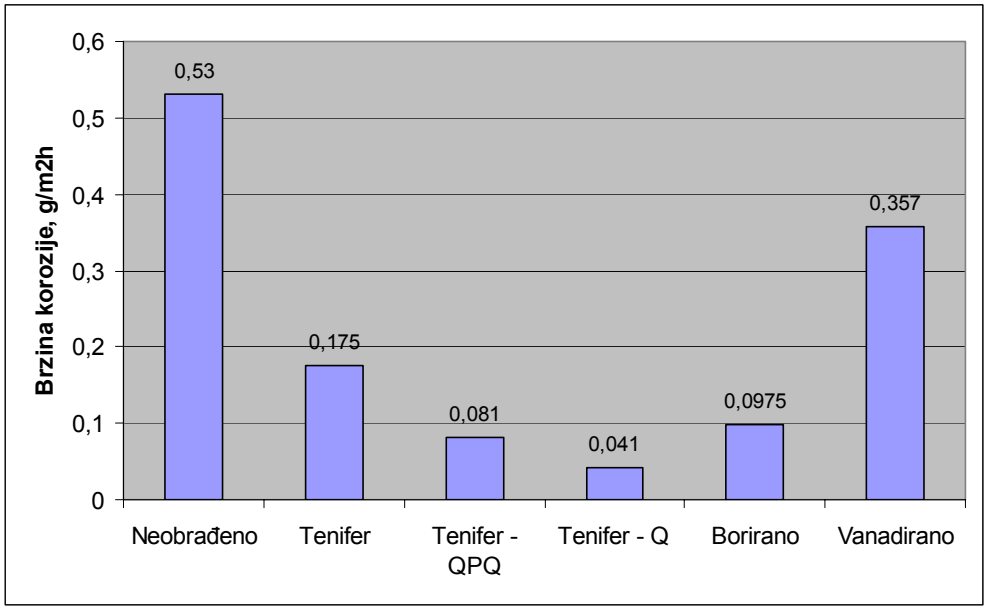
SLIKA 2: Raspored tvrdoće u rubnom sloju ispitnog uzorka od čelika Ck 45 nakon površinskog modificranja postupcima:

1. nitrokarburiranja s i bez naknadne oksidacije
2. boriranja u pasti
3. vanadiranja u solnoj kupci

Gravimetrijska metoda određivanja brzine korozije, provodila se u atmosferi koja zasićenoj kapljicama otopine elektrolita u tzv. slanoj magli. Postupak je proveden prema normi SS DIN 50 021 tzv. SS –test. Parametri ispitivanja bili su:

- Temperatura……..: 33 ^{0}C
- Otopina…….: 5% NaCl
- Vrijeme ispitivanja……...: 96 sati (4 dana)

Rezultati ispitivanja prikazani su na slici 3. Stupanj djelotvornosti zaštite određen prema jednadžbi (1) za svaku pojedinu grupu toplinski obrađenih uzoraka, prikazan je u tablici IV. U tablici V prikazan je izgled ispitanih uzoraka sa i bez produkata korozije.



SLIKA 3: Brzine korozije grupa uzoraka nakon 96 sati ispitivanja u slanoj komori prema normi SS DIN 50 021.

Tablica III: Vrijednosti stupnjeva djelotvornosti zaštite (z, %), dobivene gravimetrijskom metodom.

Vrsta toplinske obrade	**Stupanj djelotvornosti zaštite z, %**
Tenifer	**70**
Tenifer – Q	**92**
Tenifer – QPQ	**85**
Boriranje	**82**
Vanadiranje	**33**

Iz slike 3. se vidi da su svi toplinski obrađeni uzorci pokazali bolju korozijsku postojanost od osnovnog toplinski neobrađenog uzorka. Nadalje, ako se promotre postupci nitrokarburiranja Tenifer, Tenifer – Q i Tenifer – QPQ, može se uočiti da su najlošiju otpornost korozijskom djelovanju pokazali uzorci obrađeni postupkom Tenifer.

Tablica IV: Fotografije uzoraka sa i bez korozijskih produkata, nakon 96 sati ispitivanja u slanoj komori prema SS DIN 50 021 testu.

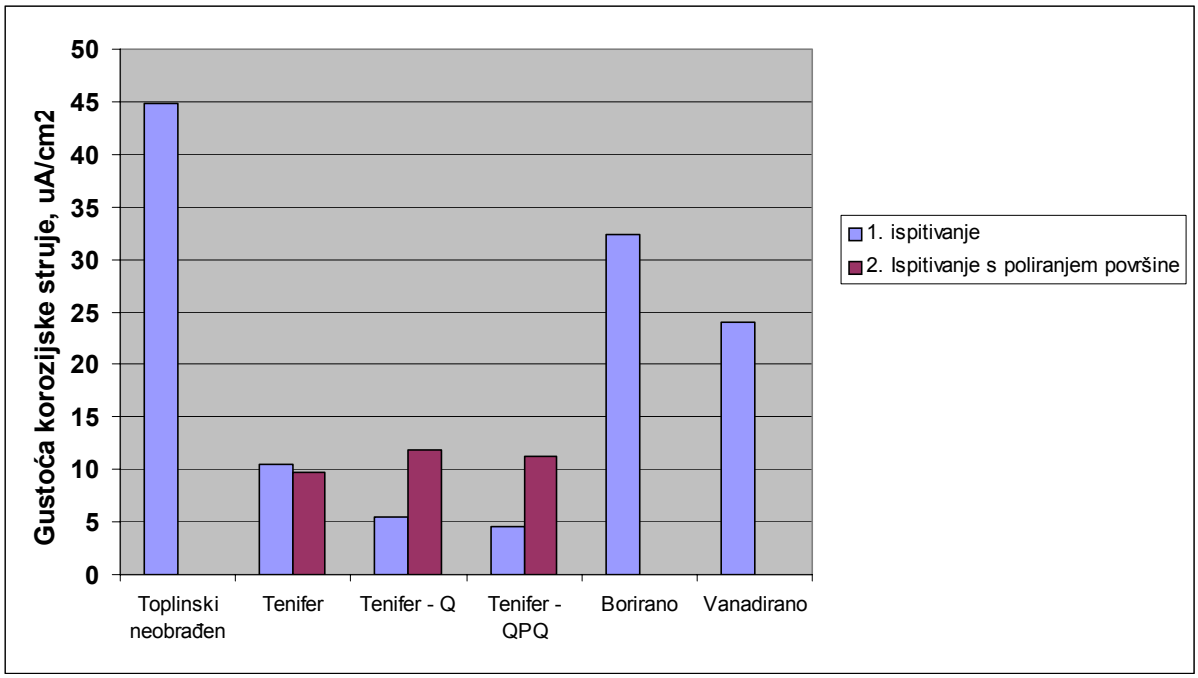
Parametri toplinske obrade	**Oznaka uzorka**	**Nakon korozije**	**Nakon skidanja korozijskih produkata**
<u>Toplinski neobrađeno</u> **Polazni materijal Č1531 (Ck45)**	**1.** **2.** **3.**		
Nitrokarburirano postupkom Tenifer **580 ^{0}C / 2h / voda**	**12.** **13.** **14.**		
Nitrokarburirano postupkom Tenifer – QPQ 580 ^{0}C/2h +AB1/380 ^{0}C/30 min/voda **poliranje AB1/380 ^{0}C/15 min/voda**	**22.** **23.** **24.**		
<u>Nitrokarburirano postupkom Tenifer – Q</u> **580 ^{0}C/2h +AB1/380 ^{0}C/30 min/voda**	**26.** **27.**		
<u>Borirano</u> **EKABOR1 / 900 ^{0}C / 4h / peć**	**32.** **34.**		
<u>Vanadirano</u> **900 ^{0}C / 4h / ulje**	**42.** **43.** **44.**		

Nakon držanja u solnoj kupki Tenifer TF1 pri temperaturi od 580 ^{0}C u trajanju od 2 sata ispitni uzorci su stavljeni u oksidacijskoj kupku AB1 na temperaturu 380 ^{0}C u vremenu od 30 min te je u tih 30 min stvorena dovoljna količina željeznog oksida čime je postignuta dobra korozijska otpornost postupka Tenifer – Q. Nakon toga su uzorci predviđeni za obradu postupkom Tenifer – QPQ polirani i oksidirani u kupci AB1 na istoj temperaturi od 380 ^{0}C ali u vremenu od 15 min. Razloge slabije korozijske otpornosti valja tražiti u činjenici da su uzorci obrađeni postupkom Tenifer – QPQ polirani i da je pri tom skinuto 2 – 3 μm površinskog sloja oksida te da je potom naknadno uranjanje u oksidacijsku kupku AB1 trajalo 15 min što izgleda nije bilo dovoljno dugo za ponovno stvaranje kvalitetnog oksidnog sloja oksida koji bi postigao najbolju korozijsku otpornost. Iz navedenoga se može zaključiti o važnost i utjecaju oksida na korozijsku postojanost nitrokarburiranih predmeta.

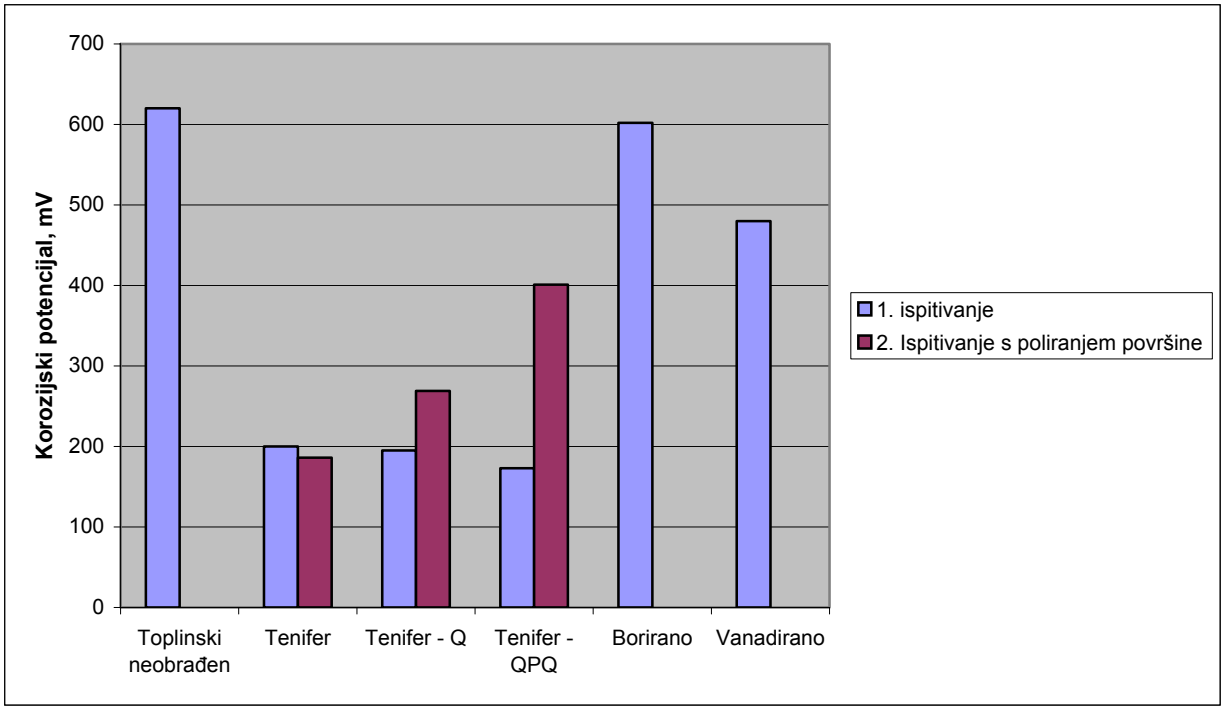
Borirani uzorak prema slici 3. pokazuje nešto lošiju otpornost koroziji od postupaka Tenifer – Q i Tenifer – QPQ, ali bolju od postupka Tenifer i vanadiranja. Stupanj djelotvornosti zaštite iznosi 82 %, što je znatno više u odnosu na 47 % koje su dane u literaturi. Razlozi mogućeg previsokog rezultata korozijske postojanosti također mogu biti prekratko vrijeme trajanja ispitivanja i povišena temperatura ispitivanja.

Vanadirani uzorak je pokazao bolju korozijsku postojanost od toplinski neobrađenog uzorka i ujedno najlošiju otpornost korozijskom djelovanju unutar grupe ispitivanih toplinski obrađenih uzoraka. Treba naglasiti da su ovi uzorci pokazali drugačiji oblik korozije tj. pitting koroziju (tablica IV.), dok su sve ostale grupe uzoraka pokazale koroziju koja ima oblik opće korozije odnosno, korodirali su jednoliko po cijelom svom presjeku.

Rezultati ispitivanja korozijske otpornosti elektrokemijskom metodom prikazani su na slikama 4 i 5. Izračunati stupanj djelotvornosti zaštite za svaku grupu toplinski obrađenih uzoraka prikazani su u tablici VI.



SLIKA 4: Kvantitativni prikaz vrijednosti gustoće korozijske struje dobivenih Tafelovom ekstrapoloacijom. Općenito vrijedi da manja vrijednost gustoće korozijske struje odgovara boljoj korozijskoj otpornosti.



SLIKA 5: Kvantitativni prikaz vrijednosti korozijskog potencijala dobivenih Tafelovom ekstrapolacijom. Općenito vrijedi da manja vrijednost korozijskog potencijala boljoj korozijskoj otpornosti.

TABLICA VI. Vrijednosti stupnjeva djelotvornosti zaštite (z, %), dobivene elektrokemijskom metodom.

Vrsta toplinske obrade	**Stupanj djelotvornosti zaštite – z, %**	
	1. ispitivanje	**2. ispitivanje s poliranjem**
Tenifer	**77**	**78**
Tenifer – Q	**88**	**74**
Tenifer – QPQ	**90**	**75**
Boriranje	**28**	**- - -**
Vanadiranje	**46**	**- - -**

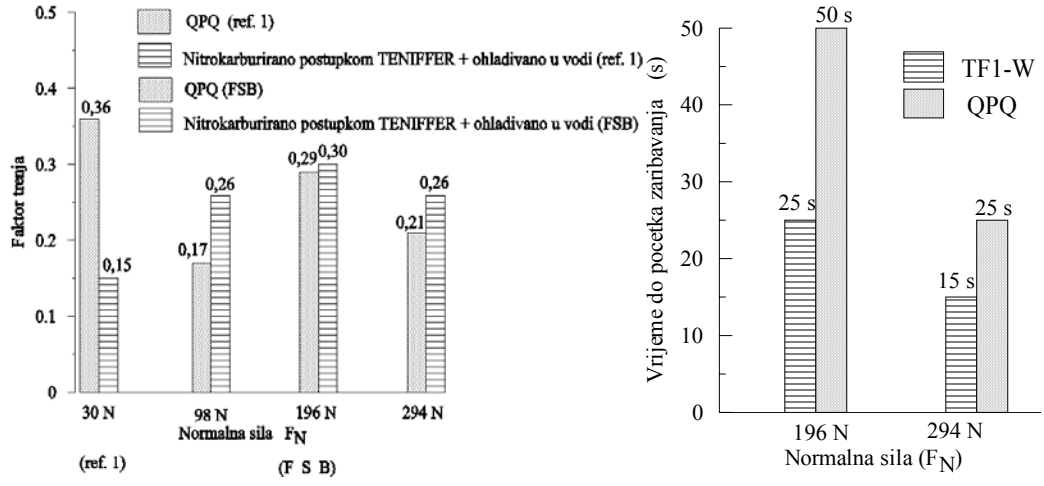
Na temelju rezultata vidi se da ispitni uzorak obrađen Tenifer – QPQ pokazuje najveću otpornost koroziji. Ostala dva postupka nitrokarburiranja (Tenifer i Tenifer - Q) pokazuju nešto lošiju korozijsku otpornost od postupka Tenifer – QPQ, ali bolju od ispitnih uzoraka obrađenih boriranjem i vanadiranjem. Zanimljivi su podaci korozijske otpornosti postupaka Tenifer – Q i Tenifer – QPQ nakon drugog ispitivanja kada se površina ispitnih uzoraka polirala prije ispitivanja čime je uklonjen dio oksida sa površine uzorka i vidi se da im je korozijska otpornost smanjena. Kod postupka Tenifer je također načinjeno drugo ispitivanje ali se korozijska otpornost nije promijenila, jer se time samo smanjio površinski sloj dok je struktura ostala ista. Iz toga se može zaključiti da sloj oksida koji nastaje prilikom oksidacije u oksidaciskoj kupki AB1 znatno poboljšava korozijsku postojanost dijelova obrađenih ovim postupcima.

Uzorci obrađeni boriranjem pokazuju najlošiju korozijsku otpornost. Kako u literaturi nisu pronađeni podaci o korozijskoj otpornosti ovih slojeva nakon ispitivanja elektrokemijskom metodom, nije ih moguće usporediti. Kao i kod ispitivanja gravimetrijskom metodom temperatura ispitivanja je bila viša (υ_0 = 32 ^{0}C) nego ona normom propisana (υ_0 = 25 ^{0}C) te treba i ovdje biti oprezan kod konačnog zaključka o korozijskoj postojanosti. Razlozi mogućeg odstupanja rezultata od stvarnih vrijednosti mogu biti i u morfologiji dobivenog sloja nakon boriranja, jer su se javile poprečne pukotine i ljuštenje sloja borida što vjerojatno ima utjecaja na korozijsku otpornost.

Uzorci obrađeni vanadiranjem pokazuju nešto bolju korozijsku otpornost od ispitnih uzoraka obrađenih boriranjem i lošiju od ispitnih uzoraka obrađenih postupcima nitrokarburiranja.

Faktor trenja u ovoj prvoj fazi istraživanja određen je za ispitne uzorke obrađene Tenifer postupkom i Tenifer QPQ postupkom primjenom nekoliko različitih opterećenja kliznog para ispitni uzorak-tarni prsten (bez podmazivanja). Uzorak obrađen Tenifer QPQ postupkom pokazao je manji faktor trenja od onoga obrađenog Tenifer postupkom. Do razlike je došlo vjerojatno zbog drugačijih uvjeta pokusa kliznog trenja u odnosu na ovo ispitivanje. Faktor trenja povećava se s porastom opterećenja jer dolazi do probijanja oksidnog sloja i sloja željeznih nitrida, te ostvarenja čistog metalnog dodira.

Kod ispitnih uzoraka obrađenih Tenifer postupkom do zaribavanja dolazi kod optrećenja normalnom silom od 196 N već nakon 25 sekunda, dok kod uzoraka obrađenih QPQ postupkom do zaribavanja dolazi tek nakon 50 sekunda. Povećanjem iznosa normalne sile na 296 N uzorci obrađeni Tenifer postupkom izdržali su do zaribavanja samo 15 sekundi , nasuprot QPQ uzoraka koji su izdržali 25 sekundi. Primjenom opterećenja većeg od 296 N do zaribavanja kod obje vrste ispitnih uzoraka dolazi samim pokretanjem uređaja, pa je to granična vrijednost opterećenja s kojim je izvođeno određivanje faktora trenja i sile zaribavanja.



a) b)

SLIKA 6: Iznos srednjeg faktora trenja (a) i trajanje ispitivanja prije zaribavanja (b) u kliznom kontaktu ispitni uzorak-tarni prsten nakon nitrokarburiranja TENIFER i TENIFER QPQ postupkom (vlastita ispitivanja i podaci iz literature)

ZAKLJUČAK

Iz rezultata provedenih ispitivanja može se zaključiti slijedeće:

- Najmanje povećanje svih parametara hrapavosti postignuto je kod postupka nitrokarburiranja s naknadnom oksidacijom (Tenifer - QPQ) što je posljedica poliranja uzoraka, uobičajene faze nakon nitrokarburiranja. Stoga je ovaj postupak posebno prikladan za alate i strojne dijelove koji se prije toplinsko – kemijske obrade strojno obrađuju na konačne dimenzije.
- Najveće povećanje svih parametara hrapavosti (oko 2 puta) pokazali su borirani i vanadirani ispitni uzorci. Povećanje parametara hrapavosti ovih uzoraka posljedica je stvaranja sloja Fe – borida odnosno vanadij karbida.
- Metalografskom analizom potvrđen je nastanak površinskih slojeva Fe – nitrida, Fe – borida odnosno vanadijevog karbida nakon primjene odgovarajućih postupaka. Nakon nitrokarburiranja dobivena je zona spojeva s porama do polovice dubine, a primjena naknadne oksidacije (postupci Tenifer – Q i Tenifer - QPQ) uzrokovala je izlučivanje iglica nitrida u difuzijskoj zoni. Kod boriranih uzoraka uočene su poprečne pukotine i ljuštenje boridnog sloja ,čini se zbog različitih koeficijenata toplinske dilatacije sloja i osnovnog materijala. Primjenom postupka vanadiranja dobiven je vrlo tanak i homogen sloj (8 μm) sloj vanadijevog karbida.
- Gravimetrijskim ispitivanjem brzine korozije u slanoj komori (DIN SS 50 021) utvrđen je najveći stupanj djelotvornosti zaštite od korozije (z = 92 %) za uzorak obrađen postupkom nitrokarburiranja sa ohlađivanjem u oksidacijskoj kupki (Tenifer - Q), ali i postupci Tenifer-QPQ (z = 85 %) i boriranje (z = 82 %) također su pokazali dobru korozijsku otpornost. Vanadirani uzorci pokazali su najslabiju korozijsku postojanost (z = 33 %) i tipičan tip pitting korozije.
- Ispitivanja korozijske postojanosti elektrokemijskim dvama metodama (metoda Tafelove ekstrapolacije i metoda mjerenja polarizacijskog otpora) pokazala su kvalitativno slične rezultate. Najveći stupanj djelotvornosti zaštite od elektrokorozije pokazali su ispitni uzorci obrađeni postupcima Tenifer – QPQ (z = 90 %) i Tenifer – Q (z = 88 %), dok su borirani (z = 28 %) i vanadirani (z = 46 %) ispitni uzorci pokazali slabiju korozijsku otpornost.
- Naknadna oksidacija nitrokarburiranog čelika (postupak TENIFER QPQ), osim što pridonosi sniženju zaostalih naprezanja, sniženju deformacija oblika, i sniženju faktora trenja, pridonosi i povišenju korozijske postojanosti pa to upućuje na mogućnost proširenja primjene ovoga postupka i na one dijelova alata i strojeva koji su u radu, izloženi istovremenom djelovanju mehanizama adhezijskog trošenja i korozijskom djelovanju

Literatura

[1]. Wahl, G.: "Salzbad-Nitrocarburieren-TENIFERQPQ-Verfahren", Technische Mitteilungen, Durferrit Gmbh

[2] T. Filetin, K. Grilec: "Postupci modificiranja i prevlačenja površina", priručnik za primjenu, HDMT, Zagreb, 2004.

[3] D. Krumes: "Površinske toplinske obrade i inženjerstvo površina', Strojarski fakultet u Slavonskom Brodu, Sveučilište J.J. Strossmayer u Osijeku, Slavonski Brod, 2004.

[4] B. Matijević, M. Stupnišek, S. Golubić: "Difuzijsko formiranje tvrdih karbidnih slojeva", Zbornik radova: Novi postupci modificiranja i prevlačenja površina, HDTOIP, Zagreb, 2004.

[5] Marušić, K., Otmačić, H., Landek, D., Cajner, F., Stupnišek-Lisac, E.: "Modification of carbon steel surface by the Tenifer process of nitrocarburizing and post-oxidation", Surface & Coatings Technology 201 (2006) 3415–3421

[6] V. Ivušić: "Tribologija", Hrvatsko društvo za materijale i tribologiju, Zagreb, 1998.

PRIMARY PROCESS SELECTION AS THE PART OF PROCESS PLANNING

ODABIR PRIMARNOG PROCESA KAO DIO PLANIRANJA TEHNOLOŠKIH PROCESA

Predrag Ćosić[1], Slavko Dolinšek[2], Valentina Gečevska[3]
[1]University of Zagreb, Faculty of Mechanical Engineering and Naval Architecture, Zagreb, Croatia
[2]University of Primorska, Faculty of Management, Koper, Slovenia
[3]Ss. Cyril and Methodius University, Faculty of Mechanical Engineering, Skopje, Macedonia
predrag.cosic@fsb.hr

Stručni članak / Professional paper

Abstract:. The field of our research is defining the main criteria for selection of primary processes and types of operations in production. Selection of primary process is based on nature of material, quantity, form complexity of the part, part size/mass and some other factors. Type and sequence operation are results of influence different factors as product shape, surface roughness and tolerance. In application will be used some aspects of knowledge base. Application will enable users to better understand procedure of selection primary process and sequence operations with possible additional technological gradation support. Self learning and testing of students is included in application. In application are used IT technologies of Visual Basic.NET.

.

Key words: process planning**,** primary process selection, distance learning

Sažetak: Područje istraživanja je definiranje glavnog kriterija za odabir primarnih procesa i vrsta operacija u proizvodnji. Odabir primarnog procesa temeljen je na svojstvima materijala, količini, složenosti oblika izratka, dimenzijama/masi izratka te nekim drugim faktorima. Vrsta i redoslijed operacija su rezultat utjecaja različitih faktora kao što su: oblik izratka, površinska hrapavost i tolerancija. U aplikaciji su korišteni neki aspekti baze znanja. Aplikacija će omogućiti korisnicima bolje shvaćanje procedure odabira primarnog procesa i redoslijeda operacija sa mogućim dodatnim tehnologijskom stupnjevanom podrškom. Samoučenje i samotestiranje studenata uključeno je u aplikaciju. U aplikaciji je su korištene tehnologije Visual Basic NET.

Ključne riječi: projektiranje tehnoloških procesa, odabir primarnog procesa, učenje na daljinu

1. INTRODUCTION

Process planning can be defined by a *sequence of activities.* A decision implementation has to be based on intuition , on partially estimated data or accurate data. As different process planners have different experience. So, it is no wonder that for the same part, different process planners will design different processes [1, 2, 3].

The experienced process planner usually makes decisions based on comprehensive data without breaking it down to individual parameters. *Good interpretation* of the part drawing includes mainly dimensions and tolerances, geometric tolerances, surface roughness, material type, blank size, number of parts in a batch, etc. *Logical approach* of a process planning, as the very complicated, multilevel and comprehensive approach of generating alternative process plans would be discussed, in this work, through *few topics*: a) selection of primary processes, b) sequencing the operations, etc.

The choice of process should be made with economic and technological factors. The other criteria for selection of initial material like ratios of material portion to the price of the blank, residual stress in the blank, scheme of stress state, productivity, anisotropy of material, etc. are too complicated and not enough general as the basis for the decision support [4].

The process of the general model creation would be more complicated by reason of: 1) necessity for quantity the whole' history and sequencing the operations, 2) necessity for continuously precision monitoring (data acquisition), 3) ''rule creation'' (implementation of AI techniques) as the basis in the process decision support. The required quantity will be a major determining factor of process selection.

The following factors would be the basis for decision support selection of the manufacturing process as the primary process (for example, forming by deformation) [5, 6]: a) *quantity*, b) *complexity of form*, c) *nature of material*, d) *size of part*, e) *section thickness*, f) *dimensional accuracy*, g) *cost of raw material*, h*) possibility of defects and crap rate*, etc [3].

2. NEW CHALLENGES IN EDUCATION FOR MANUFACTURING

Digital business has become a strategy to survive. Parts are made where conditions are most favourable. Non-core activities are out-sourced. It is observed that high education does not completely reflect real needs of the industry that faces problems of integrative nature across the traditional disciplines, such as: a) working globally in a multicultural environment, b) working in interdisciplinary, multi-skill teams, c) sharing of work tasks on a global level, d) working with digital tools for communication, e) working in an virtual environment [7].

Therefore special efforts would be done to integrate technical, humanistic field (sociology, economy, history, culture, psychology, etc.), skills of IT and web technologies.

As through a long time it is observed decreased interest for studying technical and natural sciences (especially in developed countries – the northeast part of Europe), serious efforts were done in process of questionnaire development, data collecting, analysis and development of new curriculums with great influence of interest, motivation, learning [8], multimedia, Internet, IT and web technologies (Projects PISA, ROSE), [9]). Choice of material and design solution cannot be done on purely technical and economical criteria, but must also take recycling, pollution and disassembly and reuse concerns into account.

3. SOME FEATURES AND REQUESTS IN E-LEARNING

In process of developing e-learning curriculum is deeply reciprocally integrated fields of E-Learning Management, E-Learning Tutoring and E-Learning Course Design. The most important questions in implementation e-learning courses are *models of online learning*: difference between teaching and learning, forms of collaboration, teaching strategies [10], the

role of e-tutor, learning design; *e-tutoring*: handling groups online, stimulating motivation & encouraging reflection, *quality evaluation of e-learning*: grid for the tutors and for the students, *on-line e-assessment* [11].

Online Assessment [11] and e-learning is one of the possible ways to help students during process of learning, teaching and can improve the assessment of student learning. We can expect more students with higher level of motivation, with desire to explore new web technologies for online assessment, higher level of democratization in education, possibility for more student's creativity and 'deeper' studying.

4. DEVELOPMENT WEB APLICATION E-LAPP

E – *learning application for process planning* (E – LAPP) is created to help students to better understand a matter that has been thought on our university. It is conceived in three different modules: *Selection of Primary Process*, *Exercises* and *Solved Examples.*

The first module *Selection of Primary Process* enables students to determine an appropriate primary process for manufacturing required part. There are two different methods whereby it is possible to select primary process. The first method is named by technician Gideon Halevi. During developing application for second method there were used ASM Handbook so it is called ASM [6], [3].

Halevi method [5] enables students to select a primary process only by knowing material, shape complexity and required quantity (Fig. 1). Based on input parameters application lists a process sequence. The first listed forming process is the most acceptable, but if there are some reasons why this process cannot be used a student is allowed to choose the next one on the list.

Application, also, offers student to infiltrate deeper in chosen process. For example, if student click on '*Forming from Solid by Material Removal*' and press button 'Next' it will open a new window where student can input required data about the part. By pressing a button 'Calculate' application will list required process sequences and part dimensions with tolerances and surface roughness on which required part has to be treated (Fig. 2).

ASM [6] method offers student to choose between two different approaches of primary process selection: *Simple Process Planning Method* and *Advanced Process Planning Method.* *Simple Process Planning Method* is conceived in a way that on a base of input parameters such as material, surface roughness, dimensional accuracy, complexity, production rate, production run, relative costs and size (projected area) makes a first selection and lists possible operations. In the next step application asks student to rank offered criteria: cycle time, quality, flexibility, material utilisation and operating costs and demand a last condition in order to make a last selection. The required condition is 'shape'. After the last selection is made, application lists possible solutions in table with adequate explanations. There is also a graph of process acceptability. It is important to mention that graph only suggest student which process is the most acceptable, but it is up to student and his knowledge to decide if that process is really the most acceptable (Fig. 3).

Advanced Process Planning Method [6] offers student a different approach to the problem. The first selection is, here, made only by material. Based on type of material application lists a basic operation for process planning: Forming from Solid by Material Removal, Welding, Forging, Forming from Solid by Deformation and Forming from Liquid (Casting, Moulding). Once a basic operation is chosen, all other calculation is made for that basic operation. First, application offers student to choose adequate shape according to table (Fig. 4).

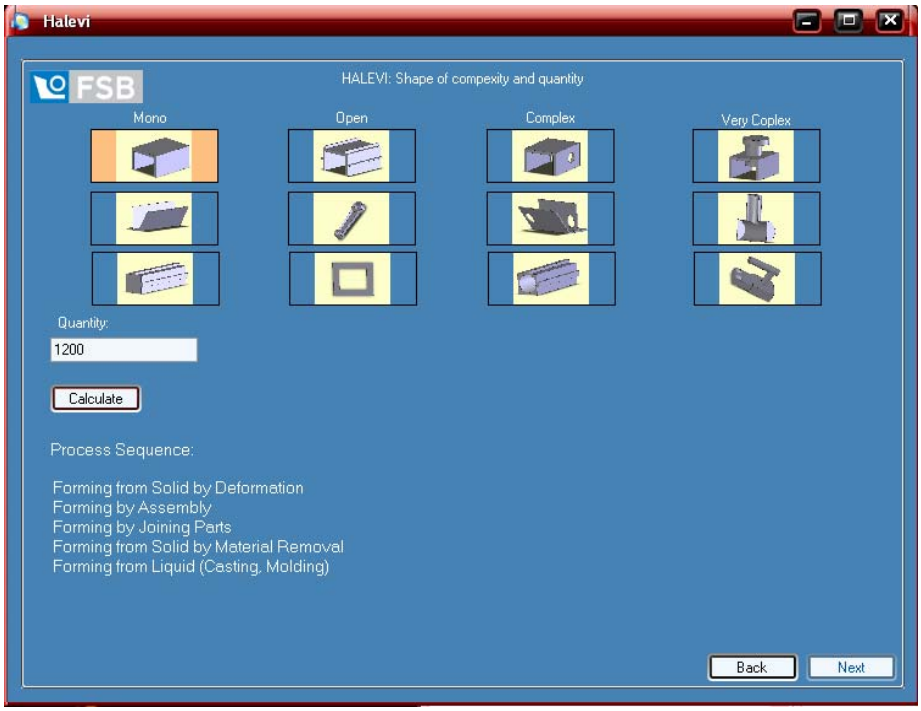


Figure 1 Primary process selection – Halevi [5] as result of decisions based on product shape and product quantity

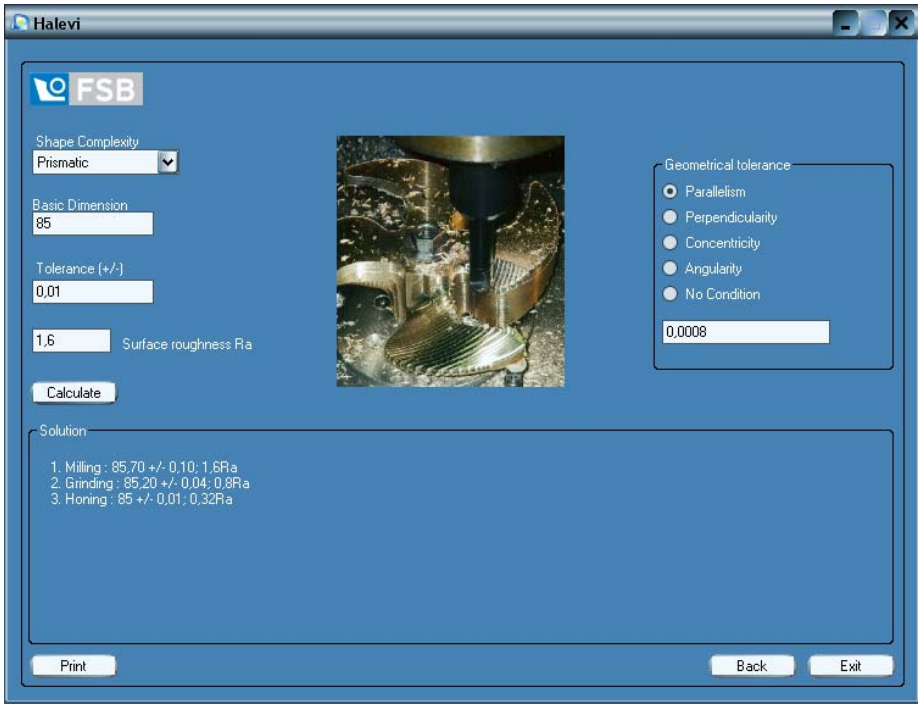


Figure 2 Process sequence solution as result of shape complexity, basic dimension, tolerance, surface roughness and selection of geometric tolerance

Next, application requires from student to input other necessary parameters and then is made a final, more deeply selection. The results are presented in graph of acceptability. It is important to mention that, same as in Simple Process Planning Method, graph only suggest student which process is the most acceptable, but it is up to student and his knowledge to decide if that process is really the most acceptable.

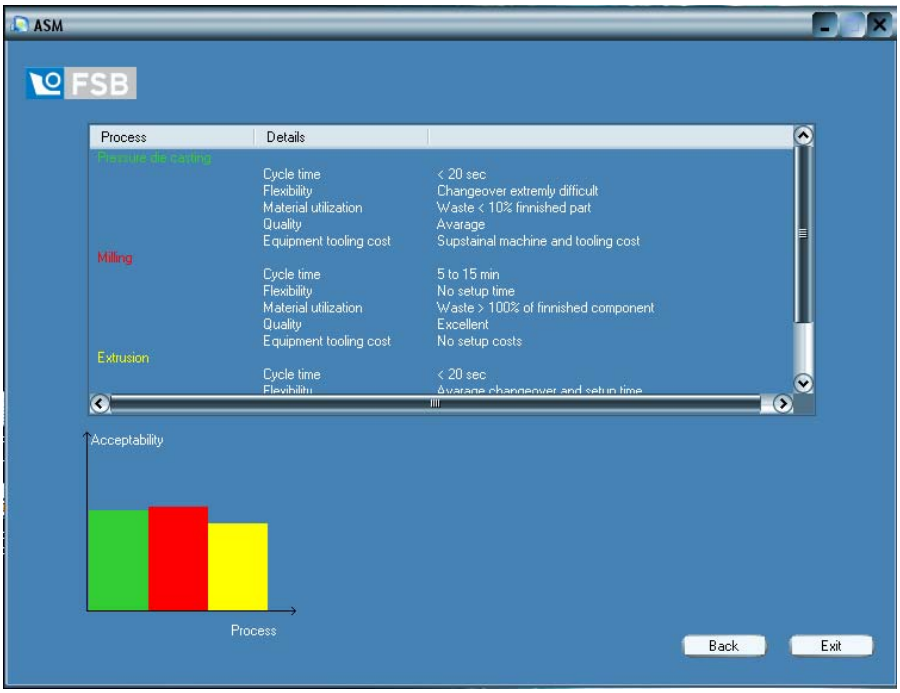


Figure 3 Suggested primary process (ASM) – *Simple Process Planning* [6]

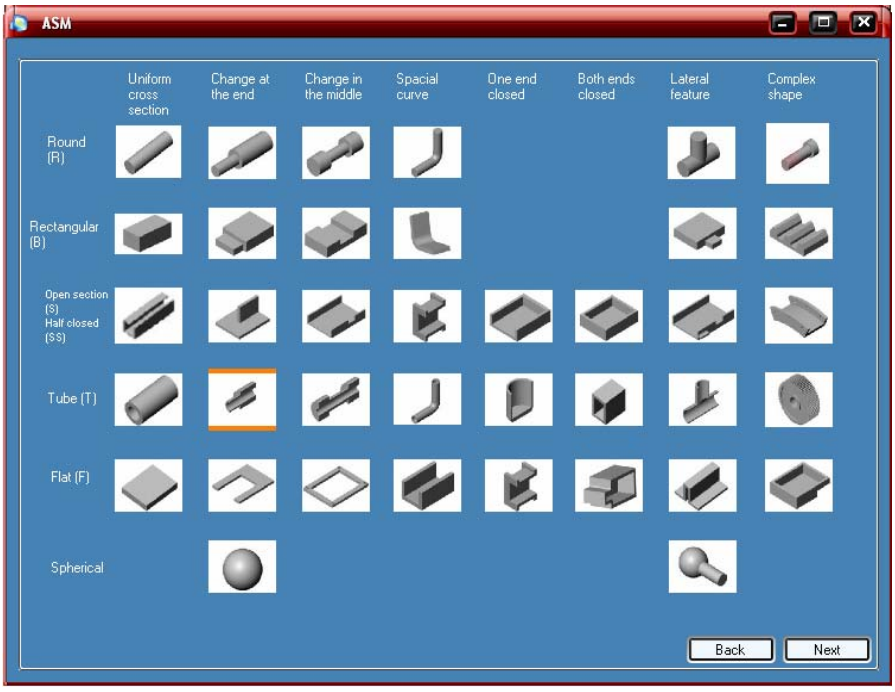


Figure 4 Suggested products shape for selection - *Advanced Process Planning Method* [6]

The second module is *Exercises*. It is divided into two entireties: *Exercise and Manager*. *Manager* (Fig. 5) enables tutors to give tasks that can be time limited. Running an option Exercise student can solve the tasks, which has been given by tutor. After every solved task student gets feedback information about how successful he was in the form of won points. For every correctly solved step students get one point.

Solved Examples (Fig. 6) is the third module in *On line Assessment module*. Here is shown few solved examples for both methods. For each example there is an explanation for every step and there are given tables which are used in code with marked solutions (Fig. 7, Fig. 8). The biggest challenge, that we came across while we were developing application,

was how to enable student to rank offered criteria (ASM method - *Simple Process Planning Method*), because in real manufacturing not every criteria are equaly ranked. So, we agreed to assign them weight. Primary criteria has weight 25, secondary 20, tertiary 15, quaternary 10 and quinary criteria has weight 5. Once criteria are ranked, application multiply each grade with weight of criteria, for obtained processes after final selections, and sum them up (Tab. 1). Description of marks (Tab. 1) is given in below (Tab. 2). In process of criteria ranking, users observed subjectivity, show on possibility using fuzzy logic in further development of our application.

Process	Shape	Cycle time	Flexibility	Material utilization	Quality	Equipment tooling costs
Pressure die casting	3D	5	1	4	2	1
Centrifugal casting	3D hollow	2	3	5	3	3
Compression molding	3D	3	4	4	2	3
Injection molding	3D	4	1	4	3	1
Sand casting	3D	2	5	2	2	1
Investment casting	3D	2	4	4	4	3
Milling	3D	2	5	1	5	5
Grinding	3D	2	5	1	5	4
Electrical discarge machining	3D	1	4	1	5	1
Blow molding	3D hollow	4	2	4	4	2
Forging	3D	2	4	3	2	2
Rolling	3D	5	3	4	3	2
Extrusion	3D	5	3	4	3	2
Powder metallurgy	3D solid	2	2	5	2	2

Table 1 Rating of characteristics for common manufacturing processes

Sums are then compared and process that has the biggest sum has the biggest acceptability in graph (Fig. 3). Sums are then compared and process that has the biggest sum has the biggest acceptability in graph (Fig. 3).

5. INSTEAD OF CONCLUSION

The biggest challenge, that we came across while we were developing application, *was how to enable student to rank offered criteria* (*ASM method - Simple Process Planning Method*), because in real manufacturing not every criteria are equally ranked. So, we agreed to assign them weight. Primary criteria has weight 25, secondary 20, tertiary 15, quaternary 10 and quinary criteria has weight 5. Once criteria are ranked, application multiplies each grade with weight of criteria, for obtained processes after final selections, and sum them up (Tab. 1). Description of marks (Tab. 1) is given in below (Tab. 2).

In process of criteria ranking, users observed subjectivity, show on possibility using fuzzy logic in further development of our application. Sums are then compared and process that has the biggest sum has the biggest acceptability in graph (Fig. 3).

REFERENCES

[1] Cosic, P., Levanic, A.: *Web Oriented Database System for Process Planning*, Pacific Congress on Manufacturing and Management (PCMM) 2004, 8, - 10 December 2004 - Gold Coast, Australia, ISBN 0-9578296-1-2, pp 922-928.

[2] P. Cosic, N. Volarevic, D. Lenac, *Variants of Process Planning – Step toward Production Planning*, ATDC'05 (Advanced Technologies for Developing Countries), Slavonski Brod, Croatia, 21 – 24. September 2005. pp. 375-380.
[3] http://ptp.fsb.hr
[4] Cosic, P., Sever, D. Milinovic, S., *Process Planning Application and Internet Connectio*n, AMST'02 Advanced Manufacturing Systems and Technology, Kuljanic, Elso (ur.). Wien New York : SpringerWienNewYork, 2002. pp 283-290.
[5] Halevi, G., *Proocess of Operation Planning*, Kluwer Academic Publishers, Dordrecht, 2003.
[6] ASM *Handbook Vol. 20, Materials Selection and Design*, ASM Int., Ohio, 1997.
[7] Rolstadås, A., Moseng, B. (2002) Global Education in Manufacturing GEM, *CIRP International Manufacturing* , Education Conference CIMEC, pp 1-13, 2002.
[8] Krapp, A. Structural and dynamic aspects of interest development: theoretical considerations from an ontogenic perspective, *Learning and Instruction* 12 383-409, 2002.
[9] Turmo A., Lie, S. *Cross-country comparability of students* , Self-reports from the PISA 2003 study, 2003.
[10] Pratt, D. D. *Good teaching: One Size Fits All?* (str. 1-11). Preuzeto 11.9.2006. s http://www.teachingperspectives.com/PDF/goodteaching.pdf, 1998
[11] Gard, E., *Emdel: a Model for Valorization of eLearning in a Knowledge Society*, Final Report, www.emdel.org, 2005.
[12] Bull, J., Computer-Assisted Assessment: Impact on Higher Education Institutions, *CAEducational Technology & Society* 2(3), ISSN 1436-4522, 1999.

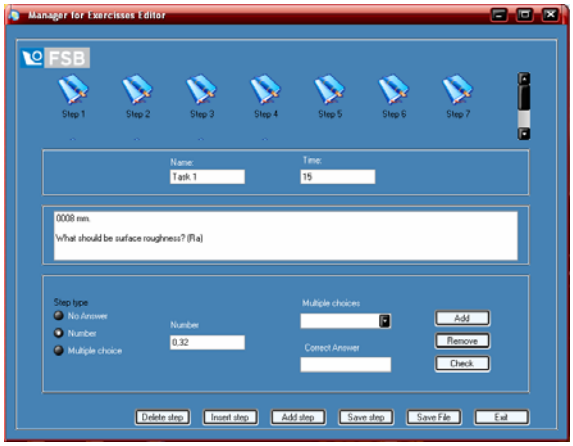


Figure 5 Example of *Manager* module work

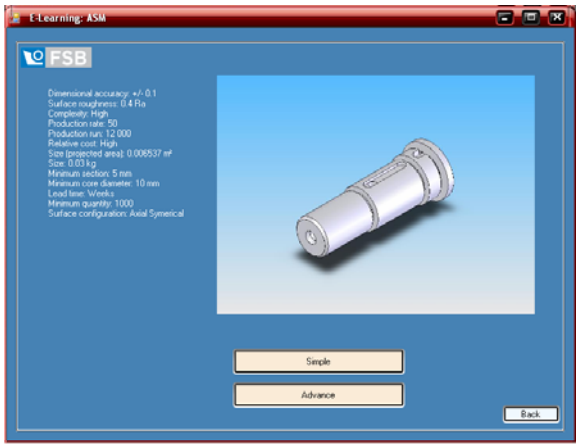


Figure 6 Solved examples with explanation for selected primary processes and final result

Rating	Cycle time	Quality	Flexibility	Materials utilization	Operating costs
1	> 15 min	poor quality, average reliability	changeover extremely difficult	waste > 100 % of finshed component	substantial machine and tooling costs
2	5 to 15 min	average quality	slow changeover	waste 50 to 100 %	tooling and machines costly
3	1 to 5 min	average to good quality	average changeover and setup time	waste 10 to 50 %	tooling and machines relatively inexpensive
4	20 s to 1 min	good to execellent quality	fast changeover	waste < 10 % finished part	tooling costs low/little equipment
5	< 20 s	execellent quality	no setup time	no appreciable waste	no setup costs

Table 2 Scale for rating manufacturing processes

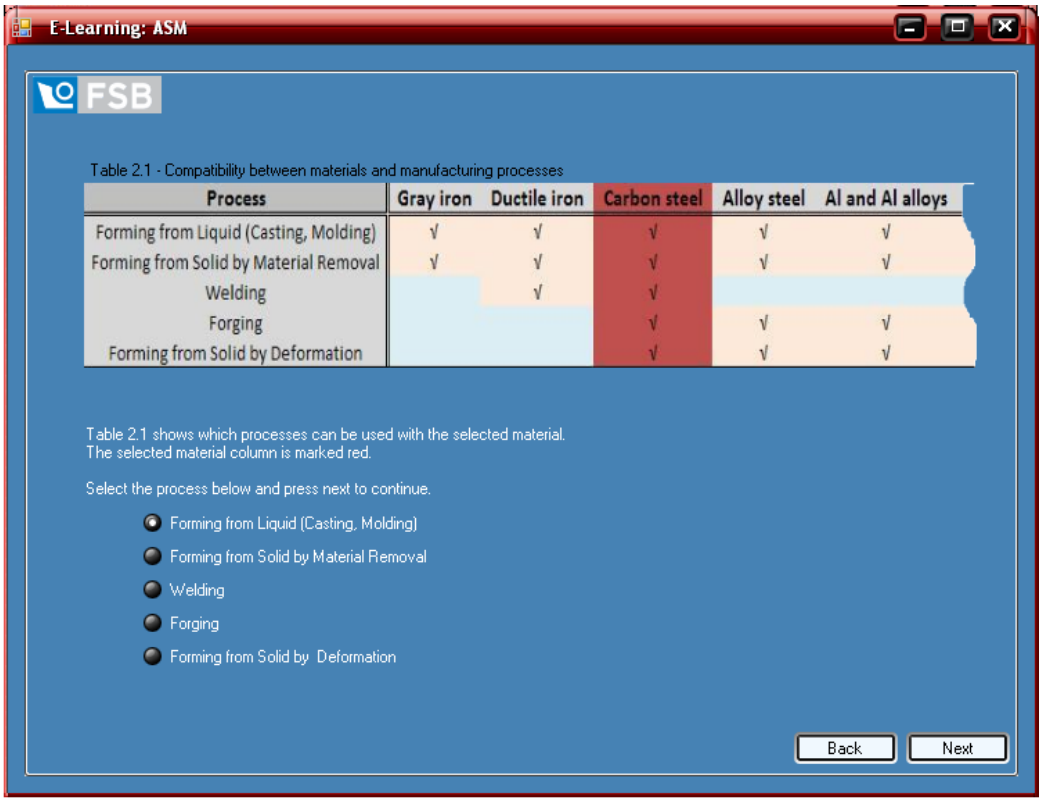


Figure 7 Possible primary processes for selected material

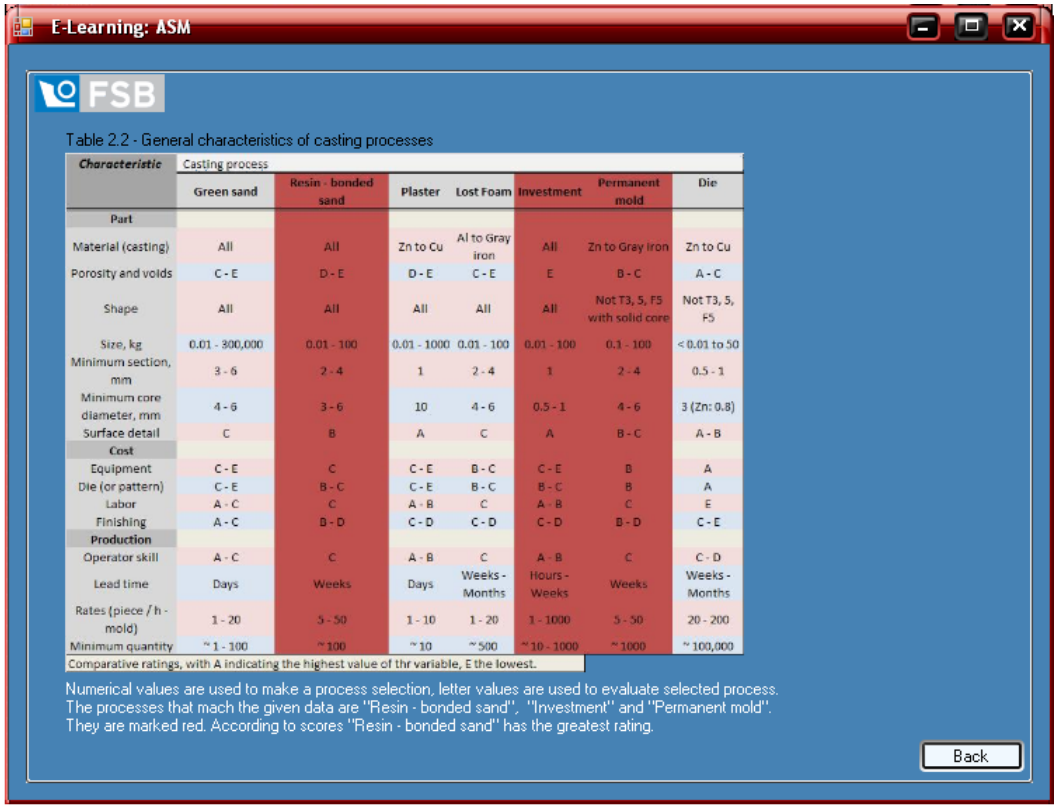


Figure 8 Final step in selection – possible casting processes

Sveučilište u Zagrebu Metalurški fakultet Sisak
Dušan.Ćurčija dipl.ing.[1]

MODELIRANJE MAZIVOGA SLOJA KOD VALJANJA BEŠAVNIH CIJEVI

Izvorni znanstveni rad / Original scientific paper

Sažetak: Iskorištena je aplikacija AutoCAD-a , kao snažnoga programa za modeliranje u 3D da bi se prezentirali crteži matematičkih izračunavanja u matematičkim programima: Mathematica , MATLAB i MathCADProfesional.Približna analitička riješenja Reynoldsove diferencijalne jednadžbe za podmazivanje predstavljena u radu ,obrađena su Excelovim Solverom i komparirana sa metodom Monte-Carlo.Matematička izračunavanja ukazuju na brzo opadanje mazivoga sloja na trnu kod kontinuiranoga valjanja bešavnih cijevi u kavezima. Dok je na početku konti pruge za procese redukcije cijevi po radijusu ispunjen uvijet stabilnoga hidrodinamičkoga podmazivanja , radni kavezi u završnim sekcijama konti pruge ukazuju prema teorijskim izračunavanjima na pojavu ″glodanja maziva″ na trnu.Izvedeno je približno analitičko riješenje u točki M koje kontrolira numeričku metodu Monte-Carlo i ukazano je na mogućnost dobivanja ostalih kontrolnih točaka..

Ključne riječi:Reynoldsova diferencijalna jednadžba , točke motrišta kamere AutoCAD-a, maziva , konti pruga , bešavne cijevi.

1.Uvod

Valjanje cijevi u okruglim kalibrima[1] je varijanta uzdužnoga valjanja , gdje zonu deformacije u pravilu stvaraju radni valjci i trn prema **slici 1**. Valjanje cijevi na dugačkom plivajućem trnu primjenjuje se kod konti-stana koji u svom sastavu imaju 7 do 9 radnih kaveza.Prije ulaganja cijevnice među valjke u nju se uvodi dugački cilindrični trn , **slika 2**., koji se giba u zoni deformacije zajedno sa cijevnicom.Brzina kretanja trna manja je od brzine kretanja prednjega kraja cijevi na izlazu iz valjaka , ali je veća od brzine kretanja zadnjega kraja cijevi na ulazu među valjke.Posebnosti brzinskih uvijeta valjanja u kalibrima dovode do toga da su brzine cijevi i valjaka u svakome poprečnome presijeku zone deformacije jednake samo u dvije točke žljeba kalibra.

Zadnjih godina razrađeni su načini realizacije procesa valjanja cijevi u konti-stanu uz primjenu dugoga nepomočnoga cilindričnog , konusnog ili stupnjevitoga trna.

Posebnost ovoga valjanja je prisustvo dviju subzona: zone redukcije promijera i zone redukcije stijenke cijevi prema **slici 1.** i **slici 3**. koje to jasno predočavaju.U vanjskome kontaktu[2,3] cijevi i valjaka gdje se ne razmatra dodavanje maziva , vladaju zakoni trenja po Kulon-Amontonu , dok između trna i unutrašnje površine cijevnice , zbog prisustva maziva , vladaju zakoni tekućinskoga trenja po Newtonu.Veličine tangencijalnih napona u mazivome sloju [4,5] opisuje se diferencijalnom jednadžbom (1):

$$\tau_x = \mu^*(v_C - v_T)\frac{1}{\varepsilon(x)} - \frac{1}{2}\varepsilon(x)*\frac{\partial p}{\partial x} \qquad (1)$$

Promijena gradijenta pritiska u mazivome sloju[4,5,6,7] opisuje diferencijalna jednadžba(2) , volumnu potrošnju maziva po perimetru[6,7] cijevi daje izraz (3) .

[1] Vanjski suradnik Metalurškoga fakulteta u Sisku

$$\frac{dp}{dx} = \frac{6\mu(v_C + v_T)}{\varepsilon^2(x)} - \frac{12\mu Q}{\varepsilon^3(x)} \tag{2}$$

$$Q(x) = \int_0^{\varepsilon(x)} udy = -\frac{1}{12\mu}\frac{dp}{dx}\varepsilon^3(x) + \left(\frac{v_C + v_T}{2}\right)\varepsilon(x) \tag{3}$$

Geometriju kontakta maziva[8,9,10] opisuje izraz (4),dužinu mazivoga klina izraz (5).

$$\varepsilon(x) = \varepsilon_0 + R_0\left[\cos\alpha_0 - \sqrt{1-\left(\sin\alpha_0 - \frac{x}{R_0}\right)^2}\right] \tag{4}$$

$$a = R_0\left[\sqrt{1-\left(\cos\alpha_0 - \frac{\varepsilon_a}{R_0} + \frac{\varepsilon_0}{R_0}\right)^2} - \sin\alpha_0\right] \tag{5}$$

$$\varepsilon(x) = \varepsilon_0 - \alpha_0 x + \frac{x^2}{2R_0} - \frac{\alpha_0 x^3}{2{R_0}^2} + \frac{x^4}{8{R_0}^3} \tag{6}$$

Izraz (6) je razvoj[11,12,13] formule (4) u Mac-Laurinov red.Karakteristike maziva za teorijska istraživanja i geometrija procesa, uzete su iz literature dosadašnjih radova[8,11] po rusko-ukrajinskim autorima i predstavljene su u **tablici 1**.

Tablica 1.Uobičajene karakteristike maziva za teorijska izračunavanja

Parametar	Vrijednost	Jedinica
γ-piezokoeficijent viskoznosti	**2,18E-7**	**Pa^{-1}**
p_0-pritisak valjanja	**20E6**	**Pa**
V_C-brzina gibanja cijevnice	**8,5**	**m/s**
V_T-brzina trna	**7,5**	**m/s**
R-radijus valjaka	**0,197 (0.4229)**	**m**
S_{C2}-debljina stijenke cijevi	**0,003 (0.0271)**	**m**
μ_0-dinamička viskoznost maziva $\mu=\mu_0 \exp(\gamma * p_0)$	**0,024-0.048**	**Pas**
α_0-kut zahvata	**0-0,02**	**rad**
ε_a-visina maziva na trnu	**0,001-0,00000001**	**m**
A-tehnološki parametar	**1,965512E6 (* 533,333)**	**m^{-1}**
$A=(1-\exp(-\gamma * p_0)/6\mu_0\gamma(v_C+v_T))$		
Pretpostavljaju se glatke površine cijevnice i trna $R_0=R+S_{CX}$		
Vrijednosti u zagradama odnose se na sliku 15.		

Radni kavez prikazan je na **slici 3**.Cijev na trnu ima izrazito konusni oblik što govori da je kavez sa početka konti pruge.

2.Riješenja diferencijalne jednadžbe (2) i grafička interpretacija

Približna analitička riješenja diferencijalne jednadžbe predstavljena su u **tablici 2**. Riješenje u oblati **Ψ** izvedeno je kao referentni kut zahvata α u radu [11] i [14] i predstavlja poznata riješenja rusko-ukrajinskih autora : A.P.Grudeva , V.L. Mazura , G.L.Kolmogorova .
Riješenje u oblasti **Ω**, **M Point** , i **Φ,Σ** , daju se u ovome radu.

Slika 4. daje rafinirani uvid u riješenja **tablice 2**.Točka **M** se realno postavlja u nizu prikaza $\{ \varepsilon_a\text{^}(1/3) ; \Delta\varepsilon_0/\varepsilon_a \}$.Za series 1. , $\Delta\varepsilon_0$ je diferencija od pilota $\boldsymbol{\varepsilon^{0.1}_{o}}$, dakle visina mazivoga sloja za bilo koji kut zahvata α , minus visina maziva za pilot 0.1 rad. Slično , series 2 je računat po relaciji: $(\varepsilon_0^1 - \varepsilon_0^*) / \varepsilon_a$.

Slika 5. daje model mazivoga sloja na trnu računat numeričkom metodom Monte-Carlo.Na ulazu **I** maziva ima u suvišku , dok na izlazu konti pruge **II** , mazivo je na trnu oglodano jer nema svježih dotoka ispod cijevi kaveza.

Slika 6.daje komparaciju približnih analitičkih riješenja i numeričkih izračunavanja.Tako je series 1. vezano uz **Φ**-područje , series 2. je **Σ**-podruje , marker kvadrata **M** je riješenje **M Point** po tablici 2. , series 3. je metoda Monte-Carlo.Brojevima: 1,2,3 i 4 označena su motrišta kamere AutoCAD-a.Po **Σ**- riješenju , $\ln(\varepsilon_A) \approx -15.414043$ kada $\varepsilon_0 \to 0$.

Tablica 3. 3D View kamera na sliku 6. Pogledi lijevo od W na slici 4.

Slika	**Oznaka**	**Napomena**
Zajednička obilježja		
Slika 7. **Slika 8.** **Slika 9.** **Slika 10.**	Marker 1	**Ω**- područje slike 4. i tablice 2.
	Marker 2	**Σ**-područje slike 4. i tablice 2.
	Marker 3	Numerička metoda Monte-Carlo
	Marker 4	Točka **M** slike 4.,marker **M** na slici 6. , **M Point** po tablici 2.
	$\text{Ln}(\varepsilon_A)$, $\text{Ln}(\varepsilon_0)$	Apscisa i ordinata u 2D , za komandu AutoCAD-a **Revsurf**
Specifična obilježja		
Slika	**Oznaka**	**Napomena**
Slika 7. i **9**.	Markeri 2 i 5	Predstavljaju "šešir " nastao rotacijom luka $P\text{-}P_I$ sa slike 6.
Slika 8.	$\mathbf{II_0}$	Prazni dio prostora gdje približno stoji kamera 3 na slici 6.
Slika 10.	**P**	Crtež piramide predstavlja točku **P** na slici 6.(presjecište **Ω** i **Σ**)

Prema slici 10. analizirati ćemo točku presjecišta P (ctrež piramide) ucrtanu u sliku 6. Po tablici 2. presjecište Ω i Φ formula predstavljeno je slijedećim algebarskim polinomom 12 stupnja:

$$\left(\frac{-4\cdot R^6}{b^6}\right)\cdot\left[\begin{array}{l} 1764\,R^2\,b^6 - 25200\,R^2\,b^5\,x + 140400\,R^2\,b^4\,x^2 - 26100\,R A^2\,b^6\,x^3 - 393600\,R^2\,b^3\,x^3 \ldots \\ + 291600\,A^2\,b^5\,R\cdot x^4 + 600000\,R^2\,b^2\cdot x^4 - 1393200\,R A^2\cdot b^4\cdot x^5 - 480000\,R^2\,b\cdot x^5 \ldots \\ + 3628800\,R A^2\,b^3\cdot x^6 + 160000\,R^2\cdot x^6 + 50625\,A^4\,b^6\,x^6 - 540000\,R A^2\,b^2\,x^7 - 607500\,A^4\,b^5\,x^7 \ldots \\ + 3037500\,A^4\,b^4\,x^8 + 4320000\,R A^2\,b\cdot x^8 - 8100000\,A^4\,b^3\,x^9 - 1440000\,R A^2\,x^9 \ldots \\ + 12150000\,A^4\,b^2\,x^{10} - 9720000\,A^4\,b\cdot x^{11} + 3240000\,A^4\,x^{12} \end{array}\right] := 0 \qquad (7)$$

Preko točke M Point on se svodi na čestični model:

$$\left[\begin{array}{l} -1 + \frac{100}{7}\cdot z - \frac{3900}{49}\cdot z^2 + \frac{34975}{147}\cdot z^3 - \frac{74300}{147}\cdot z^4 + \frac{22300}{21}\cdot z^5 - \frac{3839425}{1764}\cdot z^6 + \frac{166875}{49}\cdot z^7 - \frac{204375}{49}\cdot z^8 \ldots \\ + \frac{265000}{49}\cdot z^9 - \frac{337500}{49}\cdot z^{10} + \frac{270000}{49}\cdot z^{11} - \frac{90000}{49}\cdot z^{12} \end{array}\right] := 0 \qquad (8)$$

Čestični model ima autonomna riješenja : pet konjugirano-kompleksnih parova i dva realna riješenja

Z_1=0.272277 i Z_2=0.190923 .Pomoću Z_1 dobivamo klonirano riješenje diferencijalne jednadžbe u točki presjecišta koje se može izraziti preko riješenja u točki M Point:

$$\varepsilon_a = 0.94953\ \varepsilon_{aMAX}\ ;\quad \varepsilon_0 = 0.9895\ \varepsilon_{Mpoint} \tag{9}$$

Preko riješenja čestičnoga modela Z_2 može se klonirati nova točka riješenja diferencijalne jednadžbe, a kombinatornim razrušavanjem grupe $b^n x^m$ u (7) gdje je n= 1-6 , a m= 1-12 , može se dobiti mnogo novih kloniranih riješenja.U takvom kombinatornom pristupu pilot kloniranja je ;

$$b := \sqrt[3]{\frac{R}{A^2}}\ , \qquad x := z_1 \cdot b \tag{10}$$

Takav pristup dovodi do vezanih analitičkih relacija kloniranja kao što je to ustanovljeno u izrazu (7) pri prvom krugu prolaza kombinatornoga razrušavanja polinoma (7) i slijedi :

$$\sqrt{\frac{R_2}{R_1}} \cdot A_1 := A_2 \tag{11}$$

Vidimo određenu relaciju između radijusa valjanja izvučenih po kvadratnoj jednadžbi R i tehnoloških parametara po bikvadratnoj jednadžbi A.Točka presjecišta sada preuzima ulogu točke **M Point** čime se nastavlja kloniranje diferencijalne jednadžbe(2) prema manjim vrijednostima ε_a, također i manjim zahvatnim kutevima sa novim čestičnim modelom.Uzimajući radni primjer da je A=3131318 m^{-1} i R=0.4 m slijedi rijesenje preko(9), tocke **M Point ,** ε_0 = 0.0000053026 m , dok metoda Monte-Carlo daje ε_0 = 0.0000053028 m, za pripadni ε_a=0.00000937304 m.

Slika 7., **Slika 8** ,**Slika 9 i Slika10.** daju motrišta kamere na **slici 6**. to jest ciljane snimke. nakon što su rezultati izračunavanja u matematičkim programima modelirana u AutoCAD-u. Pojašnjenja ovih pogleda preko kamere AutoCAD-a upotpunjuje **Tablica 3**.

Slika 11.daje proračune mazivoga sloja od sredine konti pruge prema ulazu.Izvršena je linearna korekcija **Ω**-područja pomoću riješenje u točki **M Point**, po **tablici 2,** što je predstavljeno na **slici 11b**.

Tablica 4. 3D View kamera na sliku 11a.Pogledi desno od W na slici 4.

Slika	**Oznaka**	**Napomena**
Zajednička obilježja		
Slika 12 **Slika 13** **Slika 14**	Marker 1	**Ω**- područje slike 4. i tablice 2.(ili **I-Ω** na **slici 11a**)
	Marker 1a	Korekcija **Ω**- područja preko slike 11b. (ili **II-Ω** na **slici 11a**)
	Marker 3	Numerička metoda Monte –Carlo
Specifična obilježja		
Slika	**Oznaka**	**Napomena**
Slika 13	◄——►	Sferna pruga Monte-Carlo (dobivena modeliranjem u AutoCAD-u).
	●——●	Sferna pruga **II-Ω** , korekcija preko **M Point** tablice 2., **slika 11b**.

Slika 12. , Slika 13. i Slika 14. daju motrišta kamere postavljena na Slici 11a.Vidljivo je da je linearna korekcija približno analitičko riješenje privela numeričkoj metodi Monte-Carlo. Pojašnjenja daje Tablica 4.

Slika 15.daje integralnu komparaciju uzduž cijele konti pruge pa prema tome i uzduž cijele apscise na **slici 4**. uz pojašnjenja predstavljena u **Tablici 5**.

Tablica 5. Pojašnjenje markera na slici 15.

Marker	**Link**	**Napomena**
Series 1	Monte-Carlo	Numerička izračunavanja
Series 2	**Ω**-područje tablice 2	Prihvatljivo od $\mathbf{I_a}$ do $\mathbf{II_a}$
Series 3	Riješenje po **M Point** u tablici 2	Kontrolira Monte-Carlo
Series 4	**Σ**-područje tablice 2 , lijevo od točke **P**	Graf dobro prati Monte-Carlo
Točka **P**	Ima isto značenje kao na slici 10.	Presjecište **Ω** i **Σ** riješenja

Ω-I	Prelazno područje oko točke **M Point** , gdje **Ω** formula odustaje od pratnje Monte-Carlo , a **Σ** formula još nije uhvatila korak sa Monte-Carlo metodom.Pogodno za interpolacije ili **Poligonalnu metodu**[14].Unutar intervala presječna točka **P** je polinom 12 stupnja.
	Oblast primjene **Ψ** formule u tablici 2.To je početak konti pruge kada imamo maziva u suvišku i kada se odvija redukcija cijevi po promijeru.**Ω** formula i **Ψ** formula daju podudarna riješenja.

3.Zaključak

U nizu slikovitih prikaza pokazano je da približna analitička riješenja diferencijalne jednadžbe (2) , data u tablici 2. dobro prate numeričku metodu Monte-Carlo.Oblikovana u AutoCAD-u pružaju rafinirani uvid u tu komparaciju i daju realan izgled maziva na trnu kod valjanja bešavnih cijevi na konti pruzi u kavezima.Posebnu važnost ima riješenje[15,16] izvedeno u točki **M Point**, jer omogućava linearnu korekciju mazivoga sloja u području **Ω** formule a ta korekcija može se protegnuti i na područje **Ω-I slike 15**.Druga važna karakteristika **M Point** je kontrola numeričke metode Monte-Carlo u toj točki.Iznosimo primjer za uvijete slike 15.

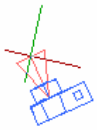
Tablica 6. Kontrola numeričke metode Monte-Carlo sa približnim analitičkim riješenjem u točki M Point za A= 2718281 m^{-1} , R= 0.314 m .

ε_A / m	α / rad	ε_0 / m Monte-Carlo.
0.057	0.0141	0.00009266
0.00577	0.001414	0.0000146154
0.0005772	0.00014142	0.000014781
0.000057721	0.0000141421	0.000013110
0.00000577215	0.000001414213	0.000005619
0.0000005772156	0.00000014142135	0.0000005756
0.000000057721566	0.0000000141421356	0.00000005765
Kontrola u tocki M preko tablice 2.		
0.00001000648	0.00588226	0.0000054324
Monte-Carlo u tocki M		
0.00001000648	0.00588226	0.0000054323

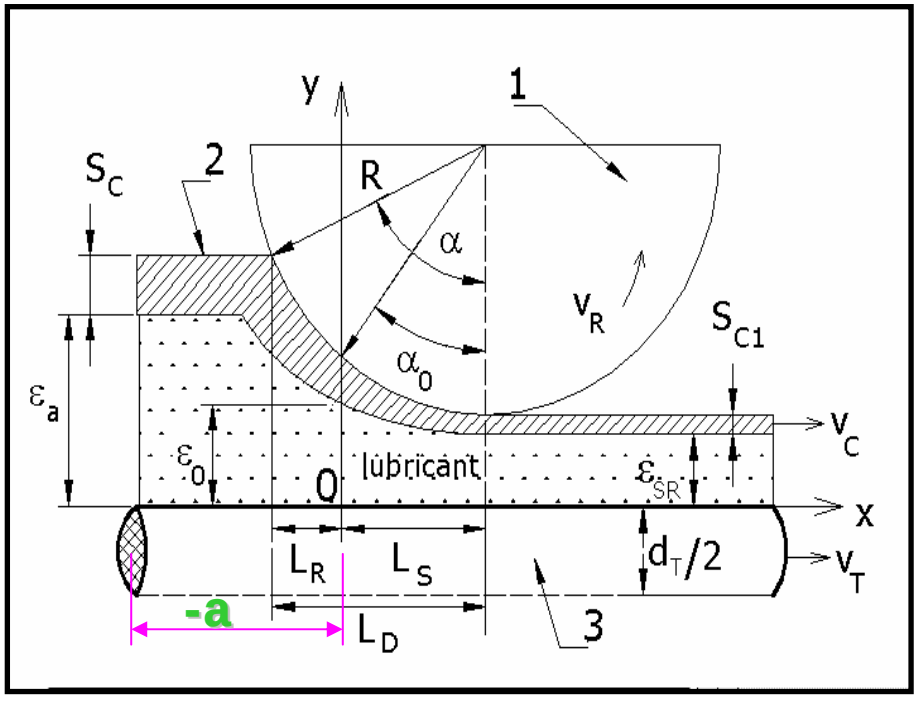
Vidljiva je dobra podudarnost analitičkoga riješenja i numeričke metode. Pomoću točke **M Point** ukazano je na mogućnost dolaženja do novih približnih analitičkih riješenja diferencijalne jednadžbe (2) , matematičkim kloniranjem(izraz(9)) u čijoj pozadini zapravo leži kriterij sličnosti tipičan za mehaniku fluida.

4.Popis simbola i pojašnjenja slika

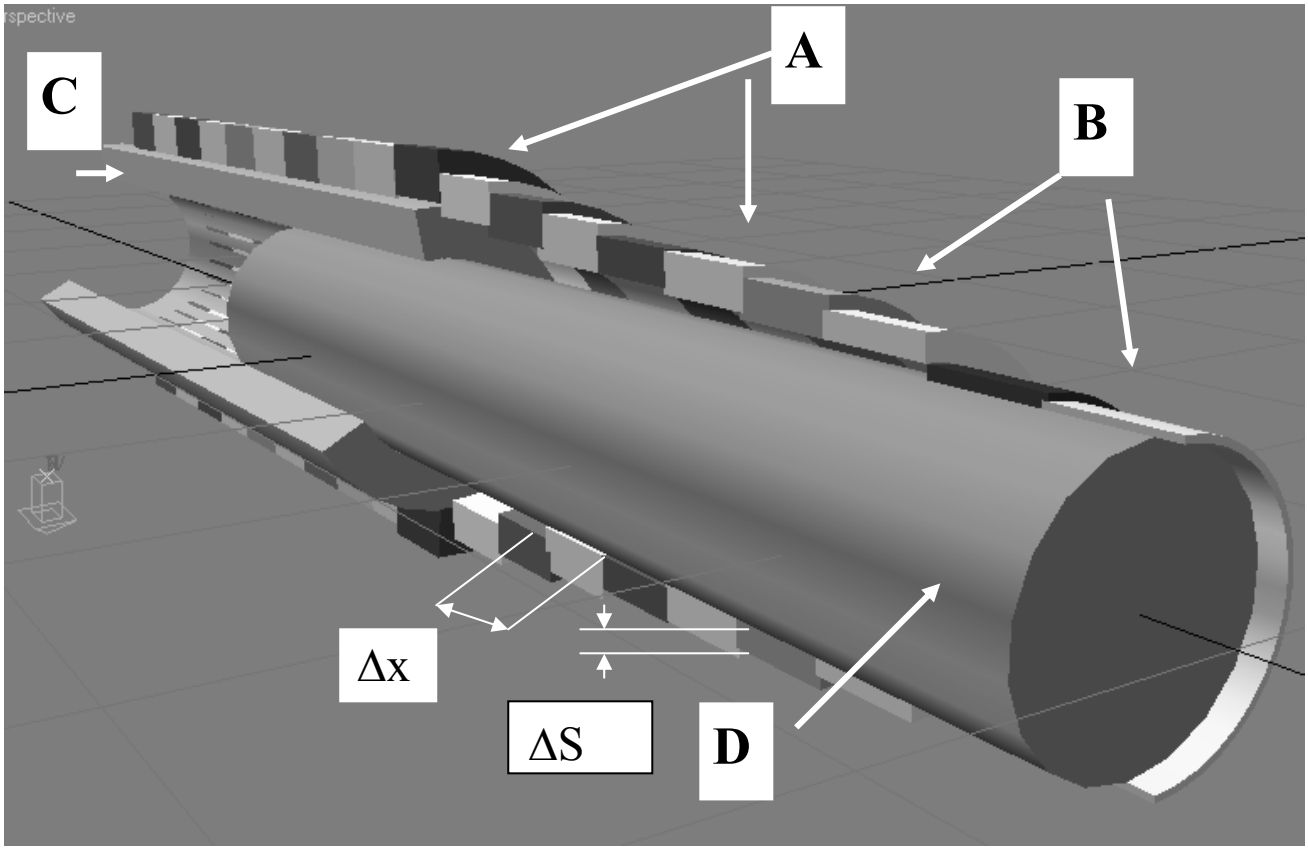
Simbol	Jedinica	Napomena
ε_0	m	Visina maziva na ulaznom presjeku zone deformacije (slika 1)
$\varepsilon^1{}_o$	m	Visina maziva kada kut zahvata α_0 teži nuli
$\varepsilon^{0.1}{}_o$	m	Visina mazivoga sloja za zahvatni kut 0.1 rad , slika 4.(series 1.).
$\varepsilon^*{}_0$	m	Karakterisrtična visina maziva kada kvadratni trinom u izrazu (6) ima diskriminantu kvadratne jednadžbe nula
$\varepsilon(x)$	m	Visina mazivoga sloja u području [-a : 0] , slike 1., formula (4).

ε_{SR}	m	Prosječna visina maziva na trnu nakon prolaza kroz kavez
ε_a	m	Visina maziva na trnu ispred ulaznoga presjeka zone deformacije
ε_{aMAX}	m	Karakteristična visina maziva na trnu u točki M
a	m	Dužina mazivoga klina (slika 1.) , formula (5).
α-α_0	rad	Kut redukcije cijevi po promijeru (slika 1.) ili opseg A (slika 2.)
α_0	rad	Kut deformacije cijevi po stijenki (slika 1.) ili opseg B (slika 2.)
α^*_0	rad	Karakteristični kut koji se pridružuje ε^*_0
v_R	m/s	Obodna brzina valjaka
v_C	m/s	Brzina gibanja cijevi
v_T	m/s	Brzina gibanja trna
$d_T/2$	m	Polumjer trna
R	m	Radijus valjaka u kavezu
R_0	m	$R_0 = R + S_{CX}$
S_{CX}	m	Debljina stijenke cijevi ovisna o apscisi x u zoni deformacije
S_C	m	Debljina stijenke cijevi na trnu prije ulaza u zonu deformacije
S_{C1}	m	Debljina stijenke nakon prolaza kroz konti prugu
L_R	m	Projekcija na apscisu područja redukcije cijevi po promijeru
L_S	m	Projekcija na apscisu zone redukcije cijevi po stijenki
L_D	m	$L_D = L_R + L_S$
.....	točkice	Prikaz maziva na slici 1. , kružni prsten 2. na slici 3., isječak C na slici 2.
D	-	Oznaka trna na slici 2.
Δx ,ΔS	m	Elementarni kružni prsten cijevi dužine Δx, debljine stijenke ΔS
τ_x	Pa	Tangencijalni napon u mayivome sloju
μ_0	Pa s	Dinamička viskoznost maziva pri pritisku valjanja
μ	Pa s	Dinamička viskoznost maziva pri atmosferskom pritisku
u	m/s	Brzina gibanja maziva uzduž apscise
γ	Pa^{-1}	Piezokoeficijent viskoznosti maziva
p	Pa	Pritisak valjanja
Q	m^2/s	Potrošnja maziva po perimetru trna –jednodimenzijski model
dp/dx	Pa/m	Gradijent pritiska u mazivome sloju , formula (2)
$\partial p/\partial x$	Pa/m	Parcijalni izvod pritiska po apscisi , formula (1)
sinα... Ln (ε_a)	rad...	Oznaka za trigonometrijske funkcije , oznaka za prirodni logaritam
		Oznake za točke motrišta kamera AutoCAD-a.Nakon što su približna analitička riješenja izračunata po tablici 1. ona se kompariraju sa numeričkom metodom Monte-Carlo iz matematičkih programa i tako dobivena modeliraju se u AutoCAD-u.Slika 6. i slika 11.
Ψ	m	Zona na konti pruzi koja se opisuje riješenjem u tablici 2. ,slika 4. po ruskim autorima[4,5] , za slučaj suviška maziva na trnu.
Ω	m	Zona na konti pruzi koja slijedi odmah iza Ψ zone gdje ε_a ima utjecaja na ε_o , i ta riješenja , nadalje , iznose se u ovome radu.To je na slici 4. područje redukcije cijevi po promijeru , pojašnjeno i na slici 2.
Σ	m	Zona konti pruge kada počinje i završava intenzivno glodanje maziva na trnu , odvija se deformacija stijenke cijevi
Φ	m	Zona oko točke M na slici 4.Na nju se mogu primjeniti interpolacijski polinomi da povežu proračun mazivoga sloja po Ω i Σ formulama date u tablici 2.

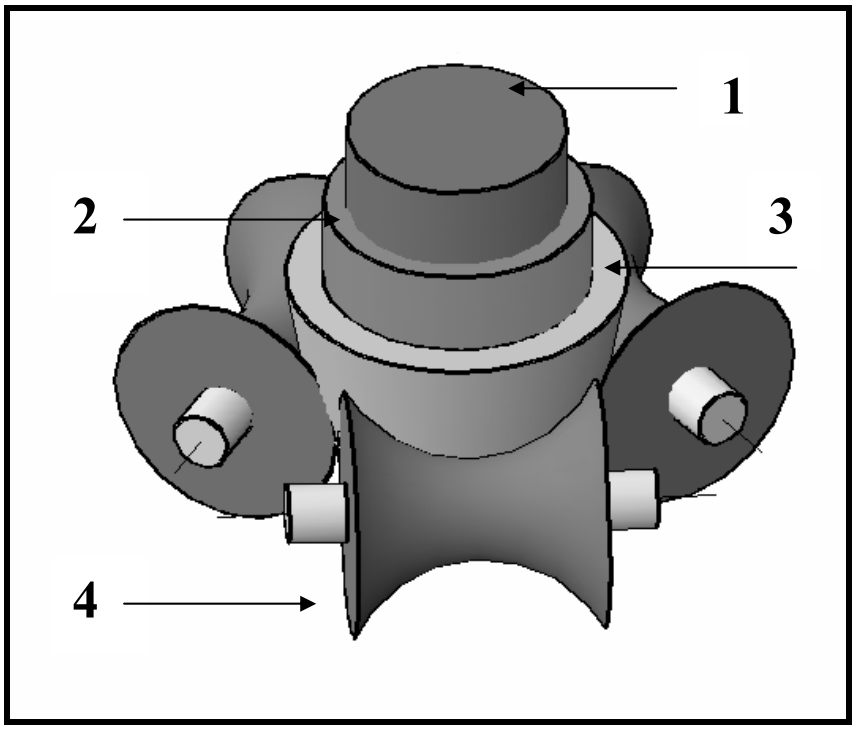
Ω-I	m	Šire područje oko točke M , predstavljeno na slici 15.pogodno je za primjenu **Poligonalne metode** otkrivene od strane autora ovoga rada[14].
M-Point	m	Točka približnoga analitičkoga riješenja u tablici 2. koja kontrolira numeričku metodu Monte-Carlo , te omogućava linearnu korekciju mazivoga sloja po slici 11b.Efekt vidljiv na slikama 12 , 13 i 14.
W	-	Referentna točka na slici 4.Desno od W je redukcija cijevi po radijusu , dok je lijevo od W deformacija stijenke cijevi .Pojašnjava problematiku i nema analitičkoga izraza.
>>, ≈ , ^{0} →, ^, E	-	Matematički simboli za: mnogo veće , približno , oznaka stupnja, teži , znak za potenciju , baza broja 10 .
A	m^{-1}	Tehnološki parametar: $A= [1- \exp(-\gamma p)] / [6\mu_0\gamma(v_C + v_T)]$
exp,[16]	-	Baza prirodnoga logaritma , oznaka za reference



Slika 1. Shema valjanja bešavnih cijevi na konti pruzi



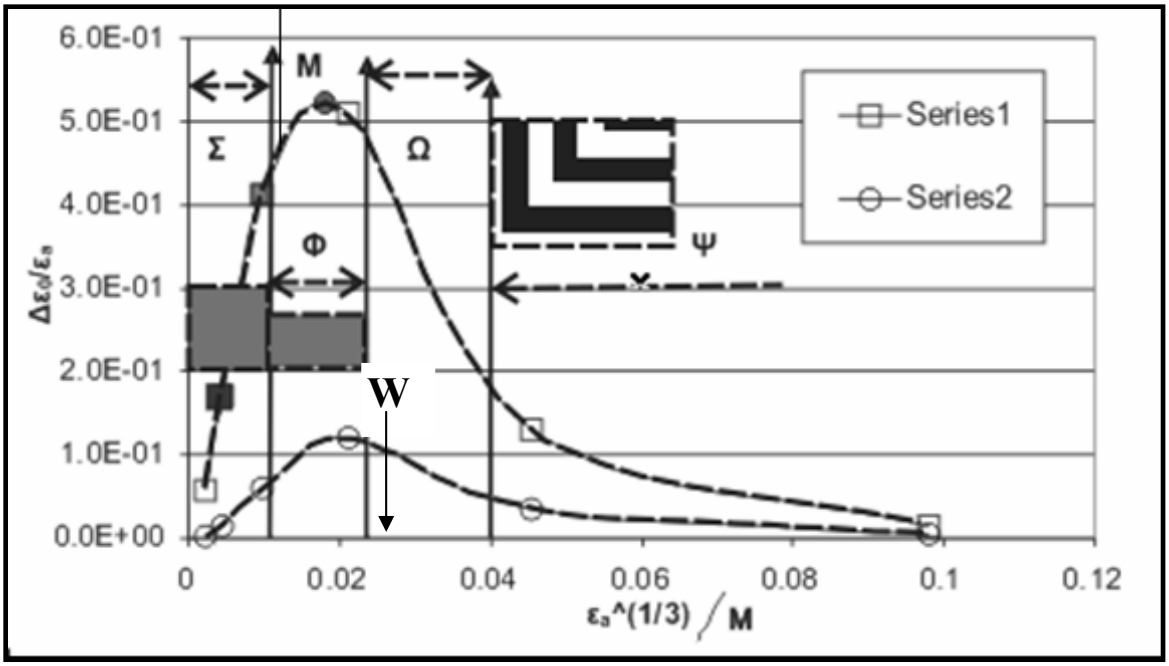
Slika 2.Prikaz 3D redukcije cijevi po promijeru i deformacije cijevi po stijenki; C-mazivo , D- trn , A i B opsezi valjanja na trnu ,Δx i ΔS elemantarni prsten cijevi na trnu.



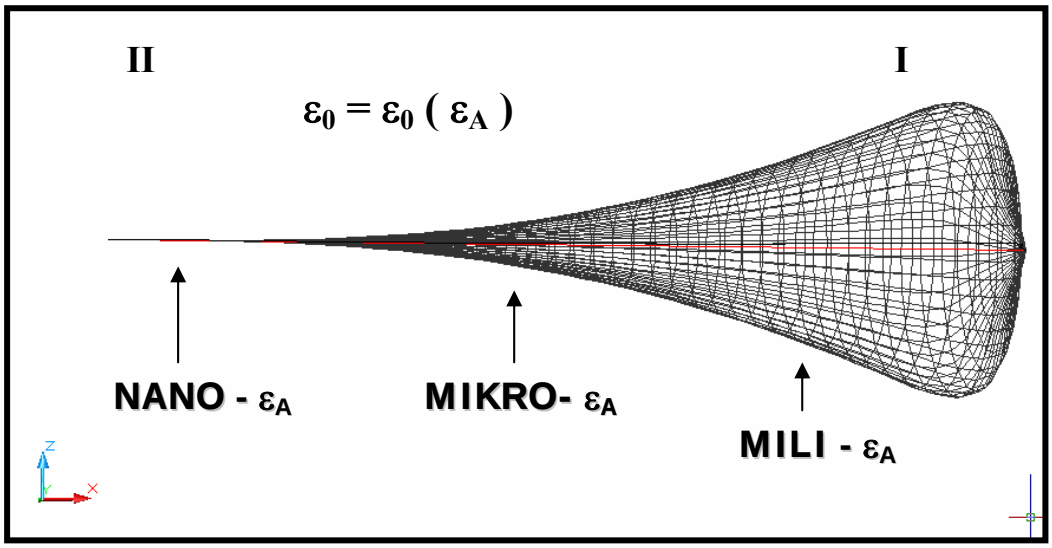
Slika 3. Izgled kaveza sa tri valjka:1-trn,2-mazivo , 3-cijev,
4- valjak.To je analizirani tribomehanički sistem.

Tablica 2.Riješenja diferencijalne jednadžbe (2).

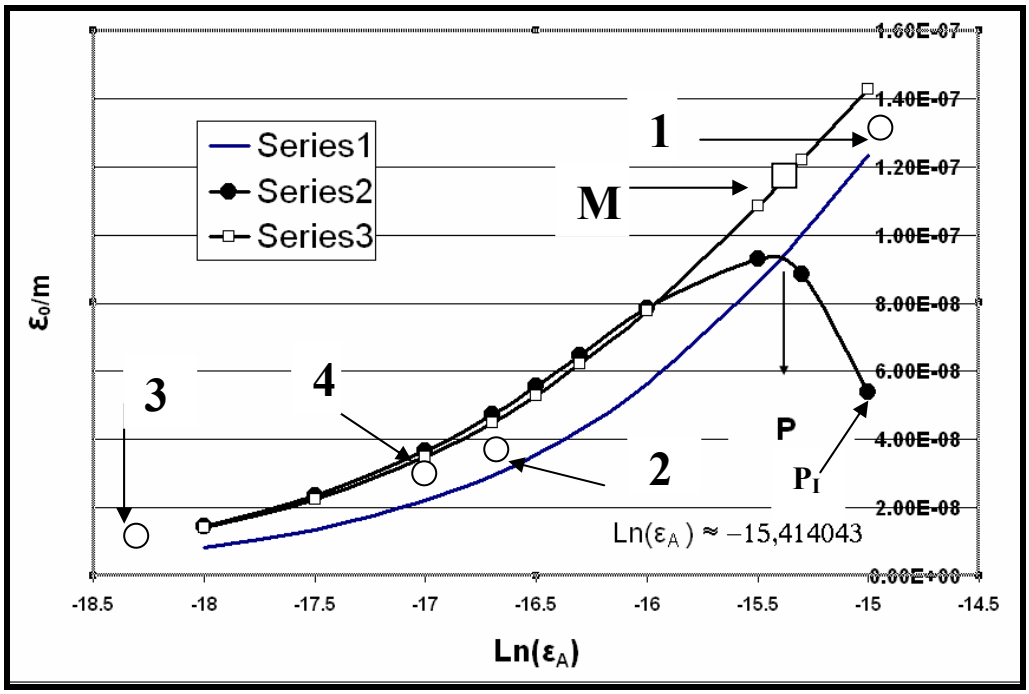
Zone of Fig. 3.	Approximate analytical solution	
Ψ	$\varepsilon_0^* = 0.7726\varepsilon_0^1 \qquad \varepsilon_0^* = 0.5R_0(\alpha^*)^2 \qquad \alpha^* = \sqrt[3]{\frac{8}{15R_0A}}$	$\varepsilon_a >> \varepsilon_0$
Ω	$\alpha^* = 2^* \sqrt[3]{\frac{\varepsilon_a\sqrt{2R_0\varepsilon_a}}{10R_0^{\,2} + 15R_0A\varepsilon_a\sqrt{2R_0\varepsilon_a}}} \qquad \varepsilon_0^* = \frac{R_0(\alpha^*)^2}{2}$	
M Point	$\alpha_0^* = \left(\frac{2}{5}\right)^2 \frac{1}{A\varepsilon_{aMAX}} \qquad \varepsilon_0^* = \frac{R_0(\alpha_0^*)^2}{2} \qquad \varepsilon_{aMAX} = 0.28674^* \sqrt[3]{\frac{R_0}{A^2}}$	
Φ Σ	$\varepsilon_0^1 = \varepsilon_a\left(1 - \frac{0.57348^*\varepsilon_a}{\varepsilon_{aMAX}}\right) \qquad \varepsilon_{aMAX} = 0.28674^* \sqrt[3]{\frac{R_0}{A^2}}$	$\varepsilon_a \to \varepsilon_0$



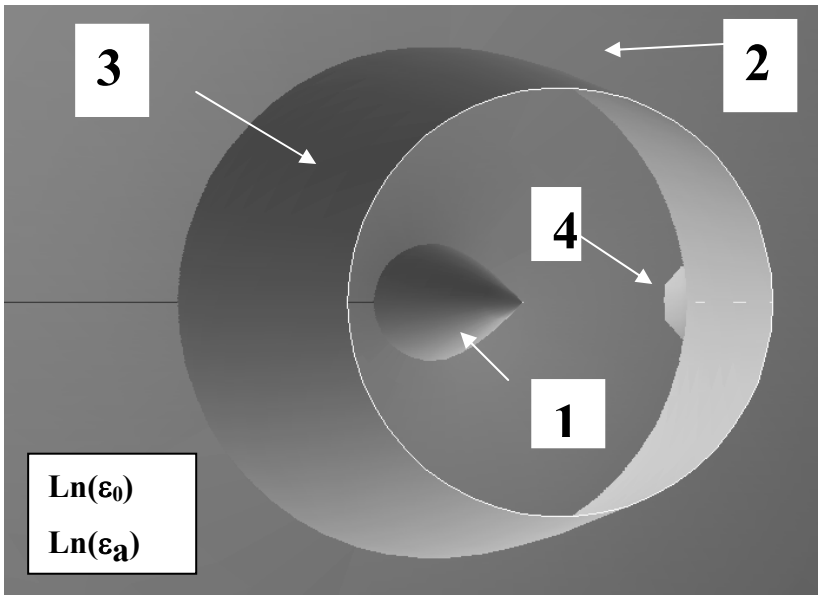
Slika 4.Raspored oblasti po dužini konti pruge prema riješenjima u tablici 2



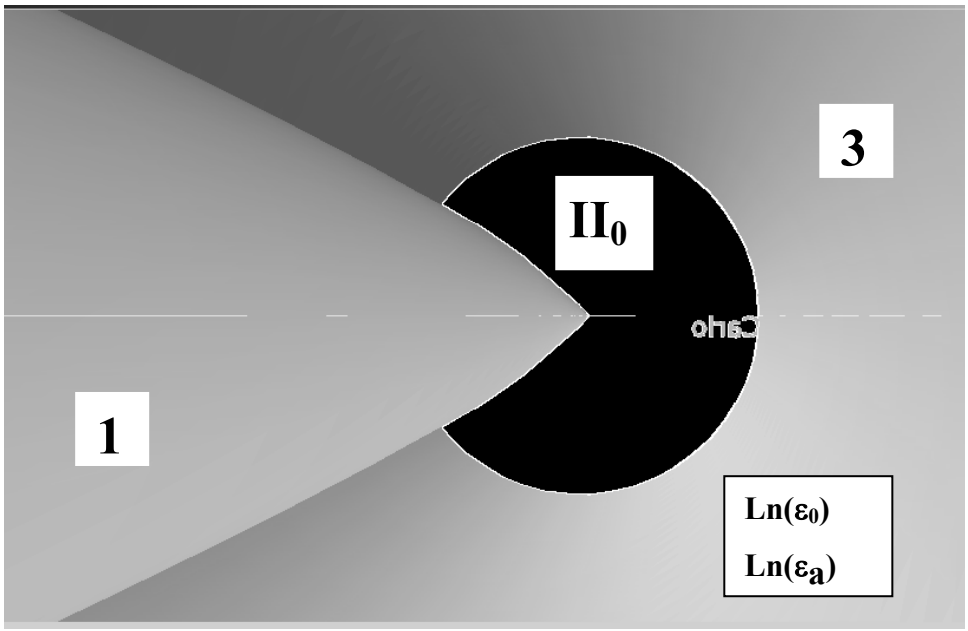
Slika 5. Modelirani mazivi sloj po dužini trna konti pruge u AutoCAD-u.($d_T/2$=0.)
I-redukcija cijevi po radijusu , II-izlazni kavezi i glodanje maziva.



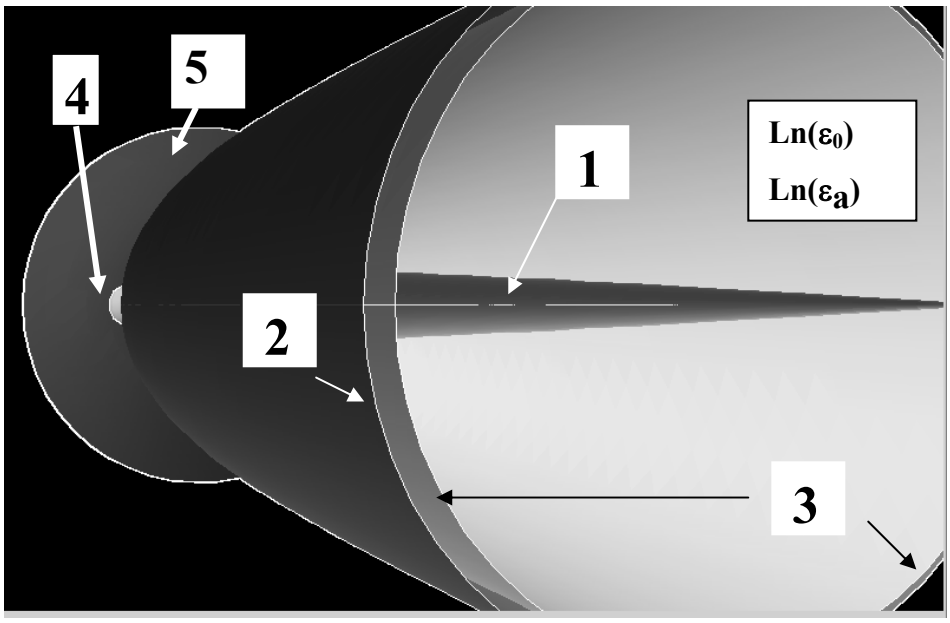
Slika 6.Usporedba približnih analitičkih riješenja u tablici 2 sa numeričkom metodom Monte-Carlo, u opsegu od približno sredine konti pruge do izlaznih kaveza.



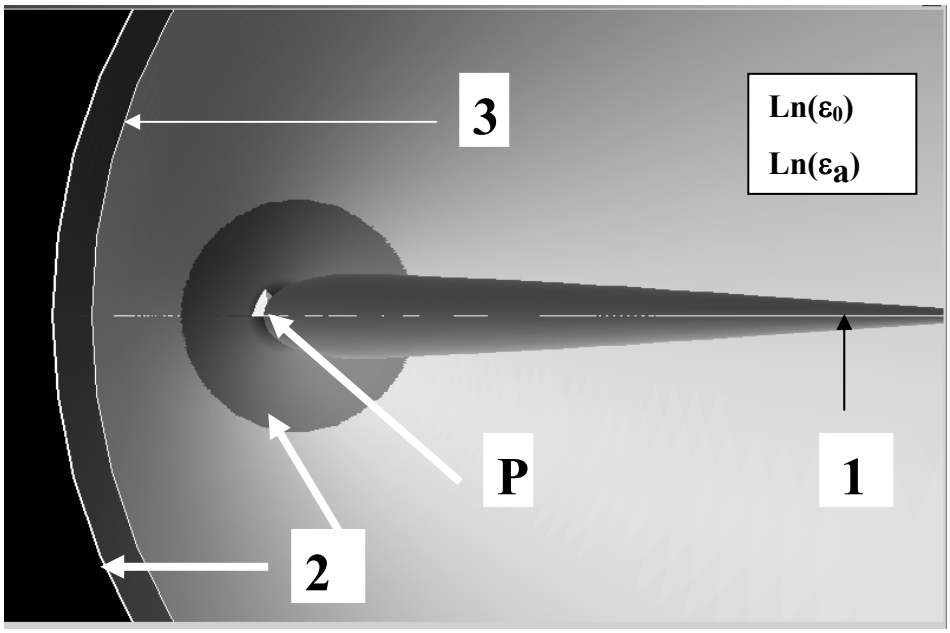
Slika 7.Točka motrišta 1. sa slike 6.Kamera hvata pogled od sredine konti pruge prema izlazu.



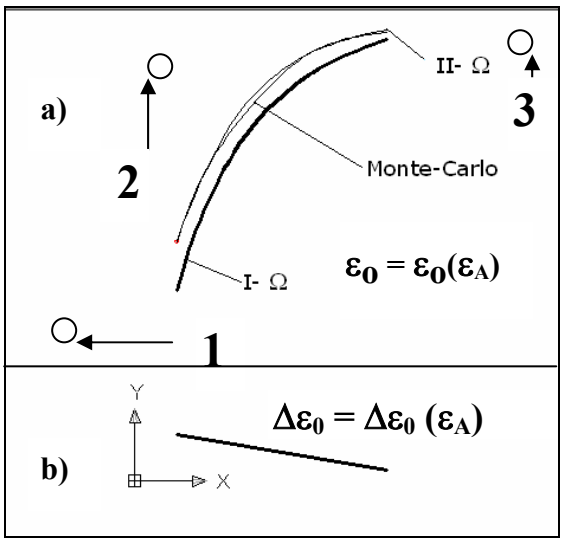
Slika 8.Točka motrišta 2. na slici 6.Kamera je usmijerena prema izlaznim kavezima konti pruge.



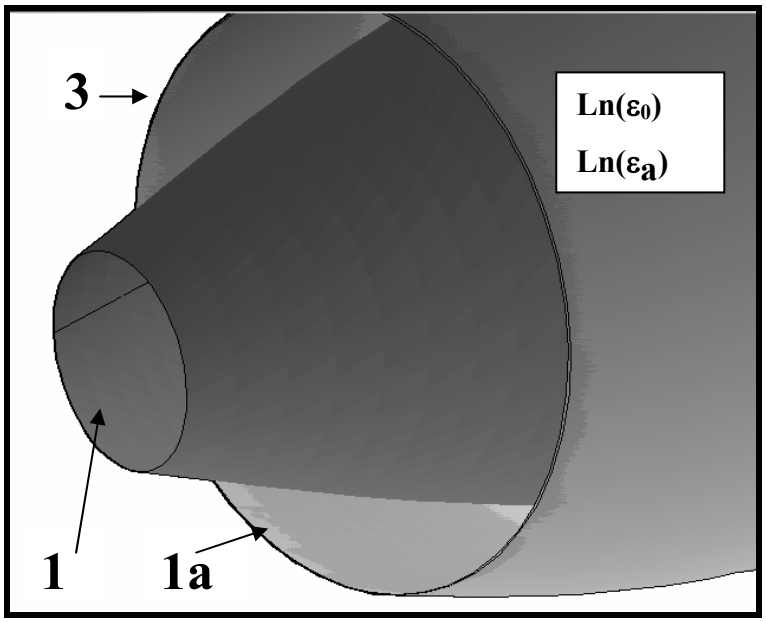
Slika 9. Točka motrišta 3. na slici 6.Kamera hvata modelirani snimak mazivoga sloja na izlaznim kavezima konti pruge(nakon svoga zaokreta za 180^0).



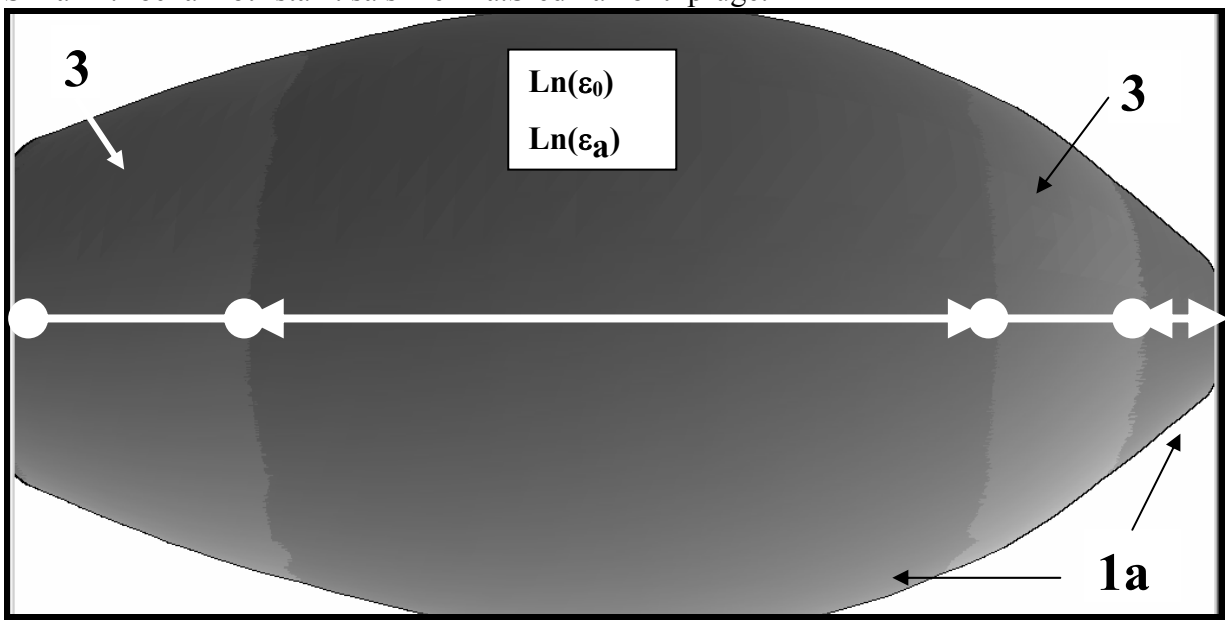
Slika 10. Točka motrišta 4 na slici 6.Kamera je usmijerena prema presijecištu približnih analitičkih riješenja tablice 2.



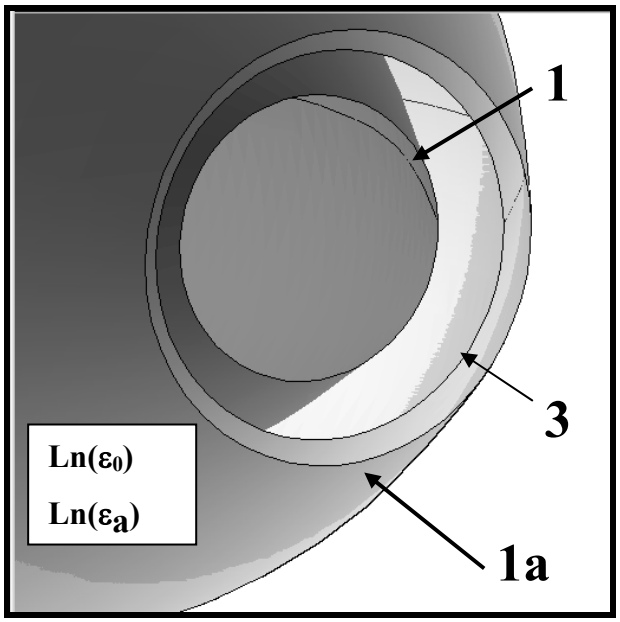
Slika 11.Usporedba približnoga analitičkoga riješenja sa metodom Monte-Carlo u opsegu ulaznih kaveza konti pruge do približno sredine konti pruge.



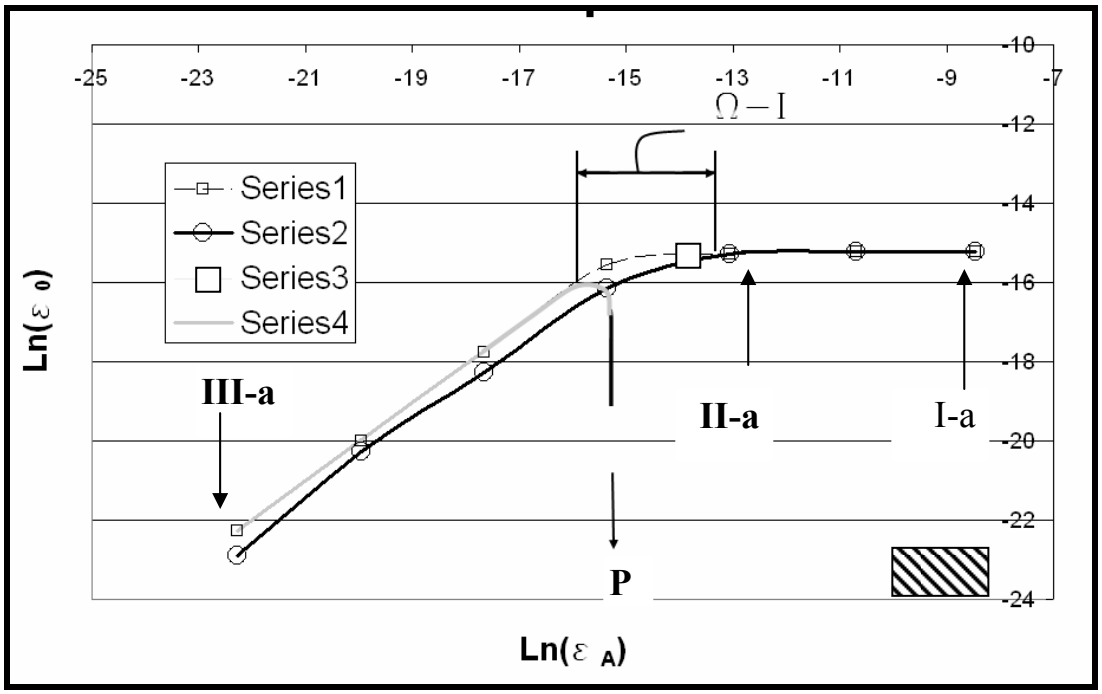
Slika 12.Točka motrišta 1. sa slike 11a.Sredina konti pruge.



Slika 13.Točka motrišta 2. sa slike 11a.



Slika 14. Točka motrišta 3. sa slike 11a.Ulazni kavezi konti pruge.



Slika 15.Usporedba analitičkih riješenja po tablici 2 sa numeričkom metodom Monte-Carlo duž cijele konti pruge.

5.Literatura

[1] .I.Mamuzić , V.M.Drujan ,Teorija ,Materijali , Tehnologija , Čeličnih cijevi, Hrvatsko Metalurško Društvo , Zagreb **1996** , 137-275.

[2] .S.V.Mazur , Postanovka zadači i zakonomernosti tečenija smazki v očage deformacii pri prokatke trub,Sučasni problemi metalurgii, tom 8, s. 447-452 Nacionalna Metallurgičeskaja Akademia Ukraine,Dnepropetrovsk **2005**, Ukrajina

[3] D.Ćurčija , I.Mamuzić , Materiali in Tehnologije , 39 (**2005**) 3, 61-77

[4] O.P. Maksimenko , A.A. Semenča , Issledovanie kontaktno-gidrodinamičeskoj smazki pri prokatke. Sučasni problemi metalurgii, tom 8, s. 99-103 Nacionalna Metallurgičeskaja Akademia Ukraine,Dnepropetrovsk **2005**, Ukrajina

[5] P.L. Klimenko , Kontaktniie naprjaženija pri prokatke s tehnologičeskoj smazkoj , Sučasni problemi metalurgii, tom 8, s. 44-49 , Nacionalna Metallurgičeskaja Akademia Ukraine,Dnepropetrovsk **2005**, Ukrajina

[6] D.Ćurčija , Materiali in Tehnologije , 37 (**2003**) 5, 237-251

[7] D. Ćurčija , I. Mamuzić, Metalurgija 44 (**2005**) 3, 221-226

[8] D. Ćurčija , I. Mamuzić, Metalurgija 44 (**2005**) 4, 295-300

[9] D. Ćurčija , I. Mamuzić , Lubricating film shape at band dressing , 38 Symposium Lubricants ,Društvo za Goriva i Maziva , Zagreb , Rovinj 19-21 10, **2005**. Croatia

[10]D.Ćurčija , I.Mamuzić , Metalurgija 43 (**2004**)249 (Summarie)

[11]D.Ćurčija , I.Mamuzić, Goriva i Maziva 46 (**2007**) 1,34-44.

[12]D.Ćurčija , I.Mamuzić , F.Vodopivec ,Metalurgija 45(**2006**) 3,250. (Summarie)

[13]D.Ćurčija , I.Mamuzić, Materiali in Tehnologije , 41(**2007**) 1,21-27.

[14]D.Ćurčija , I.Mamuzić , Tehnika RGM 34 (**1983**) 8, 1075-1078.

[15]D.Ćurčija , I.Mamuzić , Estimate of lubricant film on pipe rolling in cages/mills , 40th SCIENTIFIC SYMPOSIUM LUBRICANTS 2007 , 24.-26. 10**. 2007**, Pula , CROATIA

[16]D.Ćurčija , I.Mamuzić , Materiali in Tehnologije 42 (**2008**) 1,55-59.

Formatted

Analysis of the indentation size effect on the microhardness of alumina ceramics using different models

Analiza utjecaja opterećenja na mikrotvrdoću aluminij oksidne keramike uporabom različitih modela

Lidija Ćurković, Marijo Lalić, Sanja Šolić
Faculty of Mechanical Engineering and Naval Architecture, University of Zagreb, Ivana Lučića 5, Zagreb, Croatia

Izvorni znanstveni rad / Original scientific paper

Abstract:
The Vickers microhardness of slip-cast high purity alumina ceramics is determined as a function of the indentation load. The results show that the measured hardness depends crucially on the load, which indicates the influence of the indentation size effect (ISE). The load dependence of microhardness is analyzed by using the traditional Meyer Law; a proportional specimen resistance (PSR) model and a modified proportional specimen resistance (MPSR) model. The best correlation between measured values and used models is achieved by using a modified PSR model.

Keywords: hardness, indentation size effect, alumina ceramics.

Sažetak:
Mikrovrdoća visoko čiste aluminij oksidne keramike, dobivene lijevanjem suspenzije metodom po Vickersu, određena je u ovisnosti o primijenjenom opterećenju. Rezultati pokazuju da izmjerene vrijednosti tvrdoće značajno ovise o primijenjenom opterećenju, što ukazuje da je prisutan utjecaj opterećenja na tvrdoću. Utjecaj opterećenja na mikrotvrdoću analiziran je uporabom tradicionalnog Meyerovog zakona, modela otpornosti razmjernog svojstvima uzorka i modificiranog modela otpornosti razmjernog svojstvima uzorka. Najbolje slaganje između izmjerenih vrijednosti i primijenjenih modela postignuto je uporabom modificiranog modela otpornosti razmjernog svojstvima uzorka.

Ključne riječi: tvrdoća, utjecaj opterećenja na tvrdoću, aluminij oksidna keramika.

1. Introduction

Hardness is one of the most frequently measured properties of ceramics and it is a measure of material resistance to permanent plastic deformation. Its value helps to characterize the resistance to deformation, densification, and fracture. Hardness is usually measured on conventional microhardness machines with Vickers or Knoop diamond indenters. These machines make impressions whose diagonal size is measured with an attached optical microscope. For research purposes, Vickers, Knoop, and Berkovich (triangular pyramid) indenters are customary; Rockwell and Brinell indenters are rarely suitable for ceramics research. For engineering and characterization applications, approximately 60 % of worldwide published ceramic hardness values are Vickers hardness values, with loads typically in the range of a few newtons to 9.8 N (HV1) and occasional data for soft or high-toughness ceramics as high as 98 N (HV10). About 35 % are Knoop hardness values with loads from as low as 0.98 N (HV0.1) to 19.6 N (HV2). At low indentation loads, problems arise from the load dependence on hardness and from the measurement uncertainty due to a small indentation size. At higher loads, cracking and spalling pose problems; and in some cases they make credible measurement impossible.

Accurate measurements of the hardness of brittle materials have been difficult due the dependence of hardness on load. For ceramics, the indentation size is small and the percentage error may be larger; because of that it is crucial that the diagonal length be measured carefully. Smaller diagonal lengths are produced in ceramics than in most metals for a given load, which increases the measurement uncertainty.

A correct optical microscopy technique is crucial for ceramic hardness measurements. Reasonable skill, experience, and a careful experimental technique are necessary to measure diagonal lengths accurately and precisely.

The indenter gives a geometrically similar indentation so that the measured hardness should be independent of the applied load. But investigations have confirmed that the hardness is usually load-dependent, i.e. decreasing in a low load range [1-8] or increasing [9] with an increase in the applied load. Some materials exhibit an increase in hardness with a decreasing load (indentation size effect, ISE) while others undergo a decrease in hardness with a decreasing load (reverse indentation size effect, RISE) [1,7]. The ISE is illustrated schematically in Figure 1.

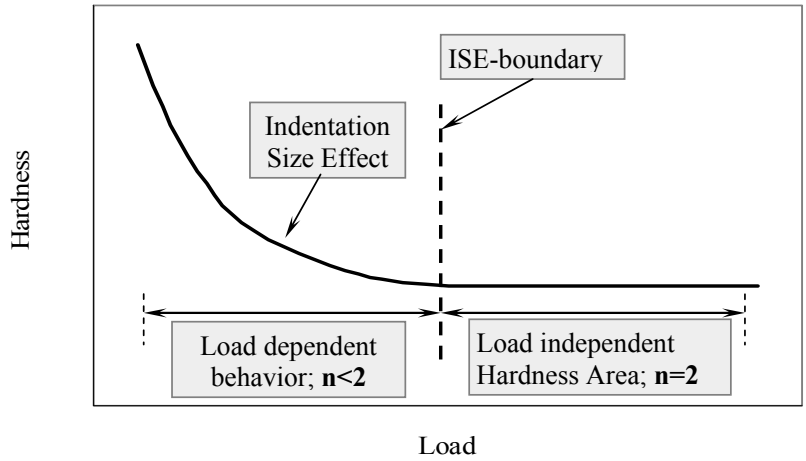


Figure 1. Shematic plot of the indentation size effect (ISE) behavior [9].

The apparent hardness is a function of the applied load at low indentation test loads, where there is no constant value for hardness (load dependent hardness). At high indentation test loads, hardness is a constant value. Load independent hardness has also been referred to as the "true" hardness in some literature.

To calculate the indentation size effect (ISE), several relationships between the applied load, P, and the resulting indentation size, d, have been suggested [1-9]. The goal of this work is to analyse the observed ISE of slip-cast alumina ceramics using the traditional Mayer Law, a proportional specimen resistance (PSR) model and a modified PSR model.

2. Experimental procedure

The material used in this study was a high purity slip-cast alumina ceramics (SC-Al_2O_3). A SC-Al_2O_3 specimen was prepared in Applied Ceramics, Inc., Fremont, California, U.S.A.

Vickers hardness measurements HV0.1, HV0.2 and HV0.5 were performed using indentation loads of 0.9807 N, 1.961 N and 4.903 N for 15 s, respectively. Indentation tests were carried out under laboratory conditions on an Instron, Wilson-Wolpert Tukon 2100B, a micro Vickers tester. Care was taken to make indentations only on those areas which had no visible pores. Thirty determinations for each load were performed on the alumina sample. The average value of diagonal lengths of the indentation for each load was used to calculate the hardness according to equation (2). Before carrying out hardness measurements, all specimens were prepared by the standard ceramographic technique [10]. The sample was mounted with a DuroFix-2 Kit, ground and then polished up to 1 μm with a diamond paste until a mirror-like surface was achieved. All the indentation tests were carried out under ambient laboratory conditions.

3. Results and discussion

The hardness number H is defined as a ratio of the applied load (P) to the contact area (A) between the indenter and the sample:

$$H = P/A \tag{1}$$

In the case of Vickers hardness tester (Figure 2), hardness numbers HV were calculated using the relation:

$$HV = P/A = \alpha F/d^2 \tag{2}$$

Where:
α = 0.1891
HV = Vickers hardness,
F = applied load (N),
d = arithmetic mean of the two diagonal length (mm).

The variation of microhardness of SC-Al_2O_3 ceramics with the applied load is shown in Figure 3. Results show that microhardness decreases with the increasing indentation test load. This dependence of hardness on the applied load is known as the ISE. The observed decrease in hardness with an increasing load is usually called a normal ISE.

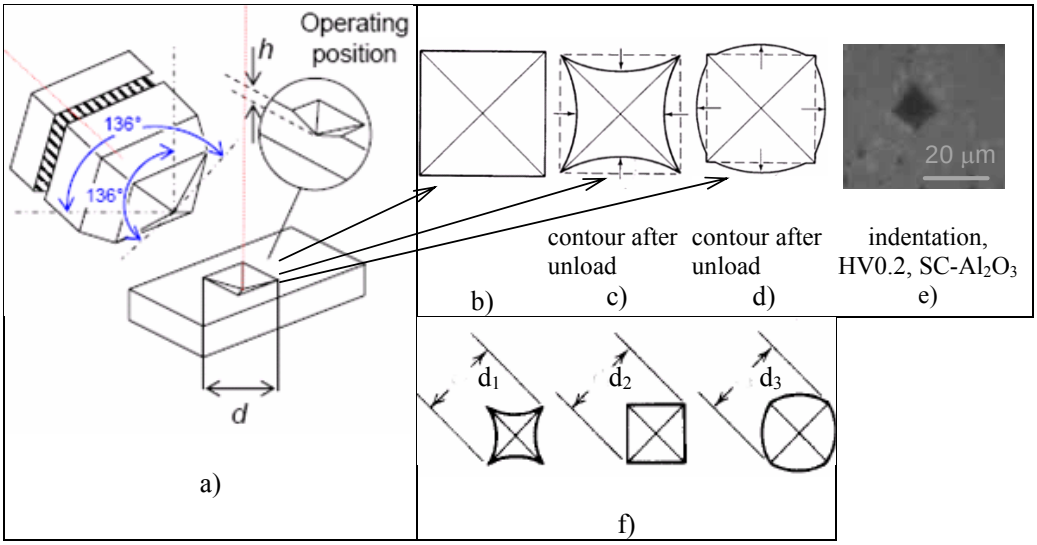


Figure 2. Vickers hardness testing: a) Schematic of a Vickers or a diamond pyramid hardness indenter (h~ d/7); distortion of diamond pyramid indentions due to elastic effects: b) perfect indentation, c) pincushion indentation due to the material sinking around flat faces of the pyramid, d) barrelled indentation due to the ridging material around the faces of the indenter; e) optical photo of a Vickers indentation at the applied load of 1.961 N for SC-Al_2O_3 ceramics; f) indentations with equal diameters but different areas ($d_1=d_2=d_3$; $A_1<A_2<A_3$) [11].

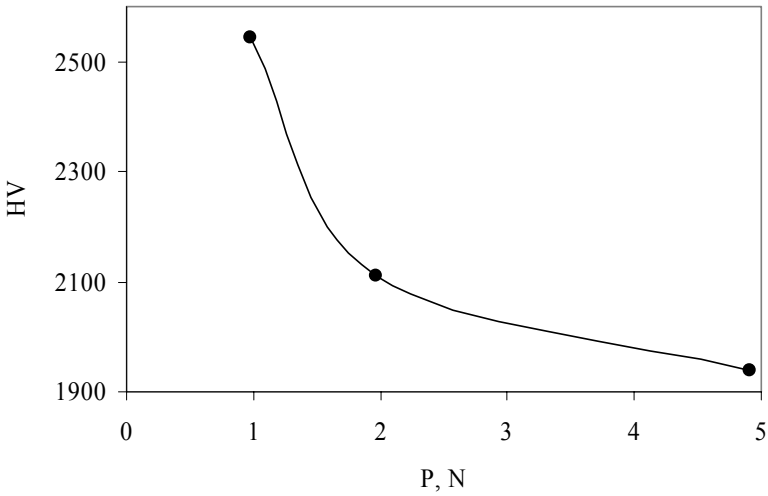


Figure 3. Vickers hardness as a function of the applied load for SC-Al_2O_3 ceramics.

The most common explanation for the ISE found in literature is directly related to the structural factor of the test material. Meyer proposed an empirical relation between the load and the size of the indentation. This relationship is usually called Meyer's Law [5]. The

Meyer Law is simply an empirical expression to describe the relationship between the indentation load, P, and the resultant indentation size, d.

$$P = Ad^n \tag{3}$$

where A is a constant parameter for a given material and n is Meyer's index (or number), which is a measure of the ISE. These parameters are obtained from the curve fitting (Figure 4) of experimental results of indentations (*log P* versus *log d*). Meyer's Law has been suitable for the representation of experimental data for a variety of ceramics, and Meyer's index n has been experimentally observed to be between 1.5 and 2.0. The A and n values in equation (3) determined by linear regression analysis and the results are summarized in Table 1. The data show a linear relationship, indicating that the traditional Meyer Law is suitable for describing microindentation data. The Meyer index n obtained experimentally is less than 2, which indicates that hardness is dependent on test loads.

Table 1. Regression analysis results of experimental data according to equation (3).

Sample	n	*log A*	A	Correlation factor (R^2)
SC-Al_2O_3	1.7139	3.5273	3367	0.9984

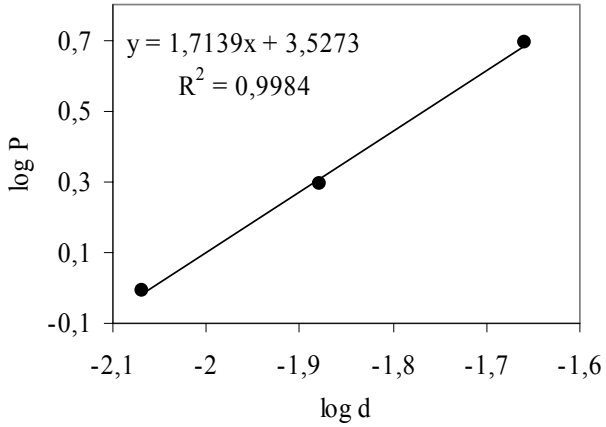


Figure 4. Vickers microhardness data on SC-Al_2O_3 ceramics according to the Meyer Law.

The Meyer Law is simply an empirical expression to describe the relationship between the indentation load and the indentation size. An alternative analysis of the ISE to the Meyer Law is a proportional specimen resistance (PSR) model and recently a number of researches have explained the ISE with this model. The proportional specimen resistance (PSR) model was introduced by Li and Bradt [4]. In this model, the applied test load (*P)*, and the resulting indentation size (*d*), were found to follow the relationship:

$$P = a_1 d + a_2 d^2 \tag{4}$$

where a_1 and a_2 were considered as constants; a_1 (N/mm) coefficient was suggested to relate to the proportional resistance of the test specimen and a_2 (N/mm^2) to the load-independent hardness, or "true" hardness. Equation (4) can be transformed into:

$$P/d = a_1 + a_2 d \tag{5}$$

The parameters a_1 and a_2 from equation (5) are evaluated through the linear regression of *P/d* versus *d.* Figure 5 shows the plot *P/d* versus *d* with a straight line with a slope equal to

the a_2 value and an intercept equal to the a_1 value. The results are presented in Table 2. Li et al. [12] concluded that this model might provide a satisfactory explanation for the origin of the ISE in microhardness tests for different materials.

Table 1. Regression analysis results of experimental data according to a PSR model.

Sample	a_1	a_2	Correlation factor (R^2)
SC-Al_2O_3	42	8255.9	0.9984

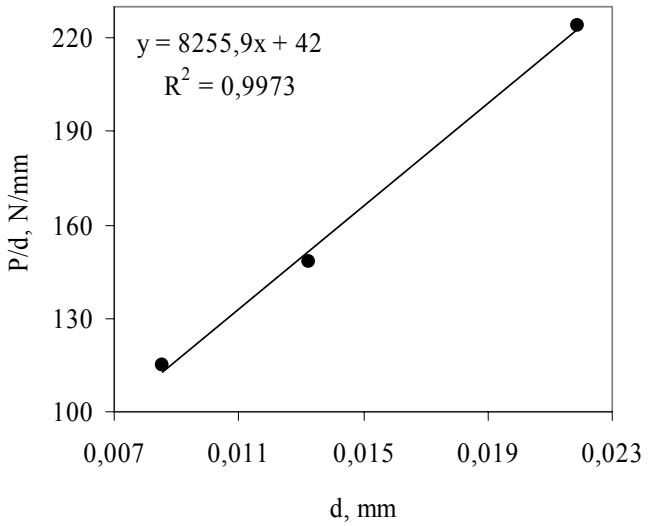


Figure 5. Vickers microhardness data on SC-Al_2O_3 ceramics according to a proportional specimen resistance (PSR) model.

Gong et al. [5] suggested a modified PSR model designed on the basis of the consideration of the effect of a machining-induced, residually stressed surface on the hardness measurements, giving

$$P=P_o+a_1d+a_2d^2 \qquad (6)$$

where P_0 is a constant related to the surface residual stresses associated with the surface machining and polishing and a_1 and a_2 are the same parameters as the ones given in equation (4). Figure 6 illustrates P versus d for alumina ceramics samples tested in the present study. The solid lines in these plots are obtained by conventional polynomial regression according to equation (6). The best-fit values of the parameters included in equation (6) for SC-Al_2O_3 ceramics sample are presented in Table 3.

Table 3. Parameters P_0, a_1 and a_2 of the MPRS model according to equation (5) for SC-Al_2O_3 ceramics.

Sample	P_0	a_1, N/mm	a_2, N/mm^2	Correlation factor (R^2)
SC-Al_2O_3	0.31	-6.02	9850.8	1

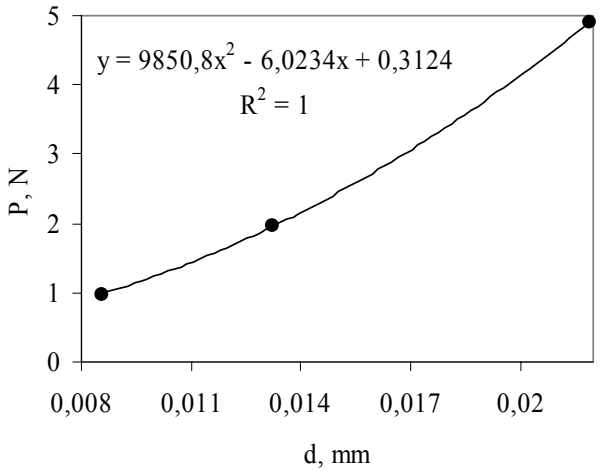


Figure 6. The applied load versus indentation size according to the modified PSR model for SC-Al_2O_3 ceramics.

P_0 is a specimen constant, rather than a material constant. Surface finishing processes (grinding and polishing), which remove the material mechanically, used in the preparation of the specimens prior to indentation can be a cause of the ISE because the finishing processes introduce plastic deformation and cracks into the material adjacent to the surface[5]. The relatively small or negative values of P_0 in Table 3 seem to be reasonable estimates of the residual of the surface stress for SC-Al_2O_3 ceramics which have been subjected to careful finishing processes (grinding and polishing).

4. Conclusions

Like many other ceramics, SC-Al_2O_3 ceramics show the indentation size effect behaviour. It means that the measured hardness values increase with decreasing indentation loads.

Meyer's Law has proved to be satisfactory for the description of experimental data with a correlation coefficient of 0.9984. The Meyer index n obtained experimentally is less than 2, which indicates that hardness is dependent on test loads.

Moreover, the PSR model can be used to analyze the ISE observed in SC-Al_2O_3 ceramics, but the best correlation between measured values and mathematical models was achieved with the MPSR model with a correlation coefficient of 1.

Acknowledgments

The presented research results were achieved within the scientific project "Structure and properties of engineering ceramics and ceramic coatings" supported by the Croatian Ministry of Science, Education and Sport. We thank Matt Sertic from Applied Ceramics, Inc. for providing alumina ceramics samples.

5. REFERENCES

[1] H. Li, A. Ghosh, Y.H. Han, R.C. Bradt, The frictional component of the indentation size effect in low load microhardness testing, *J. Mater. Res.* **8** (1993) 8(5) 1028–1032.

[2] J. Gong, Z. Guan, Load dependence of low-load Knoop hardness in ceramics: a modified PRS model, Mater. Lett., 47 (2001) 140-144.
[3] X. J. Ren, R. M. Hooper, C. Griffiths, J. L. Henshall, Indentation size effect in ceramics: correlation with H/E, J. Mater. Sci. Let., 22, 2003, 1105-1106.
[4] H. Li, R.C. Bradt, The microhardness indentation load/size effect in rutile and cassiterite single crystals *J. Mater. Sci.* **28** (1993) 917-926.
[5] J. Gong, J. Wu, Z. Guan, Examination of the indentation size effect in low-load Vickers Hardness testing of ceramics, *J. Eur. Ceram. Soc.* **19** (1999) 2625–2631.
[6] H. Kim, T. Kim, Measurement of hardness on traditional ceramics, J. Eur. Ceram. Soc., 2002, 22, 1437-1445.
[7] U. Kolemen, Analysis of ISE in microhardness measurements of bulk MgB_2 superconductors using different models, J. Alloys Compd. 425 (2006) 429-435.
[8] O. Sahin, O. Uzun, U. Kolemen, N. Ucar, Vickers microindentation hardness studies of β-Sn single crystal, Mater. Characterization, 58 (2007) 197-204.
[9] S. Sebastian, M. A. Khadar, Microhardness indentation size effect studies in $60B_2O_3$-(40-x)PbO-xMCl_2 and $50B_2O_3$-(50-x)PbO-xMCl_2 (M=Pb, Cd) glasses, *J. Mater. Sci.,* **40,** 1655-1659 (2205).
[10] R. E. Chinn, Ceramography Preparation and Analysis of Cearmic Microstructures, ASM Interantional, USA, 2002.
[11] http://bama.ua.edu/~mweaver/courses/MechBeh/M02a.pdf
[12] H. Li, Y. H. Han, R. C. Bradt, Knoop microhardness of single crystal sulphur, *J. Mater. Sci.* **29,** 5641-5645 (1994).

Analiza mikrostrukture aluminij oksidne keramike

Lidija Ćurković[1], Vera Rede[1], Peter Panjan[2], Mirjana Fudurić Jelača[3], Marijo Lalić[1]

[1]Fakultet strojarstva i brodogradnje, Zagreb, Croatia
[2] Institut Jožef Stefan, Ljubljana, Slovenija
[3]Visoka škola za sigurnost, Zagreb, Croatia

Izvorni znanstveni rad / Original scientific paper

Sažetak:

U radu je opisan postupak pripreme visoko čiste aluminij oksidne (Al_2O_3) keramike oblikovane hladnim izostatičkim prešanjem za analizu mikrostrukture. Za analizu mikrostrukture korišten je optički mikroskop, pretražni elektrosnki mikroskop (SEM) te mikroskop atomski sila (AFM). Na poliranoj površini uzroka određen je udio pora, a nakon toplinskog nagrizanja određena je veličina zrna. Prosječni promjer zrna određen je metodom kruga, metodom crte, te analizom slike.

Ključne riječi: mikrostruktura, aluminij oksidna keramika.

Microstructure analysis of alumina ceramics

Abstract:

In this paper is described a method for preparation of a cold isostatically pressed (CIP) high purity alumina ceramics (Al_2O_3) for microstructure analysis. Microstructure analysis was performed by means of optical microscopy (OM), scanning electron microscopy (SEM) and atomic force microscopy (AFM). Porosity is determined on the polished surface of sample; grain size is measured after thermal etching. The mean grain diameter is determined by means of lineal-intercept method, circular-intercept method and image analysis.

Keywords: microstructure, alumina ceramics.

1. Uvod

Mikrostruktura svih tehničkih materijala pa tako i tehničke keramike utječe na cijeli niz svojstava među kojima su mehanička, tribološka, korozijska, toplinska, električka i dr. Znanstveni radovi često pokušavaju staviti u odnos svojstva i ponašanje materijala sa karakteristikama mikrostrukture. Metode i uvjeti proizvodnje općenito se odražavaju na mikrostrukturu. Korijen uzroka mnogih nedostataka je vidljiv u mikrostrukturi. Znanost koja se bavi utvrđivanjem korelacije između strukture i svojstava materijala zove se *materijalografija*. *Keramografija* je dio materijalografije čiji je zadatak priprema, istraživanje i analiza mikrostrukture keramičkih materijala. Na temelju analize mikrostrukture moguće je unaprijed odrediti svojstva i ponašanje materijala pri određenim uvjetima opterećenja ili ukazati na optimalnu mikrostrukturu za neki proces prerade ili područje primjene.

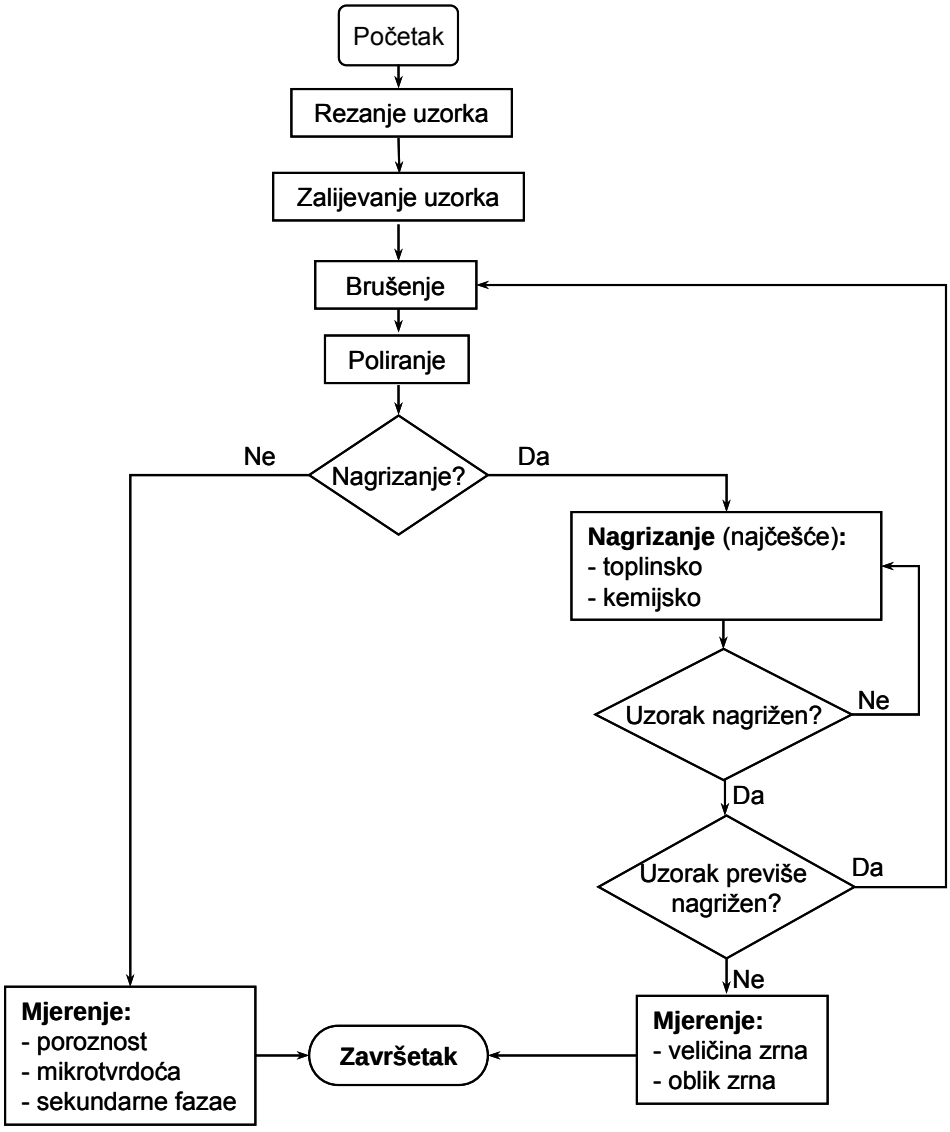
Pod pojmom *mikrostruktura* podrazumijeva se strukturna razina između 0.1 i 100 μm. Područje od približno 100 μm je granica razlučivanja ljudskim okom bez pomagala. Nivo strukture veći od 100 μm zove se *makrostruktura* i neke keramike imaju zrna i pore koje su vidljive golim okom.

Mikrostruktura obuhvaća analizu: kristalnih zrna, sekundarnih faza, granica zrna, pora i mikropukotina. U analizu mikrostrukture svrstava se i mjerenje mikrotvrdoće.

Kvalitetno pripremljen keramografski uzorak je najvažniji segment mikrostrukturne analize keramičkog materijala. To je uzorak s ravnom, glatkom i sjajnom površinom koji dobro reprezentira materijal u cijelosti. Priprema uzorka započinje utvrđivanjem mjesta na dijelu s kojeg se uzorak uzima. Pritom se osobito mora voditi računa o položaju i orijentaciji površine uzorka koja će se dalje pripremati za analizu. Uzorak se nakon toga izrezuje, zalijeva u masu, brusi i polira, po potrebi nagriza te analizira. Tijek pripreme i analize keramografskog uzorka prikazan je na slici 1 [1-3]. Na poliranom uzorku određuje se: volumni udio i veličina pora, volumni udio sekundarnih faza (neke sekundarne faze vide se u poliranom stanju, a neke nakon nagrizanja).

Na poliranom uzorku se mjeri i mikrotvrdoća. Nakon analize poliranog uzorka slijedi nagrizanje u svrhu određivanja prosječnog promjera zrna, oblika zrna i razdiobe veličine zrna. Nagrizanjem se otkrivaju i ocrtavaju granice zrne i to omogućava mjerenje ili usporedbu veličine zrna. Nagrizanje se ne provodi sve dok nije određena poroznost i izmjerena mikrotvrdoća. Za nagrizanja keramike najčešće su u uporabi tri metode: toplinsko nagrizanje, nagrizanje otopinama (kemijsko) i plazma nagrizanje. Pored ovih najčešće korištenih metoda nagrizanja u literaturi se navode i druge metode kao što su: nagrizanje u talinama soli, toplinsko bojanje, termokemijsko nagrizanje i reljefno poliranje. Aluminij oksidna keramika se nagriza toplinski i otopinama (kemijski). U ovom radu uzorak visoko čiste aluminij oksidne keramike nagrižen je toplinski zato što je toplinsko nagrizanje najpogodnije za visoko čiste jednofazne okside kao što je aluminij oksidna keramika. Toplinsko nagrizanje je najjednostavnija, najčišća i najefikasnija metoda ocrtavanja granica zrna u mikrostrukturi keramike, posebice za jednofazne okside. Ako toplinsko nagrizanje provodimo na previsokim temperaturama i dulje vrijeme postoji opasnost apsorpcije najmanjih zrna u veliko zrno. To može rezultirati sa rastom zrna i na taj način se mikrostruktura mijenja. Toplinsko nagrizanje se najčešće provodi na temperaturi oko 100 do 200 °C ispod temperature sinteriranja u trajanju do 60 min. Za neke keramičke materijale toplinsko nagrizanje može trajati nekoliko sati. Kod keramika koje se javljaju u više alotropskih modifikacija, kao što je djelomično stabilizirana zirkonij oksidna keramika (ZrO_2), sklona je raspucavanju pri višim temperatura uslijed istezanja koje se javlja s faznim transformacijama. Pri temperaturi iznad 1000 °C visoko čista cirkonij oksidna keramika podliježe displazivnim transformacijama od monoklinske (gustoća je 5,83 g/cm^3) do tetragonske faze (gustoća je 6,10 g/cm^3), a hlađenjem ispod 1000 °C transformacija je reverzibilna. Djelomično stabilizirana cirkon oksidna keramika (PSZ) ima metastabinu kubičnu primarnu fazu i sadrži najčešće malu količinu CaO,

MgO ili Y_2O_3 u čvrstoj otopini. Djelomično stabilizirana cirkon oksidna keramika koristi tetragonsku-monoklinsku transformaciju u svojoj sekundarnoj fazi da bi postigla efekt očvrsnuća. Djelomično stabilizirana i tetragonska polikristalna zirkon oksidna keramika toplinski se ne nagriza. Cirkon oksidna keramika koja sadrži 13 % itrija (ZDY) je potpuno stablilizirane kubične strukture i ona se može toplinski nagrizati. Kod višefaznih okida, koji uključuju veliki broj porculana, može se pojaviti inkongruentno taljenje ili reakcije između različitih faza koje pri visokim temperaturama mogu promijeniti mikrostrukturu. Općenito neoksidne keramike toplinski se nagrizaju u vakuumu ili inertnoj atmosferi da bi se izbjegla oksidacija na poliranoj površini. Ispravan postupak toplinskog nagrizanja može se naći u literaturi [1, 4-7].



Slika1. Dijagram tijeka priprave uzorka za keramografiju [1,3].

2. Eksperimentalni dio

Za analizu mikrostrukture korišten je uzorak aluminij oksidne keramike oblikovane hladnim izostatičkim prešanjem (CIP- Al_2O_3), čistoće 99,8 %. Uzorak CIP-Al_2O_3 je sinteriran u Applied Ceramics, Inc., Fremont, Kalifornija, SAD. Ispitivana Al_2O_3 keramika sadrži MgO kao pomoćno sredstvo za sinteriranje i uobičajene nečistoće SiO_2, CaO, Na_2O i Fe_2O_3.

Sinteriranje je obavljeno pri temperaturi od 1650 ^{o}C u plinskoj peći i kontrolu temperature uz postepeno grijanje i hlađenje.

Nakon sinteriranja i rezanja uzorka Al_2O_3 keramike slijedi zalijevanje te brušenje i poliranje uzorka.

Zalijevanje uzorka

Masa za zalijevanje uzorka je „Acry Fix Kit“, dok je vrijeme skrućivanja cca. 9 - 11 min. Prije zalijevanja uzorka masa se miješa ~ 1 min i nakon skrućivanja odnosno vađenja iz kalupa zaliveni uzorak pere se vodom.

Brušenje (Diamond Grinding Disc)

Optimalna kvaliteta brušenja ostvaruje se sljedećom kombinacijom brusnih ploča i finoće abrazivnih čestica:

1. stupanj: ploča s dijamantnim abr. česticama, 120 (~180 μm)
2. stupanj: ploča s dijamantnim abr. česticama, 220 (~65 μm)
3. stupanj: ploča s dijamantnim abr. česticama, 600 (~20μm)
4. stupanj: brusni papir kvalitete 1200, abr. čestice SiC
5. stupanj: brusni papir kvalitete 2400, abr. čestice SiC
6. stupanj: brusni papir kvalitete 4000, abr. čestice SiC.

Prije stavljanja ploča se prvo navlaži, zatim se uključi vrtnja i brusi dok se ne dobije željena ravnina. Nakon završene jedne faze brušenja, uzorak se ispire vodom uz mali dodatak deterdženta za posuđe i zatim brusi na isti način brusnom pločom finije granulacije.
Poslije brušenja slijedi poliranje.

Poliranje

Poliranje uzoraka Al_2O_3 keramike obavljeno je u tri stupnja:
1. stupanj - Podloga *DP-Mol*, lubrikant *Blue*, 5min, dijamantna pasta 6 μm
2. stupanj - Podloga *DP-Mol*, lubrikant *Blue*, 5min, dijamantna pasta 3 μm
3. stupanj-Podloga *OP-Chem*, lubrikant *Blue*, 5min, dijamantna pasta 1 μm.

Poslije svakog stupnja potrebno je uzorak dobro oprati.
Na poliranom uzorku određen je volumni udio pora. U svrhu određivanja veličine zrna aluminij oksidne keramike polirani uzorak je toplinski nagrižen na temperaturi od 1500 ^{o}C, u trajanju od 20 min, uz postepeno grijanje i hlađenje [1,2]. Optičkim mikroskopom, pretražnim elektronskim mikroskopom (SEM) te mikroskopom atomski sila (AFM) promatrana je i snimljena mikrostruktura. Prosječni promjer zrna aluminij oksidne keramike određena je metodom kruga, metodom crta, te analizom slike pomoću programa Analysis Materials Research Lab.

Nagrizanje

Nagrizanje površine uzorka slijedi nakon poliranja i provedenih mjerenja u poliranom stanju. Uzorak aluminij oksidne keramike nagrižen je toplinski zato što je toplinsko nagrizanje najjednostavnija, najčišća i najefikasnija metoda ocrtavanja granica zrna u mikrostrukturi keramike, posebice za jednofazne okside kao što je aluminij oksidna keramika [1,5-7]. Pri visokim temperaturama ravnina polirane površine je termodinamički nestabilna u području granica zrna, na visokim temperaturama tijekom toplinskog nagrizanja svako polirano zrno smanjuje svoju energiju (u području granica zrna) blagim zaobljavanjem difuzijom atoma sa granica zrna kreirajući reljefni kontrast između susjednih zrna.
Nakon toplinskog nagrizanja na uzorku se može odrediti oblik i veličina kristalnog zrna.

3. Rezultati i diskusija

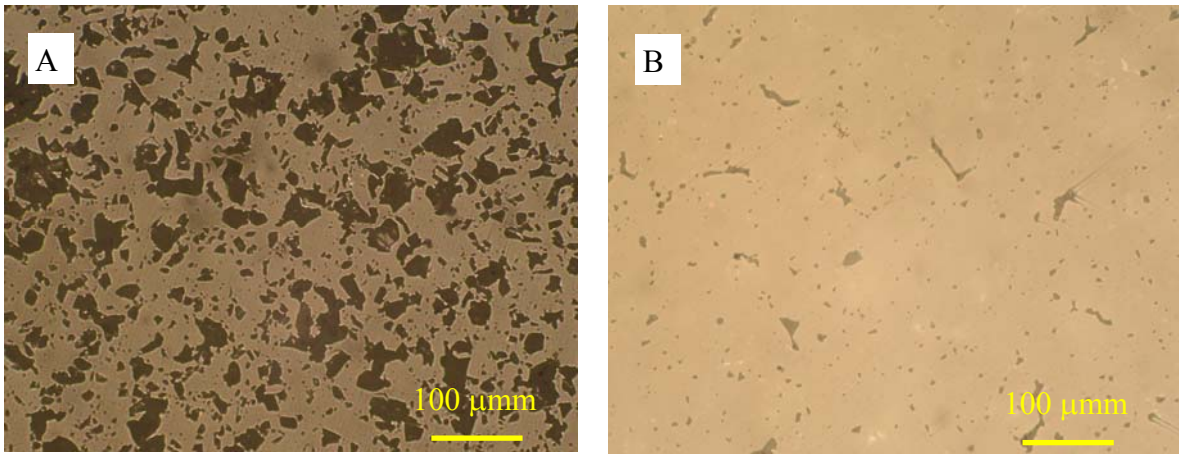
Rezultati kemijske analize aluminij oksidne keramike prikazani su u tablici 1.

Tablica 1. Kemijski sastav aluminij oksidne keramike.

uzorak	Maseni udio, %					
	MgO	Fe_2O_3	SiO_2	Na_2O	CaO	Al_2O_3
Al_2O_3 keramika	0,066	0,015	0,02	0,05	0,013	ostatak

Na temelju rezultata kemijske analize aluminij oksida (tablica 1) može se uočiti da je maseni udio Al_2O_3 99,8 %.

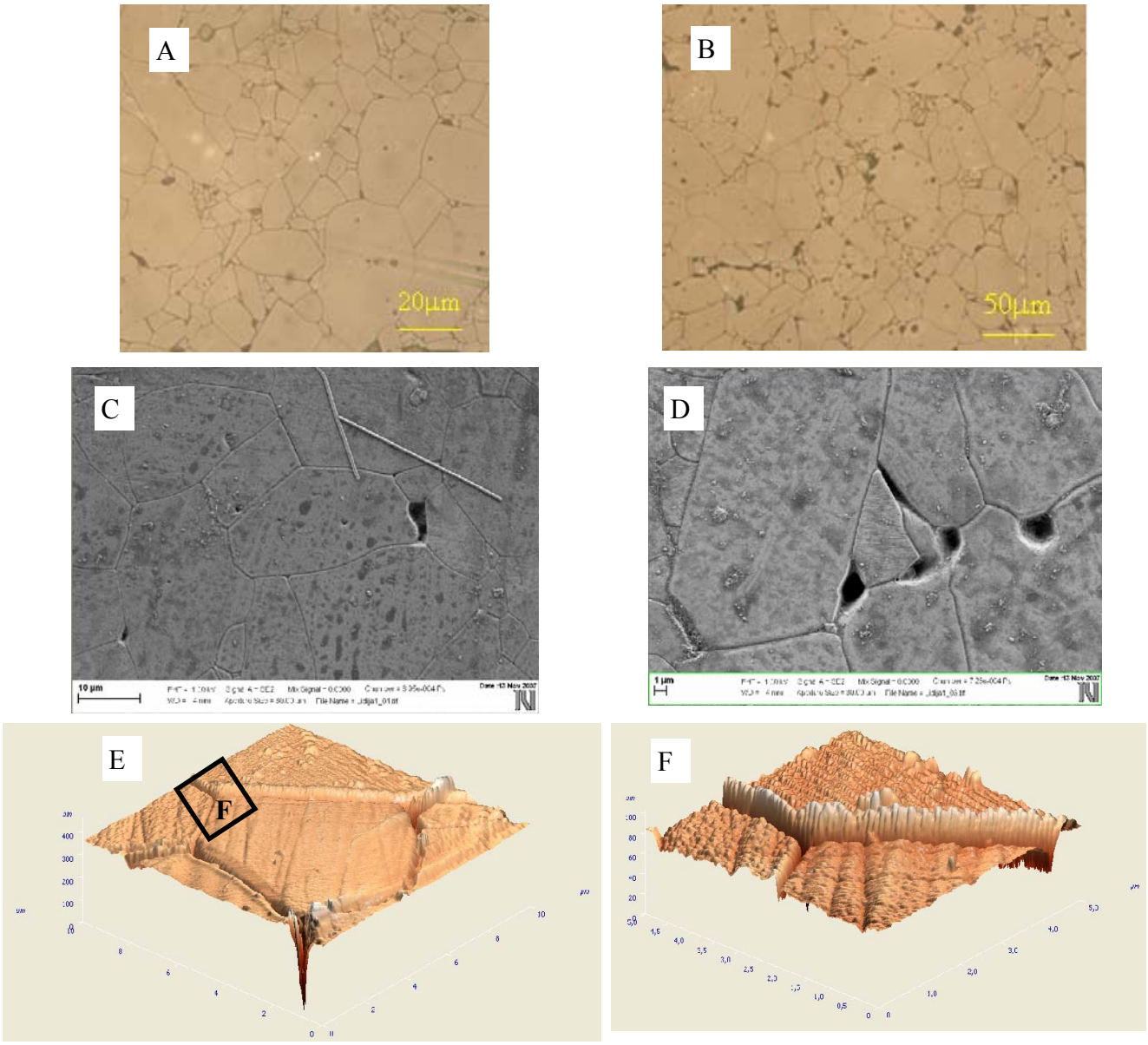
Na slici 2A prikazana je površina Al_2O_3 keramike nakon zadnjeg brušenja, a na slici 2B prikazana je polirana površina uzorka Al_2O_3 keramike. Na poliranoj površini uzorka mjeri se volumni udio pora i sekundarnih faza (ako su prisutne), mikrotvrdoća keramike i analiziraju se eventualno prisutne mikropukotine. Volumni udio pora Al_2O_3 keramike (slika 2B, pore su tamne točkice) iznosi između 1 i 2 %. Poroznost ukazuje na stupanj zgušnjavanja keramike nakon procesa sinteriranja. Prema praktičnom iskustvu, ako je poroznost ispod 8 % to ukazuje da su pore izolirane (nisu međusobno povezane), a ako je poroznost veća od 8 % tada su pore međusobno povezane [1].



Slika 2. Površina uzorka Al_2O_3 keramike nakon brušenja (A) i poliranja (B) [8].

Mikrostruktura uzorka Al_2O_3 keramike je promatrana i snimljena optičkim mikroskopom (slika 3A i 3B), pretražnim elektronskim mikroskopom (slika 3C i 3D), te mikroskopom atomski sila (slika 3E i 3F) uz različito povećanje. Na slikama su jasno vidljiva zrna i granice zrna Al_2O_3 keramike. Zrna su nepravilnog oblika i različite veličine. Na slici 3E kvadratićem i slovom E je označena je područje tromeđe (granica zrna gdje se sijeku tri zrna) koji je izdvojen i prikazan na slici 3F. Na slici 3E prikazana je skenirana površina AFM veličine 10 µm · 10 µm, a na slici 3F prikazana je skenirana površina AFM veličine 5 µm · 5 µm. Površinska hrapavost (Sa) mikrostrukture na slici 3E je 7,6 nm, a na slici 3F je 4 nn.

Nazubljena tekstura (slika 3E i 3F) aluminij oksidne keramike smatra se da je produkt dislokacija, kliznih ravnina ili nesavršenosti pod-zrna. Ova svojstva materijala nisu bila vidljiva tipičnom analizom veličine zrna pomoću optičkog mikroskopa i SEM tehnike. Ova svojstva su se mogla detektirati samo uporabom transmisijskog elektronskog mikroskopa (TEM). Primjenom mikroskopa atomskih sila karakteristike površine dimenzija od 0,1 nm do više od 10 μm mogu se kvantificirati sa točnim trodimenzijskim informacijama.



Slika 3. Mikrostruktura aluminij oksidne keramike promatrana optičkim mikroskopom (A i B), pretražnim elektronskim mikroskopom (C i D), te mikroskopom atomski sila (E i F) uz različito povećanje nakon toplinskog nagrizanja [3].

Prosječna veličina zrna metodom kruga

Na snimci mikrostrukture (slika 3B) nacrta se krug promjera 5 cm i odredi se površina kruga. Izbroje se zrna koja se cijelom svojom površinom nalaze unutar kruga (z = 41). Zatim se izbroje zrna koja su presječena kružnicom (n = 21) i pomnože Oertelovim faktorom 0,67. Ovo znači da se smatra da je 67 % zrna presječenih kružnicom unutar kruga. Pri poznatom povećanju (V = 250) izračunata je prosječna veličina zrna po sljedećoj jednadžbi:

$$F_m = \frac{F_K \cdot 10^6}{(0{,}67\ n + z) \cdot V^2}\ (\mu m^2) \qquad (1)$$

gdje je: F_K - površina kruga u mm^2, z - broj zrna koja se cijelom svojom površinom nalaze unutar kruga, n - broj zrna koja su presječena kružnicom i V – povećanje.

$$F_m = \frac{1962{,}5 \cdot 10^6}{(0{,}67 \cdot 21 + 41) \cdot 250^2} = 129{,}90\ \mu m^2 \qquad (2)$$

Iz prosječne površine zrna određen je promjer zrna d: $d_{zrna} = \sqrt{\frac{129{,}90 \cdot 4}{\pi}} = 12{,}86\ \mu m \qquad (3)$

Prosječna veličina zrna metodom crte

Kod metode crte na snimci mikrostrukture (slika 3B) je nacrtano pet paralelnih linija od kojih je svaka dužine L=70 mm. Zatim su izbrojena zrna koja svaka od linija potpuno presijeca, na to je dodano prvo zrno koje je dijelom presječeno a zadnje je izostavljeno (z = 54). Ako je p broj linija (p = 5), a V povećanje (V = 250), tada se srednji promjer zrna d dobije prema sljedećoj jednadžbi:

$$d = \frac{L \cdot p \cdot 10^3}{z \cdot V}\ (\mu m) \qquad (4)$$

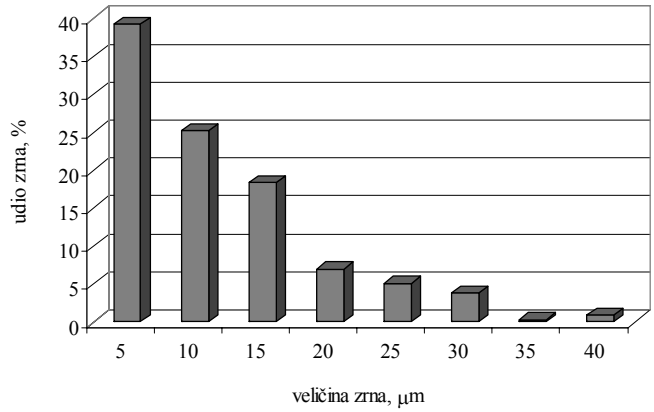
$$d = \frac{70 \cdot 5 \cdot 10^3}{54 \cdot 250} = 12{,}96\ \mu m \qquad (5)$$

Prosječna veličina zrna analizom slike

Prosječna veličina zrna analizom slike određena je pomoću programa Analysis Materials Research Lab. U tu svrhu određeni su sljedeći parametri:

- prosječna veličina zrna: 9,10 μm,
- minimalna veličina zrna: 0,62 μm,
- maksimalna veličina zrna: 40,57 μm,
- broj analiziranih zrna: 583.

Na slici 4 prikazan je histogram razdiobe veličine zrna Al_2O_3 keramike analizom mikrostrukture pomoću programa Analysis Materials Research Lab. Iz grafičkog prikaza možemo uočiti da je 39,3 % zrna sa promjerom zrna do 5 μm; 25,2 % zrna ima promjer između 5 i 10 mm, potom slijedi 18,4 % zrna sa promjerom između 10 i 15 μm, dok je najmanji udio (17,1 %) zrna promjera od 15 do 40 μm.



Slika 4. Razdioba veličine zrna aluminij oksidne keramike.

Izračunata vrijednost prosječne veličine zrna Al_2O_3 keramike metodom kruga je 12,86 μm, metodom crte je 12,96 μm i analizom slike pomoću programa Analysis Materials Research Lab je 9,10 μm. Postignuto je dobro slaganje rezultata prosječne veličine zrna metodom kruga i crte, nešto manja vrijednost je dobivena analizom slike. Rezultati dobiveni analizom slike su točniji jer je analiziran daleko veći broj zrna.

4. Zaključak

Osnovni uvjet za uspješnu analizu mikrostrukture keramike i ispravne rezultate je da analizirani uzorak bude reprezentativan i dobro pripremljen.

Na poliranom uzorku visoko čiste Al_2O_3 keramike oblikovane hladnim izostatičkim prešanjem volumni udio pora je između 1 i 2 %. Na toplinski nagriženom uzorku Al_2O_3 keramike prosječna veličina zrna metodom kruga je 12,86 μm, metodom crte je 12,96 μm, te analizom slike je 9,10 μm.

Zahvala

Prikazani rezultati proizašli su iz znanstvenog projekta „Istraživanje strukture i svojstava tehničke keramike i keramičkih prevlaka“, provođenog uz potporu Ministarstva znanosti, obrazovanja i športa Republike Hrvatske. Također zahvaljujemo se gosp. Mattu Darku Sertiću iz tvrtke Applied Ceramics, Inc., Kalifornija, USA koji je omogućio izradu ispitnih uzoraka.

5. Literatura

[1] R. E. Chinn, Ceramography Preparation and Analysis of Ceramic Microstructures, ASM International and the American Ceramic Society, 2002.

[2] H. Schumann, Metallographia, VEB Deutscher Verlag für Grundstoffindustrie, Leipzig, 1975.

[3] M. Fudurić Jelača, Mikrostruktura i svojstva aluminij oksidne keramike oblikovane izostatičkim prešanjem, Disertacija, Fakultet kemijskog inženjerstva i tehnologije, Sveučilište u Zagrebu, 2008.

[4] D. Galusek, Microstructure-property relationships in sintered alumina ceramics, Advances in Science and Technology, 45 (2006) 564-571.

[5] R. E. Chinn, Preparation of Microstructure of Alumina Ceramics, Structure, 33 (1998) 16-20.

[6] R.Z. Chen, W.H. Tuan, Thermal Etching of Alumina, Am. Ceram. Soc, Bull., 79 (10) (2000) 83-86.

[7] R. E. Chinn, Grain Sizes of Ceramics by Automatic Image Analysis, J. Am. Ceram. Soc., 77 (2) (1994) 589-592.

[8] V. Rede, Mikrostrukturna anliza keramike, 18. Savjetovanje o zaštiti materijala i industrijskom finišu, 2008, 131-137.

Strukturna i fizikalna homogenost blokova slitine EN AW-5083 proizvedenih postupkom izravnog hlađenja

Structural and Physical Homogeneity of Direct-Chill Cast Ingots of Aluminium Alloy EN AW-5083

Natalija Dolić, Ante Markotić, Faruk Unkić
Faculty of Metallurgy, University of Zagreb,

Aleja narodnih heroja 3
44 103 Sisak
Croatia

Izvorni znanstveni rad / Original scientific paper

Sažetak: U okviru ovog rada pokušala se, s aspekta fizikalnih i mikrostrukturnih svojstava ustanoviti homogenost blokova aluminijske slitine EN AW-5083 lijevanih polukontinuiranim, vertikalnim postupkom izravnog hlađenja (Direct Chill).

U eksperimentalnom dijelu ovog rada provedena su ispitivanja elektrovodljivosti i mjerenja veličine tj. broja zrna na odgovarajućim mjestima unutar poprečno izrezane ploče debljine oko 30 mm, s početka i kraja izlivenih blokova. Polazna osnovica za ocjenu homogenosti je statistički plan pokusa („latinski kvadrat“).

Statističkom obradom rezultata ustanovljeno je da se kao najznačajniji izvor varijabilnosti smatra *šarža*, dok *visina šajbe*, odnosno *debljina bloka*, pokazuje mnogo veći utjecaj od *širine šajbe*.

Ključne riječi: aluminijska slitina EN AW-5083, strukturna homogenost, veličina zrna, elektovodljivost, DC postupak

Abstract: In this thesis, the homogeneity of aluminum alloy EN AW-5083 slabs cast with the semi-continuous, vertical direct water cooling process (Direct Chill Process) has been established from the physical and microstructural aspects.

In the experimental part of his work examinations of electrical conductivity and the grain size i.e. the grain numbers on specified places within the cross sectioned 30 mm thick plate on the beginning and the end of the cast slabs were performed. The base for the homogeneity estimation was statistical examination plan (“latin square”).

By statistical processing of obtained results it has been established that the *charge* is a most significant variability source, while variability source the *slice height*, i.e. the *ingot thickness* shown the bigger influence than the *slice wideness*.

Key words: Aluminium Alloy EN AW-5083, Structural Homogeneity, Grain Size, Electrical Conductivity, Direct Chill Process

1. UVOD

Nove specijalne i precizne primjene, neprekidno tjeraju sve sudionike proizvodnog lanca na sve strože zahtjeve u pogledu kvalitete materijala, tj. njegove visoke homogenosti kemijskog sastava i strukture, uska geometrijska odstupanja, kao i njihova fizikalna, mehanička i tehnološka svojstava, koja se ocjenjuju i prihvaćaju tek nakon što su zadovoljili najstrože kriterije suvremenih metoda ispitivanja i statističkih obrada rezultata tih ispitivanja.

Homogena struktura i istoosna struktura zrna pridonose poboljšanju mnogih svojstava lijevanog metala, povećanoj sposobnosti toplinske obrade i oblikovanja tijekom kasnije prerade valjanjem ili istiskivanjem [1, 2]. Struktura zrna (srednja veličina zrna, njihova raspodjela i morfologija) ima veliki utjecaj na smanjenje nastanka površinskih grešaka, npr. vruće i hladne pukotine u rubnoj zoni blokova [3]. Polukontinuirani vertikalni postupak lijevanja izravnim hlađenjem (Direct Chill) ima veliki značaj pri proizvodnji komercijalnih aluminijskih slitina, posebno u proizvodnji blokova velikih dimenzija iz kojih se naknadnim termomehaničkim postupcima dolazi do konačnih proizvoda (valjane ploče, limovi, folije, cijevi, šipke, gredice, žica [4].

Slitina EN AW-5083, kemijskog simbola AlMg4,5Mn0,7 je teško gnječiva, toplinski neočvrstiva slitina aluminija s magnezijem koja se odlikuje visokim mehaničkim svojstvima, odličnom otpornošću na koroziju, čak i u slanoj vodi, visokom žilavošću, dobrom zavarljivošću različitim tehnikama. Aluminijske slitine serije 5xxx nalaze široku primjenu u proizvodnji traka i ploča, konstrukcijama cesta, uključujući mostove, automobilskoj industriji, brodogradnji, rezervoarima za skladištenje i posudama pod tlakom itd.

2. EKSPERIMENTALNI DIO

Metodologija ispitivanja

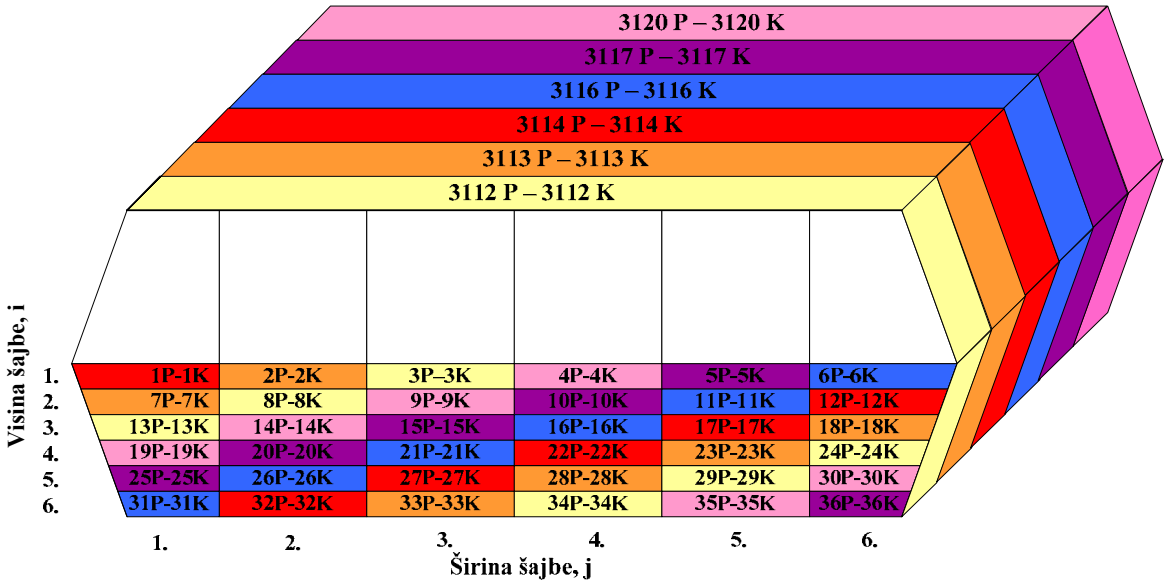
U okviru ovog rada ispitivana je strukturna i fizikalna homogenost 6 blokova lijevanih polukontinuiranim vertikalnim postupkom izravnog hlađenja (**D**irect **C**hill), proizvedenih iz 6 različitih šarži aluminijske slitine EN AW-5083 (oznaka 3112, 3113, 3114, 3116, 3117, 3120). Kemijski sastav ispitivanih šarži dan je u tablici.1.

Tablica 1. Kemijski sastav ispitivanih šarži slitine EN AW-5083

Oznaka šarže	Kemijski sastav [%]									
	Cu	**Mn**	**Mg**	**Si**	**Fe**	**Cr**	**Zn**	**Ti**	**Be**	**Na**
3112	0,01	0,465	4,355	0,14	0,415	0,105	0,0070	0,0250	nema podatka	0,00120
3113	0,01	0,450	4,065	0,11	0,355	0,085	0,0050	0,0240	0,00380	0,00020
3114	0,01	0,440	4,285	0,14	0,375	0,090	0,0070	0,0245	0,00465	0,00065
3116	0,01	0,425	4,560	0,14	0,380	0,110	0,0060	0,0205	0,00565	0,00120
3117	0,01	0,470	4,310	0,16	0,370	0,110	0,0070	0,0240	0,00370	0,00125
3120	0,01	0,440	4,280	0,14	0,360	0,100	0,0045	0,0230	0,00425	0,00020

Iz svake od 6 šarži izlivena su po dva bloka dimenzija 520 x 1430 x 5100 mm, a ispitivanja su provedena na jednom bloku od svake šarže. Sa svakog ispitivanog bloka odrezana je po jedna ploča debljine 30 mm (šajba) s njegovog početka i kraja, s koje su

uzimani uzorci prema statističkom planu pokusa „latinski kvadrat“ prema shemi na slici 1 [5]. Kao glavni mogući izvor varijabilnosti i strukturne nehomogenosti ispitivanih blokova, a time i fizikalnih i ostalih svojstava, smatra se da bi mogle biti pojedine *„šarže“* lijevanja. Uz *„šaržu“* pretpostavlja se da bi i osnovne dimenzije odlivenog bloka, tj. šajbe mogle biti izvorom neželjenih varijabilnosti, pa se i *„visina šajbe“* (*debljina bloka*) - *i*, te *„širina šajbe“* (*širina bloka*) - *j* uzimaju kao još dva moguća izvora varijabilnosti.



Slika 1. Prikaz principa uzimanja uzoraka sa šajbi po planu pokusa „latinski kvadrat“

Ispitivanja homogenosti provedena su na donjim polovicama šajbi jer se smatra da su obzirom na zrcalnu simetriju uvjeti hlađenja i skrućivanja gornje i donje polovice šajbi jednaki. Segmenti predstavljaju stupce u shemi „latinskog kvadrata“ (*„širina šajbe“, j = 1 - 6*), a da bi se dobili redovi u shemi (*„visina šajbe“, i = 1 - 6*) svaki ispitivani segment je po visini prerezan na 6 jednakih dijelova (isječaka) iz kojih su uzimani uzorci za metalografska ispitivanja i ispitivanja elektrovodljivosti. Uzorci uzeti iz šajbi rezanih sa početka blokova nose uz broj uzorka i oznaku P, a oni sa kraja oznaku K. Način uzimanja uzoraka je isti za šajbe uzete sa početka i sa kraja bloka.

Sa svakog isječka uziman je po jedan uzorak za mikrostrukturna ispitivanja. Radi otkrivanja granica zrna uzorci su nagrizani elektrolitički u Barker-ovom reagensu [6, 7]. Metalografska ispitivanja uzoraka provedena su na svjetlosnom mikroskopu sa digitalnom kamerom i sustavom za automatsku obradu slike („AnalySIS Materials Research Lab“), uz povećanje od 100X. Za određivanje prosječne veličine zrna ispitivanih uzoraka upotrijebljena je poluautomatska metoda mjerenja veličine zrna mjerenjem duljine presijecanja zrna (intercept procedura) [8, 9, 10].

Ispitivanje elektrovodljivosti svih uzoraka provedeno je na izrezanoj tankoj pločici (debljine 5 mm), dimenzija 30 x 30 mm na uređaju za mjerenje elektrovodljivosti Hocking, Auto Sigma 3000DL. Na svim uzorcima su provedena po dva mjerenja, te je uzimana njihova srednja vrijednost.

Za statističku obradu rezultata upotrijebljena je analiza varijance i korelacijska analiza (programski paket StatSoft® STATISTICA 7.1.).

3. REZULTATI I STATISTIČKA ANALIZA REZULTATA ISTRAŽIVANJA

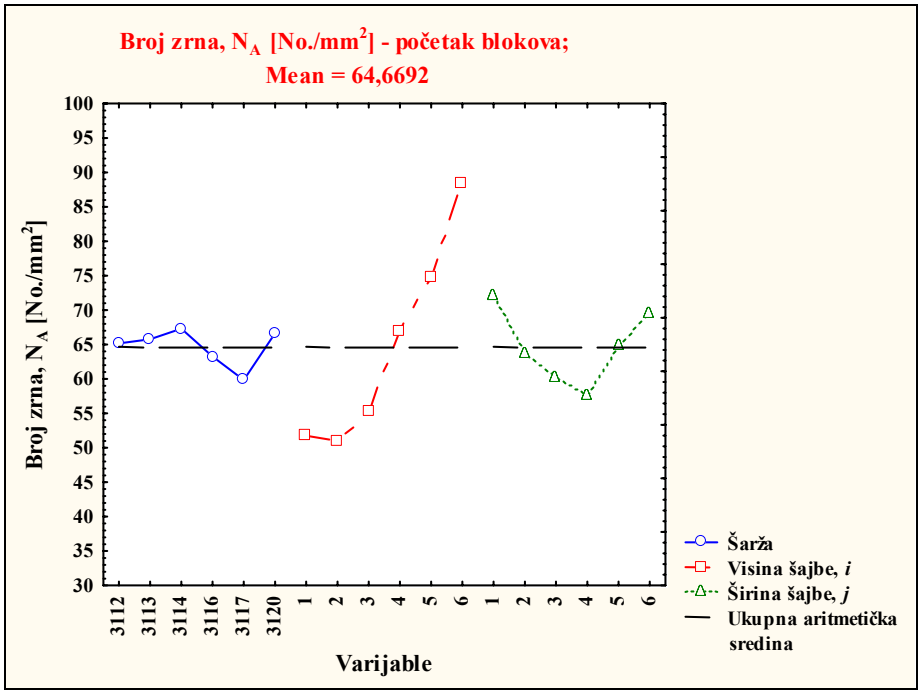
3.1. Strukturna analiza ispitivanih blokova (šarži)

Rezultati određivanja veličine, odnosno broja zrna poluautomatskom metodom mjerenja veličine zrna metodom mjerenja duljine presijecanja zrna, dani su u tablici 2., gdje $\bar{l}$ predstavlja (srednju) duljinu presijecanja iz koje se linearnom aproksimacijom [8] izračuna srednji broj zrna po jedinici ispitivane površine, $\overline{N_A}$ [No./mm^2] ili G-broj. Iz dobivene mikrostrukturne analize uočavaju se znatne razlike u veličini zrna ovisno o visini šajbe, odnosno o debljini bloka, premda su po morfologiji na sve tri pozicije zrna istoosna [11].

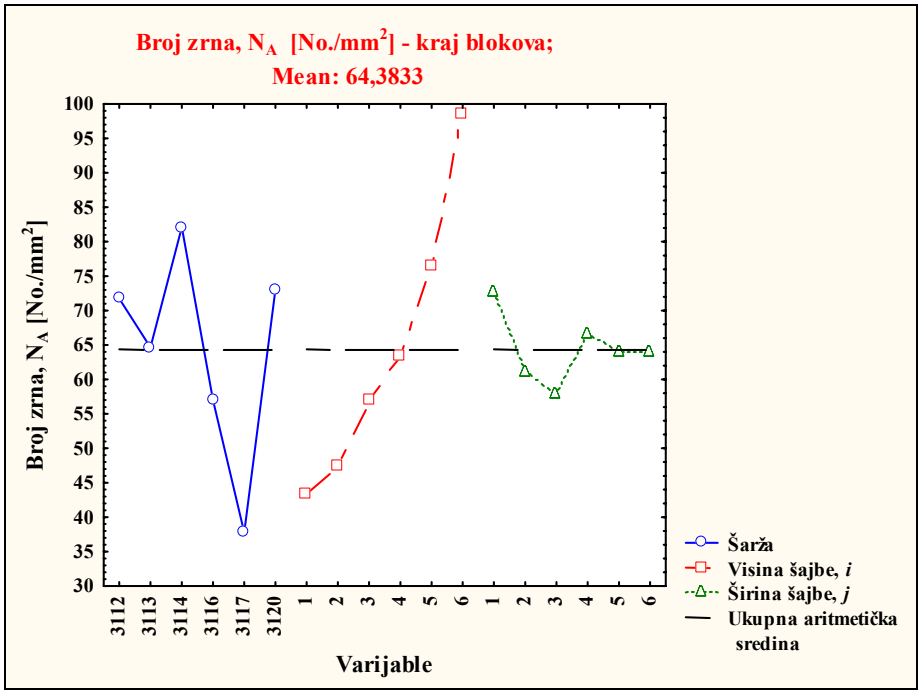
Tablica 2. Rezultati mjerenja broja zrna dobiveni poluautomatskom metodom mjerenja duljine presjeka zrna na uzorcima nagriženim Barker-ovim reagensom

Oznaka uzorka	$\bar{l}$ [μm]	Broj presjeka	G-broj	$\overline{N_A}$ [No./mm^2]	Oznaka uzorka	$\bar{l}$ [μm]	Broj presjeka	G-broj	$\overline{N_A}$ [No./mm^2]
1P	107,55	517	3,15	69,92	**1K**	96,90	496	3,45	85,11
2P	132,71	501	2,54	45,36	**2K**	170,63	530	1,82	27,81
3P	123,67	493	2,75	53,03	**3K**	173,09	499	1,78	27,04
4P	146,51	506	2,26	37,79	**4K**	123,13	509	2,77	53,49
5P	136,43	496	2,46	42,87	**5K**	222,96	528	1,05	16,10
6P	113,66	498	2,99	61,52	**6K**	126,39	519	2,69	50,72
7P	106,98	524	3,17	70,73	**7K**	107,99	501	3,14	69,29
8P	130,45	509	2,59	47,28	**8K**	136,25	504	2,47	42,96
9P	137,40	513	2,44	42,38	**9K**	121,64	523	2,80	54,75
10P	135,13	500	2,49	43,52	**10K**	193,58	540	1,45	21,34
11P	126,49	504	2,69	50,64	**11K**	137,62	493	2,44	42,27
12P	125,24	502	2,72	51,70	**12K**	122,74	519	2,77	53,82
13P	112,09	538	3,03	63,44	**13K**	104,55	510	3,24	74,20
14P	132,25	504	2,55	45,75	**14K**	109,48	519	3,10	67,16
15P	129,35	514	2,62	48,21	**15K**	168,65	535	1,86	28,41
16P	125,10	506	2,72	51,82	**16K**	123,19	506	2,76	53,44
17P	123,52	523	2,76	53,16	**17K**	116,49	526	2,92	59,12
18P	108,29	530	3,13	68,86	**18K**	114,91	503	2,96	60,46
19P	97,04	531	3,45	84,91	**19K**	104,40	498	3,24	74,41
20P	105,01	513	3,22	73,48	**20K**	135,37	503	2,48	43,40
21P	116,44	512	2,92	59,17	**21K**	120,00	508	2,84	56,14
22P	113,81	519	2,98	61,40	**22K**	109,79	501	3,09	66,72
23P	121,02	505	2,81	55,28	**23K**	107,95	506	3,14	69,31
24P	109,01	524	3,11	67,84	**24K**	107,79	514	3,15	69,58
25P	111,45	531	3,05	64,35	**25K**	126,58	522	2,69	50,56
26P	102,13	500	3,30	77,65	**26K**	116,85	504	2,90	57,12
27P	104,26	504	3,25	74,61	**27K**	90,25	496	3,66	99,35
28P	106,61	506	3,18	71,26	**28K**	100,83	513	3,34	79,51
29P	100,89	501	3,34	79,42	**29K**	93,80	505	3,54	90,81
30P	100,18	499	3,36	80,43	**30K**	98,90	529	3,39	82,26
31P	101,36	501	3,33	78,75	**31K**	98,99	501	3,39	82,13
32P	92,83	523	3,58	93,14	**32K**	78,89	510	4,04	128,49
33P	98,28	493	3,41	83,14	**33K**	99,37	516	3,38	81,59
34P	100,46	561	3,35	80,03	**34K**	79,54	503	4,02	125,86
35P	86,36	510	3,79	108,70	**35K**	87,35	516	3,76	106,32
36P	95,89	518	3,48	86,55	**36K**	109,77	510	3,09	66,75

Statističkom obradom dobivenih rezultata dobiju se grafički prikazi utjecaja pojedinih varijabli („*šarža*“, „*visina šajbe*“ i „*širina šajbe*“) na broj zrna slitine EN AW-5083, slike 2. i 3.



Slika 2. Grafički prikaz utjecaja pojedinih varijabli po nivoima za broj zrna, N_A - početak blokova



Slika 3. Grafički prikaz utjecaja pojedinih varijabli po nivoima za broj zrna, N_A - kraj blokova

Može se uočiti da utjecaj *„šarži“* za početak bloka ne pokazuje velike varijacije u odnosu na ukupnu aritmetičku sredinu (64,6692 No./mm^2), za razliku od kraja bloka gdje je njezin utjecaj značajan tj. dosta su velika odstupanja od ukupne aritmetičke sredine u oba smjera (64,3833 No./mm^2). Utjecaj *„visine šajbe“* pokazuje vrlo izraženu zakonitost po razinama. Od sredine šajbe (*i=1*) raste broj zrna prema rubu (*i=6*), što govori o značajnom utjecaju intenziteta hlađenja bloka na raspodjelu broja zrna po visini šajbe, odnosno po debljini bloka. I u primjeru utjecaja *„širine šajbe“* uočeno je da broj zrna raste od sredine prema rubovima (i za početak i za kraj blokova). Razlike broja zrna po *„visini šajbe“* su mnogo veće nego po *„širini šajbe“* što ukazuje na veći intenzitet odvođenja topline po debljini bloka nego po širini [11].

Iz tablice analize varijance za broj zrna, N_A - početak blokova, tablica 3., uočava se izrazita značajnost razlika po *„visini šajbe“* (p = 0,000008), dok izvori varijabilnosti *„šarža“* i *„širina šajbe“* nisu značajni. Pregledom tablice 4. analize varijance za broj zrna, N_A - kraj blokova, uočava se izrazita značajnost razlika između *„šarži“* i po *„visini šajbe“*, dok izvor varijabilnosti *„širina šajbe“* nije značajan.

Tablica 3. Analiza varijance latinskog kvadrata za broj zrna, N_A - početak blokova

Broj zrna N_A [No./mm^2] - početak blokova; Mean = 64,6692					
Varijable	Suma kvadrata odstupanja, SS	Stupnjevi slobode, n-1	Srednji kvadrat odstupanja, s^2	Frač	Pogreška 1. vrste
„Šarža“	227,261	5	45,452	0,46125	0,800305
„Visina šajbe“	*6654,903*	*5*	*1330,981*	*13,50690*	*0,000008*
„Širina šajbe“	891,004	5	178,201	1,80840	0,156944
Ostatak	1970,816	20	98,541		

Tablica 4. Analiza varijance latinskog kvadrata za broj zrna, N_A - kraj blokova

Broj zrna N_A [No./mm^2] - kraj blokova; Mean = 64,3833					
Varijable	Suma kvadrata odstupanja, SS	Stupnjevi slobode, n-1	Srednji kvadrat odstupanja, s^2	Frač	Pogreška 1. vrste
„Šarža“	*7243,76*	*5*	*1448,751*	*8,42068*	*0,000203*
„Visina šajbe“	*12588,90*	*5*	*2517,780*	*14,63427*	*0,000004*
„Širina šajbe“	758,06	5	151,613	0,88123	0,511561
Ostatak	3440,94	20	172,047		

Promatrajući raspodjelu broja zrna pojedinačno po šaržama unutar svake šajbe, uočava se gotovo identična srednja vrijednost broja zrna skoro za sve šarže i relativno mala odstupanja srednje vrijednosti između početka i kraja blokova. S druge strane varijacije broja zrna obzirom na poziciju unutar šajbe značajno variraju, u rasponu od oko 20 - 50 % [11]. Navedena varijacija broja zrna unutar šajbi rezultat je intenzivnog hlađenja pri rubu blokova što osigurava veći iznos pothlađenja i manje zrno, za razliku od njihove sredine gdje pod djelovanjem negativnih temperaturnih gradijenata i konstitucijskog pothlađenja nukleiraju i rastu istoosna zrna nešto većih dimenzija. Premda je cijepljenjem taline potisnuto stvaranje transkristalizacijske zone stubičastih kristala [12], nije moguće unutar cijelog presjeka jednog bloka dobiti istoosne kristale približno jednakih dimenzija. Nameće se zaključak da postignuta srednja vrijednost broja zrna i postignuta odstupanja izražena preko koeficijenata varijacije zadovoljavaju uvjete daljnje prerade blokova.

U tablici 5. prikazani su koeficijenti korelacije za broj zrna, $r_{š}$ (N_A), između šajbi s početka i kraja ispitivanih blokova za svaku pojedinačnu šaržu. Visoki koeficijenti korelacije za gotovo sve šarže ukazuju na visoku strukturnu homogenost ispitivanih blokova lijevanih DC postupkom.

Tablica 5. Koeficijenti korelacije za broj zrna, $r_{š}$ (N_A), između šajbi uzetih s početka i kraja ispitivanih blokova za svaku pojedinačnu šaržu

Šarža	3112	3113	3114	3116	3117	3120
$r_{š}$ (N_A)	0,90	0,83	0,99	0,77	0,95	0,94

T-testom dobiven je ukupni koeficijent korelacije za broj zrna za sve šarže, r (N_A) = 0,76, između početaka i krajeva blokova iz kojeg je vidljivo da je primijenjena tehnologija lijevanja i obrada taline cijepljenjem pruža zadovoljavajuću strukturnu homogenost blokova u cjelini.

3.2. Rezultati ispitivanja elektrovodljivosti

U tablicama 6. i 7. prikazani su rezultati mjerenja elektrovodljivosti, E za uzorke uzete s početka i kraja lijevanih blokova Al-slitine EN AW-5083. Na osnovu dva mjerenja elektrovodljivosti zapaža se da su na istom uzorku dobivene približno jednake vrijednosti elektrovodljivosti.

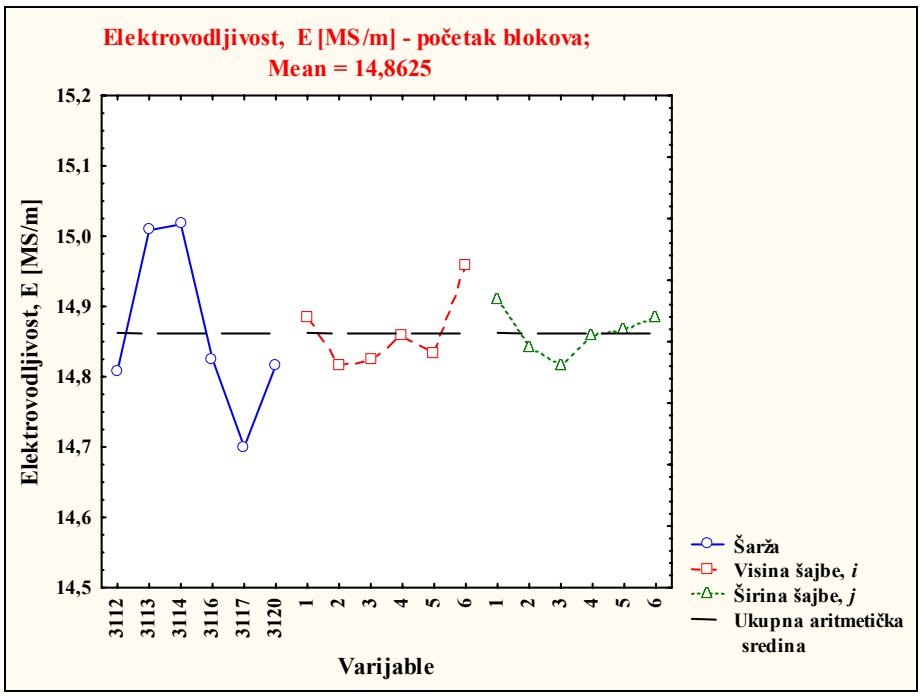
Tablica 6. Rezultati ispitivanja elektrovodljivosti za uzorke uzete s početka blokova

Oznaka uzorka	**Elektrovodljivost [MS/m]**			**Oznaka uzorka**	**Elektrovodljivost [MS/m]**		
	1. mjerenje	**2. mjerenje**	$\overline{E}$		**1. mjerenje**	**2. mjerenje**	$\overline{E}$
1P	15,00	15,00	15,00	**19P**	14,90	14,80	14,85
2P	15,00	15,00	15,00	**20P**	14,70	14,70	14,70
3P	14,90	14,90	14,90	**21P**	14,80	14,80	14,80
4P	14,90	14,90	14,90	**22P**	15,00	15,00	15,00
5P	14,70	14,70	14,70	**23P**	15,00	15,00	15,00
6P	14,80	14,80	14,80	**24P**	14,80	14,80	14,80
7P	15,00	15,00	15,00	**25P**	14,80	14,80	14,80
8P	14,80	14,70	14,75	**26P**	14,70	14,70	14,70
9P	14,60	14,70	14,65	**27P**	14,90	14,90	14,90
10P	14,60	14,60	14,60	**28P**	15,00	15,00	15,00
11P	14,80	14,80	14,80	**29P**	14,80	14,80	14,80
12P	15,10	15,10	15,10	**30P**	14,80	14,80	14,80
13P	14,70	14,80	14,75	**31P**	15,10	15,00	15,05
14P	14,80	14,80	14,80	**32P**	15,10	15,10	15,10
15P	14,60	14,60	14,60	**33P**	15,00	15,10	15,05
16P	14,80	14,80	14,80	**34P**	14,80	14,90	14,85
17P	15,00	15,00	15,00	**35P**	14,90	14,90	14,90
18P	15,00	15,00	15,00	**36P**	14,80	14,80	14,80

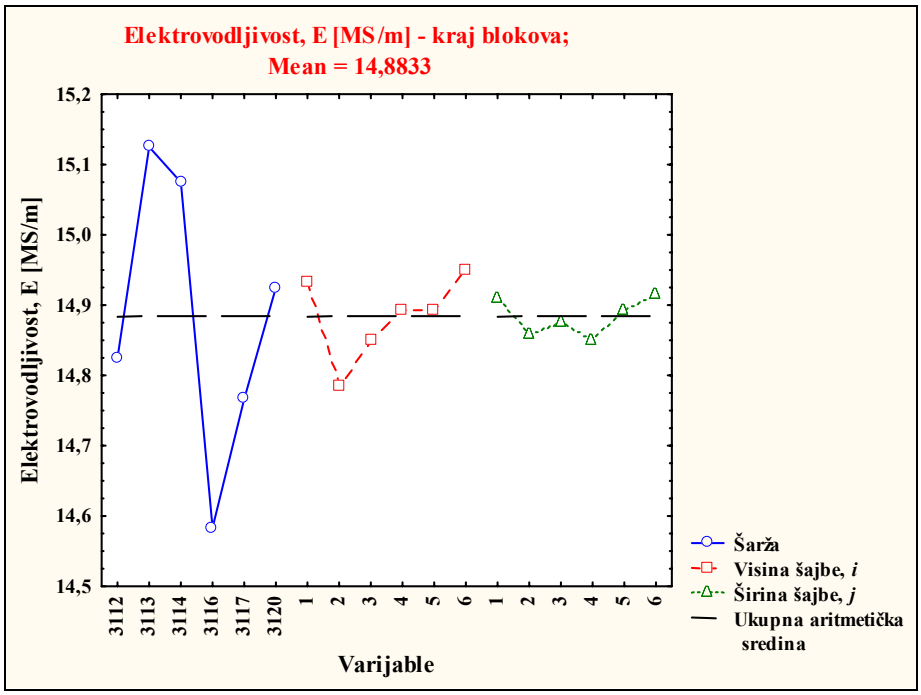
Tablica 7. Rezultati ispitivanja elektrovodljivosti za uzorke uzete s kraja blokova

Oznaka uzorka	Elektrovodljivost [MS/m]			Oznaka uzorka	Elektrovodljivost [MS/m]		
	1. mjerenje	2. mjerenje	$\overline{E}$		1. mjerenje	2. mjerenje	$\overline{E}$
1K	15,00	15,00	15,00	**19K**	14,90	14,90	14,90
2K	15,20	15,20	15,20	**20K**	14,80	14,80	14,80
3K	14,80	14,80	14,80	**21K**	14,60	14,60	14,60
4K	15,00	15,00	15,00	**22K**	15,10	15,10	15,10
5K	14,90	14,90	14,90	**23K**	15,10	15,10	15,10
6K	14,70	14,70	14,70	**24K**	14,80	14,90	14,85
7K	15,10	15,10	15,10	**25K**	14,90	14,80	14,85
8K	14,60	14,60	14,60	**26K**	14,50	14,50	14,50
9K	14,90	14,90	14,90	**27K**	15,10	15,10	15,10
10K	14,40	14,60	14,50	**28K**	15,10	15,10	15,10
11K	14,50	14,50	14,50	**29K**	14,90	14,90	14,90
12K	15,10	15,10	15,10	**30K**	14,90	14,90	14,90
13K	14,90	14,90	14,90	**31K**	14,70	14,70	14,70
14K	14,90	14,90	14,90	**32K**	15,10	15,20	15,15
15K	14,70	14,70	14,70	**33K**	15,10	15,20	15,15
16K	14,50	14,50	14,50	**34K**	14,90	14,90	14,90
17K	15,00	15,00	15,00	**35K**	15,00	14,90	14,95
18K	15,10	15,10	15,10	**36K**	14,90	14,80	14,85

Na slikama 4. i 5. dan je grafički prikaz utjecaja pojedinih varijabli po nivoima za elektrovodljivost, E za početak i kraj ispitivanih blokova koji pokazuju vrlo slične činjenice.



Slika 4. Grafički prikaz utjecaja pojedinih varijabli po nivoima za elektrovodljivost, E - početak blokova



Slika 5. Grafički prikaz utjecaja pojedinih varijabli po nivoima za elektrovodljivost, E - kraj blokova

Utjecaj *„šarži“* pokazuje velike varijacije, i to u oba smjera u odnosu na ukupnu aritmetičku sredinu i za početak i za kraj blokova, dok utjecaj *„visine šajbe“* i *„širine šajbe“* pokazuje vrlo sličnu zakonitost i za početak i za kraj blokova.

U tablicama analize varijance za elektrovodljivost, E - početak i kraj blokova (tablice 8. i 9.) uočava se izrazita značajnost razlika među *„šaržama“* uz gotovo siguran zaključak, odnosno vjerojatnost pogreške prve vrste jednaka je nuli (p = 0,000000). Izvor varijabilnosti *„visina šajbe“* također je vrlo značajan (uz p = 0,011802 za početak i p = 0,023625 za kraj blokova), dok treći izvor varijabilnosti *„širina šajbe“* nije značajan.

Srednje vrijednosti ispitivanih šarži elektrovodljivosti za početke i krajeve blokova su gotovo identične (14,8625 MS/m i 14,8833 MS/m). Iz dobivenih rezultata vidljivo je da varijabilnost elektrovodljivosti potiče od pojedine *„šarže“*. Utjecaj *„visine šajbe“* također je značajan. Kako je elektrovodljivost posljedica kemijskog sastava i postignute mikrostrukture bilo je za pretpostaviti da će ona slijediti te promjene. Treba primijetiti da su odstupanja od srednje vrijednosti elektrovodljivosti relativno mala što ukazuje na osjetljivost metode i na njenu primjenjivost u analizi homogenosti Al-blokova lijevanih DC postupkom.

Tablica 8. Analiza varijance latinskog kvadrata za elektrovodljivost, E - početak blokova

Elektrovodljivost, E [MS/m] - početak blokova; Mean = 14,8625					
Varijable	Suma kvadrata odstupanja, SS	Stupnjevi slobode, n-1	Srednji kvadrat odstupanja, s^2	Frač	Pogreška 1. vrste
„Šarža“	*0,467292*	*5*	*0,093458*	*21,99020*	*0,000000*
„Visina šajbe“	*0,083958*	*5*	*0,016792*	*3,95098*	*0,011802*
„Širina šajbe“	0,030625	5	0,006125	1,44118	0,252859
Ostatak	0,085000	20	0,004250		

Tablica 9. Analiza varijance latinskog kvadrata za elektrovodljivost, E - kraj blokova

Elektrovodljivost, E [MS/m] - kraj blokova; Mean = 14,8833					
Varijable	Suma kvadrata odstupanja, SS	Stupnjevi slobode, n-1	Srednji kvadrat odstupanja, s^2	Frač	Pogreška 1. vrste
„Šarža“	*1,223333*	*5*	*0,244667*	*37,40128*	*0,000000*
„Visina šajbe“	*0,109167*	*5*	*0,021833*	*3,33758*	*0,023625*
„Širina šajbe“	0,021667	5	0,004333	0,66242	0,656064
Ostatak	0,130833	20	0,006542		

Prema dobivenom ukupnom koeficijentu korelacije za elektrovodljivost, *r (E) = 0,70*, između početaka i krajeva blokova utvrđena je njihova zavisnost što ukazuje na statističku ukupnu homogenost blokova s aspekta elektrovodljivosti.

Neovisno o činjenici da su ispitani uzorci u primarnom ili lijevanom stanju dobiveni su relativno niski koeficijenti varijacije unutar šajbi za odgovarajuće šarže. Ti koeficijenti varijacije kreću se od 0,28 - 1,00 %. Kako je za pretpostaviti da će se homogenizacijom strukture povećati elektrovodljivost i smanjiti koeficijent varijacije, može se reći da se s aspekta elektrovodljivosti ispitanih šarži dobio odgovarajuće homogen materijal.

U tablici 10. prikazani su koeficijenti korelacije, $r_š$ *(E)*, za elektrovodljivost, E, između šajbi s početka i kraja ispitivanih blokova za svaku pojedinačnu šaržu.

Tablica 10. Koeficijenti korelacije za elektrovodljivost, $r_š$ (E), između šajbi uzetih s početka i kraja ispitivanih blokova za svaku pojedinačnu šaržu

Šarža	3112	3113	3114	3116	3117	3120
$r_š$ *(E)*	0,26	0,29	0,33	0,65	0,76	0,64

Obzirom na dobivene koeficijente korelacije za elektrovodljivost, $r_š$ *(E)*, između početka i kraja ispitanih blokova za pojedinu šaržu vidljivo je da ne postoji statistički signifikantna zavisnost između ovih varijabli. Treba također istaknuti da pretpostavljene promjene elektrovodljivosti s veličinom zrna tj. po visini, odnosno širini bloka nisu statistički potvrđene. Iz dobivenih rezultata proizlazi da se mjerenjem elektrovodljivosti ne može statistički potvrditi ovisnost elektrovodljivosti o strukturi zrna i raspodjeli izlučenih faza, odnosno općenito o mikrostrukturi, što bi sa aspekta ispitivanja bilo vrlo značajno. Može se pretpostaviti da odlučujući utjecaj na elektrovodljivost slitine EN AW-5083 u lijevanom stanju ima kemijski sastav, odnosno legirajući elementi, a da će utjecaj strukture doći više do izražaja nakon provedene homogenizacije.

4. ZAKLJUČAK

Iz rezultata ispitivanja elektrovodljivosti, te veličine i raspodjele zrna na blokovima slitine Al-Mg oznake EN AW-5083 lijevanim vertikalnim DC postupkom utvrđeno je:

1. S aspekta cijepljenja i razvoja mikrostrukture potrebno je istaći da je dobivena uglavnom jednolika sitnozrnata struktura bez izražene zone stubičastih kristala. Ova

struktura garantira i jednoliku raspodjelu izlučenih faza, kraća vremena homogenizacije i sposobnost daljnje plastične prerade.

2. Dobivene aritmetičke sredine za broj zrna za početak i kraj blokova (64,6692 i 64,3833 No./mm^2) predstavljaju relativno visoke vrijednosti broja zrna obzirom na dimenzije, što ukazuje na djelotvoran način cijepljenja taljevine i primjeren način vođenja procesa lijevanja i hlađenja.
3. Utjecaji *„visina šarže“* i *„širina šarže“* za broj zrna pokazuju vrlo izraženu zakonitost po razinama i za početak i za kraj blokova, tj. dolazi do porasta broja zrna od sredine prema rubovima šajbi. Ovo je posljedica većeg intenziteta odvođenja topline sa rubnog područja šajbi, odnosno bloka i s tim povezanog većeg pothlađenja koje predstavlja pokretačku silu skrućivanja.
4. Dobivena vrijednost koeficijenta korelacije $r\ (N_A) = 0{,}76$ upućuje na relativno visoko podudaranje broja i raspodjele zrna na početku i kraju bloka, što govori o relativno visokoj strukturnoj homogenosti blokova u cjelini, odnosno adekvatno primijenjenoj tehnologiji rafinacije i lijevanja, te učinkovitom cijepljenju taljevine.
5. Iz dobivenih rezultata elektrovodljivosti statističkom analizom uočava se veliki utjecaj *„šarže“* i *„visine šajbe“*, bez posebne povezanosti s promjenom mikrostrukture.
6. Gotovo identične srednje vrijednosti elektrovodljivosti ispitivanih šarži za početak i kraj blokova (14,8625 i 14,8833 MS/m), te relativno visok ukupni koeficijent korelacije $r\ (E) = 0{,}70$ za elektrovodljivost između početaka i krajeva blokova ukazuju na zadovoljavajuću ukupnu statističku homogenost lijevanih blokova s aspekta elektrovodljivosti.
7. Dobiveni rezultati ukazuju na konzistentnost i ponovljivost postupka taljenja, obrade taline i lijevanja blokova slitine EN AW-5083, te upućuju na važnost kontrole kako procesnih varijabli, tako i svojstava lijevanog proizvoda u cilju optimizacije navedenih varijabli.

5. LITERATURA

[1] H. E. Vatne: *Aluminium 75*, 1999, 84-90, 200-03.
[2] M. Easton and D. StJohn: *Solidification of Aluminium Alloys*, 2004, The Minerals, Metals & Materials Society (TMS), Warrendale, Pennsylvania, USA,147-56.
[3] P. D. Lee, R. C. Atwood, R. J. Dashwood, H. Nagaumi, Materials Science and Engineering A328, 2002, 213-22.
[4] R. Nadella, D. G. Eskin, Q. Du, L. Katgerman, Materials Science 53, 2008, 421-80.
[5] F. Robert and P. E. Brewer: *Design of Experiments for Process Improvement and Quality Assurance*, Engineering & Management Press, Institute of Industrial Engineers, Norcross, Georgia, USA, 1996, 115-84.
[6] E 407 – 99: Standard Practice for Microetching Metals and Alloys, American National Standard Institute/ASTM, 1999.
[7] G. F. Vander Voort: *Metallography, Principles and Practice*, 2nd ed., ASM International, Materials Park, Ohio, USA, 1999, 610-16.
[8] E 1382 – 97: Standard Test Methods for Determining Average Grain Size Using Semiautomatic and Automatic Image Analysis, American National Standard Institute/ASTM, 1997.
[9] N. Dolić, K. Terzić, J. Prgin, A. Markotić and F. Unkić, *Proceedings book of 6th International Foundrymen's Conference: Inovative Foundry Materials and technologies*, 2005, Opatija, Croatia, 160-74.

[10] N. Dolić, K. Terzić, J. Prgin, A. Markotić and F. Unkić, *Proceedings book of International Conference: Materials, Tribology, Processing, MATRIB 2005*, 2005, Vela Luka, Croatia, 301-08.
[11] N. Dolić, A. Markotić, F. Unkić, *Metallurgical and Materials Transactions, 38B,* 2007, 491-95.
[12] D. G. Altenpohl: *Aluminium: Technology, Applications, and Enviroment, A Profile of a Modern Metal, Aluminium from Within*, 6th ed., The Aluminum Association and The Minerals, Metals & Materials Society (TMS), Warrendale, Pennsylvania, USA 1999, 33-59.

A FEASIBILITY STUDY FOR A SANS INVESTIGATION OF PHASE CHANGE MATERIAL FOR ENERGY STORAGE APPLICATIONS

A. J. Farrell [1], M. Rogante [2]

[1] Optical and Semiconductor Devices Group, Dept of Electrical and Electronic Engineering, Imperial College London, South Kensington, London SW7 2AZ
[2] Rogante Engineering Office, NDT, Contrada San Michele, n. 61, P.O. Box 189, 62012 Civitanova Marche, Italy – www.roganteengineering.it

Izvorni znanstveni rad / Original scientific paper

ABSTRACT

In this paper, PlusICE^{TM} Phase Change Material mixtures of non-toxic eutectic solutions are considered for a Small Angle Neutron Scattering diagnostic study, especially concerning the phase transition (melting) measurement (micro phase separation processes, nano-crystals formation or melting). Such material can be adopted for energy storage applications, and the main aim is to improve the stability of the mixture.

The relevant temperature range and the technical details of the same powder are reported, and a description of the proposed experiment follows.

This study wishes to demonstrate the feasibility of the SANS process for examining this material on the nano-scale prior to a full materials investigation, which aims to provide both the information to both improve the characteristics and performance of the considered mixture.

Keywords: Phase Change Materials; Neutron Techniques; SANS.

1. Introduction

Phase Change Materials (PCM) are “latent” thermal storage materials that use chemical bonds to store and release heat. The thermal energy transfer happens while a material changes from a solid form to a liquid, or vice versa.

PCM can be broadly grouped into two categories, i.e. organic compounds (such as polyethylene glycol) and salt-based products. Much work has been done over the years on one particular PCM, namely Glauber’s salt or sodium sulphate decahydrate. This salt is readily available, cheap, non corrosive and non toxic. It normally freezes at 32.5°C, which has made it ideal for use in solar heating and heat rejection applications. It is possible to depress the phase transition temperature to conventional HVAC chilled water ranges of 5-13°C by the addition of other salts. However, Glauber’s salt melts incongruously; in other words, upon melting, the salt tends to separate into a saturated solution with insoluble anhydrous sodium sulphate crystal. These crystals are heavier than the saturated solution, hence they settle out of solution due to gravity. When the phase change material is next frozen these crystals are unable to recombine with the saturated solution, resulting in a loss in TES capacity. This occurs during each freeze/melt cycle, and results in continuous loss of performance. Many attempts have been made to eliminate this segregation with varying degrees of success. The fundamental behind this work has been to thicken the mixture to such an extent that crystals that form during melting are held suspended in the solution. If this can be achieved, the crystals will then be recombined into the main body of the phase change material during the next freezing cycle, so no loss of performance will occur. A recent work has concentrated on using other thickening agents, in particular synthetic polymer gels.

The material considered in this study is a blend of inorganic salts and thickening agents, ammonium chloride (5-10%), similar to: 49.3% MgCl2.6H20 and 50.7 wt% Mg (NO3)2.6H20. Chemical composition varies depending on the phase change temperature.
The same powder is a mixture of non toxic eutectic solution having freezing and melting point higher than those of water and offering thermal energy storage capability between -62°C and 117°C. This phase change mixture can be sealed, for instance, inside an Aluminium profile beam which enables heat transfer via natural convection: when the surrounding air temperature is less than the material solution, the cell freezes and later stored latent heat can be released back to the surrounding space. In the considered PCM, the majority of the salt hydrates are not subject to any volume change, i.e. expansion or contraction during the phase change process. These salt hydrates have performed reliably with no degradation in either composition or storage capacity.
The application of SANS to PlusICE^{TM} PCM is novel. PlusICE^{TM} E17 mixture has been investigated by Rogante Engineering Office adopting SANS technique. The relevant temperature range and the technical details are: phase change temperature = 17°C; Density = 1487 kg/m^3; Latent Heat = 143 kJ/kg = 213 MJ/m^3; Spec. Heat = 0.67 kJ/kg K; Thermal Cond. = 0.43 W/m K.
The latent heat of fusion from the salt hydrates allows the considered mixture to have a larger thermal energy storage capacity relative to its physical size. The scope of this thermal energy application is wide ranging of solar heating, hot water, heating rejection, i.e. cooling tower and dry cooler circuitry thermal energy storage applications.

2. Method

Neutron investigations have recently become an increasingly significant probe for materials across a wide range of disciplines, and can reveal significant properties about materials. Neutrons are becoming more and more useful in the characterisation of materials and components of industrial interest. Their peculiarity, with respect to other investigation techniques, is the possibility of giving full information down to ~Å (0.1nm) dimensions, in a non-destructive way, about the microphysical structure of the sub-surface of materials [1].
Small Angle Neutron Scattering (SANS), further to other techniques, allows the true and full characterization of materials on the nano-scale. The small energies and the weak - but not negligible - interaction of Neutrons with matter means SANS is a non-destructive technique. Thus, the same sample can be studied in-situ or measured any number of times after either further usage or heat-treatment. Averaging over a macroscopic sample volume SANS then provides information with high statistical accuracy.
The considered technique allows the investigation of various materials such as porous media, polymers, membranes, ceramics, metals and solutions of micelles. The possibility to substitute hydrogen for deuterium also makes SANS a unique technique for investigating macromolecular structures in synthetic and biological polymers. The considered technique further allows the determination of void sizes and their distributions in porous media as well as the investigation of particle agglomeration and the evolution of pores during sintering. SANS is also useful for the understanding of the thermodynamics of two-phase systems [2].
SANS is a technique which deals with elastic and coherent scattering. The scattered intensity *I(q)* is measured as a function of the incoming Neutron flux, Φ, the instrument specific constant, A, the transmission of the sample, T, and the volume of the sample, V:

$$I(\lambda,Q) = \Phi A T V_{sample} \frac{d\Sigma}{d\Omega} + bg \qquad (1)$$

where λ is the neutrons wavelength and Q is the momentum transfer:

$$Q = \frac{4\pi \sin(\theta/2)}{\lambda} \qquad (2)$$

where θ is the scattering angle. Finally, *bg* is a contrast factor due to the background for the instrument, and Σ is the total area of the interface per unit volume of the sample [1, 2]. The $d\Sigma/d\Omega$ factor is the so called form-factor $F(Q)$, which contains information about the scattering particles of the sample. The scattering particles are nano-sized inhomogeneities in the studied material, for example, micelles, pores, nano-cracks and precipitates. Thus, the form factor can be expressed using the characteristic size of the scattering particle. Two approaches are used. In the low- or so called Guinier-region ($QR_g \leq 1$), the behaviour of the scattering intensity can be written using the Guinier expression for all shapes of non-interacting scatterers. It can then be said that:

$$F(Q) = K^2 V_{particles}^2 \exp\left(-Q^2 R_g^2 / 3\right) \qquad (3)$$

where R_g is the radius of gyration of each individual scatterer and V is the total volume of the scattering particles per unit volume. K is a dependent factor of the material and is often called the contrast between the embedding medium (or matrix) and the scattering object. An important feature of this equation is that R_g can be determined even if $I(q)$ is known only in arbitrary units.
A different approach can be used in large Q regions ($QR_g \geq 4$). The Porod law describes this behaviour as follows:

$$F(Q) = K^2 \frac{2\pi A}{Q^4} + bg \qquad (4)$$

where A is the total area of the interface per unit volume of the sample [1]. See refs. [3-6] for a detailed treatment of the theoretical bases.

3. Measurements, results and discussion

The measurements for this feasibility study were performed by Rogante Engineering Office using the SANS diffractometer "Yellow Submarine" at the Budapest Neutron Centre (BNC). This device covers a Q-range from 0.004 $Å^{-1}$ to 0.5 $Å^{-1}$, which allows the density composition and magnetization fluctuations in materials to be measured on a length scale of 10 Å to 1000 Å. The scheme of the SANS diffractometer is shown in Fig. 1.

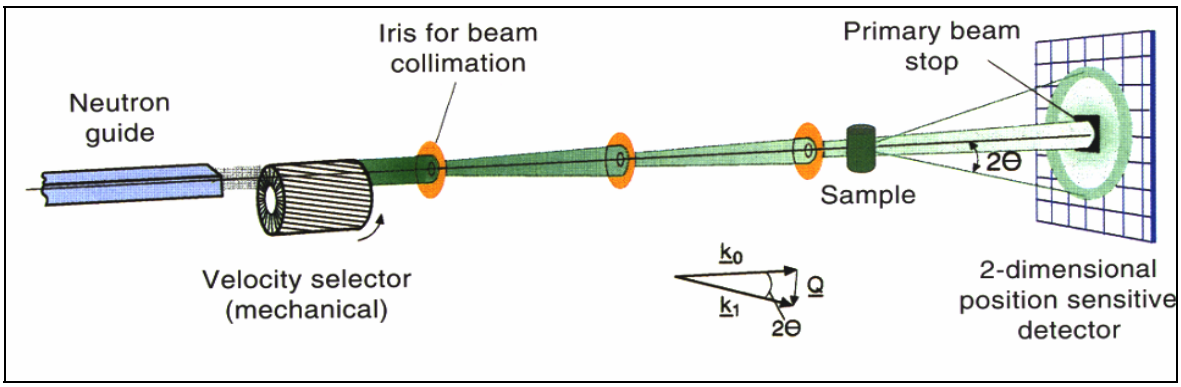


Fig. 1 - Scheme of the SANS diffractometer of the Budapest Research Reactor used by Rogante Engineering Office for the investigation of the PlusICE^{TM} E17 mixture.

The neutrons are produced by a 10MW reactor and guided to the sample by super-mirrors. The wavelength can be varied between 3.4 and 23 Å with the aid of a multi-disc type velocity selector. The beam intensity is monitored by a 64 by 64 pixel (each of 1 cm by 1 cm) two-dimensional position sensitive detector filled with BF_3 gas.
The measurements have been performed at various temperatures in the range 15-45°C. Fig. 2 shows details of the sample holder during the SANS measurement.



Fig. 2. PlusICE^{TM} E17 PCM investigated by SANS.

The investigated material was initially radiated particularly to various values of: neutron beam wavelength, selector speed, sample-detector distance. The fittest values and therefore the most indicative parameters of measurement able to underline the microstructural characteristics of the investigated material have been individualized, in such way, to allow the best resolution.
The primary data treatment have been made, after the measurement, including the regrouping of the two-dimensional scattering patterns, background subtraction, correction for transmission and normalization to standard samples, usually to 1 mm water. The scattering patterns are isotropic, as shown in figure 3.

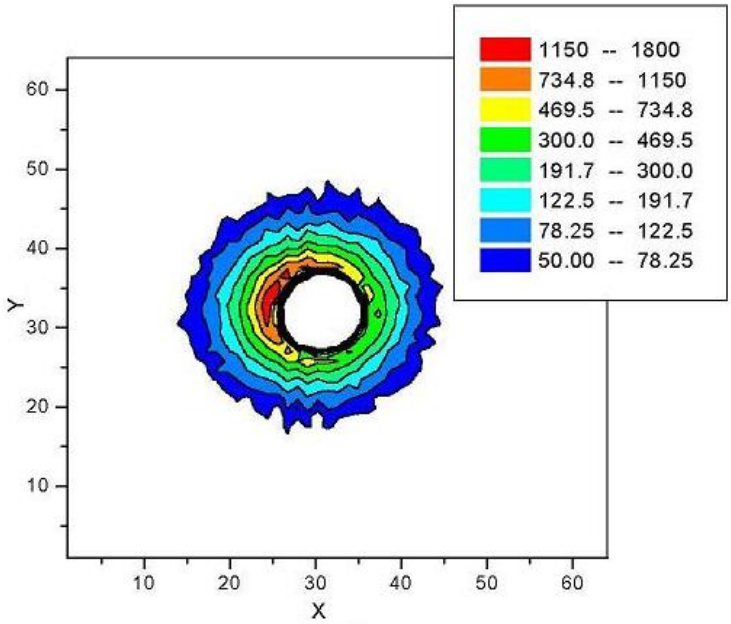


Fig. 3. SANS patterns of the investigated sample.

The same image has been obtained by the two-dimensional detector. The punctual geometry of such investigation method is shown: a beam having a circular section hits a part of the sample, producing scattered neutrons that are pointed out by the two-dimensional detector.
The scattering power of the sample resulted pretty strong, and the sample has been measured in two sample-detector positions. Such features allowed obtaining sufficiently accurate counting statistics.
Figure 4 shows a SANS curve of the investigated sample.

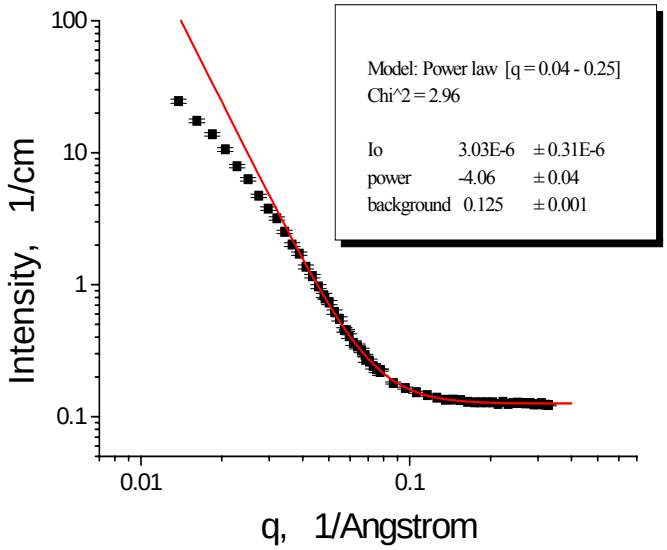


Fig. 4. SANS curve of the investigated sample.

The experimental curve indicates the presence of a Porod scattering; fitting the high-q side of the curve with the following power law plus background:

$$I(q) = I_0 * q \wedge power + Bg \qquad (5)$$

resulted in the value of the exponent power = -4.0 within the fitting error. This indicates the presence of smooth interfaces, most probably between the wet powder and the air included in the sample.
The deviation of the small q region from the Porod law indicates that there must be either small structural units of sizes 10÷1000 nm (e.g., powder grains) or to the non-homogeneous structure of the material components mixture.
The present study has verified the feasibility of the adoption of SANS technique for the characterization of PlusICE^{TM} mixtures of non-toxic eutectic solutions. The first scattering data have shown the industrial applicability of the adopted technique in the considered case.
The neutron scattering on the investigated mixture sample resulted very high. The presence of grains with smooth surface, moreover, has been detected. So, the following thermal treatment can induce some transformations of the grains to be clear visible by SANS. The nano-scale features of phase transition, consequently, should be observed (e.g. growth of new phase domains, coexistence of old and new phases also) by performing a definitive SANS measurements. Useful information on the phase transition (melting), on micro phase separation processes and nano-crystals formation or melting can be also obtained.

As the considered material concerns hydrated salts, it is desirable to prepare also deuterated samples (e.g. to exchange light water to heavy one), so the difference in scattering intensities (deuterated - protonated) can give a very interesting information on the structure of the hydrated molecules.

Conclusions

The characterization of PlusICE^{TM} PCM for energy storage applications by means of SANS technique can supply useful information at the nano-scale level, especially concerning phase transition (melting) and hydrated molecules status.

SANS measurements supplied by Rogante Engineering Office represent efficient complementary methods in the complete investigation of the considered material.

Rogante Engineering Office represents a reference point for Industry with regard to the Industrial Applications of Neutron Techniques for materials and components analysis and characterization, and in particular the non-destructive determination of inner and sub-surface RS, and the microstructural characterization by SANS.

References

[1] M. Rogante and L. Rosta, in: Proc. SPIE 5824, Opto-Ireland 2005: Nanotechnology and Nanophotonics, W. J. Blau, D. Kennedy and J. Colreavy (Eds.), pp. 294-305 (2005).

[2] A. Len, L. Rosta, E. Rétfalvi, P. Harmat and M. Rogante, Studia Universitatis Babes-Bolyai (UBB) journal, Physica XLIX/2, 81-84 (2004).

[3] O. Glatter and O. Kratky in: Small Angle X-ray Scattering, Academic Press, London (1982).

[4] C. Williams, R. P. May and A. Guinier in: Mat. Sci. and Technol., E. Lifshin (ed.), vol. 2B, pp. 611-656. VCH Verlagsgesellschaft, Weinheim (1994).

[5] H. M. Rietveld, Acta Cryst., 22, p.151 (1967).

[6] H. M. Rietveld, J. Appl. Cryst., 2, p.65 (1965).

Cooling and heating panels using aluminium foams

Roman Florek, František Simančík, Martin Nosko, Roman Uhrík, Peter Mihálka*

Institute of Materials and Machine Mechanics; Slovak Academy of Sciences Račianska 75, 831 02 Bratislava 3, Slovak Republic
**Institute of Construction and Architecture; Slovak Academy of Sciences*
Dúbravská cesta 9, 845 11 Bratislava, Slovak Republic

Izvorni znanstveni rad / Original scientific paper

ABSTRACT

Aluminium foam is a unique material possessing very high thermal diffusivity due to high thermal conductivity of the cell walls accompanied with rather low overall thermal conductivity, controlled by total porosity. On heating or cooling these properties allow reaching the uniform temperature within the foam structure very quickly without local overheating or overcooling also in quite large panels.
The heat can be transferred in or from the foam using pressed-in tubes, whereas the foam in the vicinity of tube is compressed thus allowing better heat transfer between the foam and tube and parallelly improving mechanical fixing of tube in the structure.
After impregnation of such foam (equipped with tubes) by appropriate filler (plaster, polyurethane foam, etc.) the resulting lightweight panels can be used for efficient heating of floors or walls or for cooling of ceilings. The foam contributes to quick heat spreading in the whole panel volume, giving very uniform temperature distribution also if only relatively short length of heating/cooling tube is used. Low heat capacity allows quick response to temperature changes thus saving an energy related to overheating. Moreover, ductile porous structure of aluminium foam reduces the sensitivity to cracking due to temperature changes in plasterboards, improves their mechanical properties and allows reuse after dismantling.
The paper will present the performance of heating/cooling floor and ceiling panels utilizing aluminium foam as heat spreader. Comparison with typical current solutions will be made comprising both efficiency and cost issues.

Key words: aluminium foam, lightweight heating/cooling panels, floor heating, ceiling cooling, air-conditioning

INTRODUCTION

In order to enhance the performance of cooling and heating panels, novel materials must be taken for this purpose. Efficiency of cooling or heating panels is mainly affected by their thermal conductivity, emissivity, area, geometry and weight. Aluminium foam with its properties is material which is able to enhance the cooling or heating performance further. Tubes for cooling or heating medium can be easy pressed-in aluminium foam structure or in-situ foamed (only stainless steel tubes). In addition to this, using aluminium foams can bring some additional functions as load bearing ability, electro-magnetic field shielding or sound absorption ability (2).

EXPERIMENTAL

Cooling performance measurements

Cooling performance was measured on aluminium panel with dimensions (500 x 500 x 15 mm) with pressed in aluminium tube (D_{outer} x t = 8 x 1 mm). To ensure constant conditions during the whole measurement and to avoid external temperature and air circulation influences were the measurements done in a special isolated chamber assigned for this purpose (floor area = 5 m^2). This panel was in as-received state; without any additional coating or painting. Radiation from all surfaces in the chamber and air temperature was measured by ball thermocouple. The cooling performance was measured at different water flow rates and temperature differences. Inlet and outlet temperatures of water were measured by thermocouples. The measurements were performed according to EU standard (EN 14240). Arrangement of measurement is presented in figure 1.

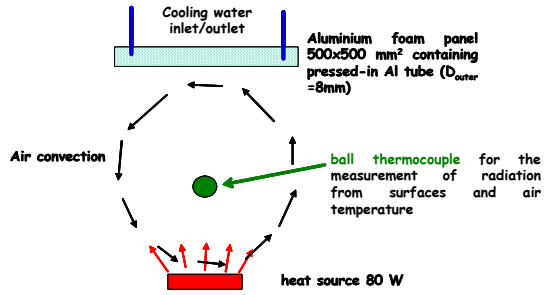


Figure 1: Arrangement of cooling performance measurement.

Surface emissivity measurements

In case of radiant heat exchangers the emissivity is an important value (1). It indicates how much heat or cold can surface radiate to surrounding surfaces. The emissivity was measured on aluminium foam samples (200 x 100 x 15 mm) in as-received as well as; in order to increase radiation ability; in painted condition. The emissivity as well as radiation properties of the panels were measured by infrared camera NEC TH 7100. In order to ensure constant conditions and to avoid any external influences (sunshine, outside temperature changes, other heat sources and reflections affecting IR-camera) were all the measurements done in a special isolated dark chamber (floor area 30 m^2). During the measurement were the samples placed on a heating panel which was pre-heated to 60°C (see figure 2). Subsequently, the influence of overall thermal conductivity on cooling ability of the panels with identical surface emissivity; gypsum plaster panel with cast-in aluminium tube (D_{outer} x t = 8 x 1 mm) and aluminium foam panel with pressed-in aluminium tube (D_{outer} x t = 8 x 1 mm) and additional gypsum plaster surface coating; was observed (see figure 3).

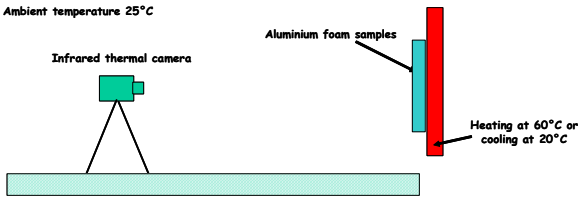


Figure 2: Arrangement of emissivity measurement during heating

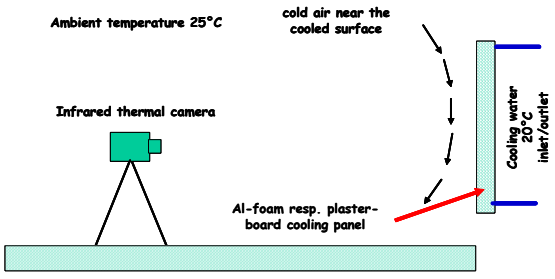


Figure 3: Arrangement of measurement on cooling panels with the identical value of surface emissivity (gypsum plaster panel with cooling tubes and aluminium foam panel with cooling tube and gypsum plaster coating).

RESULTS

The measurements on as-received aluminium foam panel have showed an excellent cooling ability. There were observed very short response times what can be attributed to very good thermal conductivity of aluminium foam structure. The tested panel reached its steady state temperature very quickly; within ~ 1 minute.

Cooling performance can be calculated according to following formula.

$$\Phi = \frac{Q}{t} \qquad (1)$$

Where **Φ** is heat flow in W, **Q** is amount of heat in J and **t** is time in seconds.

Density of heat flow **q** in W/m^2

$$q = \frac{\Phi}{A} \qquad (2)$$

Where **A** is area in m^2

The heat flow is a vector value, is characterized by numerical value and flowing direction.

In our case was the cooling performance calculated as follows

$$\Phi = c_p \cdot q_m (W_{inlet} - W_{outlet}) / 0{,}25\ m^2 \qquad (3)$$

Specific heat capacity of water at 15°C $\mathbf{c_p}$ = 4187 J/(kg.K)
$\mathbf{q_m}$ is water flow rate in (kg/3600 seconds)

The performance was calculated every 5 minutes. All calculated values were finally averaged and this value was taken as heating performance value. The averaged values from all measurements together with all parameters are listed in table I.

Table I: Parameters of the measurement and measured cooling performance of the aluminium foam panel.

Area	m2	0,25		
Heating power	W	80		
Heat transfer from periphery	W	20		
Temperature difference (ball thermocouple - cooling water)	°C	5,88	7,07	9,2
Surrounding air temperature (ball thermocouple)	°C	26,16	25,07	25,23
Water inlet temperature	°C	20,28	17,6	16,03
Water outlet temperature	°C	21,13	18,29	16,80
Water temperature difference (inlet vs. outlet)	°C	0,85	1,13	0,77
Water flow rate	l/h	20	18	43
Total cooling capacity measured per panel	W	**19,77**	**23,66**	**38,33**
Calculated cooling capacity per square meter	W/m2	**79,09**	**94,63**	**153,32**

Measurement of emissivity has showed different value for as-received as well as painted aluminium foam surface. For comparison, polished aluminium possesses emissivity ~ 0,025, in case of anodized aluminium it is ~ 0,25, as-received aluminium foam surface reaches an overall value 0,75. This value can additionally be enhanced to ~ 0,98 by painting of aluminium foam (see also figures 4b and 4d). The overall emissivity value 0,75 for as-received aluminium foam surface is caused by its porous structure, which on one hand increases a real surface and on the other hand causes a multiple reflection of radiation wave in the partial closed cells (smaller bright spots in figure 4c). Some of cells, which are almost closed, can act as a "black body"(so called "ideal radiator") and on this account are able to absorb almost whole radiation energy. Flat surface or almost flat area with lowest emissivity in figure 4c is represented by grey color. The painted surface showed higher and more uniform emissivity distribution (see figure 4d).

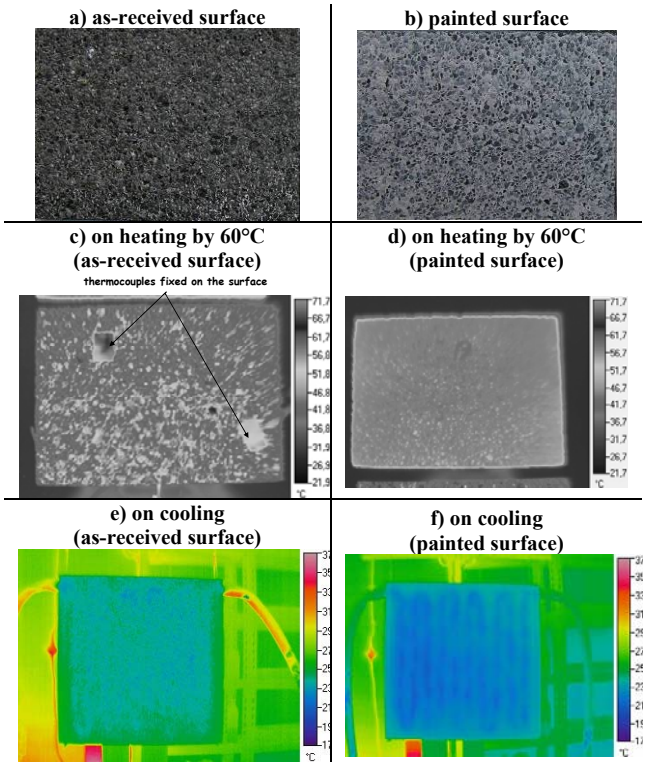


Figure 4: comparison of emissivity effect during the heating (middle) and cooling (right); as-received with emissivity ~ 0,75 vs. painted with ~ 0,98

The influence of emissivity on cooling ability can be clearly seen in figure 4e and 4f. The aluminium foam panel, which was also used for cooling performance measurements, was painted by white radiator color. (figure 4b and 4f). Figure 4e, f presents the radiation difference between the as-received and the painted aluminium foam panel. As can be seen, the radiation is significantly higher and according to this, comparing the both emissivities; it can be concluded that the cooling performance of such surface treated panel can be enhanced by about 20%. Subsequent enhancement of cooling performance can be done by allowing air convection above the cooling panels. In some cases it is possible by i.e. perforation of aluminium foam panels.

Subsequently, the measurements on panels with identical surface emissivity as well as surface treatment were performed (see figure 5). The measurements were focused on effect of thermal conductivity on cooling ability. The measurements were performed on following two panels; aluminium foam panel coated with gypsum plaster and simple gypsum plaster panel with integrated cooling tube. It is visible in figures below that the high thermal conductivity of aluminium foam is able to ensure very uniform temperature distribution (figure 5 left) compared to gypsum plaster panel (figure 5 right). In case of aluminium foam, the temperature of the cooling area is very close to the cooling water temperature. It means that also the effective area for heat exchange is larger compared to panel without aluminium foam where the cooling tube can be clearly seen because of low thermal conductivity of gypsum material.

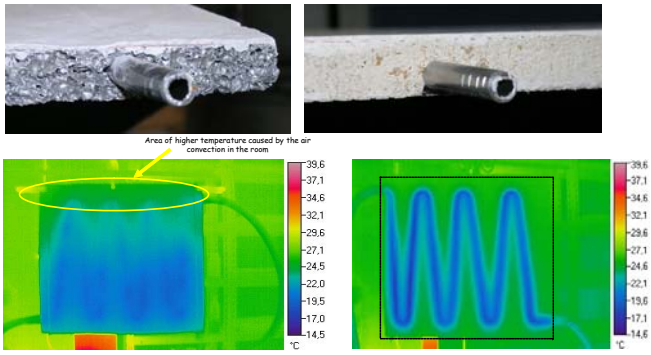


Figure 5: cooling panel of aluminium foam filled at the room facing side with gypsum plaster (left) and gypsum plaster panel with embedded aluminium tube (right).

CONCLUSION

Tube fitted aluminium foam panels exhibit exceptionally efficient heating and cooling performance when used directly as radiators or embedded as hear spreads in plasterboard or PU panels. High cooling and heating efficiency of aluminium foam is due to its high specific surface, low heat capacity and high thermal conductivity of cell walls. Cooling performance is comparable with traditional solutions (even better) for low temperature heating system or heat exchangers. In case of aluminium foam panels can be this performance enhanced by additional surface treatments (painting => emissivity enhancement) and design of panels which will allow, beside the radiation, the air convection, too.

Main benefits of aluminium foam panels are:

- Higher performance compared to conventional panels.
- Very low energy consumption compared to fan air-conditioning (in case of cooled ceilings; because of radiant heat exchange; for a sufficient thermal comfort already 26°C is enough).

- Maintenance-free,
- Fireproof (through flowing water can be even used as efficient fire protection)
- Self-supporting (load bearing) ability
- Flexibility (panel can be shaped in some extent)
- unique look adjustable with additional surface treatments
- sound absorption ability if used directly as radiator
- efficient electro-magnetic shielding
- Potential use of aluminium foam panels is in heating/cooling for ceilings or walls in various buildings but also in new generation of transport vehicles (i.e. trains, ships), utilizing also excellent stiffness-to-weight ratio of this remarkable material.

ACKNOWLEDGMENT

Financial support of ALULIGHT GmbH and GLEICH GmbH is greatly acknowledged.

REFERENCES

(1) Sálavé chladíci systémy; Ing. Vladimír Zmrhal,PhD; 2006
(2) Aluminium foam-a new lightweight material; 1997 Kovové materialy; F.Simančík, J. Kováčik, J.Jerz, P. Minár

THE PREDICTION OF THE AS-CAST DUCTILE IRON IMPACT TOUGHNESS BY USING ARTIFICIAL NEURAL NETWORK AND CHEMICAL COMPOSITION

PROCJENA UDARNE ŽILAVOSTI NODULARNOG LIJEVA U LIJEVANOM STANJU UMJETNOM NEURONSKOM MREŽOM NA OSNOVI KEMIJSKOG SASTAVA

Z. Glavaš[1)], F. Unkić[1)] K. Terzić[1)]

[1))] Metalurški fakultet Sveučilišta u Zagrebu
Aleja narodnih heroja 3, 44000 Sisak
Republika Hrvatska

Izvorni znanstveni rad / Original scientific paper

ABSTRACT

This paper present the application of artificial neural network in the production process of ductile iron. A backpropagation neural network has been established to predict the as-cast ductile irons impact toughness by using chemical compositions as inputs. The generalization property of the developed artificial neural network is very good, which is confirmed by a very good accordance between the predicted and the targeted values of the as-cast impact toughness on a new data set that was not included in the training data set.

Key words: ductile iron, impact toughness, artificial neural network

SAŽETAK

U ovom radu prikazana je primjena umjetne neuronske mreže u procesu proizvodnje nodularnog lijeva. Formirana je unaprijedna statička neuronska mreža s povratnim prostiranjem pogreške (*eng. Backpropagation Neural Network)* koja na osnovi kemijskih sastava procjenjuje udarnu žilavost nodularnog lijeva u lijevanom stanju. Generalizacija formirane umjetne neuronske mreže je vrlo dobra, što potvrđuje vrlo dobro slaganje između procijenjenih i ciljanih vrijednosti udarne žilavosti u lijevanom stanju na novom skupu podataka koji nije bio uključen u skup podataka za učenje.

Ključne riječi: nodularni lijev, udarna žilavost, umjetna neuronska mreža

1. Introduction

Ductile iron (DI) is a very specific engineering material which possesses good mechanical properties and castability. Apart from a better tensile strength, this material has a considerably better impact toughness than other cast irons, which provides a much wider range of application.

The mechanical properties of DI are primarily determined by its microstructure [1 - 8]. Chemical composition is one of the most significant factors determining the microstructure. The changes of the chemical composition result in the changes of the microstructure as well as of the mechanical properties.

The ferrite content in the metal matrix has a significant influence on the impact toughness of DI. Therefore, the presence of elements which are ferrite promoters is desirable. With the goal of producing as-cast ferritic DI, the contents of pearlite promoters and carbides promoters should be kept as low as possible. A very harmful influence on the impact toughness has P, because it has a strong embrittling effect and should be kept as low as possible [9].

The impact toughness data is important in optimizing the design parameters of a specific component. Therefore, it will be useful to create the model for the prediction of the impact toughness of DI before pouring of the melt into the moulds. This allows for corrective measures to be taken with the purpose of obtaining the required impact toughness of DI castings.

The model for the prediction of impact toughness of DI based on multiple linear regression technique could be applied, more or less successfully, only to specific process conditions under which they have arised. Meanwhile, casting production process is a complicated and nonlinear process, i.e. chemical composition, microstructure and casting properties are not in linear relationship. Therefore, in order to obtain a reliable model for the prediction of the impact toughness of DI, it is necessary to use artificial neural networks (ANN). The important features of ANN are nonlinearity, learning (training) ability and adaptability to new situations [10, 11]. A properly trained ANN is capable to map the input to the output patterns with a minimal error between the modeled and the measured output values. In recent years, ANN are many times successfully applied to correlate chemical composition and data from the cooling curve with the shape of graphite, microstructural and mechanical properties of gray and ductile iron castings [12 - 14].

In this paper, a neural network model has been established to predict the as-cast impact toughness of DI based on chemical compositions.

2. Experimental

The base melt for the production of DI was produced in an acid-lined cupola furnace (diameter 800 mm, cold air, capacity 4-5t/h). The charge materials consisted of special low-manganese pig iron, returns scrap and steel scrap. The melt was transferred to the net-frequent induction furnace, capacity 4t and power 1100kW, where its temperature was raised due to the homogenization and the correction of chemical composition. After that, the melt was desulphurized in a 3t ladle by the addition of CaC_2 and strongly mixed with inert gas (nitrogen) which was introduced through a porous plug located at the ladle bottom. After the desulphurization and the removing of slag the melt was poured into a channel-type induction holding furnace (receptor), capacity 20t and power 800kW. The nodularizing treatment of the base melt was performed by the Flotret or Osmose method via FeSiMg5 alloy. After the treatment, a sample of the melt was taken for the estimation of chemical composition and a Y-

block was cast. Chemical composition of the tested DI samples was determined with a LECO GDS-400A spectrometer. The average chemical composition of the examined DI melts is given in table 1. Deviations from the chemical composition given in table 1 were present on a few melts (a higher content of P, Cu and Cr).

Table 1. Average chemical composition (wt. %) of the DI melts used in the experiments

C	Si	Mn	P	S	Ni	Cr	Cu	Mo	Ti	Al	Sn	Mg
3,5-3,8	2,6-3,1	0,1-0,3	0,025-0,045	0,001-0,010	0,03-0,06	0,04-0,06	0,06-0,11	0,004-0,009	0,010-0,020	0,009-0,015	0,005-0,012	0,028-0,036

A Y-block was cast into the mould which had been produced by the Betaset® process. The dimensions and the form of the Y-block are specified according to the HRN EN 1563. Altogether, 139 melts have been made. All Y-blocks were poured under same conditions.

Standard test pieces with a V-notch for the estimation of the as-cast impact toughness were machined from the Y-blocks. The dimensions and the form of the test pieces are specified according to the EN 10045-1 (the length of a test piece is 55 mm; a square section with 10 mm sides; V-notch of 45°, 2 mm deep with a 0,25 mm radius of curvature at the base of the notch). Test pieces have always been taken from the same place in the Y-block. Altogether, 267 standard test pieces have been made and tested.

The impact energy is the measure of the as-cast impact toughness. The impact energy of DI samples in the as-cast condition was examined by the Charpy method at 20 °C according to HRN EN 10045-1. In this examination a testing machine with maximum striking energy of 15 J was applied.

With the goal of estimating the relationship between the microstructure properties and chemical compositions, metallographic examinations were performed after the Charpy impact test by a light metallographic microscope with a digital camera and the image analysis system (AnalySIS® Materials Research Lab). Test pieces were prepared by a standard metallographic technique. On each sample, three measurements were performed for each analyzed microstructure property.

The software used to create the ANN which predicts the impact toughness of DI using chemical compositions as inputs is Neural Network Toolbox of MATLAB® 7.0.

3. Results and discussion

The input parameters for the ANN are the contents of the estimated elements of the chemical composition of the analyzed DI melts.

In this work, the early stopping method was used to improve the network generalization and prevent the overfitting. According to this method, the experimental data set is divided into three subsets: the training data set, the validation data set and the test data set. The training data set was used for computing the gradient and updating the network weights and biases. The validation data set was not included in the training data set and was used to decide when to stop the training. The test data set error was not used during the training, but it was used for the comparison of different models, i.e. for the evaluation of the performance of networks. Network generalization is good when a network is able to perform as well on a test data set as on a training data set. To produce the most efficient training, the input and the output data are normalized before the training.

In this paper, different network architectures were examined to determine a network which has a minimum generalization error. The best results were achieved by a multilayer

Backpropagation Neural Network (BPNN) which was trained using the Levenberg-Marquardt algorithm. The parameters of the selected network (BPNN) are given in table 2.

Table 2. Architectures and parameters of the selected neural network (BPNN)

Number of hidden layers	2
Number of neurons in the first hidden layer	9
Number of neurons in the second hidden layer	15
Number of neurons in the output layer	1
Transfer function of the first hidden layer	'logsig'
Transfer function of the second hidden layer	'logsig'
Transfer function of the output layer	'purelin'
Levenberq-Marquardt parameter μ	0,001
μ increase factor	10,0
μ decrease factor	0,1

The performance of the trained BPNN was measured by regression analysis between the network outputs and the corresponding target values which had been obtained by measuring (table 3). Figure 1 show the performance of the BPNN on the test data set that was not used during the training.

Table 3. Values of performance functions and coefficients correlation (R) on training, validation, test and entire data set

Data set	Performance function				Coefficient correlation
	SSE	MSE	RMSE	NRMSE	R
Training set	2,5339	0,0189	0,1375	0,0733	0,998
Validation set	26,7861	0,4059	0,6371	0,3118	0,953
Test set	12,9842	0,1938	0,4402	0,2405	0,971
Entire data set	42,3043	0,1584	0,3980	0,2089	0,978

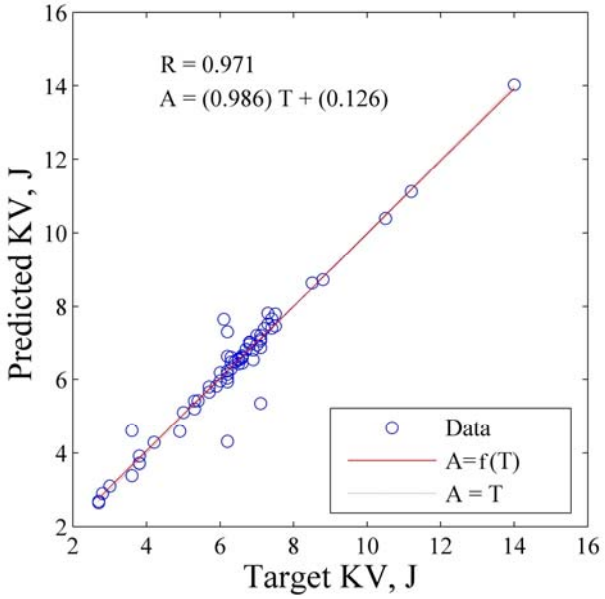


Figure 1. Performance of the BPNN on the test data set, R - coefficient correlation, A - predicted impact energy (KV), T – target impact energy (KV)

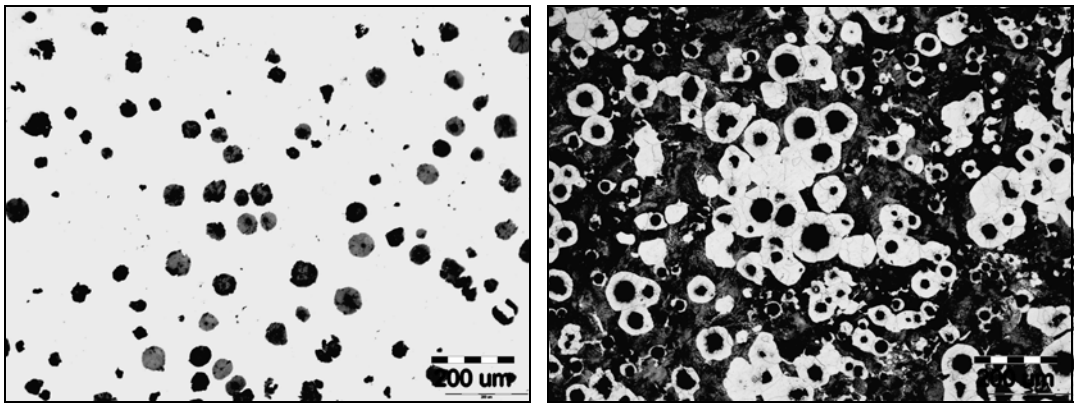
Performance functions are important measures for the evaluation of a network's performance. In this paper, performance functions used for the training of BPNN are the Sum Squared Error (SSE), the Mean Square Error (MSE), the Root Mean Square Error (RMSE) and the Normalized Root Mean Square Error (NRMSE). Values of the performance functions on the training, validation, test and the entire data set are given in table 3.

Figure 1 shows a very good network generalization which is confirmed by a high value of coefficient correlation between the network outputs and the corresponding target values obtained by measuring. This is the indication of a proper network architecture and a proper selection of the input network parameters.

The obtained results show that it is possible to predict the as-cast impact toughness of DI by neural networks using chemical compositions as inputs. Successfulness of the model is confirmed by a high value of coefficient correlation between the measured and the predicted values of the impact toughness on the test data set. In the succession of discussion, there will be considered the influence of the elements of chemical composition on the as-cast impact toughness of DI.

Ductile iron with optimum impact toughness can be obtained by producing an entirely ferritic metal matrix without carbides. A high C content can reduce carbide formation and it favors ferrite formation over pearlite. However, the combination of high C contents, i.e. carbon equivalent (CE), and slow cooling rates results in the flotation and the formation of non-spheroidal graphite forms which has a negative influence on the impact toughness of DI. The increasing of C contents may result in the increasing of nodules count per unit volume and the decreasing of the average distance between them. During the eutectoid transformation, i.e. austenite decomposition, a high nodule count acts on the decreasing of diffusional paths of C in the solid state, which results in the increasing of the ferrite content in the microstructure. Silicon promotes ferrite and has a significant influence on the achievement of carbide free as-cast structures. However, since Si strengthens the ferrite, its content should not be over about 2,5%.

In order to obtain a high ferrite content, the content of pearlite promoters (Cu, Sn, Sb, Mn, Cr, Mo, V, etc.) should be kept as low as possible. Copper, tin and antimony are strong pearlite promoters. Small additions of these elements are sufficient to produce pearlitic matrix. These elements segregates to the graphite/metal interface and retard the diffusion of C near the graphite nodules which suppresses the γ to α + graphite transformation. Figure 2 shows optical micrographs of the microstructure of a DI sample which has a high copper content (0,48%). A high pearlite content results in a low value of the impact toughness (2,6J).



a) b)

Figure 2. Optical micrographs of the microstructure of a DI sample which has a high copper content (0,48%), a) no etched, b) etched, natal. Ferrite content is 38,7%, pearlite content is 61,3%, 80 nodules/mm^2, nodularity is 70%

Phosphorus is an undesirable element in DI and should be kept as low as possible. It forms a very hard and a brittle phase (phosphide eutectic) which segregates during the solidification to the cell boundaries. Figure 3 shows the optical micrograph of the microstructure of a DI sample which has a high phosphorus content (0,085%). A high phosphorus content results in a low value of the impact toughness (3,2J).

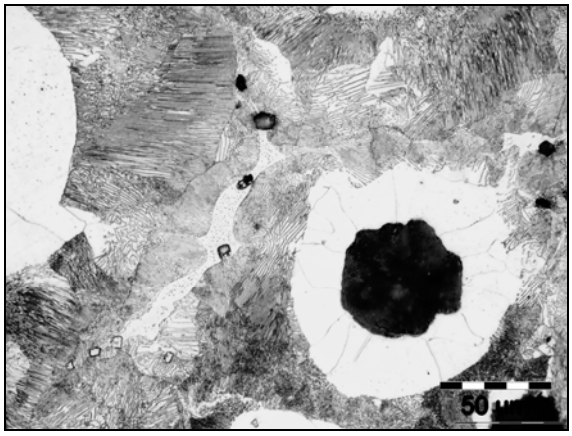


Figure 3. Optical micrograph of the microstructure of a DI sample which has a high phosphorus content (0,085%), etched, natal

Magnesium has a strong affinity for sulphur. This is the reason why it is desirable to use low sulphur base melts for DI production. High sulphur contents in the base melts require the addition of higher quantities of magnesium treatment alloys to obtain high nodularity.

Manganese, chromium, vanadium and molybdenum are carbide forming elements. Since the carbides are very hard and brittle phases, which has a negative influence on the impact toughness of DI, the contents of these elements should be kept as low as possible. Though being a pearlite promoter, nickel is a graphitizer and it reduces the formation of primary carbides. It has also been found that nickel has no harmful influence on the impact toughness of DI.

Aluminum and titanium have a significant influence on graphite morphology in DI. These elements are highly surface active and concentrate at the graphite/melt and graphite/solid interfaces. The contents of these elements should be kept as low as possible, because even very low contents results in the formation of non-spheroidal graphite forms.

4. Conclusions

The obtained results show that artificial neural networks are a powerful tool for the modeling of nonlinear processes. A developed backpropagation neural network successfully predicts the as-cast impact toughness of ductile irons using chemical compositions as inputs. A very good accordance between the measured and the predicted as-cast impact toughness was achieved. This allows for corrective measures to be taken before the pouring of the melt into the moulds with the purpose of obtaining the required microstructural and mechanical properties of castings as well as the decrease in the percentage of the waste castings.

References

[1] E. N. Pan, W. S. Hsu, C. R. Loper, Jr., Effects of Some Variables on the Matrix and Mechanical Properties of Ferritic Ductile Irons, AFS Transactions **96**(1988), 645 - 660.

[2] D. Venugopalan, A Kinetic Model of the $\gamma \rightarrow \alpha$ + Gr Eutectoid Transformation in Spheroidal Graphite Cast Irons, Metallurgical Transactions **21A**(1990) 4, 913 - 918.

[3] D. Venugopalan, A. Alagarsamy, Effects of Alloy Additions on the Microstructure and Mechanical Properties of Commercial Ductile Iron, AFS Transactions **98**(1990), 395 - 400.

[4] D. Venugopalan, Prediction of Matrix Microstructure in Ductile Iron, AFS Transactions **98**(1990), 465 - 469.

[5] T. Skaland, Ø. Grong, Nodule Distribution in Ductile Cast Iron, AFS Transactions **99**(1991), 153 - 157.

[6] F. Unkić, N. Gavranović, M. Vasilić, Utjecaj sadržaja silicija na mehanička svojstva primarnih i toplinski obrađenih uzoraka nodularnog lijeva vrste EN-1563-GJS-400-18LT, Strojarstvo **47**(2005) 1-2, 33-38.

[7] P. Mrvar, M. Trbižan, J. Medved, A. Križman, Study of the Eutectoid Transformation in the As-cast Spheroidal Graphite Cast Iron with „in-situ“ Dilatation Analysis – Method for Quality Control, Materials Science Forum **508** (2006) 287-294.

[8] X. Guo, D. M. Stefanescu, Solid Phase Transformation in Ductile Iron – A Benchmark for Computational Simulation of Microstructure, AFS Transactions **105**(1997), 533 - 543.

[9] S. Komatsu, T. Shiota, Influences of Silicon and Phosphorus Contents and Cooling Rate on J_{IC} Fracture Toughness of Ferritic Spheroidal Graphite Cast Iron, Proceedings of the Third International Symposium on the Physical Metallurgy of Cast Iron, The Physical Metallurgy of Cast Iron, ur. H. Fredriksson, M. Hillert, Elsevier Science Publishing Company, Stockholm, Sweden, 29 - 31 August 1984., 517 - 526.

[10] M. T. Hagan, H. B. Demuth, M. H. Beale, Neural Network Design, PWS Publishing Company, Boston 1996.

[11] L. Fausett, Fundamentals of Neural Networks, Prentice-Hall, Inc., New Jersey, 1994.

[12] J. L. Xu, Z. P. Wang, C. Chen, Neural Network Model in Predicting Mechanical Properties of Ductile Iron, AFS Transactions **110**(2002), paper 02-013.

[13] R. B. Yao, C. X. Tang, G. X. Sun, Predicting Gray Cast Iron Properties with Artificial Neural Network, AFS Transactions **104**(1996), 635 - 642.

[14] Z. Glavaš, D. Lisjak, F. Unkić, The Application of Artificial Neural Network in the Prediction of the As-cast Impact Toughness of Spheroidal Graphite Cast Iron, Kovove Materialy **45**(2007), 41 – 49.

FRAKTOGRAFSKA ANALIZA AUSTENITNOG NEHRĐAJUĆEG ČELIKA AISI 321 NAKON ZAVARIVANJA

FRACTOGRAPHIC ANALYSIS OF AUSTENITIC STAINLESS STEEL AISI 321 AFTER WELDING

Mirko Gojić, Stjepan Kožuh, Drago Laćman

Metalurški fakultet Sisak, Aleja narodnih heroja 3, 44103 Sisak

Faculty of Metallurgy, University of Zagreb, Aleja narodnih heroja 3, 44103 Sisak, Croatia

Izvorni znanstveni rad / Original scientific paper

Sažetak

U radu su prikazani rezultati fraktografske analize prijelomnih površina nakon ispitivanja vlačne čvrstoće i udarne radnje loma osnovnog materijala i zone taljenja austenitnog nehrđajućeg čelika AISI 321. Ispitivanja su provedena pretražnim elektronskim mikroskopom (SEM) i energetsko disperzijskim spektrometrom (EDS). Utvrđeno je da su prijelomne površine karakterizirane sitnojamičastim duktilnim prijelomom. Iniciranje prijeloma je uočeno na međupovršinama Ti-čestica/metalna osnova i Mn-uključak/metalna osnova. Mjestimično su zapažena i područja krhkog transkristalnog prijeloma.

Ključne riječi: austenitni nehrđajući čelik, zavarivanje, mehanička svojstva, prijelomna površina

Abstract

In this work the results of fractographic analysis of fracture surfaces of samples after tensile strength testing and impact energy of base and weld metals for austenitic stainless steel AISI 321 are shown. Tests were carried out using scanning electron microscopy (SEM) and energy dispersive spectrometer (EDS). It was found that fracture surfaces were characterized by ductile fracture with small dimples. Initiation of the failure was observed at interfaces Ti-particles/matrix and Mn-inclusions/matrix, respectively. Also, sporadically the field of brittle transgranular fracture are observed.

Key words: austenitic stainless steel, welding, mechanical properties, fracture surface

1. UVOD

Uporaba austenitnih nehrđajućih čelika vrlo je raširena u kemijskoj i petrokemijskoj industriji, eksploataciji nafte i plina, brodogradnji, postrojenjima za izradu lijekova i hrane. Zavareni čelični proizvodi od austenitnih čelika najčešće se izrađuju u obliku limova i cijevi. Glavne karakteristike ove skupine čelika su dobra korozijska i toplinska otpornost, zadovoljavajuća svojstva pri niskim temperaturama, povoljan odnos čvrstoća/masa, niska magnetna permeabilnost, nisu skloni povećanju zrna u zoni utjecaja topline itd. [1, 2]. Jedna od često primjenjivanih vrsta austenitnih nehrđajućih čelika je čelik AISI 321. Čelik AISI 321 pripada skupini titanom stabiliziranih nehrđajućih čelika. Stabilizacija titanom provodi se radi sprječavanja precipitacije karbida $Cr_{23}C_6$ odnosno povećanja otpornosti prema interkristalnoj koroziji [3].

Prilikom izloženosti nehrđajućih čelika visokotemperaturnim procesima (zavarivanje, toplinska obradba) može doći do promjene svojstava i mikrostrukture [4-7]. Stoga je kod odabira dodatnog materijala za zavarivanje nužno obratiti pozornost na postizanje odgovarajućeg sadržaja delta ferita u zoni taljenja radi postizanja zahtjevanih mehaničkih i korozijskih svojstava zavarenog spoja. Međutim, nekontrolirana prisutnost delta ferita predstavlja osnovu za pogoršanje mehaničkih svojstava i korozijske otpornosti zone taljenja, pogotovo ukoliko je čelik duže izložen djelovanju povišenih temperatura.

Nastanak nepovoljne mikrostrukture čeličnih materijala bitno utječe na trajnost, odnosno ″životni vijek″ ugrađenih komponenti [8]. Često tijekom uporabe austenitnih nehrđajućih čelika može doći do neočekivanih prijeloma. Zato je nužno poznavati fraktografsku analizu prijelomnih površina nakon ispitivanja mehaničkih svojstava zavarenog spoja. U ovom radu prikazani su rezultati fraktografske analize prijelomnih površina nakon ispitivanja vlačne čvrstoće i udarne radnje loma osnovnog materijala i zone taljenja čelika AISI 321.

2. EKSPERIMENTALNI DIO

Lim dimenzija 300x300x10 od austenitnog nehrđajućeg čelika AISI 321 pripremljen je u obliku V-spoja za zavarivanje ručnim elektrolučnim (REL) postupkom te postupkom s netaljivom elektrodom pod zaštitom plina (TIG). Zavarivanje korijena provedeno je TIG postupkom uz primjenu Böhler FOX SAS 2-A elektrode promjera 3,2 mm. Popuna je ostvarena REL postupkom uz primjenu Böhler FOX SAS 2-IG elektrode promjera 2,4 mm. U tablicama 1 i 2 naveden je kemijski sastav osnovnog i dodatnog materijala korištenog za zavarivanje. Dodatni materijal (elektroda) odgovara po kemijskom sastavu osnovnom materijalu. Glavni legirajući elementi austenitnog nehrđajućeg čelika AISI 321 su krom, nikal i titan.

Tablica 1. Kemijski sastav osnovnog materijala, mas.%.

C	Mn	Si	Cu	V	Mo	Al	Cr	Ni	Ti	Co	Nb
0,04	1,48	0,39	0,41	0,08	0,36	0,014	17,40	9,59	0,28	0,15	0,013

Tablica 2. Kemijski sastav Böhlerovih elektroda, mas.%.

Vrsta elektrode	C	Si	Mn	Cr	Ni
FOX SAS 2-A	0,03	0,8	0,8	19,5	10,0
FOX SAS 2-IG	0,03	0,5	1,8	19,8	10,2

Ispitivanje mehaničkih svojstava provedeno je na kidalici INSTRON tip 1196 pri sobnoj temperaturi. Uzorci za ispitivanje mehaničkih svojstava (vlačna čvrstoća, udarna radnja loma) pripremljeni su prema norni DIN 50125:2004 sa suženim dijelom u zoni taljenja. Ispitivanje udarne radnje loma provedeno je Charpy metodom na standardnim uzorcima (10x10x55 mm, V-zarez dubine 2 mm) kod sobne temperature. Nakon ispitivanja mehaničkih svojstava provedena je analiza prijelomnih površina pretražnim elektronskim mikroskopom (SEM) JEOL JSM 5610 opremljenim energetsko disperzijskim spektrometrom (EDS).

3. REZULTATI I RASPRAVA

Budući da TIG i REL postupci zavarivanja spadaju u postupke zavarivanja taljenjem tijekom zavarivanja u zoni taljenja dolazi do miješanja osnovnog i dodatnog materijala (elektrode). Poznato je da mikrostruktura određuje većinu mehaničkih, fizikalnih i kemijskih svojstava. Tijekom zavarivanja i žarenja dolazi, zbog temperaturnog i kemijskog gradijenta, do nastajanja nehomogene strukture koja je gotovo uvijek metastabilna u temperaturnim uvjetima primjene te bitno utječe na svojstva čelika.

Rezultati ispitivanja mehaničkih svojstava osnovnog materijala i zone taljenja čelika AISI 321 navedeni su u tablici 3. Usporede li se vrijednosti vlačne čvrstoće može se primijetiti da se zavarivanjem dobila zona taljenja s 33,5 N/mm^2 višom vlačnom čvrstoćom od osnovnog materijala (593,0 N/mm^2). Nasuprot tome osnovni materijal karakterizira izrazito visoka udarna radnja loma (222,2 J). Navedena razlika u mehaničkim svojstvima proizlazi iz kemijskog sastava te mikrostrukture nastale nakon taljenja i ponovnog skrućivanja područja zone taljenja.

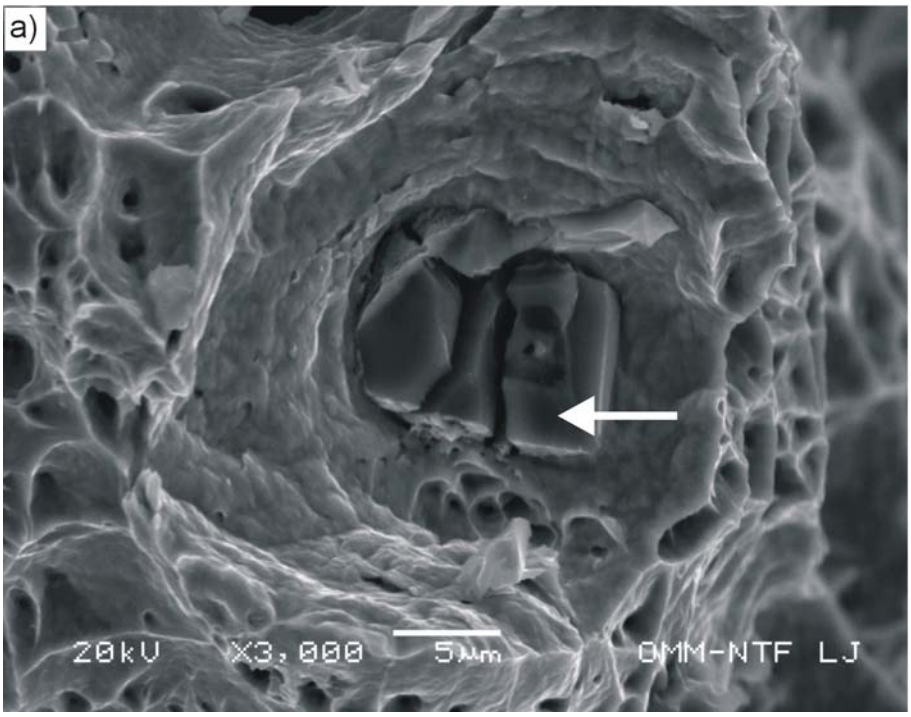
Tablica 3. Mehanička svojstva osnovnog materijala i zone taljenja čelika AISI 321.

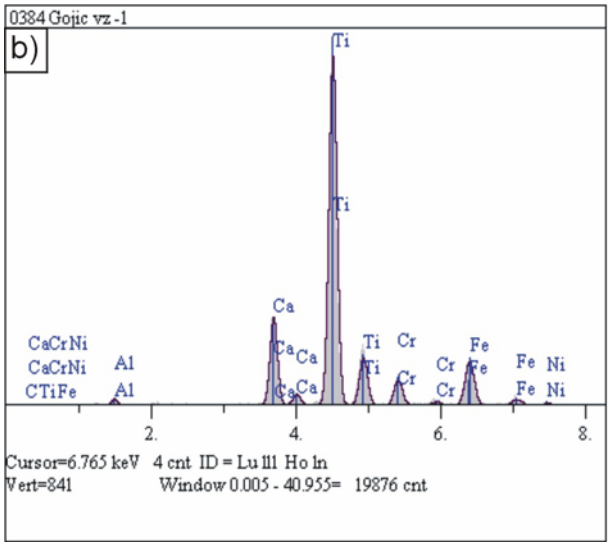
	Vlačna čvrstoća, N/mm^2	Udarna radnja loma, J
Osnovni materijal	593,0	222,0
Zona taljenja	626,5	122,3

Ispitivanje prijelomnih površina provedeno je na ostacima uzoraka dobivenim nakon ispitivanja vlačne čvrstoće i udarne radnje loma. Iz snimljenih mikrofraktografija vidljivo je da nakon ispitivanja mehaničkih svojstava na prijelomnim površinama osnovnog materijala i zone taljenja čelika AISI 321 uglavnom prevladava sitnojamičasta duktilna morfologija uz prisutnost čestica i uključaka u nastalim jamicama (slika 1 i 2). Nastanak sitnojamičaste morfologije usko je povezan s izrazito visokom vrijednosti udarne radnje loma osnovnog materijala (222 J) ali i zone taljenja (122,3 J). Također, na prijelomnim površinama mjestimično se mogu uočiti područja krhkog transkristalnog prijeloma (slika 3). Analizom

prijelomnih površina može se uočiti da je prijelom najčešće započinjao na međupovršini Ti-čestica/metalna osnova (slike 1, 3 i 4).

EDS analiza prijelomnih površina pokazala je da su Ti-čestice uglavnom sadržavale 49-68%Ti, 7-16%Cr, 15-21%Fe te oko 1%Ni i 2%V. Primijećeno je da osim na Ti-česticama prijelom započinje i na međupovršini Mn-uključak/metalna osnova (slika 2). EDS analizom utvrđeno je da se Mn-uključci sastoje uglavnom od 43%Mn, 23%Fe, 22%Cr, 6%Ti, 3%Ni i 1%Si.

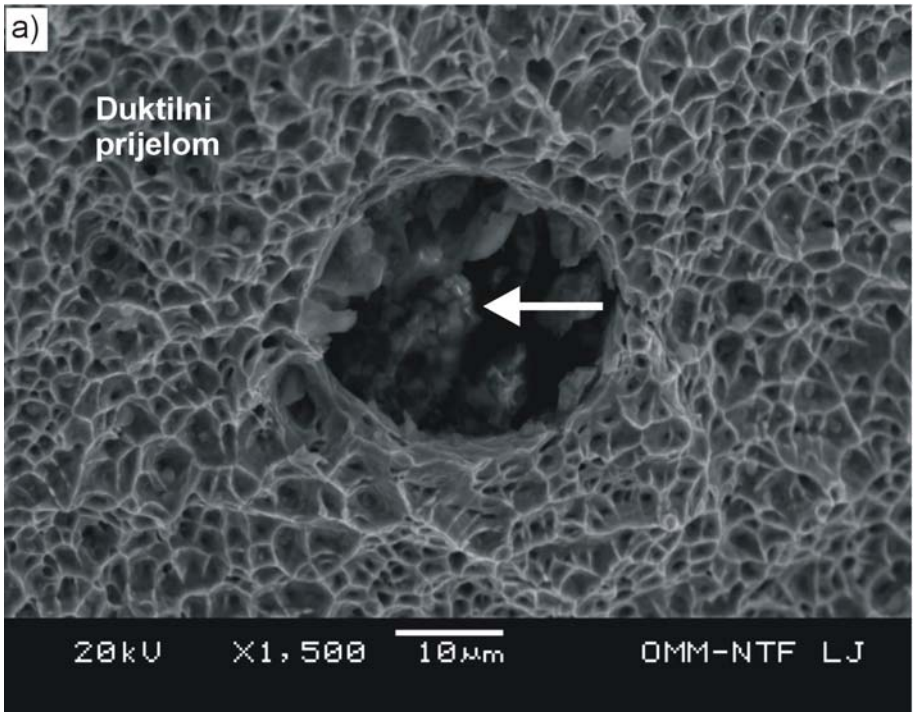


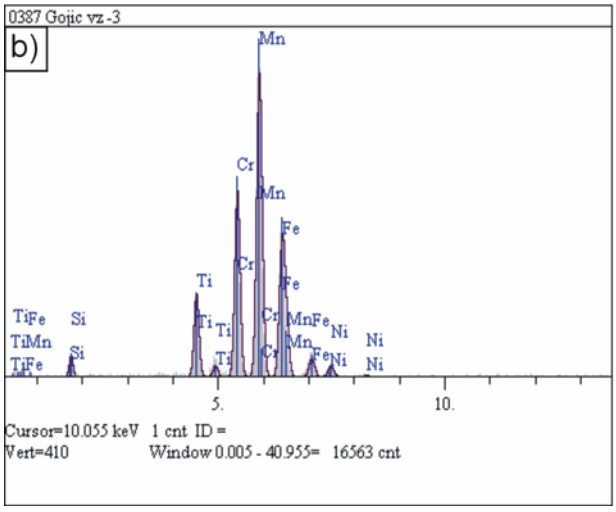


Elt.	Line	Intensity (c/s)	Error 2-sig	Atomic %	Conc		
C	Ka	0.00	0.000	0.000	0.000	wt.%	
Al	Ka	7.05	1.187	1.438	0.805	wt.%	
Ca	Ka	125.18	5.002	11.671	9.704	wt.%	
Ti	Ka	535.55	10.347	64.625	64.178	wt.%	
Cr	Ka	41.76	2.889	6.737	7.267	wt.%	
Fe	Ka	76.46	3.910	14.613	16.931	wt.%	
Ni	Ka	3.78	0.869	0.915	1.115	wt.%	
				100.000	100.000	wt.%	Total

kV	20.0
Takeoff Angle	35.0°
Elapsed Livetime	20.0

Slika 1. SEM mikrofraktografija (a) i EDS spektar Ti-čestice na prijelomnoj površini osnovnog materijala AISI 321 nakon ispitivanja vlačne čvrstoće; povećanje: 3000X

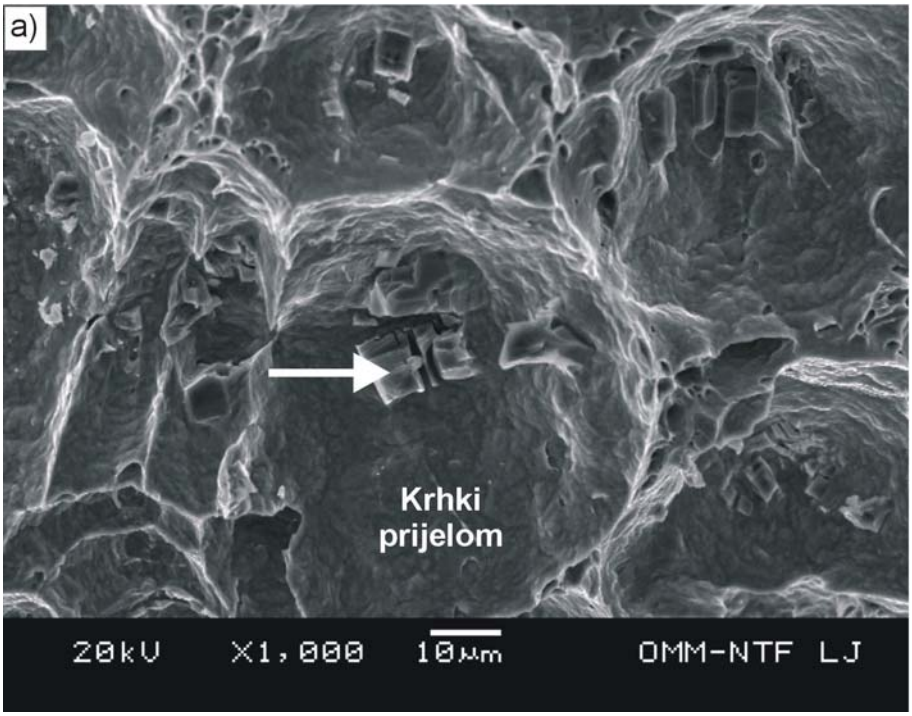


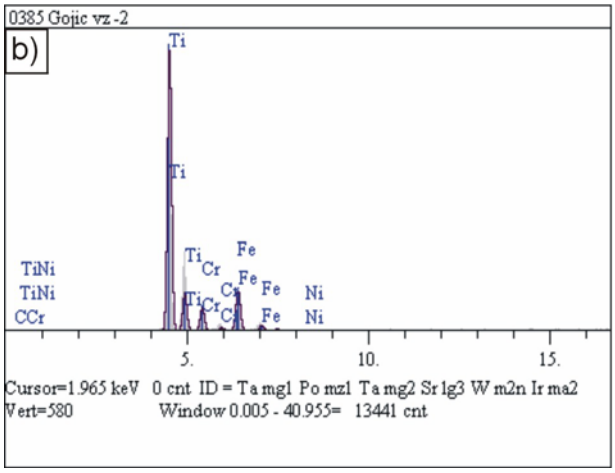


Elt.	Line	Intensity (c/s)	Error 2-sig	Atomic %	Conc		
C	Ka	0.00	0.000	0.000	0.000	wt.%	
Si	Ka	13.05	1.615	2.672	1.407	wt.%	
Ti	Ka	67.36	3.670	7.345	6.592	wt.%	
Cr	Ka	160.89	5.672	22.954	22.379	wt.%	
Mn	Ka	256.03	7.155	41.675	42.929	wt.%	
Fe	Ka	119.49	4.888	22.644	23.711	wt.%	
Ni	Ka	10.31	1.436	2.710	2.982	wt.%	
				100.000	100.000	wt.%	Total

kV	20.0
Takeoff Angle	35.0°
Elapsed Livetime	20.0

Slika 2. SEM mikrofraktografija (a) i EDS spektar Mn-uključka na prijelomnoj površini zone taljenja čelika AISI 321 nakon ispitivanja vlačne čvrstoće;
povećanje: 1500X

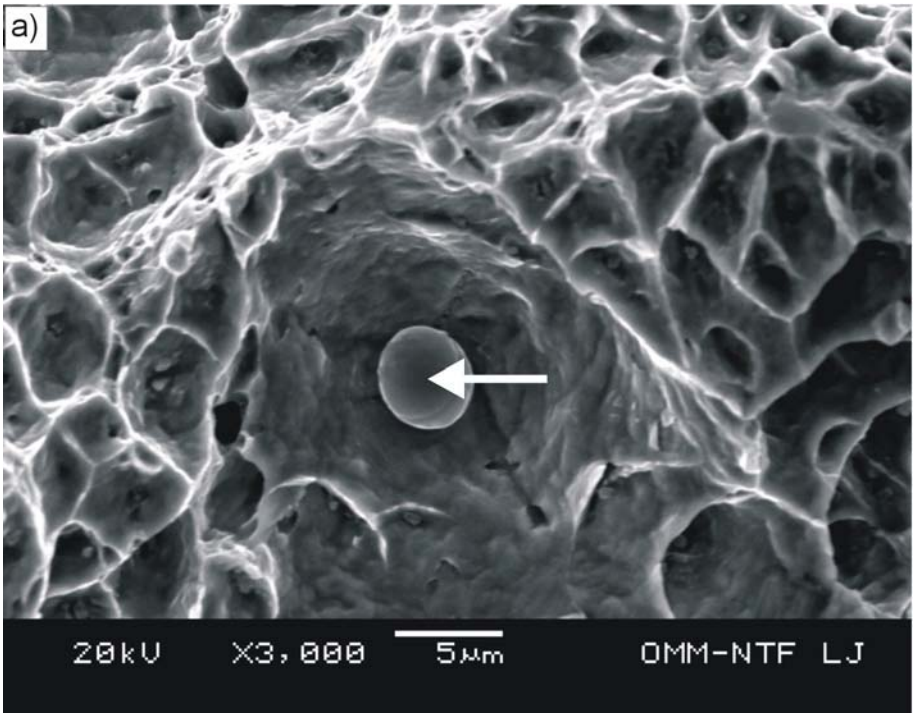


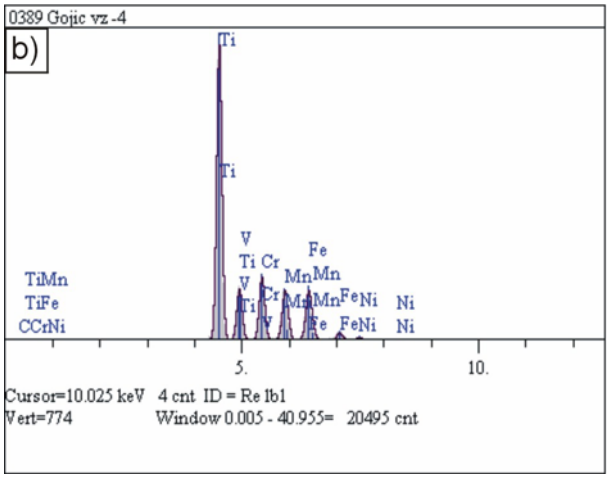


Elt.	Line	Intensity (c/s)	Error 2-sig	Atomic %	Conc		
C	Ka	0.00	0.000	0.000	0.000	wt.%	
Ti	Ka	380.51	8.723	70.940	68.077	wt.%	
Cr	Ka	34.40	2.623	8.803	9.176	wt.%	
Fe	Ka	62.24	3.528	19.077	21.359	wt.%	
Ni	Ka	3.02	0.776	1.180	1.388	wt.%	
				100.000	100.000	wt.%	Total

kV	20.0
Takeoff Angle	35.0°
Elapsed Livetime	20.0

Slika 3. SEM mikrofraktografija (a) i EDS spektar Ti-čestice na prijelomnoj površini osnovnog materijala AISI 321 nakon ispitivanja udarne radnje loma (223 J); povećanje: 1000X





Elt.	Line	Intensity (c/s)	Error 2-sig	Atomic %	Conc		
C	Ka	0.00	0.000	0.000	0.000	wt.%	
Ti	Ka	510.80	10.105	52.907	49.815	wt.%	
V	Ka	19.21	1.960	2.133	2.137	wt.%	
Cr	Ka	112.59	4.744	15.659	16.016	wt.%	
Mn	Ka	81.42	4.034	12.412	13.414	wt.%	
Fe	Ka	91.61	4.279	15.726	17.275	wt.%	
Ni	Ka	5.23	1.023	1.163	1.343	wt.%	
				100.000	100.000	wt.%	Total

kV	20.0
Takeoff Angle	35.0°
Elapsed Livetime	20.0

Slika 4. SEM mikrofraktografija (a) i EDS spektar Ti-čestice na prijelomnoj površini zone taljenja čelika AISI 321 nakon ispitivanja udarne radnje loma (128 J);
povećanje: 3000X

4. ZAKLJUČCI

Na temelju provedenih istraživanja mehaničkih svojstava (vlačna čvrstoća i udarna radnja loma) te analize prijelomnih površina osnovnog materijala i zone taljenja austenitnog nehrđajućeg čelika AISI 321 može se zaključiti slijedeće:

- Kombinacijom TIG i REL postupaka zavarivanja dobila se zona taljenja s višom vlačnom čvrstoćom i nižom žilavošću od osnovnog materijala. Udarna radnja loma osnovnog materijala je za 100 J veća od udarne radnje loma zone taljenja .
- Prijelomne površine osnovnog materijala i zone taljenja karakterizira primarno sitnojamičasti duktilni prijelom. Analizom prijelomnih površina uočeno je da prijelom najčešće započinje na međupovršini Ti-čestica/metalna osnova te na međupovršini Mn-uključak/metalna osnova.
- EDS analiza je pokazala da su Ti-čestice uglavnom sadržavale 49-68%Ti, 7-16%Cr, 15-21%Fe te oko 1%Ni i 2%V. Mn-uključci sadržavali su najčešće 43%Mn, 23%Fe, 22%Cr, 6%Ti, 3%Ni i 1%Si.
- Također, analizom prijelomnih površina mjestimično su zapažena i područja transkristalnog krhkog prijeloma koja su karakterizirana ravnim plohama.

5. LITERATURA

1. S. Kožuh, M. Gojić, *Zavarivanje* **49** (2006) 5, str. 177-185.
2. R. A. Lula, Stainless steel, American Society for Metals, Metals Park, Ohio, 1986.
3. T. Thorvaldsson, G. L. Dunlop, *Metal Science* **14** (1980), str. 513-518.
4. M. Sireesha, S. K. Albert, S. Sundaresan, *Materials Science and Technology* **19** (2003) 10, str. 1411-1417.
5. M. Gojić, L. Kosec, P. Škraba, D. Pinotić, Mikrostrukturna svojstva dupleks nehrđajućeg čelika nakon zavarivanja, Proceedings International Conference Joining of Corrosion Resistant Materials, HDTZ, Opatija, 2003, str. 205-212.
6. U. K. Mudali, R. K. Dayal, *Materials Science and Technology* **16** (2000) 4, str. 393-398.
7. K. Guan, X. Xu, H. Xu, Z. Wang, *Nuclear Engineering and Design* **235** (2005), str. 2485-2494.
8. J. C. Lippold, D. J. Kotecki, Welding Metallurgy and Weldability of Stainless Steels, John Wiley&Sons, New Jersey, 2005.

EROZIJSKO TROŠENJE NODULARNOG LIJEVA ČELIČNIM KUGLICAMA

EROSION OF DUCTILE CAST IRON WITH STEEL BALLS

Krešimir Grilec, Suzana Jakovljević, Božidar Maslać
Faculty of Mechanical Engineering and Naval Architecture, Ivana Lučića 5, Zagreb

Stručni članak / Professional paper

Sažetak: Erozija česticama je gubitak materijala s površine krutog tijela zbog relativnog gibanja (strujanja) fluida u kojem se nalaze krute čestice. Erozija kod koje je strujanje pod malim kutom u odnosu na površinu (manjim od 30°) naziva se abrazivna erozija, a kad čestice udaraju o površinu gotovo okomito (60° do 90°) to je udarna erozija.
Jedna od prednosti nodularnog lijeva u odnosu na druge ljevove je njegova dobra otpornost na trošenje. Ipak treba imati na umu da ta otpornost ovisi i o uvjetima trošenja. Kad se govori o otpornosti na erozijsko trošenje krutim česticama, ta otpornost značajno ovisi o kutu udara čestica. U ovom radu ispitivana je otpornost na erozijsko trošenje pri dva kuta upada čestica (15 i 90°) te dvije veličine čeličnih kuglica.
Ključne riječi: otpornost na erozijsko trošenje, nodularni lijev, abrazivna erozija, udarna erozija

Abstract: Particle erosion is a wear loss from surface of solid body caused by a relative motion of fluid with solid particles. When impact angle is low (between 0° and 30°) this kind of erosion is called the abrasive erosion. On the other side, if the impact angle is between 60° and 90°, it is considered the impact erosion.
One of the advantages of ductile cast iron in relation to other cast irons is his good wear resistance. However, we must consider that wear resistance depends on wear conditions. Solid particle erosion resistance is a function of an impact angle. In this paper, samples of ductile cast iron were eroded with steel balls of two different sizes at two different angles of impact (15° and 90°).
Key words: erosion resistance, ductile cast iron, abrasive erosion, impact erosion

1. UVOD

Nodularni lijev je ljevačka pseudobinarna slitina željeza i ugljika, koji se pretežnim dijelom izlučio u kuglastom obliku, [1].

Približni kemijski sastav lijeva prema [2] iznosi: 3,2…3,8 %C, 2,4…2,8 %Si, < 0,5 % Mn, < 0,045 % P i < 0,01 %Si.

Kemijski sastav nodularnog lijeva razlikuje se od sivog lijeva po tome što sadrži veći postotak ugljika i silicija, ali i magnezija (ili cerija) tako da se grafit izlučuje u obliku kuglica. Osim toga, sadržaj sumpora je znatno niži nego kod sivog lijeva. Metalna osnova u lijevanom stanju može biti monofazna: feritna i perlitna te dvofazna feritno-perlitna.

Legiranjem ili toplinskom obradom mogu se postići i druge strukture. Nodularni lijev je materijal koji osvaja tržište i zamjenjuje druge ljevove na bazi željeza. Nodularni lijev ima mnogo veću čvrstoću nego sivi lijev, ali mu nedostaje sposobnost prigušivanja vibracija i obradivost sivog lijeva. Mehanička svojstva su mu između čeličnog i sivog lijeva: bolje se obrađuje od čelika, ima bolju sposobnost prigušivanja i bolja ljevačka svojstva od čelika. Najvažnija primjena nodularnog lijeva je za izradu cjevovoda za vodu i kanalizaciju. Nadalje, nodularni lijev se između ostalog koristi za izradu auto komponenti, u industrijskim postrojenjima, klima uređajima, vjetroelektranama itd.

2. EROZIJA ČESTICAMA

Erozija česticama je gubitak materijala s površine krutog tijela zbog relativnog gibanja (strujanja) fluida u kojem se nalaze krute čestice. Od velike je važnosti kut pod kojim čestice udaraju o površinu. Erozija kod koje je strujanje pod malim kutom u odnosu na površinu naziva se abrazivna erozija, a kad čestice udaraju o površinu gotovo okomito to je udarna erozija, [3].

Valja napomenuti da je erozija česticama različita od ostalih vrsta erozije, tj. erozije fluidima i kavitacijske erozije. Razlog tome leži u činjenici da je vremenski period kontakta između erozivne čestice i materijala jako kratak, što eroziju česticama čini potpuno drugačijim procesom od abrazije i adhezije gdje je kontakt između reaktivnih površina relativno konstantan.

3. EKSPERIMENTALNI DIO

Uzorci nodularnog lijeva izliveni su u brodogradilištu Brodosplit u Splitu.

3.1. Kemijska analiza

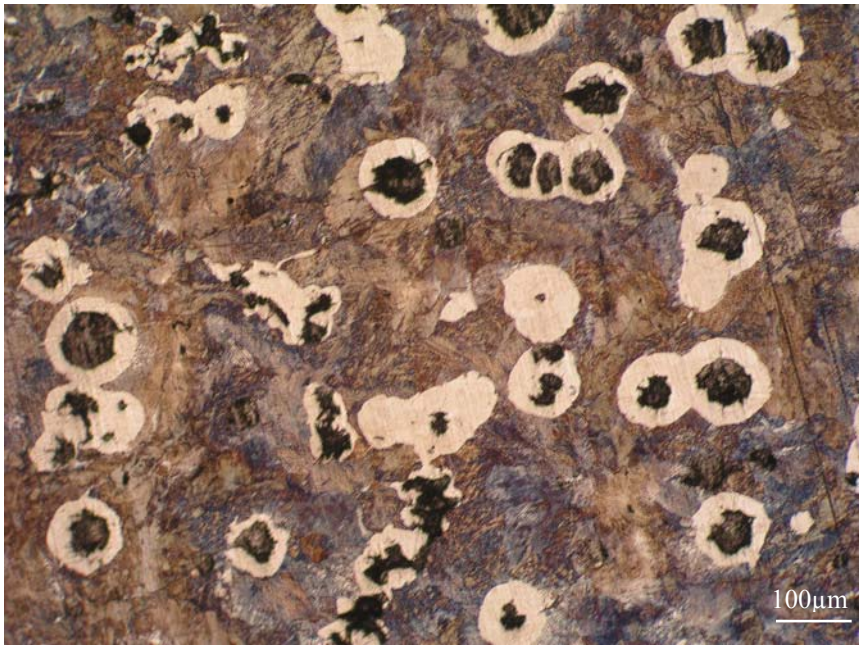
Uzorci za kemijsku analizu su izrezani iz odljevka te analizirani u Laboratoriju za analizu metala Fakulteta strojarstva i brodogradnje. Nakon analize dobiveni su sljedeći rezultati:

Tablica 1 – Kemijski sastav uzorka

	Maseni udjeli, %								
	C	Si	Mn	P	S	Cu	Ni	Mo	Mg
Nodularni lijev	2,34	2,72	0,72	0,054	0,011	1,14	0,095	0,016	0,033

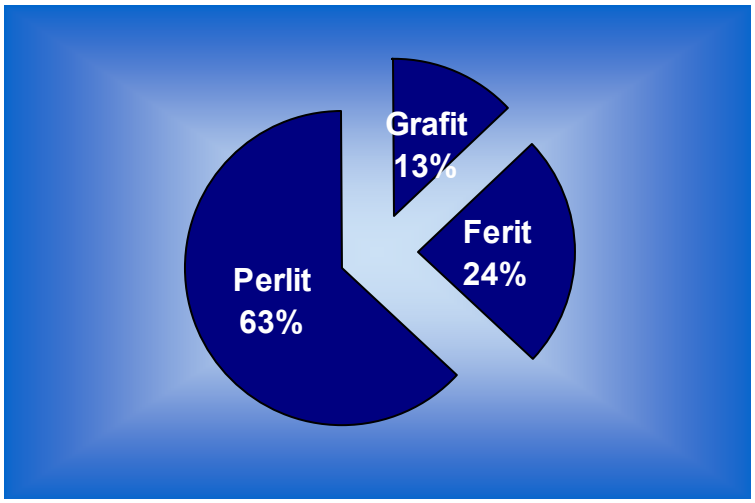
3.2. Metalografska analiza

Metalografska analiza provedena je u Laboratoriju za materijalografiju Fakulteta strojarstva i brodogradnje u Zagrebu. Na slici 1 vidljive su nodule grafita u feritno-perlitnoj matrici.



Slika 1 – Mikrostruktura nodularnog lijeva

Kao što se vidi na slici 2, u matrici prevladava perlitna struktura.



Slika 2 - Volumni udio pojedinih faza u uzorku

3.3. Ispitivanje tvrdoće

Mjerenje tvrdoće provedeno je u Laboratoriju za ispitivanje mehanička svojstva Fakulteta strojarstva i brodogradnje. Za mjerenje je korištena Brinell metoda s opterećenjem od 1840N te kuglica promjera 2,5 mm. U tablici 2 su prikazani dobiveni rezultati.

Tablica 2. Tvrdoća po Brinell-u HB 2,5/1840

X.	d, mm	HB
1.	1,00	229
2.	0,97	244
3.	0,99	234
4.	1,01	224
5.	1,00	229
srednja vrijednost	0,994	228

3.4. Ispitivanje otpornosti na erozijsko trošenje

Ispitivanje otpornosti na erozijsko trošenje provedeno je u Laboratoriju za tribologiju Fakulteta strojarstva i brodogradnje u Zagrebu. Uređaj za ispitivanje je prikazan na slici 3, a detalj ispitivanja na slici 4



Slika 3 – Uređaj za ispitivanje otpornosti na eroziju



Slika 4 – Ispitivanje otpornosti na erozijsko trošenje

Parametri ispitivanja:

- Abraziv: čelične kuglice srednjih promjera 700μm i 1100μm
- Brzina vrtnje: 1440 okr/min
- Vrijeme trajanja ispitivanja: 13min 53 sec
- Broj udara uzorka u mlaz kuglica: ~20000
- Kutovi udara uzorka u mlaz kuglica: 15°, 90°
- Dimenzije uzorka: 18×18×18 mm
- Broj uzoraka: 3

Gubici mase su dani u tablicama 3 i 4, posebno za svaku veličinu sačme.

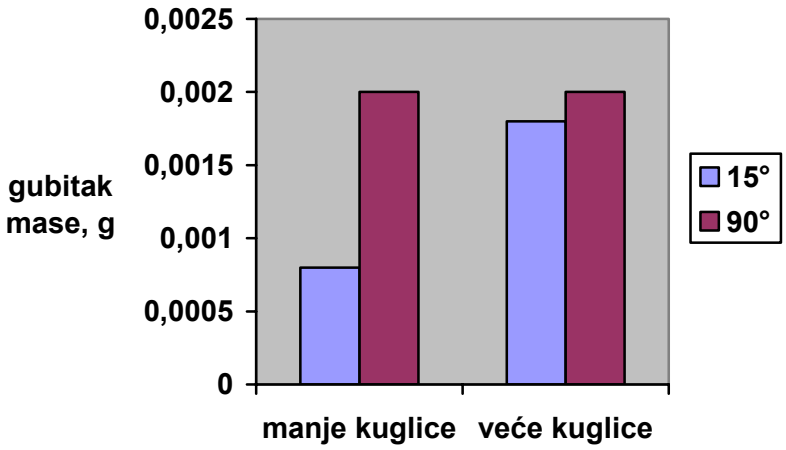
Tablica 3 - Gubitak mase ovisno o kutu upada čestica za manju sačmu (ϕ700μm)

Kut upada	Uzorak 1	Uzorak 2	Uzorak 3	Prosječni gubitak mase
	gubitak mase [g]			
15°	0,0008	0,0008	0,0008	0,0008
90°	0,0022	0,0018	0,0020	0,0020

Tablica 4 - Gubitak mase ovisno o kutu upada čestica za veću sačmu (ϕ1100μm)

Kut upada	Uzorak 1	Uzorak 2	Uzorak 3	Prosječni gubitak mase
	gubitak mase [g]			
15°	0,0032	0,0014	0,0010	0,0018
90°	0,0017	0,0016	0,0028	0,0020

Na slici 5 prikazane su srednje vrijednosti gubitaka mase ovisno o kutu upada čeličnih kuglica i njihovoj veličini.



Slika 5 - Gubitak mase ovisno o kutu upada kuglica i njihovoj veličini

Erozija kod koje je strujanje pod malim kutom u odnosu na površinu (manjim od 30°) naziva se abrazivna erozija, a kad čestice udaraju o površinu gotovo okomito (60° do 90°) to je udarna erozija. Tablica 3 i 4 te slika 5 pokazuju da nodularni lijev ima bolju otpornost na abrazivnu nego na udarnu eroziju. To je posebno izraženo kod manjih kuglica (ϕ 700μm).

4. ZAKLJUČAK

Jedna od prednosti nodularnog lijeva u odnosu na ostale željezne ljevove je njegova dobra otpornost na trošenje. Pri tome treba imati na umu da otpornost na trošenje ovisi o uvjetima trošenja. Otpornost na eroziju česticama ovisi o kutu upada čestica. Rezultati ispitivanja pokazuju da nodularni lijev ima bolju otpornost na abrazivnu nego na udarnu eroziju.

LITERATURA

[1] M. Novosel, D. Krumes: "Željezni materijali, I. dio: Lijevovi", Strojarski fakultet u Slavonskom Brodu, Slavonski Brod, 1994.
[2] T. Filetin, F. Kovačiček, J. Indof: "Svojstva i primjena materijala", Fakultet strojarstva I brodogradnje u Zagrebu, Zagreb, 2002.
[3] V. Ivušić: "Tribologija", Hrvatsko društvo za materijale i tribologiju, Zagreb, 2002.

ISPITIVANJE APSORPCIJE ENERGIJE UDARA ALUMINIJSKE PJENE

EXPERIMENTAL STUDY OF IMPACT ENERGY ABSORPTION IN ALUMINIUM FOAM

Krešimir Grilec, Pero Previšić, Gojko Marić
Faculty of Mechanical Engineering and Naval Architecture, Ivana Lučića 5, Zagreb

Izvorni znanstveni rad / Original scientific paper

Sažetak: Pjene općenito, kao i aluminijske pjene imaju mnoga povoljna svojstva zahvaljujući njihovoj poroznoj strukturi što ih čini pogodnima za brojne primjene. Mogućnost apsorpcije energije udara je jedno od najzanimljivijih uporabnih svojstava pjena. Primjena lakih poroznih materijala visoke čvrstoće u transportnoj industriji je sve zanimljivija u pogledu povećanja sigurnosti. Aluminijske pjene se sve češće koriste kao različiti apsorberi kinetičke energije (odbojnici automobila, vlakova, tramvaja). U ovom radu istraživan je utjecaj kemijskog sastava, gustoće i oblika aluminijske pjene na apsorbiranu energiju udara.

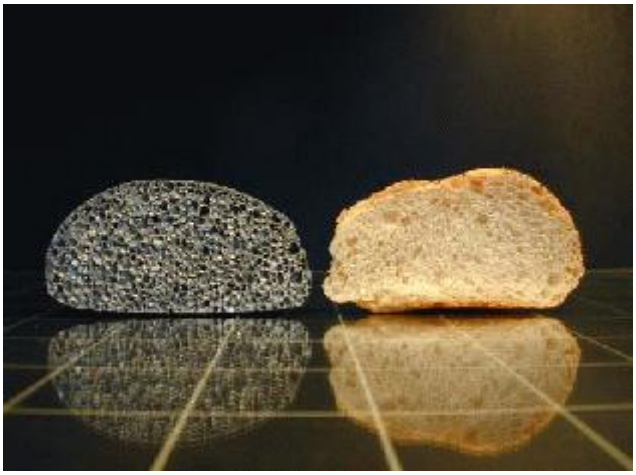
Ključne riječi: aluminijska pjena, apsorpcija energije udara, tlačno ispitivanje

Abstract: Foamed materials in general, and aluminium foams in particular, demonstrate a number of interesting properties due to their porous structure, which makes them usable in a wide range of applications. Possibility of absorbing the energy of impact is one of the most interesting properties of foams. The use of lightweight porous materials with high specific strength has attracted much interest in the transportation industry in order to improve safety. Recently, foamed aluminium is frequently used in various absorbers of kinetic energy (buffers of automobiles, trains, trams). This paper studies the influence of chemical composition, density and shape of aluminium foams on absorbing the energy of impact.

Keywords: aluminium foam, absorption of impact energy, compression test

1. UVOD

Priroda stvara ćelijaste materijale, kao što su npr. drvo, kamen, koralj i sl. čija su svojstva optimalno prilagođena okolnim uvjetima, [1]. Metalne pjene su pokušaj oponašanja takvih građa i struktura za tehničke uvjete primjene. To su porozni metalni materijali ispunjeni šupljinama (ćelijama) koje mogu varirati po obliku (otvorene, zatvorene) i veličini. Na slici 1 prikazana je usporedba metalne pjene i kruha.



Slika 1 - Usporedba metalne pjene i kruha (HMI Berlin) [2]

Metalne pjene mogu se proizvesti iz gotovo svih vrsta metala koji postoje u obliku praha, no zbog ranog stadija istraživanja komercijalno su danas najčešće dostupne metalne pjene na bazi aluminija (Al) i nikla (Ni). Po posebnoj narudžbi proizvode se i pjene na bazi magnezija (Mg), olova (Pb), cinka (Zn), bakra (Cu), bronce, titana (Ti), čelika pa čak i zlata (Au), [1]

Osnovna svojstva metalnih pjena su:

- niska gustoća (masa),
- relativno visoka krutost,
- dobra izolacijska svojstva (zvuk, toplina),
- negorivost,
- odlična apsorpcija energije udara itd.

2. APSORPCIJA ENERGIJE UDARA

Primjena lakih poroznih materijala visoke čvrstoće u transportnoj industriji je sve zanimljivija u pogledu povećanja sigurnosti, [3]. Aluminijske pjene se sve češće koriste kao različiti apsorberi kinetičke energije (odbojnici automobila, vlakova, tramvaja) [4]

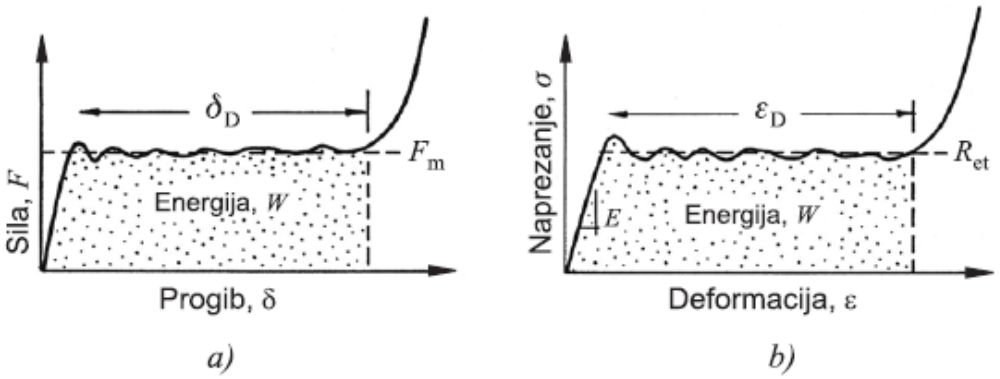
Apsorpcija energije udara po jedinici volumena (W) može se prikazati sljedećom relacijom:

$$W = \int_0^{\varepsilon} \sigma(\varepsilon) d\varepsilon$$

Gdje je:

W – apsorbirana energija udara po jedinici volumena (MJ/mm^3)
ili (N/mm^2)
σ – tlačno naprezanje (N/mm^2)
ε – deformacija (%)

Tu je bitno da granica stlačivanja (R_{et}) bude tek nešto manja od naprezanja pri kojem dolazi do loma materijala, odnosno do dosizanja kritične deformacije zgušnjavanja (ε_D). Površina ispod krivulje R_{et} – ε_D pokazuje kolika se količina energije udara može apsorbirati (slika 2).



Slika 2 - Krivulje koje prikazuju apsorpciju energije pri savijanju a) i tlaku b), [1]

3. EKSPERIMENTALNI DIO

U radu su ispitivane dvije vrste aluminijskih pjena sa zatvorenim ćelijama:

- ALULIGHT AlSi 10 TiH_2 -0,8
- ALULIGHT AlMgSi 0,6 TiH_2 -0,4

Tehnologija korištena za izradu uzoraka je plinom oslobođene čestice rastvorene u polučvrstoj fazi. Korištena je elektrootporna peć snage 2,5 kW koja se nalazi u Laboratoriju za nemetale, Fakulteta strojarstva i brodogradnje u Zagrebu.

Slika 3 prikazuje uzorke aluminijskih pjena.



Slika 3 - Uzorci aluminijskih pjena različite gustoće i materijala stjenke

Tablica 1 - Uzorci aluminijskih pjena različitih gustoća i dimenzija

Naziv	**450 MAT CIL**	**600 MAT CIL**	**900 MAT CIL**	**450 SJAJ CIL**	**600 SJAJ CIL**	**900 SJAJ CIL**
Dimenzije uzorka (mm)	Ø84,9×100					
Materijal	ALULIGHT AlSi 10 TiH2 - 0,8			ALULIGHT AlMgSi 0,6 TiH2 - 0,4		
Masa (kg)	0,45	0,60	0,90	0,45	0,60	0,90
Gustoća (g/cm^3)	0,80	1,06	1,60	0,80	1,06	1,60
Naziv	**450 MAT**	**600 MAT**	**900 MAT**	**450 SJAJ**	**600 SJAJ**	**900 SJAJ**
Dimenzije uzorka (mm)	76×76×100					
Materijal	ALULIGHT AlSi 10 TiH2 - 0,8			ALULIGHT AlMgSi 0,6 TiH2 - 0,4		
Masa (kg)	0,45	0,60	0,90	0,45	0,60	0,90
Gustoća (g/cm^3)	0,78	1,04	1,56	0,78	1,04	1,56

Ispitivanje je provedeno u Laboratoriju za ispitivanje mehaničkih svojstva na Fakultetu strojarstva i brodogradnje u Zagrebu. Za ispitivanje se koristila kidalica marke WPM, model EU 40 mod., maksimalne tlačne sila od 400 kN. Brzina ispitivanja iznosila je 6 mm/min. Slika 4 prikazuje kidalicu na kojoj je vršeno ispitivanje (statički tlačni pokus).



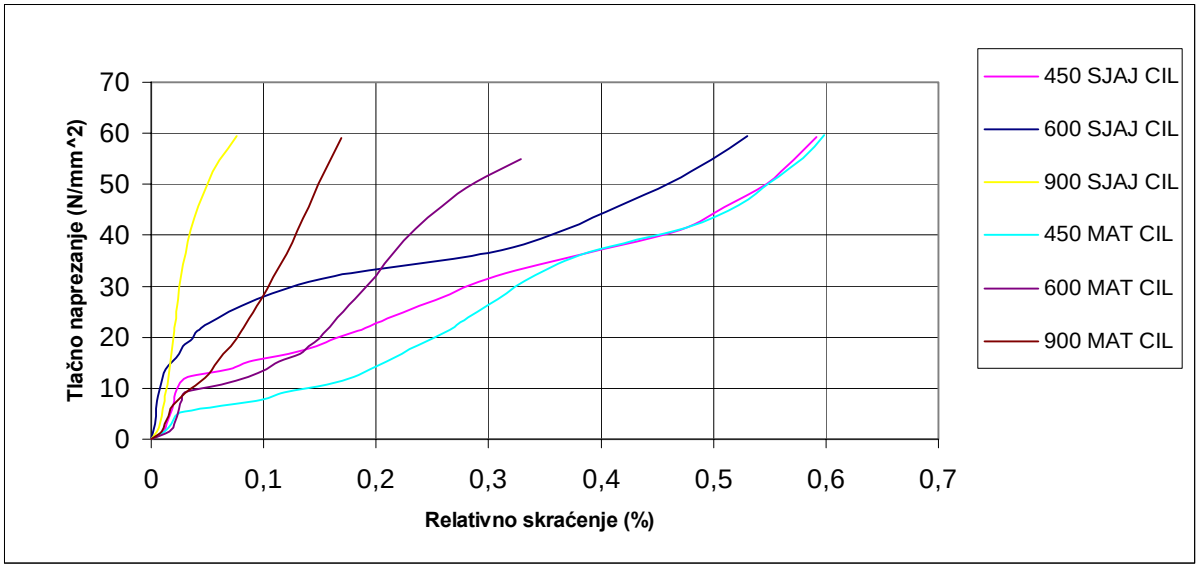
Slika 4 - Kidalica na kojoj je vršeno ispitivanje

Na slici 5 prikazan je tijek ispitivanja uzorka.

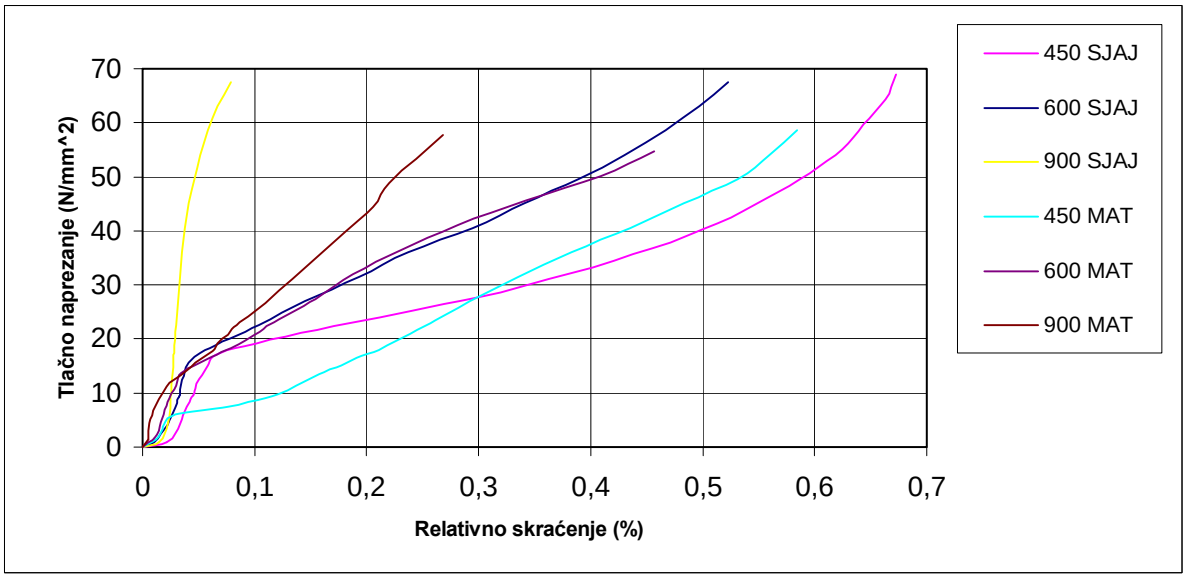


Slika 5 – Ispitivanje uzoraka

Na slikama 6 i 7 prikazani su dobiveni dijagrami „tlačno naprezanje – relativno skraćenje“.

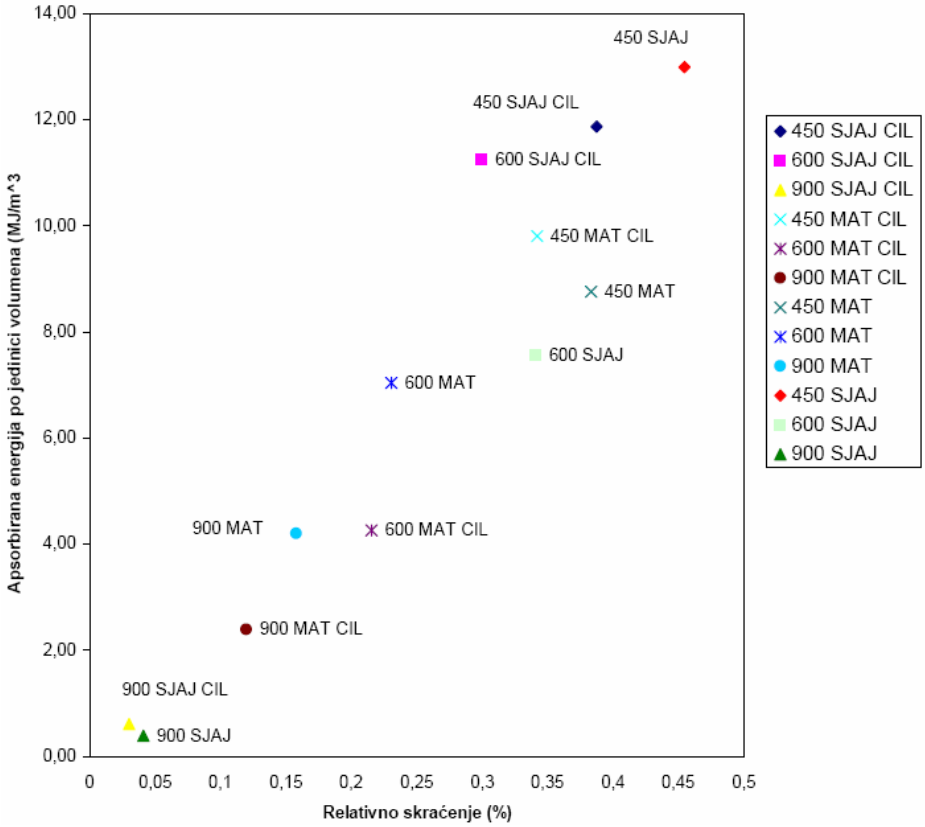


Slika 6 - Dijagram „tlačno naprezanje – relativno skraćenje“ za uzorke kružnog poprečnog presjeka



Slika 7 - Dijagram „tlačno naprezanje – relativno skraćenje“ za uzorke kvadratnog poprečnog presjeka

Kako bi se usporedili dobiveni rezultati za različite uzorke, na slici 8 prikazana je ovisnost apsorbiranog rada po jedinici volumena i relativnog skraćenja.



Slika 8 - Apsorbirani rad po jedinici volumena pri tlačnoj sili od 200 kN

4. ZAKLJUČAK

Statičkim tlačnim pokusom utvrđeno je da aluminijske pjene imaju dobra svojstva pri apsorpciji energije udara. Pri statičkom tlačnom pokusu niti jedan uzorak nije imao istaknutu fazu deformacije pri konstantnom tlaku. Ustanovljeno je da pjene niže gustoće mogu apsorbirati više energije uz veće relativno skraćenje. Pri nižim gustoćama ALULIGHT AlMgSi 0,6 TiH_2 - 0.4 pjena može apsorbirati više energije uz veće relativno skraćenje od ALULIGHT AlSi 10 TiH_2 – 0,8 pjene iste gustoće. Također ALULIGHT AlMgSi 0,6 TiH_2 - 0.4 pjena ima bolju iskoristivost energije udara od ALULIGHT AlSi 10 TiH_2 – 0,8 pjene. Prema dobivenim rezultatima nema značajnijeg utjecaja oblika poprečnog presjeka.

LITERATURA

[1] T. Filetin, I. Kramer, G Marić: "Metalne pjene", Hrvatsko Društvo za materijale i tribologiju, Zagreb, 2003.

[2] "On the road again: metal foams find favor", http://www.hmi.de/people/banhart/A-Journals/a064_banhart2002.pdf

[3] S:Y: Kim, B.Y. Hur, K.C. Kwon, S.H. Cho, C.Y. Lim, Y.M. Yoo, M.H. Lee: "Mechanical and sound absorption properties of closed cell Al foam by pot furnace method", International Conference on Cellular Metals and Metal Foaming Technology METFOAM 2003, Berlin

[4] V.I. Lebedev, V.I. Komov, D.A. Andreev: "Ability of constructions from foamed aluminium to absorb different konds of energy", International Conference on Cellular Metals and Metal Foaming Technology METFOAM 2003, Berlin

mr. Lutvo Haznadarević
V. prof. dr. Jusuf Kevelj
Univerzitet “Džemal Bijedić”
Mašinski fakultet u Mostaru

PRELIMAINARNA ISTRAŽIVANJA TEMPERATURNIH POLJA LEGURA TITANA

Prethodno priopćenje / Preliminary note

SAŽETAK

Generisana toplotna energija, locirana u relativno uskom podrižučju zone rezanja, dovodi do pojave visokih temperatura koje uslovljavaju različite fizičko-kemijske promjene u zoni rezanja. Visoke temperature pri obradi brušenjem titanovih legura, koje karakterišu trenutno postizanje maksimalnih vrijednosti sa kratkotrajnim dejstvom, imaju izrazito štetno dejstvo na karakteristike kvaliteta obrađene površine obratka i stanje radne površine tocila. Ovome treba dodati i dimenzionalne graške, što sve skupa može bitno da smanji eksploataciona svojstva gotovog dijela.
Ključne riječi: toplotna energija, brušenje, titan, naprezanje

ABSTRACT

Generated thermal energy, located in relatively small cutting area, brings to the instance of high temperatures which are the cause of the different physical and chemical change in the cutting area. High temperatures during the Titanium alloys grinding process are extremely harmful on the quality characteristics of the product grinding area and on the condition of the grindstone, desktop and these high temperatures are the cause of the instant achievement of the maximum values with the short time period of duration.

Dimensional mistakes are needed to be added here, and all these things together can significantly reduce exploitative characteristics of the made part.

Key words: thermal energy, grinding, Titanium, strain

1. UVOD

Temperatura brušenja je termodinamička veličina toplotnog stanja procesa brušenja, koja označava stepen zagrijanosti pojedinih tačaka u zoni kontakta brusa sa obratkom. U općem slučaju temperatura brušenja θ je funkcija jačine toplotnog izvora q, vremena djelovanja toplotnog izvora t, toplotno-fizičkih karakteristika elemenata obradnog sistema $\lambda\rho c$ i prostornih koordinata x, y, i z, odnosno:

$$\theta = f(q,\, t,\, \lambda\rho c,\, x,\, y,\, z)$$

Vrijednosti temperatura svih tačaka u zoni kontakta brusa sa obratkom u datom vremenskom trenutku, definišu temperaturno polje zone rezanja, izotermnu površinu i temperaturni gradijent. Izotermnu površinu čine sve tačke sa istom temperaturom dok je temperaturni gradijent najveća promjena temperature u pravcu normalnom na izotermnu površinu. Velika količina toplotne energije koja iz zone rezanja odlazi u obradak, može u

površinskom sloju materijala obratka izazvati niz nepoželjnih termičkih defekata. Usljed periodičnog dejstva visokih temperatura, sa velikim brzinama zagrijavanja i hlađenja, u površinskom sloju obratka pojavljuju se: promjene mikrostrukture, mikrotvrdoće, zaostali naponi, mikropukotine i mjestimično nagorjele površine. Da bi se odredilo temperaturno polje u površinskom sloju materijala obratka, mjere se temperature u obratku za različito odstojanje mjerne tačke od kontaktne površine brusa i obratka. Uz temperaturu pogodno je mjeriti i sile brušenja kako bi se na osnovu istih definisao tačan položaj promjene temperature u odnosu na kontaktnu površinu. Koristeći tako dobivene dijagrame promjene temperature i sila brušenja, njihovom sistematizacijom dobija se promjena temperature u zoni kontakta sa vremenom za različito odstojanje mjerne tačke od površine obratka. Promjena temperatura u zoni kontakta sa vremenom, izmjerene na različitom mjestu unutar površinskog sloja obratka, ilustruju izgled temperaturnog polja zone rezanja. Uzimajući u obzir trenutak ulaska brusa u zahvat, dimenzije i brzinu kretanja obratka, može preko vremenske promjene temperature modelirati temperaturno polje zone rezanja. Dobivene zakonitosti promjene temperature po dubini površinskog sloja materijala obratka potvrđuju karakteristike parametara toplotnog izvora, tj. utjecaja elemenata režima obrade na temperaturu brušenja.

Vidi se da veća dubina rezanja, prvenstveno zbog povećanja jačine toplotnog izvora, izrazito povećava kontaktnu temperaturu brušenja, a time i dubina toplotnog opterećenja površinskog sloja obratka. Suprotno, veća brzina obratka, zbog manjeg vremena djelovanja ukupnog toplotnog izvora na materijal obratka, smanjuje kontaktnu temperaturu brušenja i ujednačuje toplotno opterećenje površinskog sloja obratka.

2. DEFINISANJE PARAMETARA BRUŠENJA TITANA

2.1. Predmet obrade

Za definisanje temperatura brušenja korištena je legura titana TA6V, koja sve više ima komercijalnu primjenu zbog:

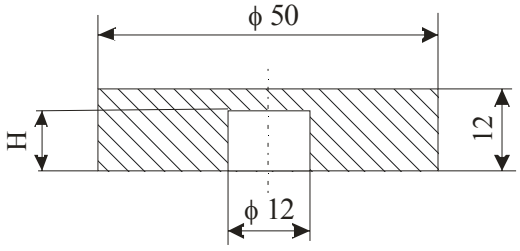
- Mala specifična težina (između aluminijuma i čelika),
- Velika mehanička otpornost, naročito za legure, udružena sa dobrim osobinama pri zamaranju,
- Otpornost na koroziju u velikom broju medija, itd.

Tabela 1.

Mehaničke i fizičke osobine		
Istezanje $\sigma_{0,2}$ (daN/mm^2)	Istezanje σ_{max} (daN/mm^2)	Gustina ρ (g/cm^3)
92	105	4,505

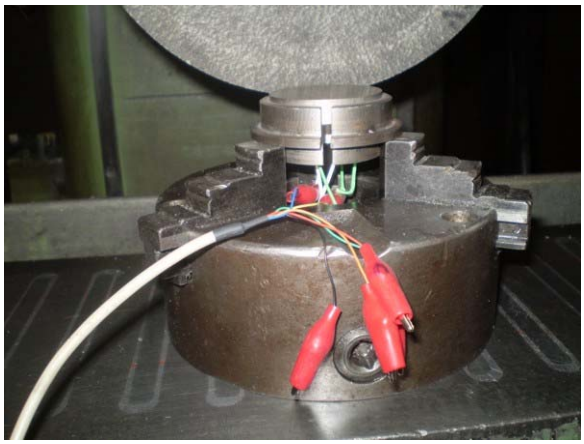
Tabela 2.

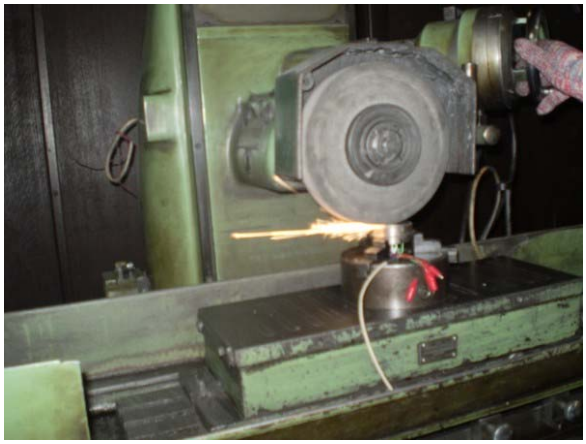
Hemijski sastav TA6V								
%	C	Fe	Al	V	H	N	O	Ti
Od			5,5	3,5				
do	0,08	0,25	7	4,5	0,01	0,07	0,2	ostatak



Slika 1. Izgled epruvete

2.2. Radno mjesto (slika 2 i 3)





Opiti su vršeni na stroju za ravno brušenje:

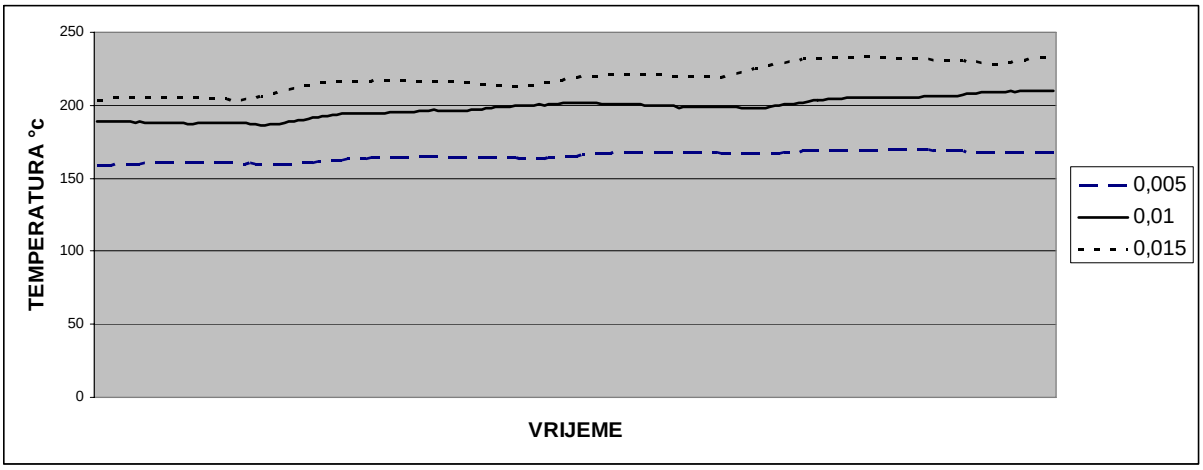
- Radni napon ..... 220/380 $[V]$,
- Maksimalna brzina stola ..... $v_R = 18\left[\frac{m}{\min}\right]$,
- Prečnik brusa ..... $D = 250\,[mm]$
- Broj obrtaja brusa ..... $3000\left[\frac{o}{\min}\right]$,
- Snaga elektromotora ..... 2,2 $[kW]$,
- Prenos pomoćnog kretanja - ..... hidraulički.

Alat korišten pri izvođenju opita je koturasti brus proizvođač SWATY – Maribor, mjere brusa 250x76x35, kvalitete B46J6V.

3. REZULTATI MJERENJA

r.b.	epruveta br. 5 δ=0,005 mm	epruveta br. 9 δ=0,01 mm	epruveta br. 3 δ=0,015 mm
	Temperatura u °C		
1.	169,5286	205,1981	231,6636
2.	169,5286	205,1981	231,6636
3.	169,5286	206,0985	231,5534
4.	169,3301	206,2986	231,333
5.	169,0324	206,0985	231,1127
6.	168,834	206,0985	231,1127
7.	168,7348	206,1985	231,1127
8.	168,6355	206,2986	231,0026
9.	168,6355	206,2986	230,8924
10.	168,5363	206,3987	230,6721
11.	168,4371	206,899	230,4518
12.	168,2387	207,5996	230,2315
13.	168,2387	207,9999	230,2315
14.	168,2387	208,4003	229,5707
15.	168,2387	208,5005	228,91
16.	168,0403	208,8008	228,5797
17.	167,9411	208,9009	228,3595
18.	167,8419	209,2013	228,2494
19.	167,8419	209,3014	228,4696
20.	167,8419	209,3014	228,7999
21.	167,7427	209,6018	229,0201
22.	167,7427	209,3014	229,5707
23.	167,7427	209,6018	230,3417
24.	167,7427	209,4015	230,8924
25.	167,7427	209,7019	231,333
26.	167,7427	210,0023	231,9941
27.	167,6435	210,2026	232,7654
28.	167,6435	210,1025	233,096
29.	167,6435	210,2026	233,647
30.	167,6435	210,3028	233,9777

$H = 9\,[mm]; v_R = 3\left[\frac{m}{\min}\right]$



Slika 4. Zapis vrijednosti temperatura za $H = 9\,[mm]$; $v_R = 3\left[\frac{m}{\min}\right]$

4. ZAKLJUČAK

- Obrada titanove legure brušenjem je otežana zbog loše toplotne provodljivosti, kao i zbrog relativno velike duktilnosti (titan je mehak, lijepi se na radnoj površini brusa), te zbog tvrdog oksidnog sloja koji nastaje dužim stajanjem na zraku.
- Promjena temperatura u zoni kontakta sa vremenom, izmjerene na različitom mjestu unutar površinskog sloja obratka, ilustruju izgled temperaturnog polja zone rezanja. Uzimajući u obzir trenutak ulaska brusa u zahvat, dimenzije i brzinu kretanja obratka, može se preko vremenske promjene temperature modelirati temperaturno polje zone rezanja.
- Pri brušenju titana većim dubinama, a relativno niskim brzinama predmeta obrade primjećena su spaljena mjesta (što se objašnjava lošom toplotnom provodljivosti titana). Primjena mekših bruseva od upotrijebljenih bi vjerovatno dala bolje rezultate.

5. LITERATURA

[1] Cebalo R.: *Optimalno područje brušenja u puno vatrootpornih Ni-legura za plinske turbine*, disertacija, FSB, Zagreb, 1985.
[2] Ekinović S.: *Obrada rezanjem*, Dom štampe, Zenica, 2001.
[3] Cebalo R.: *Possibility of Comparison and Application of Conventional and Creep Feed Grinding*, ICPR 4th International Conferance of Prodiuction Research, Tokio, 1977.
[4] Jovičevič M.: *Osvrt na istraživanja procesa obrade brušenjem*, Saopštenje IAMA, br. 18, 1973.
[5] Šavar Š.: *Obrada odvajanjem čestica*, II. dio, Sveučilišna naklada Liber, Zagreb, 1987.
[6] Bajić N.: *Identifikacija parametrov brušenja za adaptivno krmiljenje*, Doktorska disertacija, Ljubljana, 1986.
[7] Zirojević Lj.: *Termodinamski aspekti primjene rashladnog sredstva pri izradi alata za obradu rezanjem visokoučinskim brušenjem*, Doktorska disertacija, Mostar, 1982.
[8] Haznadarević L.: *Optimalno područje brušenja titanovih legura*, 3rd International Conference on Computer Aided Design and Manufacturing CADAM 2005, September 27th – October 1st 2005, Supetar – Brač, Croatia.

INFLUENCE OF ARTILLERY WEAPON BARREL SUPERHEAT ON EROSION WEAR RESISTANCE OF MATERIAL

doc. dr. sc. Mirko Jakopčić
Croatian Defence Academy ''Petar Zrinski"
Ilica 256 B, 10000 Zagreb, Croatia
e-mail: mjakopc@yahoo.com

doc. dr. sc. Krešimir Grilec
Faculty of Mechanical Engineering and Naval Architecture, University of Zagreb, Ivana Lučića 5, 10000 Zagreb, Croatia
e-mail: kgrilec@fsb.hr

Izvorni znanstveni rad / Original scientific paper

Keywords: weapon barrel, fire rate, superheat, erosion

ABSTRACT

This paper researches the influence of the artillery weapon barrel superheat on the change of erosion wear resistance of material.

A great quantity of the powder gasses evolves by the weapon firing in the weapon barrel. The temperature of these gasses reaches up to 3800 K, and their maximum pressure is up to 6000 bar. The powder gasses have a compound chemical composition, so they make a very aggressive atmosphere in relation to the barrel material. At the same time, the powder gasses contain the solid particles too: the soot particles and the unburned powder grains. These particles are moving by great speed in the strong turbulent streaming of the powder gasses. In this way, the erosive wear of the barrel material appears on the bore surface. This is the erosive wear of material by the solid particles.

At the same time, the contact pressure on the rotating band and the barrel bore surfaces appears. It results with normal force effect on the contact surfaces, so a strong sliding friction force is generated on those surfaces. The sliding friction energy transforms to the heat energy too, so the barrel material heating is very intensive in such firing conditions. Therefore, the rate of fire is determined for every artillery weapon to keep the barrel heating on the allowed level.

The test samples production was based on the previous analysis of some weapon barrel materials. So, the erosion test samples are made of heat treated steel 42CrMo4. This steel has the similar chemical, metallographic and mechanical properties as the analysed weapon barrel steel.

The test samples were tempered at 600 °C, 700 °C, 800 °C and 900 °C, over a period of one hour, and then air cooled. It's the similar way of heating and cooling as the superheating and cooling of the barrel by intensive firing.

The wear resistance is represented by the sample mass loss after 15, 30, 45 and 60 minutes of erosion wear time. The test results represent that unheated samples have got the best wear resistance in comparison with the heated samples.

The wear resistance increases as many as 3,9 times if material was previously heated at 600 °C. The heating of material at 700 °C and 800 °C causes more intensive material wear. The significant material wear increase is shown in the samples which were heated at the 900 °C. The samples heated in this way represent as many as 17,5 times bigger material loss than unheated samples.

The test results show that adhering to the determined fire rate is very important: the exceeded fire causes the weapon barrel superheat, as well as the significant decrease of the material wear resistance.

1. INTRODUCTION

The firing process is a strong and dynamic process which takes place in the weapon barrel. During this process the powder burns intensively and a great quantity of the hot powder gasses evolves. The high pressure of the powder gasses enables the projectile movement to the barrel mouth. The projectile movement time through the barrel lasts about 0,01 second and in this time the projectile reaches the maximum muzzle velocity (v_0) of up to 1800 m/s [1].

The big heat quantity is developed by the powder burning, and both the powder gasses and the barrel material are heated by this heat energy. The powder gasses may be heated up to 3800 K, and their maximum pressure is up to 6000 bar [1], [2].The powder gasses have a compound chemical composition: they contain CO, CO_2, H_2O, H_2 and N_2, so they make a very aggressive atmosphere in relation to the barrel material.

At the same time, the powder gasses contain the solid particles too: the soot particles and the unburned powder grains. Because of the strong turbulent streaming of the pressed powder gasses, these particles are moving by the high speed in the barrel bore and hit the bore surface. In this way, the erosive barrel wear by the solid particles appears. Furthermore, because of very high speed, the particles are penetrated into the material surface and make the corrosion centres.

Therefore the many hitting directions of solid particles into the bore surface, both the abrasive and hitting erosion appears in the weapon barrel: the abrasive erosion is made by the particles which hit at the smaller angle to the surface, and the hitting erosion is made when the particles hit at the higher angle to the surface.

At the same time, the contact pressure between the both centring and rotating band of the projectile and the bore surface appears. The rotating band is cut into the grooved barrel profile. So, the high contact pressure as well as the strong sliding force appears on the contact surfaces between the projectile bands and the bore surface. The sliding friction energy transforms to the significant quantity of the heat energy too.

Total amount of heat developed by the powder burning and the projectile movement through the barrel bore heats the barrel material, from the bore surface layers to the barrel's outer surface. Because of high quantity of heat energy, the temperature of bore surface layers may reach up to several hundreds degrees Celsius and even up 1000°C [1]. This superheat may cause the change of the barrel material microstructure, as well as of its mechanical properties.

The barrel heating is not uniform during the transverse section: the bore surface is heated the most, but the material layers in the direction of the barrel's outer surface are colder. In this way, the outer layers of material don't enable the thermal dilatation of the inside warmer layers. So, thermal stress increases in the direction of the barrel bore surface. Finally, this stress may cause the appearance of surface micro cracks.

In accordance with all above mentioned, the firing process has a compound tribological effect on the weapon barrel: the mechanical, thermal and chemical processes affect the barrel. It is obvious that many wear mechanisms exist in the barrel in these conditions at the same time: the abrasion, the adhesion, the fatigue and the tribocorrosion [3], so that the increase of the barrel heat level probably changes the wear resistance of material.

This paper presents the procedure and the results of the erosion wear experiment. The barrel material of chosen artillery weapon was tested. A portion of test samples wasn't

tempered previously, but the others were tempered at 600°C, 700°C°, 800°C and 900°C and air cooled. It is similar to the superheating and cooling of the barrel by intensive firing.

The influence of the weapon barrel superheat on the erosion wear resistance of material will be shown by the analysis of the obtained experiment results.

2. TEST SAMPLES PREPARATION

The chemical composition analysis and the hardness measurement of material were done for barrel of some artillery weapons: the field gun, the antiaircraft gun and the mortar. It was established that the material of each barrel is one of quenched and tempered steels [3]. The test samples used for the research in this paper were made of soft annealed 42CrMo4 steel (Figure 1).

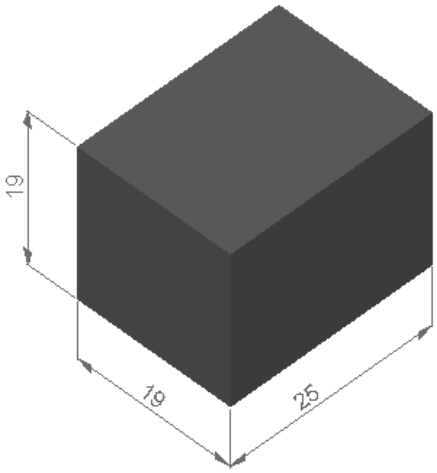


Figure 1. Test sample for erosion wear

The chemical composition of test samples is shown in Table 1.

Table 1. Chemical composition of test samples (42CrMo4)

Chemical composition (%)	C	Si	Mn	Cr	Ni	Mo
	0,41	0,20	0,75	1,05	-	0,23

The samples' surfaces have previously been ground and they have got N6 quality because the bore surface has the same machining quality [4]. The hardness of 32±2 HRC was measured on the weapon barrel bore [3]. To obtain this hardness, the samples were oil quenched at 860°C and tempered at 600°C for two hours [3], [5].

One of test samples was subsequently cross-sectioned and prepared for the metallographic recording. The cross-section surfaces were ground and polished previous to etching by NITAL. The metallographic recording of the quenched and tempered sample cross-section is shown in Figure 2.

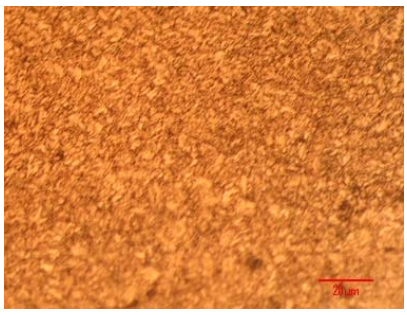


Figure 2. Metallographic recording of quenched and tempered sample (42CrMo4)

The homogeneous structure of the tempered martensite is seen in above figure.

The test samples were heated before the erosion wear by the solid particles. Therefore, four by four samples were tempered at 600°C, 700°C, 800°C and 900°C over a period of one hour and air cooled. These are the possible heating temperatures of the barrel bore surface which evolve by the intensive firing process, respectively when the allowed rate of fire is exceeded.

One sample of every tempered group was cold cross cut and prepared for the metallographic recording. The cross-sections of the samples were ground and polished and subsequently corroded by NITAL. The metallographic recordings of sample cross sections are shown in Figure 3.

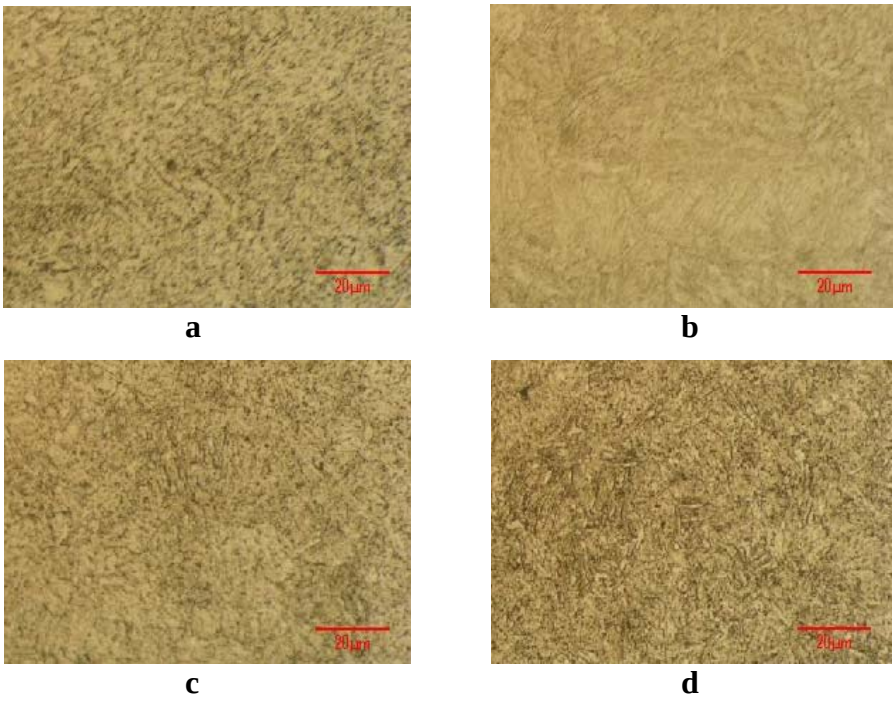


Figure 3. Metallographic recordings of tempered and air cooled test samples

a-sample tempered at 600°C, b-sample tempered at 700°C, c-sample tempered at 800°C, d-sample tempered at 900°C

The hardness was measured on the samples' surfaces and the means of the measuring results are shown in Table 2.

Table 2. Surface hardness of test samples

Temperature of previously heating (°C)	600	700	800	900
Mean hardness (HV1)	495	476	397	412

In accordance with the metallographic recordings (Fig. 3) and the values of measured hardness (Table 2), as well in accordance with CCT diagram of 42CrMo4 steel (Fig. 4), the structure of tempered martensite is kept by the material heating at 600°C and 700°C and air cooling.

The samples tempered at 800°C and 900°C maintain the uniform small-grained structure. However, with obtained hardness of about 400 HV1, the bainite may appear in

the micro structure of the test steel, as well as the ferrite-pearlite structure, along with the basic structure of martensite.

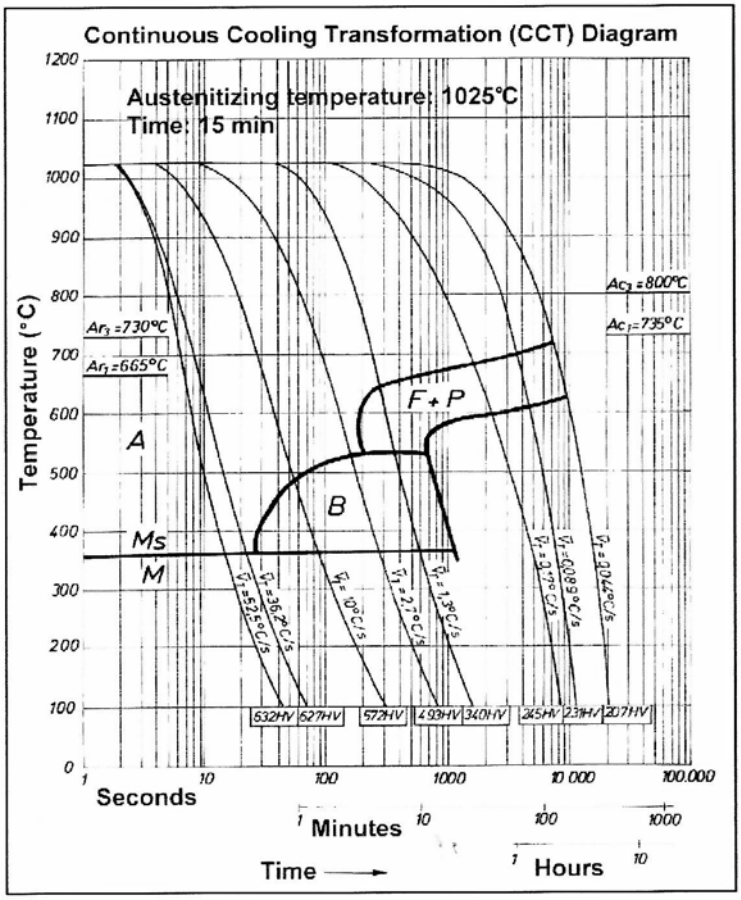


Figure 4. CCT diagram of 42CrMo4 steel [5]

Test samples were heat treated in the Laboratory for heat treating at the Faculty of Mechanical Engineering and Naval Architecture in Zagreb. Also, the samples were prepared for the metallographic recording and recorded in the Laboratory for Metallographic, and the tribological tests were performed in the Laboratory for Tribology at the same Faculty.

3. TESTING OF EROSIVE WEAR AND TEST RESULTS

The erosion wear of barrel material was tested. The quartz sand OTTAWA AFS 50/70 was used as erosive particles at the test equipment. The wear resistance is represented by the sample mass loss after 15, 30, 45 and 60 minutes wear time, at the rotational speed of the sample support of 1444 rpm.

The macro picture of the final worn surface is shown in Figure 5.



Figure 5. Sample surface after erosive wear

The wear track is well marked on the above figure.

Eight wear cycles were done for every level of previous sample tempering. The mean values of the measured mass loss are represented in Table 3.

Table 3. Mass loss (gr) in the erosion wear

Temperature of previous sample heating (°C)	Time of erosion wear (min)			
	15	30	45	60
	Mass loss (gr)			
Unheated sample [3]	0,0023	0,0042	0,0057	0,0087
600	0,0179	0,0235	0,0282	0,0340
700	0,0372	0,0431	0,0503	0,0565
800	0,0396	0,0473	0,0529	0,0581
900	0,0993	0,1314	0,1469	0,1528

The data in Table 3 shows that the heated samples have got the most significant mass loss in the first wear period. This appearance may probably be caused by the evolving of the ferric oxide layer on the sample surfaces by the heating. The ferric oxide is very brittle and very easy to wear.

The distribution of the samples' mass loss is represented in Figure 6.

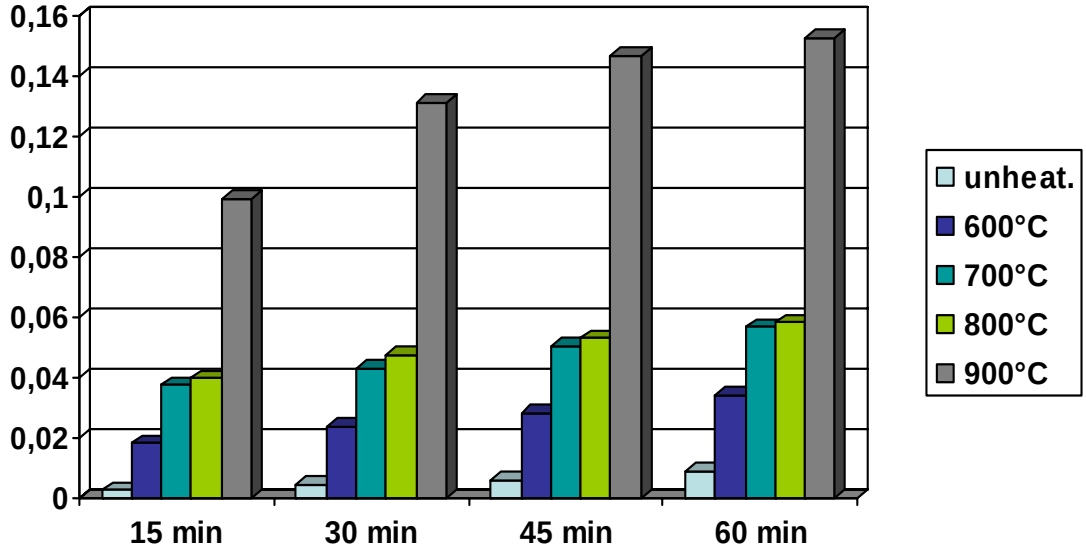


Figure 6. Distribution of samples' mass loss

The significant influence of the barrel superheat on the material wear increase is seen in Figure 6. Therefore, adhering to the determined firing rate is very important to prevent the barrel superheat and its consequent intensive wear.

4. CONCLUSIONS

This paper researches the influence of the weapon barrel superheat on the change of the material wear intensity by the particle erosion. The test samples were made of 42CrMo4 steel and quenched and tempered, to obtain the similar metallographic and mechanical properties as the weapon barrel steel. Before the testing, the samples were heated at 600ºC, 700ºC, 800ºC and 900ºC over a period of one hour and then air cooled. One group of previously unheated samples was also tested there.

The uniform structure of the tempered martensite was presented on the metallographic recordings of the samples. The measured hardness on the samples' cross-section surfaces is higher in the test samples which were tempered at 600ºC and 700ºC (495 HV1 and 476 HV1). Also, the hardness is lower in the samples tempered at 800ºC and 900ºC (397 HV1 and 412 HV1). In accordance with CTT diagram of 42CrMo4 steel, the portion of the bainite, as well as the portion of the ferite-perlite may be contained in the microstructure with the basic martensite.

The test results represent that unheated samples have got the best wear resistance in comparison with the heated samples. In comparison with the material loss of unheated samples, the material loss increases from 3,9 times if the samples were previously heated at 600ºC, up to as many as 17,5 times if the heating level was 900ºC.

These results have shown that the determined fire rate is very important to adhere to: the fire rate must not be exceeded, because it causes the weapon barrel superheat and significant decrease of the material wear resistance.

REFERENCES

[1] Jakopčić, M., 1999, "Temeljne značajke tribološkog procesa u cijevi topničkog oružja", Zbornik MATRIB '99, Trogir, p. 111-118.

[2] Viličić, J., Gajić, M., 1979, "Balistika", SSNO, Beograd.

[3] Jakopčić, M., 2002, "Otpornost na trošenje cijevi topničkih oružja", disertacija, Fakultet strojarstva i brodogradnje Sveučilista u Zagrebu, Zagreb.

[4] Pavelić, V., ‘’Specifične tehnologije u proizvodnji oružja’’, MORH, Zagreb.

[5] www.F:\Ravne\steels\vcmo135.html.

ADVANCED TECHNIQUES FOR UTILISATION OF ALUMINIUM FOAMS

Jaroslav Jerz, František Simančík, Roman Florek, Martin Nosko
Institute of Materials & Machine Mechanics SAS, Bratislava, Slovak Republic

Izvorni znanstveni rad / Original scientific paper

ABSTRACT

The unique approach to novel structural and functional applications of various aluminium foams has been presented in this contribution. Easy manufacturing of components using unconventional techniques can make the reinforced aluminium foams very attractive for various industrial applications, especially for light-weight stiff body structures of future cars, busses, trains, ships, aeroplanes, etc. and also for light and efficient heat exchangers integrated into the interior floor, wall and ceiling panels.

The metallic reinforcement can be either directly embedded during production of foamed component into its surface layer in places, where large tensile stress is anticipated, or pressed into the foam structure after foaming process. The reinforcement in both cases takes over the unacceptable tensile stresses while foamed matrix lends necessary stiffness.

Aluminium foam possesses simultaneously both very high thermal diffusivity due to high thermal conductivity of the cell walls and rather low overall thermal conductivity, controlled by total porosity. These properties allow reaching the uniform temperature within the foam structure during heating or cooling very quickly, without local overheating or overcooling even in quite large panels. Moreover, the heat can be transferred in or from the foam using tubes pressed-in to the foam by recently patented technique, whereas the foam in the vicinity of tube is compressed, thus allowing better heat transfer between the foam and tube and simultaneously improving mechanical fixing of tube in the structure. After impregnation of the foam by appropriate filler (plaster, polyurethane foam, etc.) the resulting light-weight panel can be used for the purpose of very efficient and cheap heat-exchanger. The foam contributes to quick heat spreading in the whole panel volume, giving very uniform temperature distribution, also if only relatively short length of heating/cooling tube is used. Low heat capacity allows quick response to temperature changes, thus saving the energy related to overheating.

The principles of utilisation aluminium foam have been described in this contribution as both light-weight stiff reinforced structural components and heat spreaders in various heating/cooling floor and ceiling panels. The comparison of this approach with conventional current solutions has been presented including the efficiency, cost, properties, design and further important issues.

Key words: aluminium foam, light-weight design, highly efficient heat-exchanger

INTRODUCTION

Foamed aluminium and its alloys have the best potential to be applied in various industrial applications in comparison with any other polymer, ceramic or metallic foams. There are several reasons supporting the fact that just foamed aluminium is the most perspective cellular structural material. It is first of all owing to low density and melting temperature, great stiffness, toughness and in particular sufficient corrosion endurance that aluminium is the most convenient metal for relatively low cost production of high porosity structure which can be successfully used also for structural purposes.

The performance of a structural component made of aluminium foam is limited by the properties of the alloy of which the foam is made and by the porous structure and shapes to which the foam can be foamed. Performance may mean strength for a given weight, for instance, or stiffness for minimum cost, or fatigue life, or thermal resistance, or safety, while meeting certain design requirements.

Performance of structural component is often limited by combination of material properties. For example the best material for a light, stiff tie (a tensile strut) is the one with the greatest value of the specific stiffness E/ρ (E is the Young's modulus and ρ is the density). In other modes of loading, the performance-maximising criterion can be more complicated [4]. The best material for a light stiff beam, for instance, is that with the largest value of $E^{1/2}/\rho$.

LIGHT-WEIGHT DESIGN USING ALUMINIUM FOAM

Nowadays, development of light-weight structural materials pays special attention to the field of aluminium foams, due to their unusual combination of high stiffness and low density, which cannot be effectively achieved by using of any conventional structural material (**Fig. 1**). However, insufficient ability of the foam to resist excessive tensile stresses in critically exposed surfaces of load-bearing components can initiate premature fracture of the component. That is why the foam is usually combined with bulk materials into sandwiches, foam-core castings, etc. The main role of the foam is to be a filler or space holder that increase inertial moments of initially hollow cross section. In order to use metallic foams for structural application the foamed component should have an own load-bearing ability, without need to combine them with relatively heavy and expensive bulk components. The using of aluminium foams partially reinforced by proper reinforcements (wires, meshes, stretched steel sheets, etc.) in the most exposed surface is the best approach how to extend the application potential of metallic foams for light-weight structural design.

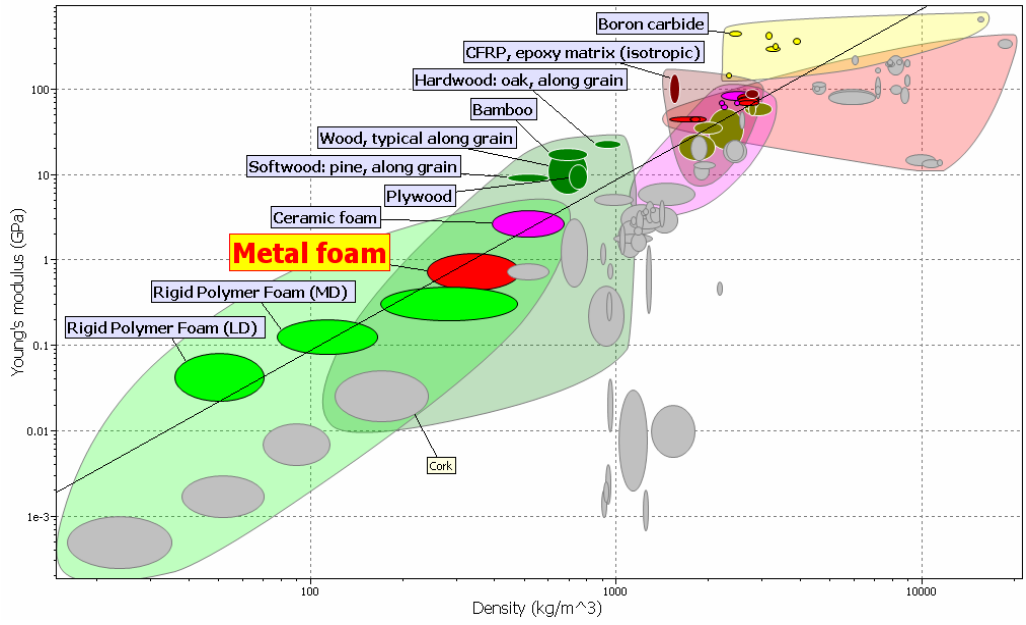


Figure 1 *A chart of Young`s Modulus vs. Density illustrating the selection of engineering materials for beam loaded in bending with high values of $E^{1/2}/\rho$. Contours of constant $E^{1/2}/\rho$ appear as a family of lines of slope 2. Materials with $E^{1/2}/\rho$ greater than a chosen value can be identified (Chart is created using CES EduPack 2007 software with the Level 1 database).*

MANUFACTURING OF ALUMINIUM FOAM

Two foaming methods are the most appropriate for production of foamed aluminium components characterized by large application potential in various industrial fields:

1. The most promising method for production of near-net-shaped structural components containing a dense aluminium surface skin and porous inner foamed aluminium structure is powder metallurgical route (**Alulight**®), which comprises foaming of the solid precursor prepared by hot extrusion of powdered aluminium with admixed powder of foaming agent (TiH_2), whereas the pore forming hydrogen is evolved during melting of this precursor. This method enable the production of light-weight structural components with partially reinforced tensile loaded surface by various metallic or ceramic stiffeners in the form of nets, perforated sheets or wires woven into the grids. There are two principally different foaming techniques for production of reinforced foamed aluminium components for structural applications by foaming of the precursor prepared by powder-metallurgical route. The first one is based on foaming in the mould and the second unique technique [12] comprises the low pressure casting process, by which the melted aluminium foam is injected by piston into the cavity of the foaming mould (**Fig. 2**).
2. Different principle is used at the method for manufacturing of aluminium foams with trade name **ALPORAS®**, where aluminium melt mixed together with foaming agent is foamed. Melt viscosity is firstly increased by calcium addition and subsequently the gases are released as a result of thermal decomposition of added foaming agent forming the pores in the melt. This process was developed by Shinko Wire Company, Amagasaki, Japan. The entire foaming process can last 15 minutes for a typical batch 2400 × 700 × 450 mm^3 with the weight about 180 kg. The panels, plates and other products can be obtained by sawing of these large blocks. Densities of these products (after cutting off continuous surface layer of the block) vary between 0.18 – 0.24 g/cm^3 and pore size is in the range ~ 2 - 10 mm.

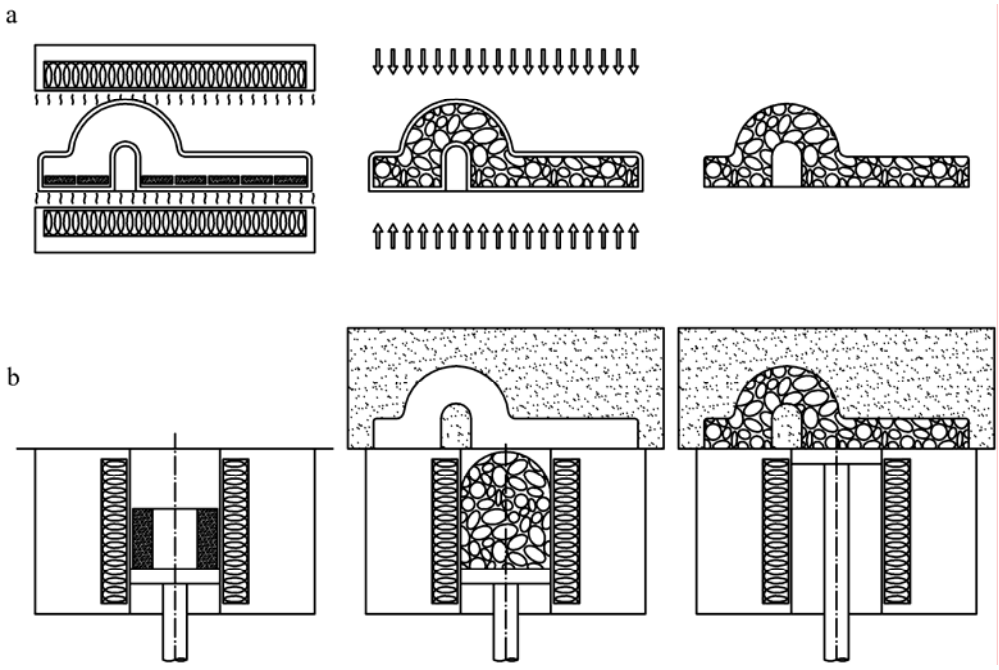


Figure 2 *Powder-metallurgical method of aluminium foam manufacturing by: (a) foaming of foamable precursor in the mould, (b) low pressure casting of melted aluminium foam.*

STRUCTURAL APPLICATIONS OF ALUMINIUM FOAM

Filling of hollow cavities with metallic foam improves the mechanical properties (resistance against buckling, torsion, transversal compression), enhances ability to absorb crash energy, protects the cavity from dirt and moisture contamination and reduces the noise and vibration of structural parts. Contemporary approved applications in the automotive industry include various motor carriers, suspension parts, body frame stiffeners (**Fig. 3**), etc. The utilisation of aluminium foam for stiffening of welded components enables cost effective stiffening of existing components for small series application submitted to increased loading (e.g. heavier engines, off-road condition etc.). In this case the foamed part is inserted into the component before welding without significant changes in a common technological process.



a b c

Figure 3 Structural applications of PM prepared aluminium foams: (a) suspension part and (b) hollow aluminium profile of car frame reinforced with aluminium foam insert; (c) aluminium foam panel reinforced with expanded stainless steel sheet.

Powder-metallurgically prepared aluminium foams are always covered by dense skin, which significantly improves the mechanical properties. However the natural skin of foamed components sometimes contains small holes or even cracks. These inevitable defects can initiate premature fracture of the foam, especially when they appear on the tensile loaded surface of foamed part. Reinforcement of tensile loaded surface skin with metallic or ceramic wires or fibres woven into grids with various mesh size can solve this problem very efficiently (**Fig. 3c**). The stresses, which usually cause the yielding or even fracture of surface skin, can be overtaken by reinforcements. The possibility to reinforce the foamed component selectively according to the expected load allows significantly to improve its stiffness, strength, plasticity and energy absorption capacity. Moreover the reinforcements simplify joining of foamed parts (welding is possible) and enable even limited shaping after foaming process.

HIGHLY EFFICIENT HEAT EXCHANGERS BASED ON ALUMINIUM FOAM

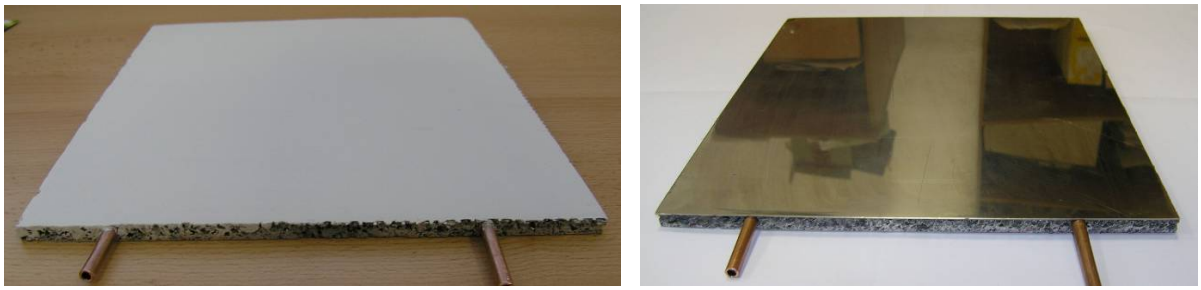
The improvement of air-conditioning efficiency in buildings or transport vehicles without demands on intensive air exchange can be effectively achieved by radiant heating and cooling systems using aluminium foam panels. Such panels could not only enhance the overall heating power as well as suppress a certain drawbacks of the present systems but also to bring some additional functions as load bearing ability, shielding of electro-magnetic field or sound absorption ability.

Above described ALPORAS® aluminium foam acts as heat exchanger and the heat can be transferred in the foam using impressed tubes [13]. An example of marble floor panel with integrated cooling (heating) system using aluminium foam exchanger is described in **Fig. 4**. Similar panels can be advantageously used also as solar collectors, if they are installed as facing of buildings.



Figure 4 *Marble panel for floor heating or cooling with impressed Cu-tube and Al-foam ALPORAS® heat exchanger (Dimensions: 600 x 600 mm).*

The most promising potential applications of heat exchangers based on aluminium foam with impressed copper tubes are expected mainly in the field of extremely ligth-weight cooling and heating panels for interior walls and ceilings (**Fig. 5**).



a b

Figure 5 *Examples of heat exchangers with aluminium foam ALPORAS®: (a) wall and ceiling panel with one site impregnated by plaster, (b) wall, ceiling or floor panel with stainless steel or aluminium cover sheet for clean rooms or various industrial applications.*

CONCLUSIONS

Easy manufacturing of structural and functional components allowing reasonable production costs can make the reinforced aluminium foams very attractive for various industrial applications, especially for light-weight stiff body structures of future cars, busses, trains, ships, aeroplanes, etc. and for light and efficient heat exchangers integrated into the interior floor, wall and ceiling panels. The reinforcements of aluminium foam surface significantly improve the strength, plasticity, energy absorption capacity and fracture toughness of foamed structural component. The powder-metallurgical method of aluminium foam manufacturing makes possible to reinforce structural component selectively in weakest points, which enables not only to obtain maximum property-to-weight ratio but reinforcements also simplify joining of foamed parts.

The heat exchangers produced using aluminium foam according to the novel principle described in this contribution are very good candidate for highly efficient heating/cooling systems where excellent performance at minimum weight and manufacturing costs is expected.

ACKNOWLEDGEMENTS

The financial support of Alulight International GmbH., Ranshofen, Austria and Gleich GmbH., Kaltenkirchen, Germany is greatly appreciated.

REFERENCES

[1] Simančík F., Rajner W., Laag R.: "Alulight - Aluminum foam for lightweight construction", SAE Tech. Paper Series 2000-01-337, Warrendale: SAE, Inc., 2000, p. 31.
[2] Kováčik J., Simančík F., Jerz J., Tobolka P.: "Reinforced aluminium foams". In: Proc. of Int. Conf. "Advanced Metallic Materials", 5-7.11.2003, Smolenice, Slovakia, p.154-159.
[3] Simančík F., Rajner W., Laag R.: "Reinforced Alulight for structural use", In: Processing and properties of Lightweight Cellular Metals and Structures (TMS Annual Meeting), Seattle, February 17 – 21, 2002, p. 25.
[4] Ashby M.F.: "Materials selection in mechanical design." Pergamon Press, Oxford, 1992.
[5] Sosnik A.: US Patent 2434775, 1948.
[6] Allen B. C.: US Patent 3087 807, 1963.
[7] Gibson L. J. and Ashby M. F.: Cellular Solids, (Oxford: Pergamon Press, 1988).
[8] Jerz J.: Foamed Aluminium and Aluminium Alloys Prepared by Powder Metallurgy, PhD thesis, TU Vienna, 1995.
[9] Jerz J., Simančík F.: Light-weight structural design using of metallic foams. In *MATRIB´05: 10. Conference on Materials, Processes, Friction and Wear, Vela Luka, 23-25 June 2005.* Zagreb: Croatian Society for Materials and Tribology, 2005, p. 95-101.
[10] Simančík F., Florek R., Tobolka P.: Reinforced aluminium foam profiles. In *Powder metallurgy 2004, Viedeň, 17-21.10.2004.* Shrewsbury: EPMA, 2004, p. 47-48.
[11] http://www.gleich.de/produkte/pdf/katalog-en.pdf
[12] Simančík F., Schörghuber F., Hartl E.: US Patent 5 865 237, 1999.
[13] Simančík F., Jerz J.: EP1611262 (Method for strengthening a component consisting of a deformable cellular material, said component and the use thereof), 2006.
[14] Florek R., Simančík F., Nosko M., Tobolka P., Uhrík R.: Heating and Cooling Panels Using Aluminium Foam *MATRIB´07: International Conference on Materials, Tribology and Processing, Vela Luka, 21-23 June 2007.* Zagreb: Croatian Society for Materials and Tribology, 2007, p. 430-437.
[15] Jerz J., Simančík F., Florek R.: Structural and functional applications of various aluminium foams. In *Aluminium 2007. Transactions of the Universities of Košice – The 5th International Conference, Doksy–Staré Splavy, 10.-12.10.2007.* Košice: TU, 2007. ISBN 1335-2334. p. 357-362.

Contact:
Dr. Ing. Jaroslav Jerz
Institute of Materials & Machine Mechanics, Slovak Academy of Sciences
Racianska 75, SK-831 02 Bratislava 3, Slovak Republic, tel.: +421-2-49268223, fax: +421-2-44223301
E-mail: ummsjerz@savba.sk,
http://www.umms.sav.sk,
http://www.matnet.sav.sk

Research and Exploitation of Surface Engineering Technology

David M. Kennedy and Kai Scholten
Department of Mechanical Engineering,
Dublin Institute of Technology, Bolton Street, Dublin 1, Ireland

Keywords: Thick and Thin Films, Surface Modification, Surface Shape Design
Pregledni članak / Subject review

Abstract

Surface engineering refers to a wide range of technologies that aim to design and modify the surface properties and characteristics of components. The applications are very broad from macro to nano and from extremely hard materials to polymeric coatings. The uses are found in many engineering, energy, gas and oil, transport, medical, cosmetic, optical, chemical and sports industries. Research in this field of technology is ongoing and the benefits that can be derived are enormous. The design, wear and tribological properties of components for instance have been greatly enhanced by surface engineering and the economic benefits to industries far outweigh the cost and use of traditional materials. Surface coatings and surface modification as depicted in Figure 1. represent developments in surface technologies. This paper discusses some of the processes and techniques of this technology and the potential benefits to be derived for those involved with Research and innovation in this field of study.

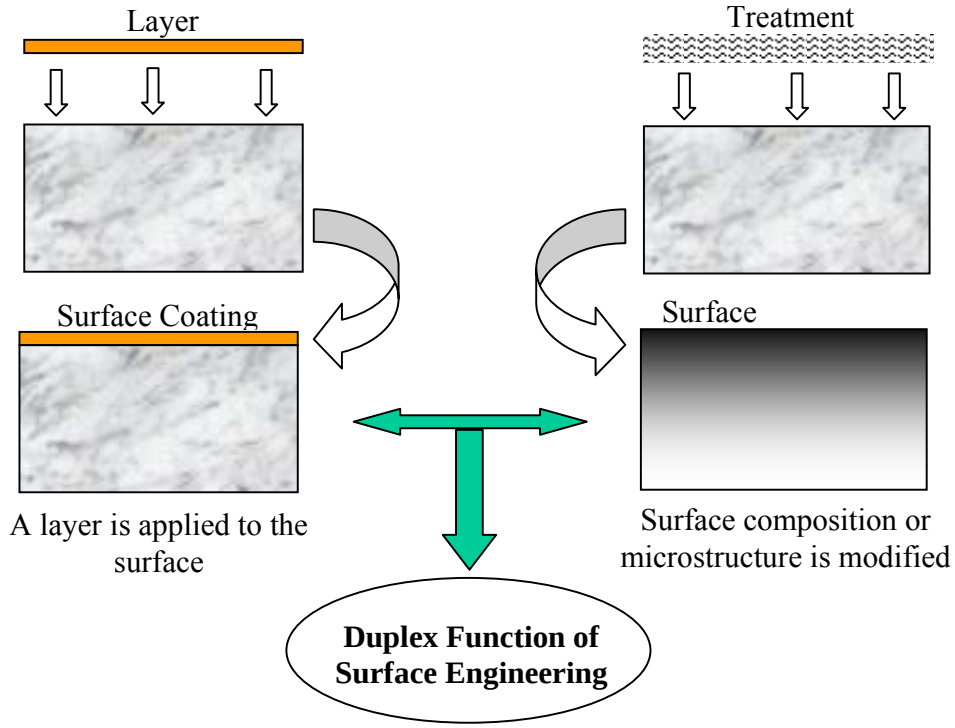


Figure 1. Surface Engineering Methods

1.0 Introduction

Considerable progress has been made over the last few decades in the development, testing and characteristics of advanced Surface Engineering and Surface Coatings. Prior to these developments, materials were subjected to heat treatments, paint, galvanising, alloying, anodising, carburising, and shot blasting which had limited effects on material properties and component enhancement. Countries such as Germany, Britain, France, United States of America, Australia, India and China have developed and exploited the uses of surface coatings for Industrial applications in many disciplines of Science and Engineering. A current report in Britain produced by the National Surface Engineering Centre (Nasurf) estimates that Surface Engineering processes could affect manufactured products worth £120 Billion and Surface Engineering is currently worth over £20 Billion to the U.K. economy. It has been estimated that the cost of wear, fatigue and corrosion amount to 4 % of GDP, the value of the UK coating market in 2005 to be in the region of UK£21.3bn and the value of products critically affected by coatings for the UK is in the order of £143bn [1]. One of the key advantages of Surface Engineering is that it is continually evolving, where researchers are exploiting new discoveries and applications for coatings, both from nature, replacing old methods and from experimentation. Common industries and sectors where surface engineering is applied include:

i) Aerospace
ii) Micro and nanotechnology
iii) Medical
iv) Mechanical and Manufacturing
v) Electronics
vi) Chemical
vii) Construction
viii) Electronics
ix) Mining
x) Offshore operations
xi) Machine Tools
xii) Sport
xiii) Aerospace
xiv) Transport
xv) Food and Packaging
xvi) Agriculture
xvii) Power generation

In practice, coatings are used to confer one or more of the following surface properties:

(i) Corrosion protection.
(ii) Decorative purposes.
(iii) Hardness.
(vi) Electrical conductivity.
(v) Solderability.
(vi) Build up of material for restoration.
(vii) Wear resistance.
(viii) Optical or thermal reflectivity.
(ix) Oil retention.
(x) Thermal conductivity.

Some important requirements of coatings at high temperatures for instance include:

(i) High melting temperature to protect the substrates.
(ii) Hardness.

(iii) Corrosion resistance.
(iv) Adhesive strength
(v) Low diffusion to prevent internal substrate corrosion.
(vi) High density, to avoid gas flux through pores to the substrate.
(vii) Stress free or in a state of compressive stress at working temperature.

The lists are extensive but not exhaustive as Surface Engineering has an impact on most standard and innovative products used today. The applications of surface coatings have been extensively explored and it is one of the fields of engineering and science that continues to offer innovative solutions to advanced technologies. Recently, surface coatings have been utilised increasingly in some specialised areas. Such applications include coatings in the sports industry, biomedical/orthopaedics, dentistry, cancer therapy, and the art industry.

2.0 Current and future applications

In the cutting tool industry, modern cutting applications cannot be accomplished without protecting the tools with a thin wear-resistant coating. These applications include high speed cutting, hard machining of high hardness (Rockwell>60C) materials, dry cutting and cutting of materials such as Titanium, AlSi alloy or other non-ferrous abrasive materials. They enhance wear resistance and hardness at the cutting edge and reduce diffusion and friction. Other applications include high toughness such as in punching applications. Examples of TiN coated machining tools are shown in Figure 2. In the transport industry, approximately 6% of the costs of manufacturing engines and transmissions are involved in coating technologies [2]. Surface coatings in the transport industry can be broken into power units, vehicle components and fixed permanent structures. Other more advanced applications include Tribochemistry, Transmission Systems and Engine Systems [3]. Coatings used in power generation units such as diesel engines and power transmission are well advanced today. They protect the power units from erosion and wear and suspension and brakes are coated with thermally sprayed coatings to improve wear resistance, extending service life. Polymer coatings are applied to exposed areas of vehicles and they act as a body coat on some vehicles to improve aesthetics, abrasion and corrosion resistance. Polymer coatings also reduce noise levels. Marine applications include bridges and oil rigs to combat saltwater corrosion and sand abrasion problems.

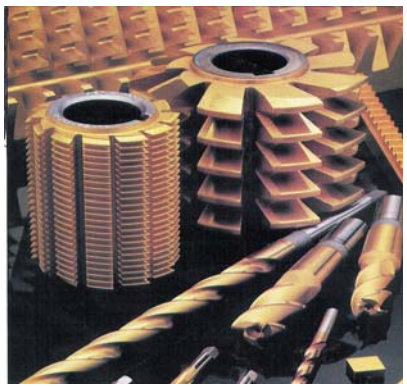


Figure 2. TiN Coated tools

In the aerospace industry, coatings on engine parts have been practised for over 50 years. Surface coated gas turbine engine provide high strength at high temperatures, corrosion resistance, abradable seals and bearing properties. Spacecraft components such as gears and ball bearings, coated with MoS_2, applied by PVD magnetron sputtering helps lower the heat generated within the transmission system. Surface modification improve the performance of many components. Some of the future applications that will require

research and development include engine and transmission design, especially for engines using hydrogen fuels.

2.1 Sports Industry Applications

Surface engineering of titanium oxide for motor sports has proved to be an effective modification to optimise the properties of engine parts, enhancing the performance of racing cars. If a reduction of inertial mass occurs in any engine, it will lead to increased speed, greater acceleration and better fuel efficiency and higher performance. Titanium alloys have an excellent combination of properties in terms of high strength/weight ratio, resistance to corrosion and bio-compatibility. As described by Bell and Dong [4], surface engineered titanium will be the material of the 21st century.

Engines should have low friction and low wear contacts at high temperatures in chemically reactive environments. Cam followers coated with DLC have a very low friction coefficient, reducing sliding friction by up to 80%. Applying surface coatings to golf clubs is a novel approach to improving contact and/or frictional effects, resulting in friction control of golf clubs, thus effecting ball spin. This will help determine the distance, spin and direction of flow of the ball. Typical surface modifications to golf clubs include TiN and Carbide coatings, shot peening and surface shape design. Other applications in the sport industry include snow ski designs, curling, cycling, soccer boots and protective clothing. Reducing or increasing friction in the competitive sports can be the difference between winning and losing. Table 1. shows a list of the current and future potential for surface engineering materials, processes and applications.

Material	**Function or role**	**R& D**	**Process**	**Coating type**	**Applications**
Metals	Corrosion	Quality	Thermal	Nano	Textiles
Ceramics	Wear	Design	PVD/CVD	Micro	Sport
Polymers	Friction	Testing	Sputtering	Thin	Marine and offshore
Powder form	Tribo corrosion	Innovation	Plasma	Thick	Machinery
Rod form	Adhesion	Colour and texture	Dipping	Multi layer	Building Industry
Atomic form	Oxidation	Thermoche-mical	Mechanical	Multi process	Renewable energy (PV)
Gaseous form	Fracture	Electrochemical	Heat Treatment	Hard	Transport
Liquid form	Optical	Paints & Organic coatings	Ion Implantation	Soft	Aerospace
Plasma	Fatigue	Characterisatio n	Laser & Electron Beam	Transparen t	Tools
	Thermal barrier	Surface modelling	Electrochemical	Insulator	Biomedical
	Diffusion barrier	Mechanics	Atmospheric & Vacuum	Conductor	Cutlery & kitchenware
		Cost reduction		Tough	Electronic
		Optical	Anodising	Hard	Mining
		Bio medical		Abradable	Military
		Sports & motor racing		Weight reduction	Porosity

Table 1. Surface Engineering diversity

3.1 Research and development

Surface engineering offers materials savings and environmental benefits in numerous applications, e.g. through increased service life, reduced emissions, energy consumption, and improved recyclability. Many modern surface engineering processes have low environmental impact as opposed to old heat treatment and chemical treatment processes. Coatings for wind, wave, solar and PV systems will be required to enhance their environmental uses and make them more efficient.

Reduction in weight, particularly for motor vehicles by using aluminium, magnesium and titanium alloys require surface engineering to improve corrosion and tribological properties. Deposition of titanium alloys has increased wear resistance substantially, permitting their use for lightweight components in Formula One vehicles and in other advanced applications in the offshore, biomedical, and sports sectors.



Figure 3. Polymer spraying

Polymer coatings for structural applications have strong potential for growth as well as being a cost effective and rapid method of depositing coatings on a wide range of materials without affecting their mechanical or physical properties. This is a rapid deposition process as shown in Figure 3.

Applications of functionally graded structures capable of a response to their environment will increase. This will involve further growth in the use of sensor technology, increasingly combined with applications such as smart oxidation resistant layers for gas turbines, and food packaging. Some 80% of aircraft vehicles and components are dependent on surface engineered components. Examples include coatings for gas turbines for power generation. Packaging such as beverage cans rely on coated form tools. Coatings have improved the quality of packaging through water and gas barriers on food products. Punch tools using Diamond Like Carbon (DLC) or Cubic Boron Nitride (CBN) have greatly extended their use and work life.

From 2005, it is predicted that 50% of all architectural glass will be coated with materials to reduce glare, heat loss and improve aesthetics. Glass products can be coated to prevent breakage by using tin oxide films. There is a need to further develop such coatings, so that the glass weight can be further reduced by using thinner walls. Surface engineering techniques make a significant impact on architectural glass, automotive glass, display panels, mirrors and packaging.

- Developments in coating technology now permit multi-layer structures with specific properties to be deposited on glass. Applications include;
- low-emissivity (Low-E) and solar control coatings on architectural glass;
- solar control and electrically conductive coatings on automotive glass;
- high reflectance coatings for solar collectors and telescope mirrors;
- moderate reflectance coatings for headlamp reflectors and rear view mirrors;
- photovoltaic coatings for solar cells; anti-scratch coatings on opthalmic lenses;
- conductive anti-reflective coatings for computer monitors and television screens.
- scratch-resistance and corrosion resistance.

The films are typically less that 1 μm thick and deposited using PVD and CVD.Biomedical devices, from prosthetic joints to substrates for tissue regeneration to advanced biosensors rely on engineered surfaces to provide both functionality and

biocompatibility. Surgical implants are coated with porous titanium or with synthetic bone to promote fixation in the body as shown in Figure 4. Almost 100% of electronic components and advanced sensors, optical coatings, etc. are fabricated using surface engineering technologies.



Figure 4. Coated implants

3.2Thermally sprayed coatings

Thermal spraying is now regarded as one of the key enabling surface engineering technologies. Applications include automobiles, aerospace, medical, marine, sports etc. Any material that has a well defined melting point and does not decompose when heated can be thermally sprayed and over 500 materials are now available for coating selection. Aerospace engineers apply these coatings at the manufacturing stage and during repair. Thermal barrier coatings are used to protect against extreme heat. Abradable coatings allow the rotating blade tip to machine its own seal. In vehicle design, cast iron liners have been replaced with a thin plasma coating and lightweight brake discs can be coated with a ceramic. Rolls used in the paper, printing and steel industries are protected against wear and corrosion. Water and chemical pump impellors and housings are now coated to prevent corrosion and wear.

4.0 Coating Techniques and Processes

Figure 5. shows the fusing of a WC-Co coating to an aluminium substrate providing a hard wear resistant coating to a lightweight material. Figure 6. shows the main components of the thermal spray gun. Some examples of coating process and their associated costs and functions are highlighted in Table 2 while Table 3. gives an outline of traditional and advanced surface coating processes and their applications.



Figure 5. WC-Co coating process

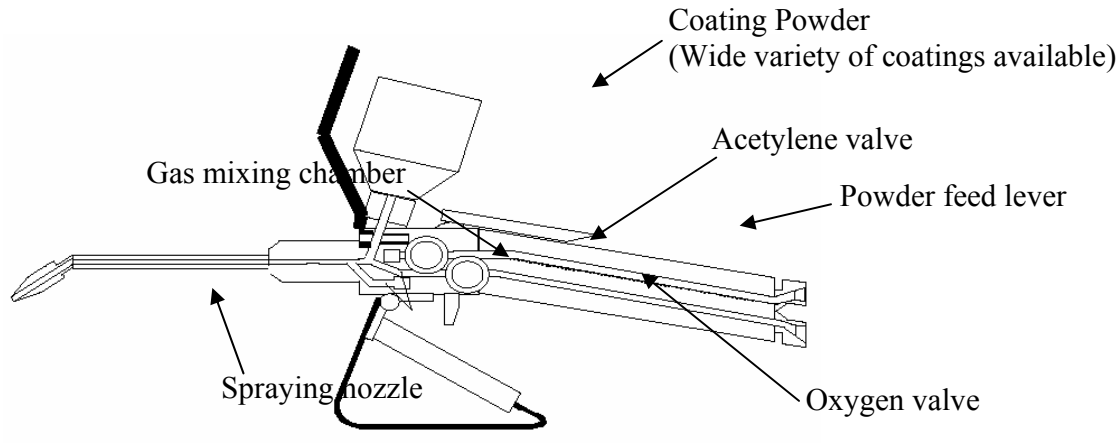


Figure 6. Thermal Spray Torch

ADVANCED SURFACE COATINGS AND INDUSTRIAL APPLICATIONS

PROCESSES	TYPES	PROPERTIES	APPLICATIONS
Chemical Vapour Deposition (CVD)	Diamond film	Hardness Wear resistance	Cutting tools and Dies Drills, Mills, Punches
Physical Vapour Deposition (PVD)	Diamond like Carbon (DLC)	Shock resistance Chemical resistance	Tapping, Reaming Extruders
Ion- plating	Titanium Nitride	High Temperature Resistance	Injection moulding Ball Bearings
Ion implantation	Titanium Carbide	Low friction	Rolling mills
Weld facing Cladding Broaching	Silicon Nitride	Toughness	Mining equipment
Thermal spray	WC-Co Tungsten carbide		Forging, Quarrying
Plasma spray	Aluminium oxide Silicone carbide Chromium carbide	Diffusion barrier Fatigue resistance	Impact resistance Pump housings Aircraft components
Laser surfacing	Chromium oxide	Corrosion resistance	Agricultural parts
Dipping		Surface finish	Electrical contactors
Electroplating		Electrical insulation	Engine parts

Table 2. Traditional and advanced applications of surface Engineering

Process	Costs	Value	Applications	Functions	User friendly	Flexibility
Plasma spraying	Expensive to setup and train staff in. High power requirement Water/Air cooling, high material consumption.	Used for high value parts such as aeronautical engines and exhaust parts, wide range of coatings and thicknesses. High/rapid deposition rates.	Wide range of thick coatings. Athmospheric Small and large components. Broad range of substrates	Wear, salvage, Corrosion Erosion, , Abrasion, Hardness, Friction coatings, thermal barriers etc	Safety precaution such as extreme noise. Mobile, High temperatures. Post treatment allowed	Very versatile, Mobile, Rapid pre treatment and post treatment, Thick and thin coatings, line of site.
Electroplating	Relatively cheap to set up but environmentally unpopular, requires skilled staff.	Broad range of coatings, low waste Can be used for metallic and non metallic surfaces. Broad range of materials can be deposited.	Decorative, wear and wide range of coatings, thick and thin, Need conductive substrates.	Decorative, wear, conductive coatings,	Need different baths and electrodes for different metals, precision control for good deposit rates and coating quality.	Limited in coating hardness, Sample sizes, non mobile, non line of site process. Limited to certain substrates, no heat treatment of substrates
CVD & PVD	Expensive to set up but relatively clean, fully automatic, requires skilled operators, expensive and slow pre cleaning	Excellent life of components, used for high value but relatively small components, not suitable for salvage,	Cutting tips and tools, implants, engine parts, high hardness, wear, impact resistant coatings	Thin coatings, high bond strength, low porosity coatings,	Fully automatic, Slow growth rate, non mobile, relatively small sample size, PVD: line of site	Restricted to small components, requires expert operators, wide range of coatings and multi-layers, not good for resalvage work.
Sheradising	Relatively cheap process but limited mainly to steels.	High corrosion resistant process where zinc is used on threads of nuts and bolts,	Steel components suchas metal casings, nuts and bolts where clogging of threads does not occur.	Thin uniform coating of zinc applied at approximat ely 370oC in rotating drum.	Simple process to develop and control. Limited to only a few applications	Relatively fast process, component size is limited by drum size. Cementation process
Carburising	Relatively cheap to develop but limited to steels in face centred cubic crystal form.	Extremely high hardness and wear resistant properties developed to appreciable surface depths. High temperatures limit the process and cause metal distortions.	Gas, solid or liquid processes make it versatile for different substrates	Wear parts, high hardness, limited to metals, namely steels, good depth of penetration.	Cyanide process is hazardous to life.	Samples can be masked if no heat treatment is required in certain areas of the surface, post heat treatment can be conducted on components.

Table 3. List of coating techniques and applications

5.0 General discussion and conclusions

Surface engineering technologies have the ability to supply added value and thus add profit. It acts as a bridge, transferring technology and expertise between end-user sectors that would not normally benefit from this cross-fertilisation. Environmental legislation continues to be an important driver for change. Surface Engineering continues to evolve, offering new opportunities for those involved in the research and applications of these coatings. The innovative approach of developing old coating methods to new techniques and applications will generate wealth and create new products for a wide range of industries. Surface engineering also represents a very efficient use of specialist materials. With a reduction in equipment costs, and improvement in knowledge and technical skills, the future research and development of surface engineering looks very promising as outlined in this paper. It is one key area where physicists, biologists and engineers have integrated knowledge and expertise to develop and apply successful solutions to dated technology. These advances, supported by environmental, health and safety, nanotechnology and innovative designs will see this industry grow and expand over the next 30 years.

References:

[1] A. Matthews, R. Artley, and P. Holiday: '2005 revisited: the UK surface engineering industry to 2010, 1998, Farnborough, NASURF

[2] http://www.iom3.org/divisions/surface/secforesight.pdf,

[3] COST Action 532, Triboscience and Tribotechnology, Superior friction and wear control in engines and transmissions, European Commission, SDME, B-1049 Brussels, 2007

[4] H. Dong and T. Bell: Final report on Link Surface Engineering Programme: 'Advanced surface engineering of titanium alloys (AdSurfEngTi)', EPSRC/DTI, 1995–1998.

Mechanical Engineering Education in Irish Context On route to becoming a Chartered Engineer

David M. Kennedy and Richard Good
Department of Mechanical Engineering,
Dublin Institute of Technology, Bolton Street, Dublin 1, Ireland

Pregledni članak / Subject review

Keywords: Bologna accord, Engineers Ireland, Programme Outcomes

Abstract

Engineering Education in Ireland and throughout Europe has changed dramatically over the last few years and the pace of change is ensuring that we, the educators are constantly keeping abreast of new developments and benchmarks. Programmes that were based on inputs from learners are now outcomes based and the onus is on the educators and facilitators to provide evidence that graduates are capable of conducting specific tasks, commonly termed as Programme Outcomes. Similarly, greater onus is now placed on the learner to take greater responsibility for their educational development. The new and current process of meeting the educational requirements of becoming a Chartered Engineer are been modified to meet new outcomes that are designed to enhance the engineering and professional development skills of the learner for 2013 and beyond. This paper discusses the development of Mechanical Engineering Programmes in Ireland, the associated programme outcomes and the alignment of engineering programmes in Europe. The paper will also discuss what the author recognises as strengths and weaknesses within the engineering education provided now and in the future. These points are addressed under some of the following headings:

- Mechanical Engineering modular programme structure
- Outcomes based programme design
- Development of transferable skills
- Semesterisation of programme
- Becoming a Chartered Engineer

1.0 Introduction

The education of an engineering student has gone through dramatic changes over recent times, influenced by the Bologna Accord [1] and more recent European educational agreements. Many changes have taken place including programme duration, the skill set of the graduate engineer and the mobility of learners. Similar to the globalisation of trade, engineering education has seen similar developments whereby students can complete modules, semesters and years at a combination of institutes and graduating from their host institute with an accumulation of credits or more commonly known as ECTS's

(European Credit Transfer System) [2]. For most European and Irish educational institutes, the most dramatic developments in recent years has been the shift from entry standards to an outcomes based system. This system has been designed and defined to identify the necessary education, technical, applied physics and professional development of the engineering graduate to meet the educational standards to become a professional engineer or chartered engineer. The programme outcomes have been developed on a European and national basis to clearly identify the skill set that students should attain on exiting a programme in order to become a chartered engineer. In Ireland, the recognised body responsible for the engineering profession is the Institute of Engineers of Ireland (Engineers Ireland or EI) [3] and this Institute, through collaboration with European and worldwide bodies are responsible for assessing the quality and accreditation of engineering programmes. On graduation from accredited engineering programmes, graduates must complete a minimum of four years of relevant engineering work or studies in order to become a chartered engineer. In Ireland, an Honours Degree at NQAI (National Qualifications Authority of Ireland) [4] that is accredited by Engineers Ireland meets the educational standard for Chartered Engineering grade of membership. The NQAI system is shown in Figure 1. This type of programme can take a minimum of four years to complete and currently carries 240 ECTS's or 60 per year.

Those entering this programme from the second level educational system normally have a high level of mathematics and/or a science subject and have attained a prescribed number of points from their second level educational studies.
From the year 2013, the aim is to increase the educational standards from an Honours Degree to a Masters Degree in line with Bologna and other countries throughout Europe and the world. Currently the Honours Degree accredited programmes are recognised on a worldwide basic for meeting the educational standards of Chartered Engineer through the Washington Accord [5]. In the Irish context, education is currently free of charge for up to a period of four years. Students pay a registration fee each year and must support themselves and pay for books etc.
Some of the questions that need to be answered are based on the need for a master's qualification to become a chartered engineer, consisting of a minimum of five years of educational study;
How will programmes be designed to meet this?
Will it be supported by government?
Will it be a turn off for students?
Will it be a turn off for parents?
Will it result in negative publicity?
Will it upgrade the status of the engineer?
Will it undermine the economy that depends on a good supply of engineers?
Will it produce better engineers?
Will it have any effects either way?

2.0 Formation of a Chartered Engineer
Currently the formation of a chartered engineer takes a minimum of eight years and consists of two main phases;

1. The first phase consists of studying and successfully completing an engineering degree programme accredited by engineers Ireland as meeting the educational standards required for the title of Chartered Engineer

2. The second phase is called Initial Professional Development and involves the achievement of the competences necessary to apply engineering principles to the solution of engineering problems. This is further defines in the literature [5].



Figure 1. NQAI Framework of Educational Qualifications

2.1 Bologna Accord

The Bologna accord was established in June 1999 with the intention of establishing by 2010 a "European Higher Education Area," based on principles of academic independence and autonomy. The major goal was to produce a more transparent system whereby the different national systems would all be structured on three cycles: Bachelor, Master and Doctorate. The resulting Bologna Declaration has been central to educational reforms among all of the EU countries. The main signatories to this agreement are: Albania - Andorra - Armenia - Austria - Azerbaijan - Belgium - Bosnia and Herzegovina - Bulgaria - Croatia - Cyprus - Czech Republic - Denmark - Estonia - Finland - France - Georgia -Germany - Greece - Holy See - Hungary - Iceland - Ireland - Italy - Latvia - Lithuania - Luxembourg - Malta - Moldova - Netherlands - Norway - Poland - Portugal - The Former Yugoslav Republic of Macedonia - Romania - Russia - Serbia and

Montenegro - Slovakia - Slovenia - Spain - Sweden - Switzerland - Turkey - UK – and Ukraine.
The Bologna Declaration aimed at ensuring that European higher education and research would be fully responsive to both social change and scientific advancement. To increase the competitiveness of European higher education, the signatories viewed these six improvements as essential;
Grades: Academic grades need to be easy to read and compare which would enhance international transparency. A system of comparable degrees emerged as a key improvement. A two-tier system-undergraduate and graduate-was adopted. The first cycle (bachelor's degree) was designed to last at least three years and the second cycle (master's degree) conditional upon the completion of the first cycle. The master's degree can lead to the third cycle, the doctorate degree. The signatories also agreed to establish a system for the easy transfer of academic credit through the European Credit Transfer System (ECTS), thus promoting student mobility, access and fostering European cooperation in assuring quality and compatibility. It also advocated the development of comparable criteria and methodologies for assuring comparable quality throughout European educational systems. These criteria and methodologies could be extended to other countries. A "European Dimension." In working toward a "European dimension of higher education," the signatories aimed at fostering a "convergence" of higher education systems by coordinating their programs of study, training and research.

2.2 Programme outcomes
The Programme Outcomes (PO's) for meeting the educational standards for Chartered Engineer (CEng) are currently broken into six main outcomes as follows:

1. The ability to identify, formulate, analyze and solve engineering problems
2. The ability to design a system, component or process to meet specified needs, to design and conduct experiments and to analyse and interpret data
3. An understanding of the need for high ethical standards in the practice of engineering, including the responsibilities of the engineering profession towards people and the environment
4. The ability to work effectively as an individual, in teams and in multi-disciplinary settings together with the capacity to undertake lifelong learning
5. The ability to communicate effectively with the engineering community and with society at large
6. The ability to derive and apply solutions from a knowledge of science, engineering sciences, technology and mathematics

2.3 Programme Area Descriptors
Engineers Ireland has determined that the study of six programme areas is necessary if engineering graduates are to achieve the programme outcomes described. These are based on the following themes;

(a) Science and Mathematics
(b) Discipline specific Technology
(c) Information and Communications Technology
(d) Design and Development
(e) Engineering Practice
(f) Social and Business Context

Combining programme outcomes and programme areas results in a matrix as shown in Figure 2. The empty spaces can be filled with relevant learning outcomes from modules, subjects or courses that address these PO's and PA's

	Programme Outcome 1 Derive & Apply solutions	Programme Outcome 2 Solve Eng. Problems	Programme Outcome 3 Design, Experiment	Programme Outcome 4 Ethical Standards	Programme Outcome 5 Work in teams, etc	Programme Outcome 6 Communicate
Programme Area (a) Science & Maths						
Programme Area (b) Discipline Specific Technology						
Programme Area (c) Info & Communications						
Programme Area (d) Design & Development						
Programme Area (e) Engineering Practice						
Programme Area (f) Social & Business						

Figure 2. Programme Outcomes and Programme Areas

2.4 Learning Outcomes

Learning Outcomes are required for each module or element of a module
A learning Outcome is a statement of achievement which may take the form of the acquisition of:

1. Knowledge
2. Understanding
3. An Intellectual Skill
4. Practical Skill

They provide a clear explanation of what is required to complete successfully a module in a programme of study providing there are strong links between the learning outcomes, the assessment criteria and the assessment methods

1. Technical Skills

Module	
Applied Thermodynamics	Control Engineering
Engineering Management	Computer Modelling
Electrical & Electronic Engineering	Fluid Mechanics
Mechanical Engineering Design	Mechanical Engineering Design
Mechanical Engineering Design	Mechanical Engineering Design
Mechanics of Machines	Mechanics of Materials
Engineering Mathematics	Engineering Materials

2. Transferable Skills
3. Work Related Attitudes
4. Development Goals

3.0 Mechanical Engineering Honours Degree Programme at DIT

The Mechanical Engineering Programme at Dublin Institute of Technology currently consists of four years or stage of study. This is divided into 8 semesters (two per year) with assessments during and examinations at the end of each semester.
The modules (subjects) for Stages 1 to 4 are shown in Figures 3 to 6 respectively.

Module Title	
Engineering Physics 1	Engineering Physics 2
Eng Applications & Introduction to Engineering	
Engineering Computing	
Engineering Chemistry 1	Engineering Chemistry 2
Mechanics 1	Mechanics 2
Engineering Drawing & CAD	Engineering Drawing (Building Services)
Engineering Drawing and Interpretation, Mechanical Machine Component / Assembly	Engineering Drawing (Structures)
Professional Development	
Engineering Mathematics 1	Engineering Mathematics 2

Figure 3. Stage 1 Modules for Mechanical Engineering

Module	
Control Engineering and Automation	Fluid Mechanics 2
Mechanical Engineering Design & CAD	Engineering Computing
Electrical & Electronic Engineering	Manufacturing Technology
Engineering Materials	Mechanics
Professional Development	Thermodynamics
Mathematics	Statistics

Figure 4. Stage 2 Modules

Figure 5. Stage 3 Modules

Figure 6. Stage 4 Modules

4.0 Assessment process

The Accreditation process is undertaken by a panel of three experienced experts, one of whom is normally from Industry. They receive the documentation form the Institutes/Universities or Colleges a few weeks prior to the visit and their report address the headings listed in Table 1. The visit of the panel to the relevant institute takes two whole days and their findings are presented to the institute where the programme resides prior to their departure. The outcome of the report may result in three results:

1. Full accreditation for the next five years
2. Three years accreditation if some deficits are found in the evidence presented to the panel.

Module	
Computer Modelling	Control Engineering
Engineering Management	Fluid Mechanics
Energy Systems (Sustainable & Renewable)	Heat & Mass Transfer
Engineering Mathematics	Mechanics of Materials 4
Mechanics of Machines	Project

3. No accreditation which can arise if there are major deficits or if the programme has never been accredited in the past

The report is then presented to Engineers Ireland where it goes before a committee responsible for programme accreditation.

ACCREDITATION PANEL REPORT
Department
Dates of Visit:
1. Programme Title:
2. Educational Standard being sought – Chartered Engineer
3. Programme Panel:
4. Compatibility with Engineers Ireland Guidelines
4.1 Entry Standard
4.2 Programme Duration and Structure
4.3 Resources including buildings, laboratories, equipment, academic and support staff
5. Analysis and Implementation of Programme Outcomes.
5.4 Programme Outcomes
Programme Outcome (a)
Programme Outcome (b)
Programme Outcome (c)
Programme Outcome (d)
Programme Outcome (e)
Programme Outcome (f)
6. Assessment of Student Performance
7. Student Transfer and Mobility
8. Features and Strengths of Programme

9. Recommendation to Accreditation Board
Conditions (mandatory) to apply to Accreditation
or
Deficits in Programme for which accreditation is not recommended
9.1 Recommendations (Non-mandatory) for Improvement of the Programme

Table 1. Accreditation Panel Report

5.0 Discussion and conclusions

From the outset, one noticeable feature of the programme outcomes is that three of them are dedicated to direct non engineering activities such as Ethics, Communication skills and working in multidisciplinary settings. The introduction of these outcomes indicate the importance such skills and attributes play in the working activities of a professional engineer. It is also fair to say that the last three programme outcomes are those that cause greatest difficulties to those running the programme and deficits normally derive from these. This shift to programme outcomes has created a change of approach for educational institutes and greater effort has been attributed to the personal development, teamwork, ethical and communication skills of an engineering syllabus.

For the future, the Bologna Accord is identifying a five year programme or Masters qualification as the educational standard for accreditation to Chartered Engineering awards. This may result in a 3+2 or 4+ 1 (Primary Degree plus Masters) configuration. It may allow greater collaboration with industry for student work placement during their educational training etc. However it is unlikely that adding extra years to a programme will result in government funding or free education for the whole five years. Decisions on this have yet to be agreed on. In conclusion, the programme outcomes approach has been welcomed by educational Institutes and has resulted in more creative ways of delivery of Honours Engineering Programmes in Engineering.

References

[1] Bologna Accord, 1999

[2] http://ec.europa.eu/education/programmes/socrates/ects

[3] Engineers Ireland Accreditation Criteria for Engineering Education Programmes, March 2007

[4] National Framework of Qualifications, A Framework for the development, recognition and award of qualifications in Ireland, Document number 2003/5, October 2003

[5] Chartered Engineer, Regulations for the title of Chartered Engineer, Engineers Ireland

RESISTANCE OF WHITE CAST IRON TO ABRASION TEST

D.Kolednjak[(1)], D.Kamenečki[(2)], Z.Schauperl[(3)]

[(1)] INP d.o.o., SR Njemačke 10, Zagreb
[(2)] PLINACROd.o.o., Savska cesta 88, Zagreb
[(3)] FSB, Ivana Lučića 5, Zagreb

Izvorni znanstveni rad / Original scientific paper

ABSTRACT

Wear tests were carried out using the method "dry sand/rubber wheel" with a group of white cast iron samples, using quartz sand as an abrasive.

The same group of materials was metallographically processed, the quantitative analysis of microstructure was performed, the microhardness was determined, and the wear resistance index identified.

Following that, it was determined whether the results obtained during the measurement of volume loss are compliant with the calculated indexes of abrasion resistance, and the conclusions were made regarding the validity of the abrasion resistance index application.

Key words:
wear resistance index, abrasion, wear, metallography

SAŽETAK

Provedeni su pokusi trošenja metodom "suhi pijesak/gumeni kotač" sa grupom uzoraka bijelog lijeva, koristeći se kvarcnim pijeskom kao abrazivom.

Ista grupu materijala je metalografski obrađena i izvršena je kvantitativna analiza mikrostrukture uz određivanje mikrotvrdoće, te je određen indeks otpornosti trošenja.

Nakon toga je ustanovljeno odgovaraju li rezultati dobiveni prilikom mjerenja gubitka volumena izračunatim indeksima otpornosti abraziji, te su doneseni zaključci o valjanosti primjene indeksa otpornosti abraziji

Ključne riječi:
indeks otpornosti trošenja, abrazija, trošenje, metalografija

1 INTRODUCTION

The term "wear" means a constant loss of material from surfaces of solid bodies caused by a mechanic cause, i.e. by a contact with solid, liquid or gaseous bodies and a relative motion between them. The wear is manifested by a separation of tiny particles of the material which is being worn and the modification of both its body shape and its surface.

This is the reason why there is a constant need for wear testing. The most comprehensive tests are the tests with the following aims:

1. optimisation of particular elements of the system, or the entire system to achieve a specific duration
2. determining the wear impact on the entire function of the machine i.e. optimisation of the construction of certain parts and tribological system to achieve a specific functionality of a machine
3. obtaining data for maintenance and the determination of maintenance and inspection intervals
4. monitoring machine functions which have impact on wear

However, due to the fact that these tests are very expensive, time consuming, and considering the fact they require specially trained staff, we are trying to replace them with somewhat simplified systems, which are faster and simpler, but which nevertheless may give the basic features of the material during the wear process.

Because of the mentioned it is necessary to compare the results obtained in the test of wear by abrasion using the method "dry sand/rubber wheel" to the results obtained in the quantitative analysis of microstructure with the determination of microhardness of separate phases and taking into account the abrasive microhardness.

2 ANALYSIS OF ABRASIVES FOR WEAR TEST

- Type of abrasive
  For wear test quartz sand was selected
- Grain size
  Fraction 0.315 – 0.200 mm was selected
- Microhardness test
  After 20 microhardness measuring tests were carried out, the average value is X = 1265 $HV_{0,1}$
- Roundness analysis

By the analysis performed in accordance with the Powers method on 200 grains – the conclusion was made that the grains are of angular shape

- Analysis of sphericity
  By the analysis performed in accordance with the Russell and Taylor method on 200 grains the conclusion was made that the grains are highly spherical

3 WEAR TEST USING THE METHOD " DRY SAND / RUBBER WHEEL "

3.1 Calculation and results presentation

Test by the method "dry sand/rubber wheel" consists of abrasion of standard test tube by sand with the controlled grain size and composition.

Abrasion test results are shown as mass loss in gram with the indication of the applied procedure. The results of mass loss may be used internally for the comparisons of materials of equivalent density. The results can also be shown through the volume loss in the following way:

$$\text{volume loss } [mm^3] = \frac{\text{mass loss } [g]}{\text{density } [g/cm^3]} \cdot 1000$$

As the diameter of rubber wheel decreases, so decreases the relative path of sliding between the wheel and test tube. The actual volume loss with this, somewhat smaller wheel shall therefore be inaccurate. The corrected volume loss takes this into consideration and provides the result which would be obtained by the use of a new wheel of a diameter 228.6 mm (9 ").

A potential discrepancy between the real and nominal number of wheel turnings is also to be taken into consideration.

The corrected volume loss is calculated in the following way:

$$KVG = \text{measured volume loss} \cdot \frac{D \cdot N}{D_1 \cdot n_1}$$

D = 228.6 mm – nominal wheel diameter

D_1 = wheel diameter after the test [mm]

n = nominal number of wheel turnings (in accordance with a procedure variety)

n_1 = actual number of wheel turnings (read after the test completion)

3.2 Selection and preparation of material for the wear test and the varieties of test procedures

White cast iron with the following composition was selected for the test performance:

- 15 % Cr
- 3 % Mo
- 2.5 % C

in four conditions:

- cast
- hardened
- vanadized
- boronized

The wear test was performed with 200 wheel turnings, and after the test the results were corrected to 6000 turnings, i.e. to the A procedure.

3.3 Results of wear test

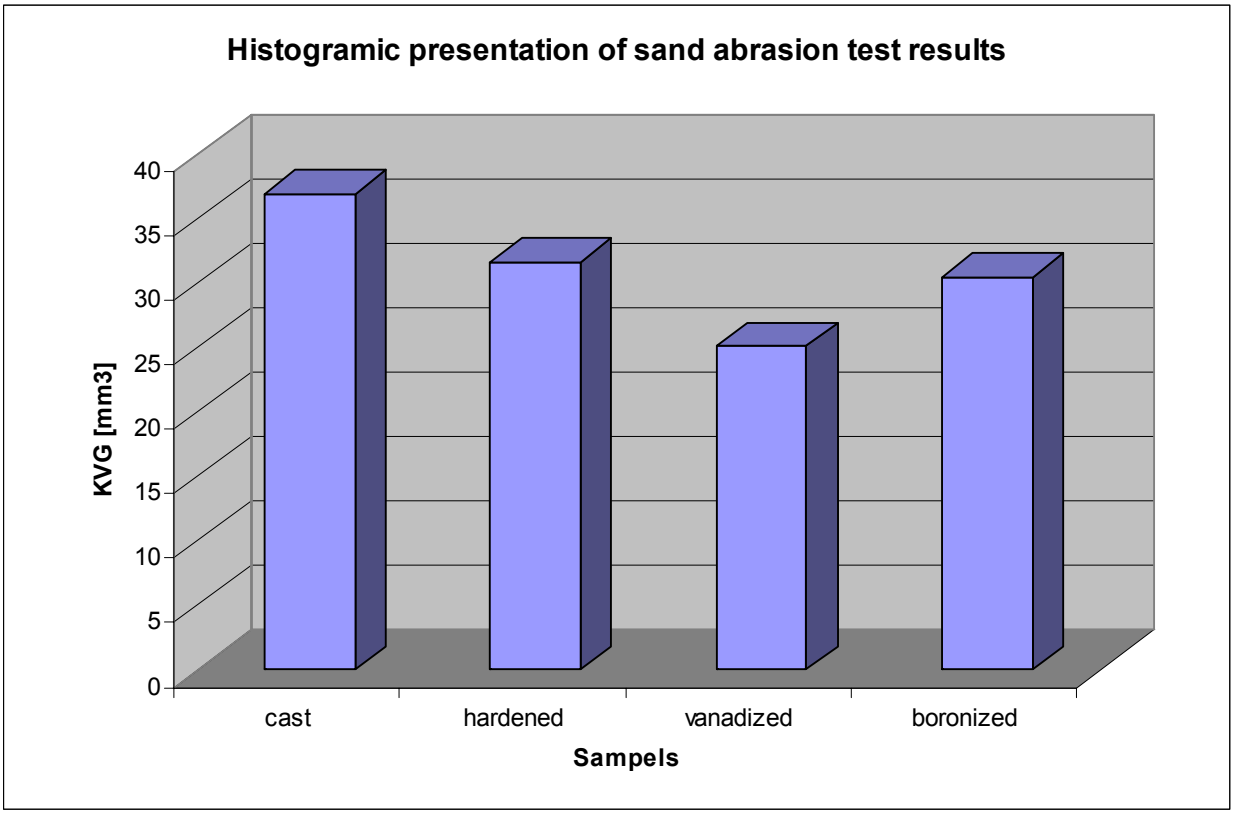


Figure 1 – Results of white cast iron abrasion test

4 DETERMINING ABRASION RESISTANCE INDEX BASED ON MICROSTRUCTURE ANALYSIS

4.1 Sample preparation

To determine abrasion resistance index it is necessary to analyse the material structure. To analyse the material structure it is necessary to perform the metallographic processing, and the preparation of samples in the following stages:

- sample cutting,
- moulding,
- grinding,
- polishing,
- etching

After the surface preparation the structure of all samples was quantified and the microhardness of each of them was measured.

4.2 Model for abrasion resistance index determination

By the analysis of material microstructure it is possible to determine the coordinates of points A, B and C in the figure, and in this way to define the dependence curve for any material. Taking into consideration the hardness of abrasive H_a, it then is possible to determine the adequate abrasion resistance index $R_{AB/a}$ for this pair (material/abrasive), in the manner shown in the figure 3. Certain elements of the dependence curve are determined in the following way:

- point A is determined by the microhardness of the hardest phase in material Hm_{max} and average value of the microhardness of a unit by adding the products of volume share of certain phases in material and the relevant microhardness, i.e. $R_{AB\ min} = H_m$;
- point B is determined by microhardness of the softest phase in material and the condition $R_{AB\ max} = 60\ R_{AB\ min}$;
- point C is determined by the share of harder phase in a way shown in the figure 2

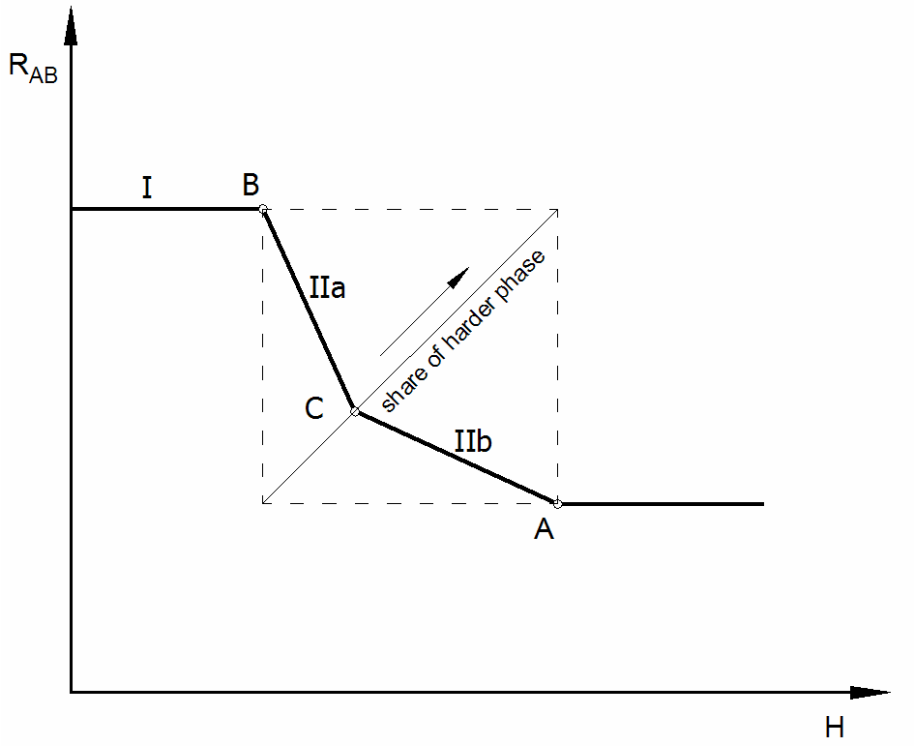


Figure 2 – Model for abrasion resistance index determination

In the area I wear is lowest, i.e. the abrasion resistance index is highest, since the abrasive is softer than the softest material constituent $H_{m\ min}$. In the area III wear is highest, i.e. abrasion resistance index is lowest, since the abrasive is harder than the hardest material constituent $H_{m\ max}$. In this area abrasion resistance is proportional to average material hardness and is not essentially dependant on the further increase of abrasive hardness, i.e. $R_{AB\ min} = H_m$.

The wear in the area I is 60 times lesser, i.e. the abrasion resistance index is 60 times higher than in the area III, i.e. $R_{AB\ max} = 60\ R_{AB\ min}$

In the transit areas IIa and IIb the position of the item C is determined by volume share of the hard phase.

The advantage of this method is relatively simple determination of abrasion resistance index of metal materials to any abrasive or a mixture of abrasives. It also enables the explanation why a certain material is more resistant than others, and thereby gives guidelines for the development and selection of materials.

4.3 Abrasion resistance index determination

4.3.1 White cast iron – cast

The microstructure of white cast iron consists of eutectic carbides of average hardness 1820 HV and austenite matrix with dispersed secondary carbides of a common microhardness 455 HV. Volume share of eutectic carbides is 17%, and of austenite matrix with secondary carbides is 83%.

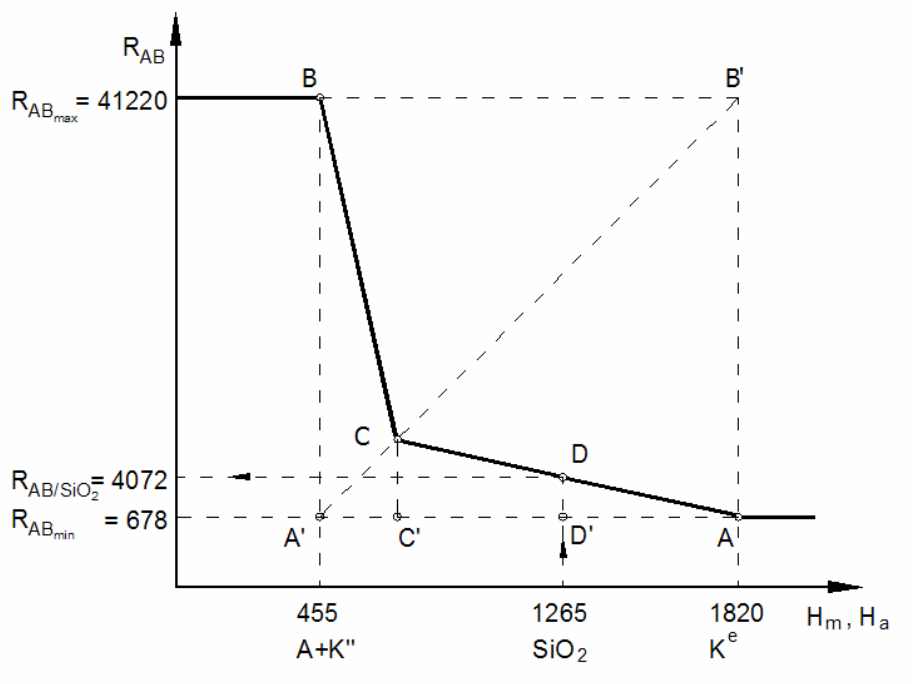


Figure 3 – Abrasion resistance index determination by quartz for white cast iron – cast

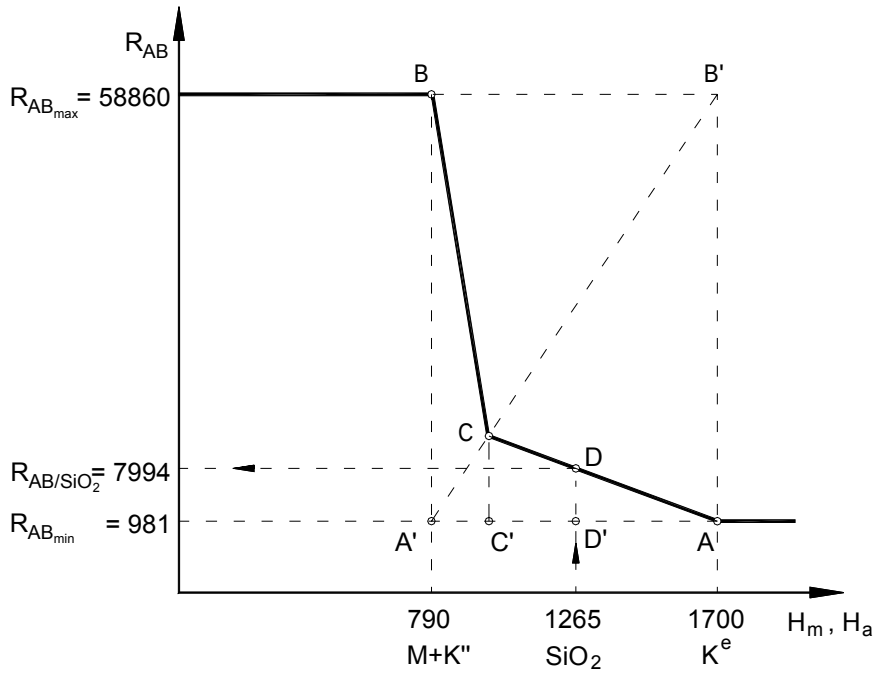
$\overline{H}_m = (A + K'') \bullet H_{A+K''} + K^e \bullet H_K^e = 0.83 \bullet 455 + 0.17 \bullet 1820 = 678\ HV_{0,2}$

$R_{ABmin} = 678$

$R_{ABmax} = 60 \bullet R_{ABmin} = 41220$

4.3.2 White cast iron - hardened

The microstructure of hardened white cast iron consists of eutectic carbides of average hardness 1700 HV and martensite matrix with dispersed secondary carbides of a common microhardness 790 HV. Volume share of eutectic carbides is 21%, and of martensite matrix with secondary carbides is 79%.



Slika 4 – Abrasion resistance index determination by quartz for white cast iron – hardened

$\overline{H}_m = (M + K'') \bullet H_{M+K''} + K^e \bullet H_K^e = 0.79 \bullet 790 + 0.21 \bullet 1700 = 981\ HV_{0,2}$

$R_{ABmin} = 981$

$R_{ABmax} = 60 \bullet R_{ABmin} = 58860$

4.3.3 White cast iron - vanadized

The microstructure of vanadized white cast iron at the surface is monophase, because the structure is 100% VC. Microhardness of this carbide layer is 1837 $HV_{0,2}$

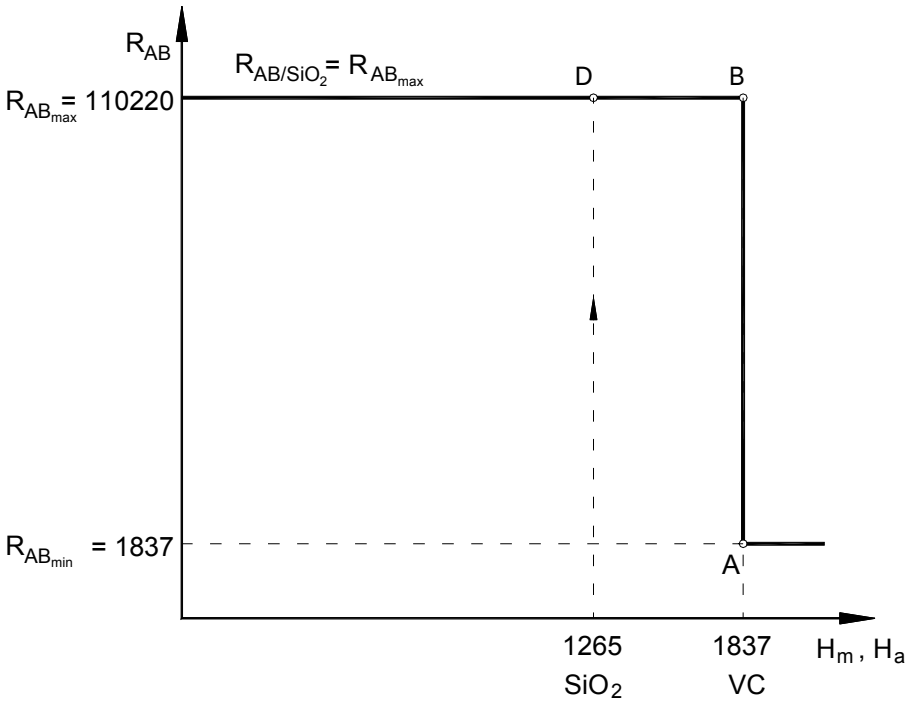


Figure 5 – Abrasion resistance index determination by quartz for vanadized white cast iron

$\overline{H}_m = R_{ABmin} = 1837\ HV_{0,2}$

$R_{ABmax} = 60 \bullet R_{ABmin} = 110220$

$R_{AB/Sio2} = 110220$

4.3.4 White cast iron - boronized

The microstructure of boronized white cast iron at the surface is monophase. Microhardness of the boronized layer is 1246 $HV_{0,2}$.

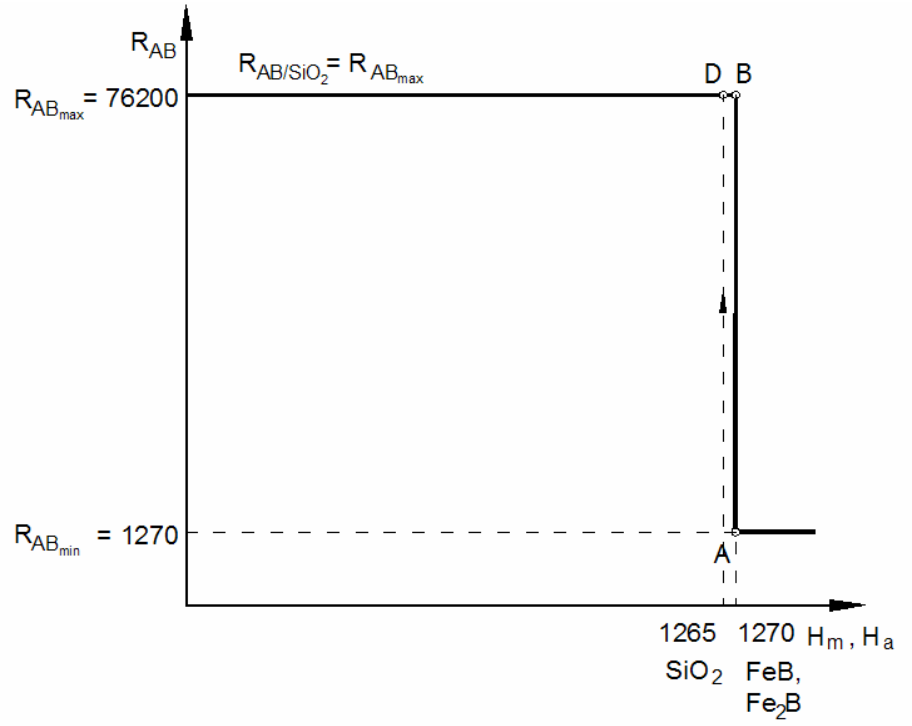


Figure 6 – Abrasion resistance index determination by quartz for boronized white cast iron

$\overline{H}_m = R_{ABmin} = 1270\ HV_{0,2}$

$R_{ABmax} = 60 \bullet R_{ABmin} = 76200$

$R_{AB/Sio2} = 76200$

4.4 Representation of the results

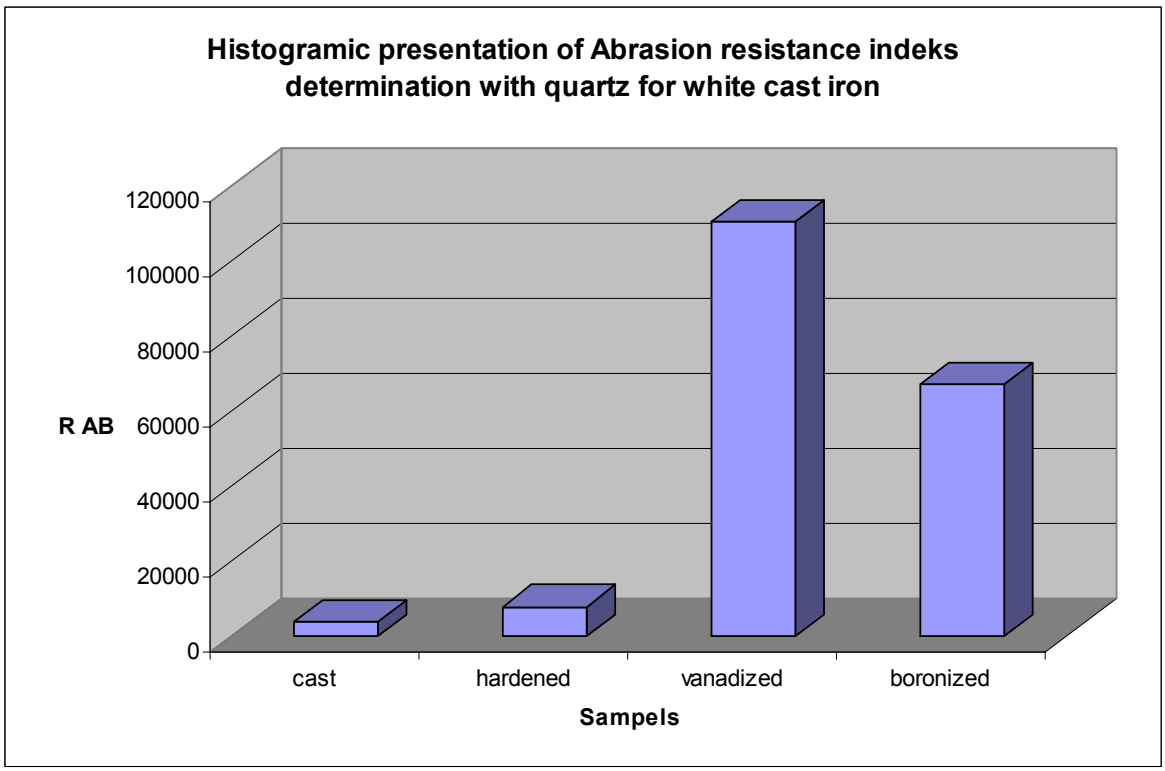


Figure 7 – Results of Abrasion resistance index determination test

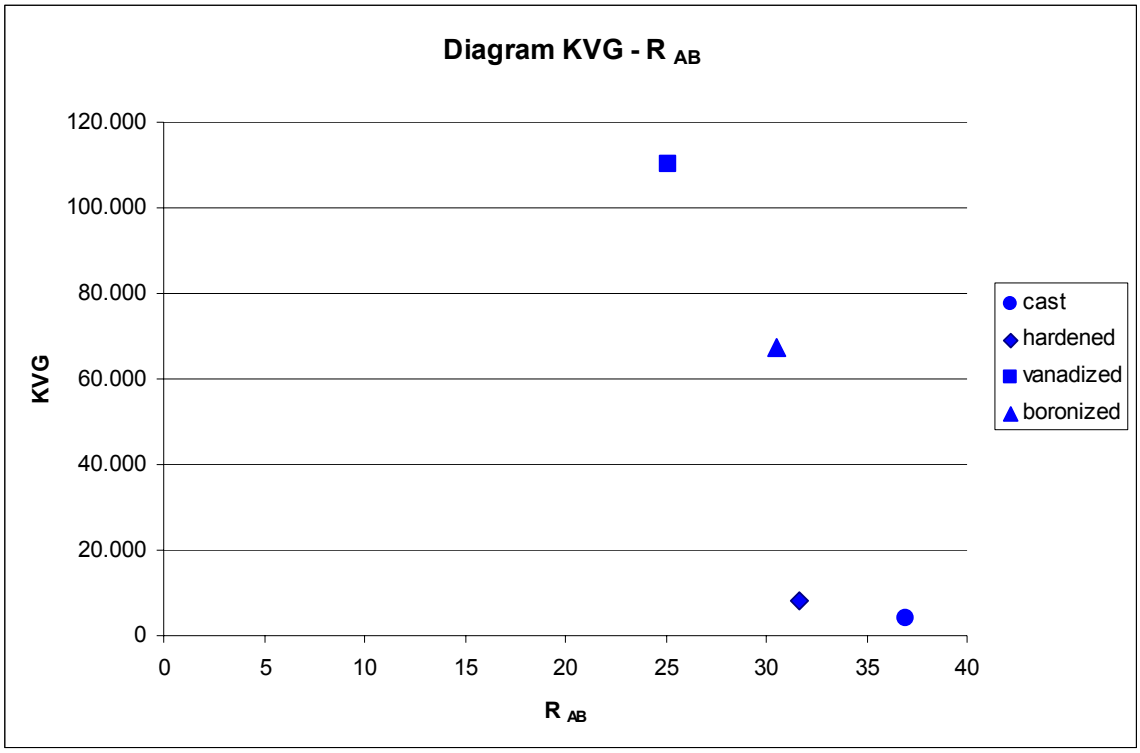


Figure 8 – Relation of values of corrected volume loss and abrasion resistance index

5 CONCLUSION

Based on the performed tests of wear by abrasion and the performed analysis of the results of wear it can be concluded that the model for determining the abrasion resistance index, which is based on the quantitative analysis of microstructure with the determination of microhardness of particular phases and taking into consideration the abrasive microhardness, is valid i.e. the obtained results during the volume loss measurement correspond to the calculated abrasion resistance indexes.

This model of abrasion resistance quantification does not take into consideration all influential factors which occur or may occur during the material abrasion, but only a few most influential.

These are the material microstructure, which is at this model necessary to quantify, and microhardness of abrasive and parts of microstructure.

However, it is not sufficient for the precise resistance index determination; therefore, by introducing new influential factors which occur during the abrasion wear, the observed model could be enhanced.

Due to the mentioned reasons, although in this quantification method of abrasion resistance certain factors are omitted, this model is applicable in practice and may give reference values at the material testing. However, due to a large number of influential factors, this wear resistance determination cannot completely replace experimental tests.

REFERENCES

[1] H. Uetz, "Abrasion und Erosion", Carl Hasner Verlag, München Wien 1986.

[2] M. Mitrovoć, "The laboratory measurement method of wear by abrasion resistance" (Graduation thesis), Faculty of mechanical engineering and naval architecture, Zagreb 1985.

[3] ASTM G65-94, Standard Practice for Conducting Dry Sand / Rubber Wheel Abrasion Tests

[5] M. Stupnišek, B. Štefotić, "Development of procedures of hard carbide layers creations on the steel by diffusion ", Papers 4. Symposium about the thermal metal-working, Paper on 4. Symposium about the thermal metal-working

[6] V. Ivušić, “Selection of material for equipment parts displayed wear by abrasion”, Comment 1 (1998), 9-13

METAL MATRIX COMPOSITES FOR FUSION REACTOR APPLICATIONS

Juraj KORÁB, Tomáš DVORÁK, Pavol ŠTEFÁNIK, Štefan KAVECKÝ

Institute of Materials and Machine Mechanics, Slovak Academy of Sciences, Račianska 75, 831 02 Bratislava 3, Slovak Republic

Izvorni znanstveni rad / Original scientific paper

Key words: copper, tungsten wires, metal matrix composite, heat sink, gas pressure infiltration, diffusion bonding, fusion reactor

Abstract

For production of the copper matrix tungsten fibres reinforced composite (Cu/W MMC) both diffusion bonding and gas pressure infiltration technology were used. In the first case the composite contained 50 vol. % of continuous fibres and in the second one it contained 63 vol. % and 78 vol. % of fibres.

Thermal expansion of unidirectional and cross-ply samples was measured in directions parallel and transverse to the fibre orientation. Although the longitudinal coefficient of thermal expansion (CTE) of unidirectional samples was low (4 - 6 ppm/K) the transverse coefficient was much higher (11 - 14 ppm/K). The composite with two-dimensional W-fibre orientation (cross-ply and W-cloth) presented slightly higher in-plane CTE (5 - 7 ppm/K) but for W-cloth it was much different: 3 - 16 ppm/K. In direction normal to the fibre orientation the CTE was 17 - 22 ppm/K.

For unidirectional infiltrated samples tensile strength was measured in direction parallel to the fibre axis (2043 MPa and 1733 MPa). Bending strength of infiltrated samples on the other hand showed slightly higher levels (2705 MPa and 3156 MPa) and diffusion-bonded material presented lower values due to its lower W-fibre content (1250 - 1430 MPa).

Introduction

Tungsten as a refractory material and copper as a very ductile and high conductive material are suitable candidates for production of metal matrix composites (MMC) that can be used in specific high temperature applications. The Cu/W composite that is going to be used for production of one part of the fusion reactor, a divertor [1], should have low thermal expansion and high thermal conductivity because it will work in the environment where very high temperature will be present (600 ^{o}C). The composite should also show good structural stability after facing to many thermal cycles that will occur during fusion reactor service.

On the other hand the fact that the material like the Cu/W MMC will be subjected to particle fluxes from the plasma (ions, electrons, atoms) and to electromagnetic radiation should be taken into account. Such materials have to show improved properties in also terms of e.g. erosion behaviour and heat flux capability [2].

Experimental

Composite preparation

In diffusion bonding technology thin monolayers of the Cu/W composite were used as the pre-material for manufacturing of the bulk composite samples. Monolayers were prepared by winding the W-wire (OSRAM) with a diameter of 50 μm on the outer surface of a steel cylinder and followed with their galvanic coating with a thin copper layer. A Cu/W layer formed on the cylinder - the monolayer - was cut into desired dimensions, placed into a steel tool and diffusion-bonded in vacuum to a bulk samples at following parameters: 700°C, 100 MPa, 900 s. Orientation of fibres in diffusion-bonded samples was both unidirectional and cross-ply and fibre fraction in both cases was of about 50 vol. %.

Another technology for the Cu/W composite preparation was the gas pressure infiltration. A W-fibre preform was prepared in the way that aligned W-fibres with diameter of 100 μm were inserted to the Mo-sheet cover and pressed together. Such a preform was infiltrated with liquid copper under following parameters: 1200°C, 1 MPa, 180 s.

Good wetting and no mutual reaction between constituents enable the Cu/W composite to be an ideal candidate for the liquid state production technology. However its disadvantage is that infiltration temperature (1200 ^{o}C) is very close to the recrystallisation temperature of W-fibres (1100 - 1400 ^{o}C) and it could later lead to degradation of some composite mechanical properties (ultimate tensile strength, σ_u, and elasticity modulus, E) [3].

Testing techniques

Coefficient of thermal expansion

Thermal expansion tests of the Cu/W composite were performed in a classical dilatometer in order to characterise relative dilatation and the coefficient of thermal expansion of the material. During each measurement were performed three heating and cooling cycles in temperature range from 20 °C up to 550 °C in argon atmosphere. Results are presented in Figures 6 - 10 and also in Table 1.

Tensile test

Tensile tests were performed at the ZWICK testing machine at the cross ram speed of 1 mm.min^{-1}. Measured gauge length l_o was 15 mm and the sample diameter was 1.13 mm.

Bending test

Bending tests were performed at the same testing machine with the cross ram speed of 1 mm.min^{-1}. The span of lower cylindrical supports with was 30 mm and their diameter was 8 mm

Results and discussion

Microstructure

Microstructure of the Cu/W composite with different fibre content and orientation is presented in Figures 1 - 5 where it is visible that diffusion bonded material contains less fibres than the infiltrated one (Fig. 1 and Fig. 2). Advantage of diffusion-bonded route is that fibre fraction can be adjusted in a larger range (e.g. from 30 to 60 vol. %) and can be controlled according to requirements. Diffusion-bonded samples were prepared from monolayers containing of about 50 vol. % of fibres and that is why the fibre content in the tested composite was the same.

For the infiltration route the fibre content was usually much higher (76 vol. %), which cannot be easily changed to lower values due to defined production route. In Figure 5 one can see the fracture surface of the Cu/W composite after tensile testing. It should be mentioned that it was very difficult to perform the test because W-fibres were very strong and Cu matrix very

ductile. This could be a reason why the sample cracked during testing also in the direction parallel to fibres.

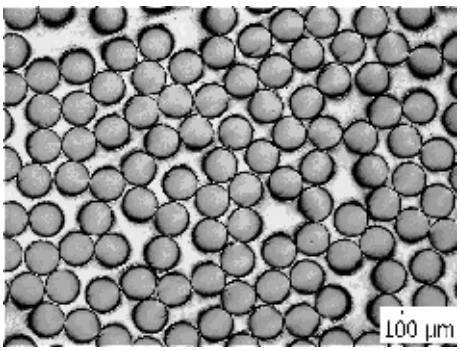


Figure 1 Microstructure of the infiltrated Cu/W composite. Volume fraction of fibres is 76 % in average.

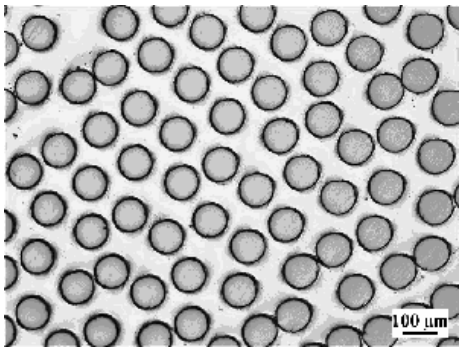


Figure 2 Microstructure of the diffusion bonded Cu/W composite. Volume fraction of fibres is approximately 50 %.

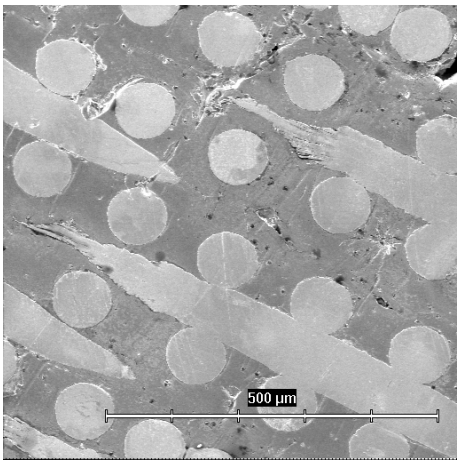


Figure 3 Microstructure of the Cu/W composite with the cross-ply (0°-90°) fibre orientation. The composite prepared by vacuum diffusion bonding of monolayers. Volume fraction of fibres is approximately 50 %.

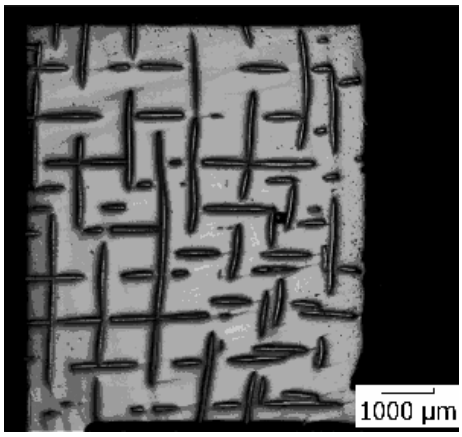


Figure 4 Microstructure of the Cu/W composite reinforced with the W-cloth (prepared by gas pressure infiltration).

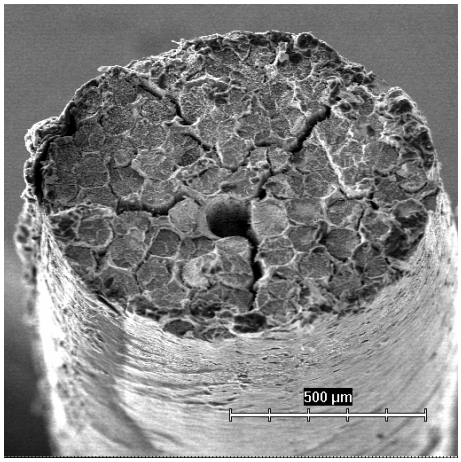


Figure 5 Fracture surface of the Cu/W composite after tensile testing.

Thermal expansion

Thermal expansion curves of different Cu/W samples are presented in Figures 6 - 9. The CTE values are then showed in Table 1.

Thermal expansion of unidirectional composites prepared by the gas pressure infiltration (fibre content 63 vol. % and 78 vol. %) is presented in Fig.6. The longitudinal CTE of the material is at the level of tungsten (4 – 5 ppm/K) and the transverse one is larger: in the range of 11 – 14 ppm/K.

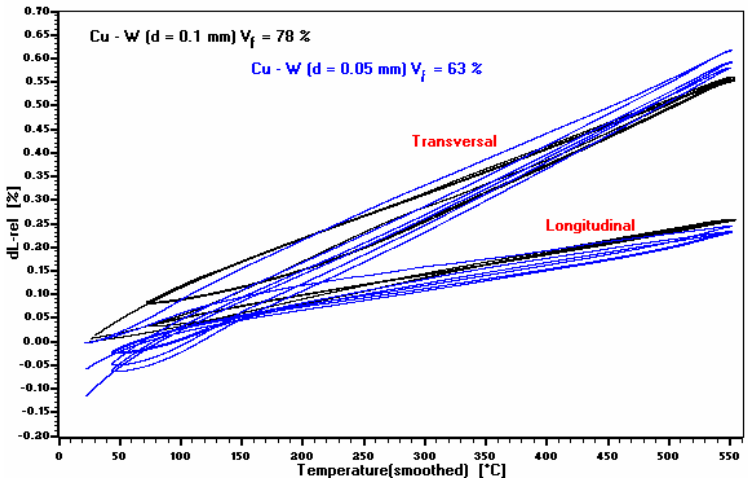


Figure 6 Thermal expansion curves of the unidirectional Cu/W composite measured in direction parallel (longitudinal) and normal (transverse) to the W-fibre orientation (produced by gas pressure infiltration)

Thermal expansion of the cross-ply composite prepared by diffusion bonding (Fig.7) showed that deformation of the composite in transverse direction is of about 0.3 %. It is not clear whether this indicates certain delamination due to insufficient adhesion between bonded monolayers or only compensation of constrained in-plane expansion. The in-plane CTE of the cross-ply composite was of about 5 - 7 ppm/K and similarly to previous cases the through-the-plane CTE was very high (17 - 20 ppm/K).

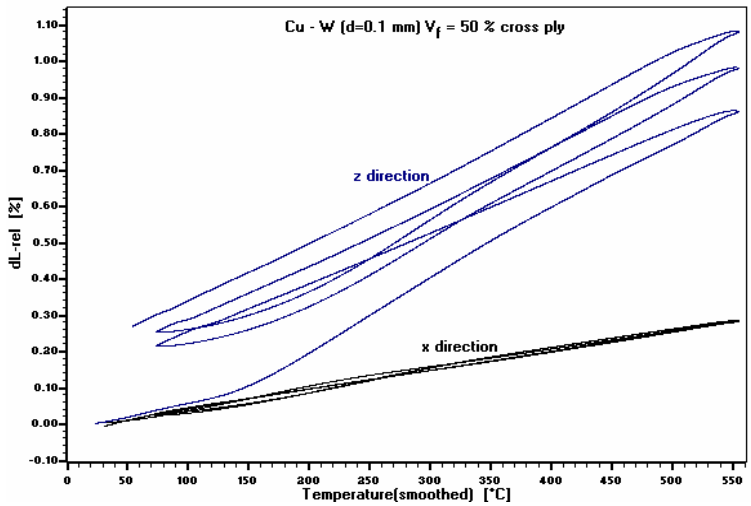


Figure 7 Comparison of thermal expansion curves of the cross-ply Cu/W composite prepared by diffusion bonding route (DB). Curves were measured in two directions: in - plane (x-direction) and normal to the W-fibres orientation (z-direction)

Comparison of thermal expansions of unidirectional samples prepared by different routes is presented in Fig.8. The longitudinal CTE of both diffusion bonded and an infiltrated material is very similar (4 - 5 ppm/K) - thermal expansion curves are nearly same. However, in transverse direction the CTE of diffusion bonded composite is much higher (18 – 21 ppm/K). Since the longitudinal CTE is stable and the chart did not reveal any deformation, shift in transverse direction can represent plastic deformation of the matrix that expand more due to limited expansion of the composite in longitudinal direction. However in transverse direction the above-mentioned poor bonding strength between monolayers could play an important role during testing.

From very large transverse thermal expansion of diffusion-bonded samples it can be concluded that the gas pressure infiltration is probably more appropriate technique for production of Cu/W composites.

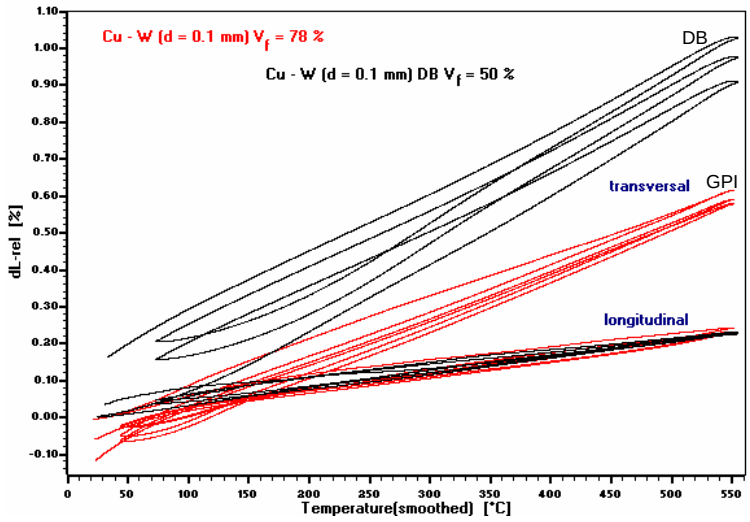


Figure 8 Comparison of thermal expansion curves of the unidirectional Cu/W composite prepared by both gas pressure infiltration (GPI) and by diffusion bonding route (DB). Curves were measured in direction parallel and normal to the W-fibre orientation

Thermal expansion of the Cu/W-cloth MMC produced by the GPI route showed quite different behaviour in two principal directions (Fig.9). The in-plane CTE was in very large range - from 3 to 16 ppm/K. The value 16 ppm/K was obtained only at high temperature (250 ^{o}C). This phenomenon might occur due to the fact that the fibre arrangement (W-cloth) is different that the one in the cross-ply composite (W-fibres were straight). The W-cloth reinforcement presented such design that fibres could stretch to a certain extent during thermal treatment and allowed the matrix to expand more. The through-the-plane CTE (z-direction) of the composite produced from W-cloth was very high (18 -22 ppm/K) and was similar to that for other samples.

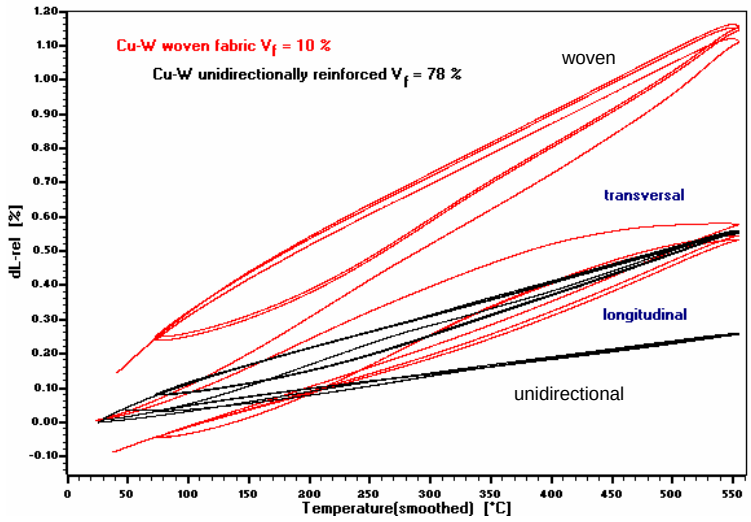


Figure 9 Comparison of thermal expansion curves of the Cu/W- woven/fabric and unidirectional Cu/W composite prepared by GPI. Curves were measured in two directions: along fibres (longitudinal and in-plane) and normal to the fibre axis (transverse).

Table 1 The coefficient of thermal expansion of different Cu/W samples

production route	fibre orientation	fibre fraction (vol. %)	CTE (ppm/K)		
			longitudinal	transverse	in-plane
gas pressure infiltration	unidirectional	63	4 - 5	12 - 14	-
	unidirectional	78	4 - 6	11 - 12	-
	woven / cloth	10	-	18 - 22	3 - 16 (higher value obtained at 250 °C)
diffusion bonding	unidirectional	50	4	18 - 21	-
	cross-ply	50	-	17 - 21	5 - 7

Tensile and bending tests

Tensile strength of unidirectional samples prepared by the GPI method was measured in direction parallel to the fibre axis (Table 2). The ultimate tensile strength values (σ_u), showed quite large scatter (2043 MPa and 1733 MPa) and they are slightly lower than those ones calculated from the rule-of-mixture (ROM): $\sigma_{u(ROM)}$ = 2300 MPa. The difference could be caused by some difficulties that occurred during testing. On one hand to clamp firmly the

Cu/W sample to the testing machine was difficult because W-fibres were very hard and on the other the composite sample was very strong to be broken. To complete the test according to standards was difficult and that is why the bending test was chosen as next testing method.
In Tables 2 and 3 mechanical testing values of Cu/W samples with similar W-fibre content are compared and from results one can see that the bending test gave higher values than the tensile test by approximately 30 %.

Table 2 Tensile test results of unidirectional Cu/W composites prepared by gas pressure infiltration method

Sample type	**76 % W fibres**	**78 % W fibres**
ultimate strength σ_u (MPa)	2043	1733
yield strength σ_Y (MPa)	1736	1526
elasticity modulus E (GPa)	356	332

Samples with different fibre content were prepared for bending test. From Table 3 one can see that volume fraction of fibres could reasonably influence mechanical properties of the composite. It should be noted that during bending test several cracks between monolayers were formed in each sample. This indicates that the interlayer shear stress was much higher than the bonding strength between monolayers. It means that diffusion-bonding temperature of about 700 ^{o}C was not sufficient to achieve a material with suitable properties.

Table 3 Bending test results of unidirectional Cu/W composites prepared by different technologies

Sample No.	**1632** **43 % W fibres** (diffusion bonded)	**B13** **78 % W fibres** (infiltrated)	**2013** **78 % W fibres** (infiltrated)
ultimate strength σ_u (MPa)	1250 - 1430	3156	2705

Conclusions

- Unidirectional Cu/W composite showed typical orthotropic properties - very low thermal expansion in direction parallel to fibres and very high thermal expansion in transverse direction. This behaviour was same for samples prepared by both gas pressure infiltration and diffusion bonding technology.
- The composite with two-dimensional fibre orientation (cross-ply and W-cloth) showed typically high through-the-plane CTE (17 - 22 ppm/K). The in-plane behaviour for the cross-ply material was according to requirements: 5 - 7 ppm/K.
- The W-cloth reinforced copper showed very different CTE in both in-plane and z-direction, 3 - 16 and 22 ppm/K, respectively. This means that the reinforcement for this type of composites needs to be optimised in order to decrease large differences.
- Tensile tests of unidirectional samples showed lower values than those calculated from the rule of mixtures.
- Bending test seemed to be more suitable for infiltrated composite.
- Interlaminar cracks occurred in diffusion-bonded samples after bending test and probably influenced the final result.

- Some difficulties during mechanical testing occurred and need to be solved in future work (poor sample clamping during tensile test and delamination during bending test).

Literature:

[1] http://www.iter.org/a/index_use_1.htm

[2] Plasma-facing Materials and Components, presentation of the Prof. Dr. Dr. Harald Bolt, Dr. Joachim Roth, Max-Planck-Institut für Plasmaphysik , Garching, Munich, Germany

[3] PLANSEE, Austria, a company leaflet, 2006

Acknowledgement:

This work has been performed within the framework of the Integrated European Project „ExtreMat“ (contract NMP-CT-2004-500253) and with financial support of the European Community. It only reflects the view of the authors and the European Community is not liable for any use of the information contained therein.
The authors acknowledge financial support from the Grant Agency of the Slovak Republic VEGA (project 2/7173/27).
Authors also thank to their former colleague Ivan Kramer for preparation of all relevant data used in this work.

SOL-GEL SYNTHESIS AND CHARACTERISATION OF NANOCRYSTALLINE GAHNITE

SOL-GEL SINTEZA I KARAKTERIZACIJA NANOKRISTALINIČNOG GANITA

S. Kurajica, E. Tkalčec, J. Šipušić, G. Matijašić, V. Mandić

University of Zagreb, Faculty of Chemical Engineering and Technology, 19 Marulićev trg, Zagreb, Croatia

Izvorni znanstveni rad / Original scientific paper

Abstract: Nanosized zinc aluminate spinel (gahnite, $ZnAl_2O_4$) powder was prepared by sol–gel technique at low sintering temperatures. The dried gel and thermally treated samples were characterized by means of Differential Thermal Analysis and Thermo-Gravimetric Analysis (DTA, TGA), X-Ray Diffraction (XRD) and Transmission Electron Microscopy (TEM). The surface area was measured by a Brunauer-Emmet-Teller (BET) adsorption-desorption isotherms. Zinc aluminate spinel powder was produced by gel heat-treatment at temperatures as low as 300 °C. The average gahnite crystallite size for the samples sintered in the temperature range of 400–1000 °C has been calculated by means of Scherrer equation revealing nanocrystalline powders were prepared. TEM micrograph of sample sintered at 700 °C for 2 h showed nano-sized particles with high level of agglomeration. The average particle sizes obtained using XRD, TEM and BET studies were compared.
Keywords: crystallite size, crystallization, gahnite, sol-gel synthesis.

Sažetak: Sol-gel metodom i sinteriranjem gela pri niskim temperaturama pripravljeni su prašci nanokristaliničnog cink aluminatnog spinela (ganita, $ZnAl_2O_4$). Osušeni gel i termički obrađeni uzorci karakterizirani su primjenom diferencijalne termičke i termogravimetrijske analize (DTA, TGA), rendgenske difrakcije (XRD) i transmisijske elektronske mikroskopije (TEM). Specifična aktivna površina određena je Brunauer-Emmet-Teller (BET) adsorpcijsko-desorpcijskom izotermom. Cink aluminatni spinel dobiven je termičkom obradom gela pri temperaturi od 300 °C. Prosječna veličina kristalita ganita u uzorcima sinteriranim u temperaturnom području 400–1000 °C izračunata je primjenom Scherrerove jednadžbe, te je utvrđeno da su pripravljeni prašci nanokristalinični. TEM mikrograf uzorka sinteriranog pri 700 °C tijekom 2h pokazuje da se prašak sastoji od jako aglomeriranih čestica nanometarskih veličina. Prosječne veličine čestica utvrđene primjenom XRD, TEM i BET metoda uspoređene su međusobno.
Ključne riječi: ganit, kristalizacija, sol-gel sinteza, veličina kristalita.

Introduction

Zinc aluminate spinel ($ZnAl_2O_4$), naturally occurring as the mineral gahnite has drown considerable attention as catalytic material (catalyst or metal support) with improved properties due to high thermal and chemical stability and high mechanical resistance [1]. In high-temperature processes, sintering resistance and chemical stability are the properties of the most significance for the catalytically active phases. Zinc aluminate spinel has been investigated as a catalyst for the numerous processes, as well as a catalyst support. Optical properties make gahnite material of interest for ceramic pigments and coatings [2].

Zinc aluminate spinel catalysts or supports and ceramics are commonly prepared by a solid-state reaction between zinc oxide and aluminum oxide [3]; however, for attaining complete reaction, a temperature of above 1000 °C has to be maintained for several days. The disadvantages of solid-state routes, such as inhomogeneity, lack of stoichiometry control, high sintering temperature and low surface area, are improved when the material is synthesized using a solution-based method [4].

Nanosized materials, in comparison with bulk materials, display improved properties such as lowered sintering temperatures, increased hardness, stability, diffusion, and ductility [5]. Aiming at nano-sized particles, different approaches are required. Compared with other techniques, the sol-gel method is a useful and attractive technique for the preparation of nanocrystalline gahnite because of its advantage of producing pure and ultrafine powders at low temperatures.

In the present paper, a sol-gel process is presented to synthesize $ZnAl_2O_4$ nanometer powders using $Al(O^sBu)_3$ (aluminium-sec-butoxide) and $Zn(NO_3)_2{\cdot}6H_2O$ (zinc nitrate hexahydrate) as starting materials. The crystal phase evolution, crystallite size and surface area have been investigated.

Experimental

The appropriate amount of $Al(O^sBu)_3$ (97%, Aldrich, UK) was dissolved in ^{s}BuOH (99%, Kemika, Croatia) using syringe to minimize exposure to air humidity. The appropriate amount of $Zn(NO_3)_2{\cdot}6H_2O$ (99%, Kemika, Croatia) was dissolved in ^{s}BuOH separately. The solutions were stirred for 1 h and then $Zn(NO_3)_2{\cdot}6H_2O$ solution was added dropwise to the $Al(O^sBu)_3$ solution. The molar ratio of $Al(O^sBu)_3$: $Zn(NO_3)_2{\cdot}6H_2O$: ^{s}BuOH was 2 : 1 : 10. The mixture was stirred in a closed reactor for 24 h at room temperature.

During synthesis the precipitation occurred and after 24 h stirring at room temperature white slurry has been obtained. The sample was poured into large Petri dish and kept at room temperature for seven days yielding fragile mass which was subsequently grinded to form a fine powder. The obtained samples were then calcined in static air at a heating rate of 10°C/h at various temperatures between 100–1000 °C for 2 h.

The thermal behavior of powder precursor was characterized with Differential Thermal Analysis (DTA) and Thermo-Gravimetric Analysis (TGA) using simultaneous DTA/TGA analyzer Netzsch STA 409. For the thermal analysis ~50 mg of material were placed in Pt crucibles and heated at a rate of 10 °Cmin^{-1} to a 1000 °C in a synthetic air flow of 30 cm^{3}min^{-1}, α-alumina was used as a reference.

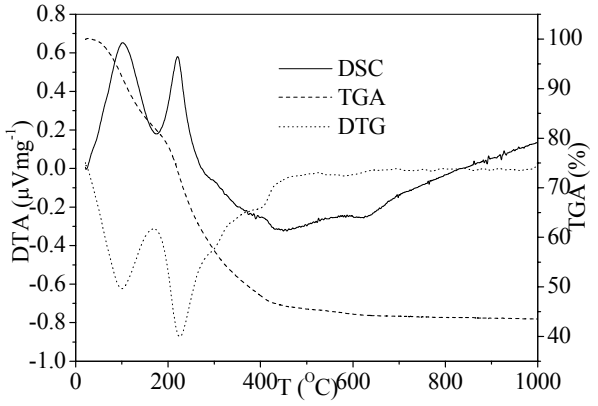


Figure 1. DTA and TGA curves of dried sample obtained with the heating rate of 10°Cmin^{-1}.

The crystal phases were identified by powder X-ray diffraction (XRD) on diffractometer Philips 1830 with CuKα radiation. Data were collected between 5 and 70^o 2θ in a step scan mode with steps of 0.02^o and counting time of 2s.

The average diameters of crystalline phase were calculated from Scherrer equation [6]: $d=(k\lambda)/(\cos\theta\times\beta)$, where d is the average crystallite diameter, k is Scherrer constant (0,89), λ is the X-ray wavelength (0,15178 nm), θ is the diffraction angle (18.453°) and β is full width at the half maximum of the strongest (311) diffraction peak corrected for the instrumental broadening.

The morphology of the sintered sample was examined using transmission electron microscopy (TEM) JEOL, JSM 6400F with an accelerating voltage of 200 kV.

Specific surface area of spinel powders and porosity were determined by a Brunauer–Emmet–Teller (BET) N_2 gas adsorption-desorption isotherm obtained at 77 K on a Micromeritics ASAP-2000 equipment. Sample was previously degassed at 400°C under a dynamic vacuum of 1.3×10^{-2} Pa. Surface areas were converted to particle sizes assuming that the particles are closed spheres with smooth surface and uniform size according to the equation: $D_{BET}=6x10^6/(\rho_{th}S_{BET})$, where D_{BET} (nm) is the average particle size in nm, ρ_{th} is the theoretical density of the powder (4.602 gcm^{-3}), and S_{BET} is the specific surface area expressed in m^{2}g^{-1} [7].

Results and discussion

Fig. 1 shows the DTA and TGA curves of the prepared dried gel. During the heating of the dried gels between room temperature and 1000°C several thermal features take place. Two endothermic effects occur with the maxima at 100°C and 220°C followed with a faint exotherm with the maxima at 623°C. The TGA curve (Fig. 1) shows two well defined weight loss steps between room temperature and 170°C, as well as between 170°C and 455°C. A continuous loss of 18 wt % and 36 wt % characterize first and second step, respectively. Additional mass loss of 3% is recorded until the 1000°C.

The dried gel was heated to temperatures between 200 and 1000°C in 100°C intervals with a soak period of 2 h. Fig. 2 shows the XRD patterns of dried and thermally treated samples. The XRD patterns of the as received powder exhibit several peaks attributed to a phase which belongs to hydrotalcite-like layered double hydroxides (LDHs). [6]. By thermal treatment at 200 °C for 2 h a new crystalline phase, $Zn(OH)(NO_3)(H_2O)$, (JCPDS 84-1907) was formed. An amorphous hump at about 6° 2θ, which can be attributed to amorphous alumina, was also observed. Complete disappearance of nitrate phase is observed in the sample thermally treated at 300 °C for 2 h simultaneously with the appearance of broad peaks with low intensity centered at 31.2,

36.8, 44.7, 55.6, 59.3 and 65.2° 2θ, which are attributed to cubic $ZnAl_2O_4$ spinel (JCPDS 82-1043). Accordingly, it could be concluded that crystallization of gahnite in sample occurs immediately after the decomposition of $Zn(OH)(NO_3)(H_2O)$ in the temperature range between 200 and 300°C. The exothermic effect of crystallization on DTA curve is overlapped by stronger endothermic effect occurring in this temperature range. Heat-treatment of the sample to higher temperatures up to a 1000°C yields no other phase beside gahnite. Therefore, additional exothermic peak at temperature of 623 °C was assigned to the additional gahnite crystallization process after complete removal of volatiles. The appearance of two crystallization processes is probably a consequence of partial segregation of nitrates in sample confirmed by XRD results (Fig. 2), as well as of the presence of organic residuals in the precursor. At higher temperatures presence of char is indicated by grayish powder appearance. The majority of zinc is not at disposal for reaction until the end of nitrate decomposition process, i.e. ~500°C. Shortly after this temperature the second crystallization step in sample GA0 occurs.

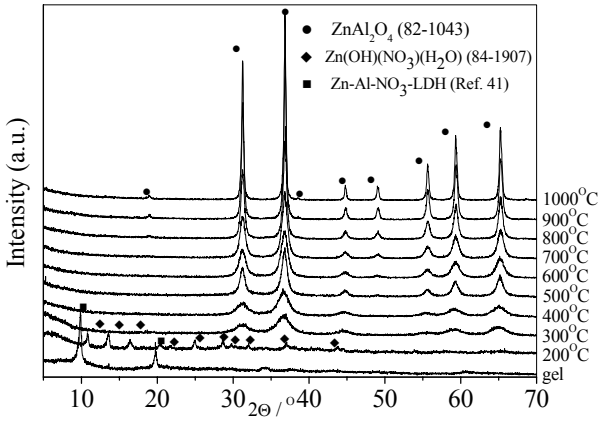


Figure 2. XRD patterns of dried gel and samples fired at different temperatures in the range of 100 and 1000°C for 2 h.

Effect of thermal treatment temperatures on spinel X-ray diffraction peaks shape is visible in Fig. 2. At lower temperatures peaks are broad pointing out to small crystallite size. With increasing heat-treatment temperature, the diffraction peaks become narrower and more intense, which is associated with an increase in the crystallite size. The average crystallite sizes of the powders sintered at different temperatures were determined from X-ray line broadening of the (311) diffraction line by means of the Scherrer formula. The dependence of the average $ZnAl_2O_4$ crystallite sizes on the annealing temperature is shown in Fig 3. The crystallite size increases up to a 500°C while for the sample fired at 600°C a decrease of crystallite size occurs. The decrease of crystallite size observed for the sample fired at 600°C (Fig 3) is in concordance with hypothesis of the second crystallization process producing a new portion of small crystallites. Described effect corroborates the conclusion that the second exothermal effect on DTA curve is a consequence of additional gahnite crystallization, i.e. that samples is characterized by two stage crystallization process. From the temperature of 600°C on, a continuous increase of crystallite size with firing temperature could be observed yielding crystallites of average size of 85 nm at 1000°C. The increase of crystallite size above 600°C is due to coarsening of particles at higher temperatures. In order to enable the crystallization of gahnite, but to restrict crystallite growth, the calcined temperature and time should be carefully controlled. Substantial crystallinity was achieved after firing the powder at 700°C for 2 h. $ZnAl_2O_4$ crystallites in samples calcined at 700°C for 2 h have an average size of about 15 nm.

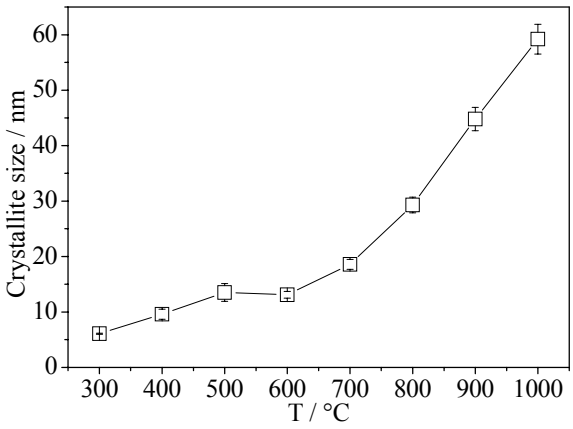


Figure 3. Crystallite size for the samples fired at different temperatures for 2 h calculated by means of Scherrer formula, vs. heat-treatment temperature.

The specific surface area and porosity has been determined for the sample fired at 700°C for 2 h. The BET specific surface area of the powder was 43.1 m^2g^{-1}. Analysis of porosity was carried out following the BJH method [9]. The pore size distribution curve (Fig. 4) displays a bimodal distribution with the most frequent pore radius (*Rp*) of 11 and 90 nm, respectively. The surface area and pore size distributions are of importance in catalysis materials determining the accessibility of reactant molecules. The average particle sizes, calculated from BET, for the sample fired at 700°C for 2 h, was 30 nm.

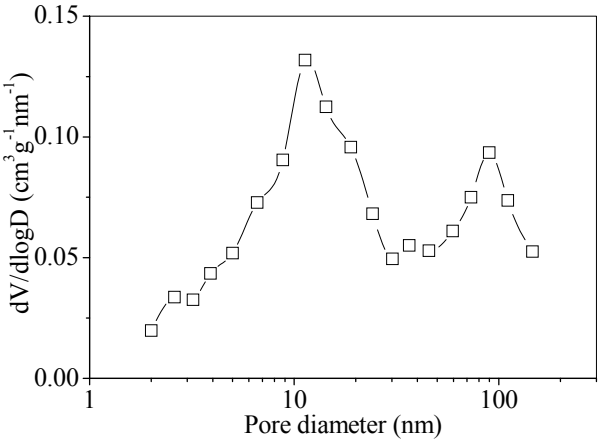


Figure 4. Pore size distribution of the sample annealed at 700°C for 2 h.

The morphology of the spinel powder thermally treated at 700°C for 2 h has been studied by transmission electron microscopy (TEM). The micrograph of the powder exhibits quasi-spherical particles with a broad size distribution (Fig. 5) having diameters in the range 10–30 nm. The micrograph revealed that powder consists of agglomerates of small primary particles with a high level of internal porosity, the pores observed represent no true porosity but voids between aggregated particles. The grain sizes from the observation of 50 particles for both samples were 10-30 nm, average 20 nm.

The average particle sizes, calculated by means of XRD and BET measurements and TEM observation, were 15, 30 and 20 nm, respectively. By the comparison of the crystallite sizes and the grain sizes calculated from BET specific surface area one can conclude that those methods do not correspond well with each other. The higher grain sizes calculated through surface area is a consequence of considerable reduction of surface area due to a higher level of aggregation. On the other hand, TEM observations show polydispersion of the samples which could be an explanation for particle size mismatch.

Conclusions

The sol-gel route for the preparation of zinc spinel nanometer powders from aluminium-*sec*-butoxide and zinc nitrate hexahydrate was presented.

The thermal evolution of precursor is characterized by two crystallization processes yielding pure zinc aluminate spinel. Zinc aluminate spinel was formed at temperatures as low as 300°C, which is lower than the most values of crystallization temperature reported in literature. Gahnite is only phase in samples determined in the temperature range of 400–1000°C.

The XRD, TEM and BET observations revealed that nano-sized particles were obtained. The surface area measured for the sample fired at 700°C for 2 h was 43.1 m^2g^{-1}. For the same sample TEM micrographs revealed high level of aggregation.

The presented process provides the obtaining of pure nanocrystalline zinc-aluminate spinel, with relatively high surface area, at very low temperatures, through a simple procedure, without need for stringent synthesis conditions.

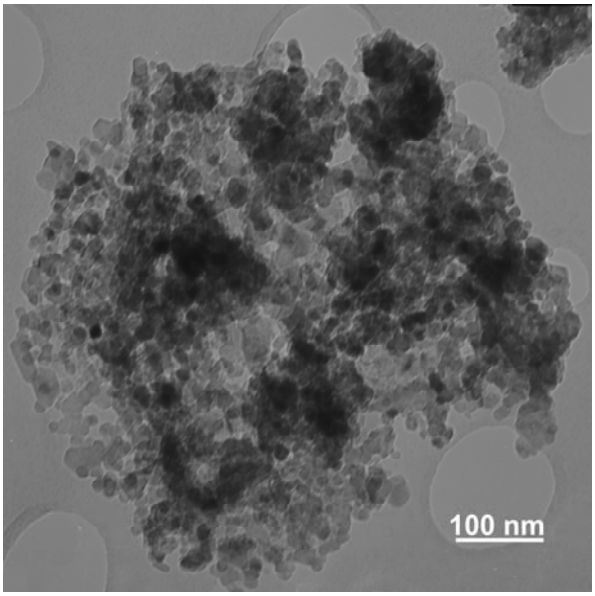


Figure 5. TEM micrograph of the sample annealed at 700°C for 2 h.

Acknowledgment

The financial support of the Ministry of Science, Education and Sports of Republic of Croatia within the framework of the project No. 125-1252970-2981"Ceramic nanocomposites obtained by sol-gel process" is greatly acknowledged.

References

1. J. Wrzyszcz, M. Zawadzki, J. Trawczynski, H. Grabowska, and W. Mista, Appl. Catal. A: Gen., 210 (2001) 263–269.
2. S. K. Sampath and J. F. Cordaro, J. Am. Ceram. Soc., 81 (1998) 649–654.
3. W.-S. Hong, L. C. De Jonghe, X. Yang, and M. N. Rahaman, J. Am. Ceram. Soc., 78 (1995) 3217–3224.
4. X. Wei, D. Chen, Mater. Lett., 60 (2006) 823–827.
5. N. Ichianose, Superfine Particle Technology. Springer-Verlag, Berlin, Germany, 1992.
6. B. D. Cullity, Elements of X-ray Diffraction, Addison-Weley, London, 1978.
7. P. Duran, J. Tartaj, F. Rubio, C. Moure, O. Pena, Ceram. Int., 31 (2005) 599–610.
8. S. Britto, A. V. Radha, N. Ravishhankar, P. Vishnu Kamath, 9 (2007) Sol. St. Sci 279
9. E.P. Barrett, G. Joyner, P.P. Halenda, J. Am. Chem. Soc. 73 (1951) 373.

PREPARATION OF ZIRCONIUM TITANATE CERAMICS BY SOL-GEL PROCESS

Jelena Macan, Suzana Markuš, Hrvoje Ivanković
Faculty of Chemical Engineering and Technology, University of Zagreb
HR-10001 Zagreb, Marulićev trg 19, p.p. 177, Croatia
e-mail: jmacan@pierre.fkit.hr

Izvorni znanstveni rad / Original scientific paper

Abstract: Zirconium titanate, $ZrTiO_4$, was synthesized by sol-gel method from zirconium butoxide and titanium isopropoxide. $ZrTiO_4$ gel was dried to obtain amorphous powder, which was ground to under 80 μm, calcined at 500 °C and milled to homogenise size distribution of the powder. Differential scanning calorimetry indicated crystallization of $ZrTiO_4$ at ~700 °C, which was confirmed by X-ray diffraction analysis. To study the influence of temperature on crystallization of $ZrTiO_4$, milled powder was also sintered at 900, 1100, 1200, 1300 and 1400 °C for 8 hours. It was found that crystallite size, as determined by Scherrer equation, increases with increasing temperature of sintering. Change of cell parameters indicates unusual transformation from disordered to ordered structure with increasing temperature. Applicability of $ZrTiO_4$ sols for preparation of thin coatings on glass substrates was also investigated. Increasing thickness of coatings leads to cracking of the coating, which can be prevented by decreasing sol viscosity or the speed of drawing the substrate from the sol.

Key words: crystallization, sol-gel process, thin coatings, zirconium titanate

Ključne riječi: kristalizacija, sol-gel postupak, tanke prevlake, cirkonijev titanat

1. INTRODUCTION

Zirconium titanate, $ZrTiO_4$, is a ceramic material with very good thermal and electrical properties and high resistance to heat and corrosive environment. This lead to its widespread use in electronic components for telecommunication purposes, such as condensers and resonators [1]. Zirconium titanate is also used for catalysts [2,3], and lately its applicability for humidity sensors is also being investigated [4]. High purity and homogeneity of ceramic material is essential for all these applications. This is difficult to achieve by classical procedure that consists of sintering a stoichiometric mixture of zirconia (ZrO_2) and titania (TiO_2) powder at temperatures up to 1600 °C for several days [1]. High-energy milling of ZrO_2 and TiO_2, which reduces crystallite size to give almost amorphous powders, can lower the transition temperature as low as 1100 °C. But this approach is also energy costly, and attrition of milling balls can increase content of impurities [5]. Because of this, sol-gel process is increasingly used to prepare homogeneous and amorphous $ZrTiO_4$ powder that crystallizes at temperatures several hundred degrees lower than in previously described methods. $ZrTiO_4$ can be prepared by hydrolysis and condensation of inorganic salts [3] or alkoxides [2]. Ceramics synthesized by sol-gel process are very pure, their microstructure is comparatively easy to tailor, and the process is also suitable for preparation of thin films [6]. In this work we investigated influence of sintering temperature on crystallization of $ZrTiO_4$ prepared by sol-gel process, and determined the best conditions for drawing thin $ZrTiO_4$ films on glass substrates.

2. EXPERIMENTAL

Zirconium titanate, $ZrTiO_4$, was synthesized by sol-gel method from zirconium butoxide ($Zr(C_4H_9O)_4$, 80 %, Fluka) and titanium isopropoxide ($Ti(C_3H_7O)_4$, 97 %, Aldrich), stabilised with 0.3 mol of acetylacetone ($C_5H_8O_2$, Fluka) per mole of alkoxide, in 2-propanol solution. Stabilised alkoxides were hydrolysed with stoichiometric amount of water for full condensation of alkoxides (2 moles per mole of alkoxide), added as 4.64 mol/dm^3 nitric acid that served as catalyst. Transparent sol was left to gel at room temperature. The resulting gel was dried at 110 °C, ground and sieved to remove particles larger than 80 μm, calcined at 500 °C to remove residual organic content, and milled. Milling was performed for 2 hours in air using a planetary ball mill Fritsch Pulverisette 6 with vial and balls of 94 % zirconia, with rotation speed of 500 rpm and powder-to-ball weight ratio of 1:10.

Table 1: Composition of sols used for preparation of amorphous $ZrTiO_4$ powder (sol A) and for drawing the thin films (sols A and B)

	Sol A	Sol B
Zr-butoxide	1 mol	1 mol
Ti-isopropoxide	1 mol	1 mol
acetylacetone	0.6 mol	0.6 mol
nitric acid	0.4 mol	0.4 mol
water	4 mol	4 mol
2-propanol	15 mol	30 mol

Thermal behaviour of the milled powder was studied by simultaneous differential scanning calorimetry and thermogravimetric analysis (DSC-TGA) on a Netzsch thermoanalyzer STA 409. Sample was heated from room temperature to

1350 °C at a heating rate of 10 °C/min in a synthetic air flow of 30 cm^3/min. Milled powder was sintered for 8 hours in a muffle furnace with Pt-PtRh thermocouple at 900, 1100, 1200, 1300 and 1400 °C. Furnace was heated to sintering temperature at 23 °C/min. X-ray powder diffraction (XRD) analysis was performed on Phillips PW 1820 instrument making use of CuKα radiation with a scanning rate of 0.12°/min. Crystallite size was determined using Scherrer equation, while crystal lattice parameters were determined from positions of diffraction maxima by computer program *Unitcell* [7]. Fully crystallized rutile, TiO_2, was used as a standard both for crystallite size and for position of diffraction maxima. Preparation and characterization of $ZrTiO_4$ powder is schematically shown in Figure 1.

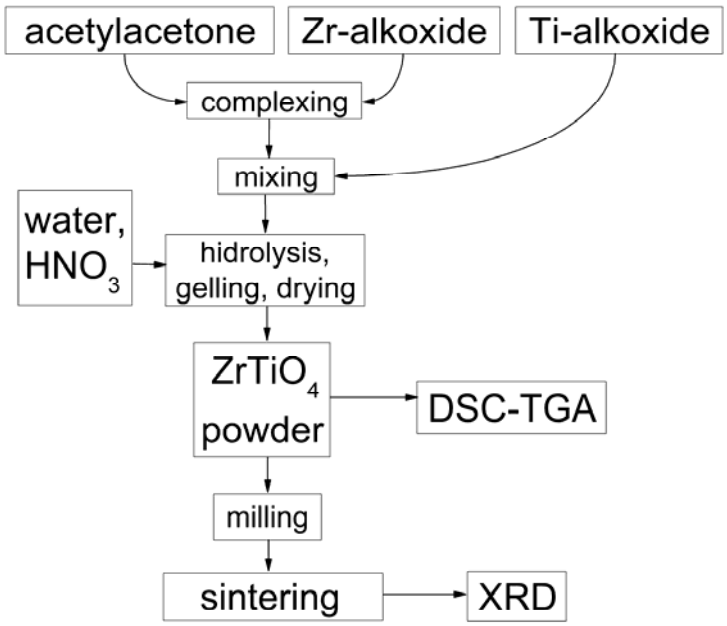


Figure 1 – Shematic representation of preparation procedure and characterisation of $ZrTiO_4$ powder

Thin $ZrTiO_4$ films were drawn on glass microscope slides previously cleaned with acetone, making use of custom-made dip-coating apparatus with drawing speeds of 0.18 and 0.05 cm/s. Viscosity of sols was modified by dilution of sol with 2-propanol, from 8.4 mPa s (sol A) to 3.3 mPa s (sol B), as determined by Höppler viscosimeter at the constant temperature of 20 °C. Viscosity of the sols increased due to condensation proceeding during 3 hours of drawing to 91.8 mPa s and 38.4 mPa s, recpectively. After drawing, coatings were dried at 110 °C for one hour, and each slide was coated from 1 to 3 times. Morphology of coatings was investigated by MOTIC BA200 optical microscope.

3. DISCUSSION OF RESULTS

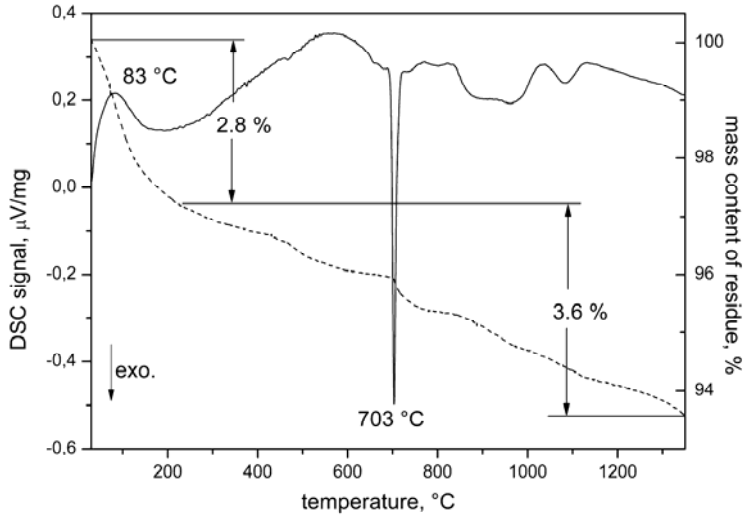


Figure 2 – Combined differential scanning calorimetry and thermogravimetric analysis of $ZrTiO_4$ amorphous powder calcined at 500 °C, taken in air at 10 °C/min

Results of DSC-TGA analysis are given in Figure 2. The first mass loss evident on the TGA curve and accompanied by a DSC endothermic maximum at 83 °C is due to evaporation of adsorbed water. The mass loss decreases approximately constantly with further temperature increase, which is ascribed to slow degradation of residual organic content. Large DSC exothermic maximum at 703 °C is due to crystallization of amorphous $ZrTiO_4$, as confirmed by XRD (Figure 3).

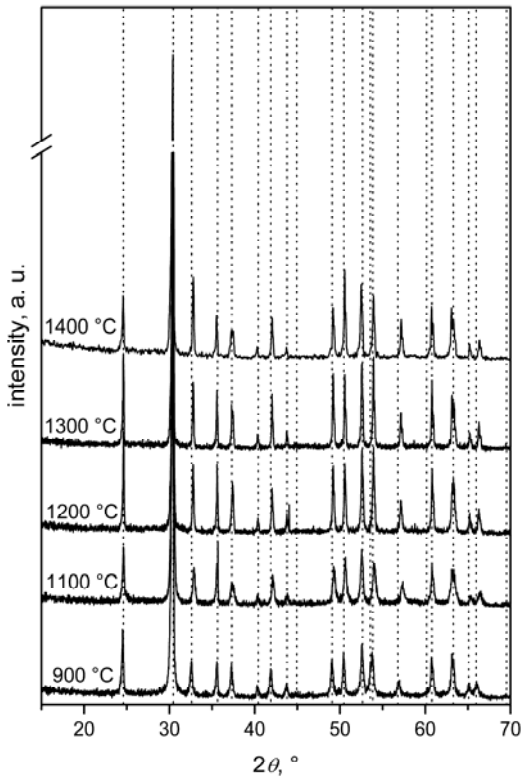


Figure 3 – X-ray diffractograms of $ZrTiO_4$ powder sintered at denoted temperatures; JCPDS data for zirconium titanate (34-415) shown as dotted lines

Table 2: Crystallite size as determined by Scherrer equation and porosity as determined by mercury intrusion, for $ZrTiO_4$ powders and tablets sintered at listed temperatures

Temperature, °C	Crystallite size, nm	Lattice parameters, Å		
		a	*b*	*c*
900	35	5.036	5.486	4.812
1100	40	5.038	5.440	4.816
1200	90	5.037	5.452	4.810
1300	130	5.034	5.442	4.814
1400	130	5.032	5.436	4.815

All sintered samples are pure crystalline $ZrTiO_4$, which crystallizes in orthorhombic symmetry. Increase in sintering temperature promotes crystallite growth, which is apparent from decreased width and increased intensity of XRD maxima. Average crystallite size in tablets and unpressed powders was determined from broadening of the XRD maxima by Scherrer equation (Table 2), using TiO_2 sintered at 1200 °C as a standard to correct for the instrumental broadening. The strain contribution to the broadening could be neglected in the calculation at low Bragg angles [8]. The apparent crystallite size expectedly increases with sintering temperature.

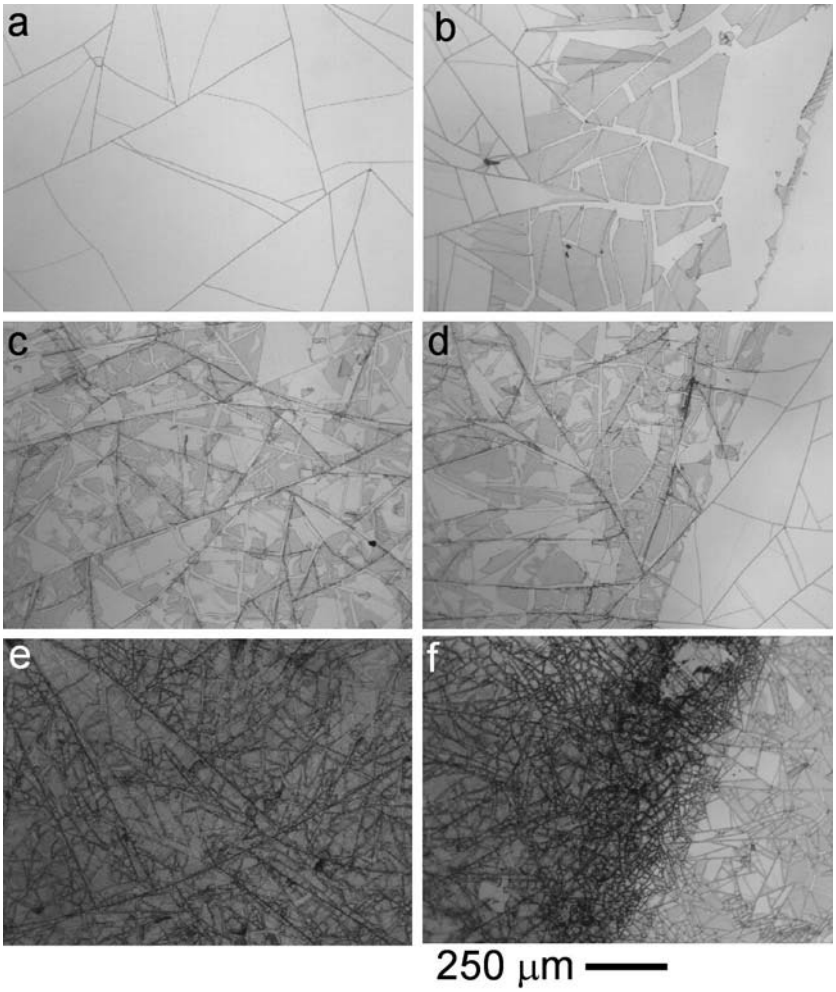


Figure 4 – Morphology of $ZrTiO_4$ coatings on glass substrate, drawn from sol A with drawing speed of 0.18 cm/s: a, b) one layer, c, d) 2 layers, e, f) 3 layers; b, d, f) edge of coating

Lattice parameter *b* decreases markedly between 900 and 1100 °C (Table 2), which could be an indication of order-disorder transformation. This is unusual since ordinarily parameter *b* decreases when disordered high-temperature form changes into more ordered low-temperature form upon very slow cooling. $ZrTiO_4$ prepared by sol-gel process crystallizes in "high-temperature" disordered state at low temperatures, because the disorder present in the initial amorphous powder is preserved in the crystalline product [9]. The ordering is most probably due to prolonged calcination at higher temperatures [10], but formation of non-stoichiometric $ZrTiO_4$ or solid solutions is also a possibility [10,11].

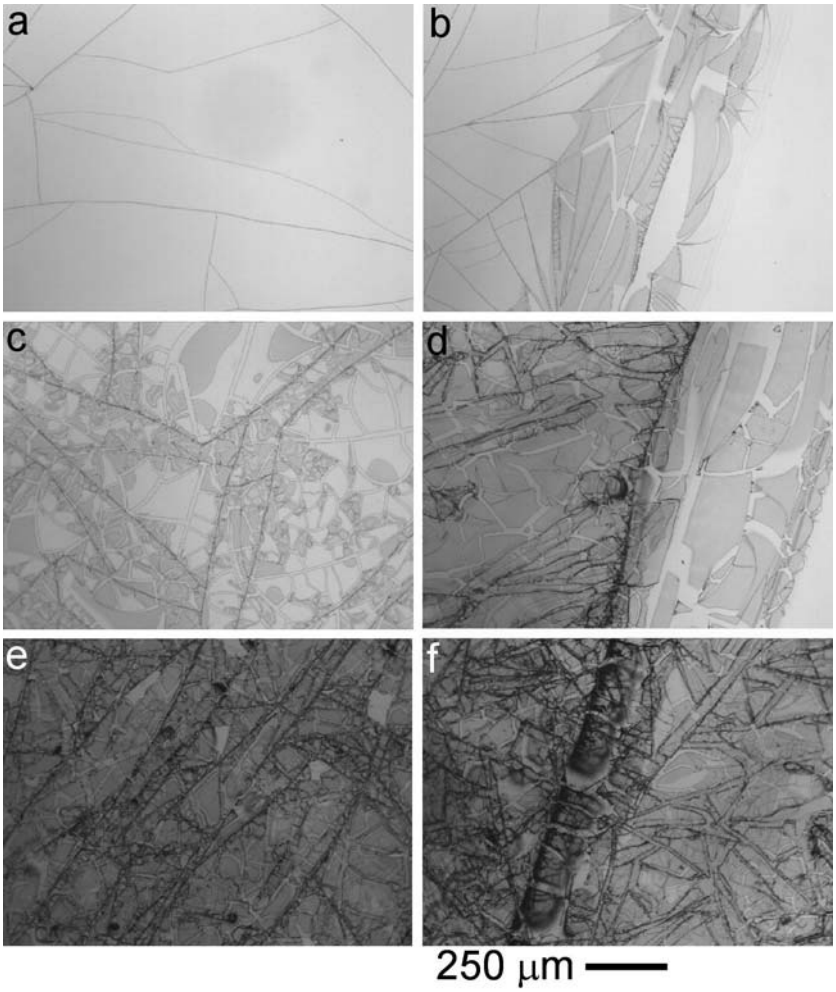


Figure 5 – Morphology of $ZrTiO_4$ coatings on glass substrate, drawn from sol A with drawing speed of 0.05 cm/s: a, b) one layer, c, d) 2 layers, e, f) 3 layers; b, d, f) edge of coating

Thickness of films depends on viscosity of sols, content of oxides or alkoxides in the sol, temperature and speed of drawing. Too thick films crack upon drying and peel from the substrate, so all of the above mentioned factors have to be optimised in order to achieve crack-free homogeneous films. Morphology of $ZrTiO_4$ coatings as a result of drawing speed and viscosity/alkoxide concentration of sols are shown in Figures 4-6.

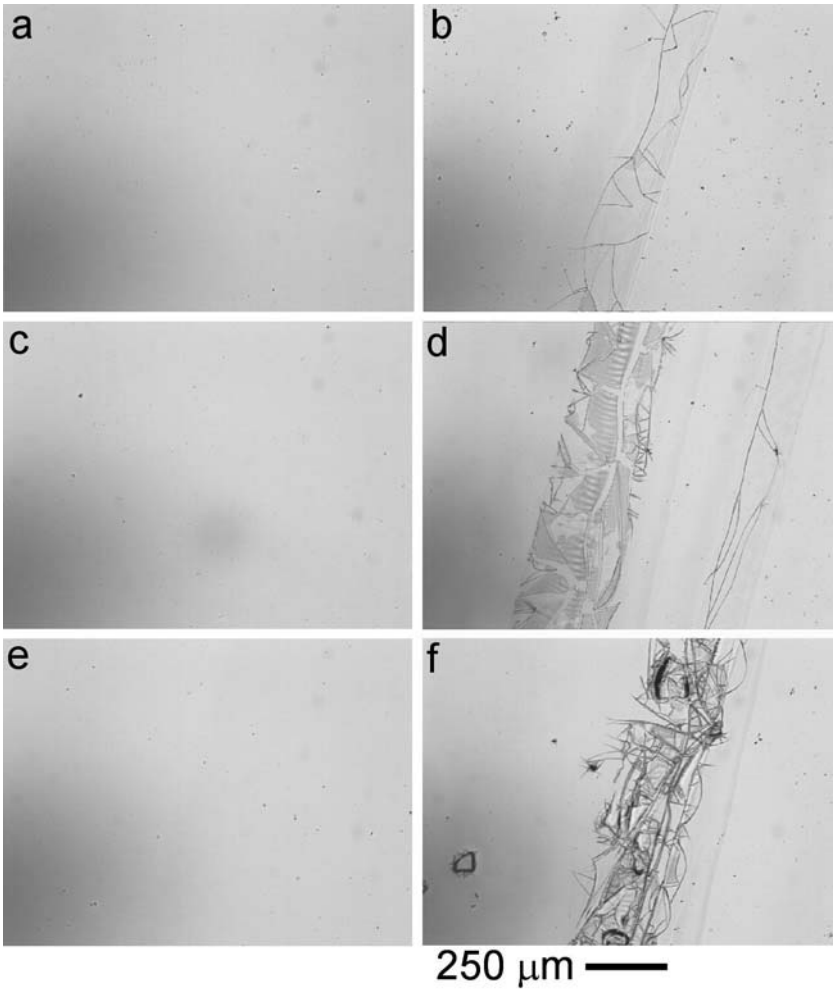


Figure 6 – Morphology of $ZrTiO_4$ coatings on glass substrate, drawn from sol B with drawing speed of 0.05 cm/s: a, b) one layer, c, d) 2 layers, e, f) 3 layers; b, d, f) edge of coating

Fast drawing speed (Figure 4) results in thick coatings that crack easily, and the cracking is more pronounced in multilayered coatings. Coatings drawn with the slowest drawing speed of the dip-coating apparatus also cracked (Figure 5). Although the cracking was somewhat less pronounced than in previous coatings, there was no practical difference. So, in order to produce crack-free coatings, viscosity and alkoxide content of sols was decreased by diluting with solute. In this manner crack-free coatings were prepared (Figure 6), even after deposition of 3 layers to prepare thicker coatings. Since viscosity increased 10 times during drawing, the decreased alkoxide content in sol was probably the key in producing crack-free coatings. Dilute sol remained stable for over 30 days when stored in tightly closed container.

4. CONCLUSIONS

Stable $ZrTiO_4$ sols were prepared by sol-gel process from zirconium butoxide and titanium isopropoxide. Powder prepared from the sol crystallizes into orthorombic $ZrTiO_4$ in one step at 703 °C. Size of $ZrTiO_4$ crystallites increases with sintering temperature, while crystalline structure transforms into more ordered form between 900 and 1100 °C. Crack-free coatings were drawn from diluted sol, and thicker coatings could be prepared by depositing several layers.

ACKNOWLEDGMENTS

Authors would like to thank the Ministry of Science, Education and Sport of the Republic of Croatia for the financial support of this study, which is a part of research project "Bioceramic, Polymer and Composite Nanostructured Materials", 125-1252970-3005.

REFERENCES

1. Y. Park, Y. H. Kim, H. G. Kim, *Mat. Sci. Eng. B* **40** (1996) 37.

2. M. C. Barrera, M. Viniegra, J. Escobar, M. Vrinat, J. A. de los Reyes, F. Murrieta, J. García, *Catal. Today* **98** (2004) 131.

3. J. Fung, I. Wang, *J. Catal.* **130** (1991) 577.

4. I. C. Cosentino, E. N. S. Muccillo, R. Muccillo, *Sens. Actuator. B* **96** (2003) 677.

6. A. Gajović, I. Djerdj, K. Furić, R. Schlögl, D. S. Su, *Cryst. Res. Technol.* **41** (2006) 1076.

6. R. W. Jones, *Fundamental principles of sol-gel technology*, The Institute of Metals, London, 1989.

7. T. J. B. Holland, S. A. T. Redfern, *Mineral. Mag.* **61** (1997) 65.

8. H. P. Klug, L. E. Alexander, *X-ray diffraction procedures*, J. Wiley, New York, 1974.

9. J. Xu, C. Lind, A. P. Wilkinson, S. Pattanaik, *Chem. Mater.* **12** (2000) 3347.

10. M. Dondi, F. Matteucci, G. Cruciani, *J. Solid State Chem.* **179** (2006) 233.

11. U. Troitzsch, A. G. Christy, D. J. Ellis, *Phys. Chem. Miner.* **32** (2005) 504.

EVALUATION OF SPECIFIC FAILURES OF SYSTEMS THIN FILM – SUBSTRATE FROM SCRATCH INDENTATION IN DETAIL

Kateřina Macháčková, Jana Palubjaková

University of West Bohemia, Universitni 22, 306 14 Pilsen, CZH, katerina.machackova@t-email.cz

Izvorni znanstveni rad / Original scientific paper

Abstract:

The paper is devoted to scratch indentation test for evaluation of properties and behaviour of systems thin film – substrate. There is used information from acoustic emission signal, coefficient of friction and the most of all evaluation of failures from surface and from cross section were used. All results are given to the correlations. Methods of evaluation are applied on analysis of systems thin film – substrate, where the basic material is from HSS and from steel with lower hardness. Thin films were deposited by low voltage reactive arc evaporation in vacuum.

1. Introduction:

The Scratch test is very often used, for evaluation of the thin films. Evaluation of the adhesion by this method is impressed with many elements. That's why it's necessary this test extend and clarify influences of these parameters. This examination is then more complex. It is necessary rather talk about evaluation adhesive - cohesive behaviour of the systems with thin films. Then it is possible evaluate of adhesion thin films to the substrate, cohesive properties of thin films and cohesive properties to surface basic material. It is important for us these failures evaluate in the details and connect more information, which we evaluate often apart.

Fulfilment SCRATCH TEST:

The samples were fixed on the sliding table. The diamond indentor (Rockwell type) had constant speed 7 mm/min. On the systems thin film - basic material was done with the diamond indentor and with the indentor of sintered carbide, normal force was from 0 N to the 80 N. With all indentors were made scratches, after 1, 2, 3, 5, 7, 10, 15, 22, 30 and 50 cycles. Complex visual evaluation is possible to determine by metallographical microscope - Nikon Optiphot 100S. By this light microscope were system image analyses performed. That makes it possible to digitize visual information to the computer over camera Sony DXC - 151 AP RGB and frame graber card Matrix Vision Pcimage - SRGB. Next part of all systems is software that scans individual scratches to the computer and pasted by using software Matlab. Scratches were documented by light microscope by using of polarizing and Nomarskeho DIC on magnification 200x on the system TiN - steel ČSN 19 830, 12 050 and 14 220.

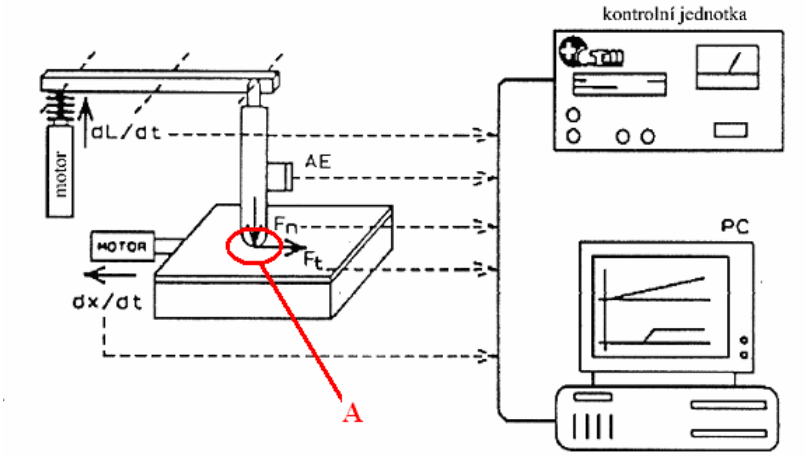


Fig.1. Schematic diagram of scratch test: Fn – normal force, F_t – tangential force in direction of indentor movement, AE - signal acoustic emission, dx / dt – sample velocity, dL / dt –growth force velocity.

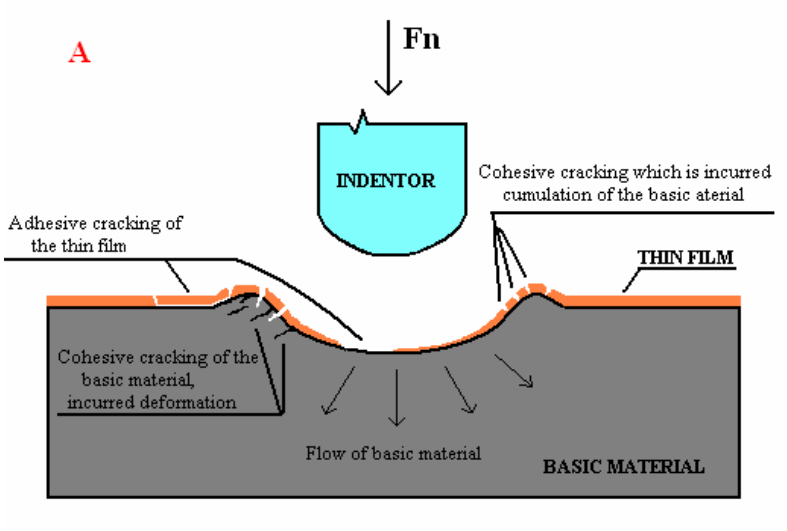


Fig.2. Schematic interface: thin film–basic material, significant line character of basic material at the scratchtest.

2. Details of significant failure

Firstly we register all the morphologies after the scratch test and we assign the given normal forces to the given failures. This evaluation we performed by measuring with the variable normal force or with the constant growing of normal force. From all morphologies we select characteristic failures.

Exhibits evaluation of failure system thin film TiN - basic material (19 830, 12 050 and 14 220), by using a light microscopy:

The failures frictional whit the diamond indentor on the systém thin film (TiN) – basic material (steel 19 830).

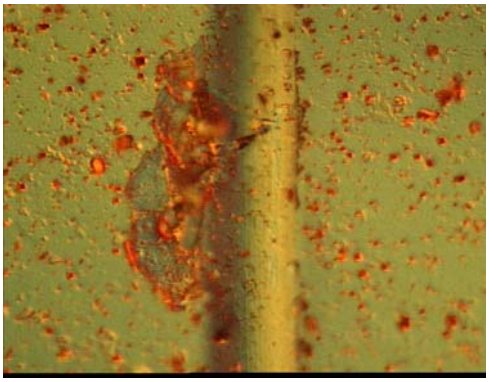


Fig.3. Detail defect after 1 cycle. Magnification 200x

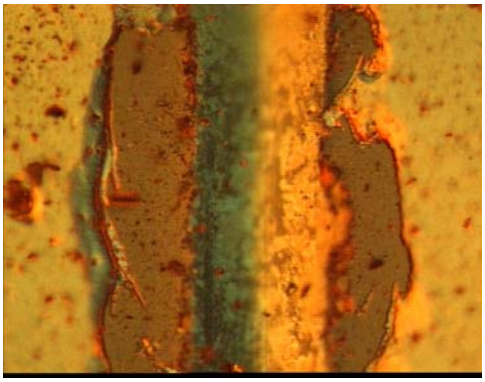


Fig.4. Detail defect after 1 cycle. Magnification 200x

The Failures frictional whit the indentor from sintered carbide on the system thin film (TiN) - basic material (steel 14 220).

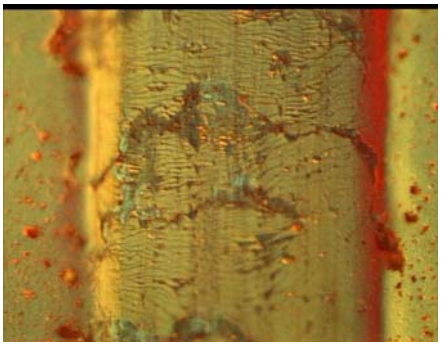


Fig.5. Detail defect after 1 cycle. Magnification 500x

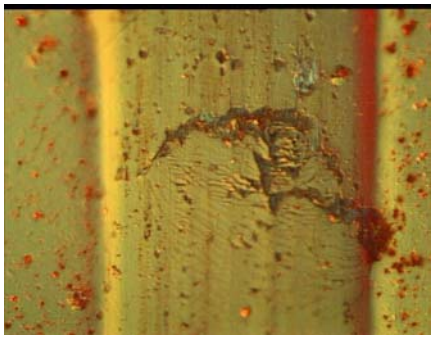


Fig.6. Detail defect after 1 cycle. Magnification 500x

<u>Exhibits evaluation of failure system thin film TiN - basic material (19 830, 12 050 and 14 220), by using a light microscopy:</u>

Documentation of cohesive defect in the scratch after 5, 10, 15 and 20 cycles on the system thin film (TiN) - basic material (19 830). The thin film has thickness 3,4µm.

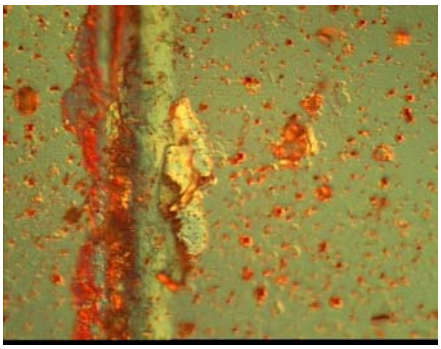


Fig.7. Detail defect after 5 cycles. Magnification 200x

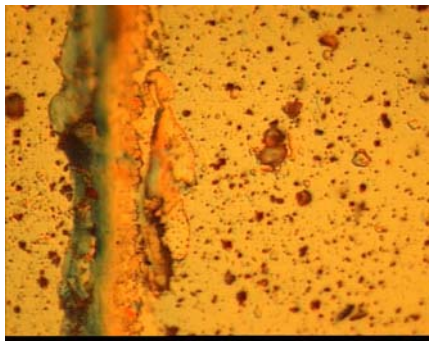


Fig.8. Detail defect after 10 cycles. Magnification 200x

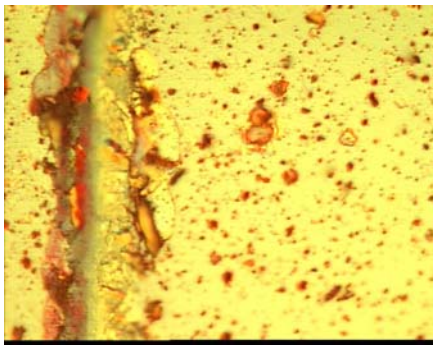


Fig.9. Detail defect after 15 cycles. Magnification 200x

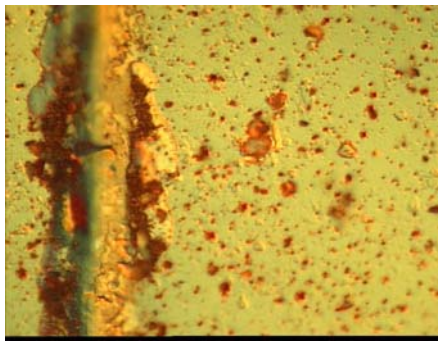


Fig.10. Detail defect after 20 cycles. Magnification 200x

3. Measuring of scratches width after the cycles

Further, for us important factor is characteristics evaluating of the scratch. From the surface we evaluate width of the scratch to the assigned normal force, it shows on the range failure in the vicinage scratch.

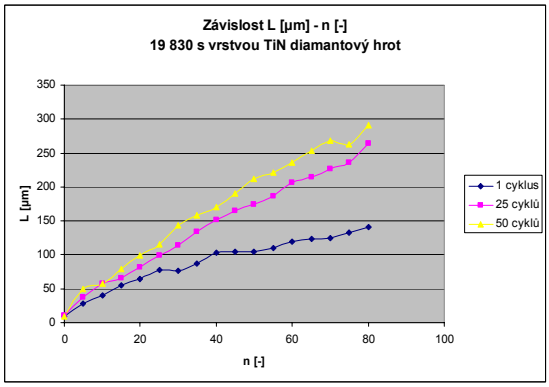


Fig.11. Graph of dependencies of width scratches on number cycles (ČSN 19 830)

In figure 11 you can see on the systems TiN - steel CSN 19 830 the changes after the cyclic scratch test. There is shown a fortification of surface by the thin film and growing width scratch with the higher cycles.

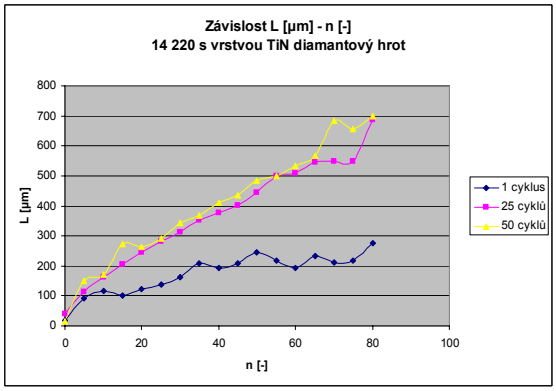


Fig.12. Graph of dependencies of width scratches on number cycles (ČSN 14 220)

In figure 12 you can see on the systems TiN - steel CSN 14 220 the changes after the cyclic scratch test. There is big contribution of thin film. The system resilience highly declines, when the indentor break into bigger depths.

4. Graphic evaluation and registration of acoustical emission

By the scratch test CSEM REVETEST we evaluate also signal of acoustical emission. The senor of acoustical emission is on the holder of diamond indentors. This signal is effected by many factors.

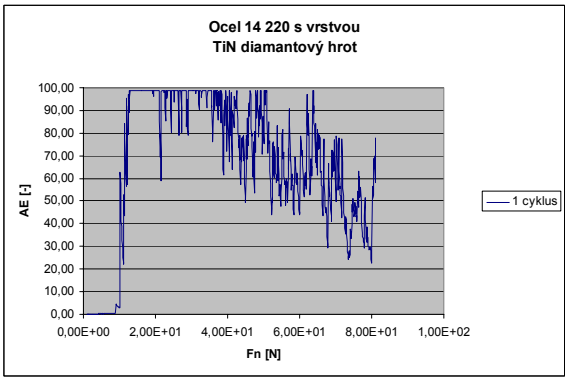


Fig.13. Graph of dependencies of acoustical emission on normal force. The system TiN – CSN 14 220

The signal of acoustic emission on the system TiN - CSN 14 220 (Fig.13) responds to cracking of surface film. This cracking is effected of plastic deformation. On the start, the acoustic emission fast increases and with the higher normal force is the signal of acoustic emission lower. It is effected by indentor, by his penetration into bigger depth. It means that stress not makes oneself felt.
On the system TiN – CSN 19 830 (Fig. 14) the acoustic emission increases when the normal force is higher. It's thereby, that the system TiN - CSN 19 830 is firmer. The signal acoustic emission thenceforth not decreases, because the substrate (CSN 19 830) cracks.

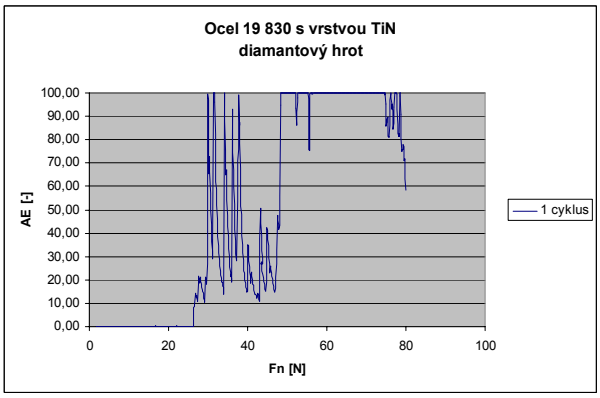


Fig.14. Graph of dependencies of acoustical emission on normal force. The system TiN – CSN 19 830

4. Exhibits evaluation failure by the help crossection

The analyse by the help crossection is for us too important. From the crossection we evaluate the characteristics failures. This method is very time - consuming and technically difficult. The crossection on the many questions answers. The crossection on the many questions can answers and then we can perfect of deposition.

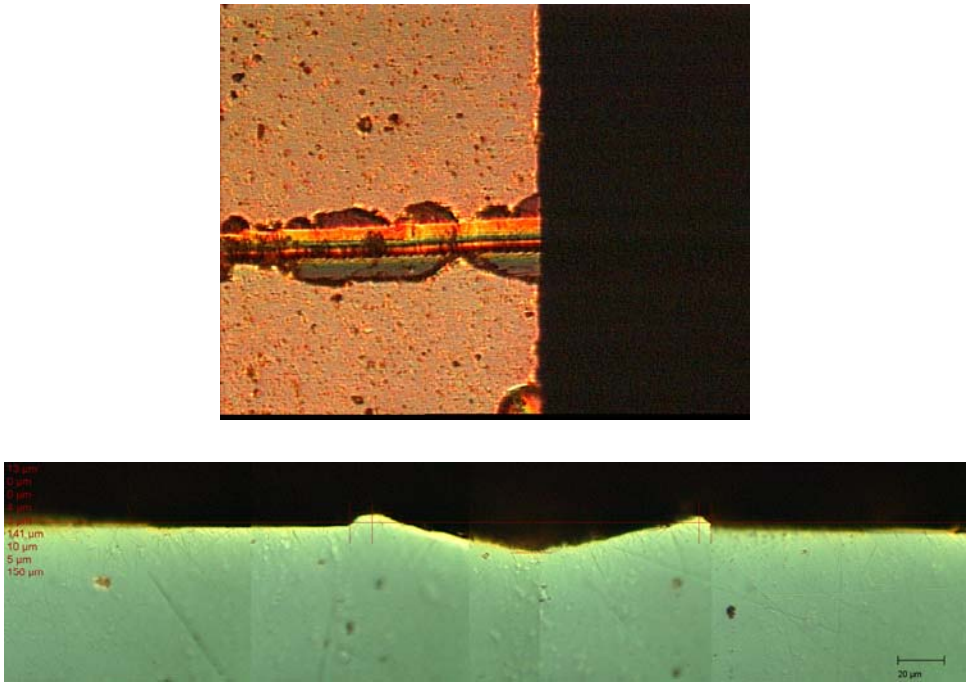


Fig.15. Tle Crossection after one cycle whit diamond indentor. Magnification 1000x

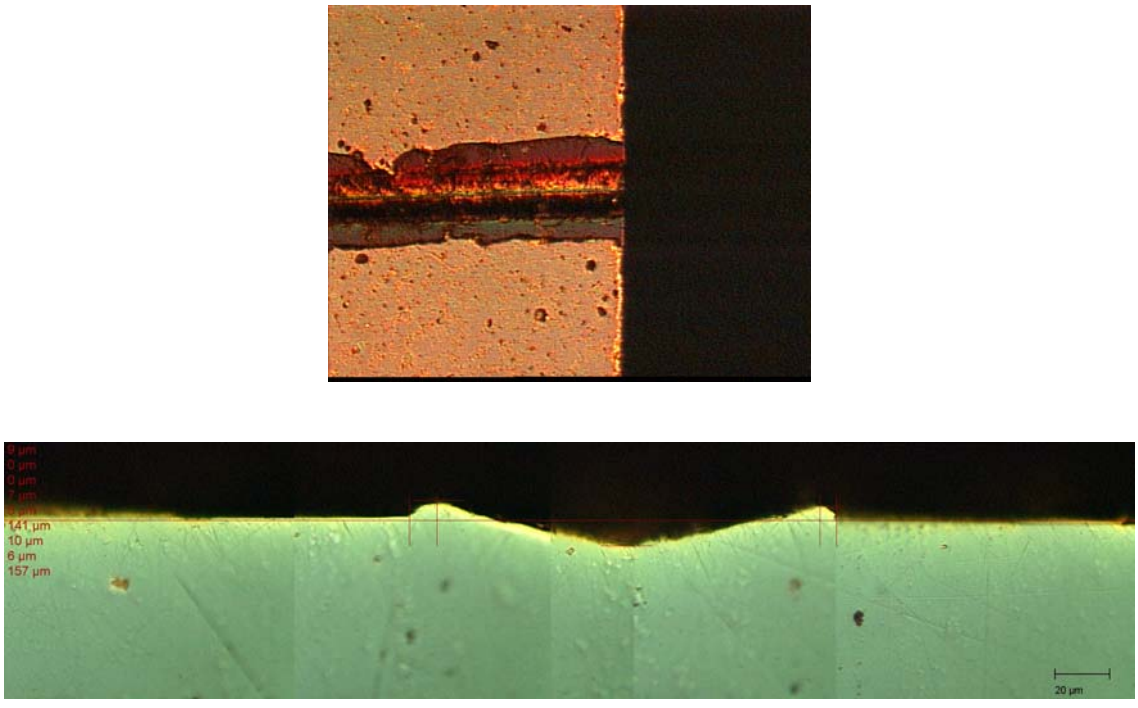


Fig.16. Tle Crossection after one cycle whit diamond indentor. Magnification 1000x

5. X-RAY fluorescent spectroscopy

This method is based on the monitoring of the secondary emission x - ray. The atoms of the sample are ionized by a primary emission x-ray and fast instil the spacer from the elektrons which are released from highers sheel and transmit characteristic the x-ray (Fig. 17). Tle emissive transition materials to the basic electron surface is called a luminescence and if this process is very fast it is fluorescence. The source of the emission x-ray is the x-ray tube. The primary emission x-rays impinges on the sample and forms a secondary fluorescent emission x-ray. Are used primarily solid samples and for the preparation are apply different technologies (grinding and polisching, forming, malting). The secondary emission enters to the monochromate. As the dispersive element is used the crystal acceprable materials. For the harder elementes we are choosen the crystal whit smaller inter plane distance (e.G. Fluor-spar lithic), for the samples whit a smaller atomic issue we are choosen the crystal whit larger inter plane distance or the artificially crystals are more often used.

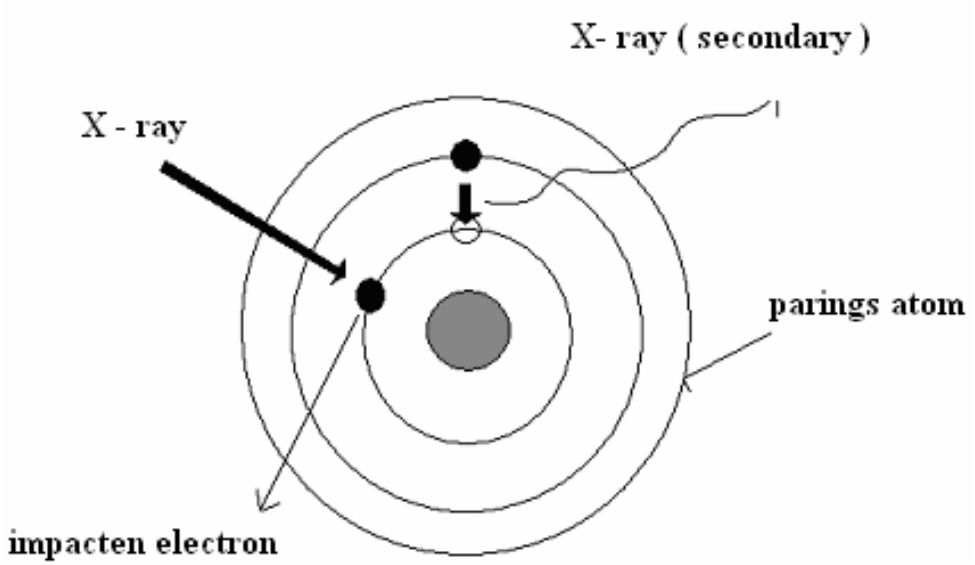
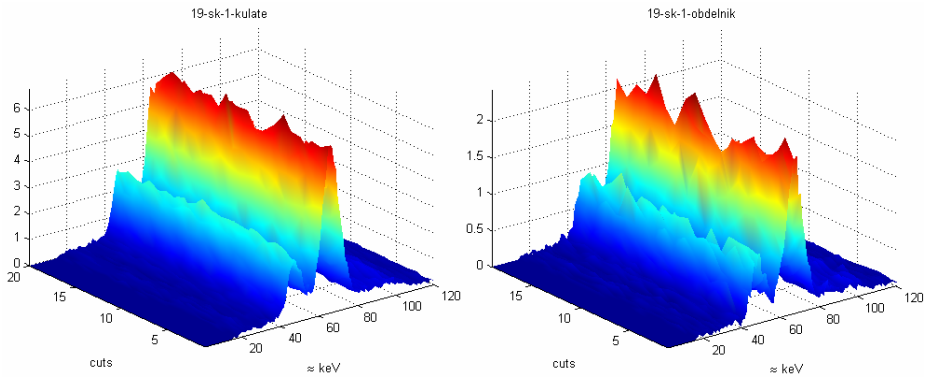
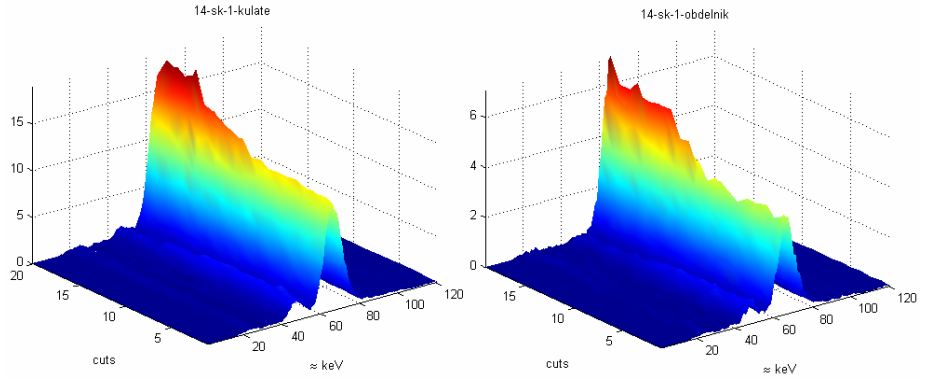


Fig. 17. Primary emission x- ray in the material and emission secundary emission x- ray.

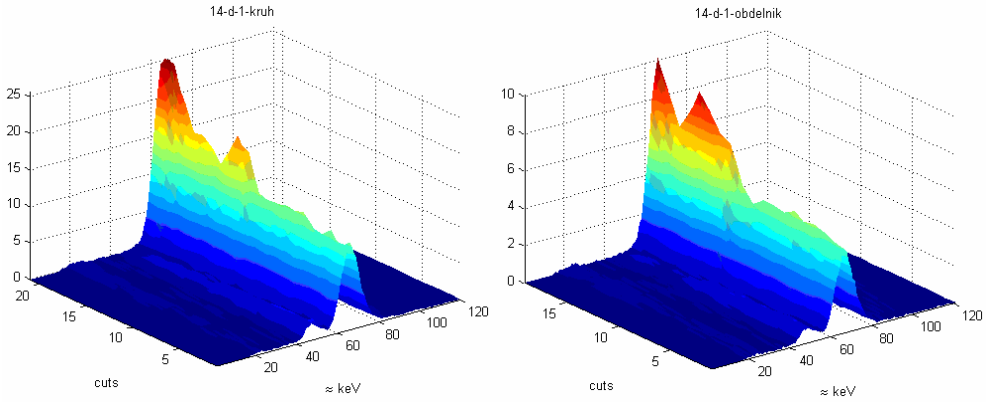
Exhibits registration thickness thin film TiN after 1 and 50 cycle on the substrate 19 830 and 14 220 on RTG fluorescent spectroscopy.



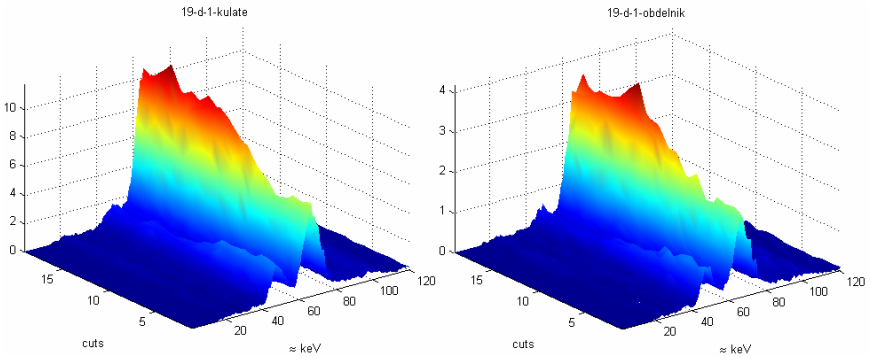
Analyse scratch after 1 cycle. Indentor from sintered carbide. Steel 19 830 whit thin film TiN



Analyse scratch after 1 cycle. Indentor from sintered carbide. Steel 14 220 whit thin film TiN



Analyse scratch after 1 cycle. Indentor from diamond. Steel 14 220 whit thin film TiN



Analyse scratch after 1 cycle. Indentor from diamond. Steel 19 830 whit thin film TiN

6. Conclusion

- The thin film TiN, has a big contribution for the both selected materials

- Whit the using of all indentors we come up the conditions. The indentors were diamond and from WC – Co.
  The geometric parameters were :
  a. Diamond indentors – R 0,2
     R 0,5
  b. Indentors from WC-Co – R 0,2
     R 0,5
- Tle evaluation was effected on three different materials, it was evaluated failure and deformation on the systém TiN – steel (CSN 19 830, 14 220 and 12 050)

- The fluorescent X – ray spectroscopy is contribution for evaluation of local fluctuation after the scratch

The paper is presented in the range of solution project n. FT-TA4/082.

Literatura

1. ŠTĚPÁNEK, I., Method for complex evaluation of properties and behaviour systems of thin film - substrate, Matrib 2000, str. 335-342, Croatia – Vela Luka, 2000, ISBN 953-96038-5-4

2. ŠTĚPÁNEK, I., KAVINOVÁ, M., HRDÝ, M., Evaluation of macroindentation statical and scratch tests in cross section in systems thin films - substrate. Matrib 2004, Croatia 2004, ISBN 953-7040-02-X

3. MACHAČKOVÁ, K., ŠTĚPÁNEK, I., Evaluation of adhesive cohesive failure from cyclic scratch test by analysis from surface and cross section of systém thin film – substrate. Switzerland 2005, poster.

THE INFLUENCE OF THE STRUCTURE OF THE OFFSET RUBBER ON THE SCREEN REPRODUCTION

Majnarić I.[1] Tahirović H.[2] Zjakić I.[1] Bolanča S.[1]

[1]Faculty of Graphic Arts, Department for Printing, Getaldićeva 2, 10 000 Zagreb, Croatia
[2]Profil International, Bužanova 20, 10 000 Zagreb

Izvorni znanstveni rad / Original scientific paper

Abstract:

During the indirect printing process, the rubber offset blanket has the function to transfer the ink from the printing form on the paper. The tiny printing elements of the dotted shape with the size between 20 and 250 μm (screen dots) are reproduced on prints. In this process, the positive deformation of the screen elements appear inevitably, which is in direct dependence on the hardness and the composition of the compressible rubber blanket. In this work it is analyzed how the rubber composition and its compressibility influence the reproduction of the screen elements, and how great is its influence in the total deformation of the screen elements. The shape of the reproduced screen elements, i.e. the circularity of the dots has also been monitored. All four printing units as well as their reproduction of the basic process inks have been tested in the work.

Key words: Offset printing, impressible rubber blanket, deformation of the screen elements, circularity,

1. Introduction

The principle of indirect printing has been used in offset lithography for the first time. Such principle is based on the prolonged ink transfer who starts from the printing form. Generally, the printing forms are composed of two kinds of elements: the non printing elements (they do not accept the ink but they accept the dampening solution) and the printing elements (they accept ink but they do not the dampening solution). The basic printing form for offset printing process is the aluminium plate whose surface is roughened and oxidized (non printing surfaces), while the printing elements were formed by selectively melting of previously coated photosensitive diazo layer (printing elements) [1].

The paste offset ink with its tackiness and density (dynamic coefficient of viscosity η= 40-150 Pa·s) is applied on the previously wetted printing form, adhering to the diazo layer. The rubber offset blanket (ROB) is the mediator in ink transfer and the dampening solution from the printing form on the printing substrate. In the contact of the printing form and the offset cylinder blanket, the first ink transfer happens during which the mirror image is formed on rubber. After that, the second ink transfer follows during which the ink is transferred on the printing substrate from the rubber offset blanket. The image is again turned and the right-reading impression is obtained whose applied ink thickness is between 0,5 – 1,5 μm. The forces in the contact zones of the cylinder are between 2,5 and 3 MPa [2].

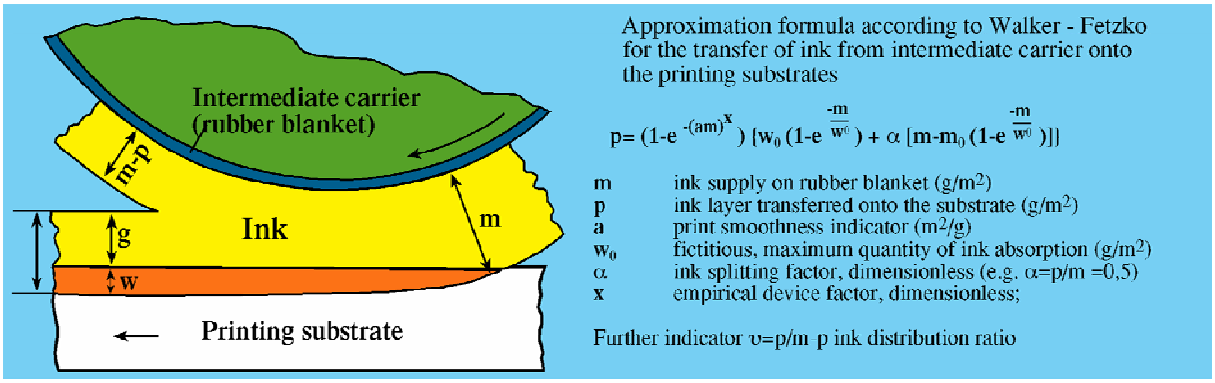


Figure 1. Printing ink transfer on the rubber offset rubber blanket, i.e. on the printing substrate

One of the factors influencing the quality of the multicolour reproduction is the composition of the offset cylinder dressing. In this work, the influence of its composition and hardness on the reproduction of the tiniest printing elements (screen dots) is analyzed.

2. Theoretical part

Offset cylinder is placed between thee printing and plate cylinder. It is composed of two parts: the productive part (it is in contact with the printing form, i.e. with the printing substrate) and the non productive part (it is not in contact with the printing form, i.e. with the printing substrate). In the non productive part there are two carriers of the offset rubber blanket which is tightened up by the tightening spindle. The production part of the offset cylinder has undercut (2,30 mm) in which the compressible i.e. non- compressible rubber blanket is placed. Because of its standard thickness (1,90 mm) the substrate is placed under the rubber offset blankets by which the total thickness is achieved which corresponds to the bearer height of the blanket cylinder (of the non compressible rubber blanket) while the total thickness in compressible blankets is for 0,05 mm higher than the bearer height [3].

Depending on the substrate composition (felt, papers, boards, rubber blanket) the tightened rubber offset blanket can have the hardness between 65° and 86° HS A. In the printing process under the influence of the same pressure, the compressible blankets will touch the printing form and the substrate in considerable longer contact zone than the conventional ones, and the print will have smaller deformations on that path. With greater hardness, the possibility of reproducing the tiniest screen elements is achieved (diameter of 8μm) with appearance of greater tribological wear [4].

Rubber offset blanket

ROB is composed of three or four layers of specially woven linen impregnated by elastomer mass and glue. The linen layers limit the elasticity of the ROB in order to extend it correctly and under control during stretching on the offset cylinder. The elastomer mass impregnated into the layers of linen determines the total hardness and deformability. The surface layer is produced by flattening especially prepared elastomer mass which is coated with the impregnated linen layers [5].

In recent times, under the surface and the first linen layer there is compressed layer of the cellular processed "spongy" polymer mass (0,03 – 0,05 mm). During the production it is formed so that the separated air or gas bubbles are blown into the hot polymer mass and compressed under pressure. The conventional linens realize the printing pressure by high elastic linen deformation in the whole thickness cross-section. The compressible surface layer deforms after to the printing form or substrate and the pressure is realized by compression of gasses in the compressible layer. Because of that reason, the conventional ROB is used only for printing on very smooth surfaces [6].

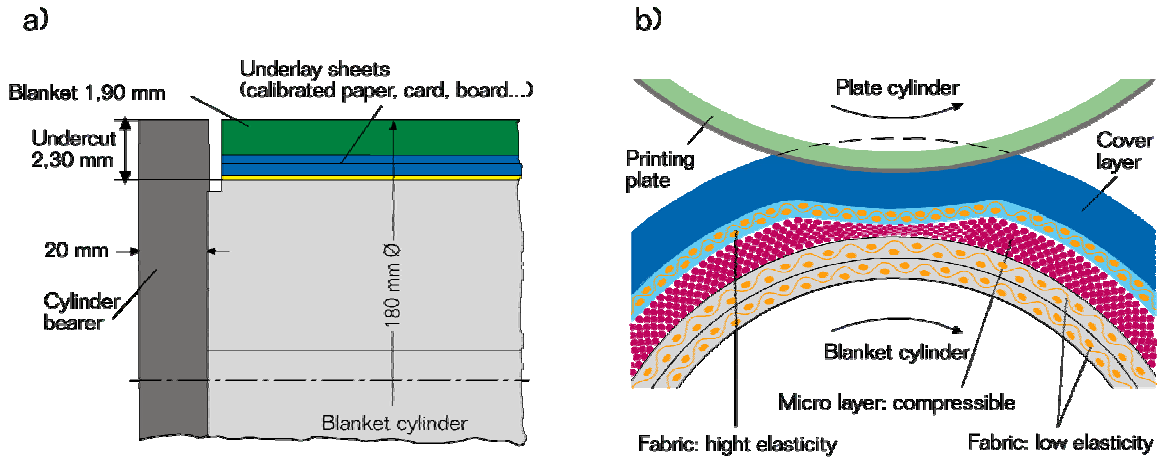


Figure 2. Cross section and deformations of the rubber offset blanket

Finally, ROB will have the direct influence on the future ink transfer, i.e. on printing appearances such as print edges deformations, doubling and extending of screen elements, picking and the angle of paper separation, mechanical deformations of paper, printing form wear, thickness and uniformity of the ink coating on the printing substrate [7].

3. Experimental part

Special printing form was made for this testing. Except the measuring and visual colour stripes there are greater CMYK patches on the form with the belonging color images. Standard fine art paper was used as the printing substrate with the grammage 115 g/m^2. Experimentally printed samples were obtained on four-colour offset printing machine Heidelberg Speedmaster 102, which prints in the following sequences KCMY (wet on wet printing). During the experiment 3 commercial types of rubber offset blankets were used: dyeGraphica 36, dyeGraphica 3000 and dyeGraphica 8213. Two basic structures were used: compressible structure and the non compressible one.

On the obtained prints, the characteristic screen patches were measured by spectrophotometer X-rite SwatchBook, which were presented as the function of the dot gain (Z%). With the device for the image analysis (Personal IAS) the increased image was obtained on which the dimension of the reproduced screen dots as well as their regularity (circularity) was measured [8].

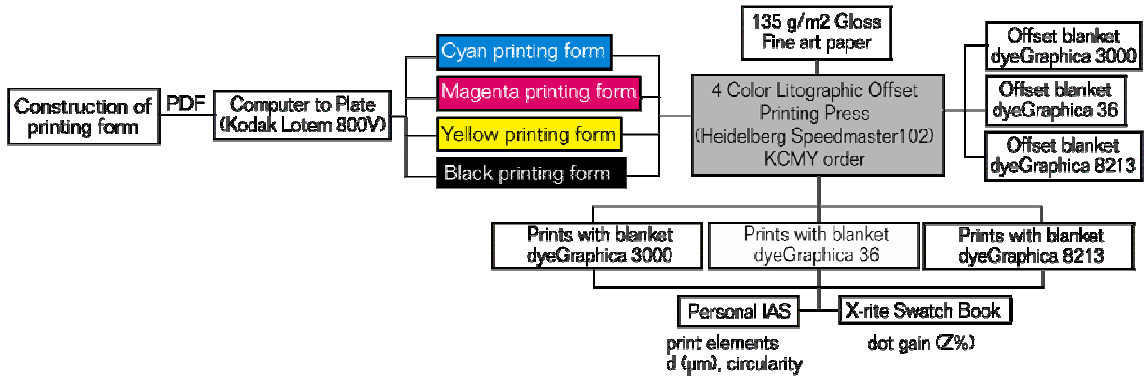


Figure 3. Schematic presentation of experiments

Table 1. Technical characteristics of the applied rubber offset blanket

Features:	dayGraphica 36	dayGraphica 3000	dayGraphica 8213
Type of blanket	compressible	compressible	uncompressible
Colour	Dark Blue	Dark Blue	Blue
Surface	Ground	Ground and Buffed	Ground
Thickness	4 Ply 1,96 mm	4 Ply 1,95 mm	3 Ply 1,95 mm
Face Compound	Solvent Reststant Rubber	Solvent Reststant Rubber	Solvent Reststant Rubber
Hardness	Overall 78° Shore A	Overall 78° Shore A	Overall 81° Shore A
Compressibility Deflection	0,220 mm at 2060 kpa	0,18 mm at 2060 kpa	0,10 mm at 2060 kpa
Elongation	1,1% at 10N/mm	0,9% at 10 N/mm	< 0,70% at 10N/mm
Tensile strength	91 N/mm	112 N/mm	> 60 N/mm



4. Results and discussion

The reproduction results of the screen values (halftones) , depending on the type of the rubber offset blanket, are presented in the form of dot gain Z (%).Only the process printing inks which were applied in printing wet on wet, were analyzed.

In all the graphs, the greatest dot gain is in the area between 40 and 60% of the screen value. In reproducing the black colour (the first printing unit) the greatest deformation of the screen elements appeared by the application of the rubber 36 ($Z_{50\%}$=17,5%), while the smallest one appeared when printing with the rubber 3000 ($Z_{60\%}$=15,5%). Both curves have similar shape which enabled the proportional tone reproduction. Black prints were made with the non-compressible rubber 8213 and have the maximal dot gain $Z_{60\%}$=17%. For the non-compressible rubber, the not sufficient dot gain in the area of 40% is characteristic, because the rubber has greater hardness which was achieved by smaller number of layers (3 layers). The dot gain curve follows the rubber gain curve 36 in darker areas (from 60% to 100% screen value) while in the lighter areas it follows the gain curve of rubber 3000.

In cyan printing (the second printing unit) the curves of the dot gain (Z%) are uniform on all tonal values. The exceptions are the compressible rubbers 36 and 3000 which form identical reproduction in the area of high tonal values. The greatest deformations appear in the area of 50%: $Z_{rubber36}$=18%, $Z_{rubber8213}$=15%, $Z_{rubber3000}$=11.5%.

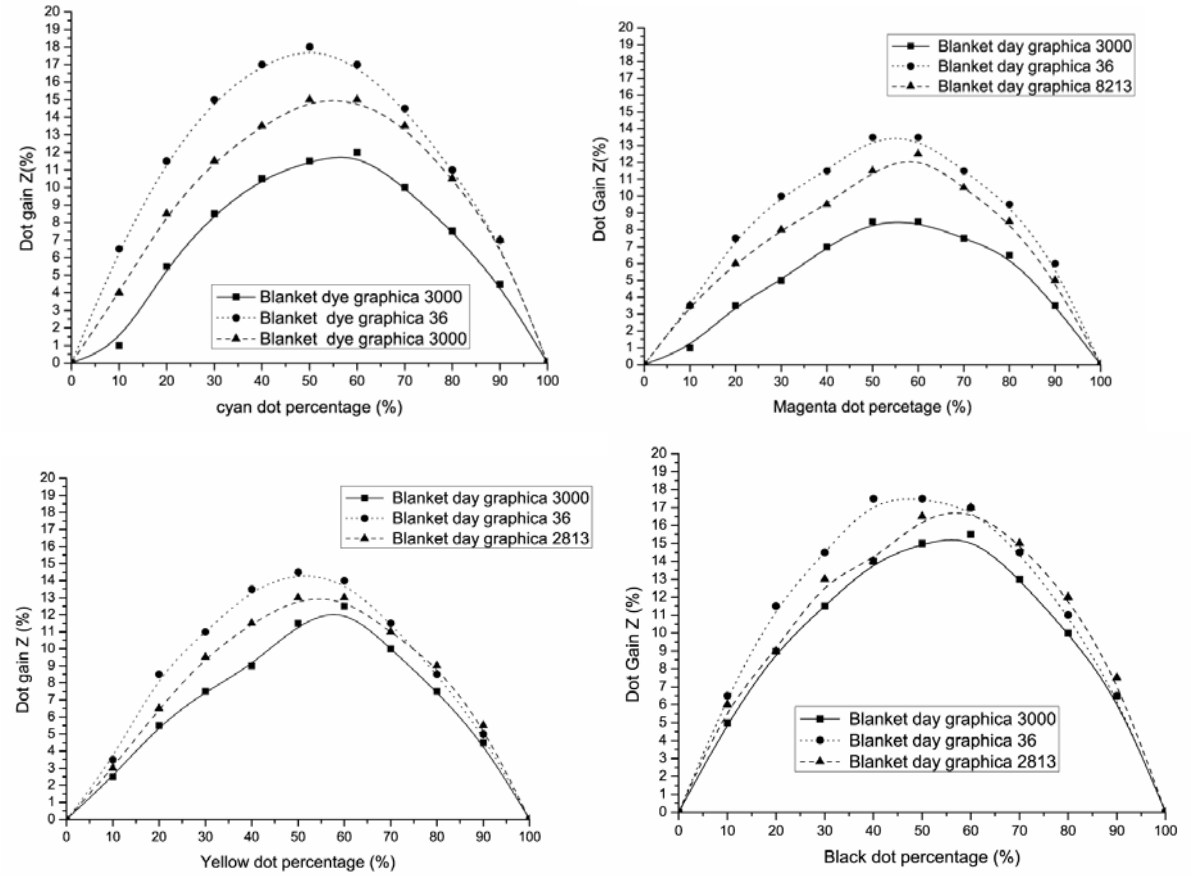


Figure 4. Dot gain on prints printed with rubber blankets dyeGraphia 36, dyeGraphia 3000, dyeGraphia 8213

The dot gain curves of magenta prints (the third printing unit) have similar shape as the curves of cyan prints. The difference is in the formed somewhat smaller maximal gains: $Z_{rubber36}$=13%, $Z_{rubber8213}$=12,5%, $Z_{rubber3000}$=8,5%.

On yellow prints (the fourth printing unit) with the different type of the rubber blanket, the greatest deviations in 40% screen area are formed: $Z_{rubber36}$=13,5%, $Z_{rubber8213}$=13%, $Z_{rubber3000}$=9,0%. With rubber 3000, the area of 40% tone value has insufficient gain. The compressible rubber 36, in comparison to the rubber 3000, has in its layers greater mechanical deformation which directly influences the dot gain.

Figure 4 presents how the tiniest image elements are reproduced, and how they are influenced by different structure of the offset rubber blanket. The dot gains in the area 10, 20 and 30% screen value are analyzed by IAS (figure 5)

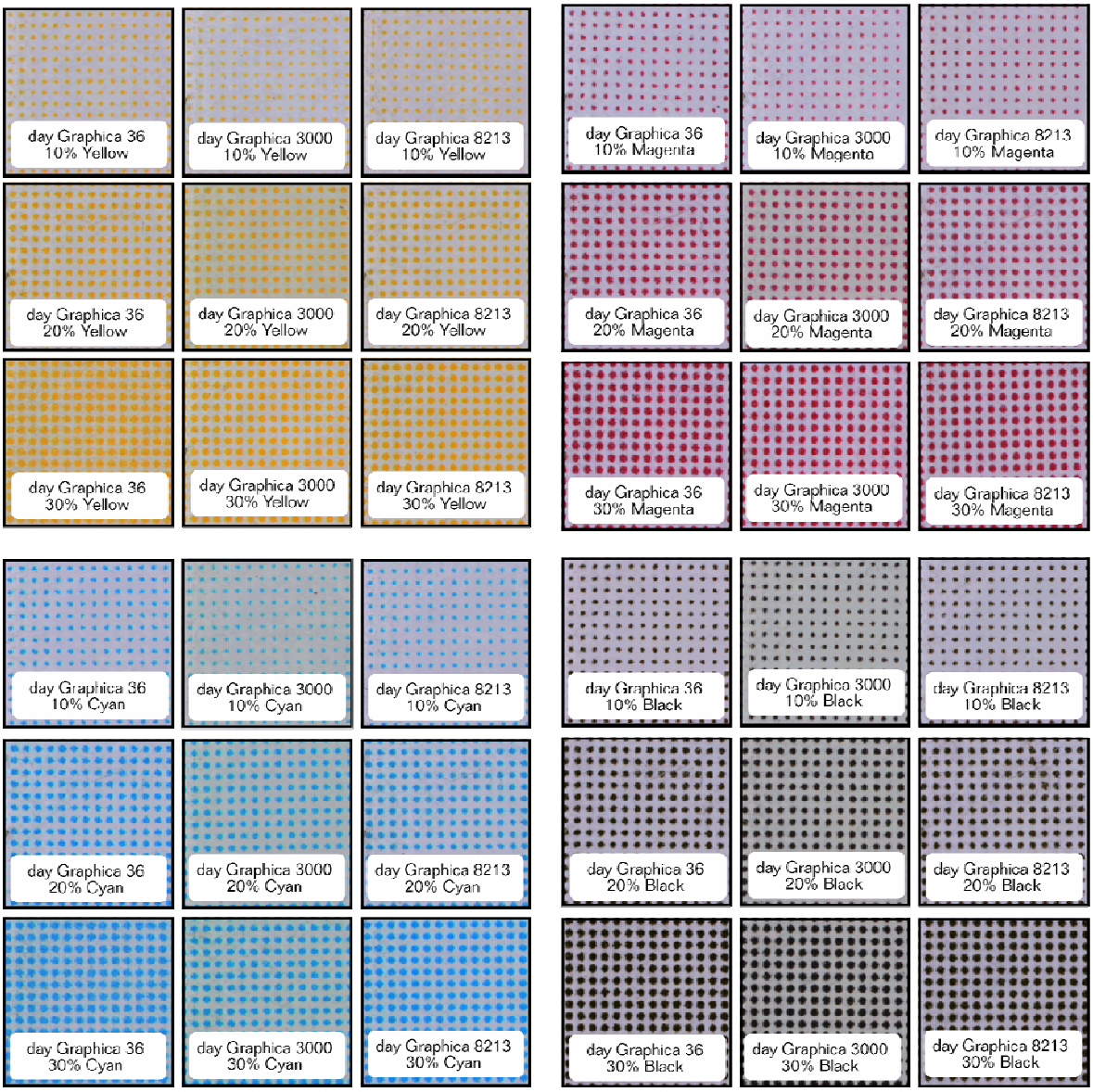


Figure 5: The magnified images of the analyzed samples printed with the rubbers dyegraphica 36, dyegraphica 3000 and dyegraphica 8213

It is generally valid for all the reproduced process inks, that the dependence of the screen value (of 10% and 30%) and the diameter of the printed elements (with different rubber blankets) is described as linear function.

The average reproduced cyan dots (for the areas 10, 20 and 30% screen value) have the greatest diameter d_{med}=91,44 μm (printed with the compressible rubber 36) while the smallest average diameter is obtained with the compressible rubber 3000 (d_{med}=80,15 μm). Non compressible rubber 8213 prints the average screen elements with the diameter d_{med}=83,42 μm and with its value it follows the linear curve of the rubber 3000. In the screen value of 30%, the deviation of the printed screen dots is the greatest. The characteristic curve of the rubber 3000 has the smallest deviation, which means that the dot gain stops to be linear ($\Delta d_{10\%-20\%}$=27,33 μm, $\Delta d_{20\%-30\%}$=15,83 μm).

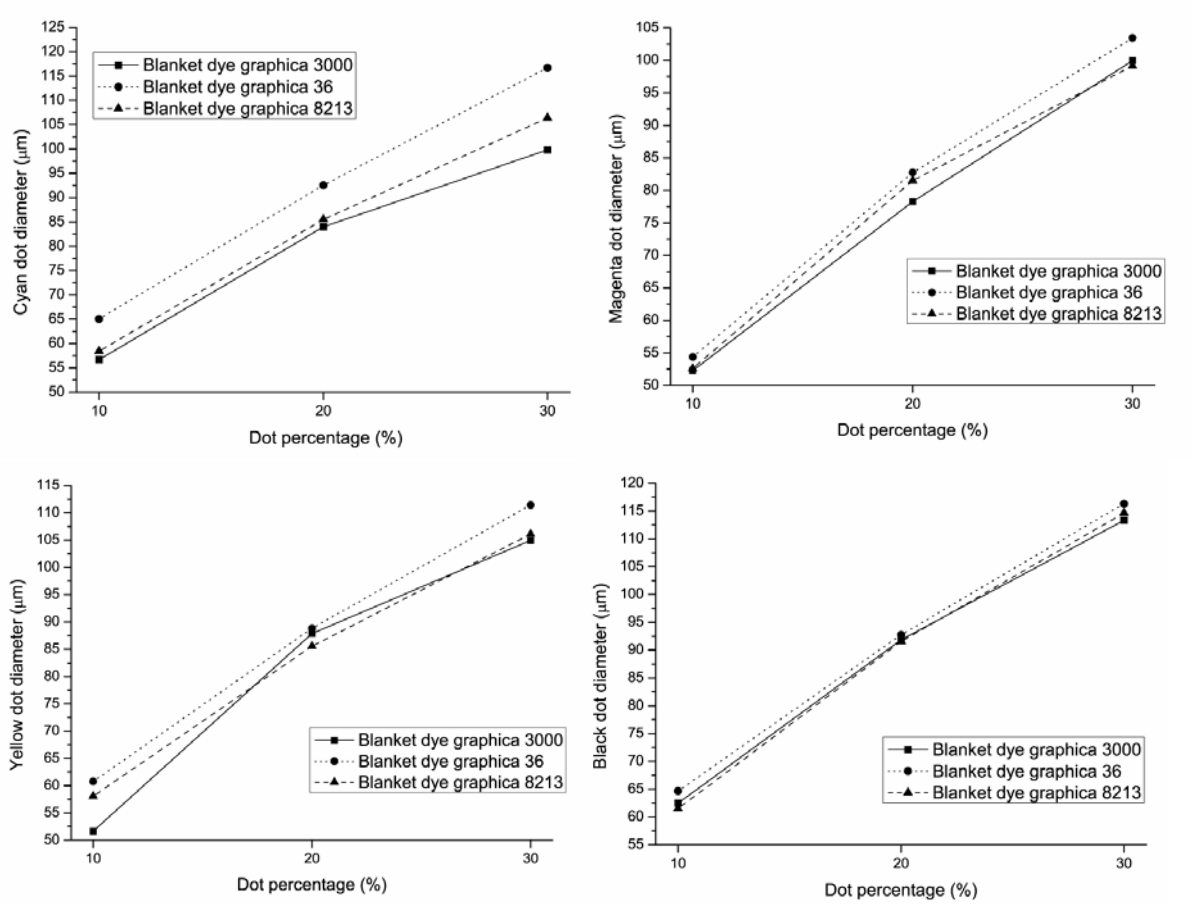


Figure 6: Graphs of dependence of the reproduced changes of the screen elements for the screen area of 10%, 20% and 30%.

For the magenta prints reproduced with the rubber 8213 the greatest oscillation of the screen elements is characteristic. By variation of the rubber offset blankets in the characteristic tested areas (10%, 20% and 30%) the following maximal deviation appears: $\Delta d_{10\%}$=2,12 μm, $\Delta d_{20\%}$=8,56 μm, $\Delta d_{30\%}$=4,3 μm. The screen elements mage by the rubber 8213 coincide with the elements made by the rubber 3000 only in the area of 10% screen value ($\Delta d_{8213-3000}$ = 0,35 μm). In the area of 20% screen value the curve of the rubber 8213 is closer to the curve of the rubber 36, forming the average deviation of the screen elements of $\Delta d_{8213-3000}$ = 3,24 μm. In

the area of 30% screen value the curve of the rubber 8213 is again closer to the curve of the rubber 3000 forming the smallest reproduced screen elements ($\Delta d_{3000\text{-}8213} = 0{,}79\mu m$).

The type of the rubber offset blanket influences the reproduction of the yellow screen elements. The greatest deviations of the screen dots diameter are per areas: $\Delta d_{10\%}$=9,08 μm, $\Delta d_{20\%}$=3,33 μm, $\Delta d_{30\%}$=6,5 μm. The rubbers 36 and 8213 show very similar deviations in comparison with the rubber 3000 which has the greatest deviation of the screen elements. In comparison to the non compressible rubber (8213 (the greatest difference is in the area of the smallest screen elements $\Delta d_{8213\text{-}3000}$ = 6,43 μm. In printing with rubber 3000, in the area of 20% screen value, the greater dot gain appears. The screen elements become greater than screen elements printed with the rubber 8213 ($\Delta d_{3000\text{-}8213}$ = 2,34 μm). With greatest printing elements (30% of the screen value) the printing with the rubber 3000 leads to the unexpected fall of the screen elements diameter ($\Delta d_{8213\text{-}3000}$ = 1,16 μm).

By variation of the three types of the rubber offset blankets, the black prints are made which are uniform in all tonal values : $\Delta d_{10\%}$=3,14 μm, $\Delta d_{20\%}$=1,18 μm, $\Delta d_{30\%}$=3 μm. In the area of 10% screen value the smallest screen elements are obtained with the non compressible rubber 8213 which is in comparison to the compressible rubber 3000 less for 0,98 μm. Their printed elements in the area of 20% screen value are equated ($\Delta d_{3000\text{-}8213}$ = 0,27 μm) so that they would become even greater in the greatest screen values obtained by non compressible rubber ($\Delta d_{8213\text{-}3000}$ = 1,28 μm). Such results can be the consequence of the ink arrangements when placing the black ink in the first printing unit and printing of black on absolutely dry paper. All other process colours have greater oscillations because of the wetting solution absorption during which smaller deviation of the printed paper substrate appear (hygroscopic paper changes its dimensional stability).

The geometric deviation of the printed screen elements is presented as the circularity (figure 6) which is defined as the ratio of the length and height of the printed printing element. In ideal case, its value is one (C=1).

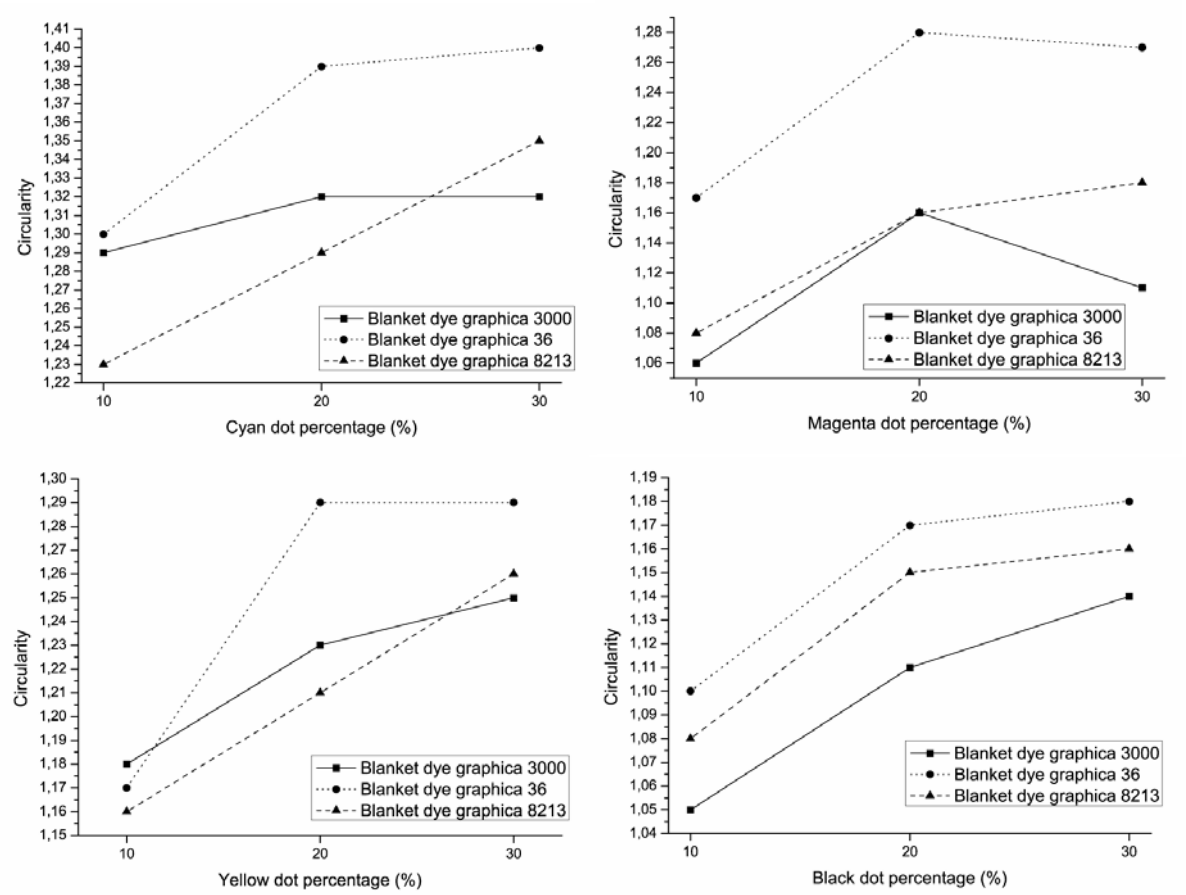


Figure 7 Circularity of the round screen elements in dependence on the ink and screen value

Generally looking, geometrically most irregularly printed screen elements are reproduced with the rubber 36. The smallest printing elements (the area of 10% screen value) keep the greatest roundness. Depending on the rubber type application, the average circularity of the cyan screen dots is C_{3000}=1,31; C_{8213}=1,36; C_{36}=1,29. The cyan dots formed with the non compressible rubber 8213 are characterized by the fact that the increase of the screen values (dot gain) influences the decrease of circularity ($\Delta C_{10\%-30\%}$=0,12). The compressible rubbers (36 and 3000) will influence the circularity increase only in the areas up to 20% screen value (ΔC_{3000}=0,03; ΔC_{36}=0,09) after which the circularity stabilizes.

Depending on the applied rubber type, the average circularity of the yellow screen dots is C_{3000}=1,22; C_{8213}=1,21; C_{36}=1,25. The yellow prints made with the rubber 8213 follow the constant decrease of circularity $\Delta C_{10\%-30\%}$=0,10. With the rubber 3000 the circularity grows somewhat slowly ($\Delta C_{10\%-30\%}$=0,07). The prints obtained with the rubber 36 have great change in circularity in the area between 10 and 20% ($\Delta C_{10\%-20\%}$=0,12), after which the circularity stabilizes $C_{30\%}$=1,29.

The measured average circularity of the magenta prints is: C_{3000}=1,11; C_{8213}=1,14 C_{36}=1,24. Magenta prints formed with the rubber 3000 are characterized with the circularity fall in the area of 20% screen value ($\Delta C_{10\%-20\%}$=0,10), so that the tonal values with greater printing elements would have better circularity ($\Delta C_{10\%-20\%}$=0,05). Variation of the rubber type will directly influence the average circularity of the black screen dots: C_{3000}=1,10; C_{8213}=1,13; C_{36}=1,15. On all black prints with the increase of screen values, the circularity decreases (the rubber 8213 $\Delta C_{10\%-30\%}$=0,08; rubber 36 $\Delta C_{10\%-30\%}$=0,07; rubber 3000 $\Delta C_{10\%-30\%}$=0,08). The

rubber 300 with its compressibility will form the smallest reproduced printing elements and it is advisable to use it for the reproduction of frequently modulated screens.

5 Conclusions

On all the experimental impressions the greatest reproduced elements are obtained with the rubber dyegraphica 36, while the smallest ones are obtained with the rubber dyegraphica 3000 (both rubbers are compressible).

By changing the rubber offset blankets it is possible to influence the reproduction directly, i.e. to influence the size of the printed screen elements. By experimental printing with the rubbers dyegraphica 36, dyegraphica 3000 and dyegraphica 8213 the greatest deviations are achieved in cyan screen elements: $\Delta d_{10\%}$=8,43 μm, $\Delta d_{20\%}$=8,56 μm, $\Delta d_{30\%}$=16,86 μm.

The smallest deviations are marked on black impressions: $\Delta d_{10\%}$=3,14 μm, $\Delta d_{20\%}$=1,18 μm, $\Delta d_{30\%}$=3 μm. On the first printing unit (black colour) the non compressible rubber dyegraphica 8213 has lower deformation of the lower tone values as well as greater deformation in greater tone values.

For printing the smallest dots the rubber 3000 is recommended, which gives especially good reproduction of the yellow screen elements. With the rubbers 8213 and 36 the printing elements are not so good reproduced.

On magenta impressions, by changing the compressible rubber (from the type 3000 to the type 36), the greatest change in circularity is obtained (ΔC_M=0,13), while the other colours will have smaller variations (ΔC_M=0,05). Rubber 36 shows identical form of the circularity curves regardless the applied type of ink.

If the non periodic screen (FM screen) is used in the printing process, the usage of compressive rubber 3000 is suggested for black and magenta, and the non compressive rubber 8213 is suggested to be used for cyan and yellow.

6. Literature

[1] Lovreček, M.; Gojo, M.; Dragčević, K.: Interfacial Characteristics of the Rubber Blanket-Dampening Solution System; Advances in Printing Science and Technology, Vol. 25, Pira International, Surrey UK 1999.
[2] Kipphan H., Handbook of Print Media, Springer - Verlag Berlin, Heidelberg 2001.
[3] Walenski, W.:Offsetdruck, Polygraph-Handbuch, Frankfurt am Main 1991.
[4] Kraut, B.: Strojarski priručnik, Tehnička knjiga, Zagreb 1975.
[5] Bosner Ž, Marošević G.: Tribosistem ofsetnog tiska, Zbornik radova 9, simpozij Intergrafija 87, Zagreb 1987.
[6] Marošević, G.; Bauer, G.: Mehanička svojstva gumenih navlaka u ofsetu, Acta Graphica 3(1991)3, Zagreb 1991.
[7] Mahović, S.; Marošević, G.: Površinska hrapavost ofsetnog gumenog platna, Acta Graphica 9(1997)1, Zagreb 1997.
[8] Majnarić I. Zadro A. Pučić I.; Screen Shapes and the Application as the Factors of Qualitative Offset printing, Scientific Book 2006: Graphic Arts Technology Design Communications, 2006, 79-88.

THE EFFECT OF ANIONIC 831A FLOCCULENT ON THE SEDIMENTATION OF MAGNESIUM HYDROXIDE OBTAINED FROM SEAWATER

UTJECAJ ANIONSKOG 831A FLOKULANSA NA SEDIMENTACIJU MAGNEZIJEVA HIDROKSIDA DOBIVENOG IZ MORSKE VODE

Vanja Martinac, Miroslav Labor, Zrinka Gadžo, Nedjeljka Petric
Faculty of Chemistry and Technology, Teslina 10/V, 21000 Split, Croatia

Izvorni znanstveni rad / Original scientific paper

Abstract: This study has examined the possibility of using the anionic 831A flocculent, produced by a Dutch firm Hercules, in tracing the rate of sedimentation of magnesium hydroxide obtained from seawater by 80% substoichiometric precipitation. The purpose of this study was to define the optimum conditions for sedimentation of magnesium hydroxide from seawater based on settling properties of magnesium hydroxide suspension in discontinuous precipitation. Examinations were made with different quantities of the 831A flocculent, and at different degrees of completeness of precipitation (70 % and 100 % precipitation) to determine the optimum quantity of the 831A flocculent during the sedimentation process. The results indicate significantly faster sedimentation of magnesium hydroxide obtained by precipitation with the smaller quantity of the precipitation agent than that required stoichiometrically, which is explained by the model of the $Mg(OH)_2$ particle. From the results obtained for discontinuous conditions, one can apply the Kynch theory to calculate the continuous thickener.

Key words: substoichiometric precipitation, sedimentation rate, magnesium hydroxide, seawater

Sažetak: U radu je ispitivana mogućnost primjene anionskog flokulansa 831A, nizozemske tvrtke Hercules, u svrhu praćenja brzine sedimentacije magnezijeva hidroksida dobivenog iz morske vode ne stehiometrijskim 80 %-tnim načinom taloženja. Svrha ovog rada je definirati optimalne uvjete pri sedimentaciji magnezijeva hidroksida iz morske vode na osnovu praćenja taložnih karakteristika suspenzije magnezijeva hidroksida u uvjetima diskontinuiranog taloženja. Ispitivanja su vršena uz različite količine 831A flokulansa, kao i pri različitim stupnjevima potpunosti taloženja (70 % i 100 %-tno taloženje) s ciljem utvrđivanja optimalne količine flokulansa 831A tijekom procesa sedimentacije. Rezultati ispitivanja ukazuju na znatno bržu sedimentaciju taloga magnezijeva hidroksida dobivenog taloženjem s manjom količinom taložnog sredstva od stehiometrijski potrebne što se objašnjava modelom čestice $Mg(OH)_2$. Na osnovu rezultata dobivenih pri diskontinuiranim uvjetima moguće je primjenom Kynchove teorije izvršiti proračun kontinuiranog taložnika.

Ključne riječi: nestehiometrijsko taloženje, brzina sedimentacije, magnezijev hidroksid, morska voda

1. INTRODUCTION

In parallel with the growth of population and exhaustion of natural resources on land, man turns to the sea to look for new sources of food and different materials, as well as for new sources of energy. In such conditions, the word's seas and oceans, covering more than 70 % of the surface of our planet, represent a great challenge and hope for all the peoples of the world with their huge food, energy, raw materials, transportation, military-strategic potentials and with their extraordinary role in the overall ecosystem. The mineral raw materials of the sea and seabed have been attracting the international attention in the last 40 – 50 years. Seawater can be economically used as raw material for obtaining magnesium hydroxide if it contains at least the following mass concentration of magnesium: γ_{Mg} = 1.3 g dm^{-3} [1]. The process of obtaining magnesium oxide from seawater [2-9] includes precipitation of magnesium hydroxide formed by the reaction of magnesium salts present in seawater with a base such as calcined dolomite or calcined lime. The sedimentation of magnesium hydroxide [10-14] is one of the most important operations in this technological process, affecting the productivity of the total plant, thereby controlling the production costs. As the suspension of magnesium hydroxide is characterized by slow sedimentation rate, the process is accelerated by addition of appropriate flocculents. This study has examined the possibility of improving the sedimentation rate and defining optimum process conditions by using the anionic powdery 831A flocculent (polyacrylamide) in obtaining the magnesium hydroxide from seawater by means of substoichiometric precipitation using 80% of he stoichiometric quantity of dolomite lime as the precipitation agent.

2. EXPERIMENTAL

The seawater used for precipitation of magnesium hydroxide had the following content of magnesium oxide and calcium oxide: 2.4576 g dm^{-3} MgO and 0.5836 g dm^{-3} CaO.

The composition of the dolomite lime used as the precipitation agent was as follows (mass %):
CaO = 57.17 % MgO = 42.27 % SiO_2 = 0.099 %
Al_2O_3 = 0.051 % Fe_2O_3 = 0.079 %

Seawater was first treated by acidifying with H_2SO_4 with on-line control through pH measurement (pH = 3.8-4.0) to remove bicarbonate (HCO_3^-) and carbonate (CO_3^{2-}) ions. At the low pH the bicarbonate and carbonate were converted to the CO_2 gas, which was stripped out of the falling water drops by the ascending air flow in the desorption tower. The flow rate of the induced air was 120 dm^3 h^{-1}, and the volumetric flow rate of seawater through the desorption tower was 6 dm^3 h^{-1}. Precipitation of magnesium hydroxide took place after pretreatment of seawater. The experimental procedure was similar to that employed in previous investigations [10-13]. The process of obtaining magnesium hydroxide took place with the addition of 80% of the stoichiometric quantity of dolomite lime as the precipitation agent. Examinations took place in a volume of 500 cm^3 of seawater, with different quantities of the 831A flocculent addition (3.8, 3.9, 4.0, 4.1, 4.2, 4.3, and 4.4 cm^3 831A flocculent per 500 cm^3 of seawater). For each individual quantity of the 831A flocculent addition, examinations were done for different degrees of completeness of precipitation (70% and 100% precipitation). Experiments were carried out in graduated glass cylinders of the same diameter. This method is suitable for tests with solid-liquid systems containing at least 0.1 mass % of solid materials.

1 mm of the height of magnesium hydroxide precipitate is equivalent to a volume of 2.9299 cm^3 of the suspension. The powdery 831A flocculent used in these examinations was an anionic flocculent (polyacrylamide) with 100 mass percent of active matter. It is a synthetic high molecular weight polymer, which is soluble in water. The prepared solution contained 0.05 mass percent of active matter (the actual activity of specific components from which it was prepared). It was prepared by dissolving 0.1 g of the flocculent in 199.9 cm^3 of distilled water, with gentle mixing. 1 cm^3 of the solution contained $5 \cdot 10^{-4}$ g of the 831A flocculent. Measurements were carried out at the constant temperature of 27 ^oC. The results obtained were within the experimental error at approx ± 0.5 mm. All the results presented are an average of 5 and have shown good reproducibility.

3. RESULTS AND DISCUSSION

Figure 1 shows the data on the settling rate of magnesium hydroxide from seawater for the 80 % substoichiometric precipitation by dolomite lime with different additions of the 831A flocculent in the amounts of 3.8, 3.9, 4.0, 4.1, 4.2, 4.3, and 4.4 cm^3 831A flocculent per 500 cm^3 of seawater.

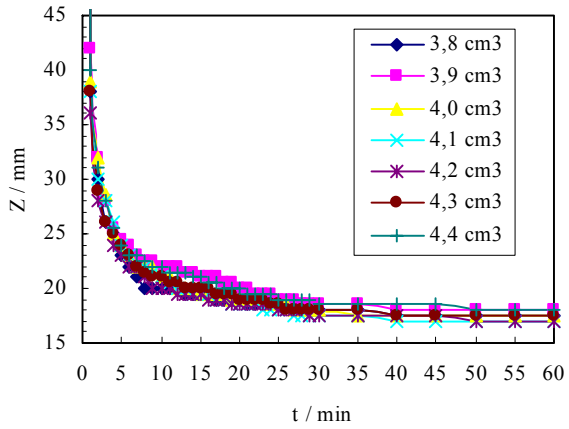


Figure 1. The dependence of the precipitate level (Z) on the setting time (t), for substoichiometric 80 % precipitation, with different additions of the 831A flocculent per 500 cm^3 of seawater.

The results obtained indicate that the best effect in increasing the sedimentation rate is attained with the addition of 4.1 cm^3 of the 831A flocculent. In these examinations the mass concentration of the solid phase in the suspension remained constant, 2.8840 g per 500 cm^3 seawater. The differences observed in individual series of experiments are due to the addition of different quantities of the 831A flocculent. In this way it is possible to use the measurements of the sedimentation rate to determine the optimum flocculent addition for the 80 % precipitation. It was necessary to determine the optimum flocculent quantity needed to achieve the best settling of the precipitate as soon as possible, and thereby the higher density of the magnesium hydroxide precipitate, with the clear boundary of separation of the clear layer from the precipitate formed.
The results indicate that the addition of the 831A flocculent in the amount of 4.1 cm^3 831A per 500 cm^3 seawater is the optimum one for improved sedimentation rate in substoichiometric 80 % precipitation of magnesium hydroxide from seawater. The precipitation curve, i.e. the graphical presentation of the dependence of the volume of the magnesium hydroxide precipitate on the settling time for substoichiometric 80 % precipitation with the addition of 4.1 cm^3 831A

flocculent per 500 cm^3 seawater (Figure 2.), shows that the zone of free precipitation is established already in the first 10 minutes from the start of tracing of the sedimentation process, followed by a zone of compression (thickening) of the precipitate.

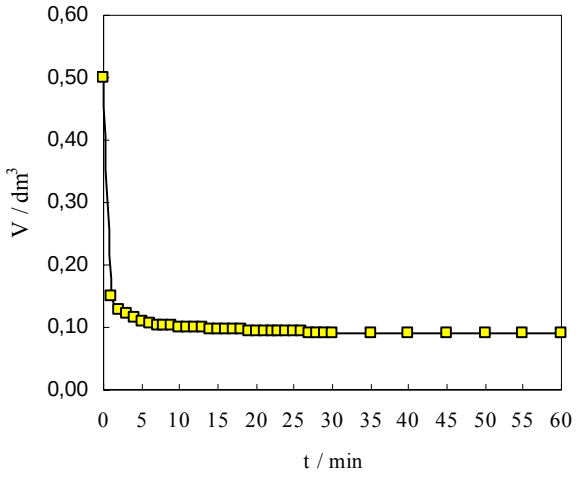


Figure 2. The dependence of the volume of the magnesium hydroxide precipitate (V) on the setting time (t) for substoichiometric 80 % precipitation, with the addition of the 4.1 cm^3 831A flocculent per 500 cm^3 of seawater.

For the results obtained to be fully confirmed, the next step in the experimental part was to examine each individual addition of the 831A flocculent (3.9; 4.0; 4.1; 4.2; 4.3; 4.4 cm^3) at different degrees of completeness of precipitation, namely at 70 %, 80 %, and 100 % precipitation. Figures 3 – 8 show the results obtained for settling properties of the magnesium hydroxide suspension in a graduated glass cylinder, for the operating conditions described.
The results obtained indicate that the sedimentation rate increases with the decrease of the initial mass concentration of magnesium hydroxide. If mass concentration of the solid phase in the suspension increases, so does the density and viscosity of the suspension, leading to reduced sedimentation rate. Porous aggregates form in concentrated suspensions, significantly reducing the sedimentation rate. Therefore the suspension properties are greatly affected by mass concentration, and by the quantity of the reagent (precipitation agent) added. In other words, the sedimentation taking place in surplus of Mg^{2+} ions (substoichiometric precipitation) is more efficient than that when there is a surplus of OH^-, both as regards the sedimentation rate and the filtering rate. Taking into consideration that mass concentrations of magnesium hydroxide, i.e. the mass of solid matter per suspension volume unit, differ for different degrees of completeness of precipitation, concentrations were mathematically equalized to eliminate their effect on the sedimentation rate. The material balance for the solid phase in suspension has the following form when used to compare the stoichiometric and substoichiometric precipitation:
$Z_o \cdot \gamma_o = Z_1 \cdot \gamma_1$, where: Z is the precipitate level, and γ the solid phase mass concentration. The index "o" denotes 100 % (stoichiometric) precipitation, and index "1" incomplete (substoichiometric) precipitation.
It then follows that Z_1 is the level that the suspension should reach for all the solid phase to be of the mass concentration γ_o. Starting from this value for Z_1, i.e. the value at which the concentrations were equalized for different degrees of completeness of precipitation, the change

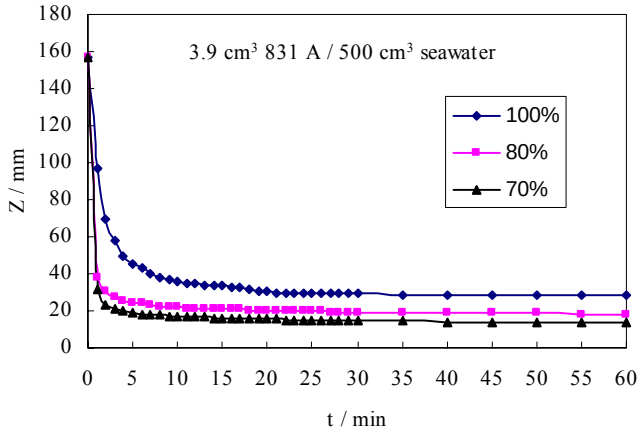


Figure 3. The dependence of the precipitate level (Z) upon the setting time (t), for different degrees of precipitation completeness, with addition of 3.9 cm^3 of the 831A flocculent per 500 cm^3 of seawater.

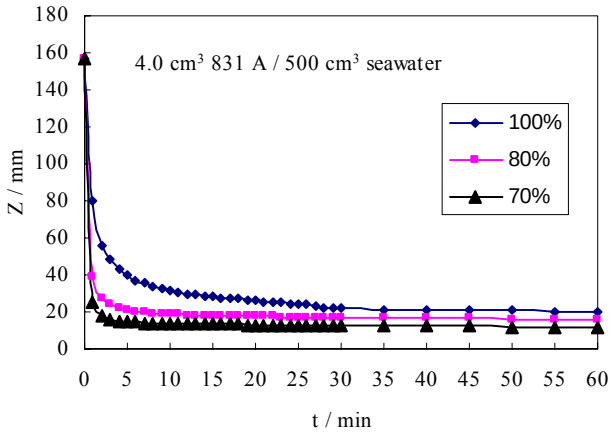


Figure 4. The dependence of the precipitate level (Z) upon the setting time (t), for different degrees of precipitation completeness, with addition of 4.0 cm^3 of the 831A flocculent per 500 cm^3 of seawater.

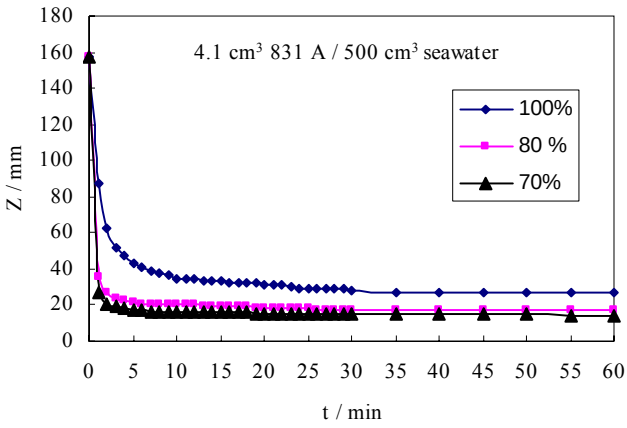


Figure 5. The dependence of the precipitate level (Z) upon the setting time (t), for different degrees of precipitation completeness, with addition of 4.1 cm^3 of the 831A flocculent per 500 cm^3 of seawater.

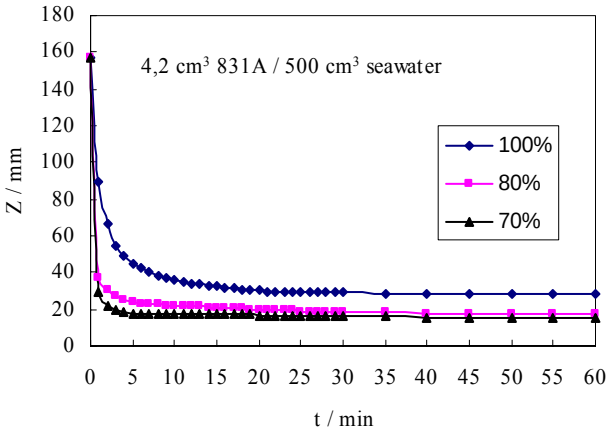


Figure 6. The dependence of the precipitate level (Z) upon the setting time (t), for different degrees of precipitation completeness, with addition of 4.2 cm^3 of the 831A flocculent per 500 cm^3 of seawater.

in the precipitate level, $\Delta Z = Z_1 - Z_2$, has been determined for the interval of 20 minutes.
It then follows that Z_1 is the level that the suspension should reach for all the solid phase to be of the mass concentration γ_o. Starting from this value for Z_1, i.e. the value at which the concentrations were equalized for different degrees of completeness of precipitation, the change in the precipitate level, $\Delta Z = Z_1 - Z_2$, has been determined for the interval of 20 minutes. Table 1 shows the values obtained for Z_1 and Z_2. The dependence $\Delta Z = f$ (% stoich.) (Figure 9) indicates the degree of completion of precipitation for which the examined flocculent addition is optimum.

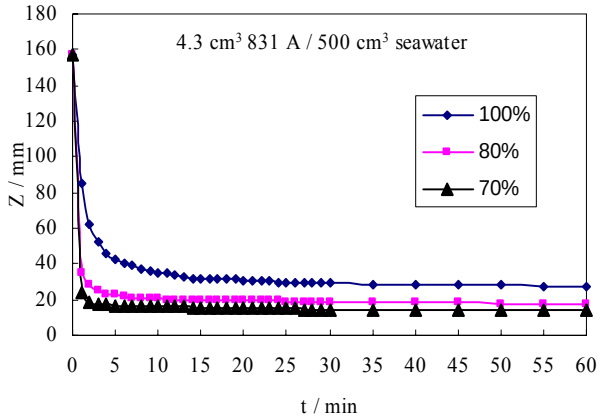


Figure 7. The dependence of the precipitate level (Z) upon the setting time (t), for different degrees of precipitation completeness, with addition of 4.3 cm^3 of the 831A flocculent per 500 cm^3 of seawater.

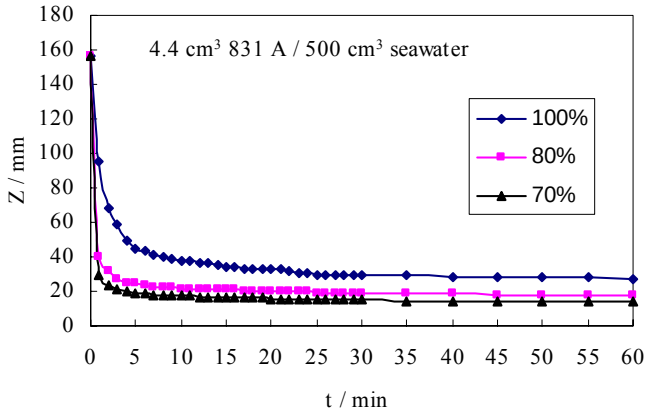


Figure 8. The dependence of the precipitate level (Z) upon the setting time (t), for different degrees of precipitation completeness, with addition of 4.4 cm^3 of the 831A flocculent per 500 cm^3 of seawater.

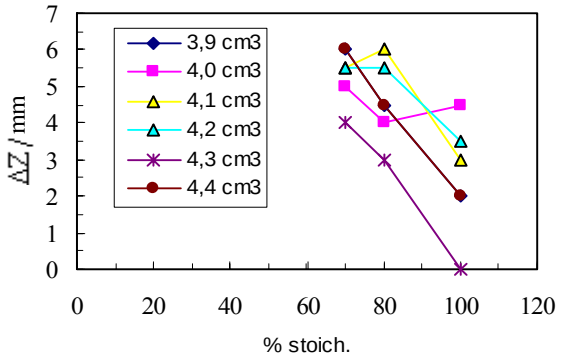


Figure 9. The dependence of the change in the precipitate level (ΔZ) on the degree of completeness of precipitation of magnesium hydroxide from seawater, with different additions of the 831A flocculent per 500 cm^3 of seawater.

Therefore, the degree of completeness of precipitation for which the sedimentation rate is highest for the examined flocculent addition is determined for the maximum value of change of the precipitate level, ΔZ. The results obtained confirm that ΔZ reaches the maximum in substoichiometric 80 % precipitation with the addition of the 831A flocculent in the amount of 4.1 cm^3 per 500 cm^3 seawater. It may then be concluded that that amount of the 831A flocculent addition is the optimum quantity needed to accelerate the sedimentation rate of magnesium hydroxide in substoichiometric precipitation with the addition of 80 % of the stoichiometrically required quantity of dolomite lime. The expenditure of the examined 831A flocculent needed to attain the maximum sedimentation rate at 80 % precipitation, expressed in mass %, amounts to $7.11 \cdot 10^{-2}$ mass %. The comparison with previously examined flocculents [11] indicates a much lower expenditure of powdery flocculents than that of gelatinous ones – Flokal-B (the expenditure of Flokal-B would be 0.248 mass %). As there are different anionic polyacrylamide-

Table 1. Dependence of Z_1 and Z_2 on the degrees of completeness of precipitation for different additions of the 831A flocculent.

cm^3 of the flocculent 831A per 500 cm^3 of seawater	Degree of completeness of precipitation %	Z_1 / mm	Z_2 / mm
3.9	70	21	15
	80	24	19.50
	100	30	28.00
4.0	70	18	13
	80	21	17
	100	26	21.5
4.1	70	21	15.5
	80	24	18
	100	30	27
4.2	70	22	16.5
	80	25	19.5
	100	31.5	28
4.3	70	19	15
	80	22	19
	100	27.5	27.5
4.4	70	21	15
	80	24.5	19
	100	30.5	28.5

based flocculents, it is necessary to determine for each of them the optimum quantity to be added to the magnesium hydroxide suspension in order to attain the maximum sedimentation rate for individual degrees of completeness of precipitation. The main purpose of the flocculent is to neutralize as much as possible the potential difference between the magnesium hydroxide particle surface and seawater, i.e. electrokinetic potential, thereby forming favourable conditions for flocculation of particles. In this way the rejection between particles is reduced. The applied 831A flocculent ($M(831A) = 6 \cdot 10^6 - 8 \cdot 10^6$ g mol^{-1}) has a medium number of active groups along the chain of carbon atoms. Examinations carried out in this study show that the 831A flocculent has outstanding flocculating properties, and can be used to improve the settling properties of the suspension of magnesium hydroxide obtained from seawater. Namely, the addition of the polyelectrolyte – 831A flocculent, causes the macromolecular chain to adsorb onto colloid particles in the magnesium hydroxide suspension.

Once one end of the molecule adsorbs onto a particle, the remainder of the molecule is still free to adsorb onto other precipitate particles in the suspension. This leads to fast agglomeration and flocculation of particles in the suspension. This effect is known as “bridging”[15,16].

4. CONCLUSIONS

- The anionic 831A flocculent, produced by the Dutch firm Hercules, has outstanding flocculating properties, and can be used to improve the settling properties of the suspension

of magnesium hydroxide obtained from seawater. The application of the 831A flocculent confirms the previously assumed model of the magnesium hydroxide particle.

- The established optimum quantity of the 831A flocculent for attaining the maximum sedimentation rate at 80 % substoichiometric precipitation of magnesium hydroxide is 8.2 cm^3 per dm^3 seawater.

- It is always necessary to supplement the examination of the settling properties of the suspension of magnesium hydroxide from seawater in discontinuous conditions in a graduated glass cylinder with different quantities of the 831A flocculent addition by the method of examining of the settling properties of the suspension of magnesium hydroxide at different degrees of precipitation completeness (70 %, 80 %, and 100 % precipitation), but with the same quantity of the 831A flocculent addition. The maximum change in the precipitate level, ΔZ, determines the degree of completeness of precipitation for which the sedimentation rate is maximum for the examined flocculent addition.

ACKNOWLEDGMENT

The results presented have originated from the scientific Project 011-0112247-2250, carried out with the support of the Ministry of science, education and sports of the Republic of Croatia.

REFERENCES

1. E. Brown et al., *Seawater*: *Its compositions, properties and behaviour, Butterworth Heinemann in associattion with The Open University*, Walton Hall, Milton Keynes, 2nd Ed., 1997, p. 104
2. M. A. Shand, *The Chemistry and Technology of Magnesia*, Wiley, New York, 2006.
3. C. Sims, *Industr*. *Minerals* **7** (1997) 21-33
4. H. Tsuge, Y. Kotaki, S. Asano: Reactive Crystallitation of Magnesium Hydroxide Obtained from Sea Water, in: H. Kakihana, H. R. Hardy JR, T. Hoshi i K. Toyokura (Ed.): *Proc*. *7th Symposium on Salt*, Vol. 2, Elsevier Science Publishers B.V., Amsterdam, 1993, pp. 219-223
5. O. Lee Maddan, US Pat. 6 267 854B1, 31 July 2001: C.A. **134** (2001) 286989M
6. N. Heasman, *Gas Wärme International*, **28** (1979) 392–397
7. R. C. Carson, J. Simandl, *Mineral*. *Eng*. **7** (1994) 511-517
8. J. C. Hicks, S. Tangney, *Ceram. Bull*. **59** (1980) 711-714
9. D. Rabadžhieva, K. Ivanova, Hr. Balarev, D. Trendafelov, *Žurnal priklačnoji himii* **70** (1997) 375-380
10. D. Barba, V. Brandani, G. Di. Giacomo, P. U. Foscolo, *Desalination* **33** (1980) 241-250
11. B. Petric, N. Petric, *Ind*. *Eng*. *Chem*. *Process Des*. *Dev*. **19** (1980) 329-335
12. V. Martinac, M. Labor, N. Petric, N. Arbunić, *Indian J*. *Mar*. *Sci*. **26** (1997) 335-340
13. V. Martinac, M. Labor, N. Petric, *Chem. Biochem*. *Eng*. *Q*. **12** (1998) 101-107
14. C. Cocheci, M. Sora, L. Taubert, S. Policec, *Filtrieren und Separieren* **9** (1995) 120-122
15. N. P. Cheremisinoff, *Handbook of Water and Wastewater Treatment Technologies*, Butterworth Heinemannin, Oxford, 2002, pp. 268-334, 73
16. L. D. Benefield, J. F. Judkins, B. L. Ewand, *Process Chemistry for Water and Wastewater Treatment*, Prentice Hall, Inc., Englewood Cliffs, New Jersey, 1982, p. 218.

SVA ČETIRI OSNOVNA MEHANIZMA TROŠENJA U JEDNOM TRIBOSUSTAVU

FOUR MAIN MECHANISMS OF WEAR IN ONE TRIBOLOGY SYSTEM

Dr. sc. Vlatko Marušić, Strojarski fakultet, Slavonski Brod
Dr. sc. Dragomir Krumes, Strojarski fakultet, Slavonski Brod
Sanja Marušić, dipl. ing., Industrijsko-obrtnička škola, Slavonski Brod

Stručni članak / Professional paper

Sažetak: Na novijoj konstrukcijskoj izvedbi pužnih preša za cijeđenje ulja uočeno je neuobičajeno brzo oštećivanje vratila pužnice. Utvrđeno je da konstrukcijska izvedba elemenata tribopara vratilo/segmenti pužnice, u uvjetima visokih pritisaka (400÷500 bara) uzrokuju njihovo (pre)brzo trošenje. Konstatirano je da do otkaza dolazi uslijed gotovo istovremenog djelovanja abrazije, adhezije, umora i tribokorozije.

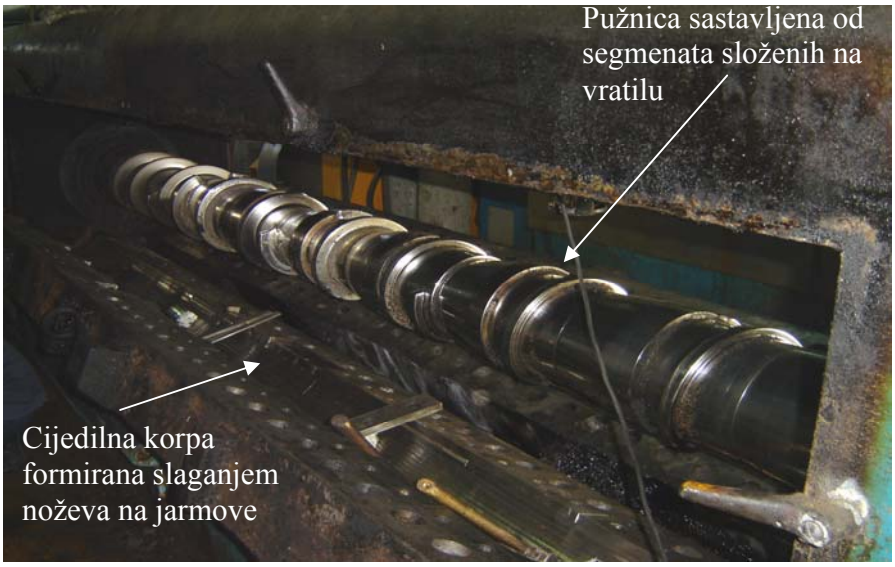
Ključne riječi: tribopar, vratilo/pužni segmenti, mehanizmi trošenja, pužna preša, konstrukcija

Abstract: On new construction process of worm press for oil squeamish it was observed uncommon rapidly damaging shaft of worm. It was determined that construction process of elements tribology pair shaft/segment of worm, in conditions of high pressure (400÷500 bar) causing their too fast wear-out. Asserted is that termination is caused by almost simultaneously activity abrasion, adhesive, weariness and tribocorrosion.

Key words: Tribology pair shaft/segment of worm, mechanisms of wear, worm press, construction,

1. UVOD

Radni dijelovi pužne preše, noževi plašta košare i segmenti pužnice, neminovno su izloženi trošenju pri cijeđenju ulja. Ti su dijelovi u kontaktu s pripremljenim uljnim sjemenjem (mlivom), a troše se abrazijom [1,2] česticama SiO_2XnH_2O sadržanog uglavnom u ljusci. Otpornost trošenju noževa i segmenata ovisi o primijenjenom postupku površinske zaštite [3], ali i o udjelu abraziva u mlivu. Za efikasno cijeđenje dovoljno je da mlivo sadrži 10÷12% ljuske. U posljednjih 5, 6 godina ističe se pristup proizvođače preša koji se sastoji u isporuci noževa i segmenata sa zaštitnim slojem za koje se deklarira vijek trajanja izražen u satima rada (!?). U pravilu je to ≈7.000 sati, odnosno koliko traje godišnja kampanja. Nakon toga proizvođač preša preporuča izvršiti njihovu zamjenu novim dijelovima. Izgled otvorene pužne preše prikazan je na slici 1.
Pri zamjeni istrošenih radnih dijelova, rasklapaju se cijedila na polutke, noževi skidaju s jarmova, a segmenti pužnice svlače s vratila (vratilo i jarmovi su svrstani u nosive dijelove preše jer, u pravilu, pri cijeđenju ulja ne bi trebali dolaziti u direktni doticaj s mlivom). Na prešama za završno prešanje novije konstrukcije, kapaciteta preko 100 tona/dan pripremljenog uljnog sjemenja, uočena je pojava, ne samo uobičajenog trošenja puževa i noževa, nego i neuobičajenog oštećivanja vratila i jarmova. Kako je do oštećenja tih nosivih dijelova preša došlo već nakon 4÷5 godina rada (!) ukazala se potreba za utvrđivanjem uzroka u cilju smanjenja negativnih efekata. Praćenjem i ispitivanjem su obuhvaćena originalna vratila iz tri pužne preše: nakon tri, četiri i nakon pet godina uporabe.



Slika 1. Otvorena pužna preša s označenim dijelovima

2. SNIMANJE STANJA OŠTEĆENIH DIJELOVA PREŠA

Nakon rasklapanja preša i pregleda demontiranih dijelova uočeno je:

- da su neki segmenti pužnice normalno istrošeni, odnosno da je potrošen samo čeoni dio vrha pužne zavojnice (slika 2a), što se s tribološke strane po definiciji naziva „normalno trošenje“,
- da je na nekim segmentima pužnice došlo do otkidanja dijela pužne zavojnice (slika 2b),
- da su na nekim konusnim segmentima pužnice ne samo dijelovi radne površine, nego i osnovni materijal u cijelosti istrošeni (slika 2c). Na slici 2d prikazan je normalno trošen konusni segment pužnice, s vidljivim utorom za brtvu.

Potrebno je istaći da se segmenti pužnice isporučuju s utorom izrađenim samo na jednoj čeonoj dosjednoj površini, a na drugu dosjeda segment s istim takvim utorom. U utore se stavljaju silikonske brtve debljine 1mm veće od dubine utora.

Međusobnom usporedbom vratila, uočeno je da postoji razlika u intenzitetu oštećenja Puno više je istrošeno, čak katastrofalno ono koje je bilo najduže u uporabi, slika 3.



Slika 2. Oštećeni segmenti pužnice

a) *pužni segment s normalno istrošenom zavojnicom; b) s otkinutim dijelom zavojnice c) konusni segment „katastrofalno“ istrošen; d) konusni segment „normalno“ istrošen*



a) *b)*

Slika 3. Izgled oštećenja na vratilima
a) vratilo nakon 4 godine uporabe (oštećeno je vratilo i pero samo djelomično)
b) vratilo nakon 5 godina uporabe (oštećeni su vratilo i pero, a utor i po dubini i bočno)

3. REZULTATI ISPITIVANJA

Analizom kemijskog sastava utvrđeno je:

- vratila su izrađena od materijala koji po sastavu odgovara Č4732, odnosno čeliku 42CrMo4 (prema EN10027-1),
- osnovni materijal tijela segmenata pužnice po sastavu odgovara Č1330, odnosno čeliku C22 (EN10027-1),
- navareni površinski sloj na segmentima sastoji se od C-Cr-Mo-Si, debljine sloja ≈ 4 mm.

Mjerenjem površinske tvrdoće, pomoću prijenosnog tvrdomjera MIC 10-D [4], utvrđeno je slijedeće:

- površinska tvrdoća vratila kretala se između 18 i 23 HRC,
- površinska tvrdoća navarenog sloja na tijelu segmenata kretala se od 50 do 55 HRC, a na pužnoj zavojnici od 41 do 55 HRC, dok se tvrdoća osnovnog materijala segmenata kretala od 130 do 160 HB.

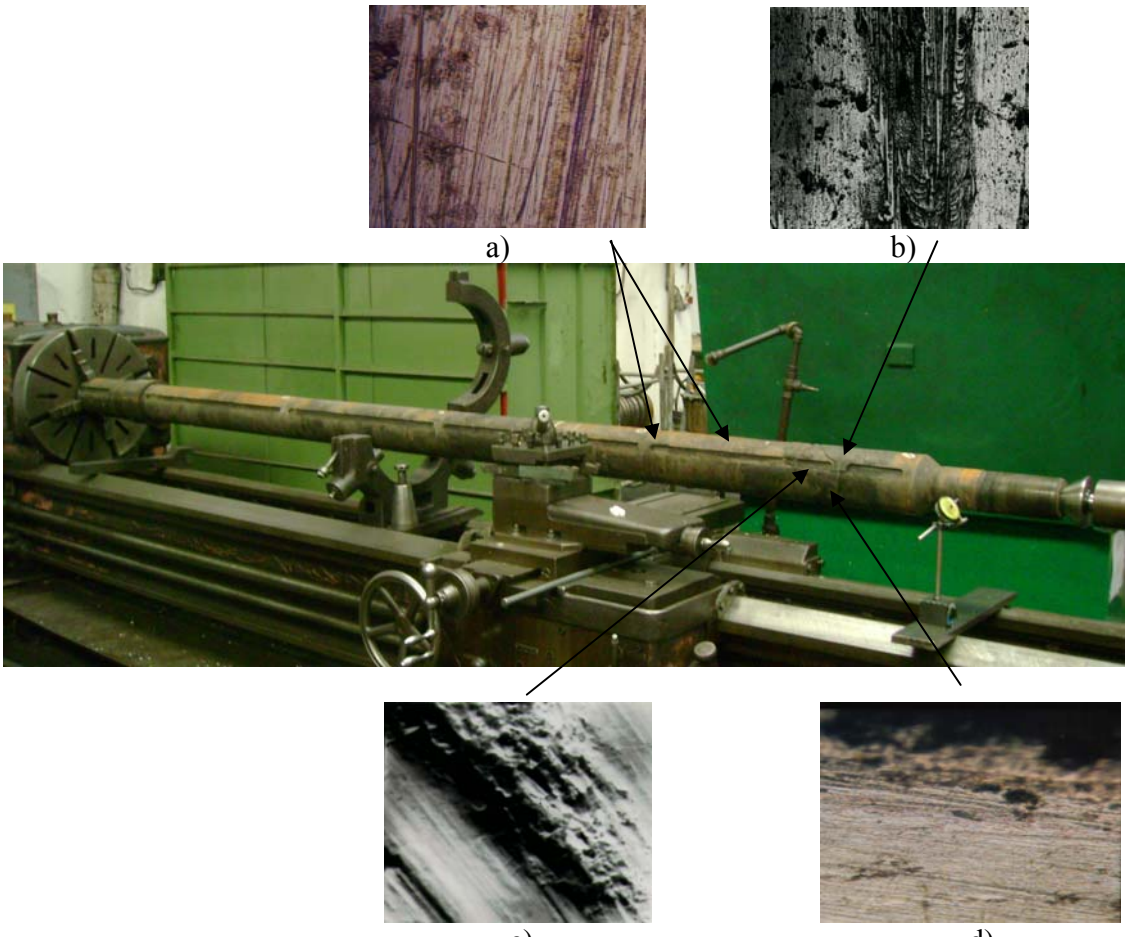
Vratila su ukupne dužine 4350 mm, pri čemu je dio na koji se navlače segmenti dužine ≈ 3350 mm. Vratilo stavljeno na tokarski stroj prikazano je na slici 4. Dimenzionalnom kontrolom utvrđeno je slijedeće:

- oštećenjem je zahvaćen samo izlazni dio vratila, u dužini ≈ 1600 mm,
- vratilo koje je u uporabi bilo 3 godine oštećeno je trošenjem u dubinu do 2 mm, a nije uočeno oštećivanje utora i pera,
- na vratilu koje je u uporabi bilo 4 godine maksimalna dubina oštećenja iznosila je do 3 mm, a uočeno je da su pera oštećena na mjestima najdubljeg istrošenja vratila, a lokalno i utori ispod pera,
- vratilo koje je u uporabi bilo 5 godina lokalno je trošenjem oštećeno u dubinu i do 8 mm, a mjestimično su pera u cijelosti istrošena, dok su utori, na nekim dijelovima svoje dužine, oštećeni u dubinu i do 3 mm,

- na vratilima koja su u uporabi bila 4 i 5 godina kontrolom pomoću komparatera utvrđeno je povećanje promjera u odnosu na nazivnu mjeru, lokalno do 2mm.

S jako oštećenih dijelova vratila uzeti su uzorci, izvršeno je snimanje tragova trošenja, te je utvrđeno da:

- postoje tragovi abrazijskog trošenja, slika 4a,
- adhezijsko trošenje izraženo je na mjestima gdje se nalaze utori i pera kojima se fiksira položaj segmenata na vratilu u cilju formiranja pužne zavojnice potrebnog koraka, slika 4b,
- umor površine (slika 4c), a i tribokorozijsko trošenje (slika 4d) vjerojatno mehanizmom tarne korozije [5], prisutni su na mjestima dosjeda segment/vratilo. Širina tih dosjeda (po unutarnjem promjeru) iznosi 40 mm na početku i na kraju segmenta, dok je sredina segmenta izrađena s 2mm većim promjerom od promjera vratila, zbog lakše montaže, a pogotovo demontaže (mlivo „zapekne“, a vjerojatno nastanu i mikrozavari pa se ponekad skidanje segmenata može izvršiti isključivo njihovim podužnim rezanjem).



Slika 4. Karakteristični tragovi trošenja na vratilu
a) – abrazija; b) – adhezija; c) – umor površine; d) - tribokorozija

4. ANALIZA REZULTATA

Pregledom konstrukcijske izvedbe segmenata pužnice i usporedbom s najizrazitije oštećenim (posve istrošenim) dijelovima konstatirano je da:

- čeone (dosjedne) površine segmenata završno se obrađuju brušenjem pri čemu se u odgovarajuće utore, pri montaži na vratilo, postavljaju silikonske brtve,
- najizrazitije, posve su istrošena tijela onih konusnih segmenata kod kojih se navareni sloj jednog segmenta oslanja na osnovni materijal susjednog,
- na položaju posve istrošenih segmenata vratilo je najdublje oštećeno, ali se oštećenje prostire i ispod segmenata čije tijelo nije posve istrošeno,
- trošenje vratila je posljedica erozijsko-abrazijskog djelovanja čestica mliva u ulju, zatim adhezije manifestirane prijelazom materijala između segmenta i vratila, ali i tribokorozije.

Na temelju toga može se konstatirati da do oštećenja segmenata pužnice dolazi uslijed neodgovarajuće izvedbe dosjednih (čeonih) površina. Ta oštećenja rezultiraju vrlo intezivnim trošenjem vratila. Međutim, pojava savijanja i uvijanja vratila ukazuje na dodatne probleme: u izboru osnovnog materijala, postupka toplinske obradbe, ali i konstrukcije cijele preše obzirom na veličine i vrste opterećenja kojima su pri cijeđenju ulja izloženi, kako radni tako i nosivi dijelovi preše.

5. ZAKLJUČAK

Rezultati ispitivanja mogu poslužiti kod izbora parametara i postupka reparaturnog obnavljanja vratila na način da površinski (novi) sloj ima puno veću tvrdoću. Na taj način je moguće produljiti njihov vijek trajanja, ali ne i otkloniti uzroke otkaza (prestanka funkcionalnog rada preše). Dodatno, rezultati ispitivanja ukazuju na to da i čeone (dosjedne) površine segmenata pužnice trebaju biti tvrde kako bi se izbjeglo njihovo mehaničko oštećivanje utiskivanjem tvrdog navara prethodnog u osnovni meki materijal narednog segmenta.

To su dvije mogućnosti za produljenje vijeka sklopa pužnice (segmenti + vratilo). U ovom trenutku teško je procijeniti da li predloženim zahvatima može biti posve spriječeno oštećivanje vratila. Razlog se nalazi u činjenici da su vratila tijekom rada izložena i savijanju i uvijanju što s konstrukcijskog pristupa neizostavno rezultira relativnim pomjeranjem dosjednih površina što ponovo može, ali u puno manjoj mjeri ili sporije, omogućiti dospijevanje mliva s uljem do vratila i njegovim trošenjem.

Proizvođači originalnih preša, a i oni koji izrađuju zamjenske dijelove, usvojili su pristup da isporučuju dijelove za koje deklariraju vijek izražen u satima rada. Najčešće je to oko 7.000 sati koliko traje godišnja kampanja. Za prešaonu kapaciteta 500 tona /dan potrebno je da u RH godišnje urodi ≈150.000 tona visokouljnog sjemenja, a hrvatska realnost je 50 do 60.000 tona suncokreta i 20 do 30.000 tona uljane repice [6,7]. Kako je na slobodnom tržištu teško naći svu preostalu potrebnu količinu sjemenja do potpune zauzetosti instaliranog kapaciteta, zasigurno da instalirana oprema tijekom godine dio vremena nije u uporabi. Iako uljno sjemenje i iscijeđeno ulje nisu korozijski agresivni, vrlo je lako moguće da se ispod naslaga zapečenog mliva u spoju vratilo/segmenti, tijekom zastoja

razvijaju i specifični korozijski procesi, npr. uvjetovani nedostatkom O_2 i/ili djelovanjem vlage sadržane u mlivu u kombinaciji s eruka kiselinama iz ulja, ali i to je oštećivanje posljedica prolaska mliva između dosjednih površina u dodiru segmenata pužnice.

Međutim, dodatnu pažnju zaslužuje totalno istrošenje dijela nekih konusnih segmenata i dijela površine vratila. Dosadašnjim je istraživanjima dokazano da vijek radnih dijelova preše ovisi i o udjelu abraziva u pripremljenom mlivu, odnosno da se hibridi suncokreta međusobno značajno razlikuju po karakteru ljuštenja [8]. Kako je na sjetvenim površinama u RH prisutno barem 20-tak hibrida, to postoji mogućnost da ponekad u preradi dominira „šarža" teško ljuštivih hibrida kod kojih se (nakon ljuštenja) udjel ljuske u mlivu penje i preko 15%. Vrlo je lako moguće da baš pri njihovoj preradi nastupi katastrofalno trošenje zaštitnog sloja segmenata pužnice, što u uvjetima zatvorenog sklopa cjedila nije moguće vizualno utvrditi. Ovo ukazuje na potrebu dodatnog opreza:

- kod prihvaćanja (naručivanja) radnih dijelova preša po principu vijeka deklariranog u satima rada,
- kod organiziranja rada službe održavanja u smislu potrebe uvođenja povremene kontrole stanja trošenju izloženih dijelova preša.

6. LITERATURA

[1] Schneider, F.H.,Khoo,D: Trennpressen-Versuch einer Bestandsaufnahme esperimenteller Arbeiten, Fette-Seifen-Anstrichmittel, 9,329-340 (1986)

[2] V. Marušić, R. Popović, S. Marušić: Mogućnost sanacije jarmova cjedila pužne prese u cilju povećanja efikasnosti rada prešaone, Uljarstvo,37,1-2:29-36(2006)

[3] V. Ivušić, V. Marušić, K. Grilec, Abrasion resistance of surface layers, COST 516 Tribology Symposium, VTT Technical Research Centre of Finland, 201-210(1998)

[4] Tvrdomjer MIC 10-D, Krautkramer, Njemačka

[5] I. Esih, Z. Dugi: „Tehnologija zaštite od korozije I - Teorija, ispitivanja korozije i ponašanja materijala", Školska knjiga, Zagreb (1990)

[6] Sortni makropokus suncokreta i soje, Agrokor-Zvijezda, Sopot Vinkovci (2006)

[7] Sortni makropokus suncokreta i soje, Agrokor-Zvijezda, Sopot Vinkovci (2007)

[8] V. Marušić, D. Štrucelj, Tribološki gubici u uljari u ovisnosti o zaštiti dijelova preša i čvrstoći sjemena nekih hibrida suncokreta, Uljarstvo, 35, 1-2(2004) 25-30

INOX 316L-materijal za sanaciju dimnjaka grada Zagreba

INOX 316L material for chimney repair in the town of Zagreb

Zdenko Meczner[1], Gojko Marić[2], Nastia Degiuli[2]
[1]Grad Zagreb, Gradski ured za prostorno uređenje, zaštitu okoliša, izgradnju grada, graditeljstvo, komunalne poslove i promet, Park stara Trešnjevka 2, 10000 Zagreb
[2]Fakultet strojarstva i brodogradnje, Sveučilišta u Zagrebu, I. Lučića 5, 10000 Zagreb
zdenko.meczner@zagreb.hr ; gmaric@fsb.hr ; nastia.degiuli@fsb.hr

Stručni članak / Professional paper

Abstract:
Gas-using devices are usually connected to a chimney without any previous interventions on the chimney to ensure safety. This is done because the conventional wisdom is that a chimney is in safe working order if it is passable, especially if it has been in use for some 40 years or more. However, the first sign of humidity on the chimney indicates that there is a great risk of intoxication.
Brick chimneys must not be used for gas fuel since porosity will definitely occur due to the composition of flue gases, and the first drop of water on the outer wall of the chimney is a sign of porosity indicating that the chimney is out of order. The chimney repair to protect it from porosity can be carried out by inserting a pipe made of inox 316 L into it.

Key words: *Chimney, flue gases, chimney repair, inox 316L.*

Sažetak:

Plinska trošila priključuju se na dimnjak bez ikakvih sigurnosnih zahvata na dimnjaku, jer je uvriježeno mišljenje da je dimnjak ispravan ako je prohodan, a pogotovo ako je bio u funkciji 40-tak i više godina. Međutim i prvi znak vlage na dimnjaku alarm je za uzbunu, jer je trovanje započelo.
Svaki cigleni dimnjak neispravan je za plinsko gorivo, jer će prije ili kasnije doći do poroznosti uzrokovane sastavom dimnog plina, a prva kapljica vlage na vanjskoj stijenki dimnjaka znak je za uzbunu i proglašenje dimnjaka neispravnim. Sanacija dimnjaka od poroznosti može se provesti umetanjem sanacijske cijevi od inox-a 316 L.

Ključne riječi: *Dimnjak, dimni plinovi, sanacija, inox 316L.*

1. UVOD

Novinski stupci puni su naslova poput: obitelj preminula u snu, ugušili se stanari, mrtvo dijete u kadi, ugušili se u kupaonici itd. Uzrok je tih smrti ugljični monoksid, plin bez mirisa, boje i okusa ali zato vrlo otrovan. Nastaje nepotpunim, zbog manjka kisika, sagorijevanjem organskih tvari kao što su drvo, ugljen, plin, petrolej, benzin. Postaje opasan kada se počne nakupljati u zatvorenim prostorima u kući, stanu, kupaonici, uredu, garaži ili skladištu. Najčešći uzrok stradavanja je neispravan rad plinskog bojlera, neispravne dimovodne instalacije te neispravna uporaba kamina i peći.
Uobičajeni simptomi trovanja su glavobolja, mučnina, kolaps, povraćanje, slabost, pospanost, koji ako se primijete na vrijeme nestaju bez posljedica. Međutim ugljični monoksid zovu tihim ubojicom jer osobe i ne primijete njegovu prisutnost te vrlo brzo uzrokuje smrt. Ugljični monoksid predstavlja veću opasnost nego svi ostali otrovi zajedno. Samo 0,2 posto ugljičnog monoksida u zraku nakon 30 minuta uzrokuje nesvijest, a nakon 2 sata smrt. Osim smrti, trovanje ugljičnim monoksidom može ostaviti i trajna oštećenja na organizmu i mozgu, nerijetko kao tešku invalidnost.
Širenjem plinske mreže po naseljima i gradovima sve više kućanstava (i ne samo kućanstava) odlučuje se zbog komparativnih prednosti plina nad ostali energentima, na grijanje i toplu vodu putem plinskih trošila. U pravilu se takva trošila priključuju na dimnjak bez ikakvih sigurnosnih zahvata na dimnjaku, jer je uvriježeno mišljenje da je dimnjak ispravan ako je prohodan, a pogotovo ako je bio u funkciji 40-tak i više godina. Međutim i prvi znak vlage na dimnjaku alarm je za uzbunu, jer je trovanje započelo.

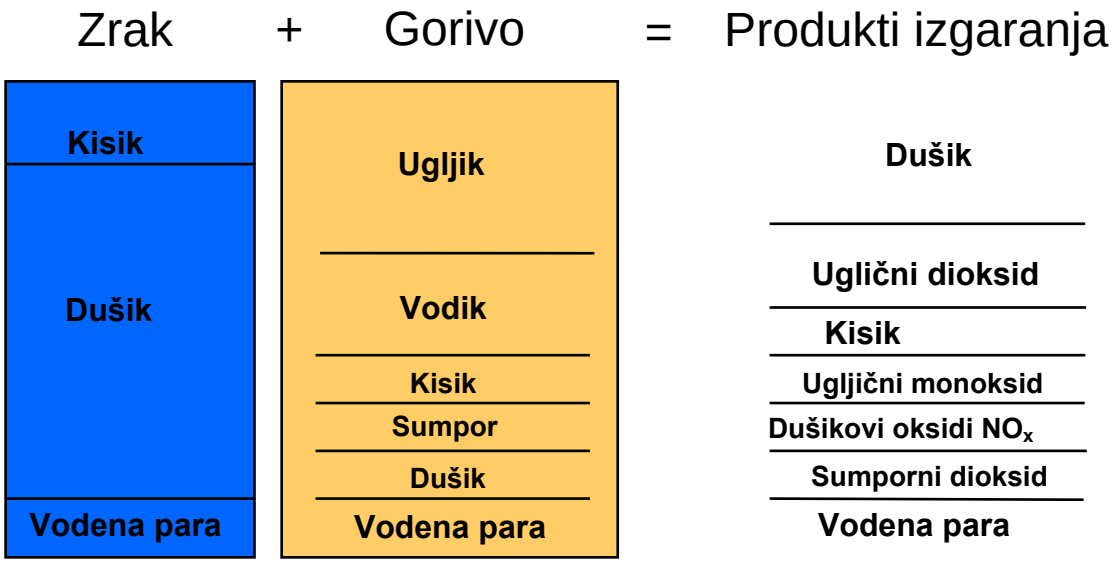


Sl. 1. Vlaga na dimnjaku

2. IZGARANJE

Produkti izgaranja molekule su različitog sastava H_2O, CO, CO_2, NO_x, itd. Te molekule nalaze se u plinovitom agregatnom stanju. Postavlja se pitanje da li neka od molekula iz sastava dimnog plina tijekom svog puta od nastanka do izlaska u atmosferu mijenja svoje agregatno stanje. Očito je da termodinamički sustav u kome se dim nalazi neće dovesti do promjene niti jedne druge molekule osim vode. Voda (H_2O) je najosjetljivija što se tiče promjene agregatnog stanja na promjene temperature.

Osim što je uvriježeno mišljenje u svijetu laika da je dimnjak ispravan ako je prohodan, postoji još jedna opasnost u procjeni ispravnosti, a to je da ako dimnjak dobro vuče (ima dobar uzgon) da je ispravan. Pri tome griješe i laici, ali i iskusni dimnjačari, jer prilaze uobičajenim probama koje su bile djelotvorne na krutom i tekućem gorivu, ali ne i na plinskom energentu.
Uobičajena provjera da li dimnjak ima uzgon, je paljenjem papira na ulasku dimovodne cijevi u dimnjak, čime se po pravcu kretanja dima, ali i po brzini kretanja dima određuje kolika je učinkovitost dimnjaka. Neke od daljnjih metoda su paljenje patrona ili prislanjanje negorivog papira na ulaz dimnjače u dimnjak, čime u slučaju dobrog uzgona, brzina kretanja zraka doslovce zalijepi papir na ulaz dimnjače u dimnjak.
Slijedeći bitan parametar je brzina kretanja zraka. U zraku kojeg dimnjak vuče nema (ili ima zanemarivo malo) vode. Uobičajeni sastav zraka kojeg je dimnjak povukao nema takav sastav da u radnim uvjetima bilo koja od molekula kondenzira, odnosno promjeni svoje agregatno stanje. No međutim u dimu nastalom izgaranjem plinovitog goriva ima jako puno vode.



Sl. 2. Proces izgaranja

Kao što se iz slike 2 vidi u produktima izgaranja nalazi se i vodena para, a u zavisnosti od temperature dima i sastava energenta njen udio bit će manji ili veći. Kod plinskog goriva imamo najveći udio vodene pare.
Kako toplinska energija prelazi samo iz stanja višeg energetskog nivoa na niži, tako će dim odnosno produkti izgaranja, u doticaju sa stijenkom dimnjaka predavati energiju dima stijenki dimnjaka. Pri tome će jedna molekula sastava dimnog plina mijenjati agregatno stanje, a to je molekula vode. U tom trenutku dimnjak ne funkcionira i neće funkcionirati tako dugo dok stijenka dimnjaka ne poprimi temperaturu koja neće više mijenjati agregatno stanje, i dimnjak će proraditi, odnosno količinu dimnih plinova odvesti u atmosferu.
Što se zapravo desilo u dimnjaku? Sve promjene agregatnog stanja bilo koje molekule događaju se u omjeru određenog tlaka i određene temperature. Ovisnost volumena plina o tlaku su neovisno jedan o drugome, ali u približno isto vrijeme, proučavali znanstvenici R. Boyle i E. Mariotte, i ustanovili obrnutu proporcionalnost volumena i tlaka plina, te se zakon po njima dvojci nazvao Boyle-Mariotteov zakon.

Mijenja li se tlak odnosno volumen plina, pri stalnoj temperaturi, što zovemo izotermnom promjenom stanja plina, tada vrijedi zakonitost pisana u slijedećem obliku:

$$p \cdot V = \text{const.} \tag{1}$$

tj. volumen plina mijenja se obrnuto proporcionalno s tlakom pri čemu su temperature i količina plina konstantni.
Boyle–Mariotteov zakon nam govori da se na svom putu od mjesta nastanka do izlaska u atmosferu produkti izgaranja nalaze u jednoj skladnoj harmoniji tj. volumen i tlak su u ravnoteži. Kako će se tlak povećavati ili smanjivati, tako će se i volumen molekule dima smanjivati ili povećavati na način da je njihov umnožak uvijek konstantan.
No međutim ovdje se pojavljuje voda i njena mala tolerancija na promjene agregatnog stanja. Molekula u plinovitom stanju ima daleko veći volumen nego ta ista molekula u tekućem stanju, a kako su umnožak volumena i tlaka uvijek konstantni, tako će i drastično smanjenje volumena molekule vode, dovesti do drastičnog povećanja vrijednosti tlaka. U tom trenutku stvoreni tlak je toliko velik da je doveo do začepljenja dimnjaka i novodolazeći dim ima samo jednu mogućnost kretanja, a to je povratak, čime počinje trovanje korisnika takvog dimnjaka.
Udisanje ugljičnog monoksida (inhalacija) je vjerojatno najlakši i najbrži put unosa otrova u organizam. Uzrok tome je što dišni put nema efikasne zaštite, osim dlačica u nosnicama koje imaju filtracijsku funkciju za velike čestice. Do neke mjere ima zaštitnu ulogu i sloj sluzi, koji prekriva cijelu površinu dišnog puta. Tu sluz izlučuju dijelom vrčaste stanice u epitelnom sloju, a dijelom male submukozne žlijezde. Sluz služi hvatanju sitnih čestica iz zraka na putu do alveola. Sama pluća sastavljena su tako da omogućavaju brz prijelaz molekula u krvotok preko velike površine od 80 m², koju čini 300 milijuna alveola.
S obzirom na posljedicu trovanja ugljični monoksid svrstavamo u kategoriju kemijskog trovanja, koji preko alveola difundiraju direktno u krvotok, pri čemu brzina difuzije ovisi o koncentracijskom gradijentu između pluća i krvi. U početnoj fazi prijelaz tvari je brži, jer je gradijent između pluća i krvi velik. Trovanje ugljičnim monoksidom može imati epidemijski karakter ako se nalazi više osoba u istom prostoru, a simptomi su glavobolja, povraćanje, koma, konvulzije, bule.
Ugljični monoksid nastaje kod nepotpunog izgorijevanje tvari u kojoj je ugljik. Ugljični monoksid je plin bez boje, mirisa i okusa, i te njegove osobine su najopasnije, jer ga ne možemo prepoznati. Nešto je lakši od zraka. U arterijskoj krvi veže se na hemoglobin. Ima otprilike 250 puta veći afinitet vezanja na hemoglobin nego kisik. Baš zbog toga se na hemoglobin veže brzo i već u vrlo niskim koncentracijama nastaje karboksihemoglobin (HbCO), koji ne može prenositi kisik. Zbog toga se u krvi smanji dio oksihemoglobina
(O_2-Hb), a na taj način i količina kisika u arterijskoj krvi. Kapacitet krvi za prijenos kisika je manji.
U trenutku kada temperatura stijenke dimnjaka dosegne temperaturu prijelaza agregatnog stanja iz plinovitog u tekuće, a to je u dimnjaku negdje oko 57˚C, dim nastavlja svoj put prema izlasku, i trovanje prestaje.
Međutim, do tog trenutka voda je već pronašla svoj put, pa je jednim dijelom tekla niz dimnjak, ali jednim dijelom i kroz vapno odnosno na mjestu spajanja cigle. Onog trenutka kada je probila voda probio je i zrak, pa je došlo do trajnog poroziteta dimnjaka, što je vidljivo pojavom vlage, odnosno vode na vanjskoj stijenki dimnjaka.
Znači svaki cigleni dimnjak neispravan je za plinsko gorivo, jer će prije ili kasnije doći do poroznosti, a prva kapljica vlage na vanjskoj stijenki dimnjaka znak je za uzbunu i proglašenje dimnjaka neispravnim, a tu poroznost zbog sastava dimnog plina može zadovoljiti umetanje sanacijske cijevi iz inox-a 316 L.



Sl. 3. Mjesto kondenzacije (strelica)



Sl. 4 Isto kao sl.3, samo drugi kut snimanja

3. IZBOR MATERIJALA ZA SANACIJU DIMNJAKA

Vodeći računa o rečenom u prethodnom poglavlju, mogu se prihvatiti samo oni materijali koji će zadovoljiti tražena svojstva, a to su keramika, legirani čelik i šamot. U praksi se kod uvlačenja cijevi u postojeći dimnjak zbog debljine stijenke šamot i keramika ne upotrebljavaju, dok je najveću primjenu našao legirani čelik koji zadovoljava tražene uvjete već kod debljine stijenke od 0,5 mm.
Sanacije dimnjaka s čeličnim cijevima već duži period se vrše na području grada Zagreba, no primijećeno je da su nakon nekih sanacija dimnjaci i dalje funkcionalno neispravni kao što su bili prije sanacije, a bilo je slučajeva i požara na tek saniranim dimnjacima.
Razlog tome su nestručno izvođenje sanacija uvlačenjem čeličnih cijevi ali i cijevi koje su načinjene od nekvalitetnog materijala, loše spajane ali i nedovoljna debljina stijenki.
Sve ovo upućuje da bi se trebalo provesti ozbiljno neovisno ispitivanje cijevi koje se ugrađuju kao i kontinuirano obrazovati izvođače takovih radova kao i dimnjačare.

Propisane norme EU su slijedeće:

- EN 1856–1 Dimnjaci – Zahtjevi prilikom obnove metalnim cijevima – Dio 1: Dijelovi dimnjaka od 01.04.2005,
- EN 1856–2 Dimnjaci – Zahtjevi prilikom obnove metalnim cijevima – Dio 2: Metalne cijevi i spojevi od 01.05.2006 (dopunjen 01.11.2007) (Uključene krute i savitljive cijevi),
- EN 1859 Dimnjaci – Metalni dimnjaci – Ispitne metode.

Ispitne metode su:

- Temperaturna klasa npr. T450 (radna),
- Plino nepropusnost/tlačnost klasa npr. N (negativna) ili P (pozitivna),
- Radni uvjeti npr. D (suho) ili W (mokro),
- Korozijski test npr. V2,
- Oznaka materijala označen uz pomoć tabele u normi (50 = 1,4404; 316L),
- Debljina stijenke npr. 050 = 0,5mm,
- Vatrootpornost npr. O ili G (G =otpornost čađenju) + udaljenost od zapaljivih materijala u mm npr. 50,

npr. ICS EN1856-1 T450 N1 W V2 L50050 G50.

Konstrukcija instaliranog dimnjaka određena je nacionalnim propisom, potvrđeno npr., "markicom" na inspekcijskim vratima dimnjaka.

4. ZAKLJUČAK

Već smo nabrojali da postoje teoretski nekoliko rješenja:

1. Srušiti stare dimnjake i na njihovo mjesto izgraditi nove.
2. Izgraditi nove dimnjake.
3. Sanirati postojeće dimnjake.

Na početku nabrajanja rečeno je da teoretski postoji nekoliko rješenja, no pragmatički postoji samo jedno rješenje, sanacija postojećih dimnjaka.

Zašto odbacujemo prva rješenja.

Ad 1. Poznato je da se dimnjaci najčešće grade tako su postavljeni u sredini zgrade, pa je rušenje postojećih i izgradnja novih na njihovom mjestu nemoguća. Naime takovim radovima trebalo bi zadirati u "srce" zgrade što bi izazvalo ogromne troškove, a veliki problem bile bi i suglasnosti svih vlasnika koji bi se trebali složiti za takav zahvat.

Ad 2. Izgradnja novih dimnjaka na fasadnoj – vanjskoj strani zgradi je teoretski vrlo rijetko moguća jer su tu postavljeni prozori, balkoni a i vizualno bi to bilo nakaradno rješenje.

Ad 3. Dakle rješenje koje je najprihvatljivije ili može se čak reći jedino rješenje je sanacija dimnjaka.

Postavlja se čitav niz pitanja vezanih uz sanaciju i njeno provođenje:

- Tko će odrediti da je sanacija potrebna (s kojom opremom)?
- Tko će izraditi plan–studiju sanacije te sugerirati način kako je izvesti i s kojim materijalom?
- Tko će sanaciju izvesti?
- I možda najbitnije tko će na kraju sanacije izvršiti pregled?

Jedno je rješenje da sve ove probleme ostavimo na rješavanje dimnjačarima! No da li je to dobar izbor?

Radi se ljudima koji u okviru svog školovanja nisu dobili dovoljno znanja da bi se nosili s ovim problemima. Velika većina njih pokušava uhvatiti se u koštac s problemom koji je nastao, te sa opremom i znanjem koji nisu dostatni pomoći građanima. No treba reći da dimnjačari, ali i drugi koji se bave sanacijama, ne bi smjeli obavljati zahvate za koje nisu izučeni i to pogotovo bez nadzora. Radi se o vrlo bitnom i osjetljivom poslu koji ako nije izveden propisno može izazvati smrtne slučajeve. Također treba naglasiti da bi sve sanacije dimnjaka trebale biti popraćene i odgovarajućim projektom i nadzorom. Svi bi materijali koji se koriste za sanaciju trebali biti podvrgnuti detaljnom ispitivanju prema EN normama koje bi bilo provedeno i popraćeno "Izvješćem o ispitivanju" – atestom u našoj zemlji. Također bi zbog svakog dana sve modernije i sofisticiranije opreme za grijanje ali i brojnih materijala dimnjaka, trebalo provoditi kontinuiranu izobrazbu dimnjačara.

LITERATURA

[1] Turk, I. : Nauka o toplini I, Udžbenici Sveučilišta u Zagrebu, Zagreb 1992.
[2] Ivušić, V.: Tribologija, Hrvatsko društvo za materijale i tribologiju, Zagreb 1998.
[3] Brkić, S.: Priručnik-nehrđajući čelici u farmacetskoj, prehrambenoj i kemijskoj industriji, Hrvatsko društvo za materijale i tribologiju, Zagreb 2007.

CONTRIBUTION TO THE PRINTING INK - PRINTING PLATE – RUN LENGHT INTERACTIONS

Slaven Miloš[1], Tomislav Cigula[2], Sanja Mahović Poljaček[2], Miroslav Gojo[2]
[1]Novi list, Rijeka
[2]Faculty of Graphic Arts, University of Zagreb, Getaldićeva 2

Izvorni znanstveni rad / Original scientific paper

Abstract

The most common printing technique today is lithography. The difference between printing and nonprinting areas on a printing plate is accomplished by opposite physical and chemical properties of those areas. The printing areas are made of photoactive layer that attracts oil and chemical substances with oil solvent – printing inks. The nonprinting areas are made of aluminium-oxide which attracts water based substances – the fountain solution.

The amount and stability of printing ink and fountain solution adsorption on these areas have direct influence on the quality level of the final product.

It is well known that different printing inks have different chemical composition and that their interaction with the printing areas and wearing of the printing plates is different. It is important to predict these interactions and more over, to predict the stability of the printing process.

The aim of this paper was to observe the changes of the coverage of image areas for four main printing colours (cyan, magenta, yellow and black) on the prints in leniency with run length. From this data it will be possible to define the changes of the printing areas on the printing plate. For detail observation of lower (0-20%) and higher coverage areas they were defined with more control fields.

The results obtained in this research confirmed the presumption. Different printing inks have various behaviours during the printing process and different role in wearing of printing plate. Black has smaller influence on wearing of photoactive layer because coverage values of black are nearly the same through the whole printing run. The highest decrease of coverage values was detected by yellow. Generally, all printing inks cause certain decrease of coverage values.

These results have been indicating that hard substances in printing inks and friction between printing plate and ink rollers reduce the areas on printing plate covered with photoactive layers.

The decreased coverage values have to be taken into consideration before the printing process starts. This information is necessary for the adjustment of all components included in printing process on time for obtaining the prints with adequate quality level.

Key words

lithography, coverage value, printing plate, wear of materials, printing ink

Sažetak

Plošni tisak je najzastupljenija tehnika otiskivanja danas na tržištu. Razlika između tiskovnih elemenata i slobodnih površina postiže se njihovim suprotnim fizikalno-kemijskim svojstvima. Tiskovni elementi su izrađeni od fotoosjetljivog sloja koji ima oleofilna svojstva i u procesu tiska privlači tiskarsku boju, dok su slobodne površine izrađene od aluminijevog oksida, polarnog karaktera, hidrofilnih svojstava i u procesu otiskivanja privlače otopinu za vlaženje.
Količina tiskarske boje odnosno otopine za vlaženje koje su adsorbirane na površini tiskovne forme, te njihova stabilnost imaju velik utjecaj na kakvoću konačnog proizvoda.
Poznato je da različite tiskarske boje imaju različit kemijski sastav, te je stoga njihova interakcija s tiskovnim elementima različita, što u konačnici može uzrokovati i različito trošenje tiskovnih elemenata.
Cilj ovog istraživanja je promotriti promjene rastertonskih vrijednosti za četiri osnovne boje na otiscima u ovisnosti o broju otisaka (veličinu naklade).
Iz izmjerenih vrijednosti moguće je definirati promjene dimenzija tiskovnih elemenata na tiskovnoj formi. S obzirom na veću osjetljivost kod niskih i vrlo visokih rastertonskih vrijednosti, u tim je područjima definirano više kontrolnih polja.
Dobiveni rezultati potvrdili su pretpostavke, različite tiskarske boje različito utječu na trošenje tiskovnih elemenata na tiskovnoj formi. Najmanji utjecaj na trošenje tiskovnih elemenata na tiskovnoj formi primijećen je kod crne boje. Izmjerene vrijednosti na otiscima nemaju znatnije razlike u rastertonskim vrijednostima bez obzira na broj otisaka. Generalno gledajući kod svih se boja rastertonske vrijednosti smanjuju povećanjem naklade, a najveće smanjenje primijećeno je kod žute boje.
Rezultati istraživanja upućuju na zaključak da čvrste čestice u tiskarskoj boji uz trenje između tiskovne forme i valjaka za nanos bojila troše tiskovnu formu smanjujući površine prekrivene fotoosjetljivim slojem – tiskovne elemente.
Smanjenje rastertonskih vrijednosti potrebno je uzeti u obzir prije početka otiskivanja. Dobivene informacije potrebne su za pravodobno podešavanje bitnih faktora u procesu tiska, te na taj način zadržavanje kvalitete otisaka kroz cijelu nakladu.

Ključne riječi

plošni tisak, rastertonska vrijednost, tiskarska boja, trošenje materijala

1. Introduction

Lithography is today the most common printing technique [1-2]. The printing areas and nonprinting areas have opposite physical-chemical properties. The printing areas attract substances with oil solvent – printing ink and the nonprinting areas attract water based substances. The majority of lithography printing plates today are made of aluminium sheets. The surface of aluminium sheets has to be mechanically and chemically processed to create characteristic rough structure on the aluminium surface. The structure consists of a thin aluminium-oxide porous film that enables good adsorption of fountain solution. Before plate making process these processed plates have to be covered with thin photoactive layer which will attract printing ink during the printing process. Considering the fact that printing plates have printing and nonprinting areas in the same level during the printing plate making process photo active layer has to be removed from the nonprinting areas.
During the printing process by friction between the printing plate and the ink rollers, fountain solution rollers and offset cylinder the surface of the printing plates is often worn. The wearing of printing plate is also influenced by chemical substances in printing ink.
The aim of this paper was to observe changes of the printing areas in leniency with print run by measuring coverage values on prints.

2. Experimental

In this research the printing plate samples were made in automated computer-controlled plate making process (Computer to plate) [3-8]. The printing plates were aluminium based with silver-halide photoactive layer [9]. The printing process was conducted on a web offset printing press. The paper used for printing was light weighted, 45 grams per square meter used in newspaper printing. Print ink used in this process was cold set printing ink. This type of printing ink is solid at room temperature and must be melted before printing. For this purpose the printing process heat ink rollers and plates and keep ink melted long enough to print and to make ink harden upon contact with cold paper[10].
To enable greater precision in measurement a special control wedge was defined. This wedge contains 26 control fields with different coverage value; difference between two neighbor fields was 5 % coverage value. For detail observation in lower (0 – 20 %) and higher (80 – 100 %) coverage area more fields were defined. In lower areas control field of 0, 2, 5, 8, 12, 15, 20 percent and in higher areas field of 80, 85, 88, 90, 92, 95, 98 and 100 percent of coverage value.
The prints to be measured were taken at the start of printing run (Sample A), the 5000^{th}, the 10000^{th}, the 21000^{th} (Sample B), the 40000^{th} (Sample C), the 60000^{th} and the 80000^{th} (Sample D) print. The measuring was performed by GretagMacbeth iCPlate II Platereader.

3. Results and discussion

Figures 1. to 4. shows coverage values on prints of four main colours, black, yellow, magenta and cyan at lower coverage areas. It can be seen that coverage values are reducing its value with increasing of nominal value by all colours. The influence of printing run length on coverage values is smallest with black colour (Fig.1.). Reduce of coverage values is most significant with yellow at the end of printing run (Sample D, Fig.2.). Coverage values of cyan do not show any change between Sample C and Sample D (Fig.4.).

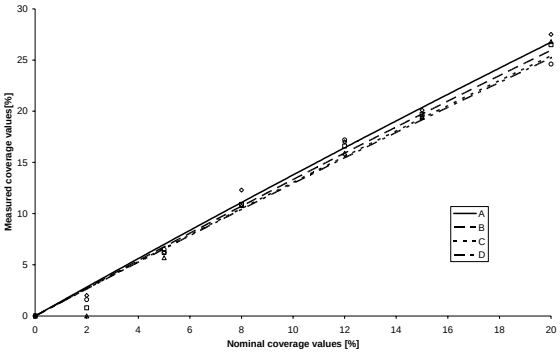


Fig.1. Coverage values of black,
A – first print, B – 21000th print,
C – 40000th print, D – 80000th print

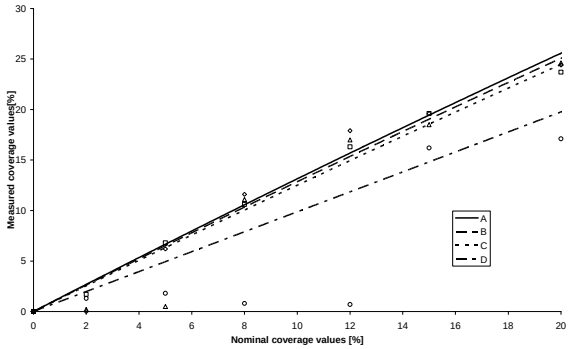


Fig.1. Coverage values of yellow,
A – first print, B – 21000th print,
C – 40000th print, D – 80000th print

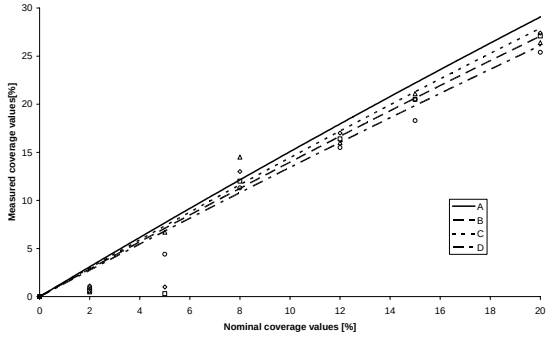


Fig.3. Coverage values of magenta,
A – first print, B – 21000th print,
C – 40000th print, D – 80000th print

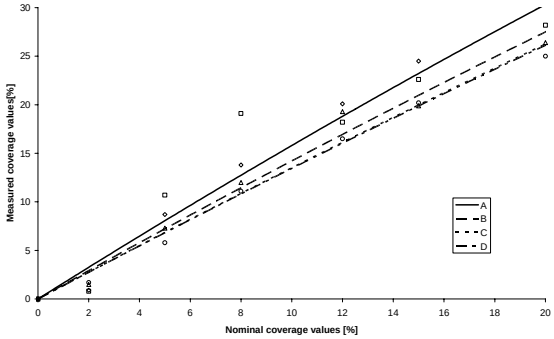


Fig.4. Coverage values of cyan,
A – first print, B – 21000th print,
C – 40000th print, D – 80000th print

In the middle coverage areas (20 – 80 % coverage value) all colours show similar behaviour as well as in lower coverage areas. Black still has smallest reduce of coverage values (Fig. 5.). With black, magenta and cyan reduce of coverage areas increases with increase of nominal coverage value (Fig. 5., 7., 8.). Yellow Sample D has largest reduce of coverage values (Fig. 6).

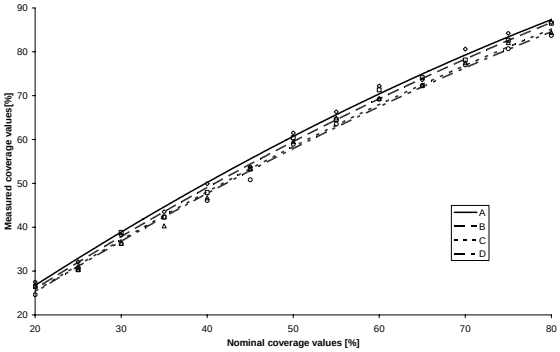


Fig.5. Coverage values of black,
A – first print, B – 21000th print,
C – 40000th print, D – 80000th print

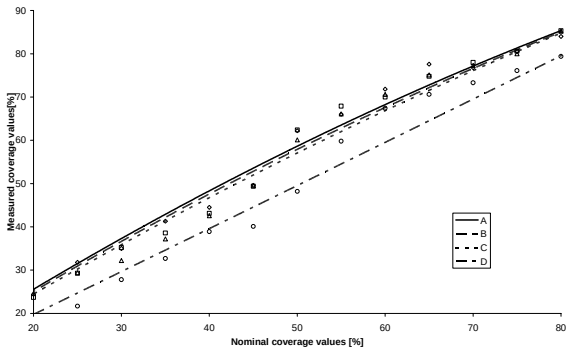


Fig.6. Coverage values of yellow,
A – first print, B – 21000th print,
C – 40000th print, D – 80000th print

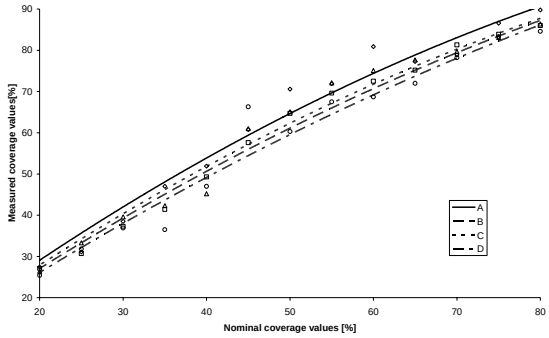


Fig.7. Coverage values of magenta,
A – first print, B – 21000th print,
C – 40000th print, D – 80000th print

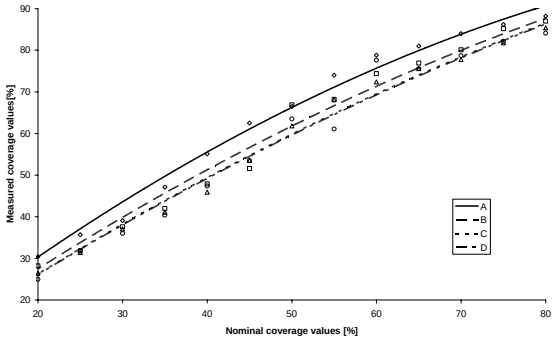


Fig.8. Coverage values of cyan,
A – first print, B – 21000th print,
C – 40000th print, D – 80000th print

One can see in Figures 10. and 12. that differences between coverage values on Samples A, B, C and D of yellow and cyan are getting smaller with increase of nominal coverage value. The largest difference between first and last (80000th) print is in very high coverage areas with black (Fig. 9.). With cyan and magenta curves of Samples B, C and D are nearly the same after 90 % nominal value.

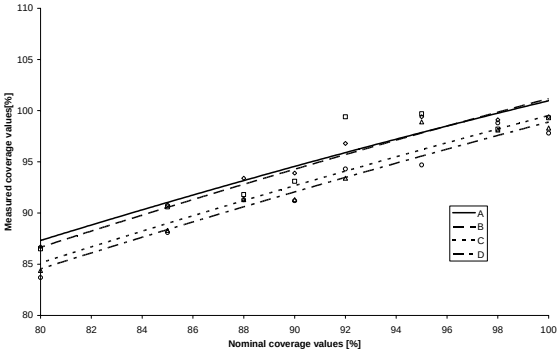


Fig.9. Coverage values of black,
A – first print, B – 21000th print,
C – 40000th print, D – 80000th print

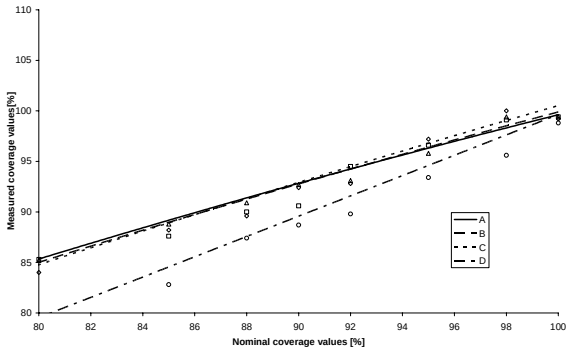


Fig.10. Coverage values of yellow,
A – first print, B – 21000th print,
C – 40000th print, D – 80000th print

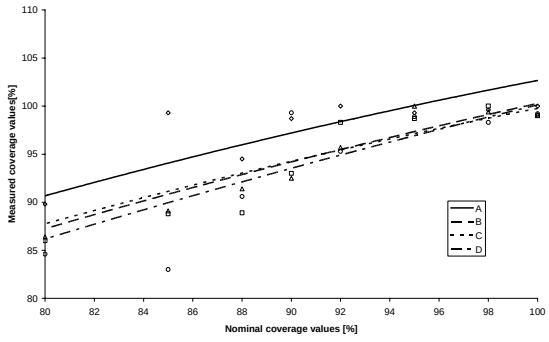


Fig.11. Coverage values of magenta,
A – first print, B – 21000th print,
C – 40000th print, D – 80000th print

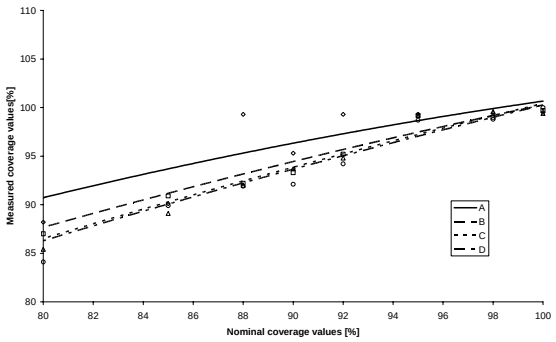


Fig.12. Coverage values of cyan,
A – first print, B – 21000th print,
C – 40000th print, D – 80000th print

4. Conclusion

The results have shown that different printing inks have different role in wearing of printing plates. It can be seen on Figures 1. to 12. that with increased printing run length the coverage values on prints decrease its value. This result can indicate that printing inks have specific hard chemical substances that in combination with friction between ink rollers and printing plate damage photoactive layer. Largest decrease in coverage value was detected in printing with yellow. The printing run length has the smallest influence on reproduction of black colour. All colours have the largest decrease of coverage value in middle coverage area.

From all these results one can concluded that for getting prints of same quality level through entire printing run, data obtained from this paper must be taken in consideration to make proper adjustments of all components included in printing process.

5. References

1. PacPhee J., Fundamentals of Lithographic Printing, Volume I, Mechanics of Printing, GATFPress, Pittsburg, 1998
2. Wilson D. G.: Lithography primer, Third Edition, PIA/GATFPress, Pittsburg, 2005
3. Adams Richard M., Romano F., Computer to Plate: Automating the Printing Industry, Graphic Arts Technical Foundation, USA, (1996)
4. Gemeinhardt, J., Belichter und Plattentechnologie, Fachhefte Grafische Industrie Bulletin Technique 4, (2001), 14-17.
5. Holland, C., CtP routing, Digital Demand 2-3, Pira International Ltd, (2002), 12-21.
6. Hutton P., Lind J., The Plate Side of Computer to Plate: Printability and Runnability, TAGA Proceedings, Rochester (NY), (1998)
7. Limburg M., Der Digitale Gutenberg – Alles was Sie über "Computer to Plate" wissen sollten, GSS-Grafik System Service, Aachen, (1994)
8. Seydel M., Computer to Plate: Digital Workflow and Integration into Quality Offset Printing, TAGA Proceedings, Rochester (NY), (1996), 634-348.
9. Mahovic S., Agic D., Gojo M., Mechanical and Optical Differences in Long Run Printing in Conventional and CtP Offset Systems, Proceedings of the 30th International Iarigai Research Conference, Croatia, (2003), 219-227.
10. http://printwiki.org/Cold_Set_Ink

Ivana Mišković
Fakultet prirodoslovno-matematičkih i odgojnih znanosti
tel: +38763955736
e-mail: ivana.miskovic@sve-mo.ba

Izvorni znanstveni rad / Original scientific paper

Sinteza i karakterizacija samoorganizirajućih monoslojeva alkantiola na zlatu

Sažetak

Površina zlata je relativno kemijski inertna, ne stvara barijerne okside i ne veže čvrsto slučajno adsorbirane molekule, pa se vrlo uređeni samoorganizirajući monoslojevi mogu lako pripremiti na zlatu. Samoorganizirajući monoslojevi pogodni su za fundamentalna istraživanja površinskih fenomena i međufaznih procesa. Na istraživanju površinskih fenomena radilo je više autora[1,2,3,4].

U ovom radu površina od zlata modificirana je samoorganizirajućim monoslojem 1-dodekantiola. Istraživana je kinetika adsorpcije 1-dodekantiola na zlatu te provedena karakterizacija površine elektokemijskim metodama i metodom kontaktnog kuta.

Ključne riječi: zlato, 1-dodekantiol, samoorganizirajući monosloj.

Synthesis and characterization of self-assembled monolayers of alkanethiols on gold

Abstract

Surface of gold is rather inert chemically, it does not make oxide barrier and it does not seize accidentaly adsorbed molecules, and highly arranged self-assembled monolayers can be easily prepared on gold. Self-assembled monolayers are suitable for fundamental analysis of the surface-phenomenon and intermediate stage of the process. Many authors has been working on the research of the surface-phenomenon.

The surface of gold in this paper is modified by self-assembled monolayer 1-dodecanethiol.

Kinetics of 1-dodecanethiol adsorption on gold has been analized, and characterization of the surface is made by electrochemical methods and by the method of the contact angle as well.

Key words: gold, 1-dodecanethiol, self-assembled monolayer

1. Uvod

Površina zlata je relativno kemijski inertna, ne stvara barijerne okside i ne veže čvrsto slučajno adsorbirane molekule, pa se vrlo uređeni samoorganizirajući monoslojevi mogu lako pripremiti na zlatu[3,4,6]. Samoorganizirajući monosloj izolira površinu vodljivog metala, ali elektroni se mogu prenositi kroz film kada se modificirana elektroda stavi u elektrokemijsku ćeliju. Jednom kada se organske molekule adsorbiraju na površinu, struktura monosloja je stabilna.

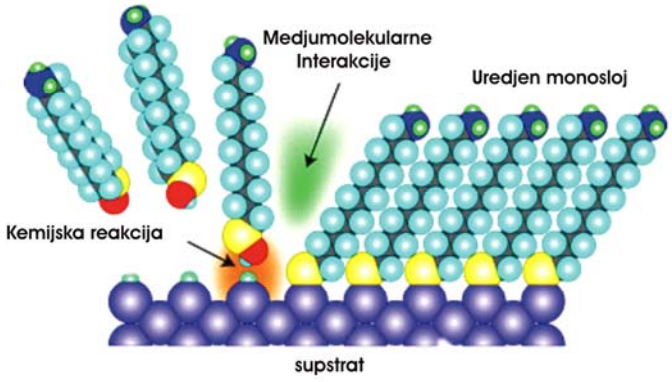
Svojstva i reaktivnost monosloja kontrolirana su završnim skupinama organske molekule koja formira film, pa su samoorganizirajući monoslojevi pogodni za fundamentalna istraživanja površinskih fenomena i međufaznih procesa. SAM nalaze široku primjenu[5,6]:

- izradba kemijskih i biokemijskih senzora,
- zaštita metala od korozije,
- mikroelektronika,
- priprava površine za kontrolirani rast kristala,
- imobilizacija DNA ili adhezija živih stanica na metalnoj površini,
- povećanje biokompatibilnosti implantata koji se ugrađuju u ljudski organizam.

U radu su izneseni (i grafički prikazani) rezultati kada je površina zlata modificirana samoorganizirajućim monoslojem 1-dodekantiola, a istraživana je kinetika adsorpcije 1-dodekantiola te provedena karakterizacija površine elektrokemijskim metodama i metodom kontaktnog kuta.

2. Samoorganizirajući monoslojevi – struktura

Samoorganizirajući monoslojevi formiraju se izlaganjem metalnih supstrata organskim molekulama s funkcionalnim skupinama. To su gusto pakirani monomolekularni slojevi visokog stupnja uređenosti.



Slika 1. Samoorganizirajući monosloj na metalnoj površini.

Na površinu supstrata adsorbira se **adhezijska grupa** koja je odgovorna za inhibicijska svojstva formiranog monosloja. Za vrijeme samoorganiziranja dolazi do umrežavanja **alkilnih lanaca** te nastaje uređen, gusto pakiran monosloj, koji osigurava mehaničku stabilnost i određuje dielektrična svojstva površinskog filma. **Završna funkcionalna skupina** određuje međufazna svojstva formiranog monosloja. Završne skupine mogu se naknadno mijenjati kako bi se promijenila svojstva monosloja ovisno o primjeni[1,3].

Samoorganiziranje se sastoji od dva odvojena procesa [1,4]:

1. *brze adsorpcije* adhezijske skupine na metalnu površinu i
2. s*pore organizacije/orijentacije i umrežavanja* alkilnih lanaca intramolekularnim van der Waalsovim interakcijama.

Nakon izlaganja zlata otopini alkantiola u apsolutnom etanolu, veza između zlata i sumpora vrlo brzo se stvara, u vremenu od nekoliko minuta:

$$RSH_{(el)} + Au \rightarrow RS - Au_{(č)} + H_{2(pl)}$$

3. Rezultati istraživanja

3.1. Elektrokemijski reaktor

Elektrokemijska mjerenja na elektrodi od zlata (Au elektroda) i elektrodi od zlata modificiranoj samoorganizirajućim mononslojem 1-dodekantiola (Au - SAM) provedena su na sobnoj temperaturi, u troelektrodnom reaktoru.

Kao radne elektrode korištene su:

- Polikristalinična Au elektroda (P = 0,074 cm^2) za elektrokemijska mjerenja,
- Polikristalinična Au rotirajuća disk elektroda (P = 0,093 cm^2) za istraživanje redoks reakcije s prijenosom elektrona,
- Monokristalna Au elektroda (P = 1cm^2) za karakterizaciju površinskih svojstava.

Kao referentna elektroda za mjerenje potencijala radne elektrode upotrijebljena je srebro – srebrov (I) klorid (Ag/AgCl) elektroda u zas. KCl, čiji je potencijal za 0,222 V pozitivniji od *standardne vodikove elektrode* (SHE). Sve vrijednosti potencijala u ovom radu dane su u odnosu na navedenu referentnu elektrodu.

Kao protuelektroda upotrebljena je elektroda od platinskog lima, savijena u polukrug, radi postizanja simetričnog električnog polja oko radne elektrode. Platinska elektroda je, prije mjerenja, žarena u redukcijskom plamenu te isprana redestiliranom vodom. Na taj su način uklonjene nečistoće poput organskih čestica s površine elektrode.

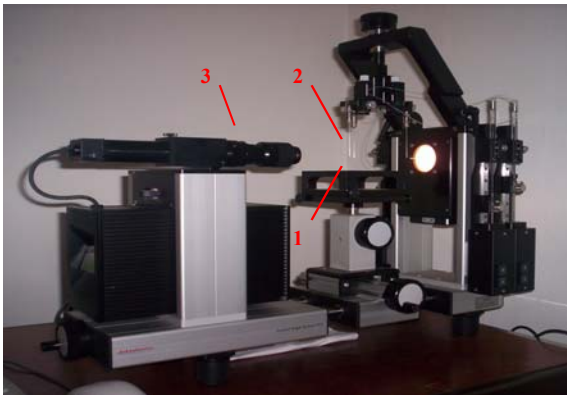
3.2. Karakterizacija samoorganizirajućih monoslojeva 1-dodekantiola na Au elektrodi

Za karakterizaciju korištene su sljedeće mjerne tehnike:

1. mjerenje kontaktnog kuta,
2. elektrokemijska impedancijska spektroskopija,
3. ciklička voltametrija.

3.2.1. Mjerenje kontaktnog kuta

Mjerenja su provedena pri 23,0°C na uređaju „Dataphysics Instruments – Conctact Angle System OCA 20“ s pripadajućom digitalnom kamerom i računalno upravljanim sustavom za doziranje različitih otapala, koji omogućava reproducibilno nanošenje kapljice volumena 1 μl (slika 2.) Upotrijebljena su sljedeća otapala: voda (H_2O), formamid ($HCONH_2$) i dijodometan (CH_2I_2). Na digitalno dobivenoj slici kapljice moguće je računalno odrediti kutove kvašenja.



Slika 2. Uređaj za mjerenje kontaktnog kuta.
1. mjesto za uzorak 2. dozator 3. kamera.

Za karakterizaciju površinskih svojstava Au i Au-SAM elektroda koristila se metoda kontaktnog kuta. Na mehanički, kemijski i elektrokemijski obrađenoj Au elektrodi i na Au-SAM elektrodi nanesene su kapljice tri različita otapala, volumena 1 μl, te su izmjerene vrijednosti kontaktnih kutova koje su prikazane u tablici 1.

Tablica 1. Srednje vrijednosti izmjerenih kontaktnih kutova vode, dijodometana i formamida na Au i Au-SAM elektrodama.

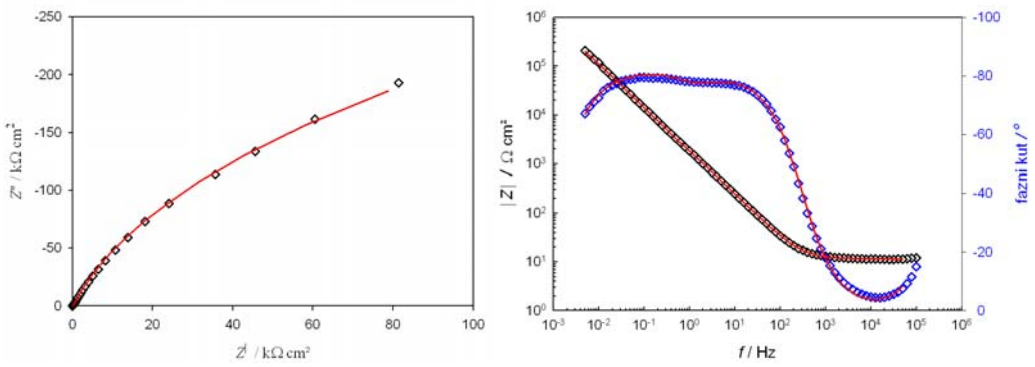
uzorak	*otapalo*	*kontaktni kut* θ_k/ °
Au	H_2O	82,1
Au	CH_2I_2	42,7
Au	$HCONH_2$	60,7
Au - SAM	H_2O	101,4
Au - SAM	CH_2I_2	53,7
Au - SAM	$HCONH_2$	86,6

Dobiveni rezultati kontaktnih kutova kvašenja dokaz su da su alkilni lanci gusto pakirani i dobro orijentirani tako da je samo završna ($-CH_3$) skupina u kontaktu s okolnom kapljevinom. [1,6].

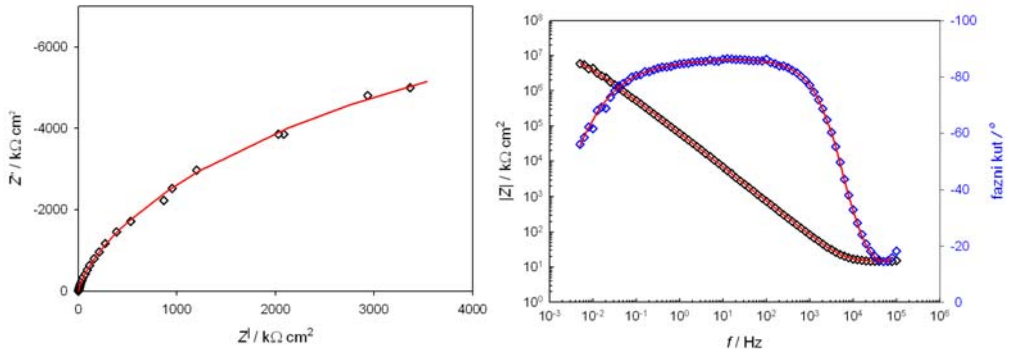
3.2.2. Elektrokemijska impedancijska spektroskopija

Impedancijski spektri snimani su u širokom području frekvencija od 10^5 Hz do $2{,}51 \times 10^{-3}$ Hz uz naponsku amplitudu pobude ± 5 mV, na potencijalu otvorenog strujnog kruga, E_{ok} nakon 30-minutne stabilizacije elektrode na istom potencijalu. Impedancijska mjerenja provedena su na računalno upravljanoj aparaturi koja se sastojala od potenciostata/galvanostata Solartron model 1287 u sklopu kojeg se nalazi FRA 1260. Impedancijski spektri analizirani su „Zview" računalnim programom, te modelirani prikladnim električnim ekvivalentnim krugovima.

Elektrokemijska impedancijska spektroskopija koristila se za istraživanje strukture međufazne granice Au/$NaClO_4$, i Au - SAM/ $NaClO_4$, te dielektričnih svojstava SAM 1–dodekantiola.



Slika 3. Nyquistov i Bodeov prikaz impedancijskih spektara snimljenih na Au elektrodi u 0,1 mol dm^{-3} otopini $NaClO_4$, pH = 5,4, na potencijalu otvorenog kruga, E_{ok} =0,3V. Simboli prikazuju eksperimentalne, a linije modelirane podatke.



Slika 4. Nyquistov i Bodeov prikaz impedancijskih spektara snimljenih na Au – SAM elektrodi u 0,1 mol dm^{-3} otopini $NaClO_4$, pH = 5,4, na potencijalu otvorenog kruga, E_{ok} =0,15V. Simboli prikazuju eksperimentalne, a linije modelirane podatke.

Matematičkom analizom eksperimentalnih podataka tj. njihovom usporedbom s EEK, primijenjena je kompleksna nelinearna metoda najmanjih kvadrata autora Boukampa uz pomoć programa *Zview*®. Rezultati analize impedancijskih spektara Au i Au-SAM elektroda sadržani su u tablicama 2. i 3.

Tablica 2. Vrijednosti elemenata električnog ekvivalentnog kruga dobivenih analizom impedancijskih spektara Au elektrode u 0,1 mol dm^{-3} $NaClO_4$, pH = 5,4 nakon 30 minuta stabilizacije na potencijalu otvorenog kruga, E_{ok} = 0,3 V.

R_Ω / Ω cm^2	$CPE_1 \times 10^6$ / F cm^{-2}	n_1	R_1 / kΩ cm^2	$CPE_2 \times 10^6$ / F cm^{-2}	n_2	R_2 / kΩ cm^2
11,67	95,38	0,90	11,58	11,44	0,97	835,44

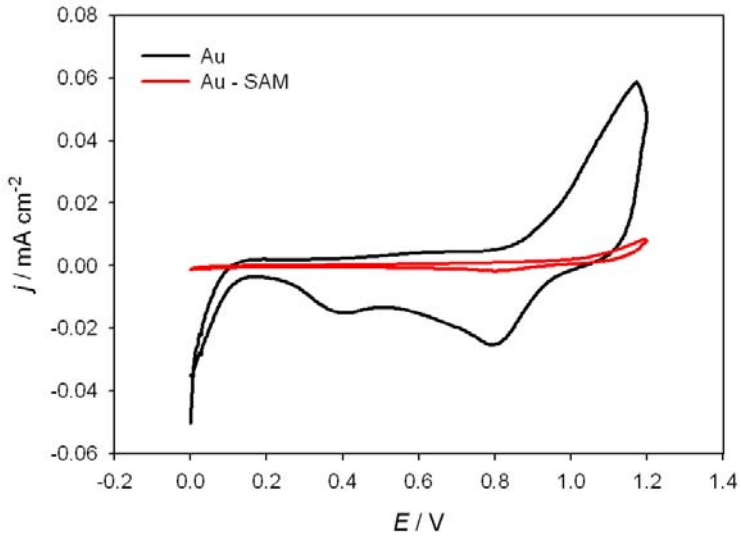
Tablica 3. Vrijednosti elemenata električnog ekvivalentnog kruga dobivenih analizom impedancijskih spektara Au - SAM elektrode u 0,1 mol dm^{-3} $NaClO_4$, pH = 5,4, na potencijalu otvorenog kruga, E_{ok} = 0,15 V.

R_Ω/ Ω cm^2	$CPE_1 \times 10^6$/ F cm^{-2}	n_1	R_1/ kΩ cm^2	$CPE_2 \times 10^6$/ F cm^{-2}	n_2	$R_2 \times 10^{-3}$/ kΩ cm^2
14,20	2,69	0,96	533,83	0,32	0,52	19,39

3.2.3. Ciklička voltametrija

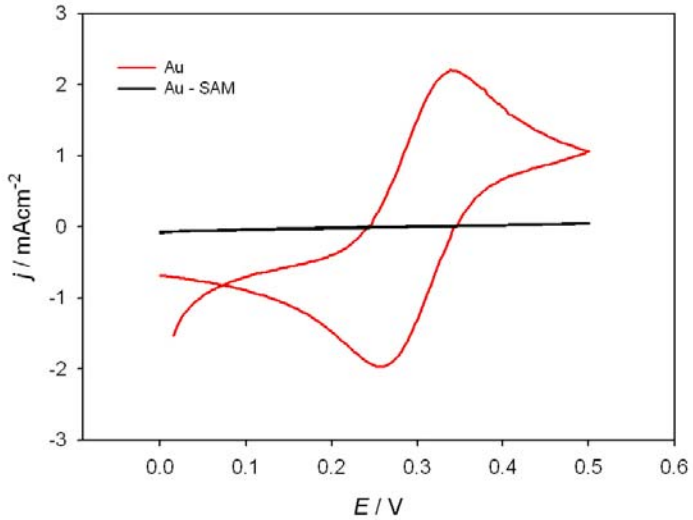
Mjerenja su provedena u širokom području potencijala: od potencijala izlučivanja vodika do potencijala izlučivanja kisika na računalno upravljanoj aparaturi koja se sastojala od potenciostata / galvanostata EG&G PAR model 273 i osobnog računala.

Elektrokemijsko ponašanje Au i Au-SAM elektroda u 0,1 mol dm^{-3} otopini Na -perklorata, pH = 5,4 ispitivano je ciličkom voltametrijom u području potencijala od 0 V do 1,2 V brzinama promjene potencijala, ν = 20 mV s^{-1}.



Slika 5. Usporedba cikličkih voltamograma snimljenih na Au i Au - SAM elektrodama u 0,1 mol dm^{-3} otopini $NaClO_4$, pH = 5,4, u području potencijala od 0,0 do 1,2 V brzinom promjene potencijala, ν = 20 mV s^{-1}. Vrijednosti struje normirane su na geometrijsku površinu elektrode (P = 0,074 cm^2).

Prijenos elektrona na Au i Au - SAM elektrodama ispitivan je u ekvimolarnoj otopini $Fe(CN)_6^{4-}$ / $Fe(CN)_6^{3-}$, koncentracije 0,01 mol dm^{-3} u 0,5 mol dm^{-3}otopini Na_2SO_4 na stacionarnoj i rotirajućoj disk elektrodi. Mjerenja su provedena u području potencijala od 0,0 do 0,5 V.

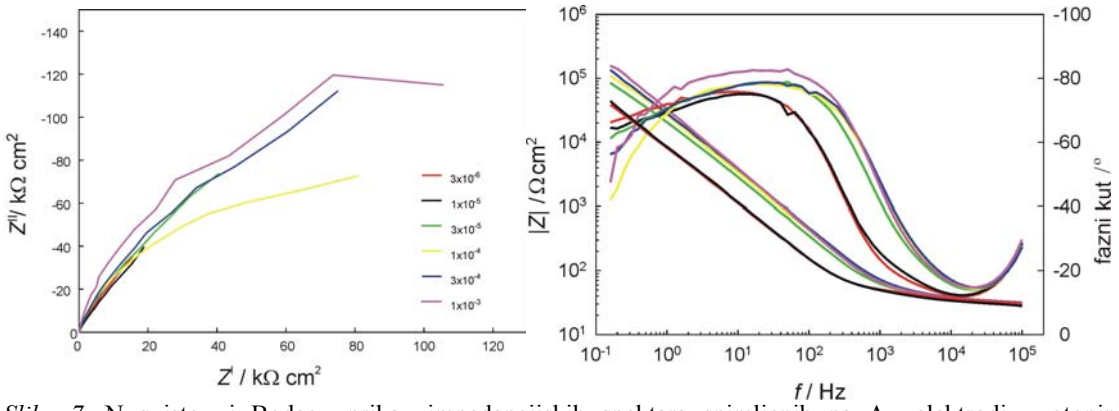


Slika 6. Usporedba cikličkih voltamograma snimljenih na Au i Au - SAM elektrodama u ekvimolarnoj otopini Fe^{2+} / Fe^{3+} u 0,5 mol dm^{-3} otopini Na_2SO_4, u području potencijala od 0,0 do 0,5 V brzinom promjene potencijala, ν = 100 mV s^{-1}. Vrijednosti struje normirane su na geometrijsku površinu elektrode (P = 0,093 cm^2).

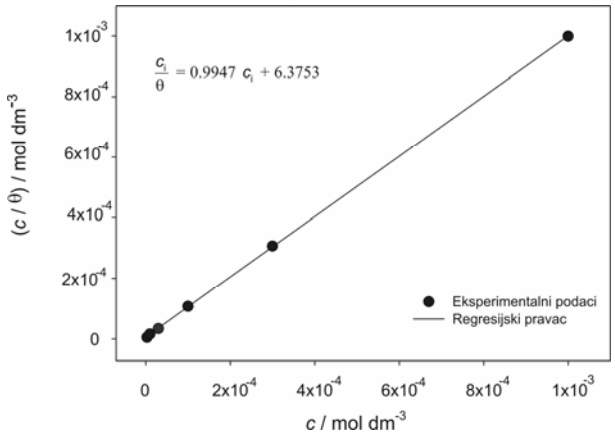
3.2.4. Kinetika i termodinamika adsorpcije 1-dodekantiola na Au elektrodi

3.2.4.1. Određivanje termodinamičkih veličina

Termodinamički parametri adsorpcije određeni su iz ovisnosti kapaciteta dvosloja, C_{DL} o koncentraciji 1-dodekantiola. Praćena je promjena kapaciteta dvosloja kod sljedećih koncentracija 1-dodekantiola: 3×10^{-6}, 1×10^{-5}, 3×10^{-5}, 1×10^{-4}, 3×10^{-4} i 1×10^{-3} mol dm^{-3} u 0,1 mol dm^{-3} $LiClO_4$ u apsolutnom etanolu.



Slika 7. Nyquistov i Bodeov prikaz impedancijskih spektara snimljenih na Au elektrodi u otopini 1–dodekantiola u 0,1 mol dm^{-3} otopini $LiClO_4$ u apsolutnom etanolu, c (DT) = 3×10^{-6}; 1×10^{-5}; 3×10^{-5}; 1×10^{-4}; 3×10^{-4} i 1×10^{-3} mol dm^{-3}, na potencijalima otvorenog kruga, $E_{ok.}$



Slika 8. Prikaz Langmuirove adsorpcijske izoterme: ovisnost c/θ o koncentraciji 1-dodekantiola u 0,1 mol dm^{-3} otopini $LiClO_4$ u apsolutnom etanolu.

U istraživanom području koncentracija 1-dodekantiola (3×10^{-6} do 1×10^{-3} mol dm^{-3}) Langmuirova adsorpcijska izoterma može se upotrijebiti za opisivanje adsorpcijskog procesa na Au elektrodi. [1,2,7]

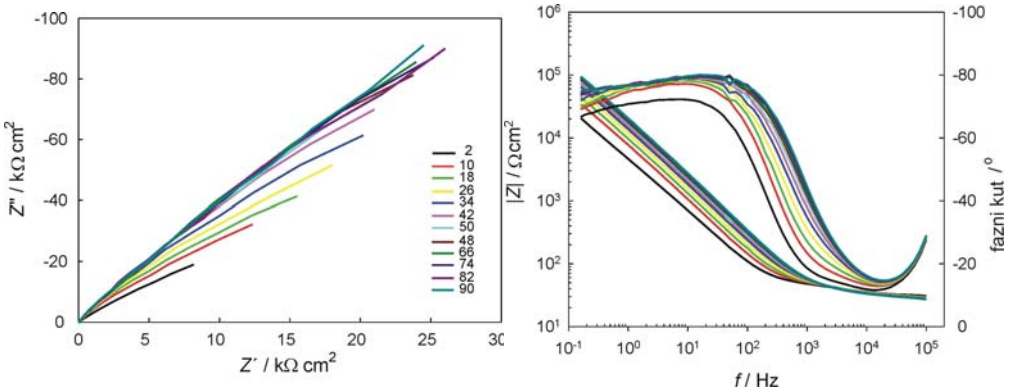
$$\frac{c_i}{\theta}=c_i+\frac{1}{\beta}$$

$$\beta = \exp\left(\frac{-\Delta G^0_{ads}}{RT}\right); \quad \beta = 1{,}5686 \times 10^5 \text{ mol}^{-1}\text{ dm}^3 \text{ – adsorpcijska konstanta}$$

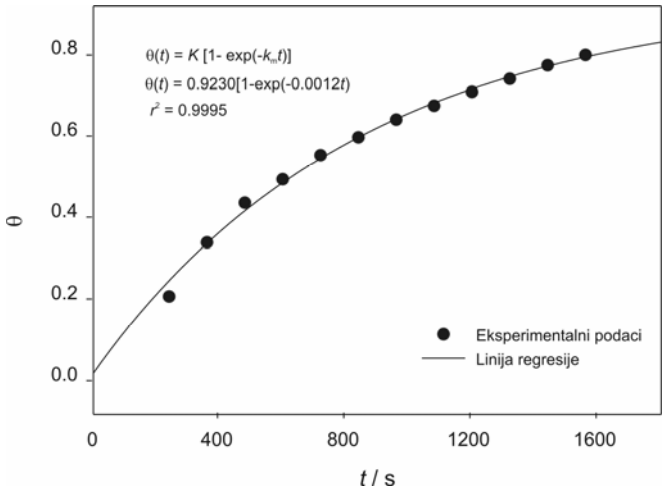
ΔG_{ads} = -29,639 kJmol^{-1} – Gibbsova energija adsorpcije

3.2.4.2. Određivanje kinetičkih veličina

Kinetičke veličine adsorpcije određene su iz vremenske ovisnosti kapaciteta dvosloja, C_{DL} kod najniže koncentracije 1-dodekantiola 1×10^{-6} mol dm^{-3} u 0,1 mol dm^{-3} otopini $LiClO_4$ u apsolutnom etanolu.



Slika 9. Nyquistov i Bodeov prikaz impedancijskih spektara snimljenih na Au elektrodi u 1 μmol dm^{-3} otopini 1–dodekantiola u 0,1 mol dm^{-3} otopini $LiClO_4$ u apsolutnom etanolu, na potencijalu otvorenog kruga, E_{ok}. Vrijeme izlaganja Au elektrode vidljivo je na slici, u min.



Slika 10. Vremenska ovisnost prekrivenosti površine Au elektrode u početnoj fazi adsorpcije (t ~ 1500 s) za c(DT) = 1×10^{-6} mol dm^{-3} u 0,1 mol dm^{-3} otopini $LiClO_4$ u apsolutnom etanolu. Simboli prikazuju eksperimentalne podatke, a linija teorijske vrijednosti.

Iz dobivenih rezultata može se zaključiti da adsorpcijska kinetika 1-dodekantiola na Au elektrodi slijedi Langmuirovu adsorpcijsku izotermu, $\theta(t) = K\left[1 - \exp\left(-k_m t\right)\right]$ kod c(DT)=1$\times$ 10^{-6}mol dm^{-3}. Vrijednosti izračunatih konstanti brzina adsorpcije i desorpcije pokazuju dobro slaganje s literaturnim podacima[1,2,8].

$$K = \frac{c}{c + \left(\frac{k_\mathrm{d}}{k_\mathrm{a}}\right)}; \qquad k_\mathrm{m} = k_\mathrm{a} c + k_\mathrm{d}$$

k_a = 1107,6 mol^{-1} dm^3 s^{-1} – konstanta brzine adsorpcije

$k_\mathrm{d} = 9{,}24 \times 10^{-5}$ s^{-1} - konstanta brzine desorpcije

4. Zaključak

Na osnovu iznijetog daju se sljedeći zaključci:

- Da bi se dobio uvid u elektrokemijsko ponašanje Au – SAM elektrode, bilo je potrebno istražiti i elektrokemijsko ponašanje Au elektrode metodama cikličke voltametrije i elektrokemijske impedancijske spektroskopije.
- Kinetika i termodinamika adsorpcije 1-dodekantiola na zlatu ispitivana je *in-situ* metodom elektrokemijske impedancijske spektroskopije.
  U početnom stupnju formiranja SAM, adsorpcija 1-dodekantiola na zlatu slijedi Langmuirovu izotermu.
- Sve mjerne tehnike potvrdile su da je na površini zlata moguće uspješno formirati kompaktni, dobro uređeni samoorganizirajući monosloj 1-dodekantiola, koji se ponaša kao neidealni dielektrik.

5. Literatura

1. I. Mišković: *Sinteza i karakterizacija samoorganizirajućih monoslojeva alkantiola na zlatu*, Diplomski rad (2006), Sveučilište u Zagrebu
2. Ž. Petrović, I. Mišković, M. Metikoš-Huković: Kinetics of adsorption of alkanethiols on gold, 13th Young Investigators' Seminar on Analytical Chemistry, July 5. – 8., 2006
3. R. K. Smith, P. A. Lewis, S. Weiss: *Progress in Surf. Sci.* **75** (2004) 1-68
4. C. D. Bain, E. B. Troughton, Y. T. Tao, J. Evall, G. M. Whitesides, R. G. Nuzzo: *J. Am. Chem. Soc.* **111** (1989) 321-335
5. A. Kudelski: *Vibrational Spectroscopy* **39** (2005) 200-213
6. Z. Hon, N. L. Abbott, P. Stroeve: *Langmuir*, **14** (1998) 3287-3297
7. D. S. Karpovich, G. J. Blanchard: *Langmuir* **10** (1994) 3315-3322
8. L. V. Protsailo, W. R. Fawcett: *Electrochimica Acta* **45** (2000) 3497-3505

Effect of foaming parameters to mechanical properties of Aluminium Foam made by P/M route and its reproducibility.

M. Nosko, R. Florek, F. Simancik, R. Uhrik

Izvorni znanstveni rad / Original scientific paper

ABSTRACT

The aluminium foam made by PM route has an advantage of high variability of its inner pore structure and porosity adjusted only by various foaming parameters. Foaming temperature and holding time at foaming temperature can affect significantly the porosity and inner pore structure of the foam. However, the variability of the pore structure is also responsible for variability of the aluminium foam properties, for example absolute values of plastic strength. This negatively affects reproducibility of the real foamed component.

Aim of the work is therefore to discover how crucially foaming parameter affects the scatter of plastic strength thus reproducibility of measured values. This study will lead to elimination of apparent non-reproducibility just by precise understanding of interconnection between the foaming parameters, pore structure and finally plastic strength of the foam component.

Keywords: Aluminium Foam, Foaming parameters, Pore structure, Plastic strength, Reproducibility

INTRODUCTION

The non-uniformities within the pore structure of aluminium foams are considered as main problem which complicates prediction of their mechanical properties and causes rather high scatter of measured values. Crucial non-uniformities such as presence of big pores or elliptical pores within the pore structure exist mainly in pore size level [1-7]. Those non-uniformities cause “premature” yielding of foamed sample and are responsible for scatter of measured values. Lot of work has been done to eliminate these non-uniformities for example by setting the manufacturing parameters: distribution of foam-able precursors, various composition of alloy in hand with heat-treating of the blowing agent or by changing the manufacturing parameters as ambient pressure, ambient atmosphere, foaming temperature, heating rate, etc. [8-14]. Every study gives valuable information how studied parameters influences the pore structure of aluminium foams in laboratory conditions. In this study, the attempt was made to investigate the influence of foaming temperature and holding time on this temperature to changes in pore structure as well as to anisotropy of compression behavior of final foam.

EXPERIMENTAL

Samples of cube shape (dimension a = 50 mm) were manufactured from 9 pieces of foam-able precursors (45x15x5 mm). The precursor distribution is schematically illustrated in Figure 1b. Foaming temperature and time was adjusted to various combinations: the foaming temperature rise from 700 up to 770°C with step 35°C; and foaming time rises from 15 up to 45 second with step 15 second for each temperature. Table of manufacturing parameters is shown in Figure 1a. Pore structure was revealed for each foaming parameters in plane

perpendicular to main precursor axis as schematically illustrated in Figure 1c. The digital camera was used for this purpose.

The uni-axial compression test was performed to reveal the effect of foaming parameters to plastic strength thus to discover effect of structural changes to scatter of measured values. The nominal displacement rate was 0.03 s^{-1}. The uni-axial compression test was done in one loading direction with regard to foaming direction.

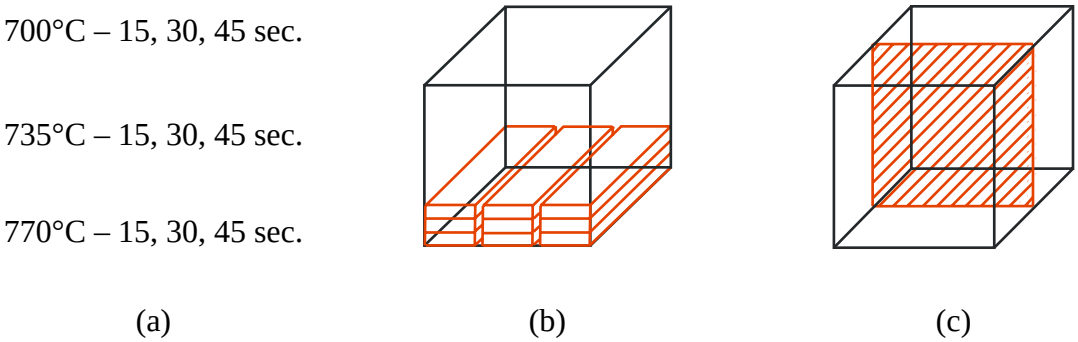


Figure 1. Foaming parameters (a), Precursor distribution (b) and Plane used for investigation of foam structure.

The values of plastic strength (Defined as first peak stress before the onset of plastic collapse [14].) obtained from stress-strain curves for various foaming parameters were than compared and evaluated with regard to reproducibility of measured values.

RESULTS AND DISCUSSION

Effect of foaming parameters to macrostructural non-uniformities

Porosity

Effect of foaming temperature and time to porosity of the foam is presented in Figure 2; higher foaming temperatures result into creation of the foam with higher porosities. The difference between porosity of samples foamed at 700°C and 735°C is significant but, only slight increase is observed between the porosity of the foam made at 735°C and 770°C.

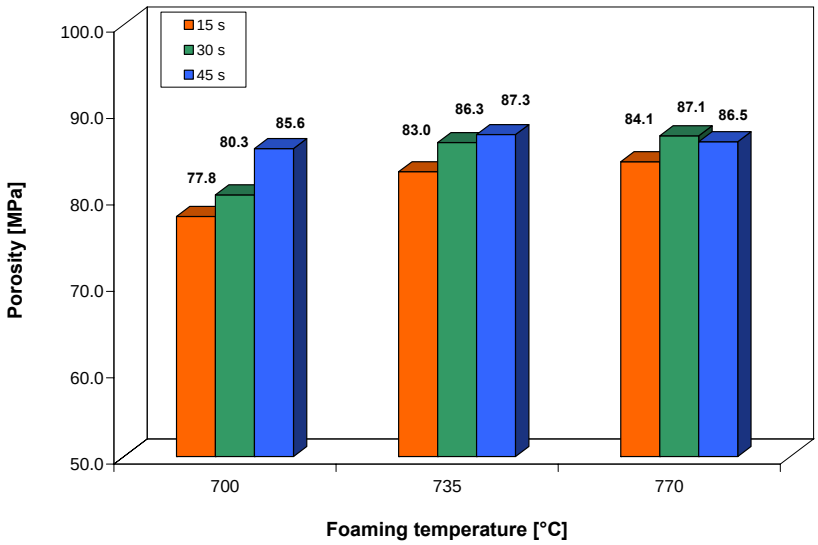


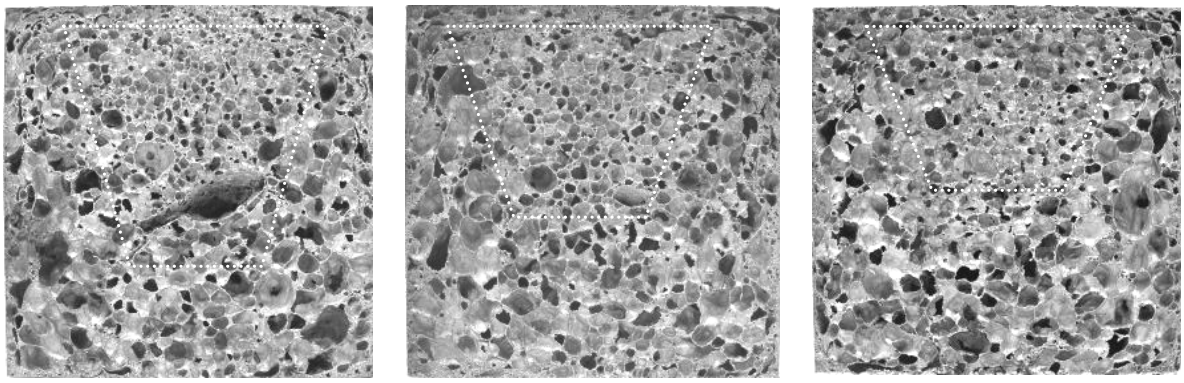
Figure 2. Effect of foaming temperature and time to final porosity of foamed sample.

Effect of foaming time to porosity of the foam is the most significant for foaming temperature 700°C; the longest foaming time is responsible for creation of the foam with the highest porosity. The porosity increases from 77.8% up to 85.6%. It means that the foaming time is responsible for 7% increase of porosity. However, in case of higher foaming temperatures (735°C and 770°C), it is only 4% increase or less. The porosity of samples for 735°C increases from 83% at 15s up to 87.3% for foaming time 45s. For temperature 770°C, the difference between the lowest and the highest porosity is only 3%.

Te foam expansion is given by the amount of evolved hydrogen during foaming. Hydrogen is evolved from blowing agent form (TiH_2) during the heating up the foam-able precursors, thus forces semi-liquid precursor to expand and create the aluminium foam. However, it takes some time for the blowing agent to decompose during foaming and amount of evolved hydrogen is influenced by the foaming temperature and time. Therefore, various foaming temperature and time, thus various amount of evolved hydrogen, affect overall porosity of the final foam component.

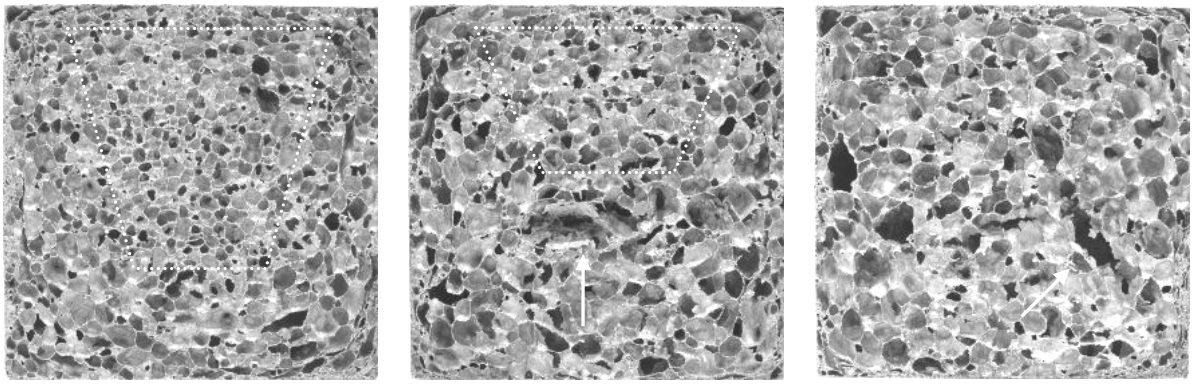
Pore structure

The pore structure developed at temperature 700°C for different foaming times is presented in Figure 3. The small-pore size area at upper part of the foam structure and large-pore area at the bottom part of the structure are characteristic for used precursor distribution [8]. The small pore size area do not disappear with increasing foaming time and remains in the structure even if foaming time is 45 seconds. However, the size of the small pore size area decreases as foaming time increases. The large pore in the pore structure is characteristic for foaming time 15 second is a result of the closed air between single precursors [8].



700°C/15s 700°C/30s 700°C/45s

Figure 3. The pore structure developed at temperature 700°C and various foaming times.

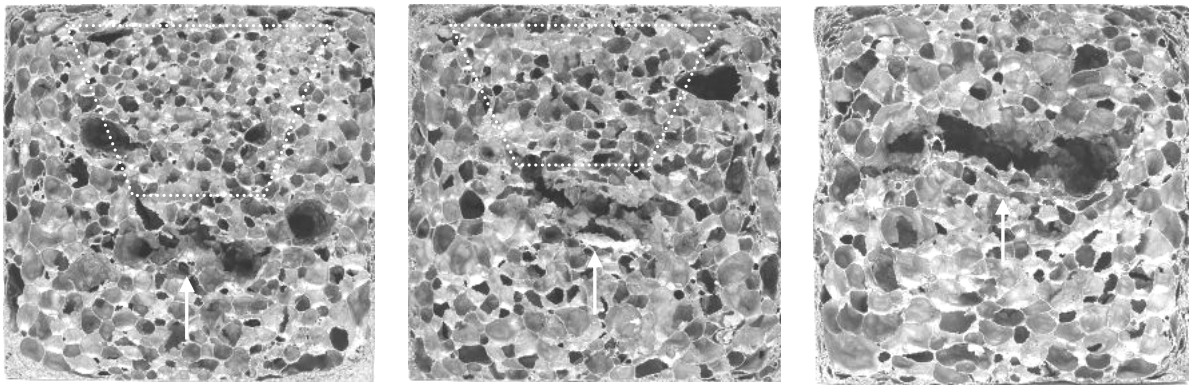


735°C/15s 735°C/30s 735°C/45s

Figure 4. The pore structure developed at temperature 735°C and various foaming times.

The changes within the pore structure in dependence on foaming time are more significant if temperature is increased up to 735°C (Figure 4). Even if time is 15s, the pore structure is more uniform in comparison with those obtained for temperature 700°C. The difference between pore size in small-pore area and large-pore area is not that significant and also, there are not large pores presented within the pore structure at this foaming time. However, if the foaming time is increased up to 30 second, the large pores with tear pore start to create. Those pores are not result of closed air between single precursors but, they are rather created by pore coalescence during expansion and their subsequent shrinking during cooling.

As can be seen in Figure 3 and Figure 4, the longer foaming time affect the existence of the small-pore area within the foam structure for foaming temperature 700°C and 735°C. This area starts to disappear with increasing time, which results into creation of the more uniform pore structure. (The small pore area is completely lost for 735°C after foaming time reach 45 seconds.) However, despite disappearing of small-pore area, the creation of large pores with tear pore faces is characteristic for the pore structure at increased temperature and foaming time. These large pores are characteristic for the pore structure developed at temperature 770°C even if holding time is 15 second (Figure 5). With increasing foaming time, they grow larger and for 45 second the large pore covers almost whole length of the pore structure.



770°C/15s 770°C/30s 770°C/45s

Figure 5. The pore structure developed at temperature 770°C and various foaming times.

The foaming temperature and time is responsible for creation and elimination of non-uniformities within the pore structure of the aluminium foam made by PM route:

a. By suitable combination of the foaming temperature and time (735°C-45s), the difference in pore size in foam volume caused by precursor distribution is eliminated.

b. The creation of large pores with tear pore faces is a result of high foaming temperature (770°C) and in some certain foaming temperature (735°C) it is result of the long foaming time too.

Effect to mechanical properties and reproducibility

On the Figure 6, there is presented scatter of absolute values of plastic strength obtained from stress-strain curves independent on porosity. The porosity of tested samples is 84.4%±3.14%. It is clear from the figure that the scatter of plastic strength values is rather high: the values of plastic strength ranges from 2.68 MPa up to 9.34 MPa with average value 4.83±1.62 MPa. Coefficient of variation is 0.336. It means that relative error of measured values is 33.6%.

However, as mentioned in chapter above, there are lots of non-uniformities within the foam structure as porosity variation and non-uniformities in pore structure (zone of small pores or existence of large pores) which are affected by foaming parameters. Their presence is

probably responsible for rather high scatter of measured values presented in Figure 6. In paragraphs below, they will be taken into account one by one and their effect to scatter of measured values will be explained.

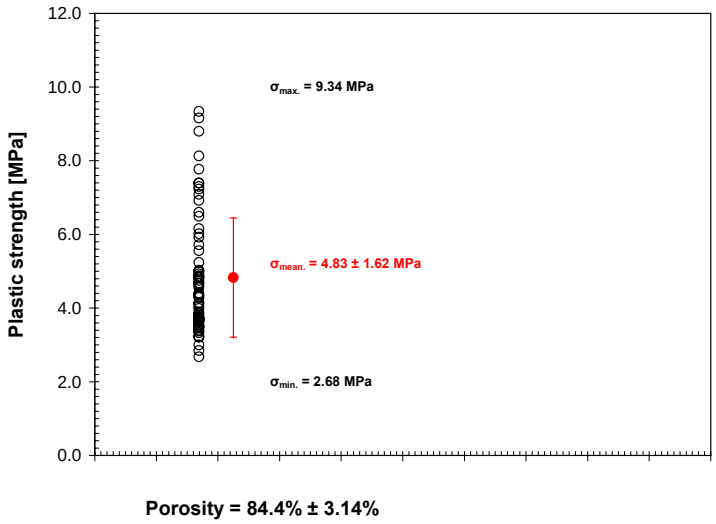


Figure 6. The absolute values of plastic strength independent on porosity.

Effect of porosity to plastic strength is presented in Table 1 and Figure 7. The average porosity 84.4%±3.14% is divided into four equal intervals. The manufacturing parameters are not taken into account in this chart. As porosity increases, the plastic strength decreases. This examination is obvious for aluminium foam [9] [14]. Moreover, this observation reveals that, if porosity of the foam sample is taken into account, the rather high scatter of plastic strength is noticeably eliminated. Coefficient of variation is decreases at least down to 0.123 for 86.5% porosity and down to 0.068 for porosity 80.5%. It suggests that the porosity is responsible for the high scatter of the absolute values and by its suitable adjusting; the relative error can be decreased more than twice below 12%. However, beside the porosity, there are some other structural features which affect deviation of measured values at certain porosity interval. In other words; they are responsible for high oscillation of the strength values around its average for certain porosity interval.

Table 1: Effect of porosity to plastic strength and coefficient of variation.

Porosity [%]	Plastic strength [MPa]	Coefficient of variation
77.5	8.38±0.87	0.104
80.5	6.94±0.47	0.068
83.5	5.11±0.45	0.088
86.5	3.71±0.46	0.123

It was already revealed that the manufacturing parameters affect the porosity of the samples and also that the approximately same porosities can be achieved by different foaming parameters. However, different foaming parameters are responsible for variation of pore structures if sample porosity is almost constant (presence of small pore zone, large pores etc. see pore structures foamed at 700°C-45s., 735°C-30s. 770°C-45s in Figure 3, Figure 4 and

Figure 5). The different non-uniformities within the pore structure are responsible for scatter of plastic strength for certain porosity interval.

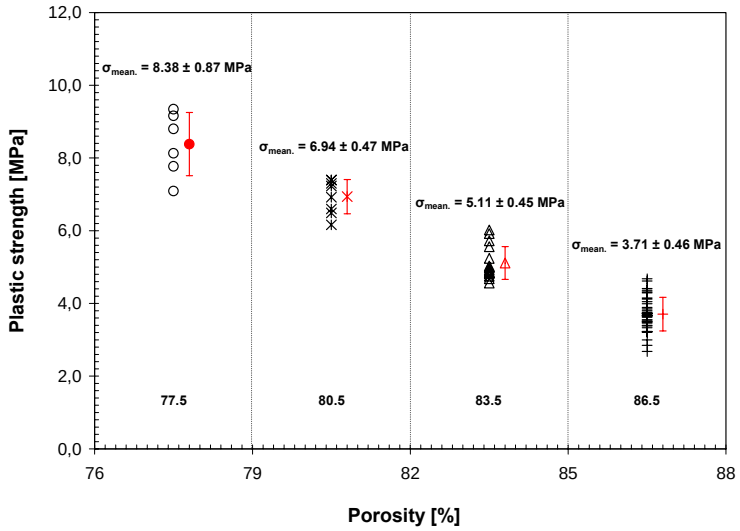


Figure 7. The absolute values of plastic strength in dependence on porosity.

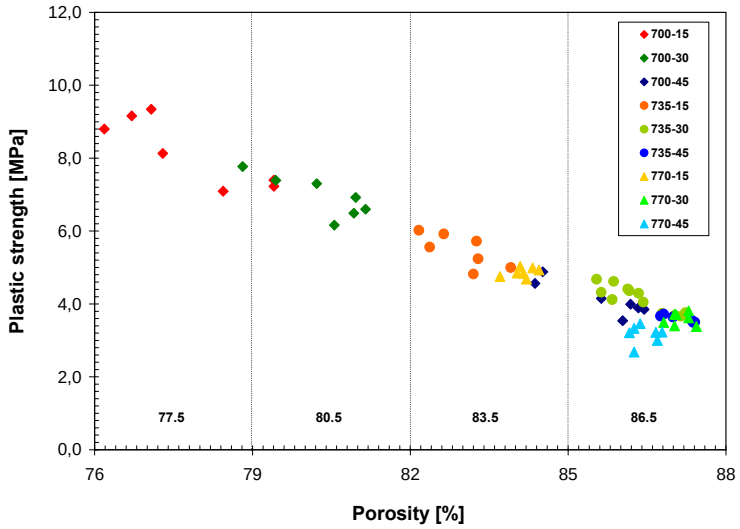


Figure 8. The absolute values of plastic strength in dependence on porosity, the different colors and shapes present different foaming parameters.

In Figure 8 and Table 2, there is presented effect of foaming parameters to plastic strength and to scatter of measured values. Only one but different combination of manufacturing parameters covers porosity intervals 77.6% and 80.6%. Therefore; from the chart, the main contribution to scatter of measured values in those intervals can be attributed to porosity variation. The non-uniformities in pore size level are constant due to same manufacturing parameters thus their effect to plastic strength is rather negligible.

However, different situation occur in case of porosity interval 83.5% and 86.5%. There are at least two manufacturing combinations which cover those intervals. For porosity 83.5% it is 735°C-15s. and 770°C-15s. Rest of combination of manufacturing parameters (735°C-30,45s. and 770°C-30,45s.) covers the interval 86.5%. Despite of this fact, the coefficient of variation

is only slightly decreased (see Table 1 and Table 2). However, the important fact is, that the coefficient of variation for single manufacturing combination is lower as one obtained only for certain porosity interval. If non-uniformities in the pore structure specific for certain combination of manufacturing parameters is taken into account, the coefficient of variation is decreased in some cases down to 0.026 for 770°C-15s.

Table 2: Effect of manufacturing parameters to plastic strength and scatter of measured values.

Man. Parameter	Porosity [%]	Pl. strength [MPa]	Coefficient of variation
700_15	77.8±1.30	8.16±0.95	0.116
700_30	80.3±0.87	6.95±0.57	0.082
700_45	85.7±0.86	4.12±0.46	0.111
735_15	83.0±0.61	5.47±0.46	0.084
735_30	86.4±0.59	4.14±0.36	0.088
735_45	87.3±0.48	3.49±0.29	0.084
770_15	84.1±0.24	4.87±0.13	0.026
770_30	87.1±0.21	3.59±0.17	0.047
770_45	86.5±0.25	3.16±0.25	0.080

CONCLUSIONS

The changes in manufacturing parameters are responsible for porosity variation of the foam sample.

Moreover, they are also responsible for the creation of various non-uniformities within the foam volume specific for certain manufacturing parameters.

By taking those facts into account during evaluation of plastic strength, the relative error can be decreased from 33.6% down to 2.6%.

ACKNOWLEDGEMENTS

The financial supports of ALULIGHT GmbH Ranshofen and Gleich GmbH are gratefully acknowledged.

LITERATURE

[1] Ashby, M.F. – Evans, A.G. – Gibson, L.J. – Hutchinson, J.W. – Wadley, H.N.G.: Metal Foam: A Design Guide, 2000, Butterworth-Heineman.

[2] Simancik, F.: Reproducibility of aluminium foam properties. In: J. Banhart, M. F. Ashby, N. A. Fleck, editors. Int. Conf., Bremen, Germany, 14-16 June, MIT Press-Verlag, Bremen, 1999, p.235.

[3] Degisher, H.P. – Kriszt, B.: Handbook of Cellular Metals, Production, Processing, Applications. 2002, Wiley-WCH.

[4] Simancik F. and col.: Basic Research in Optimalization of Mechanical Properties of Aluminium Foam and Joining Technology. Final Report, IMSAS SAS, 2002.

[5] Simone, A.E. – Gibson, L.J.: Effects of solid distribution on the stiffness and strength of metallic foams. Acta Materialia, 46, 1998, p.2139–2150.

[6] Andrews, E. – Sanders, W. – Gibson, L.J.: Compressive and tensile behaviour of aluminium foams. Material Science and Engineering, A/270, 1999, p. 113–124.

[7] Koza, E. – Leonowicza, M. – Wojciechowskia, S. – Simancik, F.: Compressive strength of aluminium foams. Materials Letters, 58, 2003, p. 132–135.

[8] Nosko, M. – Florek, R. – Simancik, F. – Uhrik, R.: Effect of precursor arrangement to foaming kinetics and pore morphology of aluminium foams made by PM route. Matrib 07, Vela Luka, 21-23 jun, 2007.

[9] Simancik, F. –Behulova, K. – Bors, L.: Effect of ambient atmosphere on metal foam expansion. In: J. Banhart, M. F. Ashby, N. A. Fleck, editors. Int. Conf., Bremen, Germany, 18-20 June, MIT Press-Verlag, Bremen, 2001, p.89.

[10] Simancik, F. – Minarikova, N. – Culak, S. – Kovacik, J.: Effect of foaming parameters on the pore size. In: J. Banhart, M. F. Ashby, N. A. Fleck, editors. Int. Conf., Bremen, Germany, 14-16 June, MIT Press-Verlag, Bremen, 1999, p.105.

[11] Duartre, I. – Banhart, J.: A study of aluminium foam formation-kinetics and microstructure. Acta Materialia 48 (2000), 2349-2362.

[12] Matijasevic, B. – Banhart, J.: Improvement of aluminium foam technology by tailoring of blowing agent. Acta materialia 54 (2006), 503-508.

[13] Matijasevic-Lux, B. – Banhart, J – Fiechter, S. – Gorke, O. – Wanderka N.: Modification of titianium hydride for improved aluminium foam manufacture. Acta Materialia 54 (2006), 1887-1900.

[14] Ramamurty, U. – Paul, A: Variability in mechanical properties of metal foam. Acta Materialia, 52, 2004, p. 869–876.

KARAKTERIZACIJA KOVARINE TOPLO VALJANE TRAKE IZVALJANE IZ KONTI SLABA

CHARACTRIZATION OF THE SCALE ON THE HOT ROLLING STRIP WHICH ROLLING FROM CONTINUOS SLAB

Vjera Novosel – Radović, Nikol Radović*, Katica Dužić, Franjo Šafar
Željezara Sisak d. o. o., 44000 Sisak, Hrvatska
*Geodetski fakultet Sveučilišta u Zagrebu, 10000 Zagreb, Hrvatska
nradovic@geof.hr

Izvorni znanstveni rad / Original scientific paper

Abstract
In this investigation structure and phase composition of film scale formed on hot rolled strip dim. 325 x 2 mm steel St. 37.8 hot rolling from slab 350 x 190 is systematically investigates by x – ray diffraction aimed to evaluate the process of rescaling. The samples for investigation were pieces of the hot rolled strip, collected at their ends, middle and beginning of the coiler. For each position of 20 x 325 mm were cut out. Every piece was further cut in plates 10 x 10 mm, and measurement directly using Philips diffractometer system (the counting technique and CoK_{α} radiation. Also film scale was scraped off, ground and homogenized for ten minutes in a WC attachment of Spex mixer mill. Prepared samples were measured photographic technique (Debye Scherrer camera). The observed Debye Scherrer patterns were microphotometered by microphotometer, type Officina Electronica di Tenno. For quantitative determination concentration the method of external standard were used. The intensities of 220 Fe_3O_4, 211 αFe_2O_3 and 200 FeO were measured and calculated by Statistica software.

Key words: scale, x – ray diffraction, hot rolled strip, coiler

Sažetak: U svrhu uklanjanja nastalog filma kovarine pri valjanju toplo valjane trake dim. 325 x 2 mm čelika St. 37.8 iz konti slaba 350 x 190 mm film je sistematski istražen uporabom metode rentgenske difrakcije. Za istraživanje uzeti su dijelovi toplo valjane trake na početku, sredini i kraju koluta. Na svakom mjestu isječen je uzorak dim. 325 x 20 mm. Svaki dio je dalje isječen u pločice dim. 10 x 10 mm izravno mjeren tehnikom brojenja na uređaju za difrakciju, tipa Philips. Film kovarine je također strugan, usitnjavan i homogeniziran 10 minuta u priključku mlina za usitnjavanje i homogenizaciju, tipa Spex. Pripremljeni uzorci su snimani tehnikom filma (Debye Scherrer kamera). Dobiveni rendgenogrami su fotometrirani na mikrofotometru, tipa Officina Electronica di Tenno. Za kvantitativno određivanje masenog udjela faza je uporabljena metoda vanjskog standarda. Izmjereni su relativni intenziteti difrakcijskih linija: 220 Fe_3O_4, 211 αFe_2O_3 i 200 FeO. Dobiveni rezultati obrađeni su matematički uporabom programa Statistica.

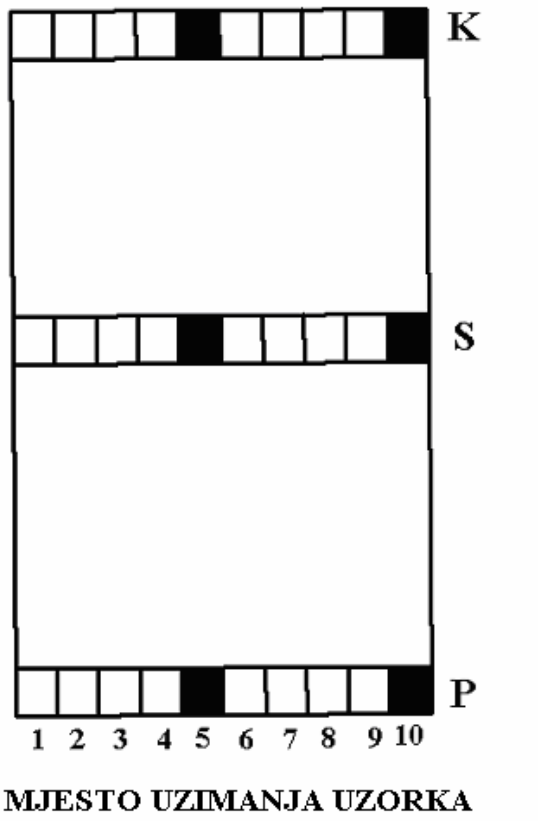
Ključne riječi: kovarina, rentgenska difrakcija, toplo valjana traka, kolut

UVOD

Tijekom valjanja toplo valjane trake iz konti slabova njena površina je neravnomjerno prekrivena filmom kovarine. Debljina nastalog filma kovarine[1] te strukturni i fazni sastav[2] (koji utječe na koheziona i deformacijska svojstva filma) izravno ovise o temperaturnim uvjetima valjanja[3]. Oni uvjetuju uspješnost uklanjanja filma kovarine sa površine toplo valjane trake u procesu njene izrade. U suprotnom, za njeno uklanjanje primjenjuje se jedan od mehaničkih i/ ili kemijskih postupaka. Korozionisti (koji proučavaju koroziju na visokim temperaturama) za uklanjanje nastalog filma kovarine u cijelosti preporučuju uporabu postupka dekapiranja[4]. No, za uspješnost postupka potrebno je istražiti: raspodjelu filma kovarine po dužini, širini i rubu toplo valjane trake; fazni sastav i maseni udio pojednih faza. U tu svrhu izvršena su istraživanja filma kovarine toplo valjane trake dim. 325 x 2 mm, čelika St. 37.8 iz konti slaba dim 350 x 190 mm uporabom metoda rentgenske difrakcije. Dobiveni rezultati istraživanja u cijelosti su dani u ovom radu.

EKSPERIMENT

Za istraživanje nastalog filma kovarine tijekom valjanja toplo valjane trake dim. 325 x 2 mm, čelika St. 37.8 iz konti slaba dim. 350 x 190 mm i namatane u kolut su uporabljeni model uzorci. Oni su pripremljeni iz isječenih dijelova, dim. 20 x 325 mm po širini toplo valjane trake na početku, sredini i kraju koluta, slika 1.



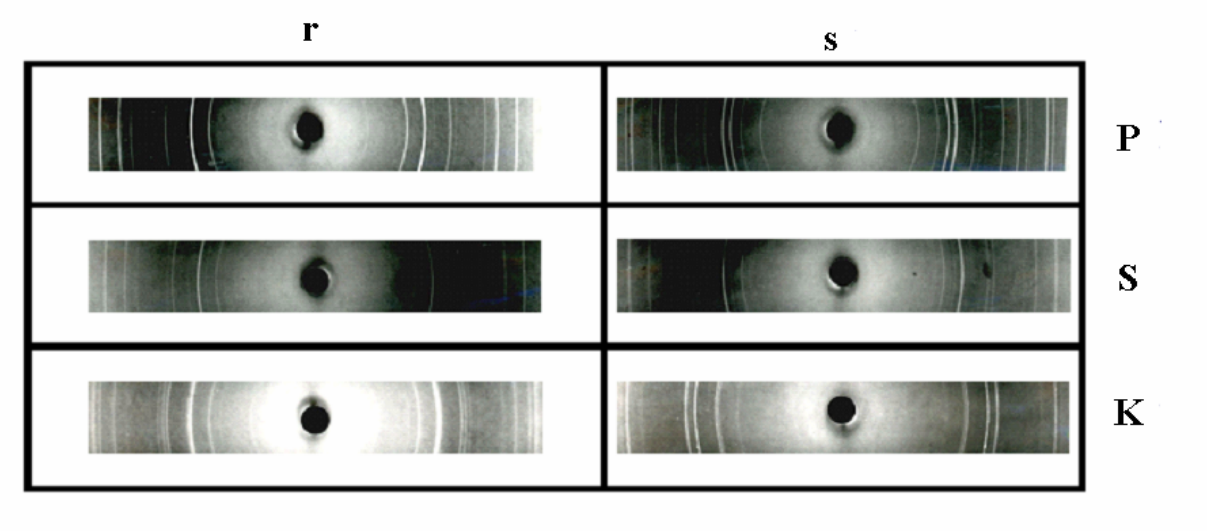
Slika 1. Prikaz uzimanja uzorka po dužini i širini toplo valjane trake na početku – **P**, sredini – **S** i kraju – **K** koluta. **1**, **2**, **3**, **4**, **5**, **6**, **7**, **8**, **9**, **10** mjesta sukcesivno uzimanih uzoraka.

Svaki uzeti dio trake dalje je isječen u pločice dim. 10 x 10 mm i izravno mjeren tehnikom brojenja na uređaju za difraktometriju, tipa Philips uz uporabu CoK_{α} zračenja.

Uzorci kovarine uzeti mehaničkim struganjem pod lupom tipa Zrak dodatno su usitnjeni i homogenizirani u WC priključku mlina za usitnjavanje i homogenizaciju, tipa Spex. Pripremljeni uzorci su snimani tehnikom filma (Debye Scherrer kamera). Dobiveni rendgenogrami su fotometrirani na mikrofotometru tipa Officina Electronica di Tenno. Maseni udio faze: Fe_3O_4, 211 αFe_2O_3 i 200 FeO je određen metodom vanjskog standarda[5, 6] mjerenjem relativnog intenziteta difrakcijske linije refleksa: 211 Fe_3O_4, 211 αFe_2O_3 i 200 FeO. Dobiveni rezultati mjerenja su obrađeni matematički uporabom programa *Statistica.*

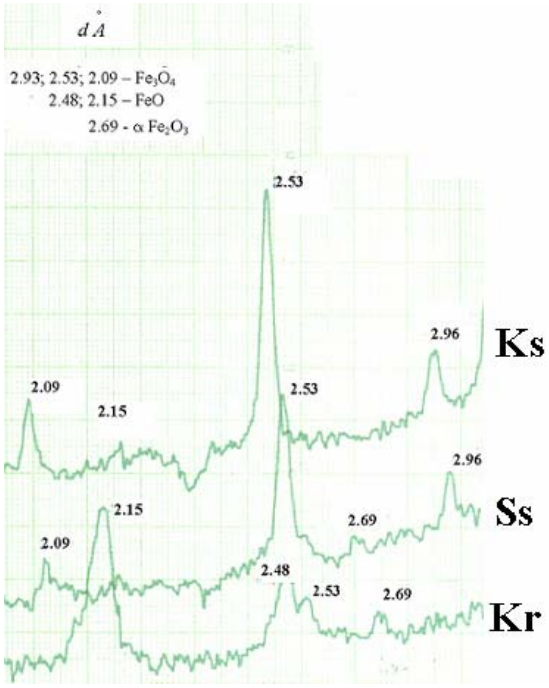
REZULTATI

Dobiveni rezultati analize filma toplo valjane trake dim 325 x 2 mm, čelika St. 37.8 valjane iz konti slaba dim. 350 x 190 mm uporabom metoda rentgenske difrakcije upućuju na promjenu njegova faznog sastava po dužini, širini i rubovima toplo valjane trake, te na početku, sredini i kraju koluta. Na ovu tvrdnju upućuju i rezultati izvršenih preliminarnih ispitivanja uzoraka uzetih u obliku praha, slika 2. i 3. Na slici 2. dobiveni rentgenogrami upućuju na promjenu broja intenziteta zabilježenih debyevskih prstena sa mjestom uzimanja uzoraka.



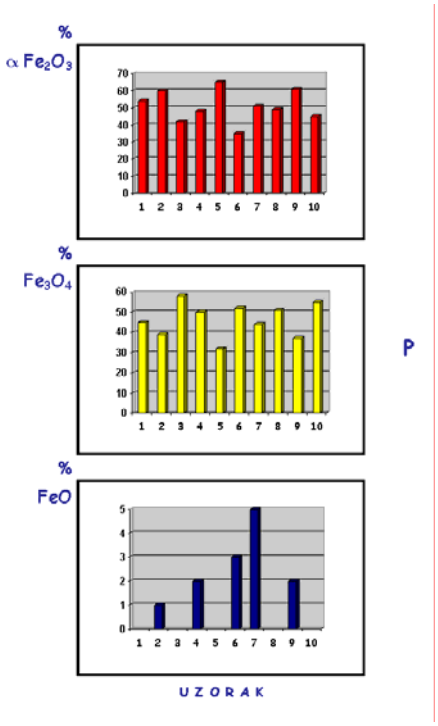
Slika 2. Rentgenogrami uzorka filma kovarine uzetih na rubu – **r** i sredini – **s** toplo valjane trake na početku – **P**, sredini – **S** i kraju – **K** koluta.

Na analogna zapažanja upućuju i dobiveni mikrofotometrijski zapisi relativnog intenziteta debyevskog prstena koji odgovara međuplošnom razmaku za fazu Fe_3O_4: 2.96, 2.53 i 2.02 $\mathring{A}$; αFe_2O_3 – 2.96 $\mathring{A}$ i FeO – 2.48 i 2.15 $\mathring{A}$.

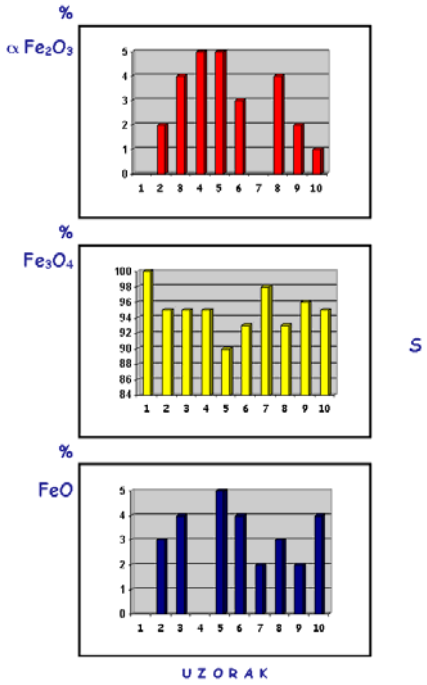


Slika 3. Mikrofotometrijski zapis rentgenograma slike 2 – **Ks**, Ss i **Kr** uzoraka uzetih na sredini **Ss** i kraju koluta **Ks** i njegovu rubu **Kr**.

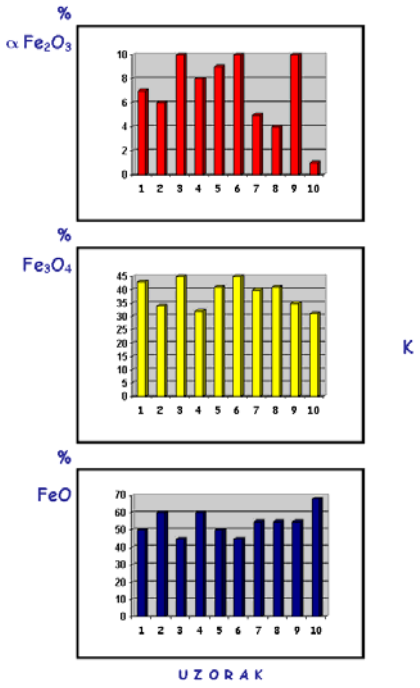
Prema dobivenom mikrofotometrijskom zapisu može se tvrditi da faza Fe_3O_4 je prisutna na svim istraživanim uzorcima u dovoljnom masenom udjelu, αFe_2O_3 u neznatnom, a FeO u uzorku **Kr** poprima maksimalnu vrijednost. Na stvarnu prisutnost masenog udjela faza te njihovu promjenu po dužini i širini toplo valjane trake upućuju dobiveni rezultati kvantitativne fazne analize, slika 4 – 7. Prema njima maseni udio faze: Fe_3O_4, αFe_2O_3 i FeO nejednoliko se mijenja po širini i dužini toplo valjane trake te rubu i sredini. Tako na početku koluta po širini toplo valjane trake maseni udio faze Fe_3O_4 se mijenja od 30 do 58 %, αFe_2O_3 od 30 do 62 % i FeO od 0 do 5 %. Na sredini koluta maseni udio faze Fe_3O_4 se mijenja od 90 do 100 % a faze αFe_2O_3 od 0 do 5 %. Na kraju koluta maseni udio faze FeO znatno je porastao u udnosu na početak i kraj koluta od 48 do 68 % faze Fe_3O_4 se smanjuje na 30 do 40 %, a faze αFe_2O_3 se neznatno povečava od 1 do 10 %.



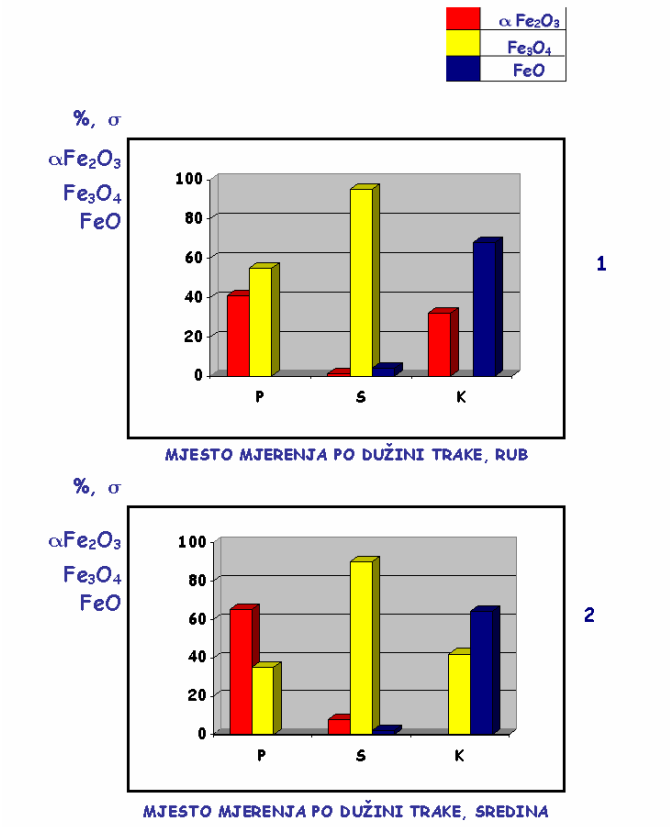
Slika 4. Promjena masenog udjela faze Fe_3O_4, αFe_2O_3 i FeO po širinu trake na početku koluta, **P**.



Slika 5. Promjena masenog udjela faze Fe_3O_4, αFe_2O_3 i FeO po širinu trake na sredini koluta, **S**.

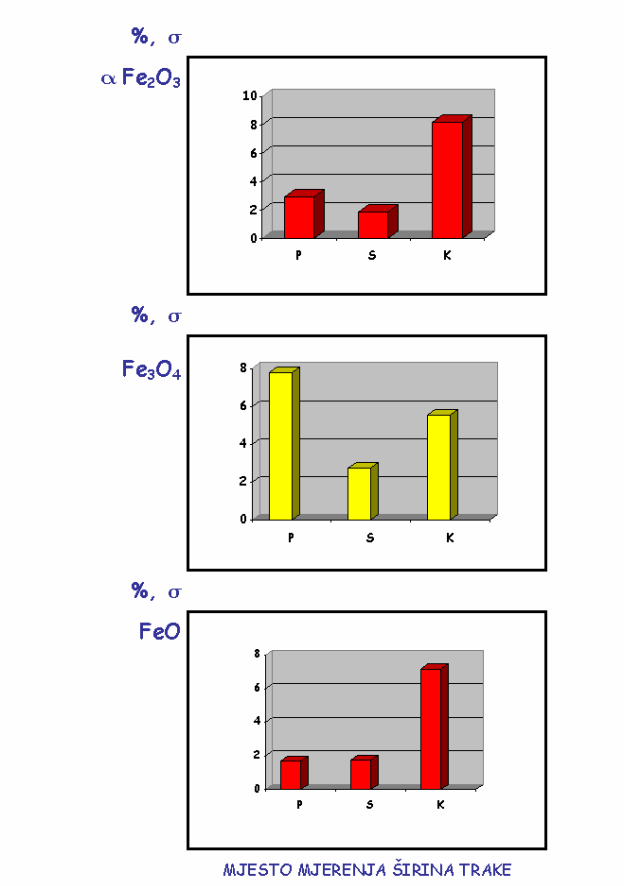


Slika 6. Promjena masenog udjela faze Fe_3O_4, αFe_2O_3 i FeO po širinu trake na kraju koluta, **K.**

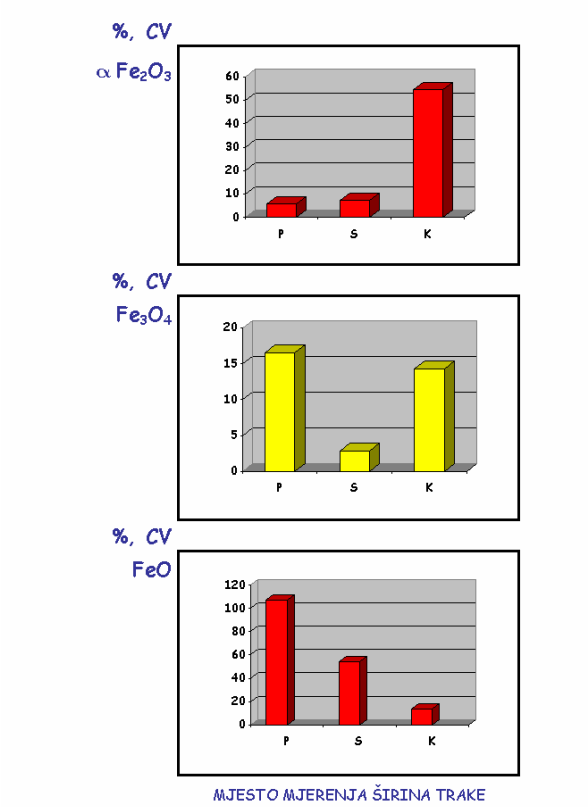


Slika 7. Promjena masenog udjela faze Fe_3O_4, αFe_2O_3 i FeO po dužini toplo valjane trake na rubu – **1** i sredini – **2** na početku – **P**, sredini – **S** i kraju – **K** koluta.

Na analogna zapažanja upućuju i izračunate vrijednosti koeficijenata standardne devijacije, σ i varijance CV, slika 8 i 9.



Slika 8. Standardna devijacija, σ masenog udjela faza po širini toplo valjane trake na početku – **P**, sredini – **S** i kraju – **K** koluta.



Slika 9. Koeficijent varijance, CV masenog udjela faza po širini trake toplo valjane trake na početku – **P**, sredini – **S** i kraju – **K** koluta.

Najveće razlike u izračunatim vrijednostima koeficijenata varijance su zapažene na početkui i kraju koluta u odnosu na njegovu sredinu. Tako CV vrijednost za maseni udio faze Fe_3O_4 iznose 16.20 %, αFe_2O_3 – 5 % i FeO 121 % na početku, te 12.5 % Fe_3O_4, αFe_2O_3 – 53.2 % i FeO – 12.5 % na kraju koluta. U sredini koluta ove vrijednosti su dosta manje. Tako su maseni udio faze Fe_3O_4 iznose 2.60 %, αFe_2O_3 – 7.25 % i FeO – 45.60 %. Prema literaturi[7] zapažene razlike u nehomogenosti faznog sastava filma kovarine, te masenog udjela faze: Fe_3O_4, αFe_2O_3 i FeO posljedica su neravnomjernog hlađenja toplo valjane trake u fazi njena namatanja u kolut. Početak i kraj toplo valjane trake namotane u kolut naglo se hladi, pa fazni sastav filma kovarine ostaje gotovo nepromijenjen. Sredina namotane trake u kolut, hladi se polagano, te faza FeO filma kovarine se polagano transformira u faze Fe_3O_4. Budući da se prisutne faze FeO i Fe_3O_4 filma kovarine međusobno razlikuju po svojstvu kohezije i deformacije to njihovo uklanjanje sa površine toplo valjane trake postupkom pjeskarenja nije ujednačeno. Naime uporabljenim postupkom se uklone samo dijelovi filma u kojima je većinski udio faze FeO. Preostali dio filma sa većinskim udjelom faze Fe_3O_4 i dalje u obliku nakupina (početak i kraj koluta toplo valjane trake) i/ ili kontinuiranog filma (sredina koluta trake) prekriva površinu toplo valjane trake. Za uklanjanje preostalog dijela filma u cijelosti korozionisti predlažu uporabu postupka dekapiranja. Za provođenje tog postupka uporabljuju se jedna i/ ili smjesa kiselina (H_2SO_4, HCl, HNO_3, HF) uz dodatak inhibitora ovisno o debljini filma kovarine i masenom udjelu faze Fe_3O_4, αFe_2O_3 i FeO.

ZAKLJUČAK

Rezultati istraživanja filma kovarine nastalog tijekom valjanja toplo valjane trake dim. 325 x 2 mm, čelik St. 37.8 iz konti slaba dim. 350 x 190 mm upućuju na nehomogeni fazni sastav i raspodjelu po dužini, širini i rubu trake na početku, sredini i kraju koluta. Unutar filma kovarine maseni udio faze se mijenja:

- Fe_3O_4 od 38 do 58 % na početku koluta, 90 – 100 % na sredini koluta 30 – 40 % na kraju koluta;
- αFe_2O_3 od 10 % na sredini i kraju koluta, te 32 do 62 % na početku koluta;
- FeO od 0 do 5 % na početku koluta, te 48 do 68 % na kraju koluta.

Na početku i kraju koluta namotana toplo valjana traka se naglo hladi, što ima za posljedicu nepromijenjeni maseni udio faze Fe_3O_4 i FeO unutar filma kovarine. No, u sredini koluta toplo valjana traka se sporo hladi te faza FeO se postepeno transfomrira u fazu Fe_3O_4. Nastaje velika razlika u masenom udjelu faza Fe_3O_4 i FeO po dužini, širini i rubu trake, kao i nemogućnost cjelovitog uklanjanja filma kovarine. Za cjelovito uklanjanje filma sa površine toplo valjane trake korozionisti predlažu uporabu postupka dekapiranja, optimalnih uvjeta određenih na osnovi izvršene karakterizacije filma kovarine.

LITERATURA

[1] Larin, Y. J., Polykov, N. V., Chernou, P. P., *Proizvod Prokatka*, 2001, **12**, 35.
[2] Du, F. C., Zhou, W. H., *J. Iron Steel Res. Inst*., 2002, **9**, 21.
[3] Kim, B. K., Szpunov, J. A., *Mater. Sci. Forum*, 2002, **2**, 1711.
[4] Kovačić, Đ., Definiranje optimalnih uvjeta rada u svim fazama kemijsko – tehnološkog procesa vrućeg pocinčavanja šavnih i bešavnih cijevi u Željezari Sisak, II. dio, Institut za metalurgiju Sisak, 1969.
[5] Novosel – Radović, Vj., Nenadić, N., Šafar, F., "*Detectability of iron oxide phases in protective magnetite film samples*" in Materials Science Forum, Mitemeier, E. J., Delhez, R., Trans. Tech. Publications, Munich, 1991, **78** – **82**, 53.
[6] Novosel – Radović, Vj., Balen, M., Radović, N., "*Determination of Fe_3O_4 phases concentration in a protective magnetite film*" in Abstract EPDIC - 3, Vienna - Austria, Sept. 25 – 28, 1993, 133.
[7] Chen, R. Y., Yuew, W. Y. D., *Oxid. Mat*., 2001, **56**, 89.

EKSPERIMENTALNO ODREĐIVANJE SILE TRENJA

Doc.dr.Mirna Nožić
Univerzitet "Džemal Bijedić", Mašinski fakultet
Maršala Tita bb, 88 000 Mostar, BiH

Prof.dr.Himzo Đukić
Sveučilište u Mostaru, FSR
Matice Hrvatske bb, 88000 Mostar, BiH

Stručni članak / Professional paper

Sažetak:

U svim procesima obrade deformiranjem značajnu ulogu ima komponenta trenja.
Pri analizi naprezanja tih procesa sila trenja se može eksperimentalno mjeriti sa specijalnim davačima. U literaturi postoji čitav niz rješenja davača za mjerenje kontaktnih naprezanja preko igle za mjerenje vertikalne komponente. U novije vrijeme javljaju se složenije konstrukcije davača, koji pored vertikalne komponente mogu mjeriti i tangencijalne komponente.
U radu je prikazana konstrukcija specijalnog davača, koji može mjeriti vertikalne i tangencijalne komponente naprezanja, sa dimenzioniranjem svih bitnih elemenata davača.
Za konstrukciju davača se koriste mjerne trake, a mjerni lanac se sastoji od: davača, univerzalnog mjernog mosta i računala sa specijalnim softverom.

Ključne riječi: davač, trenje, mjerne trake

1. UVOD

Svi procesi obrade materijala deformiranjem baziraju se na unošenju neophodne količine mehaničke energije u materijal koji se preoblikuje.
Ovo unošenje energije, odnosno stvaranje potrebnog spoljašnjeg opterećenja na obradak, ostvaruje se neposrednim dejstvom radnog tijela-alata (nosioca energije i kretanja) na njega, tj. prenošenje energije sa radnog tijela na obradak se ostvaruje preko njihovih kontaktnih površina.
Kako pri ovome dolazi do klizanja obratka po kontaktnoj površini radnog tijela-alata, to se na tim površinama javlja trenje, koje se suprotstavlja klizanju materijala koji se obrađuje.
Neophodno je uočiti razliku između trenja od klizanja na kontaktnim površinama u strojarskih konstrukcija (stroja, uređaja, i sl.) i trenja na kontaktnim površinama alata i predmeta obrade u procesima obrade deformiranjem.
Pri obradi materijala plastičnim deformiranjem dodirne površine obratka se plastično (trajno) deformiraju i poprimaju oblik radnih površina alata, dok se alat samo elastično deformira.
Sve neravnine radnih površina alata odslikavaju se na kontaktnim površinama obratka, što ima za posljedice:

- da je stvarna dodirna površina daleko veća;
- da u uslovima visokih pritisaka nastaju znatne sile molekularnog zahvata i
- da pri klizanju obratka po alatu, njegove radne površine „grebu“odgovarajuću površinu predmeta obrade.

Iz svega navedenog, nameće se zaključak da se koeficijent trenja, koji odgovara uvjetima u strojarskim konstrukcijama, ne može prihvatiti pri procesima obrade materijala deformiranjem.
U približnim inžinjerskim proračunima može se sila trenja izračunati pomoću izraza $F_T = \mu_D \cdot F_N$, pri čemu je $\mu_D > \mu$.

2. POSLJEDICE TRENJA

Posljedica klizanja materijala po radnim površinama alata je pojava sila spoljašnjeg trenja, tj. pojava tangencijalnih sila koje dejstvuju u kontaktnim površinama suprotstavljajući se klizanju materijala.
Trenje u procesima obrade materijala deformiranjem predstavlja jedan od glavnih negativnih faktora.
Kao posljedica postojanja spoljašnjeg trenja dolazi do:

- pojave neravnomjernosti deformacije i
- transformacije određene količine mehaničke energije u toplotu.

Unutrašnje trenje ima za posljedicu samo transformaciju odgovarajuće količine mehaničke energije u toplotu.
Dobijena toplotna energija ima negativan efekat na tehnološki proces obrade materijala deformiranjem zbog:

- smanjenja stepena iskorišćenja raspoložive mehaničke energije sredstava rada i
- povećanja temperature obratka.

3. TRENJE I GUBICI ENERGIJE

U procesima obrade materijala deformiranjem trenje na kontaktnim površinama alata i predmeta obrade dovodi do gubitaka energije. Na veličinu gubitaka energije utiče niz faktora, od kojih su najvažniji:

- vrsta materijala obratka i alata,
- vrsta tehnološkog postupka,
- kvalitet kontaktnih površina alata i predmeta obrade,
- temperatura na kojoj se proces odvija,
- brzina deformacije,
- način podmazivanja i vrsta sredstava za podmazivanje, i dr.

4. ODREĐIVANJE KOEFICIJENTA TRENJA

U proračunima procesa obrade materijala deformiranjem polazi se od diferencijalnih jednačina ravnotežnog stanja. Granični uvjeti na dodirnim površinama alata i obratka zadaju se u vidu promjene tangencijalnog napona po hipotezi najvećeg tangencijalnog napona u obliku:

$$\tau_S = \frac{\sigma_1 - \sigma_2}{2} \qquad (1)$$

gdje su:

τ_S – tangencijalni napon tečenja materijala;
σ_1 i σ_2 - glavni normalni naponi.

Analizom tehnoloških procesa obrade materijala deformiranjem i primjenom obrasca (1), izdvajaju se tri granična slučaja, i to:

1. U tehnološkim procesima obrade deformiranjem, u kojim je normalni napon na dodirnim površinama uvijek manji od specifičnog deformacionog otpora ($\sigma_n < \beta \cdot k$), granični uvjet se može izraziti sa:

   $$\tau_k = \mu_D \cdot \sigma_n \qquad (2)$$

   Izraz (2) predstavlja Kulonov zakon trenja primjenjen na procese obrade materijala deformiranjem kod kojih materijal klizi po kontaktnim površinama alata bez lijepljenja uz iste i bez utiskivanja reljefa radne površine alata u dodirnu površinu predmeta obrade, kao npr. pri dubokom izvlačenju.

2. U slučaju kada tangencijalni naponi na najvećem dijelu dodirne površine alata i obratka ne dostižu svoju maksimalnu vrijednost ($\tau_k < 0{,}5 \cdot \beta \cdot k$), granični uvjet se može izraziti sa:

   $$\tau_k = \mu_D \cdot \beta \cdot k \qquad (3)$$

Iz ovog uvjeta proizilazi da na kontaktnim površinama dolazi do djelimičnog klizanja i djelimičnog lijepljenja materijala koji se obrađuje po radnim površinama alata, kao što je slučaj npr: pri sabijanju u hladnom stanju, pri izradi tankih limova valjanjem sa velikim stepenom deformacije i dr.

3. Kada na najvećem dijelu kontaktnih površina alata i obratka tangencijalni napon dostiže svoju maksimalnu vrijednost:

$$\tau_k = \frac{\beta \cdot k}{2} \qquad (4)$$

Ovaj uvjet se koristi u proračunima sa istoimenim prostornim naponskim stanjem pritiska, u kojih je na najvećem dijelu dodirne površine alata i obratka normalni napon:
$\sigma_n >> \beta \cdot k$, kao što je slučaj npr. pri kovanju ili presovanju u kalupima bez podmazivanja ili sa podmazivanjem koje ima mali efekat.
U ovom slučaju klizanja materijala koji se obrađuje po radnim površinama alata nema, tj. po cijeloj dodirnoj površini odvija se lijepljenje materijala po kontaktnoj površini alata.

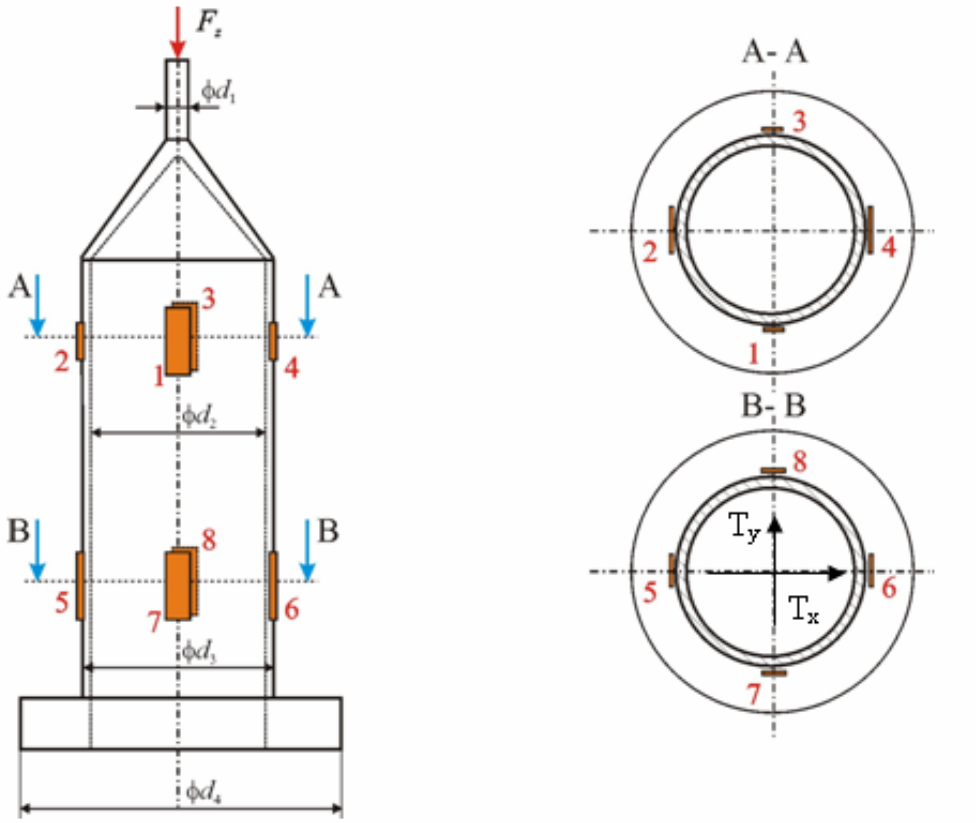
Na osnovu iznesenih graničnih slučajeva, može se zaključiti:

- da vrijednost koeficijenta (μ_D) ne može biti veća od 0,5.

  $\mu_D \leq 0{,}5$;
- da koeficijent (μ_D) ima smisla poistovjetiti sa koeficijentom trenja (μ), tj. Kulonovim trenjem samo u prvom graničnom slučaju i
- da se deformiranje materijala u trećem slučaju obavlja klizanjem unutrašnjih slojeva materijala obratka, i to jednog sloja u odnosu na drugi sloj.

5. KONSTRUKCIJA DAVAČA ZA MJERENJE KONTAKTNIH SILA

Davač za mjerenje kontaktnih sila prikazan na Slici 1. može mjeriti vertikalnu komponentu (F_z) i tangencijalne komponente (T_x i T_y). U općem slučaju ukupna sila F u bilo kom procesu obrade deformiranjem može se razložiti na vertikalnu komponentu (F_z) i tangencijalnu komponentu (T), koja se razlaže na dvije tangencijalne komponente (T_x i T_y).



Slika 1. Konstrukcija davača

Davač se sastoji iz jednog dijela. Igla davača prečnika ød$_1$ bira se u granicama između 1,5 i 2,5 mm. Manja vrijednost prečnika ød$_1$ bolje opisuje proces obrade deformiranjem koji mjerimo.
Zazor između igle i kanala u koji se ona postavlja bira se u granicama od 0,02 do 0,04 mm. Pri izboru materijala davača mora se voditi računa da sila trenja na vrhu igle ne izaziva progib veći od 0,003 do 0,005 mm.
Vanjski prečnik cilindričnog dijela davača ød$_3$ zavisi od veličine zalijepljenih mjernih traka. Minimalna vrijednost prečnika ød$_3$ za trake baze 1,5 mm iznosi 7 mm, a za trake baze 6 mm minimalni prečnik je 20 mm.
Prema preporukama proizvođača mjernih traka za prečnik ød$_3$ manji od 13 mm mora se voditi računa o uticaju zakrivljenosti površine na tačnost mjerenja. Pri lijepljenju mjernih traka na male radijuse može doći do pojave prividnih deformacija zbog malog radijusa krivine. Na vrijednost prividnih deformacija utiče: radijus zakrivljenosti površine, vrsta ljepila, debljina sloja ljepila, vrsta podloge mjerne trake, debljina podloge i vrsta osnovnog materijala.
Uticaj svih navedenih faktora na promjenu prividnih deformacija može se izraziti jednačinom:

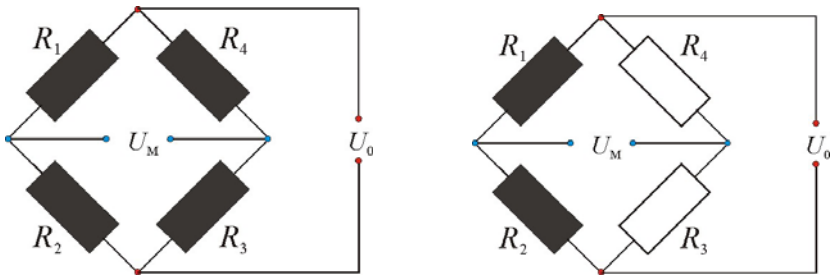
$$\varepsilon = \frac{1}{R}(1+2\nu_{AB})(h_A\alpha_A + h_B\alpha_B) - 2\nu_{AB}\alpha(h_A + h_B)\Delta T \qquad (5)$$

gdje su:

R – radius zakrivljenosti površine na koju je zalijepljena mjerna traka;
h_A – debljina sloja ljepila;
h_B – debljina podloge mjerne trake;
α_A - koeficijent toplotnog izduženja ljepila
α_B - koeficijent toplotnog izduženja podloge mjerne trake;
α - koeficijent toplotnog izduženja osnovnog materijala;
ν_{AB} - Poisson-ov koeficijent veze ljepila i podloge mjerne trake;
ΔT - prirast temperature.

Vrijednost navedenih parametara može se naći kod proizvođača mjernih traka, a cjelokupan uticaj svih parametara proizvođači obično daju u obliku dijagrama za različite veličine mjernih traka i različita ljepila.

Unutarnji prečnik cilindričnog dijela ød$_2$ određuje se iz uslova da se poprečni presjek A-A pod dejstvom vertikalne sile F_z i tangencijalnih komponenti T_x i T_y nalazi u elastičnom području.
S obzirom da je prečnik igle uglavnom manji od 2 mm, debljina stjenke cilindričnog dijela, po navedenom proračunu, je mala, pa se zbog toga mora izraditi elektrokemijskim putem. Debljina stjenke cilindričnog dijela u praksi najčešće iznosi 0,5 mm. Prečnik oslonca davača ød$_4$ prilagođava se mjestu ugradnje davača u alat za obradu deformiranjem.
Mjerenje vertikalne komponente sile kontaktnog trenja F_z vrši se na presjeku A-A, na koji su nalijepljene četiri mjerne trake, povezane u puni most. (Slika 2.a)

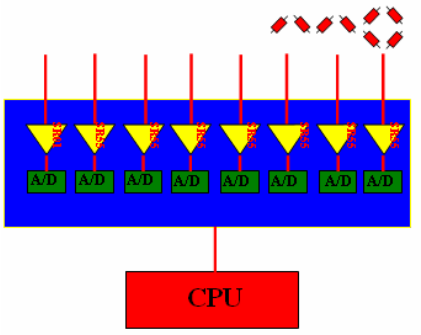


a. Presjek A-A b. Presjek B-B

Slika 2. Šeme vezivanja mjernih traka

Otpori R_1-R_4 odgovaraju mjernim trakama 1-4 prikazanim na Slici 1. (presjek A-A).
Mjerenje tangencijalne komponente T_x vrši se sa dvije mjerne trake (5 i 6), a mjerenje tangencijalne komponente T_y sa mjernim trakama (7 i 8) prema Slici 1. (presjek B-B). Mjerne trake (5 i 6) i mjerne trake (7 i 8) vežu se u polumost prema Slici 2.b. Trake (5 i 7) odgovaraju otporu R_1, a trake (6 i 8) odgovaraju otporu R_2.
Prije ugradnje davača vrši se kalibracija istog sa poznatim opterećenjem. Opterećenje davača bira se u granicama od minimalne do pretpostavljene maksimalne vertikalne komponente F_z. Kalibracijom davača uzimaju se u obzir sve eventualne greške nastale pri lijepljenju mjernih traka, kao i uticaj dužine kabla od davača do pojačivača.

Šema mjernog lanca za jednan davač prikazana je na Slici 3.



Slika 3. Šema mjernog lanca za jedan davač

Sa Slike 3. se vidi da je za jedan davač na pojačivaču potrebno imati tri kanala, i to: jedan za puni most i dva za polumost.
Korištenjem savremene mjerne opreme, kao što je Spider 8 i pripadajućeg softvera moguće je u veoma kratkom vremenu snimiti veliki broj podataka vezanih za veličinu aksijalne sile F_z i tangencijalnih sila na davaču.

6. ZAKLJUČAK

Prikazana konstrukcija specijalnog davača omogućava istovremeno mjerenje aksijalne sile i tangencijalnih komponenti trenja pri procesima obrade deformiranjem.
Korištenjem navedenog davača može se odrediti vrijednost koeficijenta trenja, odnosno izvršiti izbor najboljeg sredstva za podmazivanje za ispitivani proces. Na taj način bitno se utiče na vijek trajanja alata i stabilnost procesa.

LITERATURA:

[1] H.Đukić, P.Popović Obrada deformisanjem, Univerzitet „Džemal Bijedić“ u Mostaru, Mostar, 1988.
[2] A.P.Grudev, i dr. Trenie i smazki pri obrabotke metallov davleniem, Moskva 1982.
[3] V.Določek i dr. Elastostatika, Univerzitetska knjiga, Bihać-Banja Luka-Sarajevo-Mostar, 2004.

PREPARATION OF SILICON DOPED HYDROXYAPATITE

Klaudia Paljar, Sebastijan Orlić, Emilija Tkalčec, Hrvoje Ivanković
Faculty of Chemical Engineering and Technology, University of Zagreb
HR-10001 Zagreb, Marulićev trg 19, p.p. 177, Croatia
e-mail: sorlic@fkit.hr

Izvorni znanstveni rad / Original scientific paper

Abstract

The disadvantage of using hydroxyapatite implant is its low reactivity with human bone. An interesting way to enhance the bioactivity is addition of silicon to hydroxyapatite structure. Silicon plays important role on bone formation and calcification of implant. In this study Si-hydroxyapatite is prepared from cuttlefish bone (Seppia Officinalis L, from Adriatic Sea) by hydrothermal method. The phase composition of the converted bone samples depend on the conditions of hydrothermal treatment, on Si content in Si substituted hydroxyapatite and additional heat treatment. X-ray diffraction and Fourier transform ATR infrared spectroscopy were used to study the transformation processes during hydrothermal conversion of cuttlefish bone.

Key words: bioceramics, hydroxyapatite, hydrothermal method, silicon

1. INTRODUCTION

The requirement for biomaterials to assist in many medical applications replacing original musculoskeletal tissues and improve quality of life is rapidly increasing. Hydroxyapatite, $[Ca_{10}(PO_4)_6(OH)_2]$, has achieved significant application as a bone graft material in a range of medical and dental applications. However, a disadvantage of using pure Hydroxyapatite (HA) implants is that its reactivity with existing bone is low [1] and therefore it integrates relatively slowly with bone [2]. These properties could have implications for the time required for patient rehabilitation [3]. A way to enhance the bioactive behavior of HA ceramic is to obtain substituted HA, which resemble the chemical composition and structure of the mineral phase in bones [4,5] An interesting way to improve the bioactivity of HA is the addition of silicon to the apatite structure [6]. The earliest studies on the role of silicon in bone dates back to the early 1970s, when a series of experiments were published by Carlisle [7], using electron probe microanalysis. He found the presence of silicon (0.5 wt%) in vivo within the mineralizing osteoid regions, i.e. the active calcification sites, of normal tibiae from young mice and rats. This study suggested that silicon plays a critical role in the bone calcification process. Tanizawa and Suzuki [8] and Sugiyama *et* al. [9] tried hydrothermal methods obtaining materials with a Ca/(P+Si) ratio higher than that of pure calcium hydroxyapatite, but they did not mention about stability of Si substituted hydroxyapatite above 145°C. Kim et al [10] reported preparation of silicon-incorporated hydroxyapatite by hydrothermal treatment of natural corals. To the best of our knowledge hydrothermal treatment of Si-substituted hydroxyapatite obtained by hydrothermal technique of cuttlefish bones has not been reported in literature till now. The aim of the present study is to prepare Si-substituted hydroxyapatite by hydrothermal treatment of cuttlefish bones, Seppia Officinalis L, from Adriatic Sea. Additionally, structural characterization of the Si-substituted hydroxyapatite has been carried out.

2. MATERIALS AND METHODS

As the starting material peaces of native cuttlefish bones, Seppia Officinalis L, from Adriatic Sea were used. For hydrothermal treatment only the peaces, cut from internal cuttlebone matrix (lamellae spacing) were used, since by the pre-treatment at 350°C the

aragonite in external wall (dorsal shield) partially transforms into calcite. The content of aragonite ($CaCO_3$) in cuttlebones was determined by DTA-TG analysis. Small peaces of bones (about 2 cm^3) were put with the required volume of an aqueous solution of 0.6 M $NH_4H_2PO_4$ (Ca/P =1.67) in teflon lined stainless steel pressure vessel and sealed at 200°C for 24 hours in the electric furnace. The converted HA was washed with boiling water and dried at 110°C. Only completely converted cuttlefish bone into hydroxyapatite were used for further preparation of Si substituted hydroxyapatite. The Si substitution was performed hydrothermal (at 200°C for 24 hours) adding about 15 cm^3 solutions of $Si(CH_3COO)_4$ saturated with acetone, or aqueous solution of $Na_2Si_3O_7$, or tetraetoxysilane ($Ca_6H_2O_4Si$).

The conversion of hydrothermal transformation of the cuttlefish bone and the phase composition of the Si-converted HA samples were studied by: X-ray diffraction analysis (Philips PW 1820 counter difractometer with Cu Kα radiation) and Fourier transform infrared spectroscopy (FTIR- Bruker Vertex 70). The FTIR analysis was performed by attenuated total reflectance (ATR) spectroscopy for solids with a diamante crystal. Samples were scanned on resolution $4cm^{-1}$ with 16 scans.

3. RESULTS and DISCUSSION

3.1. X-Ray diffraction analysis

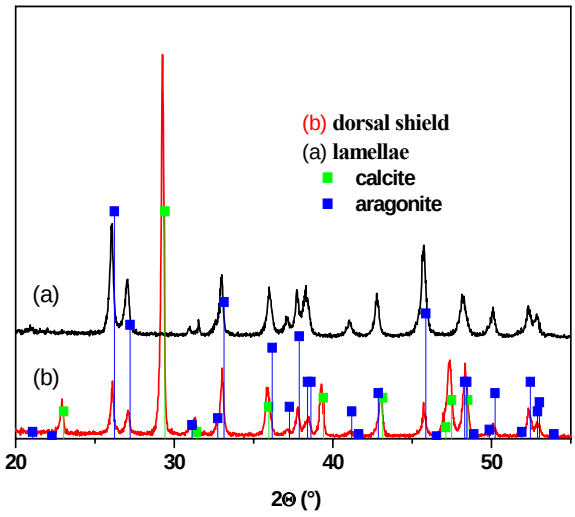


Fig 1. XRD patterns of (a) lamellae and (b) dorsal shield of cuttlefish bone heat-treated at 350°C for 3 hours.

Powder X-ray diffraction analysis (PXRD)of the internal lamellae part of bones have aragonitic structure even after heat treatment at 350°C for 3 hours, as seen on Fig 1, while the external wall (dorsal shield) partially transforms into calcite. Therefore for hydrothermal treatment only peaces of internal cuttlefish bone matrix (lamellae spacing) were used. As can be seen on Fig. 2 aragonite transforms rapidly into HA, and for complete transformation into HA at 200°C 24 hours were needed.

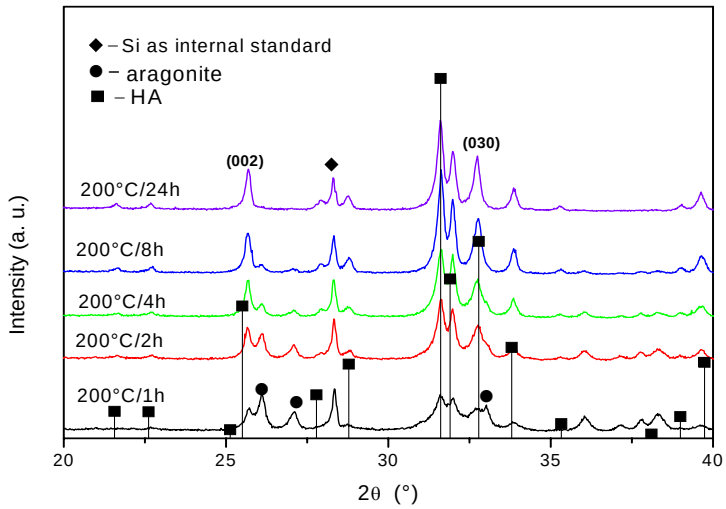


Fig. 2. XRD patterns of hydrothermal treated cuttlefish bone at 200°C at different times. For purpose of clarity the HA lines are not marked

HA with addition of TEOS; or calcium acetate, or sodium silicate were then hydrothermally treated at 200°C during 24 h washed with water and then analyzed by XRD. Si-substituted hydroxyapatite is compared with pure HA in Fig. 3.

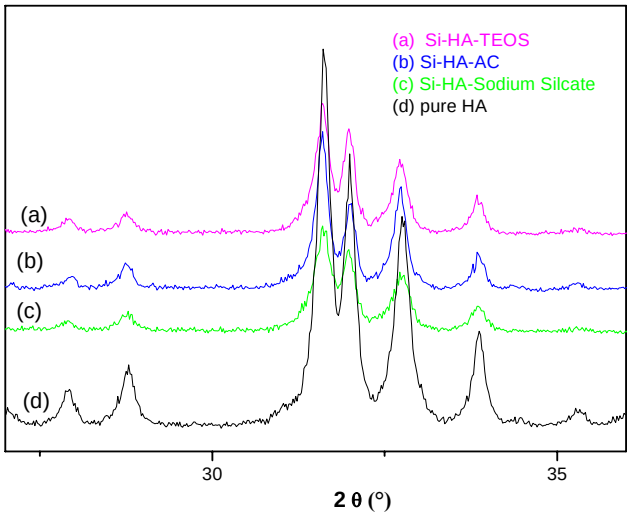


Fig. 3. XRD patterns of hydrothermal transformed Si-substituted HA (a) Si-HA-TEOS, (b) Si-HA-AC, (c) Si-HA-Sodium Silicate and (d) pure HA

The intensity of XRD pattern is the smallest by treatment of pure HA with TEOS as shown in Fig. 3. Unit cell parameters of Si-substituted HA are determined in the sample treated with TEOS using Si as internal standard. Silicon substitution results in a decrease of *a*-axis, and increase in the *c*-axis of the unit cell of hydroxyapatite as seen in Table 1.

Table 1. Lattice parameters of HA and Si-HA treated with TEOS

Sample	*a* /nm	c/nm
5 wt% Si (added as TEOS)	0.94182(3)	0.68937(3)
Pure HA	0.94259(3)	0.68898(2)

.

The evidence of incorporation of Si into the HA is obvious by measuring the unit cell parameters and is proposed by Gibson *et* al. [11]:

$$10Ca^{2+} + (6-x)\,PO_4^{3-} + x\,SiO_4^{4-} + (2-x)\,OH^- \rightarrow Ca_{10}(PO_4)_{6-x}(SiO4)_x(OH)_{2-x} \quad (1)$$

XRD analysis of patterns calcined at 1200°C (Fig. 4) shows the presence of tricalcium-phosphate as the result of system instability caused by Si–incorporation into hydroxyapatite and changing of Ca/P molar ratio. The samples with different wt% content of silicon were prepared in order to determine the effect of silicon ratio on stability of Si-HA. There is clearly seen that intensity of HA peaks reduce with silicon increase incorporated into Si-HA, and simultaneously increase the amount of TCP formed in the samples. It has to be mentioned that with Si increase also other phosphates occur in the system, most probable monetite, $CaHPO_4$; JCPDF 75-1520, and brushite $CaPO_3$ (OH) $2H_2O$; JCPDF 11-0293.

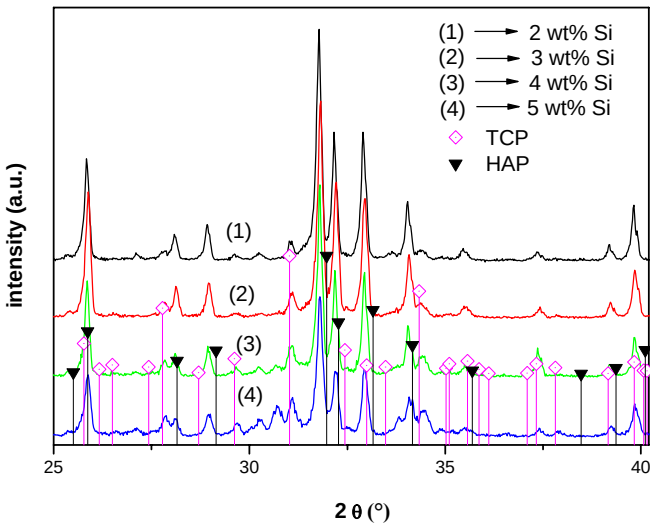


Fig. 4. XRD patterns of Si-HA samples with different wt% of silicon calcined at 1200°C

3.2. FT-IR spectroscopy

FTIR spectra were used to quantify the effect of the silicon substitution on the different functional groups, such as hydroxyl and phosphate groups of hydroxyapatite. Fig. 5. shows that the bands at 3571 and 631 cm^{-1} correspond to the stretching and vibrations modes, of hydroxyl groups, respectively. The doublet at 1471-1413 cm^{-1} is assigned to CO_3^{2-} groups. In the HA spectrum (spectrum (a) in Fig. 5) the intense bands at 1085, 1014 and 960 cm^{-1} correspond to P-O stretching vibration modes, whereas the doublet at 593-572 cm^{-1} corresponds to O-P-O bending mode, whose wavelengths are in accordance with the literature [12]. The additional band at about 872 cm^{-1} can be assigned to the SiO_4^{4-} groups [13]. The decrease in intensity of the peak in the FTIR spectra that corresponds to OH- groups on Si-HA at 630 cm-1 was expected since the substitution of phosphate groups for the silicate group leads to some loss of OH^- in order to maintain the charge balance.

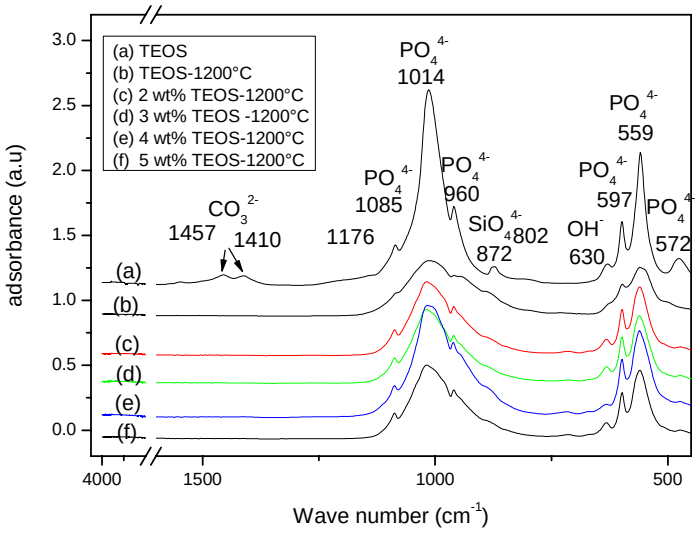


Fig. 5. FTIR spectra of (a) HA, (b) HA-1200°C, (c) 2 wt% TEOS-1200°C (d) 3 wt% TEOS-1200°C, (e) 4 wt% TEOS-1200 and (f) 5 wt% TEOS-1200 °C .

4. CONCLUSION

Hydroxyapatite and silicon substituted hydroxyapatite can be prepared by hydrothermal conversion of aragonite from cuttlefish bone. Incorporation of silicon into hydroxyapatite structure is successful and TEOS appears as the most suitable for in situ reaction of preparation of Si-HA. XRD diffraction and FTIR analysis confirmed substitution of PO_4^{3-} with SiO_4^{4-} groups. Incorporation of silicon results in removal of OH^- groups in order to maintain the charge balance, which causes the changes and defects in structure of HA. The heat-treatment of Si-substituted HA at about 1200°C partially transforms into tricalcium phosphate, however the greater amount of Si incorporation causes the appearance of other calcium phosphates, preferable monetite, $CaHPO_4$; JCPDF 75-1520, and brushite $CaPO_3$ (OH) $2H_2O$; JCPDF 11-0293.

5. ACKNOWLEDGMENTS

The financial support of the Ministry of Science, Education and Sport of the Republic of Croatia within the framework of the project No 125-1252970-3005. “Bioceramic, Polymer and Composite Nanostructured Materials” is gratefully acknowledged.

6. REFERENCES

1. Ducheyne P, Radin S, King L. *The effect of calcium-phosphateceramic composition and structure on in vitro behaviour*. I. Dissolution. J Biomed Mater Res 1993;**27**:25–34.

2. Schepers E, Declercq M, Ducheyne P, Kempeneers R. *Bioactive glass particulate material as a filller for bone lesions*. J Oral Rehab 1991;**18**: 439–52.

3. Porter A.E., Patel N., Skepper J.N., Best S.M., Bonfield W., Biomaterials 25 (2004) 3303..

4. LeGeros R.Z., Nature 206 (1965) 403.

5. Jha L.J. Best J.C., Knowles L., Rehman I., Santos, J.D., Bonfield W., J. Mat.Sc., Mater. 8 (1997) 185

6. Balas F., Perez-Pariente J., Vallwt-Regi M.; J Biomed. Mater. Res. 1 (2004) 133.

7.Carlisle E.M., Science 167 (1970) 179.

8. Tanizawa Y., Suzuki, J. Phosphorus Res. Bull. 4 (1994) 83.

9. Sugiyama K., Suzuki T., Satos T., Antifung Agents 23 (1995) 67.

10. Kim Y.H., Song H., Riu D.H., Current Appl. Phys. 5(2005) 538.

11. Gibson, I.R., Best, S.M., Bonfield: W., *J. Biomed. Mater. Res.* **4** (1994) 422.

12. Rehman I. and Bonfield w., J. Mater. Sci..: Mater. In Med. 8 (1997) 1.

13. NyQuist¸R.A., PutzigC.L. and Leugers M.A., Infrared and Raman Spectral Atlas of Inorganic Compounds and Organic Salts 3 (1995).

INFLUENCE OF CONVENTIONAL AND POWDER METALLURGY COLD WORK TOOL STEEL SUBSTRATES ON MICROSTRUCTURAL AND TRIBOLOGICAL PROPERTIES OF PVD HARD COATINGS

[1]P. Panjan, [2]Đ. Goršćak, [3]L. Ćurković, [4]M. Godec, [1]M. Čekada, [1]D. Kek Merl, [1]M. Panjan, [1]S. Paskvale

[1]Jožef Stefan Institute, Ljubljana, Slovenia
[2]Končar-Alati, Zagreb, Croatia
[3]University of Zagreb, Faculty of Mechanical Engineering and Naval Architecture, Zagreb, Croatia
[4]Institute of Metals and Technology, Ljubljana, Slovenia

Izvorni znanstveni rad / Original scientific paper

Abstract: It is well known that properties of hard coatings do not only depend on deposition process parameters (substrate temperature, ion bombardment during growth), but also critically depend on the tool material (composition, crystal structure and microstructure) and its pretreatment. It is thus important to choose the substrate material and its pretreatment very carefully. In this work, microstructural and tribological investigations of TiAlN-coated conventional and powder metallurgy cold work tool steel substrates (Vanadis 4, Vanadis 6, Sleipner, Vancron 40, D2, ASP30) are presented. Deposition system CC800/7 (CemeCon) equipped with four unballanced magnetron sputter sources was used for preparation of TiAlN hard coating.

In this paper, special emphasis is given on surface topography of uncoated and coated substrates and on the influence of tool steel substrate on microstructural and mechanical properties of hard coating. The topography of samples was analysed by optical microscope, field emission scanning electron microscope (SEM), atomic force microscope (AFM) and stylus 3D-profilometer.

Keywords: cold work tool steel, powder metallurgy steel, PVD hard coatings, microstructure, adhesion, hardness, surface topography

1 Introduction

In automotive and in other industries cold work steels are used for drawing, punching, blanking, fine blanking, shearing, cold forming, cold extrusion, cold forging, cold rolling and

powder pressing [1]. For all these applications high mechanical forces and sliding contact between the tool surface and the workpiece material are characteristic. In cold work machining, typical failure mechanisms of tools are: a) abrasive wear, b) plastic deformation, c) chipping/cracking, d) galling (built-up edge). However, the main problem with cold work is abrasive wear (scratching particles) and adhesive wear (micro-welds). Therefore there are high demands on tool hardness to enable wear resistance and resistance against plastic deformation. Therefore, tool material selection is the first and very important step in the successful design of such type of tools. In general the steels for cold work have a high carbon content and can be hardened to a very high hardness. In order to further improve the wear resistance, some of the cold work steels are highly alloyed, forming hard carbide particles in the matrix.

Besides conventional tool steels, powder metallurgy (PM) steels are also a very attractive material for such kind of applications. Powder steels have fine grain carbides (the average lateral size of carbides is 1–2 μm) uniformly distributed in the steel matrix. They are tougher than most conventional steels and therefore they are capable of machining new high strength materials.

The wear resistance of fully hardened steels can be further improved by various surface treatment techniques. The most advanced technique is deposition of a few μm thick PVD hard coating. However, the full benefits of hard protective coatings can be realised only if the coatings are supported by tool material of proper mechanical properties (high hardness and toughness) and microstructure [2-4]. Namely, the density and distribution uniformity of the carbides in steel affects the adhesion of hard coating. From the application point of view, the first demand regarding hard protective coatings is excellent adhesion to the tool material in order to withstand the high loads and shearing forces without chipping or peeling.

Beneficial influence on adhesion have only those carbides which have equal crystal structure as TiAlN hard coating (f.c.c.), while the lattice mismatch must be less then few percent. It is thus clear that the substrate surface structure is an important factor for the structure of deposited films.

Surface preparation of tools is also very important. Rough surface improves the adhesion by interlocking the depositing material with the substrate. Therefore from this point of view, some microscopic pits and hillocks would be beneficial. However, it should not be too rough, because the porosity of the coating increases due to geometrical shadowing of features on the substrate surface. High surface roughness also causes a higher coefficient of friction. Especially in the case of forming tools, the pick-up tendency can be reduced or avoided by making the chemical affinity of the counter surface low or by giving the tool surface a smooth topography. Namely, the workpiece material which adheres to any microscopic imperfections on the tool surface causes galling.

The in situ cleaning of the substrate surface by ion etching prior to the deposition is known to be essential for the coating adhesion and therefore the coating performance. Sputter etching not only influences the adhesion of the film, but also affects the nucleation and growth of the hard coating. The ion etching also alters the morphology on the micrometer and submicrometer scale. Therefore we must avoid too intensive ion etching.

In this study we selected six different tool steels, which were coated with TiAlN hard coating in the same batch. We analysed the coating microstructure on the fracture cross section as well as topography and mechanical properties.

2 Experimental

Standard laboratory tests were performed to investigate the performance of TiAlN hard coating on test tools made of six different tool steels: a cold work, high carbon, high chromium type tool steel D2 (hardened and tempered to 59 HRC), a Cr-Mo-V alloyed tool steel Sleipner (hardened and tempered to 61 HRC), Cr-Mo-V alloyed steel PM cold work tool steels Vanadis 4 and Vanadis 6 (hardened and tempered to 62 and 64 HRC, respectively), a Cr-Mo-W-V-N alloyed cold work PM tool steel Vancron 40 (hardened and tempered to 59 HRC), and PM Co-alloyed APS30 tool steel (hardened and tempered to 66 HRC). The steel samples were finally polished with diamond paste to R_a=10–14 nm, ultrasonically cleaned and degreased in bath of hot alkali solution, de-ionized water and then dried in hot air before mounting on the substrate holders. They were in situ cleaned by ion etching prior to coating deposition. The CemeCon CC800/7 sputtering system with four unballanced magnetron sources was used for deposition of TiAlN hard coatings. During substrate cleaning an RF bias was applied for 85 min (maximum RF power was 2 kW). During deposition process the substrate temperature was about 450 °C. The substrates undergo a two-axis planetary rotation.

Field emission scanning electron microscope was used for study of substrate surface morphology. Topography of uncoated and coated substrates as well as surface roughness were characterized by atomic force microcope (AFM) and 3D-stylus profilometer (Taylor Hobson Talysurf). Depth sensing indentation was used to evaluate the mechanical properties using a maximum load of 100 mN. Rockwell indenter and Revetest scratch tester was used for adhesion measurement. Five critical loads were considered for evaluation: Lc_3 (flaking at the scratch edge), Lc_4 (partial delamination of the coating), Lc_5 (total delamination of the coating), Lc(AE) (onset of acoustic emission) and Lc(F_t) (scratching force jump)

3 Results

3.1 Surface topography

The roughness of uncoated and coated substrate surface can be analyzed on several size scales [5]. While the macrofeatures (scratches, waviness and pin-holes) are mostly an inheritance from earlier grinding and polishing procedures, the morphology on micro- and submicroscale is a consequence of ion etching and deposition [6,7]. Some of the macrofeatures also originate from deposition process. They are caused by microparticles that flake during heating, etching and deposition from shields, rods, fixtures and heaters. All these surface irregularities increase the surface roughness and influence the tribological performance. Therefore a polishing treatment of coated tool surface is often used in order to reduce the material pick-up.

Fig. 1 shows backscattering micrographs of five different tool steel surfaces after polishing. The size and distribution of carbides is clearly visible. The composition of carbides was determined by EDX analysis. All PM tool steels show uniformly distributed carbides, which have a diameter of 1–2 μm. On the other hand D2, and Sleipner tool steels have much larger and nonuniformly distributed carbides.

Fig. 2a,b shows AFM images of polished ASP30 and D2 tool steel substrates. Small hillocks with a typical height in the range of 4–8 nm are visible. Their lateral dimensions are 1–2 μm and 5–15 μm for ASP30 and D2 tool steel, respectively. These dimensions

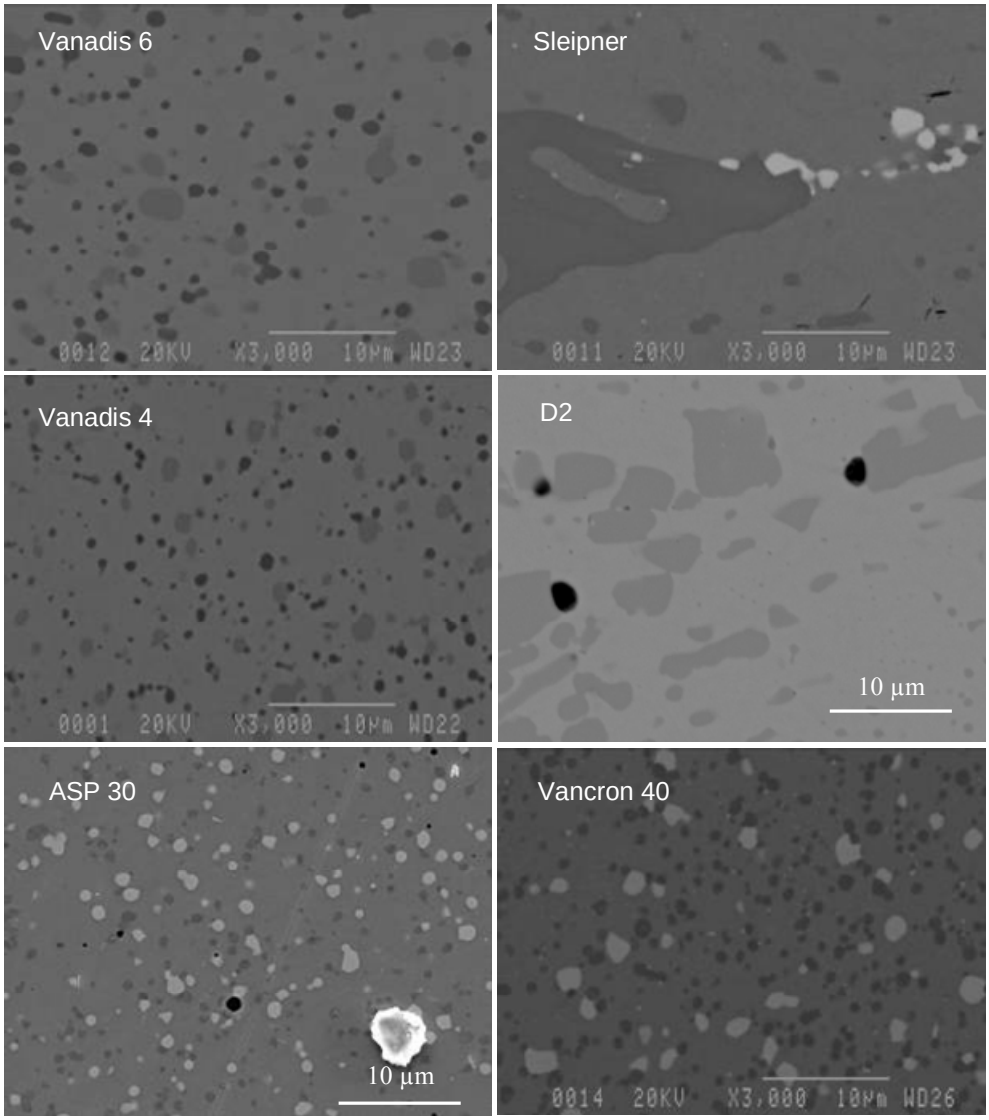


Fig. 1 SEM micrographs of a Vanadis 6, Vanadis 4, ASP30, Vancron 40, Sleipner and D2 substrate surfaces after polishing

correspond to size of carbides in ASP30 (VC and (Mo,W)C) and D2 (CrC). The height of hillocks depends on polishing time. After polishing, such hillocks were formed, while the hardness values of carbides are much higher (VC, (Mo,W)C and CrC have a hardness of 72–77 HRC, 82–84 HRC and 66–68 HRC, respectively) than the hardness of matrix (50–65 HRC). Therefore during polishing, the matrix was removed at a more rapid rate than the carbides. If the tool steel consists of two or more types of carbides (e.g. ASP30, then hillocks of various height can be observed on AFM image of steel surface.

AFM images of tool steel surface after ion etching show pronounced pits and hillocks **(**Fig. 2c,d). The reason for this effect is the fact that different carbides and the matrix have different sputtering rates. For example, the sputtering rate of (Mo,W)C is higher than that of the matrix, while the sputtering rate of CrC or VC is lower. After ion etching of D2 tool steel we observed large hillocks (their height is over 50 nm) at the position of CrC. Similar hillocks with typical height of about 60–90 nm were observed also on ASP steel at the position of VC, while pits with typical depth of about 60–80 nm were found at the position of (Mo,W)C.

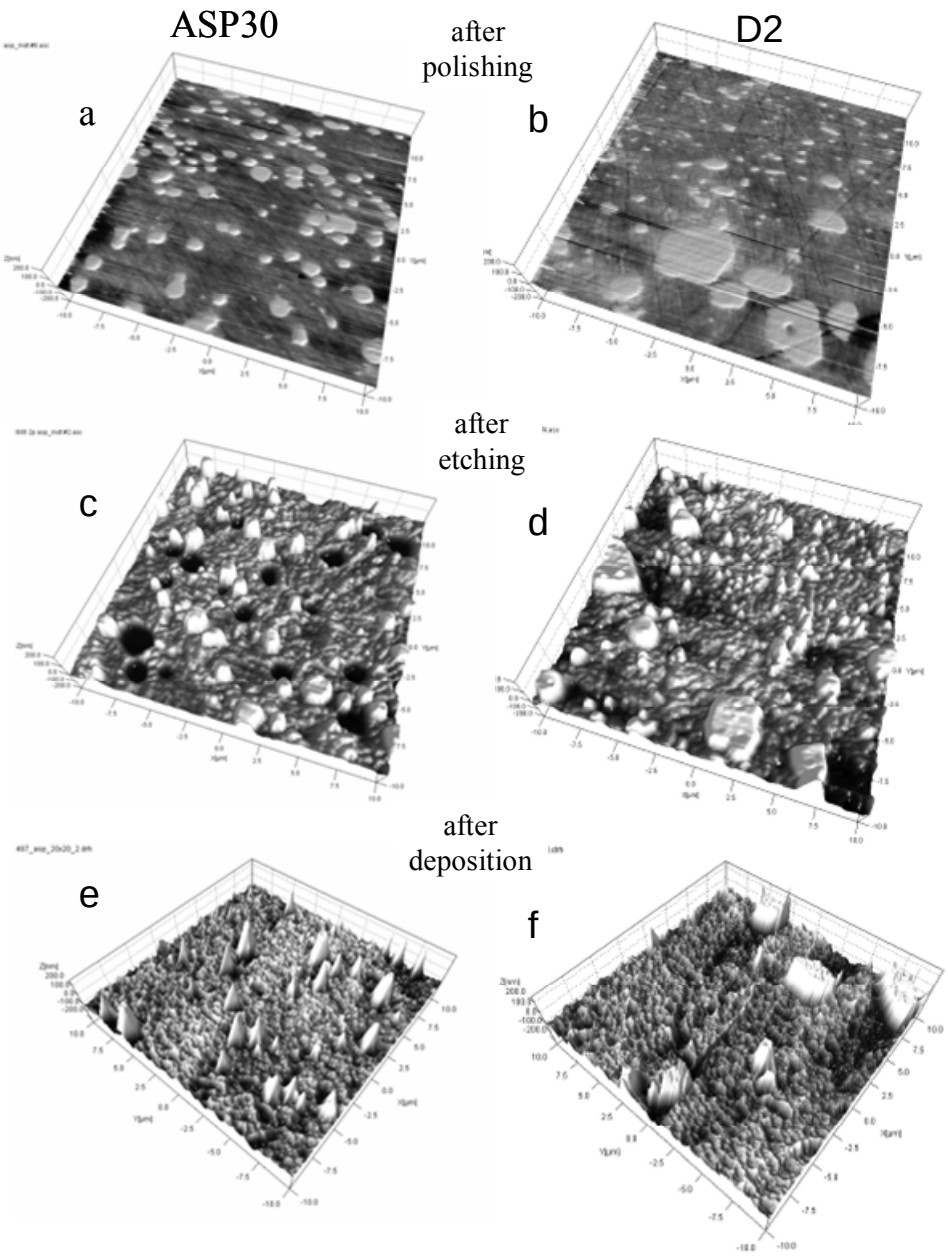


Fig. 2 AFM images of ASP30 (left) and D2 (right) substrate surfaces after polishing (a,b), ion etching (c,d) and after deposition of TiAlN hard coatings (e,f).

Surface morphology, which formed during the etching step due to preferential sputtering of various materials, was retained after deposition of hard coatings with standard thickness. The hillocks and pits at the position of carbides are clearly visible. After deposition the roughness of all substrates did not change substantially. We have to stress that during the roughness measurements we avoided the largest defects which appear during the deposition process (droplets and microparticles which are incorporated in the coating).

The surface topography of coated samples was analysed also by 3D-profilometer. Scan area of 10×10 mm and more was performed. Thus we obtained 3D-images of the coating surface on large scanning area with all the micrometer-sized details. From the 3D-image we estimated the surface density and the height distribution of the defects. We found that the density of defects depends strogly on the substrate type (Table 1). The average diameter of defects is larger for Vancron 40, D2 and Vanadis 6 tool steels than for ASP30, Sleipner and Vanadis 4.

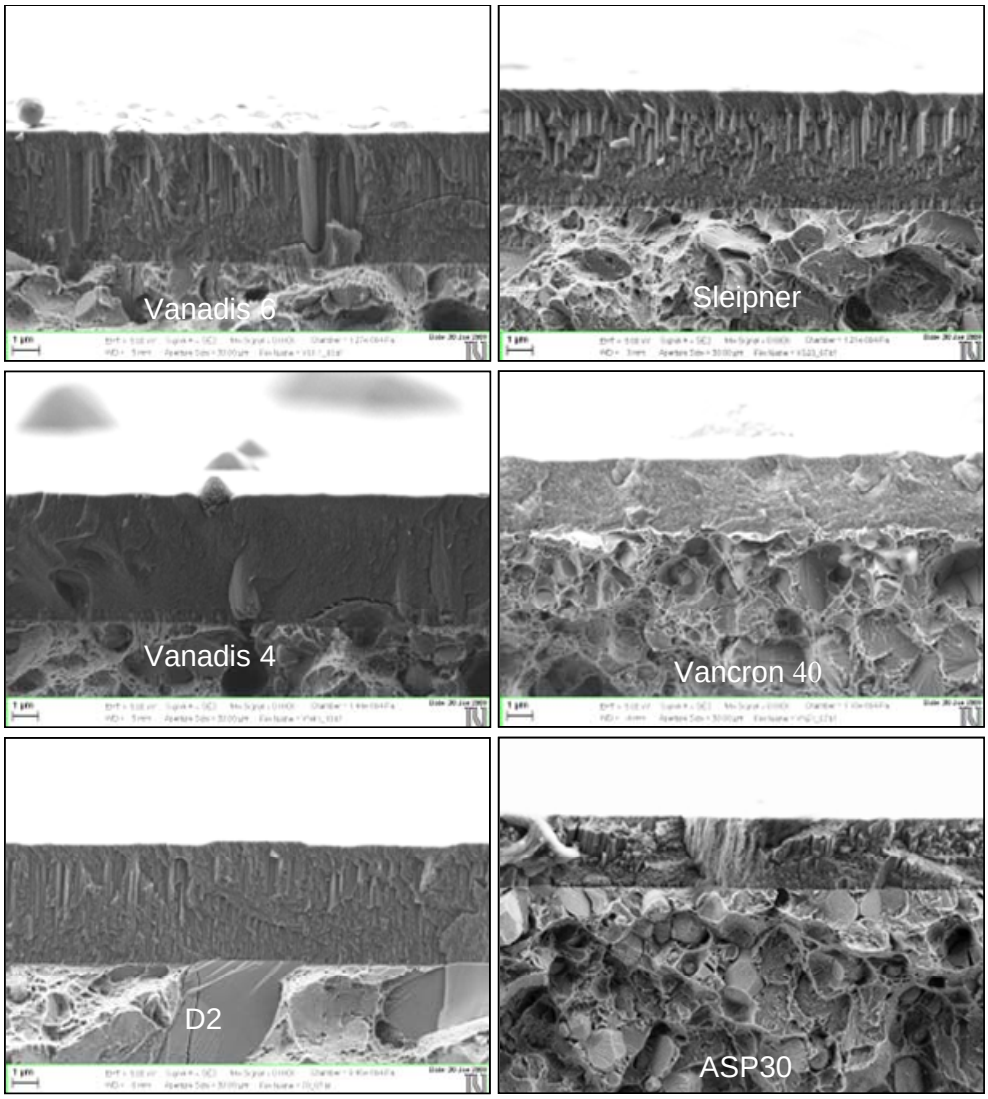


Fig. 3 Fractured cross-section of TiAlN coating on different tool stel substrates.

3.2 Coating microstructure

It is well known [8] that VC, but not $(Mo,W)_6C$ carbides have a large infuence on hard coating microstructure, while TiAlN can grow epitaxialy on the vanadium carbide phase due to a close structural matching (both of these phases have a f.c.c. crystal structure and the lattice mismatch is below 2 %). Such growth is not possible on the steel matrix, and on the $(Mo,W)_6C$ phase, because the structural mismatch is too large. Hard coatings with matching lattice structures have a higher adhesion. The sputter etching effect of substrate with different compositions was different. Therefore the fracture cross-section micrographs of TiAlN coating deposited on various substrates show different microstructure features (Fig. 3). It is much more fine grained and compact on the PM tool steel than on conventional substrates.

3.3 Mechanical properties

The results based on Rockwell adhesion test give limited but still useful information. The indentation on the ASP30 steel experienced the least damages, whereas on the D2 the damage was extensive. We estimated the level of damages (Table 1) from 1 (no damage) to 6 (extensive damages). The scratch test gives much more information. Some results of scratch test are presented in Table 1. The lowest critical loads were encountered at D2 steel, which is in accordance to the Rockwell results.

Depth sensing indentation was used to evaluate the mechanical properties. The maximum load was 100 mN. At 100 mN the highest hardness was obtained on ASP, Sleipner and Vancron 40 tool steels, while the lowest one on D2 and Vanadis 4 tool steels (Table 1). The hardness of TiAlN coating correlates with substrate hardness (see Table 1).

Table 1 Basic properties of tool materials and TiAlN (HRC-Rockwell hardness, S_a-surface roughness, HV-Vickers hardness, L_{c5}- total delamination of the coating, N-number of defects)

Sample	HRC	S_a (nm)	HV_{100mN}	HRC-adhesion	L_{c5} (N)	$N_{hillocks}$	$N_{craters}$
ASP30	66±1	68±12	3400±300	1	130±5	75	23
Vanadis 6	62,5±1	128±20	3267±300	3	120±5	592	168
Vanadis 4	59±1	144±20	2838±250	4	85±5	677	66
Vancron 40	62,5±1	144±20	3295±300	5	80±5	577	324
Sleipner	62±1	42±10	3395±300	2	116±5	247	30
D2	59±1	375±30	2740±250	6	100±5	1673	140

4. Conclusions

Based on the measurements of the mechanical properties of TiAlN hard coatings sputter deposited on 5 different tool steel substrates, it was found that the best adhesion was obtained for TiAlN/ASP30 combinations. The highest microhardness was also obtained for TiAlN/ASP30 combination. The most dense microstucture of TiAlN was observed on PM tool steels. Also the lowest number of defects (hillocks and craters) was found on TiAlN coating on ASP30 substrate.

Acknowledgements

This work was supported by the Slovenian Research Agency. It was done within the bilateral Slovene-Croatian project BI-HR/07-08-001.

References

[1] D. Goršćak, P.Panjan, M. Čekada, L. Ćurković, Surf. Eng. 2007, 23(3), 177

[2] M. Lattermann, A.P. Ehiasarian, J. Bohlmark, P.A.O. Persson, U. Helmersson, Surf. Coat. Technol. 2006, **200**, 6495

[3] C. Schonjahn, D.B. Lewis, W.D. Munz, I. Petrov, Surf. Eng. 2000, **16(2)**, 176

[4] "Handbook of hard coatings", Ed. R.F. Bunshah, Chapter 4, Noyes Publications, New Jersey, 2001, p. 146–149

[5] D.M. Matox, Surf. Coat. Technol. 1996, **81**, 8

[6] P. Panjan, D. Kek Merl, F. Zupanič, M. Čekada, M. Panjan, Surf. Coat. Technol. **202** (2008) 2302–2305

[7] M. Čekada, P. Panjan, D. Kek-Merl, M. Panjan, G. Kapun, Vacuum **82** (2008) 252–256

[8] U. Helmersson, M. Latterman, J. Bohlmark, A. Ehiasarian, J.T. Gudmundsson, Thin Solid Films 513 (2006) 1-24

UTJECAJ CITRATNIH OMEKŠAVALA NA TOPLINSKA SVOJSTVA KOMPOZITA POLI(L-LAKTID)/MLJEVENE KOŠTICE MASLINE

INFLUENCE OF CITRIC PLASTICIZERS ON THERMAL PROPERTIES OF POLY(L-LACTIDE)/OLIVE STONE FLOUR COMPOSITES

Sanja Perinović*, Branka Andričić, Tonka Kovačić, Vedrana Vučenović
Zavod za organsku tehnologiju, Kemijsko-tehnološki fakultet u Splitu, Teslina 10/V, 21000 Split, e-mail: sanja@ktf-split.hr

Izlaganje sa znanstvenog skupa / Conference paper

Sažetak: Cilj rada bio je pripremiti polimerne kompozite s poli(L-laktidnom) (PLLA) matricom te odrediti utjecaj dodataka na toplinska svojstva PLLA. Organsko punilo je brašno mljevenih koštica masline (OSF), a omekšavala su tributil citrat (TBC) i tributilacetil citrat (TBAC). Sadržaj punila je do 30 phr, a omekšavala do 20 phr i to u odnosu na PLLA. Polimerni kompoziti pripremljeni su u laboratorijskom vertikalnom dvopužnom ekstruderu, te prešanjem na injekcijskoj preši. Toplinska svojstva dobivenih materijala određena su diferencijalnom pretražnom kalorimetrijom (DSC). Utvrđeno je da staklište (*Tg*), talište (*Tm*) i temperatura hladne kristalizacije (*Tcc*) PLLA ne ovise o sadržaju punila. Sniženje tališta u PLLA kompozitima omekšanim TBC-om i TBAC-om nešto je veće nego kod samo omekšanog PLLA, ali nedovoljno da bi se zaključilo o sinergističkom učinku punila i omekšavala. Svaki od dodataka pojedinačno, tj. OSF, TBC i TBAC, povećava kristaličnost PLLA s 14% na 24…29%, dok se u omekšanim kompozitima kristaličnost povećava iznad 40%. Rezultati pokazuju da je utjecaj TBC-a i TBAC-a na toplinska svojstva PLLA kompozita podjednak.

Ključne riječi: PLLA kompoziti, mljevene koštice maslina, citratna omekšavala, diferencijalna pretražna kalorimetrija

Abstract: The thermal properties of PLLA composites containing olive stone flour (OSF) and plasticizers such as tributyl citrate (TBC) and tributylacetyl citrate (TBAC) were investigated. The content of OSF was up to 30 phr and the plasticizers up to 20 phr relative to PLLA. Polymer composites were prepared on the laboratory vertical twin-screw extruder and the injection molding machine and characterized by differential scanning calorimetry (DSC). It was determined that the glass transition temperature (T_g), the melting temperature (T_m) and the temperature of cold crystallization (*Tcc*) of PLLA are independent regarding to the content of organic filler in the samples. The melting point depression of PLLA composites plasticized with TBC or TBAC is higher than that of plasticized PLLA without the filler, but there is not enough evidence of a synergistic effect of the filler and the plasticizer. Each of the additives: OSF, TBC and TBAC, individually, increases crystallinity of PLLA from 14% to 24…29%, while in plasticized PLLA composites it increases above 40%. From the results it is evident that used plasticizers exhibit almost the same affect on the thermal properties of PLLA.

Keywords: PLLA composites, olive stone flour, citric plasticizers, differential scanning calorimetry

Uvod:

Porastom mase nerazgradljivog polimernog otpada i njegovog štetnog utjecaja na okoliš raste i interes za proizvodnjom biorazgradljivih polimera. Biorazgradljivi polimeri imaju svojstva slična polimerima dobivenim iz petrokemikalija, nisu biorazgradljivi tijekom uporabe a nakon uporabe mogu se razgraditi na niskomolekulske spojeve. Imaju veliku primjenu u medicini i/ili kao ekološki polimeri.U grupu biorazgradljivih polimera sa takvom dvojnom funkcijom ubraja se i polilaktid (PLLA). PLLA je biorazgradljiv, termoplastičan, alifatski poliester proizveden iz obnovljivih sirovina (šećerna trska, kukuruzni škrob itd.). Razgradljiv je u ljudskom tijelu i u okolišu, a toksičnost produkata razgradnje je vrlo niska[1].

Iako je interes velik, godišnja proizvodnja u svijetu sintetskih biorazgradljivih polimera manja je od očekivane, a osnovni razlog su visoki troškovi proizvodnje. Uvođenjem različitih punila, a posebice punila iz obnovljivih izvora može se sniziti cijena polimernih materijala uz zadržavanje potpune biorazgradljivosti na kraju životnog ciklusa[1], te poboljšati neka mehanička i termomehanička svojstva osnovnog materijala[2,3]. Organska punila predstavljaju vrlo interesantnu alternativu anorganskim jer omogućavaju proizvodnju jeftinijih materijala koji su manje štetni za okoliš. Ipak, organska punila ne koriste se često u polimernoj industriji, zbog slabe disperzije u polimernoj matrici i slabe adhezije s matricom.[2] Kao organsko punilo može se upotrijebiti škrob[4], drvno brašno[4], vlakna jute[4], vlakna ananasa[4], brašno pšenične slame[4], bambusova vlakna,[4] te mljevene koštice maslina. Koštice maslina dobiju se iskoštavanjem maslina ili su dio komine koja zaostaje u proizvodnji maslinova ulja. Koštice se usitnjavaju do čestica prosječnog promjera 315 μm. Brašno koštica masline spada u skupinu organskih punila i sastoji se od otprilike 8% lignina, 26% hemiceluloze i 66% celuloze.[2]

Osim visoke cijene, nedostatak biorazgradljivih polimernih materijala je mala mehanička čvrstoća i fleksibilnost. Dodatkom omekšavala smanjuje se viskoznost, modul elastičnosti i temperatura stakliša (T_g) polimernih materijala čime oni dobivaju željenu fleksibilnost. Učinkovita omekšavala poli(L-laktida) su različiti esteri limunske kiseline (citrati), koji su biorazgradljivi i neškodljivi što ih uvelike čini zanimljivim u različitim poljima primjene.[5] U mnogim radovima uz citrate istraživani su poli(etilen glikol)[6], triacetin,[6] oligomerne laktidne kiseline[7], glicerol[7] itd.

Cilj ovog rada bio je pripremiti PLLA materijal s različitim sadržajem mljevenih koštica maslina, tributil citrata (TBC) i tributilacetil citrata (TBAC), te odrediti utjecaj tih dodataka na toplinska svojstva PLLA kompozita.

Eksperimentalni dio:

Za pripremu uzoraka upotrebljen je PLLA u granulama BIOMER L9000, $M_v \cong 58700$ $gmol^{-1}$,[8] (BIOMER, Njemačka), tributil citrat, tributilacetil citrat (Merck KgaA, Njemačka) i mljevene koštice maslina JELUXYL OM 3000 (Jelu-Werk, Njemačka), promjera čestica manjih od 110 mm. PLLA je omekšan s 10 i 20 phr TBC-a odnosno TBAC-a. Neomekšanom i omekšanom PLLA-u dodano je zatim 5, 10, 15, 20, 25 i 30 phr punila (u odnosu na PLLA).

Priprema polimernih kompozita provedena je u laboratorijskom vertikalnom dvoopužnom ekstruderu (XPLORE, Nizozemska), a polimerni izradci dobiveni su injekcijskim prešanjem (XPLORE, Nizozemska). Optimalni uvjeti rada bili su: temperatura preradbe 180 °C (temperatura 6 grijaćih zona ekstrudera, struja dušika), broj okretaja pužnih vijaka 70 o/min, temperatura prihvatnog cilindra 180 °C i temperatura kalupa injekcijske preše 25 °C.

Analiza toplinskih svojstava dobivenih uzoraka provedena je diferencijalnim pretražnim kalorimetrom, DSC-4 (Perkin-Elmer, USA), zagrijavanjem uzoraka u temperaturnom području od 30…200 ˚C, brzinom od 10 ˚C/min u struji dušika (50 ml/min). Da bi se izbjegao utjecaj prethodne toplinske i mehaničke obrade uzorci su najprije zagrijani

do 200°C, (RUN 1), ohlađeni na 30°C brzinom od 10°C / min (RUN 2) i opet zagrijani na 200 °C (RUN 3). Iz DSC krivulja određena su toplinska svojstva PLLA. Iz prvog zagrijavanja određena je temperatura hladne kristalizacije (*Tcc*), kristalizacija prije tališta (*Tpc*), talište (*Tm*), entalpija hladne kristalizacije (Δ*Hcc*), entalpija kristalizacije prije taljenja (Δ*Hpc*), entalpija taljenja (Δ*Hm*). Iz drugog zagrijavanja (RUN 3) određeno je staklište (*Tg*) i promjena specifičnog toplinskog kapaciteta u staklištu (Δ*Cp*). *Tg* je određen iz polovine vrijednosti staklastog prijelaza dok ostale temperature predstavljaju točku u kojoj se tangenta sječe sa baznom linijom.

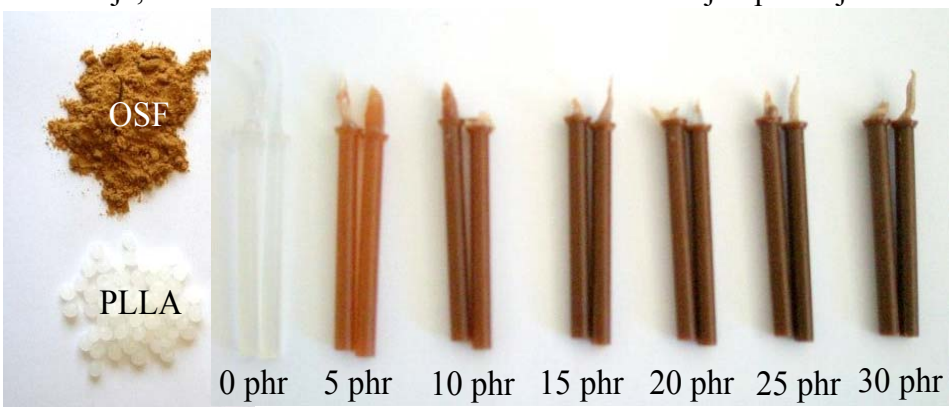
Udjel kristalične faze u PLLA (X_c) izračunat je prema izrazu:[9]

$$X_c(\%)=\frac{(\Delta H_m+\Sigma\Delta H_c)}{(\Delta H_{100\%}\times w_{PLLA})}\times 100$$

gdje je:
ΔHm - entalpija taljenja PLLA / Jg^{-1}
ΔHc - entalpija kristalizacije PLLA / Jg^{-1}
$\Delta H_{100\%}$ - entalpija taljenja 100% kristalnog PLLA (93 Jg^{-1})
w_{PLLA} - maseni udio PLLA

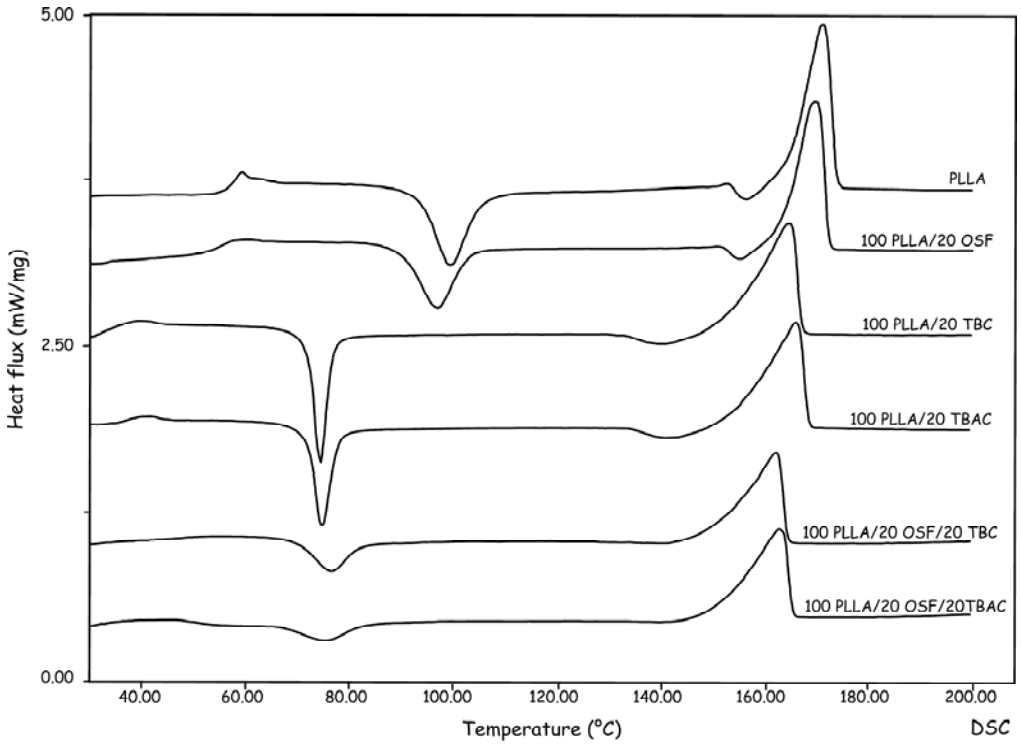
Rezultati i rasprava:

Na slici 1 prikazane su polazne komponente (PLLA i OSF) te isprešani kompoziti s različitim dijelovima punila. Obojenost otpresaka mijenja se, ovisno o sadržaju punila, od bijele do smeđe boje, a dodatak omekšavala olakšava ekstrudiranje i prešanje PLLA.



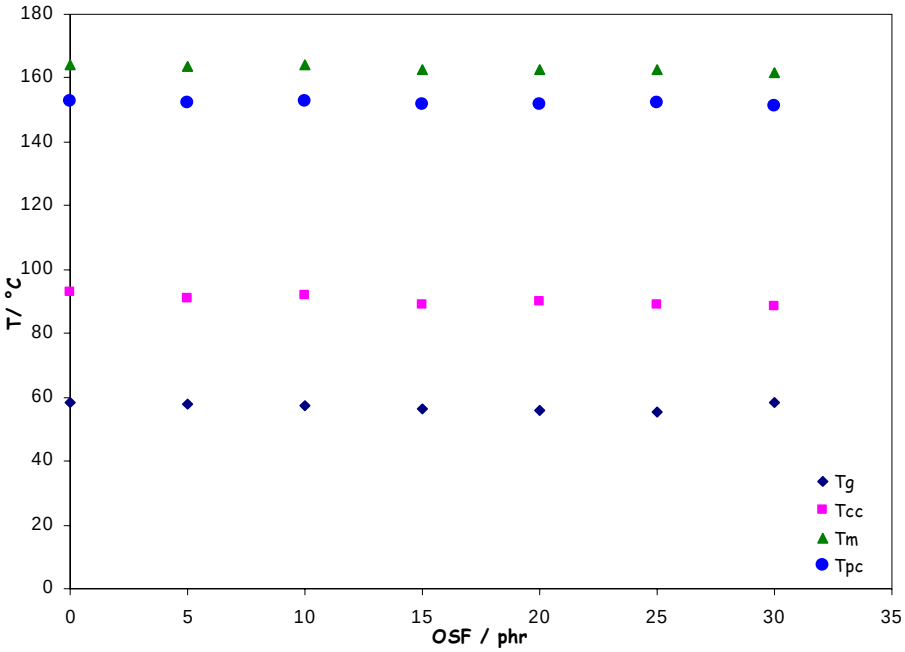
Slika 1. Čisto brašno koštica masline (OSF), PLLA i isprešani uzorci kompozita sa različitim dijelovima OSF

Analizom DSC krivulja od kojih su neke prikazane na slici 2, utvrđeno je da je PLLA kristalast polimer, sa staklištem pri 58 °C i talištem pri 164 °C. Toplina taljenja je 44,8 Jg^{-1} iz čega slijedi da je udjel kristalične faze 14%. Tijekom zagrijavanja, nakon staklišta dolazi do hladne kristalizacije pri 95 °C i kristalizacije prije tališta pri 153 °C.



Slika 2. DSC krivulje kompozita različitog sastava

Utjecaj punila na temperature prijelaza PLLA prikazan je na slici 3. Vidljivo je da punilo nema utjecaj na *Tg*, *Tcc*, *Tpc* i *Tm* PLLA. Promjene entalpija kristalizacije tijekom zagrijavanja vjerojatno su rezultat djelovanja punila kao nukleacijskog agensa, ali mogu biti i rezultat promjene kristalične strukture polimerâ, pa tako i PLLA.[10] Izgled DSC krivulja se u odnosu na čisti PLLA bitno ne mijenja.



Slika 3. Ovisnost stakliša, temperature hladne kristalizacije, temperature prije taljenja i tališta PLLA u PLLA/OSF kompozitima o sadržaju OSF-a

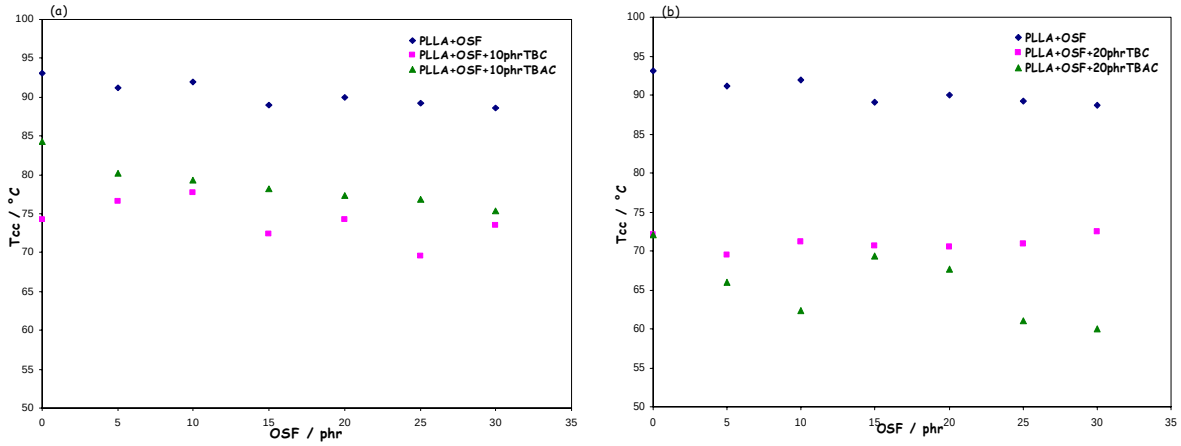
U tablici 1 prikazan je utjecaj omekšavala na toplinska svojstva čistog PLLA. Dodatkom omekšavala (TBC ili TBAC) *Tg* se snižava ispod temperaturnog područja rada DSC-4 i ne može se odrediti, ali se u pravilu povećanjem sadržaja pomiče k nižim temperaturama. Ostale karakteristične temperature prijelaza (*Tcc*, *Tpc*, *Tm*) omekšanog PLLA također se snižavaju dodatkom omekšavala. U prisustvu omekšavala temperaturno područje hladne kristalizacije se sužava i pomiče k nižim temperaturama iz čega se može zaključiti da omekšavalo također djeluje kao nukleacijsi agens jer povećava pokretljivost molekulskih lanaca amorfnog dijela kristalastog polimera. Dodatkom omekšavala širi se područje kristalizacije prije taljenja i povećava pripadajuća entalpija (slika 2, tablica 1).

Tablica 1. Rezultati DSC analize neomekšanog PLLA i omekšanog PLLA

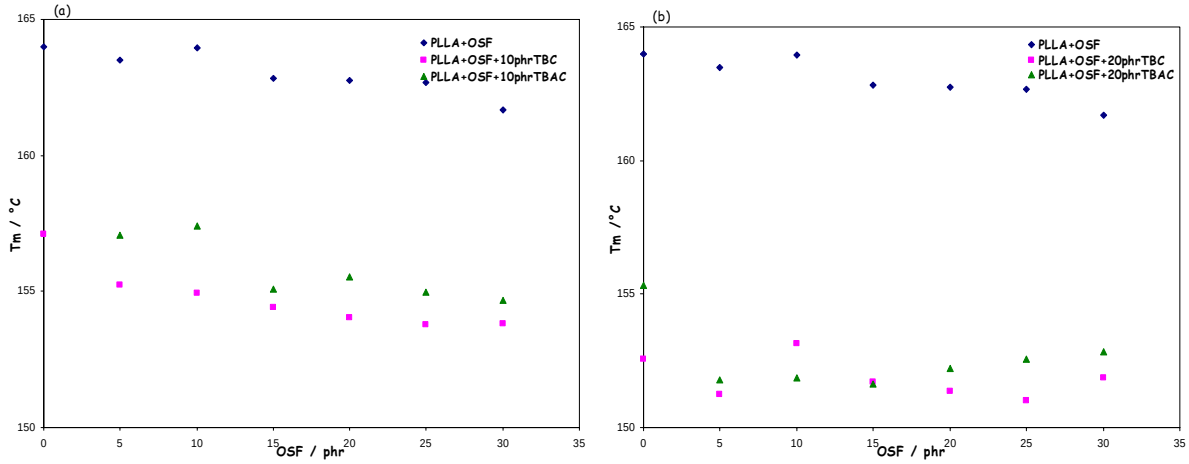
Sastav / phr	**Tg/ °C**	**ΔCp/ $Jg^{-1}°C^{-1}$**	**Tcc/ °C**	**ΔHcc/ Jg^{-1}**	**Tpc/ °C**	**ΔHpc/ Jg^{-1}**	**Tm/ °C**	**ΔHm/ Jg^{-1}**
PLLA	58	0,3003	93	-29,0	153	-2,6	164	44,7
PLLA/TBC								
100 / 10	-	-	74	-19,5	140	-2,5	157	46,3
100 / 20	-	-	72	-22,0	133	-3,4	153	45,9
PLLA/TBAC								
100 / 10	-	-	84	-24,4	143	-3,5	165	43,9
100 / 20	-	-	72	-20,2	135	-3,7	155	42,1

Analizom omekšanih PLLA/OSF kompozita s TBC-om ili TBAC-om nije uočena značajna razlika između navedenih omekšavala, što se vidi iz DSC krivulja na slici 2. U prisustvu obaju omekšavala uočava se pomak temperature kristalizacije i tališta prema nižim vrijednostima kao što je bio slučaj i kod omekšanog PLLA. Intenzitet pikova hladne kristalizacije se smanjuje, te se ne uočava kristalizacija koja prethodi taljenju. Istovremeni dodatak punila i omekšavala rezultirao je na neki način sinergističkim djelovanjem.

Utjecaj omekšavala i punila na *Tcc* i *Tm* PLLA/OSF kompozita prikazan je na slikama 4 i 5. Promjena, odnosno snižavanje *Tcc* i *Tm* u omekšanim PLLA/OSF kompozitima rezultat je uglavnom dodatka omekšavala i tek se neznatno snižavaju povećanjem sadržaja OSF.



Slika 4. Ovisnost Tcc o sadržaju TBC(TBAC) u omekšanim PLLA/OSF kompozitima: (a) 10 phr TBC(TBAC), (b) 20 phr TBC(TBAC)



Slika 5. Ovisnost Tm o sadržaju TBC(TBAC) u omekšanim PLLA/OSF kompozitima: (a) 10 phr TBC(TBAC), (b) 20 phr TBC(TBAC)

Svaki od ovih dodataka (OSF, TBC i TBAC), pojedinačno povećava kristaličnost PLLA s 14% na 24…29%. U kompozitima gdje su prisutni OSF i TBC(TBAC) kristaličnost doseže još veće vrijednosti, tablica 3.

Tablica 3. Kristaličnost PLLA kompozita određena na temelju rezultata DSC analize

Sastav / phr PLLA/OSF/TBC	**X_c / %**
100 / 0 / 0	14
100 / 5 / 0	19
100 / 10 / 0	15
100 / 15 /0	18
100 / 20 / 0	20
100 / 25 / 0	20
100 / 30 / 0	24
100 / 0 / 10	29
100 / 0 / 20	26
PLLA/OSF/10TBC	
100 / 5 / 10	24
100 / 10 / 10	25
100 / 15 / 10	25
100 / 20 / 10	27
100 / 25 / 10	32
100 / 30 / 10	29
PLLA/OSF/20TBC	
100 / 5 / 20	32
100 / 10 / 20	35
100 / 15 / 20	37
100 / 20 / 20	35
100 / 25 / 20	32
100 / 30 / 20	37

Sastav / phr PLLA/OSF/TBAC	**X_c / %**
100 / 0 / 0	14
100 / 5 / 0	19
100 / 10 / 0	15
100 / 15 /0	18
100 / 20 / 0	20
100 / 25 / 0	20
100 / 30 / 0	24
100 / 0 / 10	19
100 / 0 / 20	24
PLLA/OSF/10TBAC	
100 / 5 / 10	21
100 / 10 / 10	21
100 / 15 / 10	22
100 / 20 / 10	20
100 / 25 / 10	23
100 / 30 / 10	25
PLLA/OSF/20TBAC	
100 / 5 / 20	31
100 / 10 / 20	39
100 / 15 / 20	46
100 / 20 / 20	45
100 / 25 / 20	42
100 / 30 / 20	44

Vidi sa da kristaličnost raste povećanjem sadržaja i jednog i drugog omekšavala u kompozitima. Ova pojava može se objasniti i naknadnom hladnom kristalizacijom tijekom stajanja (starenja) zbog temperatura staklastog prijelaza bliskih sobnoj temperaturi, pri čemu se volumen amorfne faze smanjuje, a kristalizacija prisiljava omekšavalo na migraciju[11]. Porast kristaličnosti dodatkom punila rezultat je činjenice da se punila ponašaju kao nukleacijski centri.[2] Čini se da pri manjem sadržaju omekšavala (10 phr) veći utjecaj na kristaličnost ima TBC, a pri većem (20 phr) veći je utjecaj TBAC-a.

Nepravilnosti u rezultatima, tj. osipanje rezultata, vjerojatno su posljedica neravnomjerne disperzije punila unutar matrice polimera zbog načina preradbe i/ili slabe adhezije između polarnog punila i nepolarne matrice. Poboljšanje disperzije punila i adhezije između punila i matrice može se postići odgovarajućim kompatibilizatorom.

Zaključak:

Optimalni uvjeti ekstruzije PLLA kompozita bili su 180°C i broj okretaja pužnih vijaka od 70 o/min. Obojenost ekstrudata mijenja se sa povećanjem sadržaja punila od bijele do smeđe boje.

Staklište, talište i temperatura hladne kristalizacije PLLA u uzorcima ne ovisi o sadržaju punila.

U PLLA/OSF kompozitima omekšanim TBC-om i TBAC-om sniženje tališta je nešto veće nego kod samo omekšanog PLLA, ali nedovoljno da bi se zaključilo o sinergističkom učinku punila i omekšavala.

Svaki od dodataka OSF, TBC i TBAC, pojedinačno, povećava kristaličnost PLLA s 14% na 24…29%, dok u uzorcima gdje su prisutni i OSF i TBC(TBAC) kristaličnost se povećava iznad 40%.

Analizom rezultata vidi se da ne postoji značajna razlika u utjecaju TBC-a i TBAC-a na toplinska svojstva PLLA kompozita.

Literatura:

1. Y. Ikada, H. Tsuji, *Macromol. Rapid Comm.* **21** (2000) 117-132
2. F. P. La Mantia, N. Tzankova Dintcheva, M. Morreale, *Workshop on Recycling of Polymeric Materials*, 3 i 4. 07. 2003., Karlsruhe, Njemačka, Zbornik radova, A2-1.
3. M. S. Huda, L. T. Drzal, M. Misra, A. K. Mohanty, *J. Appl. Polym. Sci.* **102** (2006) 4856–4869
4. L. Averous, N. Boquillon, Carbohydrate Polymers **56** (2004) 111–122
5. L. V. Labrecque, R. A. Kumar, V. Dave´, R. A. Gross, S. P. Mccarthy, *J. Appl. Polym. Sci.* **66** (1997) 1507-1513
6. Z. Kulinski, E. Piorkowska, *Polymer* **46** (2005) 10290–10300
7. N. Ljungberg, B. Wesslen, *J. Appl. Polym. Sci.* **86** (2002) 1227–1234
8. M. Erceg, T. Kovačić i I. Klarić, *Matrib 2003.*, 26.-28.06.2003. V. Luka, Zbornik radova, str. 33-37.
9. T. Ke, X. Sun, *J. Appl. Polym. Sci.* **81** (2001) 3069-3082
10. M. L. Di Lorenzo, *J. Appl. Polym. Sci.* **100** (2006) 3145-3151
11. N. Ljungberg, B. Wessle´n, *Polymer* **44** (2003) 7679–7688

OTPORNOST NA ABRAZIJSKO TROŠENJE KERAMIČKIH PREVLAKA NA ALUMINIJSKIM PJENAMA

ABRASION RESISTANCE OF CERAMIC COATINGS ON ALUMINIUM FOAMS

Denis Prusac, Tehnička škola Zadar, 23000 Zadar, Nikole Tesle 9c
Krešimir Grilec, Sveučilište u Zagrebu, Fakultet strojarstva i brodogradnje, Ivana Lučića 5, 10000 Zagreb

Izvorni znanstveni rad / Original scientific paper

Sažetak:

U radu su ispitivane dvije različite kvalitete, tj. različite poroznosti aluminijskih pjena, AlSi10, koje su proizvedene u Laboratoriju za nemetale, FSB. Na epruvetama tih pjena postupkom plamenog naštrcavanja nanesene su tri različite vrste prevlaka, i to:

METACERAM 28030 (oksidno-keramički prašak na bazi Al_2O_3),
METACERAM 28085 (oksidno-keramički prašak na bazi ZrO_2),
METACERAM 28095 (metalni prašak na bazi molibdena).

Tako pripremljenim epruvetama ispitivana je otpornost na abrazijsko trošenje u Laboratoriju za tribologiju, Zavoda za materijale, FSB.

Pokazalo se da su utjecajni faktori primjenjena sila i vrsta sloja.
Ključne riječi: metalne pjene, oksidno – keramičke prevlake, plameno naštrcavanje, abrazija

Abstract:

The work studies two different qualities, i.e. different porosities of aluminium foams, AlSi10, which have been produced at the Laboratory for non-metals, Faculty of Mechanical Engineering and Naval Architecture. Three different types of coating were applied on the test specimens of those foams by flame spraying, which are:

METACERAM 28030 (Al_2O_3- based oxide ceramic powder),
METACERAM 28085 (ZrO_2 - based oxide ceramic powder),
METACERAM 28095 (molybdenum – based metal powder).

The specimens prepared in this manner were tested for resistance to abrasive wear at the Laboratory of Tribology, Department for Materials, Faculty of Mechanical Engineering and Naval Architecture.

It has been shown that influencing factors include the applied force and the type of layer.
Key words: metal foams, oxide ceramic coatings, flame spraying, abrasion

1. UVOD

Metalne pjene predstavljaju relativno novu vrstu i oblik materijala koji se razvijaju na osnovu oponašanja strukture i svojstava prirodnih ćelijastih materijala kao što su: drvo, kosti, koralji, pčelinje saće, i sl. Njihova najvažnija svojstva temelje se na vrsti materijala stijenke ćelija, obliku ćelija (otvorene ili zatvorene) i procesu proizvodnje kojim se dobijaju, [1].

U odnosu na druge konstrukcijske materijale, metalne pjene imaju sljedeće prednosti: mala gustoća (relativna gustoća ρ/ρs – omjer gustoće pjene i gustoće metala), prilagodljiva toplinska svojstva (ovisno o strukturi), vatrootpornost, dobra električna svojstva, izuzetno prigušenje energije udara, vibracija i zvuka, relativno visoka krutost sendvič-konstrukcija s jezgrom od metalne pjene, itd., [1].

U ovom radu proučavat će se aluminijske metalne pjene na koje će se plamenim naštrcavanjem nanositi slojevi oksidnih keramika i prevlake od Mo. Njihova uloga će biti povišenje površinske tvrdoće uz istovremeno povećanje otpornosti na trošenje. Zadatak je:

- ispitati otpornost na abrazijsko trošenje prevlaka (oksidne keramike Al_2O_3, ZrO_2 i prevlaka od Mo), nanesenih naštrcavanjem plamenom na metalne pjene dvije različite poroznosti.
- nagovijestiti nove mogućnosti primjene aluminijskih pjena zaštićenih prevlakama.

2. EKSPERIMENTALNI DIO

Početne sirovine za proizvodnju metalnih pjena mogu biti u obliku taljevine ili praha. Samo upjenjavanje materijala uvijek se događa iz tekuće faze tako da se i prah povišenjem temperature dovodi u tekuću fazu. Metalne pjene mogu se proizvesti iz gotovo svih vrsta metala koji postoje u obliku praha. Danas su najčešće dostupne metalne pjene na bazi aluminija i nikla. Kombinacijom više metala može se dobiti širok raspon svojstava. Jedan od češćih načina proizvodnje metalnih pjena je taj da se pjena oblikuje u rastaljenoj fazi. Mješavina rastaljenog praha i agensa (TiH_2) zagrijava se pri čemu se oslobađaju mjehurići u taljevini i stvara pjena. Time se može utjecati na oblik, veličinu i stupanj otvorenosti ćelija te na relativnu gustoću (ρ/ρ_s).

ρ – gustoće metalne pjene

ρ_s – gustoća neporoznog materijala

Njime je proizvedena i legura AlSi10 koju će se koristiti za izradu uzoraka.

Tehnologija korištena za izradu uzoraka je "Nastajanje pjene plinom oslobođenim raspadom čestica agensa u polukrutoj fazi", [2]. Korištena je elektrootporna peć snage 2,5 kW, koja se nalazi u Laboratoriju za nemetale, FSB Zagreb (slika1.).



Slika 1. Peć za proizvodnju pjena

Prekursor (u ovom slučaju AlSi10) reže se na komade i stavlja u kalup (slika 2.).



Slika 2. Punjenje kalupa prekursorom

Potrebno je dobiti aluminijsku pjenu različitih poroznosti. Poroznost ovisi o količini prekursora (manje prekursora - veća poroznost, više prekursora - manja poroznost).

U ovom slučaju masa prekursora za uzorak U_1 je 440 g što je 35,9 % volumena uzorka, a volumen šupljina je 64,1 % volumena uzorka (slika 3.). Masa prekursora za uzorak U_2 je 660 g, 53,9 % volumena uzorka, volumen šupljina je 46,1 % (slika 4.).

Kalup se puni prekursorom, zatvara i steže da ne dođe do istjecanja prilikom upjenjavanja. Tako pripremljen kalup stavlja se u prethodno zagrijanu peć (800 °C), gdje se zagrije na temperaturu između solidus i likvidus temperature legure. To treba obaviti što je moguće brže da pad temperature u peći bude minimalan. Izradak je gotov kada se na otvoru za izlaz plinova pojavi prva kuglica taljevine, nakon čega slijedi vađenje kalupa iz peći i intenzivno hlađenje vodom, čime se pjena stabilizira.



Slika 3. Uzorak U_1



Slika 4. Uzorak U_2

Na sve ispitne epruvete postupkom plamenog naštrcavanja, [3] nanošena je vezivna prevlaka XUPER ULTRA BOND 51000, podaci preuzeti iz kataloga, [4].

Primjenjuje se za izradu osnovnih prianjajućih slojeva na svim željeznim, materijalima od aluminija i nikla; bakrenim (sadržaj bakra niži od 95 %); stakla; keramičkih materijala.

Na vezivnu prevlaku plameno se naštrcavaju METACERAM specijalni prašci za postupak nanošenja na bazi metalnih oksida (keramika) i čistog Mo: METACERAM 28030, METACERAM 28085, METACERAM 28095. Za sve prevlake napravljeno je po šest epruveta (od kojih su prve tri izrezane iz U_1 a preostale tri iz U_2). Dimenzije epruveta iznosile su 48x18x21 mm. Na prvih šest epruveta naštrcan je METACERAM 28030, na drugih METACERAM 28085 i na preostalih šest METACERAM 28095. Svi podaci i karakteristike naštrcanih prevlaka također su preuzeti iz već spomenutog kataloga («Castolin Eutectic – dodatni materijali i aparati za specijalna reparaturna zavarivanja», A.M.I. COMMERCE, Zagreb).

METACERAM 28030

Za slojeve otporne na trošenje

Standard	K5 – 4 DIN 32529
Mikrotvrdoća djelića praška	cca 1600 HV

Oksidnokeramički prašak na bazi Al_2O_3. Najčešće se primjenjuju kao zaštitni slojevi protiv trošenja na valjcima u tiskarama, valjcima za transport papira, vodilicama niti, i sl.

METACERAM 28085

Zaštitni slojevi otporni na trošenje i dobri toplinski izolatori

Standard	K10 – 4 DIN 32529
Tvrdoća djelića praška	cca 700 HV

Sivobijeli oksidnokeramički prašak na bazi ZrO_2.

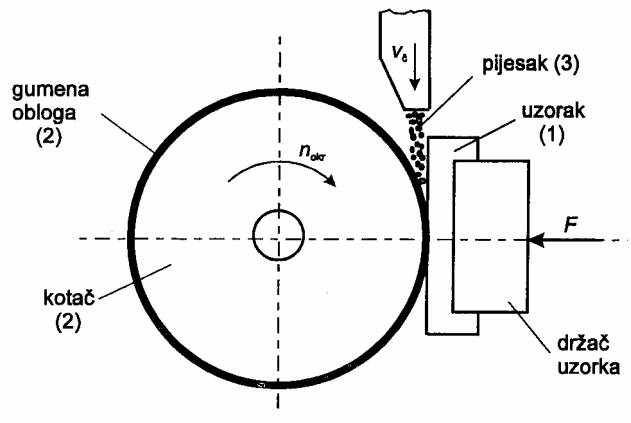
METACERAM 28095

Metalni prašak na bazi molibdena za nanošenje zaštitnih slojeva otpornih na trošenje, nanošenje plamenom

Standard	C 5 – 1 DIN 32529
Mikrotvrdoća nanošenog sloja	cca 900 HV

Normalne debljine slojeva su oko 0,3 mm. Kod slojeva debljih od 0,5 mm postoji opasnost drobljenja (ljuštenja), naročito kod mehaničkih opterećenja.

Nakon nanošenja vezivne prevlake i plamenog naštrcavanja slojeva pristupilo se samom abrazivnom trošenju pripremljenih epruveta na uređaju „suhi pijesak/gumeni kotač“ (slika 5.).



Slika 5. Skica uređaja „suhi pijesak/gumeni kotač“, [5]

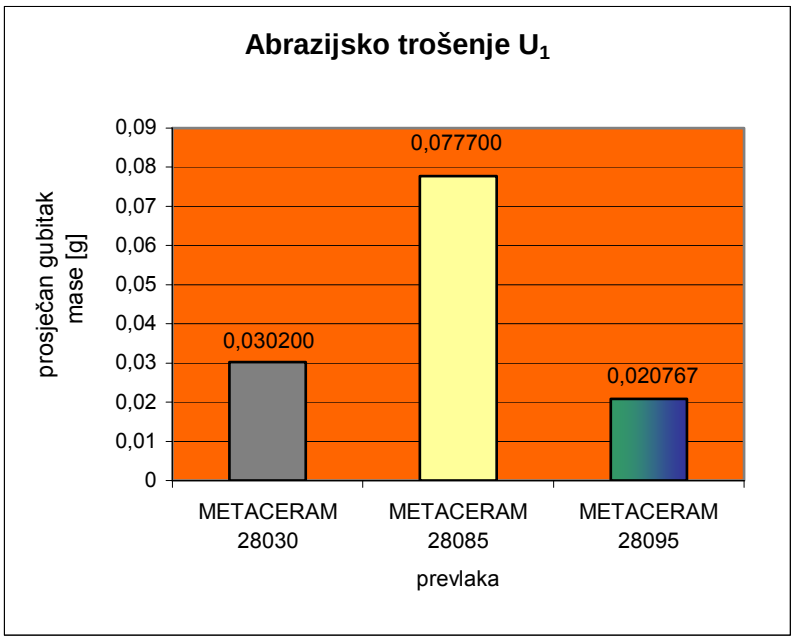
Test se sastoji od abradiranja epruveta standardnim zaobljenim kvarcnim pijeskom Ottawa AFS 50/70. Epruveta se naslanja na kotač (2) obložen gumom tvrdoće oko 60 Shore A, a opterećena je utezima preko koljenaste poluge. Korištene sile F su 15 i 45 N, broj okretaja kotača n je 100. Nakon završetka ispitivanja na uzorcima ostaje trag kao na slici 6.



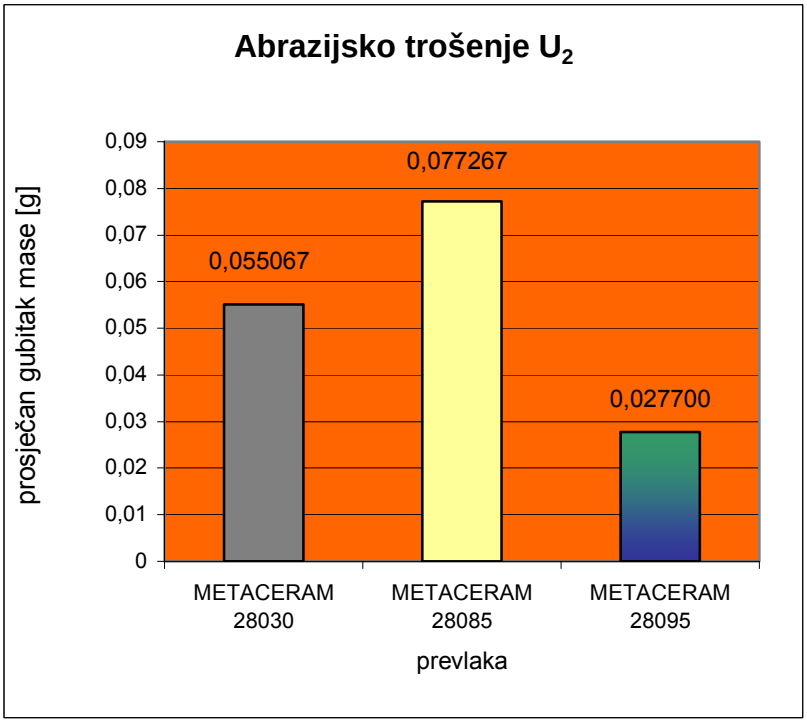
Slika 6. Trag od ispitivanja na uzorcima na uređaju „suhi pijesak/gumeni kotač“

Vaganjem epruvete prije i poslije testa utvrđuje se gubitak mase. Najveća prednost ove metode je to što je standardizirana. Dobiveni rezultati prikazani su dijagramski na slikama 7., 8., 9. i 10.

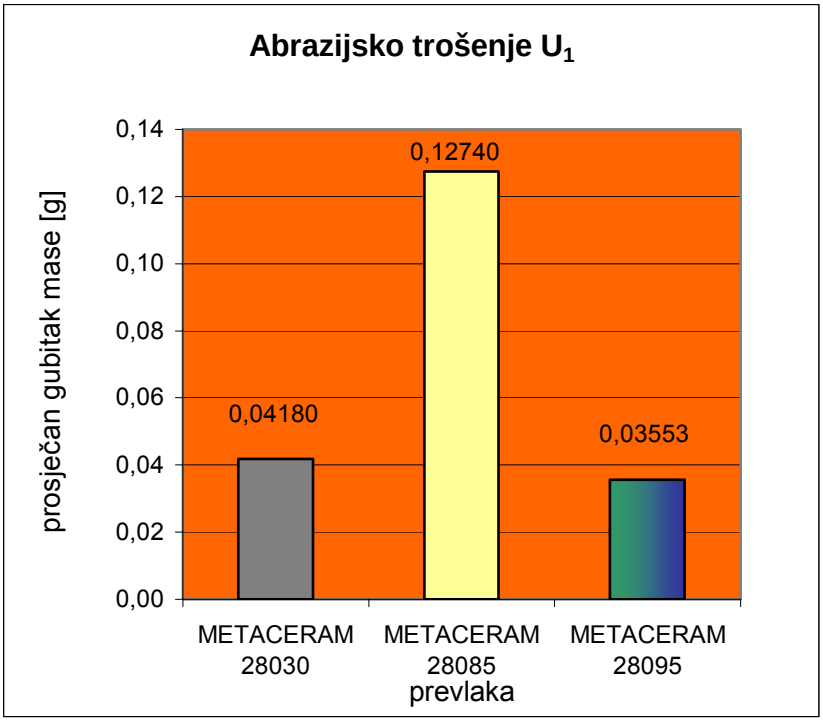
3. REZULTATI ISPITIVANJA



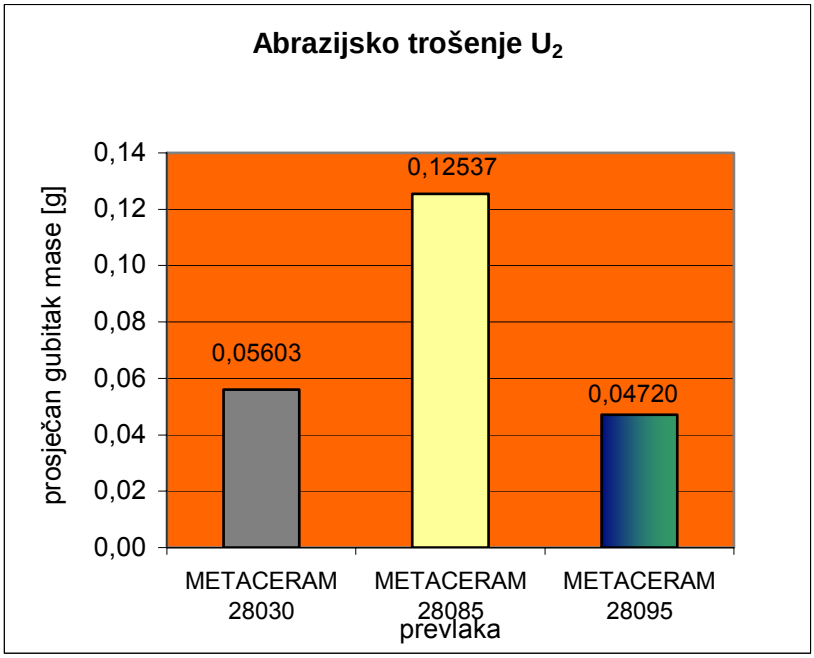
Slika 7. Dijagramski prikaz prosječnog gubitka mase epruveta od uzorka U_1 za pojedine prevlake, primijenjenu silu F = 15 N i n = 100 okretaja



Slika 8. Dijagramski prikaz prosječnog gubitka mase epruveta od uzorka U_2 za pojedine prevlake, primijenjenu silu F = 15 N i n = 100 okretaja



Slika 9. Dijagramski prikaz prosječnog gubitka mase epruveta od uzorka U_1 za pojedine prevlake, primijenjenu silu F = 45 N i n = 100 okretaja



Slika 10. Dijagramski prikaz prosječnog gubitka mase epruveta od uzorka U_2 za pojedine prevlake, primijenjenu silu F = 45 N i n = 100 okretaja

4. ZAKLJUČAK

Analizom rezultata, očigledno je da najveći utjecaj na abrazijsko trošenje prevlaka imaju primijenjena sila i vrsta prevlake.

Kod primjene prevlake METACERAM 28095 (metalni prašak na bazi molibdena) postižu se najbolji rezultati otpornosti na trošenje u slučaju abrazije. Pokazalo se da je prevlaka METACERAM 28085 (oksidnokeramički prašak na bazi ZrO_2) najmanje otporna na abrazijsko trošenje.

Povećanjem primijenjene sile dolazilo je do značajnog gubitka mase na svim prevlakama. Zanimljivo je i to da se prevlake METACERAM 28030 i METACERAM 28095 slično ponašaju pri abrazijskom trošenju pa bi u ovom slučaju značajan faktor mogla predstavljati i poroznost pjene. Očigledno je da na tim uzorcima postoji utjecaj poroznosti, ali da bi se došlo do zaključaka, bilo bi potrebno ispitati uzorke s više različitih poroznosti metalne pjene.

Primjena ovako zaštićenih aluminijskih pjena bila bi moguća na manje tribološki zahtjevnim konstrukcijama u čijoj bi se okolini nalazile sitne abrazivne čestice (npr. prašina, ugljena prašina, i sl.).

5. LITERATURA

[1] T. Filetin, I. Kramer, G. Marić: „Metalne pjene - proizvodnja, svojstva i primjena“, Hrvatsko društvo za materijale i tribologiju, Zagreb, 2003.

[2] John Banhart: „Manufacture, characterisation and application of cellular metals and metal foams“, Progress in Material Science 46 (2001) 559 – 632, Pergamon.

[3] T.Filetin, K.Grilec.: „Postupci modificiranja i prevlačenja površina – priručnik za primjenu“, Hrvatsko društvo za materijale i tribologiju, Zagreb, 2004

[4] Katalog „CastolinEutectic – dodatni materijali i aparati za specijalna reparaturna zavarivanja“, A.M.I. COMMERCE, Zagreb

[5] V. Ivušić: „Tribologija“, Hrvatsko društvo za materijale i tribologiju, Zagreb, 2002.

ADSORPTION OF NICKEL IONS ON THE BLAST FURNACE SLUDGE

ADSORPCIJA IONA NIKLA NA VISOKOPEĆNOM MULJU

A. Rađenović, J. Malina, A. Štrkalj
University of Zagreb, Faculty of Metallurgy
Aleja narodnih heroja 3
44 000 Sisak
Croatia

Izvorni znanstveni rad / Original scientific paper

ABSTRACT

This paper describes to possibility use of the blast furnace sludge (BFS) as adsorbent for removing nickel ions from aqueous effluent solutions. The effect of time and the metal solutions concentration on adsorption efficiency was evaluated. The adsorption process is analyzed using the adsorption isotherm. The BFS was shown to be effective adsorbent for the nickel cations in aqueous solution within the range of investigation concentrations.
BFS is could be alternative to the application of more expensive adsorbents like activated carbon.

Key words: blast furnace sludge, Ni^{2+} ions, adsorption, adsorption isotherm

SAŽETAK

U radu je opisana mogućnost upotrebe visokopećnog mulja kao adsorbensa za uklanjanje iona nikla iz vodenih otopina. Promatran je utjecaj vremena i koncentracije na efikasnost adsorpcije. Adsorpcijski proces analiziran je adsorpcijskom izotermom. Visokopećni mulj se pokazao kao efikasan adsorbens za uklanjanje kationa nikla iz vodenih otopina u području ispitanih koncentracija.
Visokopećni mulj bi se mogao koristiti kao zamjena za puno skuplje adsorbense poput aktivnog ugljika.

Ključne riječi: visokopećni mulj, ioni Ni^{2+}, adsorpcija, adsorpcijska izoterma

UVOD

Obrada otpadnih voda danas se uglavnom temelji na postupcima taloženja, koagulaciji/flotaciji, ekstrakciji, elektrokemijskim tehnikama, ionskoj izmjeni, osmozi i adsorpciji. Najčešće korišteni adsorbens je aktivni ugljik koji se pokazao vrlo efikasnim čak i za uklanjanje teških metala u tragovima. Zbog visoke cijene, aktivni ugljik se nastoji zamijeniti drugim, jeftinijim, a dovoljno djelotvornim adsorbensima. U posljednje vrijeme sve je učestalija primjena nekih sekundarnih produkata proizvodnih procesa koji istovremeno predstavljaju industrijski otpad. Jedan od njih je visokopećni mulj (VPM), nusprodukt industrije željeza i čelika koji nastaje u obliku taloga vrlo sitnih mikro i nanočestica nakon čišćenja dimnih plinova iz procesa proizvodnje sirovog željeza. Sastoji se uglavnom od željeza i ugljika, a zbog prisutnosti štetnih tvari (npr. Pb i Zn) ne može se potpuno reciklirati te dio visokopećnog mulja predstavlja metalurški otpad [1]. Problem odlaganja i zbrinjavanja VPM može se ublažiti njegovom daljnjom upotrebom. Sorpcijske sposobnosti VPM korištene su u postupcima uklanjanja metalnih iona i organskih boja iz vodenih otopina [2-5].
U otpadnim vodama mnogih industrijskih postrojenja sadržaj nikla iznosi od 3,4-900 mg/l [6]. Zbog toksičnog djelovanja na ekosisteme, sadržaj ovog elementa u vodenim otopinama nastoji se smanjiti.
Svrha ovog rada je bila ispitivanje adsorpcije iona nikla iz vodenih otopina na visokopećnom mulju kao mogućem adsorbensu. Interakcija adsorbata i adsorbensa u sistemu vodena otopina Ni^{2+}/VPM vrednovana je primjenom Freundlichove adsorpcijske izoterme.

EKSPERIMENT

Adsorbent

Za adsorpciju iona nikla iz vodenih otopina koristio se visokopećni mulj s odlagališta bivše Željezare u Sisku. Uzorak mulja je sušen 4 sata na 105°C, a za ispitivanja su korišteni uzorci s veličinama čestica ≤ 56 μm.
Karakterizacija VPM je provedena i opisana ranije [7]. Analizom kemijskog sastava ustanovljeno je da VPM sadrži najviše Si, Fe, Al, Ca, Mn, Pb, Zn, a od nemetala kisik i ugljik. Rezultati fazne analize su pokazali da je najveći udjel amorfne faze (76%), slijede karbonati, oksidi i alumosilikati metala. Primjenom BET metode određena je specifična površina (31,46 m^2g^{-1}) i ustanovljeno da je VPM, obzirom na veličinu i volumen pora, mezoporozan materijal.

Adsorbat

Otopine nikla su pripravljene otapanjem $NiCl_2 \cdot 6H_2O$ analitičke čistoće u deioniziranoj vodi. Početne koncentracije otopina nikla iznosile su od 50-550 mg/l. Sadržaj nikla u vodenoj otopini određen je spektrofotometrijski mjerenjem apsorbancije kod 435 nm.

Adsorpcijski eksperimenti

Adsorpcija iona nikla iz vodenih otopina na VPM provedena je statičkim postupkom. Za eksperimente je korišteno 50 ml otopine nikla poznate koncentracije i 0,25 g VPM. Ravnotežno stanje je uspostavljeno nakon 24 sata nakon čega su otopine filtrirane za određivanje sadržaja nikla. Mjerenja su provedena kod konstantne pH vrijednosti otopine (7,86) pri različitim temperaturama (20, 40 i 60°C).

REZULTATI I DISKUSIJA

Slika 1 prikazuje ovisnost kapaciteta adsorpcije (q_e, mg/g) visokopećnog mulja o početnoj koncentraciji iona nikla u otopini. Kapacitet adsorpcije je pokazatelj adsorpcijske moći adsorbensa, a iskazuje se količinom ili masom tvari adsorbirane na adsorbensu. Određen je iz izraza: $q_e = \frac{c_0 - c_e}{m} \cdot V$, gdje su c_0 i c_e početna i ravnotežna koncentracija nikla (mg/l), V je volumen otopine nikla (l) i m je masa VPM (g).
Iz slike je vidljiv porast kapaciteta adsorpcije u odnosu na veće početne koncentracije iona nikla u otopini. Porastom temperature, q_e je veći, naročito za otopine većih koncentracija.

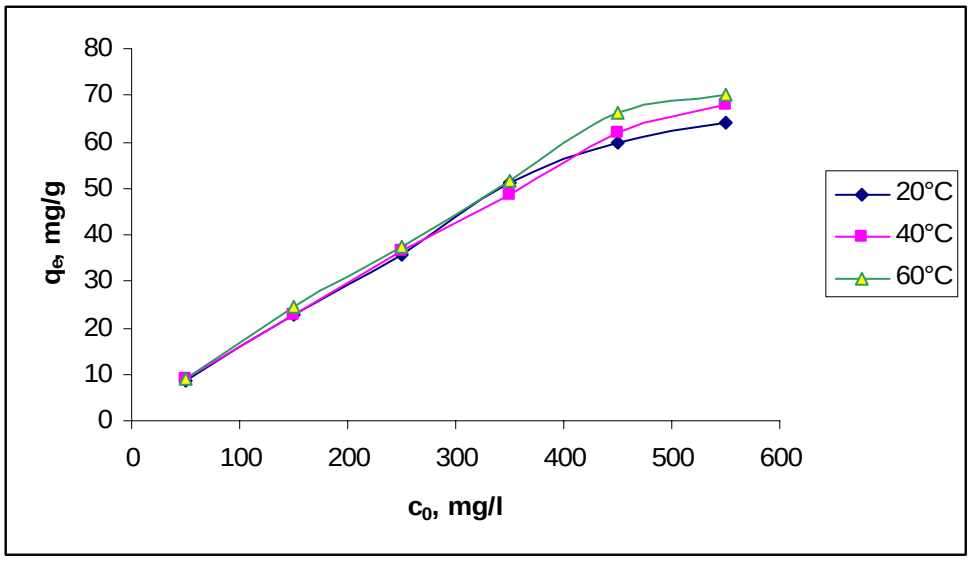
Adsorpcija iona nikla na VPM kao adsorbensu opisana je Freundlichovom adsorpcijskom izotermom koja se, uz Langmuirovu adsorpcijsku izotermu, najčešće upotrebljava za interpretaciju eksperimentalnih podataka. Jednadžba Freundlichove adsorpcijske izoterme je uglavnom bazirana na sorpciji koja se zbiva na heterogenoj površini. Predstavljena je izrazom: $q_e = K_F \cdot c_e^{1/n}$ u kome je q_e kapacitet adsorpcije adsorbensa, c_e je ravnotežna koncentracija adsorbata, a K i n su konstante. Za grafički prikaz korišten je linearni oblik Freundlichove adsorpcijske izoterme iz kojeg su izračunate vrijednosti konstanti K_F i n:

$$lnq_e = lnK_F + 1/n\ lnc_e$$

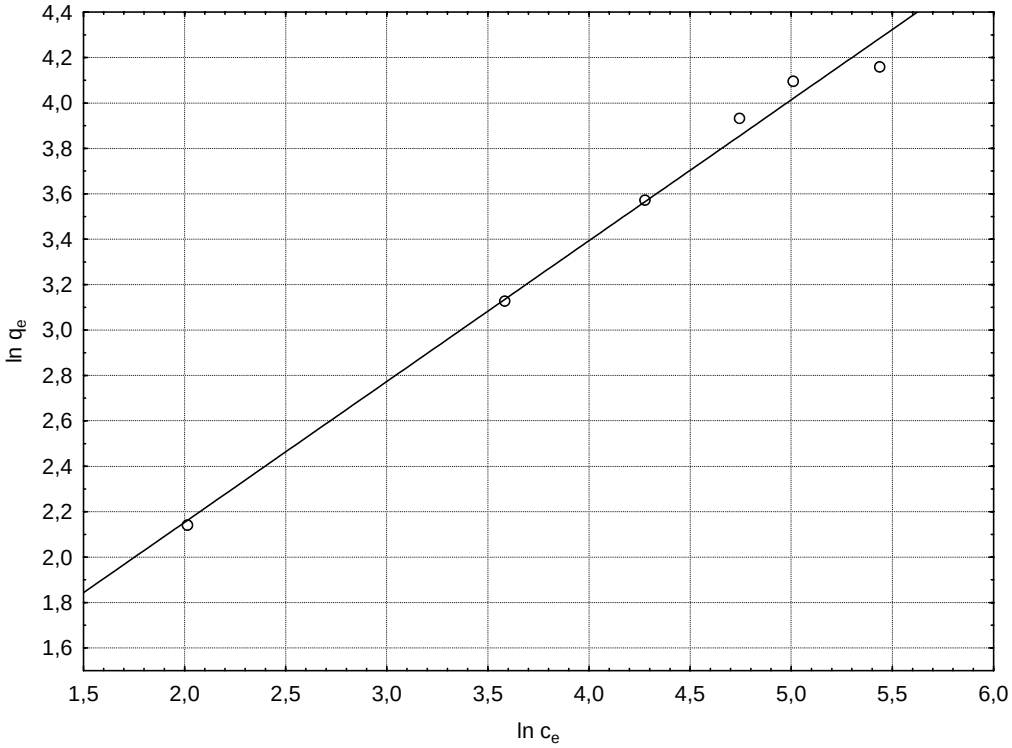
Obradom eksperimentalnih podataka dobivena je linearna ovisnost lnq_e o lnc_e kako pretpostavlja jednadžba Freundlichove izoterme za opis adsorpcijskih procesa (slike 2, 3 i 4). U tablici 1 se nalaze dobivene vrijednosti za konstante Freundlichove adsorpcijske izoterme (K_F *i* n) ovisno o temperaturi. Konstanta K_F predstavlja doseg adsorpcije, a konstanta n ukazuje na afinitet prema adsorpciji. Obzirom na dobivene rezultate prikazane u tablici, može se zaključiti da porast temperature povoljno utječe na adsorpciju iona nikla na VPM.
Vrijednosti za korelacijske koeficijente (r^2 = 0,9688 – 0,9903) ukazuju na dobru podudarnost primijenjene izoterme s eksperimentalnim podacima.

Tablica 1. Konstante K_F i n kod različitih temperatura

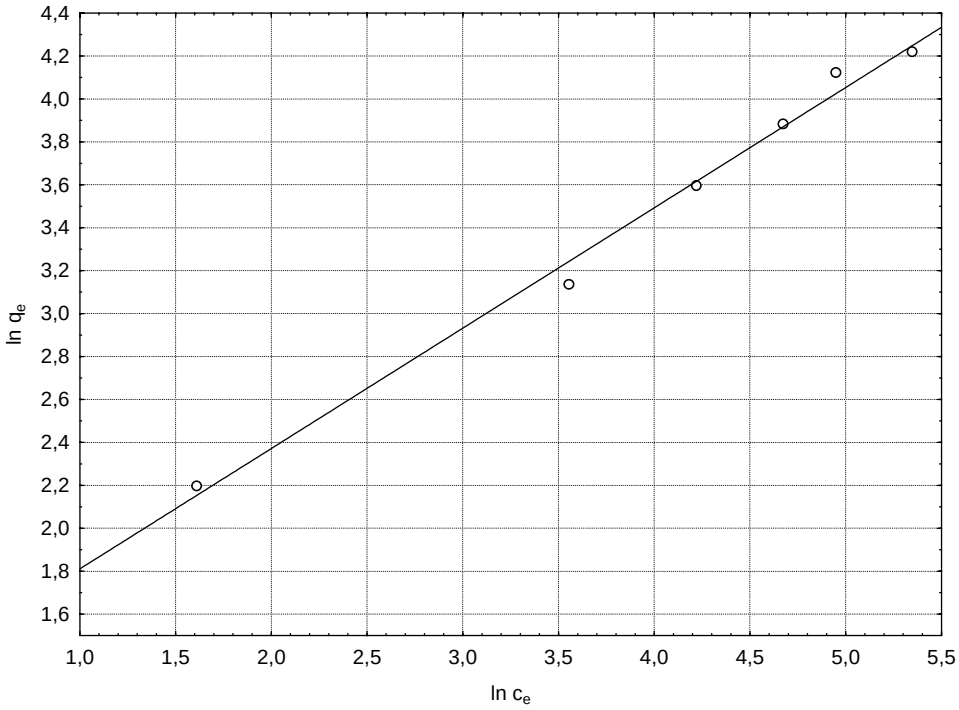
FAI	*T/°C*	*n*	K_F, $(1^{1/n}g^{-1}mg^{1-1/n})$	r^2
$lnq_e=f(lnc_e)$	20	1,623	2,553	0,9903
	40	1,783	3,489	0,9914
	60	2,140	3,835	0,9688



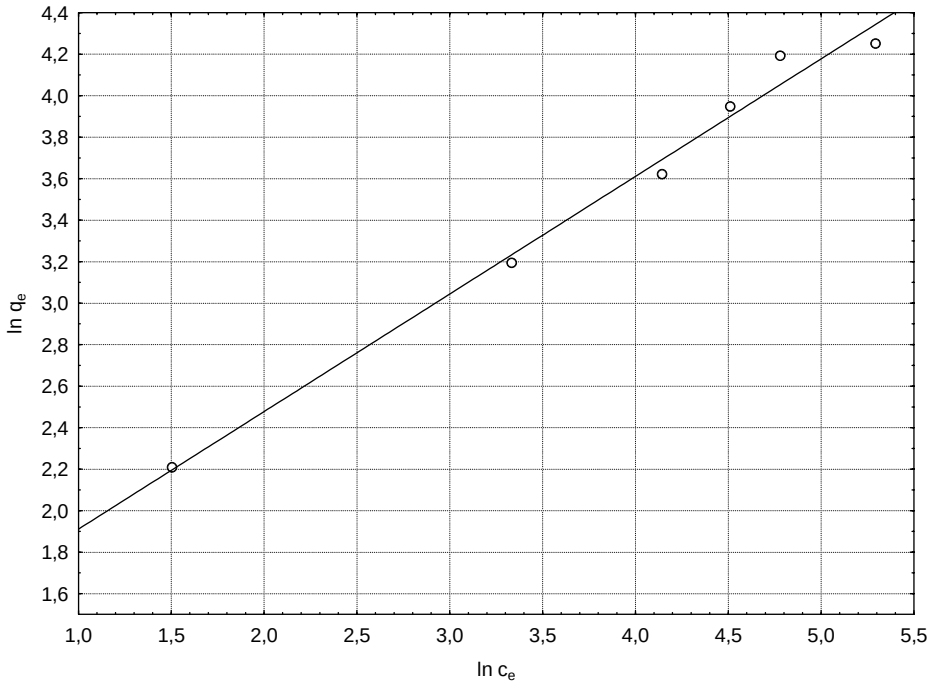
Slika 1. Ovisnost kapaciteta adsorpcije o početnoj koncentraciji iona nikla u otopini i temperaturi



Slika 2. Freundlichova adsorpcijska izoterma kod 20°C



Slika 3. Freundlichova adsorpcijska izoterma kod 40°C



Slika 4. Freundlichova adsorpcijska izoterma kod 60°C

ZAKLJUČAK

Rezultati provedenih ispitivanja su pokazali da adsorpcija Ni^{2+} na VPM ovisi o koncentraciji iona u otopini i temperaturi. Veći kapacitet adsorpcije visokopećnog mulja je postignut za otopine većih koncentracija nikla. Porastom temperature povećava se kapacitet adsorpcije.
Eksperimentalni podaci dobro se podudaraju s linearnim oblikom teorijske Freundlichove adsorpcijske izoterme na što ukazuju vrijednosti korelacijskih koeficijenata (r^2=0,9688-0,9903). Porastom temperature rastu vrijednosti konstanti K_F i n koje su povezane s intenzitetom procesa i afinitetom prema adsorpciji.
Visokopećni mulj, sekundarni i otpadni materijal industrije željeza i čelika, mogao bi zamijeniti skuplje adsorbense u postupcima uklanjanja toksičnog nikla iz vodenih otopina.
Dobiveni rezultati upućuju na opravdanost nastavka ispitivanja upotrebe visokopećnog mulja kao adsorbensa u postupcima uklanjanja i drugih, a naročito iona teških metala, iz vodenih otopina.

LITERATURA

1. P. Van Herck, C. Vandecasteele, R. Swennen, R. Mortier, Environ. Sci. Technol. 34, 3802.
2. J. Malina, A. Rađenović, Đ. Nikolić, Proc. Of 12 International Conference MATRIB 07/Grilec, Krešimir(ur.). Hrvatsko društvo za materijale i tribologiju Zagreb, 2007, Vela Luka, 133.
3. A. K. Jain, V. K. Gupta, A. Bhatnagar, Suhas, J. Hazard. Mater. B 101 (2003) 31.
4. F. A. Lopez, C. Perez, E. Sainz, M. Alonso, J. Chem. Tech. Biotechnol. 62 (1995) 200.
5. A. Lopez-Delgado, C. Perez, F. A. Lopez, Carbon, 34, 423.
6. J. W. Patterson, In: Industrial Wastewater Treatment Tehnology, Butterworth, Boston, 1988, 217.
7. J. Malina, A. Rađenović, G. Matijašić,12 International Conference MATRIB 07/Grilec, Krešimir(ur.). Hrvatsko društvo za materijale i tribologiju Zagreb, 2007, Vela Luka, 180.

DISTRIBUTION COEFFICIENT OF NI^{2+} IONS REMOVING FROM AQUEOUS SOLUTIONS BY BLAST FURNACE SLUDGE

DISTRIBUCIJSKI KOEFICIJENT UKLANJANJA NI^{2+} IONA IZ VODENIH OTOPINA POMOĆU VISOKOPEĆNOG MULJA

Ankica Rađenović, Jadranka Malina, Anita Štrkalj
University of Zagreb, Faculty of Metallurgy
Aleja narodnih heroja 3
44 000 Sisak
Croatia

Izvorni znanstveni rad / Original scientific paper

ABSTRACT

Blast furnace sludge is generated during the production of pig iron and recognized as metallurgical waste. Although sludge consists mainly of iron and carbon, in some cases it also contains harmful substances and therefore it cannot be completely recycled. In the last time, this by-product of steelmaking industry has been used for removing metallic ions and organic dyes.
The subject of this work was the investigation of possibility to use blast furnace sludge for removing Ni^{2+} ions from aqueous solution. Distribution coefficient value as indicator of the removing efficiency of Ni^{2+} was determined. The influence of controlling parameters on distribution coefficient value is shown. The results obtained have been shown that investigated blast furnace sludge is could be considered as promising material for removing of toxic Ni^{2+} ions from aqueous solutions.

Key words: blast furnace sludge, Ni^{2+} ions, aqueous solution, distribution coefficient

SAŽETAK

Visokopećni mulj nastaje za vrijeme proizvodnje sirovog željeza i smatra se metalurškim otpadom. Premda se sastoji uglavnom od željeza i ugljika, visokopećni mulj ponekad sadrži štetne tvari i stoga se ne može potpuno reciklirati.
U posljednje vrijeme ovaj nusproizvod industrije željeza i čelika je upotrebljavan za uklanjanje metalnih iona i organskih boja. U radu je ispitana mogućnost upotrebe visokopećnog mulja za uklanjanje Ni^{2+} iona iz vodenih otopina. Određen je distribucijski koeficijent kao pokazatelj efikasnosti uklanjanja Ni^{2+} iona, te pokazan utjecaj nekih procesnih parametara na njegovu vrijednost. Zbog obećavajućih dobivenih rezultata može se smatrati da je moguća upotreba visokopećnog mulja za efikasno uklanjanje toksičnih Ni^{2+} iona iz vodenih otopina.

Ključne riječi: visokopećni mulj, Ni^{+2} ioni, vodena otopina, distribucijski koeficijent

UVOD

Visokopećni mulj (VPM) je nusprodukt industrije željeza i čelika koji nastaje u obliku taloga vrlo sitnih mikro i nanočestica nakon čišćenja dimnih plinova nastalih tijekom procesa proizvodnje sirovog željeza. Sastoji se uglavnom od željeza i ugljika, a zbog prisutnosti štetnih tvari (npr. Pb i Zn) ne može se potpuno reciklirati te dio visokopećnog mulja predstavlja metalurški otpad [1]. Problem odlaganja i zbrinjavanja VPM može se ublažiti njegovom daljnjom upotrebom. Sve češće se iskorištavaju sorpcijske sposobnosti VPM u postupcima uklanjanja metalnih iona i organskih boja iz vodenih otopina [2-5].
U radu je ispitana mogućnost upotrebe visokopećnog mulja za uklanjanje Ni^{2+} iona iz vodenih otopina. Određen je distribucijski koeficijent kao pokazatelj efikasnosti uklanjanja Ni^{2+} iona adsorpcijom na VPM, te pokazan utjecaj nekih procesnih parametara na njegovu vrijednost.

EKSPERIMENTALNI DIO

Ispitivanja su provedene na uzorcima VPM s odlagališta bivše Željezare Sisak. Uzorci su sušeni 4 sata na 105°C. U tablici se nalaze podaci o kemijskom i mineraloškom sastavu i površinskim svojstvima VPM čija je karakterizacija provedena ranije [6].

Tablica 1. Karakteristike visokopećnog mulja

KARAKTERISTIKA		VRIJEDNOST	
Kemijski sastav, %			
O	42,23	Pb	0,99
C	31,74	K	0,66
Si	6,00	Mn	0,66
Zn	4,52	S	0,62
Na	3,00	P	0,14
Al	3,00	Cl	0,05
Fe	2,90	Ti	0,05
Ca	2,30	Cu	0,01
Mg	1,00		
Mineraloški sastav, %			
x-ray amorfan			76,2
Kalcit	$CaCO_3$		9,9
Magnetit	Fe_3O_4		6,3
Kaolinit	$Al_2Si_2O_5(OH)_4$		2,2
Smitsonit	$ZnCO_3$		2,1
Dolomit	$Ca,Mg(CO_3)_2$		1,6
α-kvarc	α-SiO_2		1,1
α-hematit	α-Fe_2O_3		0,4
α-elementarno željezo	α-Fe		0,2
Specifična površina (BET), m^2g^{-1}			31,46
Ukupni volumen pora, cm^3g^{-1} (1,7-300 nm)			0,157
Prosječan promjer pora, nm			17,88

Adsorpcija Ni^{2+} iona na visokopećnom mulju provedena je „bach“ postupkom. Praćen je utjecaj koncentracije otopine, vremena i temperature na adsorpciju iona nikla na VPM kao adsorbensu. Za eksperimente je korišteno 50 ml otopine nikla poznate koncentracije i 0,25 g VPM kao adsorbensa koji su najprije potresivani 30 minuta na tresilici. Nakon uspostavljanja ravnotežnog stanja, otopine su filtrirane za određivanje sadržaja nikla. Koncentracija nikla u otopini određena je spektrofotometrijski mjerenjem apsorbancije kod 435 nm.

Morfologija površine VPM je određena pretražnom elektronskom mikroskopijom (SEM metoda).

Kapacitet adsorpcije (mgg^{-1}) određen je iz izraza: $q_e = \frac{c_0 - c_e}{m} \cdot V$, a distribucijski koeficijent K_D (lg^{-1}) izračunat je iz izraza: $K_D = \frac{c_0 - c_e}{c_e} \cdot \frac{V}{m}$ gdje su c_0 i c_e početna i ravnotežna koncentracija nikla (mgl^{-1}), V je volumen otopine (l) i m je masa VPM (g).

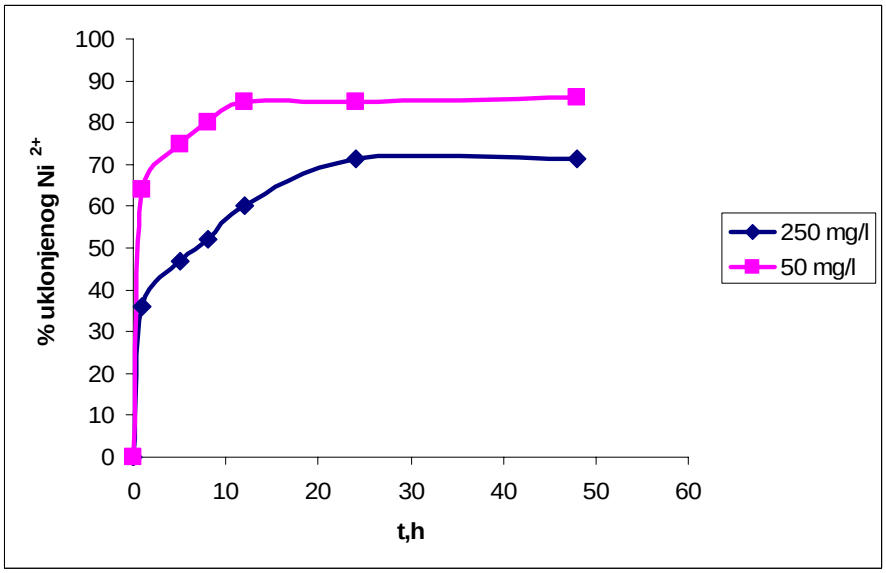
REZULTATI I DISKUSIJA

Promjena udjela izdvojenog nikla ovisno o vremenu kontakta otopine s visokopećnim muljem prikazana je na slici 1. Rezultati ispitivanja dinamike uklanjanja nikla iz vodene otopine pokazuju da se adsorpcija odvija u dva stadija; prvi je relativno brz, a drugi sporiji. Ravnotežno stanje se uspostavlja nakon 24 sata. Brzi prijenos tvari u prvom stadiju može se objasniti velikom nezauzetom površinom adsorbensa. U drugom stadiju brzina adsorpcije je manja vjerojatno uslijed sporije difuzije metalnih iona u pore VPM [7].

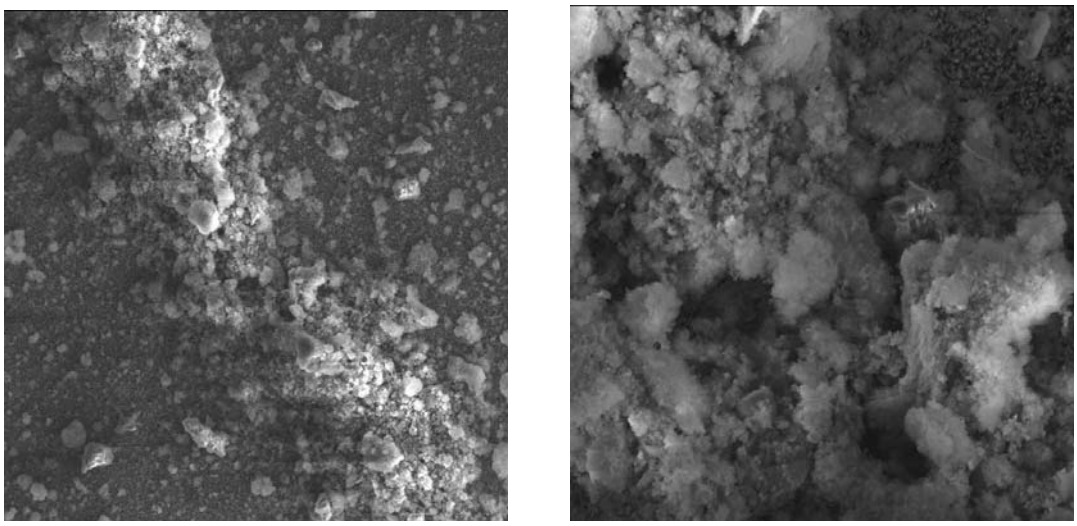
Brzina adsorpcije povezana je s površinskim svojstvima visokopećnog mulja o kojima ovise procesi difuzije i transporta adsorbata u pore adsorbensa. Od površinskih svojstava VPM značajni su velika specifična površina (31,46 m^2g), prosječni promjer pora (17,88 nm) i ukupni volumen pora (0,157 cm^3g^{-1}).

Veća efikasnost uklanjanja iz vodenih otopina je postignuta za nižu koncentraciju nikla (c_0 = 50 mg/l).

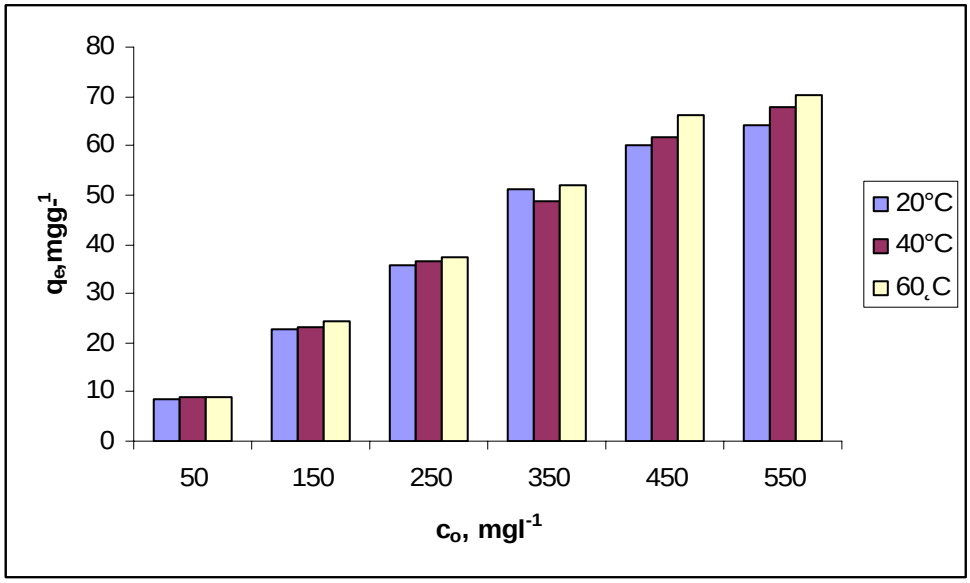
Na slici 2 prikazan je izgled površine visokopećnog mulja. Heterogenost uzorka se uočava i kod malog povećanja (50x) na slici 2a.



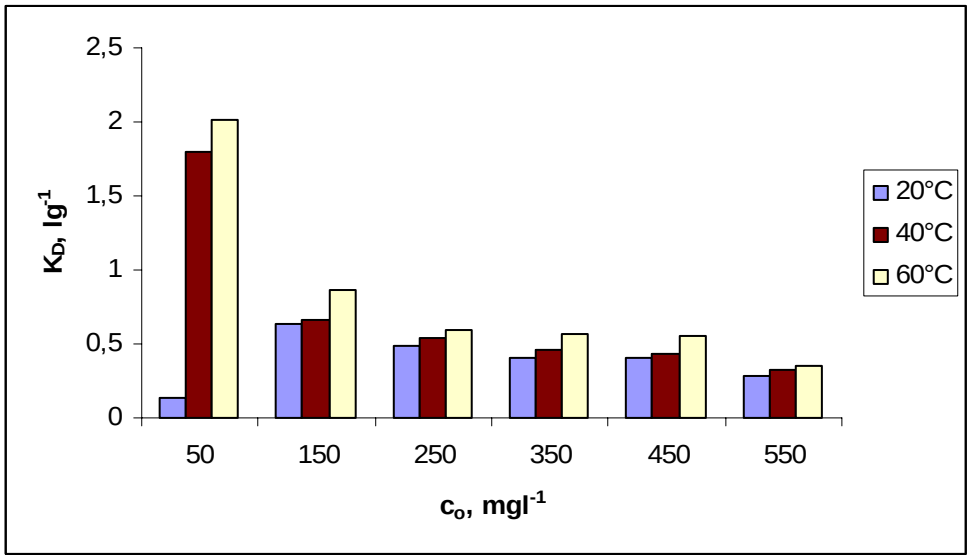
Slika 1. Ovisnost udjela izdvojenog nikla o vremenu za dvije različite početne koncentracije u otopini pri temperaturi od 20°C



Slika 2. SEM mikrografije: a) uzorka visokopećnog mulja-50x; b) visokopećnog mulja nakon kontakta(24 sata) s otopinom nikla (c_0 = 150 mgl^{-1})-300x



Slika 3. Promjena kapaciteta adsorpcije visokopećnog mulja ovisno o početnoj koncentraciji nikla i temperaturi



Slika 4. Prikaz ovisnosti distribucijskog koeficijenta o početnoj koncentraciji nikla u otopini i temperaturi

Na slici 2b prikazan je izgled površine istog uzorka koji je 24 sata bio u kontaktu s otopinom nikla koncentracije c_0 = 150mg/l. Heterogenost površine je i dalje prisutna, a pore su djelomično prekrivene adsorbatom.

Promjena kapaciteta adsorpcije visokopećnog mulja o početnoj koncentraciji nikla u otopini i temperaturi prikazana je na slici 3. Kapacitet adsorpcije, q_e (mg Ni^{2+}/g VPM) raste s porastom početne koncentracije metalnog iona i temperature.

Ovisnost distribucijskog koeficijenta nikla o početnoj koncentraciji otopine i temperaturi prikazana je na slici 4. Distribucijski koeficijent je pokazatelj efikasnosti uklanjanja iona nikla jer je povezan odnosom početne i ravnotežne koncentracije. Porastom početne koncentracije odnosno porastom ravnotežne koncentracije nikla u otopini, smanjuje se K_D.

Dobiveni rezultati pokazuju da se visokopećni mulj, kao nusproizvod industrije željeza i čelika, može koristiti za uklanjanje toksičnih iona nikla iz vodenih otopina. Pored površinskih svojstava, na adsorpcijska svojstva visokopećnog mulja utječu njegov kemijski i mineraloški sastav. Ranija ispitivanja su pokazala da je povoljan utjecaj metalnih oksida (naročito oksida željeza) i ugljika na dobra adsorpcijska svojstva visokopećnog mulja [1, 4].

ZAKLJUČAK

- Rezultati ispitivanja dinamike uklanjanja iona nikla iz vodene otopine pokazuju da se adsorpcija odvija u dva stadija; prvi je relativno brz, a drugi sporiji.
- Veća efikasnost uklanjanja iz vodenih otopina je postignuta za nižu koncentraciju nikla (c_0 = 50 mg/l).
- Kapacitet adsorpcije visokopećnog mulja raste s porastom početne koncentracije metalnog iona.
- Distribucijski koeficijent izdvajanja iona nikla iz vodene otopine, smanjuje se s porastom početne koncentracije.
- Temperatura povoljno utječe na izdvajanje nikla iz vodene otopine.

LITERATURA

1. T. Mansfeldt, R. Dohrmann, Environ. Sci. Technol. 38(2004)5 977.
2. T. Rennert, T. Mansfeldt, Wat. Res. 36(2002) 4877.
3. A. K. Jain, V. K. Gupta, A. Bhatnagar, J. Hazard. Mat. B101 (2003) 31.
4. A. Lopez-Delgado, C. Perez, F.A. Lopez, Carbon 34(1996) 423.
5. J. Malina, A. Rađenović, Đ. Nikolić,Proc. of12 International Conference MATRIB 07/Grilec, Krešimir(ur.). Hrvatsko društvo za materijale i tribologiju Zagreb, 2007, Vela Luka, 133.
6. A. Rađenović, J. Malina, G. Matijašić,12 International Conference MATRIB 07/Grilec,Krešimir(ur.). Hrvatsko društvo za materijale i tribologiju Zagreb, 2007, Vela Luka, 180.
7. A. Dabrowski, Adv. Colloid Interface Sci. 93 (2001) 135.

A NARROW DISTRIBUTION PROVIDES MORE UNIFORM PROPERTIES POLYMERS

Prof.dr.Nedžad Repčić
Faculty of Mechanical Engineering
University of Sarajevo
tel. 65 31 92, 65 65 62 fax. 65 30 55
e.mail: repcic@mef.unsa.ba,
Sarajevo,Vilsonovo 9, B&H

Pregledni članak / Subject review

Abstract: Esters in the allyl family consist principally of diallyl phthalate (DAP) and diallyl isophthalate (DAIP). Both are used as monomers and as prepolymers, which are readily converted to thermoset molding compounds and resins for preimpregnated glass cloth and paper. Allyls are also used as crosslinking agents for unsaturated polyesters. Compounds based on allyl prepolymers are reinforced with fibers (glass, polyester, or acrylic) and filled with particulate materials to improve properties. Glass fiber imparts maximum mechanical properties, acrylic fiber provides the best electrical properties, and polyester fiber improves impact resistance and strength in thin sections. Compounds can be made in a wide range of colors because the resin is essentially colorless.
Prepregs (preimpregnated glass cloth) based on allyl prepolymers can be formulated for short cure cycles. They contain no toxic additives, and they offer long storage stability and ease of handling and fabrication. Properties such as flame resistance can be incorporated. The allyl prepolymers contribute excellent chemical resistance and good electrical properties. Properties: Allyl molding compounds do not corrode copper or plated inserts or contacts, even in hot, humid environments. Molded parts maintain their high electrical properties at high temperature (to 188 °C for DAP and 205 °C for DAIP) and humidity levels. Allyl materials are also characterized by excellent dimensional stability and resistance to moisture, chemicals, and liquid oxygen. They withstand strong and weak acids, alkalies, and organic solvents, even at elevated temperatures.
Allyl moldings have low mold shrinkage and postmold shrinkage -- attributed to their nearly complete addition reaction in the mold -- and have excellent stability under prolonged or cyclic heat exposure. Advantages of allyl systems over polyesters are freedom from styrene odor, low toxicity, low-evaporation losses during evacuation cycles, no subsequent oozing or bleed-out, and long-term retention of electrical-insulation characteristics. Applications: Diallyl phthalate monomer is used as a nonvolatile crosslinker in polyester compounds to improve properties and handling characteristics. Deflection temperature is raised to 205 °C or higher, dimensional stability and electrical properties are upgraded, and flexural properties are retained for long periods at elevated temperatures. DAP is also used in combination with polyester resin systems for low-pressure decorative laminates. Allylic resins in powder and liquid form are used for coatings and for impregnating materials. Allyl prepolymers are particularly suited for critical electronic components that serve in severe environmental conditions.

Key words: materials, extrusion, injection, molding

INTRODUCTION

Chemical inertness qualifies the resins for molded pump impellers and other chemical-processing equipment. Their ability to withstand steam environments permits uses in sterilizing and hot-water equipment. Because of their excellent flow characteristics, diallyl-phthalate compounds are used for parts requiring extreme dimensional accuracy. Modified resin systems are used for encapsulation of electronic devices such as semiconductors and as sealants for metal castings.

A major application area for allyl compounds is electrical connectors, used in communications, computer, and aerospace systems. The high thermal resistance of these materials permits their use in vapor-phase soldering operations. Uses for prepolymers include arc-track-resistant compounds for switchgear and TV components. Other representative uses are insulators, encapsulating shells, potentiometer components, circuit boards, and housings. Allyl-based prepregs are used to make lightweight, intricate parts such as radomes, printed-circuit boards, tubing, ducting, and aircraft parts. Another use is in copper-clad laminates for high-performance printed-circuit boards.

FEP resin applications include wire and cable insulation for computer and electronic systems, telephone and alarm systems, and business-machine interconnects, FEP resin is also supplied as extruded sheet and film for release surfaces, roll covers, linings for chemical-processing tanks, and piping.

The homopolymers are available in several viscosity ranges that meet a variety of processing and end-use needs. The higher viscosity materials are generally used for extrusions and for molded parts requiring maximum toughness; the lower viscosity grades are used for injection molding. Elastomer-modified grades offer greatly improved toughness. Properties: Acetal homopolymer resins have high tensile strength, stiffness, resilience, fatigue endurance, and moderate toughness under repeated impact.

Properties of low moisture absorption, excellent creep resistance, and high deflection temperature suit acetal homopolymer for close-tolerance, high-performance parts. Long-term behavior in various environments can be predicted from design handbook data. Applications: Automotive applications of acetal homopolymer resins include fuel-system and seat-belt components, steering columns, window-support brackets, and handles.

Typical plumbing applications that have replaced brass or zinc components are shower heads, ballcocks, faucet cartridges, and various fittings. Consumer items include quality toys, garden sprayers, stereo cassette parts, butane lighter bodies, zippers, and telephone components. Industrial applications of acetal homopolymer include couplings, pump impellers, conveyor plates, gears, sprockets, and springs. Acrylic thermoplastics are known for their crystal clarity and outstanding weatherability. They are available in cast sheet, rod, and tube; extruded sheet and film; and compounds for injection molding and extrusion.

Cell-cast sheet is produced in several sizes and thicknesses. Alkyd molding compounds are based on unsaturated polyester-type resins, which are combined with crosslinking monomers, catalysts, reinforcements, lubricants, and fillers. The formulations are similar to those of thermosetting polyesters but with lower amounts of monomers.But each process may create stresses in different areas. Sometimes, processing conditions are so severe that there is no choice but to redesign the shape and change to a different plastic. Designers used to take little interest in the molding of parts they designed.

They sent the drawings to the molder in another department or another company and expected perfect parts to emerge. But design and processing have become so interrelated that this separation can no longer exist if products are to be consistently successful. Molders can usually be relied upon to detect and correct visible problems or readily measured factors such as color, surface condition, and dimensions.

NO TOTALLY ACCEPTED DEFINITION EXISTS

Yet another way to create more variations in plastics is alloying -- an effective and economical method to improve a weak property in a base resin. Plastic alloys, also called blends or polyblends, are usually designed to retain the best characteristics of each material. Properties that have been found to be most responsive to improvement are impact strength, heat-deflection temperature, flame retardance, chemical and weather resistance, and processibility.

A study by Battelle reports that research on polymer blending generates about 1,000 patents per year. Although no totally accepted definition exists, most engineers and chemists in the plastics industry agree that a plastic alloy is identified by most of these characteristics: The combination of polymers does not depend on chemical bonds; the mixture is entirely mechanical. Thus, copolymers (some acetals and polyolefins) and terpolymers are not alloys. Nor are epoxy compounds that copolymerize with hardeners that contribute to the properties of the cured resins.The mixture has a single melt-transition temperature. At least one property or characteristic of the base polymer is improved synergistically by the addition of the other polymer(s). The property may be physical or mechanical, or the improvement may be in processibility or cost. If synergistic improvement is not achieved, at least the best properties of all constituents are retained. Each minor component of a plastic alloy constitutes at least 5% of the mix. Many are nearer the 50:50 range. This "requirement" differs considerably from those involving metal alloys.

There, only enough of an alloying element need be present to effect a change in a mechanical or physical property. The magnitude of such a change is not important. A new technology that combines incompatible polymers to form blends called interpenetrating polymer networks (IPNs) promises to provide cost/performance benefits not previously available in engineering plastics. Several companies are working on IPN development, but only a few have made developmental IPN materials available. IPNs consist of an interwoven matrix of two polymers. A typical method for producing these alloys involves crosslinking one of the monomers in the presence of the other polymer. The need for chemical similarity between the two types of molecules is thus reduced because the crosslinking physically traps one phase within the other. The result is a structure composed of two different materials intertwined together, each retaining its own physical characteristics.

The relationship is similar to that between small blood vessels and the surrounding tissue in the human body. Patented IPN technology by Shell Chemical Co. is based on the capability of the company's Kraton G thermoplastic elastomer (styrene-butadiene-block copolymer) to form stable and reproducible structures when properly mixed in the melt stage. The blends provide properties of the individual phases of the mixture and have few or no property losses that might be expected from combining incompatible materials. The results are materials having the best performance features of both an engineering thermoplastic and a thermoplastic rubber.Although Shell was the first to come out with injection-moldable IPNs, Allied and Du Pont are also working on similar materials. Research at Allied-Signal Corp., for example, is focused on combining the toughness of thermoplastics with the solvent resistance, heat resistance, and dimensional stability of thermoset resins. Allied researchers feel that, when the IPNs become fully commercial, they will likely be processed by reaction-injection molding (RIM), by injection molding with a postmolding oven cure, or by a sheet-molding process followed by a cure cycle. Other current thermoplastic IPN technology is based on crystalline resins such as nylon 6, 6/6, and 6/10, PBT, acetal, and polypropylene, with silicone as the IPN. These IPNs can be further modified with reinforcements and lubricants such as glass or carbon fibers and PTFE. The silicone IPN functions as a nonmigratory silicone lubricant, release agent, and flow modifier. It also plays an important role in controlling shrinkage and warpage of resins and composites.

IPNs provide excellent wear performance in gears and bearings and superior dimensional control in parts such as keyboard frames for electronic typewriters. Another way to improve the compatibility of two dissimilar polymers often involved a third material. The "compatibilizer" material is a grafted copolymer consisting of one of the principal components and a material similar to the other principal component. The functional groups in segment A of the third material will have an affinity for the polymer produced from monomer A, and the functional groups in segment B an affinity for polymer B. The mechanism is similar to that of soap improving the solubility of a greasy substance in water. The soap contains components that are compatible with both substances.

MOISTURE ABSORPTION IS LOW

Alkyd molding compounds are based on unsaturated polyester-type resins, which are combined with crosslinking monomers, catalysts, reinforcements, lubricants, and fillers. The formulations are similar to those of thermosetting polyesters but with lower amounts of monomers. Alkyds are part of the group of materials that includes bulk-molding compounds (BMCs) and sheet-molding compounds (SMCs). They are processed by compression, transfer, or injection molding. Fast molding cycles at low pressure make alkyds easier to mold than many other thermosets. Alkyds are furnished in granular compounds, extruded ropes or logs, bulk-molding compound, flake, and puttylike sheets. Except for the putty grades, which may be used for encapsulation, these compounds contain fibrous reinforcement. Generally, the fiber reinforcement in rope and logs is longer than that in granular compounds and shorter than that in flake compounds. Thus, strength of these materials is between those of granular and flake compounds. Because the fillers are opaque and the resins are amber, translucent colors are not possible. Opaque, light shades can be produced in most colors, however.Properties: Low-moisture absorption and excellent dimensional stability and electrical properties are the outstanding characteristics of most alkyd molding compounds. For electrical-grade materials, absorption can be as low as 0.5%. Alkyds are relatively low-loss materials, especially the mineral-filled and glass-filled grades.Those containing cellulose may have higher loss characteristics and "drift" with temperature and humidity changes. Molded alkyd parts resist weak acids, organic solvents, and hydrocarbons such as alcohol and fatty acids; they are attacked by alkalies. Glass and asbestos-filled compounds have better heat resistance than the cellulose-modified types. Depending on type, alkyds can be used continuously to 177 °C and, for short periods, to 232 °C. Alkyd molding compounds retain their dimensional stability and electrical and mechanical properties over a wide temperature range. Halogen and/or phosphorus-bearing alkyd molding compounds with antimony trioxide added provide improved flame resistance. Other flame-resistant compounds are available that do not contain halogenated resins. Acrylic thermoplastics are known for their crystal clarity and outstanding weatherability. They are available in cast sheet, rod, and tube; extruded sheet and film; and compounds for injection molding and extrusion. Cell-cast sheet is produced in several sizes and thicknesses. Acrylic sheet cast by the continuous process (between stainless-steel belts) is more uniform in thickness than cell-cast sheet. Other formulations are opaque to UV light or provide reduced UV transmission. Mechanical properties of acrylics are high for short-term loading. However, for long-term service, tensile stresses must be limited to avoid crazing or surface cracking. The moderate impact resistance of standard formulations is maintained even under conditions of extreme cold. High-impact grades have considerably higher impact strength than standard grades at room temperature, but impact strength decreases as temperature drops. Special formulations ensure compliance with Underwriters' Laboratories standards for bullet resistance. Although acrylic plastics are among the most scratch resistant of the thermoplastics, normal maintenance and cleaning operations can scratch and abrade them.

Special abrasion-resistant sheet is available that has the same optical and impact properties as standard grades. Toughness of acrylic sheet, as measured by resistance to crack propagation, can be improved severalfold by inducing molecular orientation during forming. Jet-aircraft cabin windows, for example, are made from oriented acrylic sheet. Acrylic sheet and moldings resist solutions of inorganic acids and alkalies and aliphatic hydrocarbons such as VM&P naphtha, as well as most detergent solutions and cleaning agents. They are attacked, however, by chlorinated and aromatic hydrocarbons, esters, and ketones. Transparency, gloss, and dimensional stability of acrylics are virtually unaffected by years of exposure to the elements, salt spray, or corrosive atmospheres.

PROPERTIES ESTERS IN THE ALLYL FAMILY

Esters in the allyl family consist principally of diallyl phthalate (DAP) and diallyl isophthalate (DAIP). Both are used as monomers and as prepolymers, which are readily converted to thermoset molding compounds and resins for preimpregnated glass cloth and paper. Allyls are also used as crosslinking agents for unsaturated polyesters. Compounds based on allyl prepolymers are reinforced with fibers (glass, polyester, or acrylic) and filled with particulate materials to improve properties. Glass fiber imparts maximum mechanical properties, acrylic fiber provides the best electrical properties, and polyester fiber improves impact resistance and strength in thin sections. Compounds can be made in a wide range of colors because the resin is essentially colorless. . Properties: Acrylic plastics transmit and control light, resist weather, are stable against discoloration, and have superior dimensional stability and an excellent combination of structural and thermal properties.Allyl moldings have low mold shrinkage and postmold shrinkage -- attributed to their nearly complete addition reaction in the mold -- and have excellent stability under prolonged or cyclic heat exposure. Advantages of allyl systems over polyesters are freedom from styrene odor, low toxicity, low-evaporation losses during evacuation cycles, no subsequent oozing or bleed-out, and long-term retention of electrical-insulation characteristics. Applications: Diallyl phthalate monomer is used as a nonvolatile crosslinker in polyester compounds to improve properties and handling characteristics. Deflection temperature is raised to 205 °C or higher, dimensional stability and electrical properties are upgraded, and flexural properties are retained for long periods at elevated temperatures. DAP is also used in combination with polyester resin systems for low-pressure decorative laminates. Allylic resins in powder and liquid form are used for coatings and for impregnating materials. Allyl prepolymers are particularly suited for critical electronic components that serve in severe environmental conditions. Chemical inertness qualifies the resins for molded pump impellers and other chemical-processing equipment. Their ability to withstand steam environments permits uses in sterilizing and hot-water equipment. Because of their excellent flow characteristics, diallyl-phthalate compounds are used for parts requiring extreme dimensional accuracy. Modified resin systems are used for encapsulation of electronic devices such as semiconductors and as sealants for metal castings.A major application area for allyl compounds is electrical connectors, used in communications, computer, and aerospace systems. The high thermal resistance of these materials permits their use in vapor-phase soldering operations. Uses for prepolymers include arc-track-resistant compounds for switchgear and TV components. Other representative uses are insulators, encapsulating shells, potentiometer components, circuit boards, and housings. Allyl-based prepregs are used to make lightweight, intricate parts such as radomes, printed-circuit boards, tubing, ducting, and aircraft parts. Another use is in copper-clad laminates for high-performance printed-circuit boards. FEP resin applications include wire and cable insulation for computer and electronic systems, telephone and alarm systems, and business-machine interconnects, FEP resin is also supplied as extruded sheet and film for release surfaces, roll covers, linings for chemical-processing tanks, and piping.

CONCLUSIONS

Even here, there is the danger that these sources may not be aware of the many compromises a company must make internally among production, engineering, purchasing, and marketing considerations to produce a product that will sell at a profit. Also, a molder might be inclined to recommend the material that works best in his equipment, rather than the best for the application.The copolymers have an excellent balance of properties and processing characteristics. Melt temperature can range from 182 to 232 °C with little effect on part strength. The resin is available in natural (translucent white) and in a wide range of colors. UV-resistant grades (also available in colors), glass-reinforced grades, low-wear grades, and impact-modified grades are standard. Also available are electroplatable and dimensionally stable, low-warpage grades. Properties: Acetal copolymers have high tensile and flexural strength, fatigue resistance, and hardness. Lubricity is excellent. They retain much of their toughness through a broad temperature range and are among the most creep resistant of the crystalline thermoplastics. Moisture absorption is low, permitting molded parts to serve reliably in environments involving humidity changes. Good electrical properties, combined with high mechanical strength and a UL electrical rating of 100 °C, qualify these materials for electrical applications requiring long-term stability. A new acetal copolymer resin, Ultraform S 1320X-003, is available from BASF Corporation Plastic Materials. It has a combination of high mechanical and heat deflection properties (close to those of acetal homopolymers) and the good thermal stability and processing properties of acetal copolymer resins. The tensile strength, modulus of elasticity, impact strength, heat-deflection temperature, and surface hardness are about 10% higher than those of general-purpose acetal copolymers. The impact-modified acetal copolymer resins have a good balance of toughness and rigidity. Acetal copolymers have excellent resistance to chemicals and solvents. For example, specimens immersed for 12 months at room temperature in various inorganic solutions were unaffected except by strong mineral acids -- sulfuric, nitric, and hydrochloric. Continuous contact is not recommended with strong oxidizing agents such as aqueous solutions containing high concentrations of hypochlorite ions. Solutions of 10% ammonium hydroxide and 10% sodium chloride discolor samples in prolonged immersion, but physical and mechanical properties are not significantly changed. Most organic reagents tested have no effect, nor do mineral oil, motor oil, or brake fluids. Clear acrylic plastic is as transparent as the finest optical glass. It has a light transmittance of 92%, exceptionally low haze level of approximately 1%, and an index of refraction of 1.49 -- high enough for use in lenses and other optical applications.Colorants produce a full spectrum of transparent, translucent, or opaque colors. Most colors can be formulated for long-term outdoor durability. Acrylics are normally formulated to filter ultraviolet energy in the 360-nm and lower band. . Lower molecular-weight grades flow more readily and are designed for making complex parts in hard-to-fill molds. Also available are high-impact molding grades, which provide the same transparency and weatherability as the conventional acrylics

REFERENCES

[1] Brown, R.: Handbook of Polymer Testing, RAPRA Technology Limited, 2006.
[2] Culter, J.: Plastics Packaging:Properties, Processing, Applications,RAPRA,2001.
[3] Massey,L.: Permeability Properties of Plastics and Elastomers, England, 2000.
[4] Herman, M.: Encyclopedia of Polymer Science and Technology, Amazon, 2007.
[5] Malloy,R.: Plastic Part Design for Injection Molding , Pergamon press , Oxsford , 2004.
[6] Tres,P.: Designing Plastics Parts for Assembly, England, 2002.
[7] Zweifel, H.: Plastics Additives Handbook, Springer Verlag, 2000.
[8] Catalogues and standards: ISO, EN, DIN, SKF, FAG, SHELL, ASME, SAE, VDI, FAM, INA.
[9] Web sites - http:// www / science / engineering / design / tribology/ plastics

RESIDUAL STRESS DETERMINATION BY NEUTRON DIFFRACTION IN TUNGSTEN CARBIDE COATED AND SHOT PEENED STEEL SAMPLES

M. Rogante [1] *, G.P. Marconi[2]

[1] Rogante Engineering Office, NDT, Contrada San Michele, n. 61, P.O. Box 189, 62012 Civitanova Marche, Italy
[2] 2Effe Engineering, Via Brescia n. 45, 25080 Soiano del Lago, Italy
* Corresponding author www.roganteengineering.it

Stručni članak / Professional paper

ABSTRACT

The information on residual stresses (RS) can be revealed useful in order to optimize the performances and the reliability of industrial components, machines and plants, supplying data of considerable importance in order to plan the production processes, to analyze the service conditions and to control the maintenance phases.

Knowledge of RS, beyond carrying out a fundamental role in the study of the microstructure, can contribute to the solution of several problems connected to materials and coatings. The existing stresses between interface and substrate, in particular, have a special importance, because strictly related to the adhesion of the same coating.

In this study, the results are presented of RS measurement of two 13CrNi4 martensitic stainless steel samples - material usually used in the hydroelectric field -, of which one with tungsten carbide HVOF coating, the other with one surface submitted to shot blasting. The technique of neutron diffraction, employed by Rogante Engineering Office, and that x-rays, employed by 2Effe Engineering, have exactly revealed complementary in determining the stress status of the samples through-the-thickness.

Keywords: Residual stress; Neutron Diffraction; 13CrNi4 steel; HVOF coating; Erosion.

1. Erosion and protective coatings

The phenomenon of the erosion assumes significant importance in the management and in the costs assessment of the hydroelectric systems for power generation. Components of Pelton turbines operating in presence of water containing elevated abrasive particle amount (glacial silt), in particular, are submitted to high levels of erosion, as evidenced in Figure 1.



Figure 1. Pin tip with erosion due to glacial silt.

The top of Francis impellers, similarly, in presence of water with elevated content of glacial silt, show erosion problems, as represented in Figure 2.



Fig. 2. Francis impeller top, showing erosion due to glacial silt. Particular.

The adoption of protective coatings against wear helps to lengthen the life of components submitted to erosion, reducing, consequently, the intervention and maintenance costs. The said coatings are constituted essentially from tungsten carbides, and have an Hv hardness ~1200-1500. They are made by 2Effe Engineering by means of High Velocity Oxygen Fuel (HVOF) thermal spraying, employing anthropomorphic robots. Figure 3 represents a HVOF system with anthropomorphic robot of 2Effe Engineering, during the coating of a Francis impeller, while Figure 4 is referred to the operative phase.



Fig. 3. HVOF plant and Francis impeller.

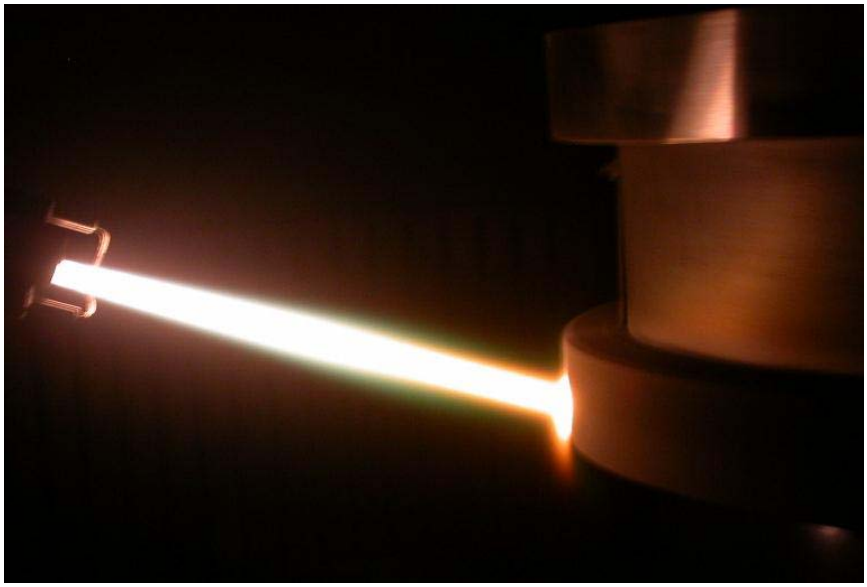


Fig. 4. HVOF plant in the operative phase. Particular.

2. Residual stresses and coatings

Knowledge of directional and spatial RS distribution in a wide diversity of industrial plants is necessary to determine their influence on the material, being a decisive factor for quality, life assessment and safety. Stress concentration – in particular, tensile stresses – should be avoided in order to increase fatigue life and keep away from stress corrosion cracking (SCC) and creep. Neutron diffraction represents almost certainly the most complete method for non-destructive stress measurement of components, helping to reduce the conservative estimates which increase material and replacement costs [1, 4-8].

The deposition of superficial coatings obtained through various productive techniques originates, in the coatings, strong RS gradients involving a variation of the coating material reticular parameters. The RS in the case of coated samples can appear with formation of delamination at the interface (in the case of compressive stress in the coating), superficial cracks (tensile stress in the coating, associated to a strong interface) and separation of the coating (tensile stress in the coating, associated to an weak interface).

RS created in the coatings by means of HVOF thermal spraying technique have received a particular consideration in the literature, having shown to assume important roles inherent to the performances of the same coatings. The duration of said coatings, in fact, has a primary importance for their crucial function to protect the substrate of the component. Defects close to the interface coating-substrate, in presence of RS, can originate cracks [2], and the RS induced in the substrate from the coating process can influence the life determination of the component [3].

RS near the interface coating-substrate, in particular, are closely correlated to the adhesion of the same coatings, therefore it is important to determine their values in function of the deposition parameters, with the aim to produce coatings with greater values of adhesion. Such values can help the deposition of coatings having greater thickness, with consequent remarkable increase of the resistance to the erosion of the considered components.

3. Neutron and x-ray diffraction of neutrons for the complete determination of the residual stresses in coated materials

Neutron Techniques have supplied more and more, in the last years, a valid contribution for the solution of industrial-type problems [4-8]. The same techniques are based on important property of neutrons, elementary particles substantially without any electric charge, constituent - together to

protons - the atomic nucleus. The characteristic of neutrons not to interact electrically with electrons and the nuclei in the matter introduces the great advantage of being able to penetrate in depth. X-ray offer an excellent resolution, but they can penetrate the matter only through superficial layers of the depth of some tens of microns), while neutrons, possessing a linear absorption coefficient approximately 1000 times weaker, penetrate the matter until various centimetres (as an example, approximately 2 or 3 cm the steels, and 5 or 6 cm the aluminium and its alloys).
Neutron diffraction technique can be employed in order to obtain in non-destructive way the RS profiles through industrial components submitted to working processes or heat and/or mechanical treatments. Knowledge of RS spatial distribution, obtainable in the material's bulk only through neutron diffraction, can allow a more correct evaluation on how the component has been influenced from the previous treatments, and supply useful information either for the planning, or for the production of industrial components [4-8].
X-ray diffraction [9-12] can be employed, in complementary way to that one of neutrons, for RS determination in metallic materials. Due to the insufficient penetration of x-rays in such materials, in fact, the determined RS represent the average carried out on one depth of few tens of microns. When the RS data obtained through x-ray diffraction are not sufficient for the understanding of the phenomena, neutron diffraction can be successfully used.
Concerning coated materials, in particular, neutron diffraction measurements supplied by Rogante Engineering Office, and x-ray diffraction measurements supplied by 2Effe Engineering, exactly reveal their complementary in determining the through-the-thickness RS status.
In this study, the results are presented of RS measurement of two 13CrNi4 martensitic stainless steel samples - material usually used in the hydroelectric field -, of which one with tungsten carbide HVOF 0,3 millimetre thickness coating (88% WC in a 12% Co matrix), the other with one surface submitted to shot peening employing ASH230spheres at a 12/14 Almen intensity. Figure 5 shows the coated sample obtained, like the latter, directly from the specimen used for the mechanical properties characterization of the cast.

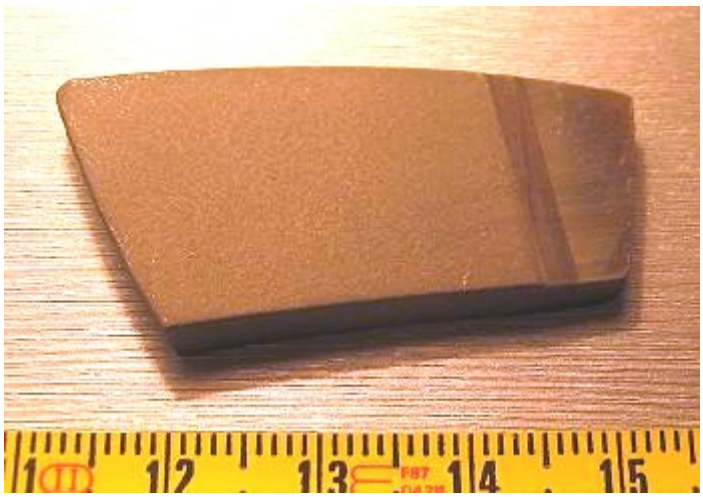


Fig. 5. The investigated 13CrNi4 martensitic stainless steel sample, HVOF coated with tungsten carbide (88% WC in a 12% Co matrix).

The RS determination by neutron diffraction has been carried out by Rogante Engineering Office, which has developed appropriate data treatment procedures for the Industrial Applications of Neutron Techniques.
For the RS calculation, the following values have been employed: Young modulus E = 225.5GPa; Poisson coefficient = 0.28.

In Figure 6 the diagrams are displayed of the RS determined by neutron diffraction for both samples. Detailed measurements have demonstrated that RS, in the considered case, are coplanar to the interface surface and bi-axially symmetrical.

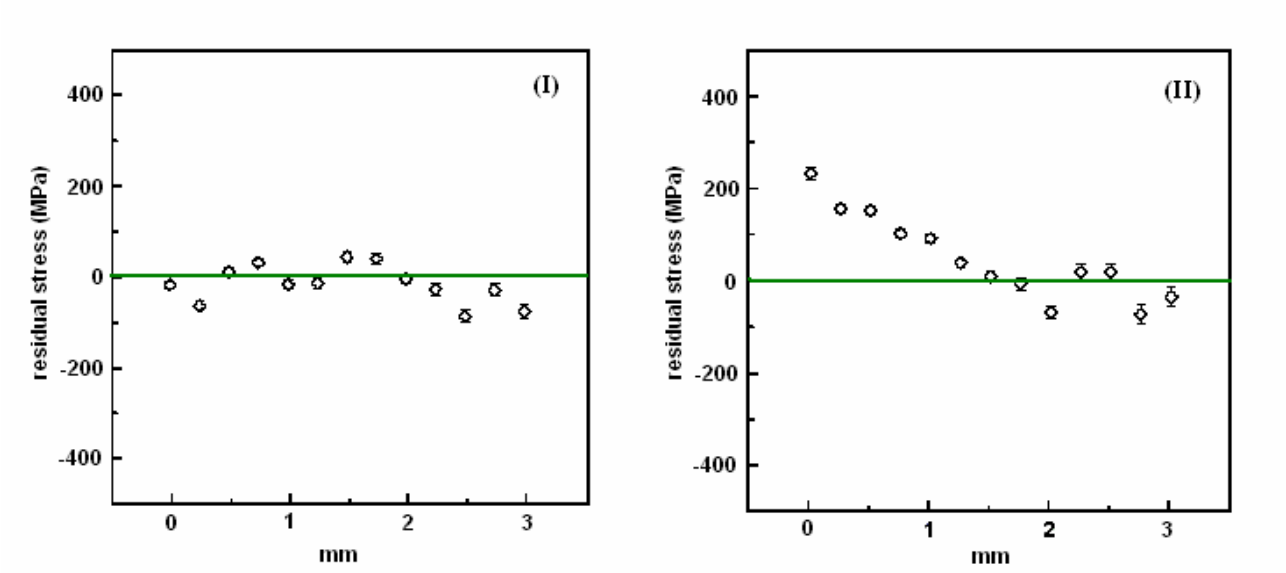


Fig. 6. RS diagrams determined by neutron diffraction by Rogante Engineering Office, for 13CrNi4 martensitic stainless steel samples, without (I) and with (II) HVOF tungsten carbide coating (88% WC in a 12% Co matrix). The values refer to RS parallel to the interface surface, and regard the base material, i.e. 13CrNi4 steel.

The sample without coating shows not relevant RS, included in a limited range of values, while in the coated sample the RS decrease from the maximum value of ~250 MPa in correspondence of the coating (0 mm) to values next to the zero in correspondence of the opposite surface (3 mm).
The RS in the coating surface have been determined, complementarily, by x-ray diffraction by 2Effe Engineering, and the maximum RS value has been found of ~-500 MPa, demonstrating the self-equilibrium of RS in the considered sample. The results obtained from the employment of both the considered techniques allowed determining in a complete way the RS status in the sample due to the coating process.

Conclusions

The characterization of HVOF coatings by means of the RS determination can clarify multiple cases of malfunctioning of coated components due to the separations of coating portions, not interpretable through the single employment of mechanical tests or traditional microstructure analysis.
Neutron diffraction measurements supplied by Rogante Engineering Office, and x-ray diffraction measurements supplied by 2Effe Engineering, represent efficient complementary methods in the complete determination of the RS status of coated materials.
Rogante Engineering Office represents a reference point for Industry with regard to the Industrial Applications of Neutron Techniques for materials and components analysis and characterization, and in particular the non-destructive determination of inner and sub-surface RS, and the microstructural characterization for the residual life evaluation.
2Effe Engineering executes HVOF coatings and shoot peening processes, and adopts X-ray diffraction for surface RS determination.

References

[1] M. Rogante, Misurazione delle tensioni residue mediante diffrazione neutronica, Rivista Italiana della Saldatura, Istituto Italiano della Saldatura, Ed., Genova, Vol. 4 (2001), pp. 461-465.
[2] B.S. Yilbas, A.F.M. Arif, M.A. Gondal, HVOF coating and laser treatment: three-point bending tests, Journal of Materials Processing Technology, 164/165 (2005), pp. 954-957.
[3] T.C. Totemeier, R.N. Wright, W.D. Swank, Residual Stresses in High-Velocity Oxy-Fuel Metallic Coatings, Metallurgical and Materials Transactions A, Volume 35A (2004), p. 1807-1814.
[4] M. Rogante, La diffrazione dei neutroni al servizio dell'industria, Lamiera, ed. Tecniche Nuove, Milano, Feb. 1998, pp. 114-120.
[5] M. Rogante, Caratterizzazione, mediante scattering neutronico, di materiali e componenti per l'impiantistica nucleare ed industriale, Tesi di dottorato di Ricerca in Ingegneria Nucleare, Università di Bologna (1999), pp. 223.
[6] M. Rogante, Misurazione delle tensioni residue mediante diffrazione neutronica, Impiantistica Italiana, Animp, Ed., Milano, Vol. 2 (2001), pp. 43-46.
[7] M. Rogante, Industrial applications of neutron techniques: a recent overview related to materials and components of technological interest, Proc. Int. Conf. "MATRIB '03", Vela Luka, Croatia, 26-28/06/2003, K. Grilec, Ed., Croatian Society for Materials and Tribology, Zagreb, Croatia (2003), pp. 235-241.
[8] M. Rogante, L. Rosta, Nanoscale characterisation by SANS and residual stresses determination by neutron diffraction related to materials and components of technological interest, Proc. SPIE Vol. 5824, (2005), p. 294-305.
[9] B. D. Cullity, Elements of X-ray diffraction 2nd Ed., Addison-Wesley Ed., Boston, USA (1978), p. 555.
[10] M. Gelfi, E. Bontempi, R. Roberti, L.E. Depero, X-ray diffraction Debye Ring Analisis for Stress measurement (DRAST): a new method to evaluate residual stresses Acta Materialia 52, (2004), pp. 583-589.
[11] B. E. Warren, X-Ray Diffraction, Addison Wesley Ed., Boston, USA (1969), pp. 252-275.
[12] R. Jenkins, R. L. Snyder, Introduction to X-Ray Powder Diffractometry, John Wiley and Sons Ed., New York (1996), pp. 544.

ADSORPTION OF PRINTING DYE ON ORGANO-ZEOLITE
ADSORPCIJA TISKARSKOG BOJILA NA ORGANO-ZEOLIT

Mirela Rožić[1], Snežana Miljanić[2], Jasna Hrenović[2], Lavoslav Sekovanić[3], Tanja Gracaković[1], Vesna Kropar Vančina[1], Stanislav Kurajica[4]
[1]Faculty of Graphic Arts, Getaldićeva 2, Zagreb, Croatia
[2]Faculty of Science, Horvatovac 102a, Zagreb, Croatia
[3]Geotechnical Faculty, Hallerova aleja 7, Varaždin, Croatia
[4]Faculty of Chemical Engineering and Technology, Marulićev trg 19, Zagreb, Croatia

Izvorni znanstveni rad / Original scientific paper

Abstract: Adsorption of quaternary ammonium surfactant; hexadecyltrimethylammonium (HDTMA) bromide on a synthetic zeolite mordenite was studied. Clarification of artificial wastewater by the surfactant-modified zeolite samples was examined too. Artificial wastewater was prepared with ink-jet dye with addition of organic solvent. To characterize surfactant on zeolite surface FT infrared spectroscopy using attenuated total reflection (ATR) and KBr pressed disk techniques as well as FT Raman spectroscopy were used. While FTIR spectra indicated sorption of HDTMA molecules with chains adopting mainly gauche conformation, ATR and FT Raman spectra of HDTMA modified mordenite could not be obtained. The organic cation replaced inorganic Na^+ cations on the external and internal zeolite surface. This modification resulted in an alteration in the surface property of zeolite – it changed from hydrophilic to more hydrophobic. Untreated zeolite showed little affinity for wastewater clarification. With 0,5 % (w/w) of surfactant-modified zeolite samples, from the solution with dye concentration of 20 mg/l efficiency of clarification is more than 95 %.

Key words: surfactant, zeolite, mordenite, printing dye

Sažetak: Ispitana je adsorpcija kvaternog amonijevog tenzida; heksadeciltrimetilamonijevog (HDTMA) bromida na sintetski zeolit mordenit. Ispitano je i bistrenje sintetske otpadne vode tenzidom modificiranim uzorcima zeolita. Sintetska otpadna voda pripremljena je s ink-jet bojilom uz dodatak organskog otapala. Za karakterizaciju tenzida na zeolitnoj površini, korištene su FT infracrvena spektroskopija tehnikama prigušene ukupne refleksije (attenuated total reflection, ATR) i KBr pastile te FT Ramanova spektroskopija. Dok FTIR spektri upućuju na adsorpciju HDTMA molekula s lancima većinom u *gauche* konformaciji, ATR i FT Ramanove spektre mordenita modificiranog s HDTMA nije bilo moguće snimiti. Organski kation izmjenjuje se s anorganskim Na^+ kationom u unutarnjim i vanjskim površinama zeolita. Posljedica modifikacije je promjena površinskog svojstva zeolita – površina se mijenja iz hidrofilne u hidrofobniju. S 0,5 % (w/w) tenzidom modificiranih uzoraka zeolita, iz otopine bojila s koncentracijom 20 mg/l djelotvornost obezbojenja veća je od 95 %.

Ključne riječi: tenzid, zeolit, mordenit, tiskarsko bojilo

1. UVOD

Zeoliti su sekundarni minerali i mogu se definirati kao hidratizirani kristalinični alumosilikati alkalijskih i zemnoalkalijskih kationa (uglavnom, Na^+, K^+, Ca^{2+}). Beskonačna trodimenzijska kristalna polianionska slagalina alumosilikata zeolitnog tipa sastoji se od $(Al,Si)O_4$ tetraedara, koji su međusobno povezani zajedničkim atomima kisika. Nastajanje takve kristalne strukture može se zamisliti izomorfnom zamjenom iona Si^{4+} trodimenzijske mreže $(SiO_2)_n$ s ionima Al^{3+}: $(SiO_2)_n + m(Al^{3+}) \rightarrow (AlO_2)_m(SiO_2)_{n-m}$. Negativni naboj alumosilikatne strukture, nastao izomorfnom zamjenom silicija aluminijem, neutraliziran je najčešće alkalnim i zemnoalkalnim kationima.

Zeoliti su sorbensi i mogu zadržati unutar svojih šupljina i kanala molekule određene veličine, što posebno vrijedi za polarne molekule (Breck D.W., 1984).

Svojstva kristaliničnih alumosilikata (zeolita) mogu se modelirati u reakcijama s tenzidima, posebno kvaternim alkil aminima, pri čemu se mogu dobiti mineralno-tenzidne matrice (organo-alumosilikati) za vezivanje anionskih i neutralnih molekula-posebno važni materijali u zaštiti okoliša (Bowman R.S., i ost. 2000; Li Z., Bowman R.S., 1998; Haggerty G.M., Bowman R.S., 1994; Li Z., Bowman R.S., 2001).

Za modifikaciju prirodnih i sintetskih zeolita i njihovu transformaciju u neionske i anionske adsorbense učestali su reaktanti kationski tenzidi: (heksadecil, oktadecil, benzil, fenil)-trimetilamonijev-(bromid, klorid) i metil-4-fenilpiridinijev-(bromid, klorid), od kojih se najviše rabi monokvaterni jednolančasti heksadeciltrimetilamonijev (HDTMA) bromid (ili klorid).

U ovom radu ispitana je adsorpcija heksadeciltrimetilamonijevog bromida na sintetski zeolit - mordenit. Ispitano je i bistrenje sintetske otpadne vode tenzidom modificiranim uzorcima zeolita. Sintetska otpadna voda pripremljena je s ink-jet bojilom uz dodatak organskog otapala.

Radi ispitivanja strukture adsorbiranih HDTMA molekula, rabljene su FT infracrvena i FT Ramanova spektroskopija.

2. EKSPERIMENTALNO

Metodologija

Za provedena ispitivanja upotrijebljen je kationski tenzid – heksadeciltrimetilamonijev bromid, $C_{16}H_{33}N^+(CH_3)_3Br^-$ ($HDTMA^+Br^-$), molarne mase 364,46 g/mol, s 99% aktivne supstance. Kritična micelarna koncentracija $HDTMA^+Br^-$ na 30 ^{0}C je 342,2 mg/l. Adorpcije heksadeciltrimetilamonijevog bromida izvedene su na sintetskom zeolitu mordenitu (JM Hubber Corp., USA). Uzorak mordenita je u natrijevom obliku s veličinom čestica manjom od 15 μm. XRD-analiza pokazala je, da uzorak sadrži manju frakciju amorfnog alumosilikata. Ispitivanja bistrenja otpadne vode provedena su na sintetskoj otpadnoj vodi pripremljene u laboratoriju. Za pripremu se rabila destilirana voda. Ispitivanja su provedena s ink-jet bojilom magenta. Pripremljena je otopina bojila koncentracije 500 mg/l uz dodatak 2,0 % (v/v) organskog otapala (etilen glikol monoetil eter acetat). Iz dobivene otopine razrijeđenjem s destiliranom vodom priređena je otopina bojila koncentracije 20 mg/l (0,08% organskog otapala).

Adsorpcija $HDTMA^+Br^-$ na zeolit i priprema uzoraka organo zeolita

Otopine heksadeciltrimetilamonijevog bromida različitih masenih koncentracija pripremljene su u destiliranoj vodi. Masene koncentracije tenzida bile su manje i veće od kritične micelarne koncentracije: od 15 do 1500 mg/l. Suspenzije koje su pripremljene miješanjem 2,0 g zeolita i 100,0 ml otopine tenzida, mućkane su 48 sati na 30 ^{0}C (mućkalica Innova 4080). Alikvoti od 10 ml suspenzije su centrifugirani, a otopinama iznad taloga određene su koncentracije preostalog tenzida mjerenjem sadržaja ukupnog organskog ugljika (Shimadzu TOC-5050A analyser). Mjera mineralno-tenzidne reakcije iskazana je omjerom masa adsorbiranog $HDTMA^+Br^-$ i mordenita, a izračunata je kao razlika početne i konačne ravnotežne koncentracije tenzida u otopini. Eksperimentalni rezultati prikazani su na slici 1. Uzorci mordenita modificirani $HDTMA^+Br^-$ ispirani su destiliranom vodom uzastopnim dekantiranjem do negativne reakcije na bromidne ione i sušeni su na zraku.

Određivanje elektrokinetičkog (zeta) potencijala uzoraka organo-zeolita

Suspenzije organo-zeolita priređene su miješanjem 0,01 g organo-zeolita i 0,05 dm^3 destilirane vode. Izmućkavanje suspenzija trajalo je 15 minuta. Alikvoti koloidno-disperznih otopina iznad taloga uzeti su za određivanje zeta potencijala. Izmjerene elektroforetske pokretljivosti čestica automatski se pretvaraju u zeta potencijal upotrebom Helmholz-Smolukhowske jednadžbe. Za svaki pojedinačni konačni numerički podatak zeta potencijala uzeta je srednja vrijednost od deset mjerenja. Rezultati su prikazani na slici 2.

Vibracijska spektroskopija

Za snimanje FT infracrvenih spektara tehnikom prigušene ukupne refleksije (attenuated total reflection, ATR) rabljen je FTIR spektrometar Vertex 70 tvrtke Bruker. Spektri uzoraka nanešenih na ATR dijamantnu pločicu snimani su u apsorpcijskom režimu u spektralnom području od 400 do 4000 cm^{-1}, 64 puta uz razlučivanje od 1 cm^{-1}. FTIR spektri uzorka pripravljenih tehnikom KBr pastile snimljeni su pomoću FTIR interferometra Bruker Equinox 55. KBr pastile pripravljene su vaganjem 1 mg sintetskog zeolita mordenita i 100 mg kalijeva bromida, miješanjem u tarioniku od ahata i prešanjem u pastilu. Spektri su snimani u spektralnom području između 400 i 4000 cm^{-1}, 32 puta uz razlučivanje od 4 cm^{-1}.

Ramanovi spektri snimljeni su na FTIR interferometru Bruker Equinox 55 s FT Raman modulom FRA 106/S. Uzorci su pobuđivani zračenjem NIR lasera Nd-YAG pri 1064 nm, snage 100 mW. Spektri su snimani u području između 0 i 3500 cm^{-1}, 64 puta uz različivanje od 4 cm^{-1}. Rezultati su prikazani na slikama 3 i 4.

Bistrenje otpadne vode

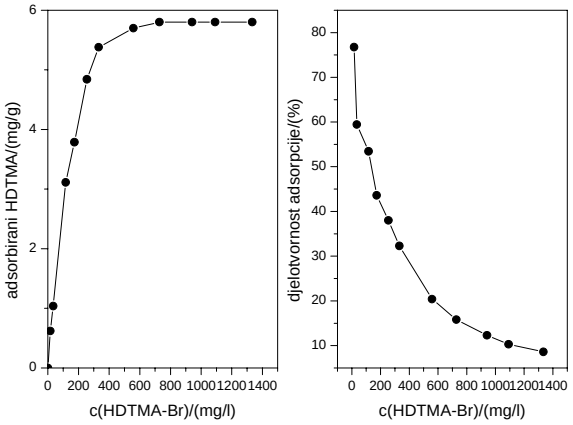
0,250 g organo-zeolita s točno poznatim HDTMA-opterećenjem vanjske površine, dodano je u 50,0 ml otpadne vode. Ovako dobivene suspenzije miješane su na magnetskoj miješalici 15 minuta brzinom od 350 rpm. Alikvoti svakih od tih suspenzija su centrifugirani te im je određena boja u Pt Co skali (DR/2500 Hach spektrofotometar). Djelotvornost obezbojenja otpadne vode izračunata je prema jednadžbi (1):

$$\%\ obezbojenja = \frac{(boja)_1 - (boja)_2}{(boja)_1} x\,100 \qquad (1)$$

gdje su $(boja)_1$ i $(boja)_2$ – boje otopina prije i nakon obezbojenja. Rezultati su prikazani na slici 5.

3. REZULTATI I RASPRAVA

Na slici 1 prikazani su rezultati određivanja adsorpcije tenzida na zeolit, a na slici 2 zeta potencijali uzoraka organo-zeolita. Djelotvornost adsorpcije smanjuje se povećanjem koncentracije tenzida u otopini. Tako je u otopini tenzida koncentracije 16,0 mg/l adsorbirano 0,61 mg HDTMA/g zeolita, odnosno 76,8 % tenzida. Ravnotežna maksimalna vrijednost adsorbiranih molekula HDTMA postignuta je u otopinama čija je koncentracija nešto veća od kritične micelarne koncentracije. U otopini tenzida koncentracije 170 mg/l adsorbirano je 3,8 mg HDTMA/g zeolita (44 %), a u otopini tenzida koncentracije 558 mg/l adsorbirano je 5,7 mg HDTMA/g zeolita (21 %).



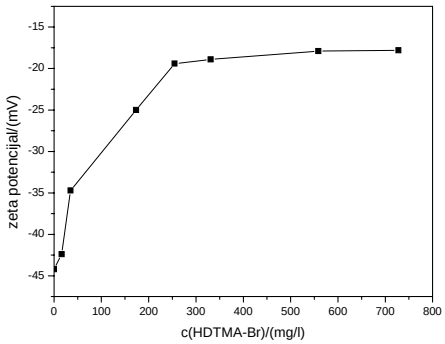
Slika1. Adorpcija i djelotvornost adsorpcije HDTMA na sintetskom mordenitu

Prema literaturnim podacima, može se pretpostaviti da je u otopinama kationskih tenzida čije su koncentracije manje od pripadnih kritičnih micelarnih koncentracija, adsorpcija tenzida rezultat interakcija izoliranih kationa s aktivnim mjestima na površini zeolita (Ogino K., Abe M., 1993; Rupprecht, Gu T., 1991; Somasundaran P., Krishnakumar S., 1997). Kationi $HDTMA^+$ ulaze u reakcije ravnotežne ionske zamjene s kompenzirajućim kationima koji su smješteni na vanjskim izmjenjivim pozicijama trodimenzionalne alumosilikatne mreže (Bowman R.S., i ost. 2000; Li Z., Bowman R.S., 1998).

Otvor najvećeg elipsoidnog 12-teročlanog prstena kanala mordenita, $(Na_2,Ca,K_2)_4[Al_8Si_{40}O_{96}] \cdot 28\ H_20$ je 0,65 · 0,70 nm, a volumen strukturnih šupljina 0,26 $[(cm^3)H_2O/(cm^3)_{MOR}]$). To je u slučaju manjih anorganskih i organskih molekula idealni prostor za inkorporaciju, enkapsulaciju i nastajanje nano – klastera (Meier W. M., 1978). Pokazano je da u vodenoj otopini molekula kationskog bojila - metilenskog modrila (MB^+), može u ravnotežnom procesu ionske zamjene zauzeti kationsko mjesto u mordenitu, gdje se nalazi kao monomerna kationska molekula koja kompenzira naboj izmjenjenog kationa (Simončić P., Armbruster T., 2005). Na aktivnim sorpcijskim mjestima na površini mordenita, MB^+ nalazi se u obliku dimernih molekula. Kvaterna amonijeva skupina kationa $HDTMA^+$ promjera 0,694 nm, ima mogućnost slobodne

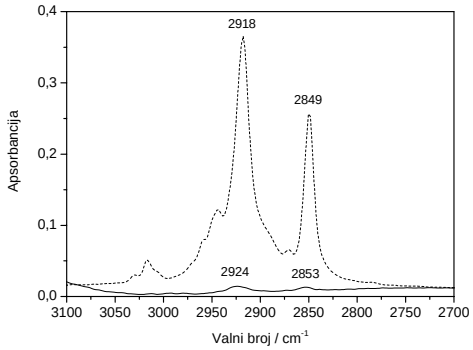
rotacije oko σ-veze -C –N^+- $(CH_3)_3$ koja povezuje alkilni lanac s dušikom i mogućnost slobodne rotacije metilnih skupina.
Mordenit spada u visokosilicijske zeolite, jer je udio T_{Si} tetraedarskih mjesta koja su zauzeta silicijevim atomima 0,80-0,85, što znači da su veze –Si-O-Si- dominantnije i u većem brojčanom iznosu u odnosu na veze –Si-O-Al-. Veza Si-O-Si je fleksibilna s dozvoljenom ograničenom rotacijom tetraedarskog para oko veznog Si-Si vektora. Fleksibilnost 12-teročlanog elipsoidnog prstena je na granici prostornih mogućnosti za djelomičnu inkorporaciju $HDTMA^+$ u poliedarski kanal mordenita. Kationima koji bi na taj način, difuzijom, bili samo djelomično inkorporirani procesom ravnotežne ionske zamjene, umanjila bi se atraktivnost za međudjelovanje s alkilnim lancima drugih kationa $HDTMA^+$ i mogućnost da pod djelovanjem disperznih sila nastaje stabilan dvosloj na međupovršini mordenit/otopina. Kako nije postignuta promjena naboja površine mineralne polianionske matrice niti kod najvećih koncentracija reaktanta $HDTMA^+Br^-$ i kako je u međupovršini mordenit/otopina dokazan relativno mali broj monomernih molekula i asocijata, onda je ovaj mehanizam realan.
Ovakva fenomenologija nije moguća npr. kod zeolita - klinoptilolita zbog stereokemijskih ograničenja gdje je pokazano da se promjenom koncentracije $HDTMA^+Br^-$ može mijenjati arhitektura opteretne površine od monoslojne do višeslojne (Bowman R.S., i ost. 2000, Haggerty G.M., Bowman R.S., 1994; Li Z., Bowman R.S., 2001, Rožić M., i ost. 2007; Sekovanić L., i ost. 2007).
Veći udio molekula HDTMA koje se adsorbiraju na uzorak nemodificiranog sintetskog mordenita, može se pripisati i adsorpciji na amorfne alumosilikate kojih ne rijetko ima u reakcijskoj suspenziji u industrijskim kristalizacijama zeolita. Ova je fenomenologija vezana uz vremensko trajanje indukcijskog perioda, temperaturu, tlak, agitaciju ili pH. Zbog velikog broja pora relativno velikog promjera i velike unutrašnje površine moguća je sorpcija polarnih organskih molekula i organskih kationa kao što je $HDTMA^+$.
Treba uzeti u obzir i da sorpcija kvaternog amina $HDTMA^+$ može biti usmjerena i na aktivna mjesta gdje kristalna struktura zeolita ima neuređenosti nastale u brzim industrijskim neravnotežnim procesima kristalizacije (npr. kutne dislokacije, ravninski defekti, nepopunjena mjesta kationskih ili anionskih strukturnih mjesta itd.). Neutralizacijom suspenzija na kraju procesa kristalizacije zeolita s mineralnim kiselinama (npr. H_2SO_4) može doći do lokalnog prezasićenja s H_3O^+ ionima i dealuminacije jednog ili više molekulskih slojeva mordenita. Pri tome mogu nastati reaktivni Si-oksoanioni i amorfni SiO_2 koji mogu sudjelovati u adsorpciji organskog kationa $HDTMA^+$ (Filipović-Vinceković N., i ost. 1980).
Mogući su dakle procesi ionske zamjene s kompenzirajućim kationima na površini mordenita, adsorpcija na aktivna mjesta, adsorpcija na amorfne alumosilikate i sterički otežani procesi ionske zamjene u poliedarskim kanalima mordenita: $Na^+_{(MOR)} + HDTMA^+_{(aq)} \Leftrightarrow HDTMA^+_{(MOR)} + Na^+_{(aq)}$.
Kod niskih koncentracija tenzida dominantna je adsorpcija monomernih kationa $HDTMA^+$, a pri višim koncentracijama tenzid je prisutan kao asocijat koji djeluje kao elektrostatski suprotno nabijena čestica i može izazvati uzajamnu koagulaciju. Polianionska anorganska matrica, pod djelovanjem suprotno nabijenog tenzidnog asocijata gubi odbojne elektrostatske sile pri čemu je podložna aglomeraciji (Despotović R., i ost. 1976).
Na slici 2 prikazani su zeta potencijali uzoraka dobivenih u reakciji mineral-tenzid, tretiranih s otopinama HDTMA-Br rastućih koncentracija. Zeta potencijali

nemodificiranog zeolita i organo-zeolita s HDTMA opterećenjem 0,61; 1,04; 3,80; 4,84; 5,40; 5,70 i 5,80 mg HDTMA /g zeolita, redom su: -44,2; -42,4; -34,7; -25,0; -19,4; -18,9; -17,9 i –17,8 mV. Zeta potencijal postiže približno konstantnu vrijednost nakon postizanja kritične micelarne koncentracije u otopini.



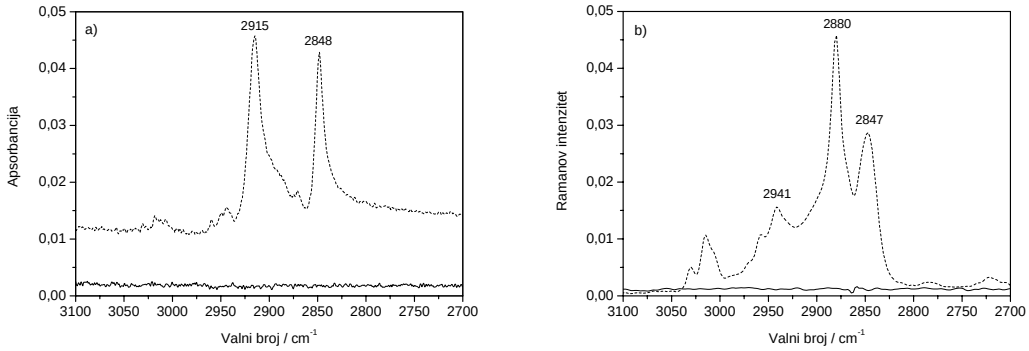
Slika 2. Zeta potencijali uzoraka modificiranog sintetskog mordenita (organo-zeolita) u ovisnosti o masenoj koncentraciji organskog reaktanta $HDTMA^+Br^-$ u suspenziji

Struktura molekula HDTMA adsorbiranih na površini sintetskog zeolita mordenita istražena je primjenom FT infracrvene i FT Ramanove spektroskopije. Najintenzivnije apsorpcijske vrpce u FTIR spektru čiste kristalne supstancije $HDTMA^+Br^-$ pri 2918 i 2849 cm^{-1} pripisane su antisimetričnom i simetričnom istezanju C–H veza metilenskih skupina (Hongping H., i ost. 2004). Frekvencije spomenutih modova ovisne su o konformaciji i gustoći slaganja metilenskih lanaca (Vaia R.A., i ost. 1994; Li Y., Ishida H., 2003). Pri visokoj koncentraciji adsorbiranih molekula, lanci poprimaju *all-trans* konformaciju, a apsorpcijske vrpce u FTIR spektrima nalaze se pri valnim brojevima odgovarajućih vrpci u spektru čistog tenzida. Kao posljedica niske koncentracije lančanih molekula na površini zeolita, javlja se konformacijski nered, pri čemu se frekvencije CH_2 modova istezanja pomiču prema većim valnim brojevima ukazujući na prisutnost *gauche* conformera. U FTIR spektru zeolita s adsorbiranim tenzidom koncentracije 5,8 mg/g, apsorpcijska vrpca antisimetričnog CH_2 istezanja zapažena je pri 2924 cm^{-1}, dok je vrpca simetričnog CH_2 istezanja zabilježena pri 2853 cm^{-1} (Slika 3).



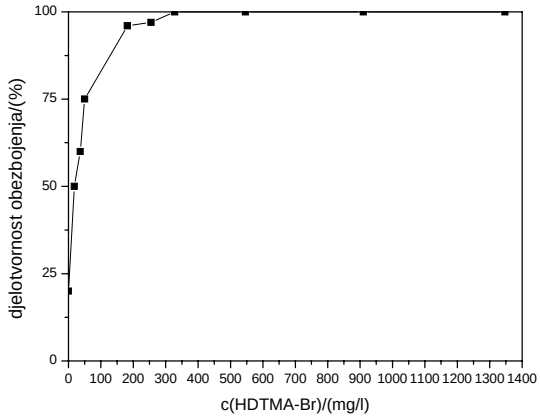
Slika 3. FTIR spektri uzoraka $HDTMA^+Br^-$ (---) i mordenita s adsorbiranim HDTMA (—) pripravljenih tehnikom KBr pastile

Slabi intenzitet i položaj vrpci u spektru upućuju na nisku koncentraciju HDTMA molekula na površini mordenita, većinom u obliku *gauche* konformera.
U FTIR ATR i FT Ramanovim spektrima mordenita s adsorbiranim tenzidom nisu uočene vrpce koje odgovaraju vibracijskim modovima HDTMA molekule (Slike 4.a i 4.b). Za pretpostaviti je da niska koncentracija molekula na površini zeolita nije dostatna za učinkovitu refleksiju odnosno raspršenje zračenja koje se bilježe ATR odnosno Ramanovim spektrom.



Slika 4. a) FTIR spektri uzoraka $HDTMA^+Br^-$ (---) i mordenita s adsorbiranim HDTMA (—) snimljeni tehnikom prigušene ukupne refleksije (attenuated total reflection, ATR) i b) Ramanovi spektri uzoraka $HDTMA^+Br^-$ (---) i mordenita s adsorbiranim HDTMA (—)

Na slici 5 prikazane su djelotvornosti tenzidom modificiranih uzoraka zeolita za obezbojenje otpadne vode. Nemodificirani zeolit pokazuje mali afinitet za obezbojenje otpadne vode. Djelotvornost obezbojenja je 20%. Za obezbojenje otpadne vode najdjelotvorniji su uzorci zeolita na kojima je adsorbirano više od 4,0 mg HDTMA/g, što odgovara početnim koncentracijama tenzida u otopini većim od 180 mg/l. S masenim udjelom od 0,5 % (w/w) tih modificiranih uzoraka zeolita djelotvornost obezbojenja veća je od 95%.



Slika 5. Djelotvornost obezbojenja otpadne vode u reakciji: modificirani sintetski mordenit (organo-zeolit)-otopina ink-jet bojila magenta, u ovisnosti o masenoj koncentraciji organskog reaktanta $HDTMA^+Br^-$ u suspenziji

4. ZAKLJUČAK

Najveća brojnost adsorbiranih molekula kationskog kvaternog tenzida na sintetskom zeolitu mordenitu postignuta je u otopinama čije su masene koncentracije manje od kritične micelarne koncentracije (342,2 mg/l). U međupovršini dvofaznog disperznog sustava; zeolit/vodena otopina heksadeciltrimetilamonijevog bromida, adsorbiraju se izolirani momomerni ioni $HDTMA^+$ elektrostatskim Coulombovim (ionskim) vezama na aktivna sorpcijska mjesta. Promjena zeta potencijala od negativnog na pozitivniji mijenja prirodu zeolita koji poprima svojstva adsorbensa organskih polutanata. Za obezbojenje ispitivane otpadne vode najbolji učinci dobiveni su s uzorcima zeolita modificiranih otopinama $HDTMA^+Br^-$ koncentracija većih od 180 mg/l. Rezultati ispitivanja pokazali su da je djelotvornost obezbojenja veća od 95 %, ako je maseni udio organo zeolita u otopini bojila 0,5 %.

5. LITERATURA

Breck D.W., (1984), *Zeolite Molecular Sieves*, Wiley, New York.

Bowman R.S., Sullivan E.J., Li Z., (2000), *Natural Zeolites for the Third Millennium,* Colella C., Mumpton F.A. (Eds.), De Frede Editore, Napoli, Italy.

Li Z., Bowman R.S., *Environ. Sci. Technol*. Vol. 32 (1998) 2278.

Haggerty G.M., Bowman R.S., *Environ. Sci. Technol*. Vol. 28 (1994) 452.

Li Z., Bowman R.S., *Wat. Res*. Vol. 35 (2001) 322.

Ogino K., Abe M., (1993), *Mixed Surfactant Systems*, Marcel Dekker, Inc., New York.

Rupprecht H., Gu T., *Colloid & Polymer Science*. Vol. 269 (1991) 506.

Somasundaran P., Krishnakumar S., *Colloids and Surfaces A: Physicochemical and Engineering Aspects.* Vol. 123-124 (1997) 491.

Meier W. M., (1978), u: Sand L.B., Mumpton F.A. (Ured.), *Natural Zeolites, Occurrence, Properties, Use*, p. 99.

Simončić P., Armbruster T., *Microporous and Mesoporous Materials* Vol. 81 (2005) 87.

Rožić M., Kropar Vančina V., Anić-Vučinić A., Sekovanić L., Košutić K., (2007), *Proceedings/11th International Conference of Printing, Design and Graphic Communications Blaž Baromić*, Grafički fakultet Sveučilišta u Zagrebu; Ogranak Matice Hrvatske Senj; Pulp and Paper Institute, Ljubljana, Slovenija, Zadar, 131.

Sekovanić L., Rožić M., Hrenović J., Malus D., Sekovanić L., (2007), *Znanstveno-stručni skup, Tehnologije obrade voda*, Akademija Tehničkih znanosti, Zadar, 14.

Filipović-Vinceković N., Sekovanić L., Žitnik D., *Powder Technology.* Vol. 27 (1980) 251.

Despotović R., Filipović N., Peček N., *Colloid & Polymer Sci.* Vol. 254. (1976) 895.

Hongping H., Ray F.L., Jianxi Z., *Spectrochim. Acta* A Vol. 60 (2004) 2853.

Vaia R.A., Teukolsky R.K., Giannelis E.P., *Chem. Mater.* Vol. 6 (1994) 1017.

Li Y., Ishida H., *Langmuir* Vol.19 (2003) 2479.

This work is done in the framework of the project No. 125-1253008-3009: Membrane and adsorption processes for organics removal in water treatment, supported by the Croatian Education, Science and Sport

KARAKTERIZACIJA MATERIJALA ZA RAD NA VISOKIM TEMPERATURAMA

CHARACTERIZATION OF HEAT-RESISTING ALLOY

J.Selanec, D. Ćorić, Z.Schauperl
Fakultet strojarstva i brodogradnje
Sveučilište u Zagrebu
Ivana Lučića 5, Zagreb

Stručni članak / Professional paper

Sažetak:
U izradi strojnih dijelova i kućišta koja su u eksploataciji izložena visokim temperaturama koriste se specijalne vrste materijala, a najčešća je primjena Ni-legura, poznatih po komercijalnim nazivima Inconel ili Nicrofer.
U ovom radu ispituju se mehanička svojstva i mikrostruktura Ni-legure, kvalitete Ni300 koja je u eksploataciji provela 72,000 sati na temperaturama većim od 1000°C. Dobiveni rezultati uspoređuju se sa svojstvima i mikrostrukturom istog materijala prije puštanja u pogon. Na temelju rezultata ispitivanja doneseni su zaključci o promjeni svojstva i strukture materijala tijekom eksploatacije.

Ključne riječi: Inconel, mehanička svojstva, mirkostruktura

Abstract:
In production of mechanical parts and housing which are exposed in exploitation to high temperatures is important to use special kinds of materials. In use most common materials are Ni alloys, with commercial names Inconel or Nicrofer.
This paper describes the results of characterization of Inconel Ni300 with 72.000 operating hours on temperatures higher than 1000°C. These results are compared to the properties of the same material, before exploitation.

Key words: Inconel, Mechanical properties, microstructure

1. UVOD

U izradi strojnih dijelova i kućišta koja su u eksploataciji izložena visokim temperaturama koriste se posebne vrste materijala. S obzirom na temperaturno područje primjene koriste se neke vrste ugljičnih (nelegiranih), niskolegiranih, visokolegiranih martenzitnih te visokolegiranih austenitnih čelika. Kod onih dijelova kod kojih se ne traži visoka statička i dinamička izdržljivost, najčešća je primjena Ni-legura, poznatih po komercijalnim nazivima Inconel ili Nicrofer.

Glavno obilježje legura na osnovi nikla je FCC kristalna struktura. U tehničkoj primjeni to znači da kod njih sa sniženjem temperature ne dolazi do prelaska žilavog u krhki prijelom, pa se mogu nazvati žilavim materijalima. Niklove su legure ponajprije razvijene zbog njihove korozijske i toplinske postojanosti. One zadržavaju dobru vlačnu čvrstoću i otpornost na puzanje pri povišenim i visokim temperaturama.

U ovom radu određuju se svojstva Ni-legure, kvalitete Ni300 (Inconel 617 ili Nicrofer 5520Co), koja je u eksploataciji provela 72,000 h. Materijal je toplinski obrađen na temperaturi 1125°C, u trajanju 5 h, uz brzinu hlađenja od 250°C/h. Uzorak materijala izrezan je s gornje polovice kućišta vrućih plinova na ulazu u plinsku turbinu i to s bočne strane kućišta, odmah uz prvi red rupa za hlađenje (*slika 1*). Na dobivenom uzorku provedena su laboratorijska ispitivanja koja uključuju ispitivanje mehaničkih svojstava te analizu mikrostrukture pomoću svjetlosnog mikroskopa.



(a) *(b)*

Slika 1: Dio kućišta vrućih plinova

2. ISPITIVANJE MEHANIČKIH SVOJSTAVA I MIKROSTRUKTURE

Ispitivanje mehaničkih svojstava i mikrostrukture provedeno je na Fakultetu strojarstva i brodogradnje u Zagrebu. Od mehaničkih svojstava određivala se vlačna čvrstoća, konvencionalna granica razvlačenja, istezljivost, kontrakcija, žilavost i mikrotvrdoća. Statički vlačni pokus i ispitivanje udarnog rada loma provedeno je na sobnoj temperaturi.

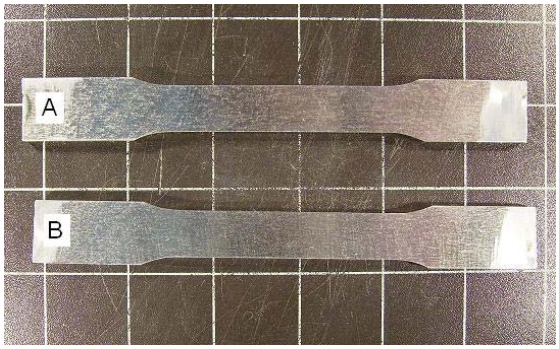
2.1 Ispitivanje mehaničkih svojstava

Slika 2 prikazuje uzorak Ni-legure (Inconel 617), iz kojeg su izrezane epruvete za vlačno ispitivanje i ispitivanje žilavosti, te uzorci za metalografska ispitivanja.

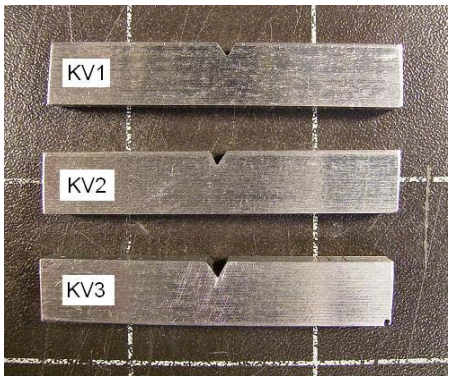


Slika 2: Uzorak Ni-legure (Inconel 617) izrezan s kućišta vrućih plinova s označenim mjestima rezanja epruveta za mehanička ispitivanja i metalografiju.

Statički vlačni pokus je proveden na računalom vođenoj elektronskoj kidalici, (proizvođač: WPM, Njemačka; vrsta: EU 40mod), koja u potpunosti omogućava provođenje ispitivanja i registriranje rezultata sukladno normi HRN EN 10002-1. Epruvete za statički vlačni pokus prikazane su *slikom 3*. Ispitivanje udarnog rada loma (žilavosti) provedeno je Charpyevim batom na nestandardnoj epruveti s V utorom dimenzija 5x10x55 mm (*slika 4*). Mikrotvrdoća je mjerena po Vickersu mikrotvrdomjerom PMT3 s utegom mase 200 g (HV0,2). Mjerenje se izvodilo u 3 niza: od unutarnjeg ruba, koji je bio izložen vrućim plinovima prema sredini, u sredini uzorka, te od vanjskog ruba prema sredini. Rezultati statičkog vlačnog ispitivanja prikazani su *tablicom 1*, dok su *tablicom 2* prikazani rezultati ispitivanja udarnog rada loma. Dijagram naprezanje - istezanje, dobiven statičkim vlačnim pokusom prikazan je *slikom 5,* a rezultati ispitivanja mikrotvrdoće dijagramski su prikazani na *slikama 6 i 7.* Na temelju dobivenih rezultata mikrotvrdoće, za svaki niz izračunata je srednja vrijednost. Ona za unutarnji rub iznosi 226 HV, za vanjski 272 HV, dok u sredini iznosi 198 HV.



Slika 3: Epruvete za statičko vlačno ispitivanje



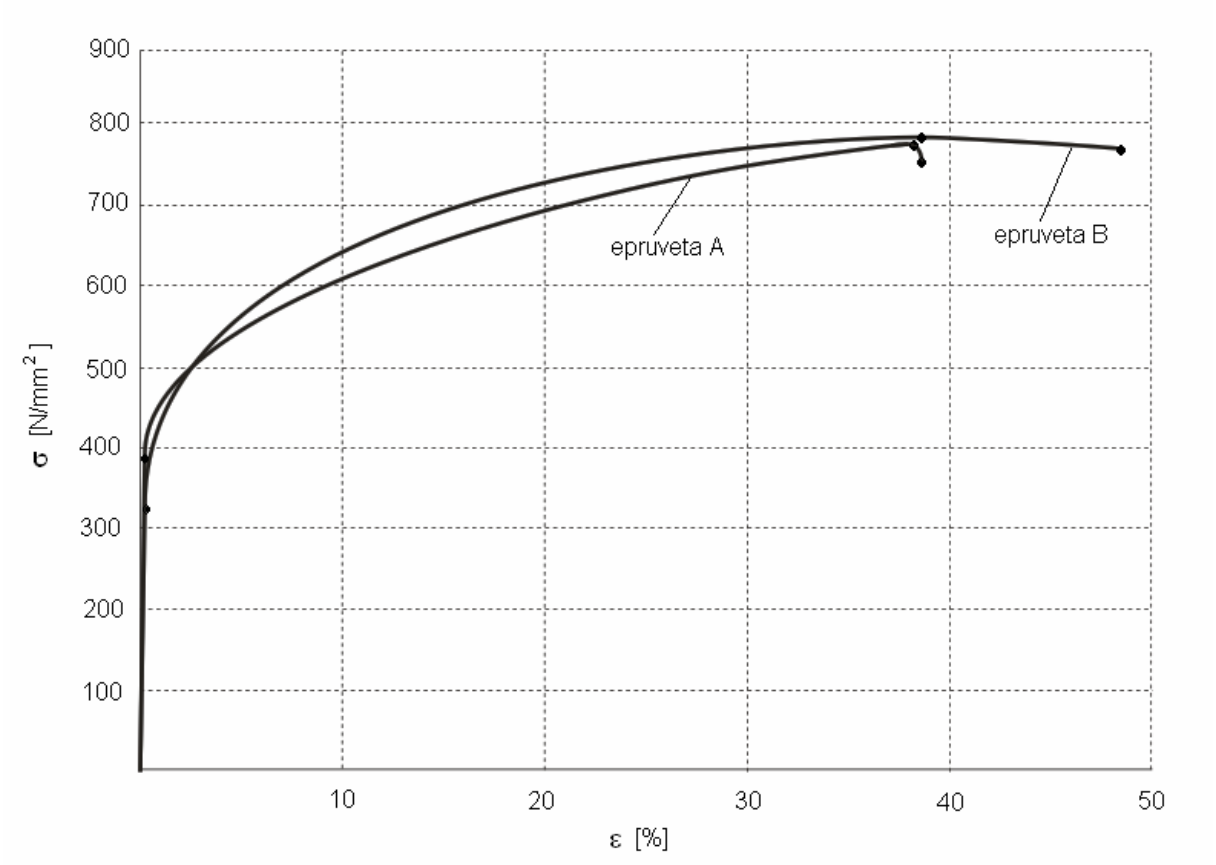
Slika 4: Epruvete za ispitivanje žilavosti po Charpyu

Tablica 1: Rezultati ispitivanja mehaničkih svojstava

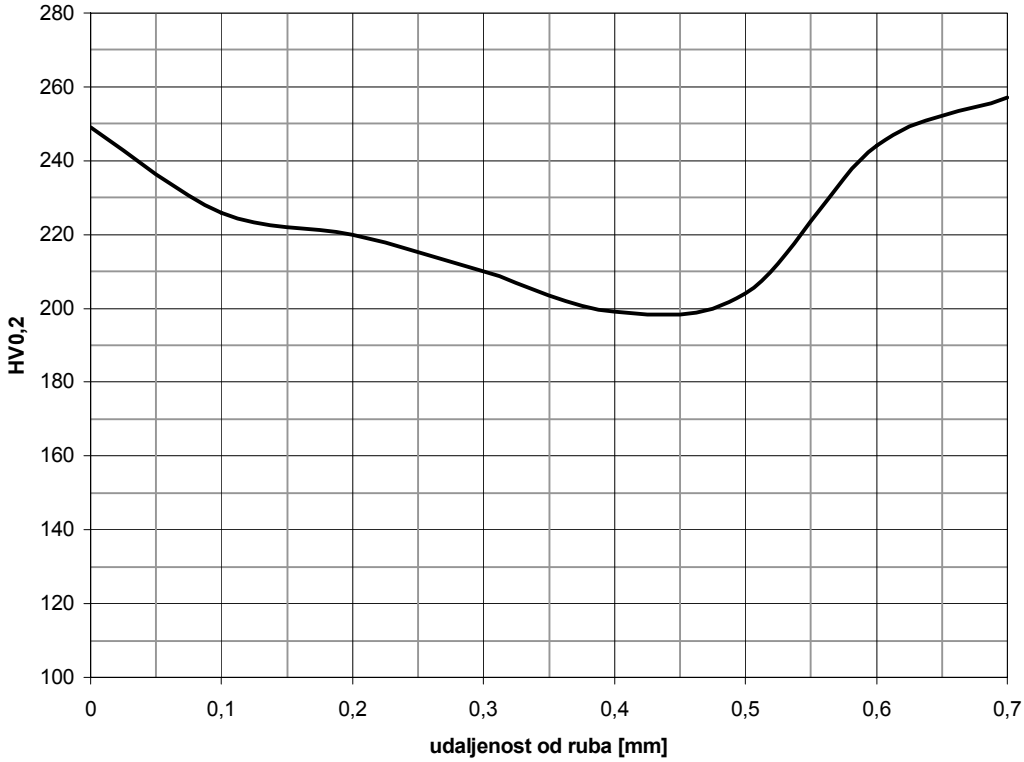
	A	**B**
konvencionalna granica razvlačenja $R_{po,2}$ [N/mm^2]	386	335
vlačna čvrstoća R_m [N/mm^2]	773	777
istezljivost A [%]	37,7	47,0
kontrakcija Z [%]	29,1	35,0

Tablica 2: Rezultati ispitivanja udarnog rada loma

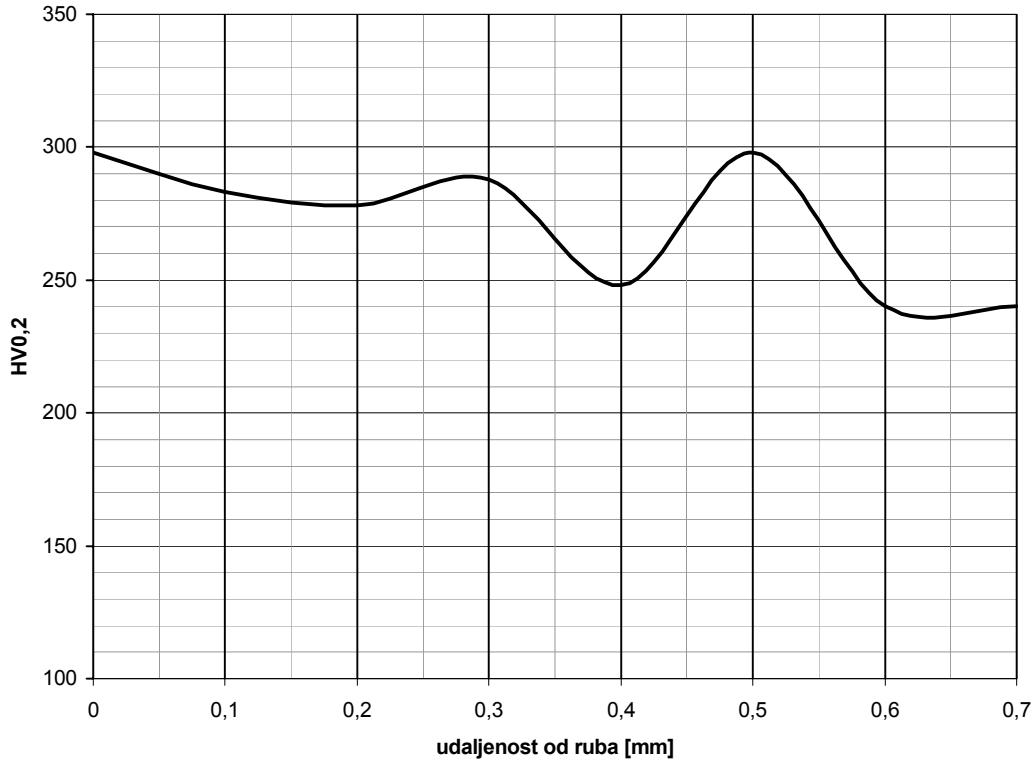
udarni rad loma [J]	**KV1**	**KV2**	**KV3**
	26,0	25,5	24,0



Slika 5: Dijagram naprezanje – istezanje



Slika 6: Promjena mikrotvrdoće od unutrašnjeg ruba, izloženog vrućim plinovima prema sredini



Slika 7: Promjena mikrotvrdoće od vanjskog ruba prema sredini

Prema dobivenim specifikacijama ovog materijala, udarni rad loma trebao bi iznositi 40 J za nestandardnu epruvetu s V utorom dimenzija 5x10x55 mm. Rezultati statičkog vlačnog pokusa trebali bi biti slijedeći:

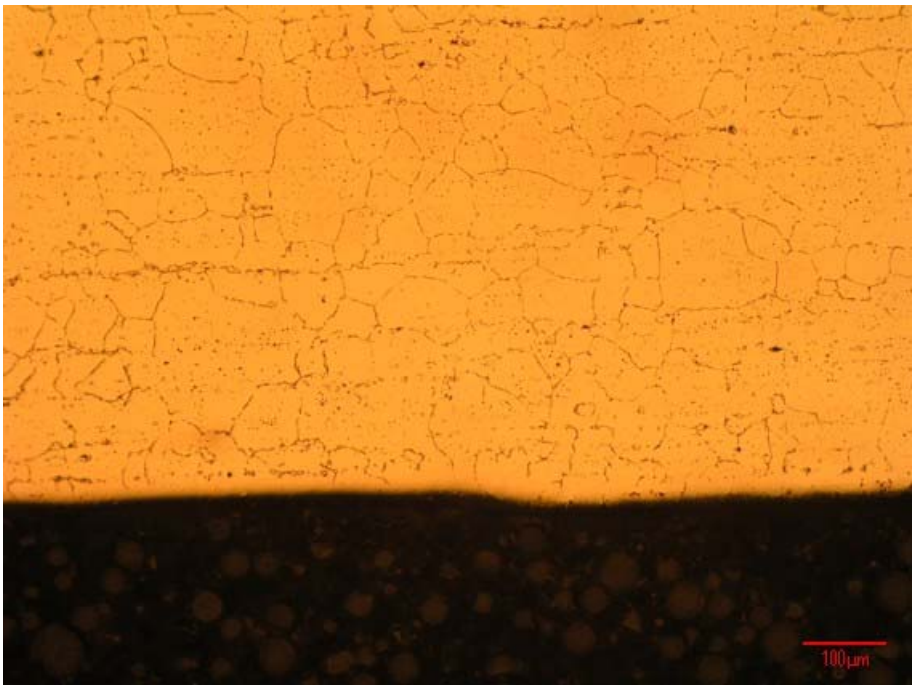
- konvencionalna granica razvlačenja $R_{p0,2}$: min. 300 N/mm^2
- vlačna čvrstoća R_m: min. 700 N/mm^2
- istezljivost A: min. 35 %

Kako se vidi iz *tablice 2*, dobivena vrijednost udarnog rada loma niža je od propisane, dok konvencionalna granica razvlačenja i vlačna čvrstoća zadovoljavaju vrijednosti propisane za taj materijal.

2.2 Analiza mikrostrukture

Analizirana je mikrostruktura materijala uz površinu koja je izložena visokim temperaturama, mikrostruktura u sredini stjenke te uz površinu materijala koja se hladi. Uzorci su pripremljeni u skladu s preporukama za tu vrstu materijala: izrezani uz intenzivno hlađenje i podmazivanje, zaliveni u odgovarajuću masu, brušeni, polirani i nagriženi u sredstvu naziva gliceregia.

Mikrostruktura u nagriženom stanju je prikazana na *slikama 2.5, 2.6* i *2.7*.



Slika 2.5 Mikrostruktura materijala uz unutrašnju površinu izloženu visokim temperaturama



Slika 2.6 Mikrostruktura materijala u sredini stjenke



Slika 2.7 Mikrostruktura materijala uz vanjsku hlađenu površinu

Na *slikama 2.5, 2.6 i 2.7* vidljivi su kristali mješanci s mjestimično izlučenim precipitatima i karbidima po granicama zrna. Analizom mikrostrukture materijala nisu vidljive značajne greške niti eventualne transformacije strukture. Ne postoji značajna razlika u veličini zrna i strukturi na analiziranim mjestima.

3. ZAKLJUČAK

Kako je već navedeno, jedno od glavnih obilježja Ni-legura je, što pri povišenim i visokim temperaturama zadržavaju dobru vlačnu čvrstoću i otpornost na puzanje. Zbog toga se u ovom istraživanju ispituju svojstva navedenog materijala (Inconel 617) izrezanog s kućišta vrućih plinova, koji je u eksploataciji proveo 72,000 h.

Ispitivanjem žilavosti po Charpyu, dobivena je puno manja vrijednost udarnog rada loma od specificirane, dok konvencionalna granica razvlačenja i vlačna čvrstoća zadovoljavaju propisane vrijednosti. Može se reći da se vrijednosti istezljivosti nisu puno promijenile. Rezultati dobiveni mjerenjem mikrotvrdoće pokazuju da se ona drastično ne mijenja od unutarnjeg ruba koji je bio izložen struji vrućih plinova prema sredini, te od vanjskog ruba prema sredini. Analizom mikrostrukture materijala nisu vidljive značajne greške niti eventualne transformacije strukture.

Modelling of high-speed steels' hardness using catalogue data

W. Sitek*
Division of Materials Processing Technology, Management and Computer Techniques in Materials Science, Institute of Engineering Materials and Biomaterials,
Silesian University of Technology, Konarskiego St. 18a, 44-100 Gliwice, Poland
*Corresponding author, e-mail address: wojciech.sitek@polsl.pl

Izvorni znanstveni rad / Original scientific paper

ABSTRACT

The paper presents the method of high - speed steels' secondary hardness modeling, based on chemical composition and heat-treatment parameters. Computer modeling using neural network were carried out using data included in steels maker catalogues containing information about high-speed steels. The model developed in the work was numerically verified. The verification procedure consists of the evaluation of the conformity of the computational results with the catalogue data. The worked out model may be used in computer systems of steels' designing for cutting tools.

Keywords: high-speed steels, hardness, neural network, modelling

1. INTRODUCTION

High-speed steels are still an important group of engineering materials. Their common industrial application justifies carrying out research on new types of steel with better functional qualities. A fast development in computer science and its widely spread modern technologies brings about the successful application of steels in research concerning the material engineering. Artificial intelligence method, including neural networks, as well as advanced computational methods make it possible to broaden the examinations over the high-speed steels in order to reduce costs of their manufacturing by replacing laborious and expensive metallurgical processes with computer analyses and simulations. Another vital factor is a significant reduction of time of analyses done, as the application of new technologies makes it possible to avoid lots of laborious empirical research and replacing it by computer simulations whose correct results are often a basic source of consecutive analyses. Modern applications of computer sciences in the material engineering including the artificial intelligence methods are more and more of the interest of the materials science environment. Years to come will definitely bring new solutions that will indicate other areas of practical use of these methods, and our own works [1-8] are an example.

In the paper there has been a neural network model presented, helpful when calculating the secondary hardness of high-steels after the heat-treatment on the basis of the chemical composition and heat treatment parameters.

2. MATERIALS AND EXPERIMENTAL METHODOLOGY

The base of the neural network model are the data included in the Erasteel world-wide high-speed maker standard catalogues embracing information about 20 grades of the high-

speed steels [9]. This catalogue involves information concerning the chemical composition shown as average concentration of particular alloy elements (Table 1). Moreover, it presents approximate diagrams of tempering curves (for different values of tempering temperatures) for the different austenitising temperature for a given type of steel. The examples taken from the catalogues are presented on Figures 1-2. Ranges of the austenitising and tempering temperatures for particular steels are presented in Table 2. This way the appropriate set of data has been obtained which describes the secondary steel hardness' values depending on the chemical composition and heat–treatment parameters containing 936 results. Next, the neural network has been designed and numerically verified that made possible to calculate the hardness of the steel on the basis of the chemical composition and heat-treatment temperatures.

3. CALCULATIONS OF STEELS' HARDNESS

For modelling of the high-speed steels secondary hardness basing only on steels chemical composition and austenitising and tempering temperatures, the multi-layer feedforward neural networks with learning rule based on the error back-propagation algorithm and conjugate gradient were employed. The 8-X-1 two-layer and 8-X-Y-1 networks were considered where X and Y denotes number of nodes in hidden layer 1^{st} and 2^{nd} respectively. There are eight nodes on the input of the network and 6 of them represent the values of the concentration of particular alloying element occurring in the analysed steels. Next two inputs represent austenitising and tempering temperatures. The node on the output network layer represents the value of the secondary steel hardness.

The model developed in the work was experimentally verified. The verification procedure consists of the evaluation of the conformity of the computational results with the data included in catalogues.

The data set was divided into three sub-sets: training, validating and testing one. The training set was used for development of the neural network model, the validating set was used for checking the model during establishing the values of weights, and the testing set was used for verifying the model when the network training was completed. Allocation of data to the particular subsets was done randomly. The following quantities determined for the data sets were used as the basic coefficients for evaluation of the neural network model performance:

- average network prediction error,
- ratio of standard deviations of errors and data,
- Pearson correlation coefficient.

These coefficients have been calculated for the consecutive distances from the quenched end. The best quality coefficients have been obtained for the MLP (multilayer perceptron) network. The analysis of the quality coefficients calculated for the training, validating, test and verifying sets has proved that the smallest error occurs in the network with one hidden layer of neurons. The structure, method, training parameters and the error value, ratio of standard deviations and the correlation coefficient values of the neural network for which the most beneficial values of the coefficient factors have been obtained are presented in Table 3. The approximate values of the mentioned coefficients for particular data sets indicate the ability of the network to generalize the knowledge acquired in the training process. The mean error value, ratio of standard deviations and the correlation coefficient for the selected distances from the quenched end have been compared in Table 3.

Table 1.
Chemical composition of analysed high-speed steels

Erasteel brand name	EN designation	Average mass concentration of the alloying element, %					
		C	Cr	Mo	W	Co	V
ABC III	HS 3-3-2	0.99	4.1	2.7	2.8	0	2.4
EM 1	HS 1-8-1	0.83	3.8	8.5	1.8	0	1.2
E M3:1	HS 6-6-2	1.05	4	6.3	6.3	0	2.5
E M4	HS 6-5-4	1.3	4.2	4.5	5.6	0	4
E M50	HS 0-4-1	0.84	4	4.2	0	0	1.1
E T1	HS 18-0-1	0.75	4.1	0	18	0	1.1
M9V	HS 4-8-3	1.2	4.2	8.5	3.5	0	2.7
E M2	HS 6-5-2	0.9	4.2	5	6.4	0	1.8
E M3:2	HS 6-5-3	1.2	4.1	5	6.2	0	3
E M7	HS 2-9-2	1.02	3.8	8.6	1.8	0	1.9
E M52	HS 1-4-2	0.89	4	4.5	1.2	0	1.9
GRINDAMAX V3	HS 7-5-3	1.2	3.9	5.2	7	0	2.7
BiMax42+	HS 2-9-1-8	1.08	3.8	9.4	1.5	8	1.2
E 945	HS 2-5-1-2	0.91	3.7	5	1.8	2.5	1.2
E M42	HS 2-9-1-8	1.08	3.8	9.4	1.5	8	1.2
WKE 42	HS 10-4-3-10	1.27	4	3.6	9.5	10	3.2
C8	HS 6-5-2-8	1.05	4	6	5	7.8	1.6
E M35	HS 6-5-2-5	0.93	4.2	5	6.4	4.8	1.8
E MAT II	HS 1-5-1-8	0.72	4	5	1	8	1
WKE 45	HS 9-4-3-11	1.41	4.2	3.6	8.8	11	3.4
ACTIUM 74 Co[1)]	-	0.9	3.9	2.75	1.8	2	1.8
[1)] No standard, TM grade							

Table 2.
Heat-treatment temperatures of analysed high-speed steels (in °C)

Erasteel brand name	EN designation	Austenitising temperature		Tempering temperature	
		Min	Max	Min	Max
ABC III	HS 3-3-2	1100	1180	520	620
EM 1	HS 1-8-1	1100	1200	520	620
E M3:1	HS 6-6-2	1150	1200	520	620
E M4	HS 6-5-4	1100	1220	520	620
E M50	HS 0-4-1	1080	1120	520	620
E T1	HS 18-0-1	1150	1280	520	620
M9V	HS 4-8-3	1160	1220	520	620
E M2	HS 6-5-2	1050	1220	520	620
E M3:2	HS 6-5-3	1120	1220	520	620
E M7	HS 2-9-2	1100	1200	520	620
E M52	HS 1-4-2	1150	1200	520	620
GRINDAMAX V3	HS 7-5-3	1120	1240	520	620
BiMax42+	HS 2-9-1-8	1100	1190	520	600
E 945	HS 2-5-1-2	1070	1170	520	620
E M42	HS 2-9-1-8	1150	1190	520	600
WKE 42	HS 10-4-3-10	1100	1230	480	620
C8	HS 6-5-2-8	1050	1200	520	620
E M35	HS 6-5-2-5	1050	1220	520	620
E MAT II	HS 1-5-1-8	1050	1100	520	620
WKE 45	HS 9-4-3-11	1100	1220	520	620
ACTIUM 74 Co	-	1050	1180	520	620

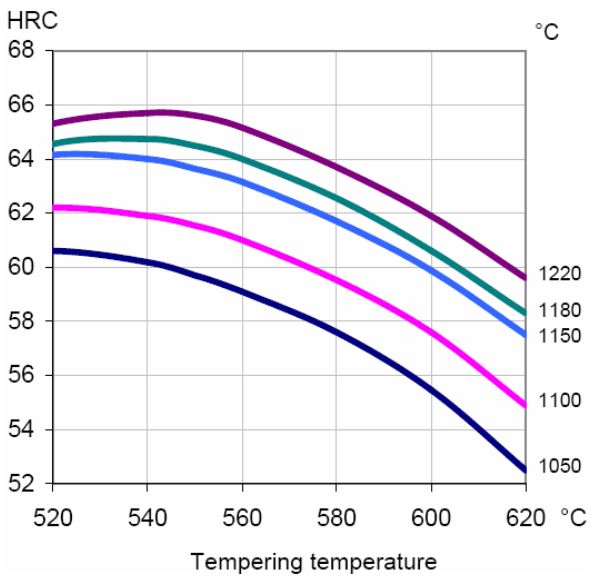


Fig. 1. Examples of data sheet used in modeling of steels' hardness (HS 6-5-2)

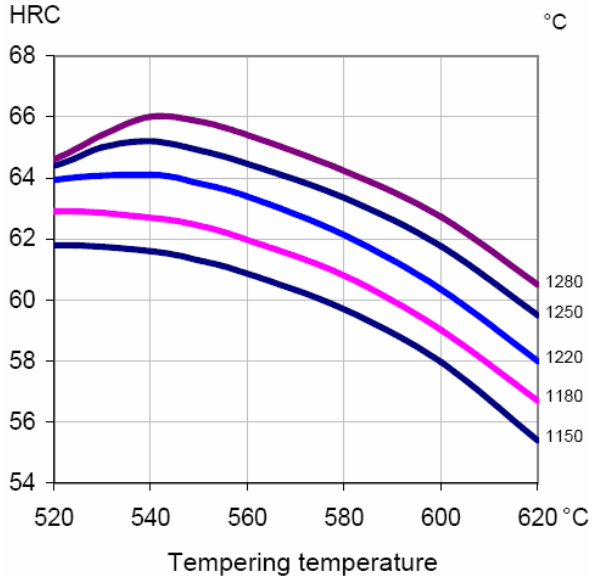


Fig.2. Examples of data sheet used in modeling of steels' hardness (HS 18-0-1)

Table 3.
The structure, training parameters and the quality coefficients for network designed for calculating the hardness

Network structure	Training method / No of epochs	Data set	Quality coefficient		
			Relative error, HRC	Ratio of standard deviations	Correlation coefficient
8-8-1	BP/50 CG/455b	training	0,33	0,13	0,99
		validating	0,37	0,14	0,99
		testing	0,37	0,14	0,99
BP – back-propagation error algorithm, CG - conjugate gradients					

The verifying calculations have shown that the neural network model allows for calculating the secondary hardness of steel with accuracy up to 0.4 HRC. It is the average error of calculations and its maximal values do not exceed 1.1 HRC (for one steels grade - BiMax42+). Moreover, the error for 65% of the calculated values is smaller than the 0.4 HRC value. These results allow accepting that the worked out model is adequate. In figures 3-8 there has been presented the example comparison of the calculation of tempering curves for selected steels.

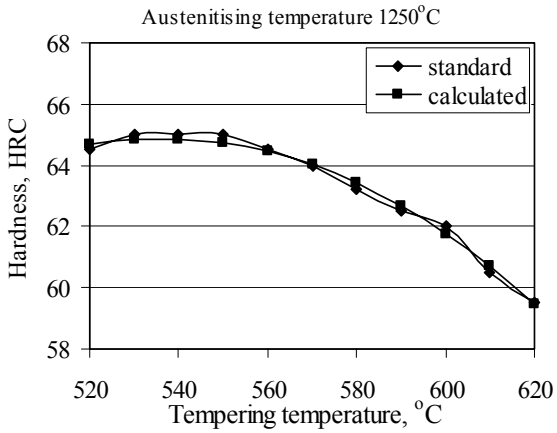


Fig. 3. Comparison of the tempering curves of the HS 18-0-1 steel grade, error of calculations 0.17 HRC

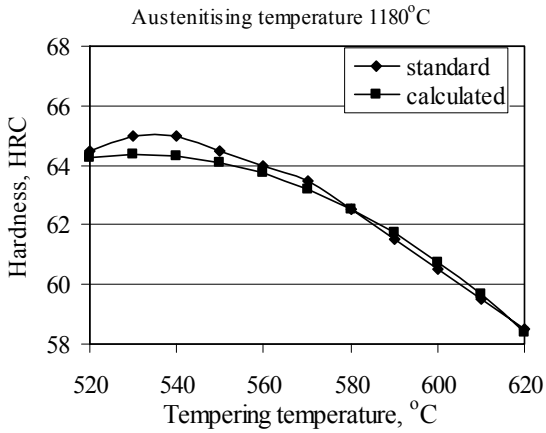


Fig. 4. Comparison of the tempering curves of the HS 6-5-2 steel grade, error of calculations 0.32 HRC

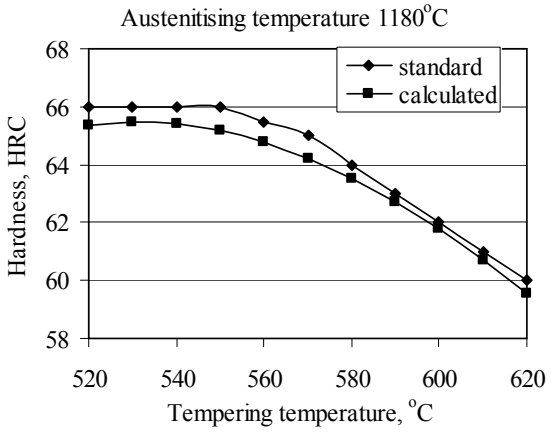


Fig. 5. Comparison of the tempering curves of the HS 2-9-2 steel grade, error of calculations 0.53 HRC

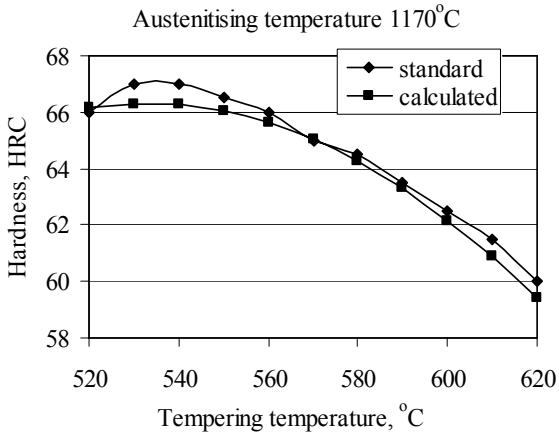


Fig. 6. Comparison of the tempering curves of the HS 2-5-1-2 steel grade, error of calculations 0.80 HRC

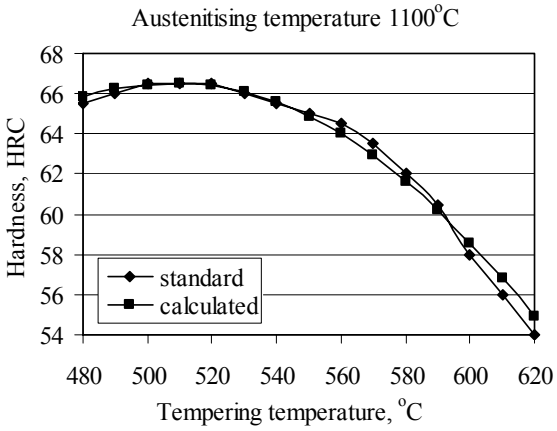


Fig. 7. Comparison of the tempering curves of the HS 10-4-3-10 steel grade, error of calculations 0.34 HRC

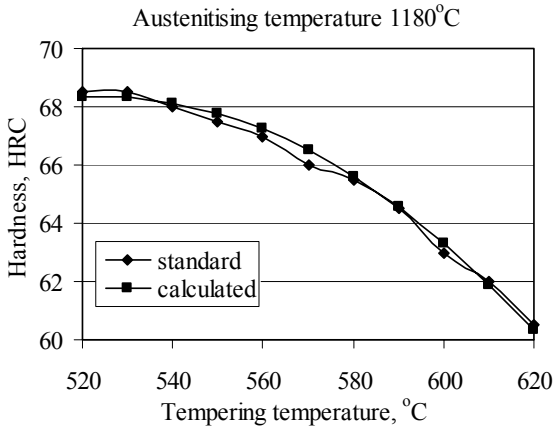


Fig. 8. Comparison of the tempering curves of the HS 6-5-2-8 steel grade, error of calculations 0.2 HRC

4. FINAL REMARKS

In the paper there has been presented the worked out model of the neural network that enables calculating the hardness of high-speed steels on the basis of the chemical composition and the heat-treatment parameters. The obtained calculation results point at the satisfactory conformity of the model with the empirical data, as the calculation error is about 0.4 HRC.

ACKNOWLEDGEMENTS

Investigations were financed in part within the framework of the research project of the Polish Ministry of Science and Higher Education KBN N N 507 2070/33 headed by Dr. W. Sitek.

REFERENCES

[1] W. Sitek, L.A. Dobrzański: Application of genetic methods in materials' design, Journal of Materials Processing Technology, Vols. 164-165, 2005, p. 1607-1611
[2] W. Sitek, L.A. Dobrzański, J. Zacłona: The modeling of high-speed steels properties using neural networks', Journal of Materials Processing Technology, Vol.157-158, 2004, p. 245-249
[3] L.A. Dobrzański, W. Sitek, M. Krupiński, J. Dobrzański: Computer aided method for evaluation of failure class of materials working in creep conditions, Journal of Materials Processing Technology, Vols. 157-158, 2004, p. 102-106
[4] L.A. Dobrzański, W. Sitek: The modelling of hardenability using neural network, Journal of Materials Processing Technology, Vols. 92-93, 1999, p. 8-14
[5] L.A. Dobrzański, W. Sitek: Designing of the chemical composition of constructional alloy steels, Journal of Materials Processing Technology, Vols. 89-90, 1999, p. 467-472
[6] L.A. Dobrzański, W. Sitek: Application of neural network in modelling of hardenability of constructional steels, Journal of Materials Processing Technology, Vol. 78 (1-3), 1998, p. 59-66
[7] W. Sitek, J. Trzaska, L.A .Dobrzański: An artificial intelligence approach in designing new materials, Worldwide Journal of Achievements in Materials and Manufacturing Engineering, 2006, Vol. 17, p. 277 – 280
[8] J. Trzaska, W. Sitek, L.A. Dobrzański: Selection metod of steel grade with required hardenability, Worldwide Journal of Achievements in Materials and Manufacturing Engineering, 2006, Vol. 17, p. 289 – 292
[9] http://www.erasteel.com/us/produits/hss.php

MEHANIČKA I ELEKTROKEMIJSKA SVOJSTVA SLITINE EN AW 8006

THE MECHANICAL AND ELECTROCHEMICAL PROPERTIES OF EN AW 8006 ALLOY

Sanja Slavica Matešić*, Jagoda Radošević, Nikša Krnić**
* TLM d.d. Narodnog preporoda 12, 22000 Šibenik, sanja.slavica@tlm.hr
Kemijsko-tehnološki fakultet, Teslina 10/V, 21000 Split, jagoda.radosevic@ktf-split.hr
** Fakultet elektrotehnike, strojarstva i brodogradnje, 21000 Split

Izvorni znanstveni rad / Original scientific paper

Sažetak: Konačne performanse folije za pakiranje ne ovise samo o mehaničkim već i o elektrokemijskim svojstvima slitine. U svrhu ispitivanja mehaničkih i elektrokemijskih svojstava slitine EN AW 8006 pristupilo se lijevanju velikih aluminijskih blokova slitine EN AW 8006 s četiri različita masena postotka Fe (1.20, 1.50, 1.70 i 1.90% Fe), te procesu industrijske prerade u svrhu dobivanja folije konačne debljine 0.030 mm. Određena su mehanička svojstva u različitim fazama prerade slitina. U analizi rekristalizacijskog ponašanja ove slitine korišten je oporavak mehaničkih vrijednosti nakon hladne deformacije prilikom završnog žarenja. Obzirom da se folija u konačnoj namjeni koristi za pakiranje u prehrambenoj industriji primjenom elektrokemijskih mjernih tehnika određena su elektrokemijska svojstva navedenih uzoraka u otopini NaCl i CH_3COOH.

Ključne riječi: EN AW 8006 slitina, mehanička svojstva, elektrokemijska svojstva.

Abstract: The final performance of the packaging foils depends not only on the mechanical but also on the electrochemical properties of alloy. In the purpose of the study, large aluminium blocks of EN AW 8006 alloy with four different levels of Fe content (1.20, 1.50, 1.70 and 1.90% Fe) were cast and industrial processed into 0.030 mm thick foil. Mechanical properties of the alloy were determined at different stages of the industrial processing. The restoration of the mechanical properties was used in the analysis of the recrystallization behaviour of this alloy previously deformed under cold-working conditions and subsequently annealed. Since the foil is going to be used in the food industry, electrochemical measurement methods were also carried out to determine the corrosive resistance of stated samples in NaCl and CH_3COOH solution.

Key words: EN AW 8006 alloy, mechanical properties, electrochemical properties.

1. UVOD

Aluminijska folija je valjani ravni proizvod pravokutnog presjeka s jednolikom debljinom manjom od 0.2 mm. Isporučuje se kupcima kao poluzavršni proizvod namotan u svitkove. U većini slučajeva ova se folija kasnije koristi kao konstrukcijski materijal za fleksibilna pakiranja koja se sastoje od kombinacije slojeva papira, aluminija i plastičnih slojeva međusobno povezanih adhezivima. Aluminijska folija koja se obično koristi u fleksibilnim pakiranjima može očuvati osjetljivu svježinu hrane mjesecima bez upotrebe hladnjaka, također štiti proizvod od vanjskih utjecaja kao što su migracija kisika, vlažnost, razne kontaminacije, svjetlo [1].

Otprilike 75% proizvedene aluminijske folije se koristi za pakiranje u prehrambenoj, kozmetičkoj, kemijskoj, farmaceutskoj industriji i za foliju za domaćinstvo, dok se 25% koristi u industriji: za izmjenjivače topline, u industriji automobila i elektro industriji.

Tipične serije slitina koje se koriste za izradu folija su 1xxx, 3xxx i 8xxx. Mn je tipični element u seriji 3xxx, a Fe i Si su tipični elementi za serije 1xxx i 8xxx. Serija slitina 8xxx sve više istiskuje seriju slitina 1xxx u području folija jer sadrži veće vrijednosti Fe, Cu, Mn, Mg, Zn i Si čime se poboljšavaju mehanička svojstva [2], ali smanjuje otpornost prema koroziji [3].

Tri različite grupe slitina aluminija za proizvodnju folija su trenutno na raspolaganju na tržištu, svaka s različitim svojstvima. Stoga je važno izabrati najprikladniju slitinu za konačnu primjenu, maksimalnim doprinošenjem fleksibilnom pakiranju.

Grupe slitina za proizvodnju folije sadrže:

- Čisti aluminij (serija 1xxx), koji daje niže mehaničke vrijednosti, ali je prikladan za proizvodnju vrlo tankih folija,
- Slitine aluminij–željezo (serije 8xxx), kod kojih dodatak Fe povećava čvrstoću i duktilnost aluminijske folije,
- Slitine aluminij–željezo–mangan (serije 8xxx), kod kojih mangan poboljšava čvrstoću folije, za proizvode gdje smanjenje izduženja nije kritično.

Konačne performanse folije za pakiranje ne ovise samo o mehaničkim svojstvima, već i o elektrokemijskim svojstvima. Izvjestan broj legirajućih elemenata i nečistoća slabo su topljivi u aluminiju, te se prilikom lijevanja precipitiraju u obliku međumetalnih spojeva. Čestice međumetalnih spojeva su mikroskopskih dimenzija i njihov korozijski potencijal često je različit od korozijskog potencijala aluminijeve matrice u kojoj se ove čestice nalaze. Zbog toga postoji mogućnost nastanka mikrogalvanskih članaka između međumetalnih čestica i aluminijeve matrice ukoliko je legura u dodiru s otopinom elektrolita, što za posljedicu ima nastanak lokaliziranog oblika korozije.

Svrha ovog rada je bila ustanoviti optimum kemijskog sastava (obzirom na sadržaj Fe), mehaničkih i elektrokemijskih svojstava ispitivane slitine, a koji će dovesti do ušteda bilo da se radi o reduciranju debljine folije ili uštedi otklanjanjem nekih slojeva unutar višeslojnog sloga u procesu oplemenjivanja folije [4].

2. EKSPERIMENTALNI DIO

Materijal:

U svrhu ispitivanja mehaničkih i elektrokemijskih svojstava slitine EN AW 8006 (Al-Fe-Mn) pristupilo se lijevanju velikih aluminijskih blokova slitine s četiri različita masena postotka Fe (1.20, 1.50, 1.70 i 1.90% Fe), te su podvrgnuti procesu industrijske prerade u svrhu dobivanja folije konačne debljine 0.030 mm. Prema Europskoj normi EN 573-3 sadržaj Fe u slitini EN AW 8006 može varirati u granicama od 1.2 do 2.0 %.

Mehanička ispitivanja:

U različitim fazama industrijske prerade slitine (nakon toplog valjanja, hladnog valjanja, međužarenja, te završnog žarenja) vlačnim ispitivanjima utvrđena su elastična i plastična ponašanja materijala u uvjetima jednoosnog statičkog vlačnog naprezanja. Vlačna ispitivanja izvršena su na uzorcima uzdužno u smjeru valjanja (UV) i poprečno na smjer valjanja (PV). Korištenjem univerzalnih hidrauličkih kidalica "Losenhausenwerk" i "Zwick" maksimalne sile od 2.5 kN ispitivani uzorci (tzv. epruvete) kontinuirano su vlačno opterećivani do loma. Vlačnim ispitivanjima utvrđena su temeljna mehanička svojstva materijala, kao što su granica razvlačenja (R_{p02}), vlačna čvrstoća (R_m) i izduženje (A). U analizi rekristalizacijskog ponašanja slitine korišten je oporavak mehaničkih vrijednosti folije debljine 0.030 mm nakon izvršene hladne deformacije tj. redukcije debljine od 96%, prilikom završnog žarenja koje je izvršeno u laboratorijskoj peći u intervalu temperatura od 0-320 ^oC u trajanju od 1 sata.

Elektrokemijska ispitivanja:

Za laboratorijska elektrokemijska ispitivanja od velikih aluminijskih blokova izrađene su elektrode u obliku kockica brida 10 mm, a elektrodni kontakt je ostvaren pomoću izolirane bakrene žice. Uzorci su sa svih strana, osim s jedne zaštićeni epoksi smolom. Slobodna površina koja je bila u kontaktu s elektrolitom iznosila je cca 1 cm^2. Prije svakog mjerenja površina radne elektrode je mehanički i kemijski obrađena. Elektrode su brušene brusnim papirima različite finoće: 360, 600 i 800. Završna glatkoća i zrcalni sjaj dobiveni su naknadnim poliranjem s brusnim papirom finoće 1000. Da bi se odstranio površinski oksidni sloj i eventualno unesene nečistoće, elektrode su držane 1 minutu u alkalnoj otopini 0.1 M NaOH, zagrijanoj na 40 ± 0.1 ^oC. Potom su elektrode ispirane destiliranom i redestiliranom vodom, te što je moguće brže, postavljene u standardni elektrokemijski reaktor s protuelektrodom od platine i zasićenom kalomel elektrodom kao referentnom, koja je preko Luginove kapilare bila u kontaktu s radnom elektrodom. Ispitivanja su provedena u deaeriranoj 0.5 M otopini NaCl i 0.05 M otopini CH_3COOH pri temperaturi 25 ± 0.1 ^oC.

Potenciodinamičke polarizacijske krivulje dobivene su pomoću potenciostata ("PAR M273A") uz brzinu promjene potencijala od 2 mV s^{-1} vođenog računalom. Mjerenja su vršena nakon uspostavljanja stabilne vrijednosti potencijala otvorenog strujnog kruga (E_{OCP}) u potencijalnom području $E=E_{OCP}\pm250$ mV u smjeru od katodne do anodne strane.

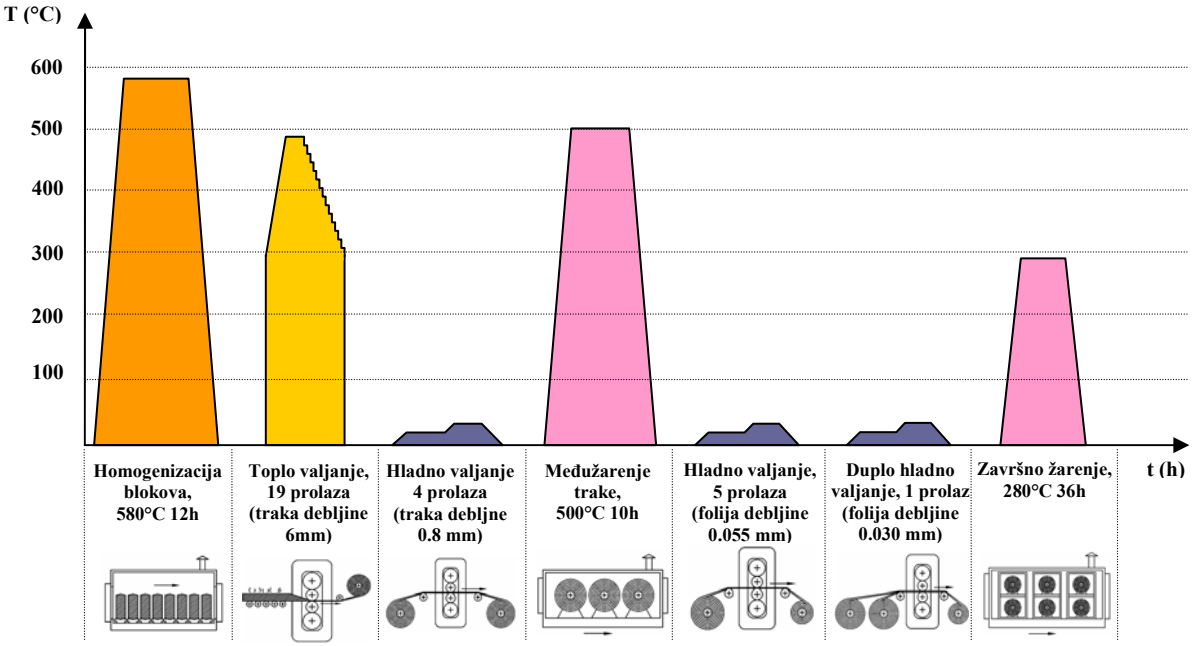
3. REZULTATI I RASPRAVA

Poznato je da željezo ima visoku topivost u rastaljenom aluminiju. Međutim, topivost željeza u aluminiju u krutom stanju je vrlo mala (≈ 0.05%) [5]. Upravo zbog ograničene topivosti u krutom stanju, kod većih sadržaja Fe dolazi do izlučivanja zasebne faze na granici zrna (najčešće je riječ o pojavi sekundarne intermetalne faze tipa Al_3Fe koja djeluje kao katoda u odnosu na osnovnu matricu aluminija) [5-11]. Takve promjene u strukturi utječu kako na mehanička i fizikalna svojstva tako i na elektrokemijska svojstva i korozijsko ponašanje slitine EN AW 8006 (Al-Fe-Mn).

Probni blokovi slitine EN AW 8006 s četiri različita masena postotka Fe (1.20%, 1.50%, 1.70% i 1.90%) su homogenizirani, toplo valjani, zatim hladno valjani u nekoliko faza do konačne debljine od 0.030 mm s jednim međužarenjem i završnim žarenjem.

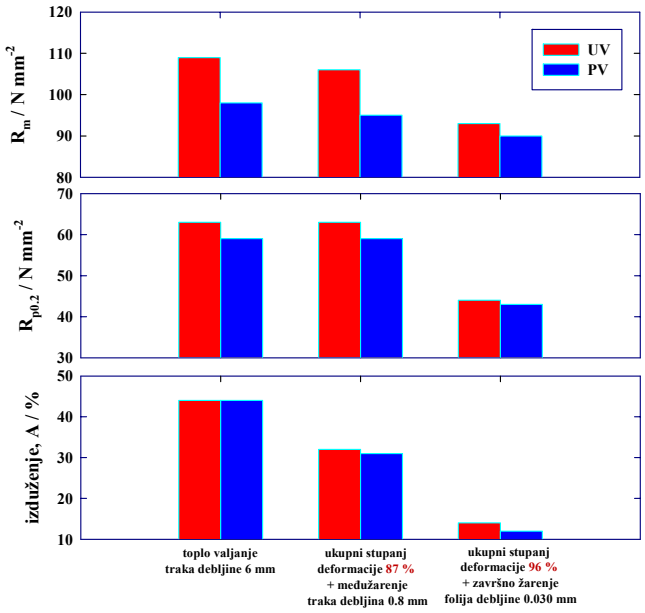
Zbog pojave pukotina pri valjanju tanjih traka iz blokova slitine s 1.70 i 1.90 % Fe zaključeno je da je opasno nastaviti s valjanjem (opasnost od požara) te su isključeni iz mehaničkih ispitivanja [4].

Na slici 1. prikazan je termomehanički model prerade slitine EN AW 8006 (Al-Fe-Mn).



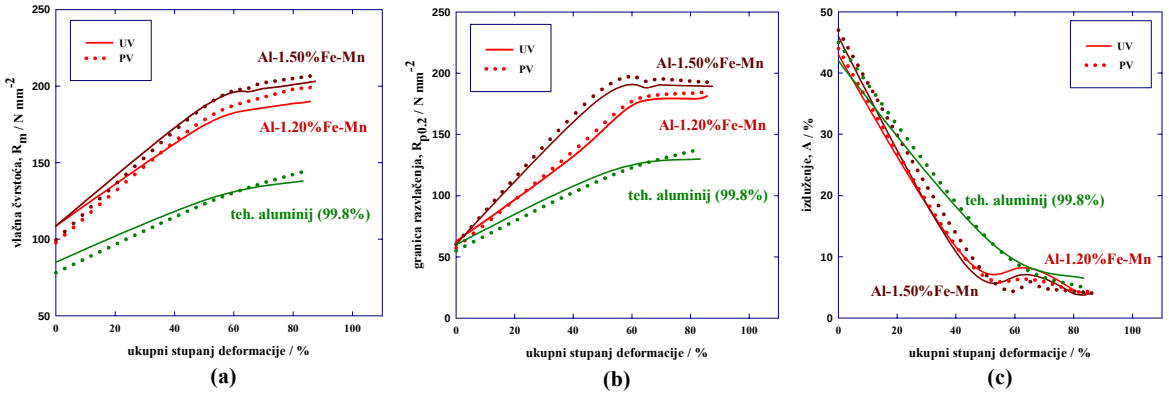
Slika 1. Termomehanički model prerade slitine EN AW 8006 (Al-Fe-Mn) [12-14].

Slika 2. prikazuje utjecaj izabranog termomehaničkog modela prerade na mehanička svojstva žarenih traka/folije sa sadržajem Fe od 1.20%. Vlačna čvrstoća i granica razvlačenja toplo valjane trake i trake međužarene nakon 87% redukcije se bitno ne razlikuju. U drugom ciklusu hladnog valjanja-žarenja vlačna čvrstoća slitine sa sadržajem Fe od 1.20% se smanji za ≈ 12%, a granica razvlačenja za ≈ 30%. Slitina u sva tri promatrana slučaja pokazuje veće vrijednosti vlačne čvrstoće i granice razvlačenja uzdužno u smjeru valjanja jer je došlo do rekristalizacije materijala. Izduženje materijala u prvom ciklusu hladno valjanje-međužarenje smanji se za ≈ 28%, a u drugom ciklusu za ≈ 55%.



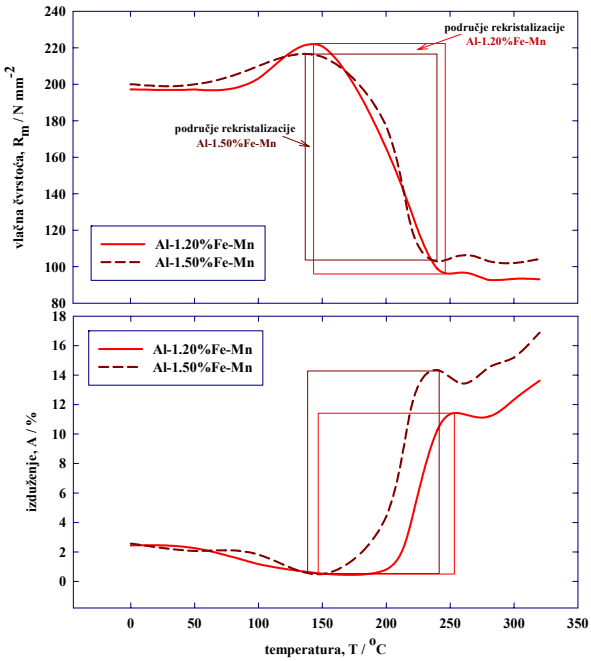
Slika 2. Ovisnost mehaničkih svojstava o ciklusu hladnog valjanja-žarenja za slitinu sa sadržajem Fe od 1.20% (UV - ispitivanja uzdužno u smjeru valjanja i PV -poprečno na smjer valjanja).

Na slici 3. prikazan je utjecaj stupnja hladne deformacije na mehanička svojstva slitine s dva različita sadržaja Fe (1.20 i 1.50%) i tehničkog aluminija (99.8%). Utjecaj stupnja hladne deformacije na mehanička svojstva je praćen tokom hladnog valjanja toplo valjanih traka debljine 6.0 mm do debljine od 0.8 mm. U toku hladne deformacije dolazi do očvršćavanja materijala, odnosno porasta vlačne čvrstoće i granice razvlačenja i smanjenja plastičnosti, odnosno izduženja materijala. Vlačna ispitivanja izvršena su na uzorcima uzdužno u smjeru valjanja (UV) i poprečno na smjer valjanja (PV). Ispitivanja su pokazala da je vlačna čvrstoća toplo valjane trake izrađene iz slitine s dva različita sadržaja Fe (1.20 i 1.50%) za ≈ 20% veća u odnosu na vlačnu čvrstoću toplo valjane trake iz tehničkog aluminija (99.8%).



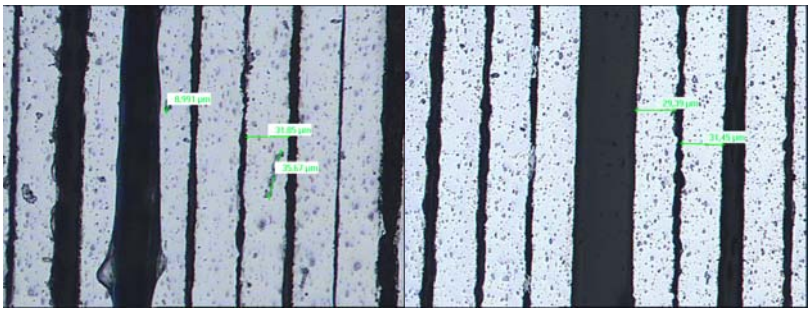
Slika 3. Ovisnost vlačne čvrstoće (a), granice razvlačenja (b) i izduženja (c) slitine sa sadržajem Fe od 1.20% i 1.50% i tehničkog aluminija (99.8%) o ukupnom stupnju hladne deformacije
(UV - ispitivanja uzdužno u smjeru valjanja i PV -poprečno na smjer valjanja).

S porastom stupnja hladne deformacije raste razlika u mehaničkim svojstvima između slitine s dva različita sadržaja Fe (1.20 i 1.50%) i tehničkog aluminija (99.8%). Zbog izduživanja zrna metala i primjesa s porastom stupnja hladne deformacije sve tri slitine pokazuju veće vrijednosti vlačne čvrstoće i granice razvlačenja poprečno na smjer valjanja. Slitina sa sadržajem Fe od 1.50% u odnosu na slitinu sa sadržajem Fe od 1.20% pokazuje ≈ 6% veće vrijednosti vlačne čvrstoće i granice razvlačenja što je u skladu sa razlikom u kemijskom sastavu. Hladno valjana traka tehničkog aluminija (99.8%) pokazuje nešto veće vrijednosti izduženja.



Slika 4. Oporavak mehaničkih vrijednosti folije sa sadržajem Fe od 1.20% i 1.50%, debljine 0.030 mm, prilikom završnog žarenja.

Na slici 4. prikazan je oporavak mehaničkih vrijednosti folije debljine 0.030 mm nakon izvršene hladne deformacije tj. redukcije debljine od 96%, prilikom završnog žarenja koje je izvršeno u laboratorijskoj peći u intervalu temperatura od 0-320 °C u trajanju od 1 sata. Područje rekristalizacije se nalazi između 140 °C i 250 °C. Nakon rekristalizacije slitina sa sadržajem Fe od 1.50% pokazuje ≈ 10% veće vrijednosti vlačne čvrstoće i ≈ 20% veće izduženje u odnosu na slitinu sa sadržajem Fe od 1.20%.

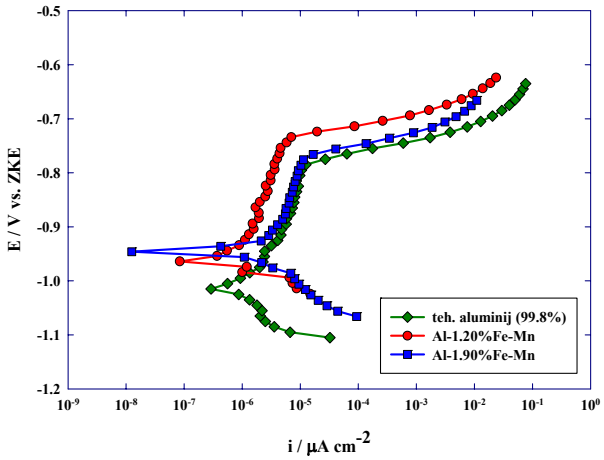


Slika 5. Mikro snimak folije sa sadržajem Fe od 1.20% i 1.50%, debljine 0.030 mm, nakon završnog žarenja (povećanje 200x).

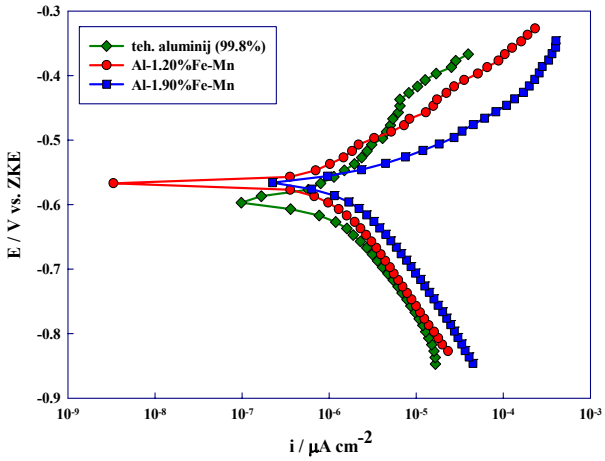
Na slici 5. prikazana je mikrostruktura folije sa sadržajem Fe od 1.20% i 1.50%, debljine 0.030 mm nakon završnog žarenja pri povećanju od 200x.

Konačne performanse folije za pakiranje ne ovise samo o mehaničkim svojstvima, već i o elektrokemijskim svojstvima. Ispitivanja su obuhvaćala praćenje vrijednosti elektrokemijskih parametara primjenom elektrokemijskih mjernih tehnika u otopinama NaCl i CH_3COOH. Kao referentno polazište na isti način praćene su vrijednosti elektrokemijskih parametara i za tehnički aluminij (99.8%).

Slike 6. i 7. prikazuju potenciodinamičke polarizacijske krivulje za slitine s dva različita sadržaja Fe (1.20 i 1.90%) i tehnički aluminij (99.8%) ispitivane u 0.5 M otopini NaCl i 0.05 M otopini CH_3COOH.



Slika 6. Polarizacijske krivulje za tehnički Al (99.8%) (◆), Al-1.20%Fe-Mn (●) i Al-1.90%Fe-Mn (■) u 0.5 M otopini NaCl.



Slika 7. Polarizacijske krivulje za tehnički Al (99.8%) (◆), Al-1.20%Fe-Mn (●) i Al-1.90%Fe-Mn (■) u 0.05 M otopini CH_3COOH.

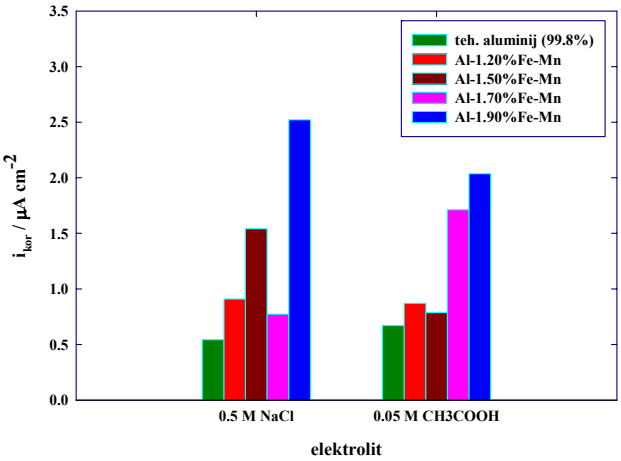
Kao što se može vidjeti na slici 6. kod ispitivanja u 0.5 M otopini NaCl u području potencijala od ≈ -0.93 do ≈ -0.73 V slitina Al-Fe-Mn pokazuje pasivno ponašanje zbog stvaranja zaštitnog oksidnog filma na metalu. Kod potencijala iznad ≈ -0.73 V dolazi do naglog porasta struje i značajnijeg otapanja metala. Kod tehničkog aluminija pasivno ponašanje je u području potencijala od ≈ -0.97 do ≈ -0.78 V, s naznakom piting potencijala kod vrijednosti od ≈ -0.78 V. Kako raste sadržaj Fe u slitini korozijska struja se povećava, a korozijski potencijal se lagano pozitivira. S porastom sadržaja Fe u slitini uočava se i da katodna struja postaje veća, dok se anodna smanjuje. U odnosu na tehnički aluminij vidimo da se legiranjem bitno povećava korozijska struja i korozijski potencijal pomiče u anodnu stranu tj. smanjuje se otpornost prema koroziji. Kod ovog ispitivanja optimalni sadržaj Fe u slitini, s obzirom na otpornost prema koroziji iznosi 1.70% na što nas upućuje dobivena najmanja vrijednost korozijske struje i brzine korozije (tablica 1.).

Na slici 7. prikazane su polarizacijske krivulje dobivene kod ispitivanja u 0.05M otopini CH_3COOH. Za razliku od ispitivanja u 0.5 M otopini NaCl nema izraženog pasivnog područja i korozijski potencijali su ≈ 350 mV pozitivniji. Uočava se da s porastom sadržaja Fe u slitini korozijski potencijal postaje lagano pozitivniji i korozijska struja se povećava. Kod ovog ispitivanja optimalni sadržaj Fe u slitini, s obzirom na otpornost prema koroziji iznosi 1.50% (najmanja vrijednost korozijske struje i brzine korozije) (tablica 1.).

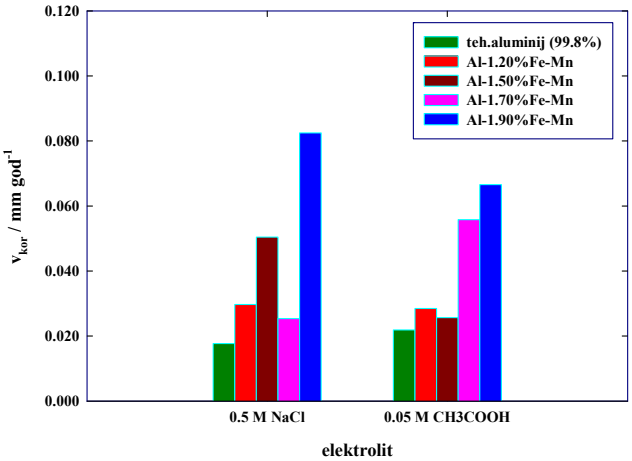
U tablici 1. dani su elektrokemijski parametri (korozijski potencijal E_{kor}, korozijska struja i_{kor}, nagibi Tafelovih pravaca b_k i b_a, i brzina korozije v_{kor}) određeni iz polarizacijskih krivulja, tj. ekstrapolacijom Tafelovih pravaca (Slika 6. i 7.).

Tablica 1. Elektrokemijski parametri određeni iz polarizacijskih krivulja za tehnički aluminij i EN AW 8006 (Al-Fe-Mn) slitinu.

elektrolit	uzorak	E_{kor} (mV)	i_{kor} ($\mu A\ cm^{-2}$)	b_k ($mV\ dec^{-1}$)	b_a ($mV\ dec^{-1}$)	v_{kor} ($mm\ god^{-1}$)
0.5 M NaCl	**Teh. aluminij (99.8%)**	-1014	0.543	-83	122	0.0177
	Al-1.20%Fe-Mn	-954	0.908	-45	278	0.0297
	Al-1.50%Fe-Mn	-932	1.542	-51	301	0.0504
	Al-1.70%Fe-Mn	**-838**	**0.772**	**-100**	**100**	**0.0254**
	Al-1.90%Fe-Mn	-945	2.522	-94	231	0.0825
0.05 M CH_3COOH	**Teh. aluminij (99.8%)**	-594	0.670	-100	100	0.0219
	Al-1.20%Fe-Mn	-566	0.870	-179	97	0.0285
	Al-1.50%Fe-Mn	**-547**	**0.787**	**-94**	**75**	**0.0257**
	Al-1.70%Fe-Mn	-601	1.712	-164	102	0.0558
	Al-1.90%Fe-Mn	-569	2.035	-200	90	0.0666



Slika 8. Korozijska struja za Al-Fe-Mn slitinu i tehnički aluminij (99.8%) u 0.5 M otopini NaCl i 0.05 M otopini CH_3COOH.



Slika 9. Brzina korozije za Al-Fe-Mn slitinu i tehnički aluminij (99.8%) u 0.5 M otopini NaCl i 0.05 M otopini CH_3COOH.

Vrijednosti korozijske struje i brzine korozije pokazuju analogno ponašanje. Slitina Al-Fe-Mn pokazuje veće vrijednosti korozijske struje i brzine korozije u odnosu na tehnički aluminij u oba ispitna elektrolita.

Kod ispitivanja u 0.5 M otopini NaCl vrijednosti korozijske struje i brzine korozije su veće za ≈ 40% kod Al-1.20%Fe-Mn, odnosno za ≈ 78% kod Al-1.90%Fe-Mn u odnosu na tehnički aluminij. Najmanju razliku u odnosu na tehnički aluminij pokazuje slitina Al-1.70%Fe-Mn, čije vrijednosti korozijske struje i brzine korozije su za ≈ 30% veće od vrijednosti izmjerenih kod tehničkog aluminija.

Kod ispitivanja u 0.05 M otopini CH_3COOH te razlike su nešto manje, tako da su vrijednosti korozijske struje i brzine korozije veće za ≈ 23% kod Al-1.20%Fe-Mn, odnosno za ≈ 67% kod Al-1.90%Fe-Mn u odnosu na tehnički aluminij. Najmanju razliku u odnosu na tehnički aluminij pokazuje slitina Al-1.50%Fe-Mn, čije vrijednosti korozijske struje i brzine korozije su za ≈ 15% veće od vrijednosti izmjerenih kod tehničkog aluminija.

4. ZAKLJUČAK

- Optimalni sadržaj Fe u EN AW 8006 slitini, s obzirom na mehanička i elektrokemijska svojstva iznosi 1.50%.
- Slitina sa sadržajem Fe od 1.50% pokazuje ≈ 10% veće vrijednosti vlačne čvrstoće i ≈ 20% veće izduženje u odnosu na slitinu sa sadržajem Fe od 1.20%.
- Obzirom da se folija u konačnoj namjeni koristi za pakiranje u prehrambenoj industriji ispitivanja u 0.05 M otopini CH_3COOH pokazala su da slitina sa sadržajem Fe od 1.50% ima najbolju otpornost prema koroziji na što nas upućuje dobivena najmanja vrijednost korozijske struje i brzine korozije.

5. LITERATURA

[1] S. Bogoll, Proceedings of 6th German Technology Symposium and Exibition, Bangkok/Thailand (1999) 1-24.
[2] M. Leoni, R. Zocchi, C. Sinagra, Allumino Mag. 78 (1990) 6.
[3] H. Leth-Olsen, K. Nisancioglu, Corr. Sci 40 (1998) 1179.
[4] S. Slavica Matešić; J. Radošević; S. Gudić; M. Kliškić, "Ispitivanje mehaničkih i elektrokemijskih svojstava slitine EN AW 8006", MATRIB (2007) 198-205.
[5]J.R. Davis, “Alloying understanding the basic”, ASM International (2001) 351.
[6] M. Leoni, R. Zocchi, C. Sinagra, Allumino Mag., 78 (1990) 6.
[7] L. De Rosa, T. Monetta, F. Bellucci, D.B. Mitton, A. Atienza, C. Sinagra, Progress in Organic Coatings, 44 (2002) 153.
[8] H. Leth-Olsen, K. Nisancioglu, Corr. Sci., 40 (1998) 1179.
[9] K. Nisancioglu, J. Electrochem. Soc., 137 (1990) 69.
[10] R. G. Buchheit, J. Electrochem. Soc., 142 (1995) 3994.
[11] A. Afseth, J.H. Nordlien, G.M. Scamans, K. Nisancioglu, Corros. Sci., 44 (2002) 2542.
[12] R.V. Singh, "Aluminium - Rolling (Process, Principles & Applications)", A publication of TMS, (2000).
[13] A.E. Barten, "Aluminium Rolling Mill Technology: Future Concepts in Thin-Strip and Foil Rolling", Landsberg (2002).
[14] I. Duplančić, "Obrada deformiranjem", FESB, Split (2007).

NIOBIUM AND COBALT INFLUENCE ON THE MICROSTRUCTURE AND HARDNESS OF Ti-Cr ALLOYS

Ljerka Slokar, Tanja Matković, Prosper Matković
University of Zagreb
Faculty of Metallurgy, Aleja narodnih heroja 3, 44103 Sisak, Croatia

Izvorni znanstveni rad / Original scientific paper

Abstract:

Due to their outstanding properties, such as low elastic modulus, high strength, corrosion resistance and excellent biocompatibility, pure titanium and its β-type alloys are currently widely used as structural biomaterials. Over the last three decades, the development of titanium alloys containing niobium for biomedical implant applications has continued to increase. Niobium as non-toxic element is an attractive β-stabilizer for titanium alloys. Chromium is also the β- phase improving element, while cobalt is a strengthener.

This paper presents the comparison of niobium and cobalt influence on the microstructure and hardness of Ti-Cr-based alloys for biomedical use. For this purpose Ti-Cr-Nb and Ti-Cr-Co alloys are produced from pure elements by an arc melting method. As-cast specimens are metallographycally prepared for microstructural examinations by optical and scanning electron microscopy (SEM). Microphotographs were taken with digital camera and analyzed with the corresponding programs. Hardness tests were carried out by Vickers method.

According to the obtained results, some alloys, designed in this study, have potential use as biomaterials.

Key words: biomaterials, as-cast Ti-Cr-Nb and Ti-Cr-Co alloys, microstructure, hardness

Sažetak:

Zahvaljujući izvanrednim svojstvima, kao što su: niski modul elastičnosti, visoka čvrstoća, otpornost prema koroziji i izvrsna biokompatibilnost, čisti titan i njegove β-slitine trenutno se najviše upotrebljavaju kao strukturni biomaterijali. Zadnjih tridesetak godina kontinuirano se povećava razvoj slitina titana koje sadrže niobij za biomedicinske implantate. Niobij kao ne-toksični element je atraktivan stabilizator β-faze titana. Krom je isto tako element koji pospješuje formiranje β-faze, dok se kobalt koristi za očvršćivanje slitine.

Ovaj rad prikazuje usporedbu utjecaja niobija i kobalta na mikrostrukturu i tvrdoću Ti-Cr slitina za biomedicinsku primjenu. U tu su svrhu slitine Ti-Cr-Nb i Ti-Cr-Co pripremljene taljenjem čistih elemenata u elektrolučnoj peći. Lijevani uzorci su metalografski pripremljeni za mikrostrukturna ispitivanja pomoću optičkog (OM) i scanning elektronskog mikroskopa (SEM). Mikrostrukture slitina snimljene su digitalnom kamerom i analizirane odgovarajućim programima. Ispitivanje tvrdoće provedeno je Vickersovom metodom.

Prema dobivenim rezultatima, neke slitine dizajnirane u ovom radu imaju potencijalnu primjenu kao biomaterijali.

Ključne riječi: biomaterijali, lijevane Ti-Cr-Nb i Ti-Cr-Co slitine, mikrostruktura, tvrdoća

INTRODUCTION

Among various metallic materials, including stainless steels and cobalt-based alloys, the pure titanium and its alloys are now the most attractive for biomedical applications. They exhibit the most suitable characteristics such as an excellent biocompatibility, low density, high strength and very good corrosion resistance.

The most widely used titanium alloy for biomedical applications Ti-6Al-4V contains vanadium, which is known as a cytotoxic element. Therefore, the alternative Ti-based alloys with another alloying elements are currently the subject of intensive study.

Though, the titanium alloys have a low shear strength and wear resistance, and the elastic modulus (100-120 GPa) which is remarkably higher than that of bone (10-30 GPa). In order to solve this problems, many new β- type Ti-alloys have been designed.

The usual method for improving the performance of titanium alloys, in terms of their biomedical and mechanical properties, is to modify their chemical composition. In the present work, this has been attempted by alloying with niobium as strong β-phase forming element and with cobalt as a strengthener /**1-5**/.

MATERIALS AND METHODS

Six Ti-Cr –based alloys, with addition of cobalt and niobium in the range of 10 to 20 at. % (Table 1) were investigated. The samples were prepared in a laboratory arc-furnace under argon atmosphere by melting the pure elements. Their purities were better than 99.9%.

Table 1. Chemical compositions and Vickers hardness of experimental Ti-Cr-Nb and Ti-Cr-Co alloys

Sample No.	Alloy composition, at.%	HV3
1	$Ti_{80}Cr_{10}Nb_{10}$	574
2	$Ti_{70}Cr_{10}Nb_{20}$	412
3	$Ti_{70}Cr_{20}Nb_{10}$	522
4	$Ti_{80}Cr_{10}Co_{10}$	466
5	$Ti_{70}Cr_{10}Co_{20}$	805
6	$Ti_{70}Cr_{20}Co_{10}$	558

To achieve the chemical homogeneity, the samples in form of “buttons” were remelted three times. The casting of alloys was realized in the same equipment by means of a specially constructed copper anode that served also as a casting mould. In this way, as-cast cylindrical specimens with dimensions about 7x12 mm were produced directly.

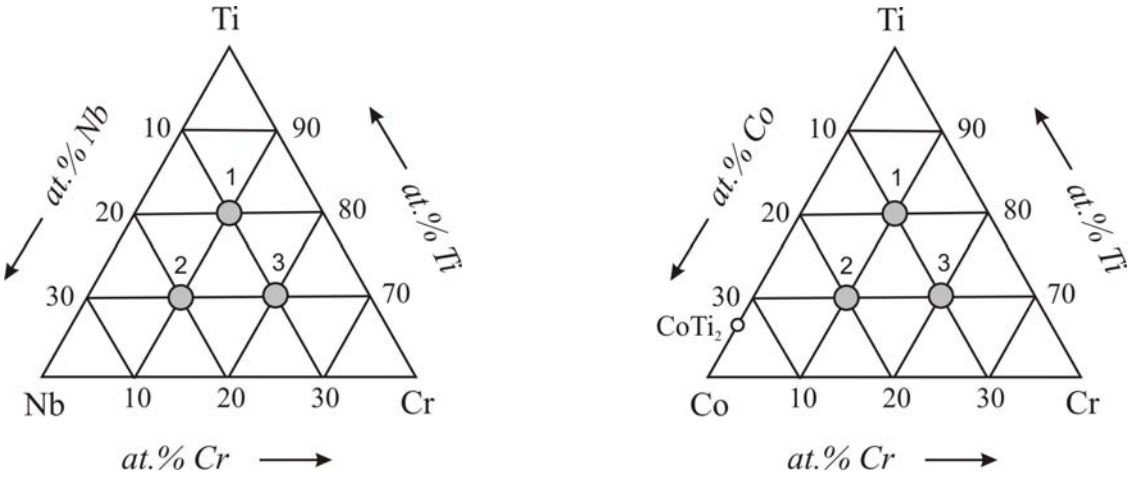
After embedding in epoxy resin, the samples are metallographically prepared with wet grinding on SiC paper and final polishing with Al_2O_3 water suspension. There was no need for etching because the microstructure was remarked easily.

The microstructure of the as-cast alloys was observed by optical microscope Leitz, Ortholux at the magnification of 280x. Microphotographs were taken with digital camera Olympus DP11 and used for optical metallography. Quantitative analysis was carried out with the computer programs Olympus DP-Soft and UTHSCA Image Tool. In addition, microstructural examination was realized by scanning electron microscopy (SEM).

Hardness measurements were performed by Vickers method (HV3) on the equipment of Otto-Wolpert-Werke.

RESULTS AND DISCUSSION

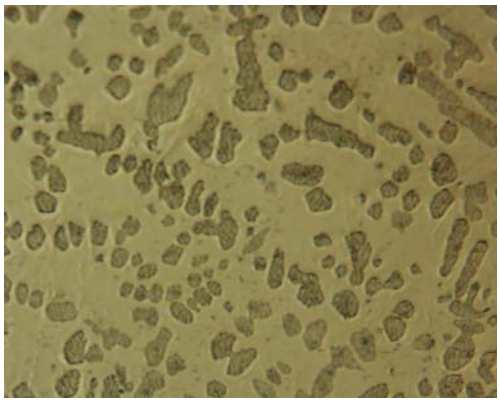
Niobium and cobalt influence on the microstructure and hardness of Ti-Cr alloys were investigated. For this purpose, three Ti-Cr-Nb and three Ti-Cr-Co alloys were prepared. Their positions are shown in the portion isothermal sections of corresponding ternary diagrams at the room temperature in Figure 1.



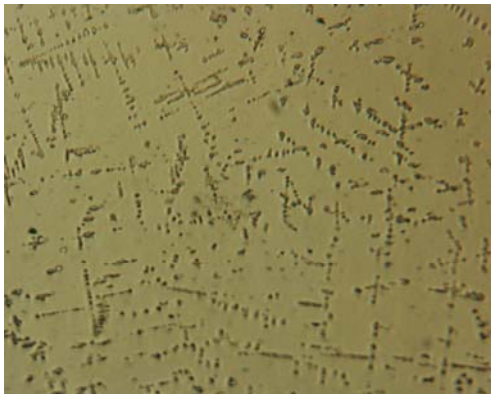
(a) Ti-Cr-Nb (b) Ti-Cr-Co

Figure 1. Compositions of experimental alloys presented in the portion isothermal sections of ternary diagrams at the room temperature

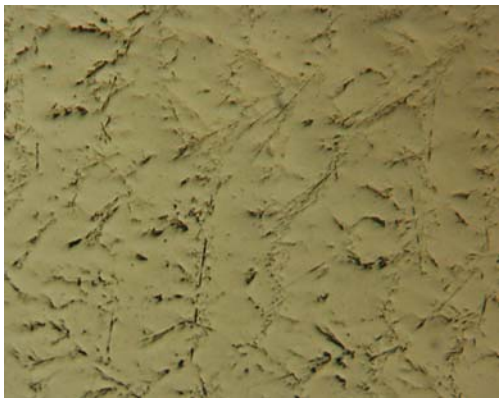
Observation by optical microscopy shows that alloys $Ti_{80}Cr_{10}Nb_{10}$ and $Ti_{70}Cr_{20}Nb_{10}$ have typical dendritic solidification microstructure, which consists of dendritic and interdendritic region (dark and light areas on microphotographs in Figure 2a and b). Alloy $Ti_{70}Cr_{10}Nb_{20}$ (Figure 2c) have multi-phase microstructure.



(a) $Ti_{80}Cr_{10}Nb_{10}$



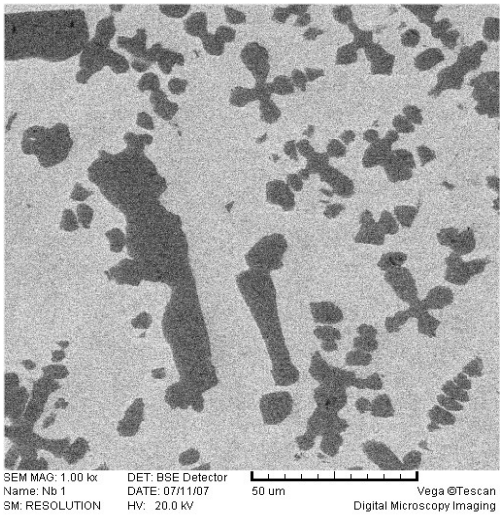
(b) $Ti_{70}Cr_{20}Nb_{10}$



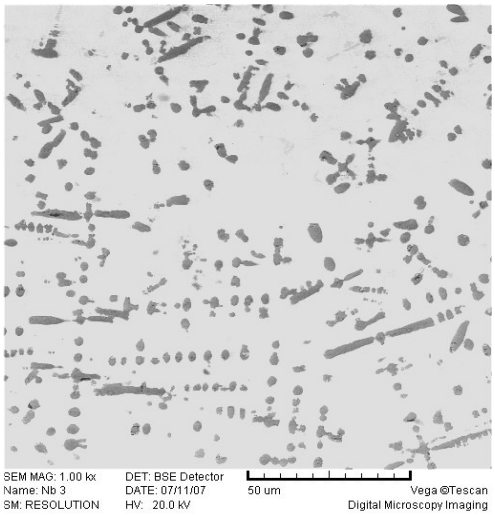
(c) $Ti_{70}Cr_{10}Nb_{20}$

Figure 2. Optical micrographs of as-cast Ti-Cr-Nb alloys (280x)

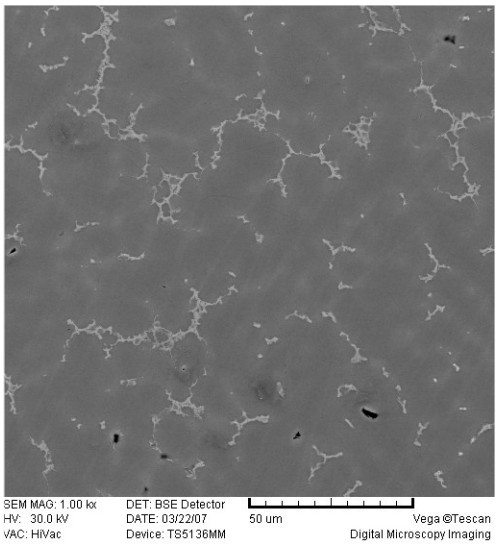
A detailed analysis by scanning electron microscopy with backscattered electrons (BSE) confirms that alloys $Ti_{80}Cr_{10}Nb_{10}$ and $Ti_{70}Cr_{20}Nb_{10}$ are two-phases (Figs. 3a and b). The alloys $Ti_{80}Cr_{10}Co_{10}$ and $Ti_{70}Cr_{20}Co_{10}$ are nearly single-phases (Figs. 3c and d), until alloys $Ti_{70}Cr_{10}Co_{20}$ and $Ti_{70}Cr_{10}Nb_{20}$ (Figs. 3e and f) have multi-phase microstructures.



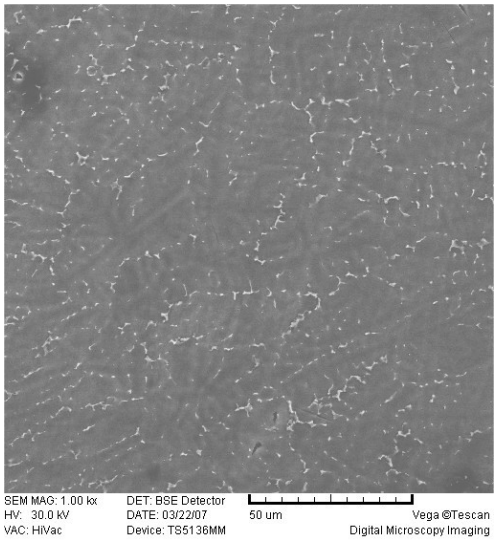
(a) $Ti_{80}Cr_{10}Nb_{10}$



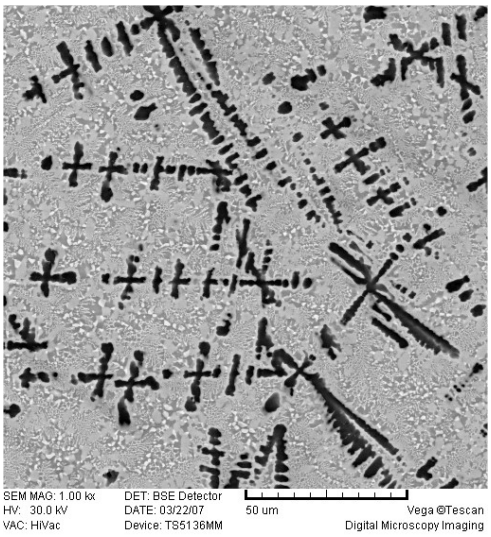
(b) $Ti_{70}Cr_{20}Nb_{10}$



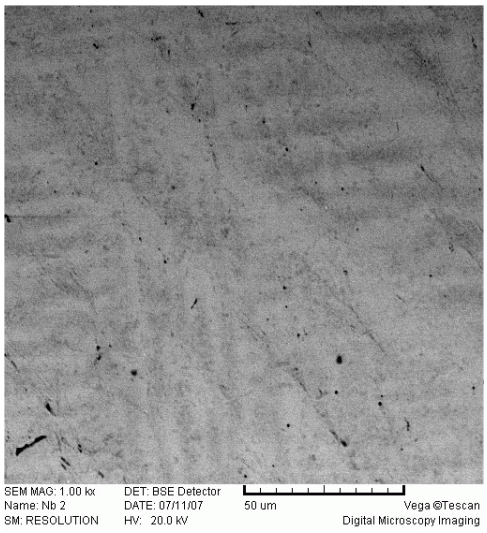
(c) $Ti_{80}Cr_{10}Co_{10}$



(d) $Ti_{70}Cr_{20}Co_{10}$



(e) $Ti_{70}Cr_{10}Co_{20}$



(f) $Ti_{70}Cr_{10}Nb_{20}$

Figure 3. SEM backscattered electron images of investigated alloys

The results of quantitative metallography (Table 2) indicate that the dendrites portion depends on alloy composition. Thus, among Ti-Cr-Nb and Ti-Cr-Co alloys the highest percentage of dendrites have alloys with the highest titanium content (80 at.%). These alloys have also the biggest average areas of grains. Contrary to this, dendrites portion decreases with niobium and cobalt content (20 at.%).

Table 2. The results of quantitative optical metallography (Image Tool program)

Sample No.	Alloy composition, at. %	% dendrites	% interdendritic region	Average area of grains, μm^2	Perimeter of grains, μm
1	$Ti_{80}Cr_{10}Nb_{10}$	37,84	62,13	105,11	18,10
2	$Ti_{70}Cr_{10}Nb_{20}$	14,62	85,38	80,84	9,51
3	$Ti_{70}Cr_{20}Nb_{10}$	18,44	81,56	77,51	9,40
4	$Ti_{80}Cr_{10}Co_{10}$	68,95	31,05	42,88	35,67
5	$Ti_{70}Cr_{10}Co_{20}$	49,34	50,66	26,96	40,03
6	$Ti_{70}Cr_{20}Co_{10}$	61,47	38,35	24,14	28,56

The results obtained from the Vickers hardness tests for experimental alloys (Table 1) are schematically delineated in Figure 4. They indicate that hardness of Ti-Cr-Nb alloys increases with percentage of dendritic phase, but decreases with niobium content /**6**/. So, the highest value of 574 HV3 has alloy $Ti_{80}Cr_{10}Nb_{10}$.

Among Ti-Cr-Co alloys the maximal value of 805 HV3 has alloy $Ti_{70}Cr_{10}Co_{20}$ with the lowest percentage of dendritic phase and with the highest cobalt content.

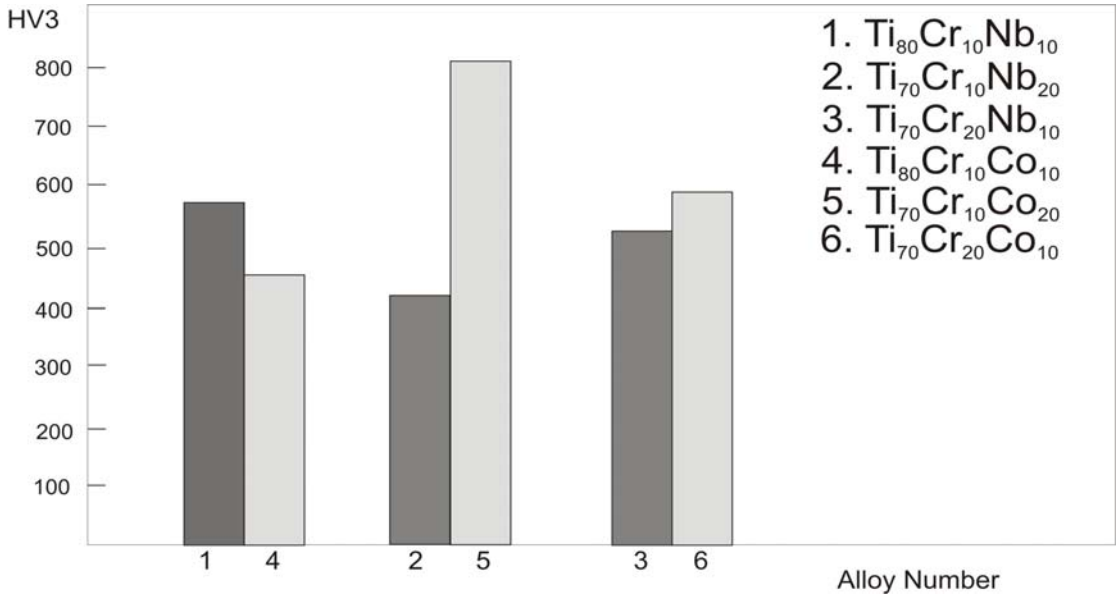


Figure 4. Comparison of Vickers hardness values for investigated alloys

CONCLUSIONS

From the represented study of niobium and cobalt influence on the microstructure and hardness of Ti-Cr alloys can be concluded as follows:

- Optical and scanning electron microscopy showed that the heterogeneity of the microstructure increases with niobium and cobalt content, so that alloys with 20 at.% niobium and 20 at. % cobalt have a multi-phase microstructures.
- Quantitative metallography indicated that the percentage of dendritic phase depends on alloy composition; the portion of dendritic phase increases with titanium content and decreases with niobium and cobalt content.
- Hardness measurements showed that alloy $Ti_{70}Cr_{10}Co_{20}$ with the highest cobalt content has also the highest hardness value.

Finally, according to the microstructure and hardness values two Ti-Cr–base alloys with niobium ($Ti_{80}Cr_{10}Nb_{10}$ and $Ti_{70}Cr_{20}Nb_{10}$) and two Ti-Cr-base alloys with cobalt ($Ti_{80}Cr_{10}Co_{10}$ and $Ti_{70}Cr_{20}Co_{10}$) designed in this study have potential use as biomaterials.

REFERENCES

1. G. He, M. Hagiwara, *Ti alloy design strategy for biomedical applications,* Materials Science and Engineering C 26 (2006) 14-19
2. M. Long, H. J. Rack, *Titanium alloys in total joint replacement – a material science perspective,* Biomaterials 19 (1998) 1621-1639
3. M. Niinomi, *Fatigue performance and cyto-toxicity of low rigidity titanium alloy, Ti–29Nb–13Ta–4.6Zr*, Biomaterials 24 (2003) 2673-2683
4. M. Niinomi, *Recent metallic materials for biomedical applications,* Metallurgical and Materials Transactions A 33 (2002) 477-486
5. A. Gutiérrez et al., *Surface microstructure of oxide protective layers grown on vanadium-free Ti alloys for use in biomedical applications,* Surface Science 600 (2006) 3780-3784
6. L. J. Xu, Y. Y. Chen, Zh. G. Liu, F. T. Kong, *The microstructure and properties of Ti-Mo-Nb alloys for biomedical application,* Journal of Alloys and Compounds 453 (2008) 320-324

PREDICTION OF WORKING STRESS OF COLD-WORK TOOL STEEL

PREDVIĐANJE DOPUŠTENOG RADNOG NAPREZANJA ALATNOG ČELIKA ZA RAD U HLADNOM STANJU

Božo Smoljan, Sunčana Smokvina Hanza, Dario Iljkić

University of Rijeka, Faculty of Engineering, Department of Materials Science and Engineering, Croatia

Izvorni znanstveni rad / Original scientific paper

Abstract

Working stress depends on fracture resistance and on deformation resistance. Fracture toughness represents fracture resistance, whereas yield strength and modulus of elasticity characterize deformation resistance.

Fracture toughness and yield strength directly depend on steel microstructure, opposite modulus of elasticity, which is the most insensitive property to structure transformations in steel.

The main influence factors on fracture resistance and on deformation resistance are presented in this paper, as well as the methods of fracture and deformation resistance usage in design of safety of engineering component application.

Keywords: mechanical properties, working stress, plastic deformation, fracture, tool steel

Sažetak

Dopušteno radno naprezanje ovisi o otpornosti na krhki lom i otpornosti na deformaciju. Lomna žilavost predstavlja otpornost krhkom lomu, a granica razvlačenja i modul elastičnosti karakteriziraju otpornost deformaciji.

Lomna žilavost i granica razvlačenja direktno ovise o mikrostrukturi čelika, dok je modul elastičnosti najneosjetljivija veličina na strukturne promjene u čelika.

U radu su opisani osnovni čimbenici koji utječu na veličinu otpornosti krhkom lomu i deformaciji te su naznačene metode kako se te veličine uključuju u ocjenu nosivosti materijala, odnosno konstrukcije.

Ključne riječi: mehanička svojstva, dopušteno radno naprezanje, plastična deformacija, lom, alatni čelik

1. Introduction

The allowable stress considered safe in the design of an engineering component is called the working stress. Each type of engineering component failures is related with characteristic mechanical property, and in designing of engineering components it is

necessary to understand types of failure. Characteristic material properties must be used with an appropriate failure criterion.

Generally, engineering components can fail due to fracture, or due to excessive deformation [1]. Fracture toughness and yield strength as well as modulus of elasticity are fundamental properties, which are used in design of safety of engineering components applications. Fracture toughness represents fracture resistance, whereas yield strength and modulus of elasticity characterize deformation resistance. When mechanical behavior is understood in terms of metallurgical structure, it is generally possible to improve the mechanical properties of metals or at least to control them.

Usually, cold-work tool steels are medium to high carbon steels which are quenched and tempered to obtain the desired strength, toughness and hardness. Cold-work tool steels should have resistance to excessive deformation and distortion, fracture, shock, wear, and softening [2].

2. Determination of working stress

The mechanical behavior of metals can be generally predicted as a function of stress-strain state and temperature. The stresses, the strains and the displacements have to be determined to solve an elastic-plastic problem. There are 15 unknowns, but there are 15 equations: the three equilibrium equations, the six equations relating displacements with strains, and the six constitutive equations relating strains with stresses. These equations are independent of the material properties, and will hold whether the body behaves elastically or whether plastic flow occurs. These equations is possible to reduce to three equations, involving only the displacements u, v, w [3]:

$$\mu\nabla^2 u_i + (\lambda+\mu)\theta_{,i} + F_i = 0 \tag{1}$$

where ∇^2 is the Laplacian operator, F_i are the body forces, invariant θ can be written as $\theta = (\partial u/\partial x)+(\partial v/\partial y)+(\partial w/\partial z)$, and λ and μ are Lame's constants.

The stress-strain relations can be written with thermal strains. If the total loading path is divided into N increments of load, the total strains at the end of the mth increment can be written as:

$$\varepsilon_{ij} \approx \frac{1}{2\mu}\sigma_{ij} - \delta_{ij}\left(\frac{\nu}{E}\Theta - \alpha T\right) + \sum_{k=1}^{m-1}\Delta\varepsilon_{ij,k}^{p} + \Delta\varepsilon_{ij,m}^{p} \tag{2}$$

where σ_{ij} and ε_{ij} are the stress and the strain tensors, respectively; $\Theta = \sigma_{11}+\sigma_{22}+\sigma_{33}$; E is the modulus of elasticity, ν is the Poisson's ratio; α is the coefficient of linear thermal expansion; T is the temperature above some arbitrary reference temperature. The forth term on the right side of Equation 2 is the plastic strain accumulated in the first mth-1 increments of load, and the fifth term is the plastic strain due to the mth increment of load. The plastic strain increments for the current or mth increment of load for the von Mises

criterion are: $\Delta\varepsilon_{ij}^{p} = (3/2)(\Delta\varepsilon_{p}/\sigma_{e})\sigma'_{ij}$; σ' is the deviatoric stress tensor, and $\Delta\varepsilon_{p} = \left(2/3\Delta\varepsilon_{ij}^{p}\Delta\varepsilon_{ij}^{p}\right)^{1/2}$. Values of $\Delta\varepsilon_{\mathrm{p}}$ and σ_{e} are related to each other through the uniaxial tensile true stress-true strain curve. Usually an elastic-plastic problem can be solved by application of numerical methods. In order to carry out such calculations in thermal processes, it is necessary to know the material properties in terms of temperature.

Since high strength materials usually have a low fracture resistance, the conventional design criteria are non adequate when there cracks are exist. In this case, equations of fracture mechanics have to be used. The catastrophic crack growth occurs when stress exceeds a certain critical value σ_{c}:

$$\sigma_{c}(\pi a)^{1/2} = (EG_{Ic})^{1/2} = (1-\nu)^{1/2}K_{Ic} \tag{3}$$

where a is the crack length, G_{Ic} is the so called critical value of elastic energy release rate per crack tip, and K_{Ic} is the fracture toughness.

Under the cyclic loads, engineering components can fail at stresses which are less than short time strength. The rate of fatigue crack propagation per cycle is usually in the relation with the stress intensity factor [4]:

$$(da/dN) = C(\Delta K)^{n} \tag{4}$$

where C and n are constants. Values of n usually vary between 2 and 4.

Deformation at constant stress defined as creep could be represented by the following empirical equation [5]:

$$\varepsilon = \varepsilon_{0} + \varepsilon_{t}\left(1-e^{-rt}\right) + \dot{\varepsilon}_{s}t \tag{5}$$

where t is the time, ε_0 is the instantaneous strain on loading, ε_{t} is the limit for transient creep, r is the ratio of transient creep rate to the transient creep strain, $\dot{\varepsilon}_{s}$ is the steady-state creep rate.

The classical approaches of theory of plasticity and fracture mechanics some times can not be successfully applied in prediction of the progressive deterioration of material preceding the macroscopic fracture. Recently, theory of damage mechanics is applying in prediction of the progressive deterioration of material preceding the macroscopic fracture. Damage evolution is due to lot of mechanisms, such us ductile plastic damage, brittle viscoplastic or creep damage, fatigue damage, macrobrittle damage, and so on. The theory of damage is concerned with all materials at low or high temperatures under any kind of load. The damage theory provides the time or the number of cycles corresponding to the initiation of such a crack at the most stressed point of the structure.

3. Micromechanisms of plastic deformation and fracture

The strength of metal is basically determined by its crystal structure, which determines the number and the type of slip systems, fixes the Burgers vector, and determines the lattice friction stress (Peierls stress) which sets the base strength level.

The most well documented strengthening measures in steels are associated with the refinement of grain size. As the grain size decreases and strain increases, the deformation becomes more homogeneous. The strain hardening of a fine grain size metals is more intensive than in those of a coarse-grain. The unique characteristic of grain refining strengthening lies in that it is the only one strengthening method that also increases the toughness. Hall and Petch have been established that the tensile yield stress, σ_Y, is related to grain size by [6]:

$$\sigma_Y = \sigma_i + k_Y d^{-1/2} \tag{6}$$

where σ_i is resistance of lattice to dislocation movement, d is the grain diameter, and k_Y is the constant which depends on dislocation pile-up properties and plays an important role in controlling the mechanical properties of steels. The Hall-Petch equation has been found to express the grain-size dependence of the flow stress at any plastic strain out to ductile fracture.

For brittle fracture, fracture stress, σ_f, can be expressed by [6]:

$$\sigma_f = \left(4\mu\gamma_s\right)/\left(k_Y d^{1/2}\right) \tag{7}$$

where μ is the shear modulus, d is the microcrack length, and γ_s is the effective surface energy. General expression of microstructural aspect for nucleation and propagation of brittle crack can be written in form [6]:

$$\left(\tau_i d^{1/2} + k_Y\right) \cdot k_Y = \beta\mu\gamma_s \tag{8}$$

where factor β depends on stress-strain condition, and τ_i is equal to the friction stress opposing motion of dislocation. A high value of friction stress τ_i lowers ductility. If the left side of Equation 8 is smaller than the right side, a microcrack can be formed but it cannot grow. If the left side of the equation is greater than the right, brittle crack will propagate at stress equal to yield stress. In steels most solutes decrease the ductility, and interstitial solutes have commonly more effects than substitutional solutes. The effective surface energy will depend on the contribution of plastic deformation, which depends on number of available slip systems and on number of mobile dislocations at the tip of the crack.

Strengthening mechanisms based on dislocation locking, such as increasing dislocation density and presence of fine second phase particles result in brittleness. Increasing of vacancies concentration with temperature can result in greater mobility of dislocations and material can softening. However, microstructural changes may occur in certain temperature ranges to alter metal behavior.

4. Algorithm of mechanical properties estimation

Mechanical properties of quenched steel directly depend on the degree of quenched steel hardening. Oriented values of investigated mechanical properties are estimated by following algorithm [7,8]:

$$R_e = 2.3HV \text{ , Nmm}^{-2} \tag{9}$$

$$R_m = \frac{R_e - 170C + 200}{0.8 + 0.1C} \text{ , Nmm}^{-2} \tag{10}$$

$$K_{Ic} = \sqrt{\frac{\varepsilon_f n^2 E R_e}{60}} \text{ , MPam}^{1/2} \tag{11}$$

$$\varepsilon_f = \ln\left(1 - \frac{Z}{100}\right)^{-1} \tag{12}$$

$$Z = 96 - (0.062 - 0.029C)R_m \text{ , \%} \tag{13}$$

$$\frac{R_m}{R_e} - \left(\frac{n}{0.002e}\right)^n \approx 0 \tag{14}$$

HV is the hardness, R_e is the yield strength, R_m is the tensile strength, C is the ratio between actual hardness and martensite hardness in HRC, ε_f is the true fracture strain, n is the strain-hardening exponent, and Z is the reduction of area.

Fracture toughness depends on microstructural constituents, as well as on size and distribution of the usual intermetallic particles and non-metallic inclusions. Limited fracture toughness can be attributed to the presence of these particles, which are virtually impossible to eliminate by any usual heat treatment once they have formed. Properties of matrix may also have an important influence on fracture toughness behavior.

Generally, any change that increase yield strength results in a decrease in fracture toughness. The fracture toughness increases with increasing of amount of retained austenite in the microstructure. The retained austenite phase is crack arrester and crack blunter, since it is softer and tougher than the martensite phase.

Numerical calculation and experimental results have been compared in order to test performance of established algorithm. Fig. 1 shows computed and experimentally estimated results of the fracture toughness and tensile strength of the hardened specimen based on the ratio between actual hardness and martensite hardness in *HRC*, martensite factor C. The comparison of fracture toughness calculated by mathematical modeling and determined by experiment, showed that the presented model has a good performance of

fracture toughness estimation based on hardness. For efficient estimation of fracture toughness, additional data about microstructure are needed.

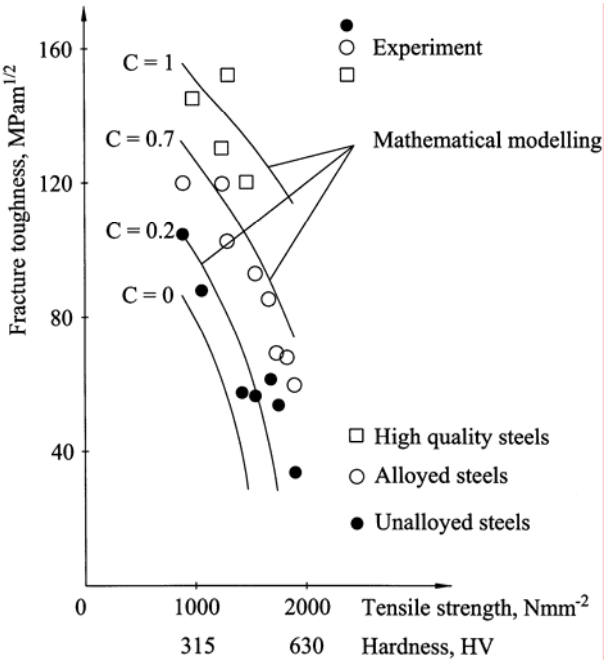


Figure 1: Hardness vs. fracture toughness [8]

5. Application

The presented algorithm is applied in computer simulation of the mechanical properties of quenched and tempered die made of high-hardenability cold-work tool steel 60WCrV7 [9]. A chemical composition of steel 60WCrV7 is shown in Table 1.

Table 1: Chemical composition of steel 60WCrV7 (DIN)

Chemical composition [wt. %]	C	Si	Mn	P	S	Cr	Mo	Ni	V	W
	0.55	0.94	0.34	0.015	0.012	1.27	0.05	0.12	0.18	2.10

Steel 60WCrV7 is one of the shock resisting tool steel types with very good toughness and wear resistance in combination with high hardenability. This steel is impact-resistant, tungsten-alloyed cold-work tool steel. In addition, it can be used as hot-work tool steel at moderate temperatures. Geometry of quenched die is shown in Fig. 2.

After heating to 950 °C for 2 hours, the die was quenched in agitated oil with the severity of quenching H = 0.45. Because of high hardenability of investigated steel, prediction of hardness distribution has been based on JM®-test [10]. After quenching, the die was tempered at 200 °C.

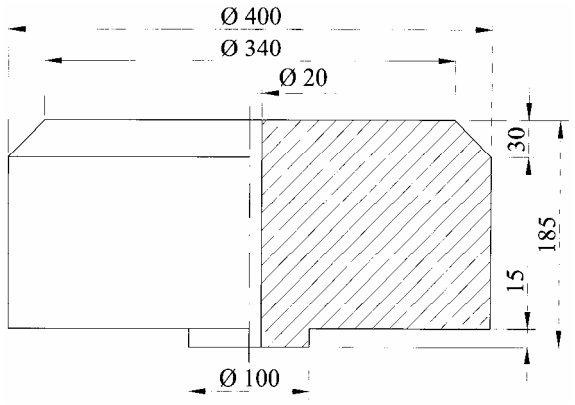


Figure 2: Geometry of die

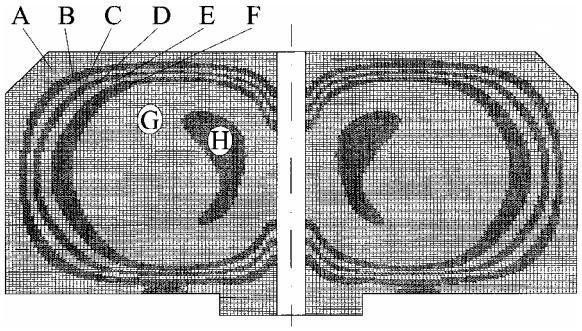


Figure 3: Distribution of mechanical properties fields

6. Results and discussion

Distribution of mechanical properties fields is shown in Fig. 3. The predicted values of mechanical properties of the quenched and tempered die are given in Table 2.

Table 2: Predicted mechanical properties of the quenched and tempered die

Mechanical properties		Field in Fig. 3							
		A	**B**	**C**	**D**	**E**	**F**	**G**	**H**
After the quenching	*HV*	820-774	773-744	743-714	713-684	683-654	653-624	623-594	593-564
	R_e Nmm^{-2}	1886-1780	1778-1711	1709-1642	1640-1573	1571-1504	1502-1435	1433-1366	1364-1297
	K_{Ic} MPam$^{1/2}$	72-76	76-84	84	84-88	88-91	91	91-95	95-100
After the tempering at 200 °C	*HV*	784-745	744-718	715-686	685-662	661-632	631-602	601-573	572-546
	R_e Nmm^{-2}	1803-1714	1711-1651	1645-1578	1576-1523	1520-1454	1451-1385	1382-1318	1316-1256
	K_{Ic} MPam$^{1/2}$	76-84	84	84-88	88	88-91	91-95	95-100	100-102

7. Conclusions

The mechanical behavior of cold-work tool steel depends nearly of all known mechanisms of steel strengthening, such as solid solution hardening, strengthening by heat treatment, grain refinement, second-phase hardening and precipitation hardening by

undeformable particles and deformable particles. Cold-work tool steels must have the fine grained microstructure with optimum distribution of fine carbides in a matrix of tempered martensite.

Presented algorithm of estimation of yield strength, R_e, and fracture toughness, K_{Ic}, is based on steel hardness, *HV*. The hardness distribution in quenched die was estimated based on relevant time of cooling, $t_{8/5}$, as well as on results of modified Jominy-test, which is designed for hardenability prediction of high-hardenability steels.

The algorithm is applied in computer simulation of the mechanical properties of quenched and tempered die made of high-hardenability cold-work tool steel 60WCrV7. By the numerical simulation of fracture toughness was established that the fracture toughness of investigated steel in both as-quenched state and tempered at 200 °C is very low and the application of these steel in mentioned states must be taken with additional caution.

It can be concluded that mechanical properties of quenched and tempered steel dies can be successfully calculated by proposed method. For efficient estimation of fracture toughness from hardness, additional data about microstructure are needed.

References

1. Gdoutos, E.E., Fracture Mechanics: An Introduction: Solid Mechanics and Its Application, Vol. 123, Springer, 2005.
2. Roberts, G., Krauss, G., Kennedy, R., Tool Steels, ASM International, Materials Park, 2000.
3. Mendelson, A., Plasticity: Theory and Application, Macmillan Company, New York, 1968.
4. Paris, P., Erdogan, F., A Critical Analysis of Crack Propagation Laws, Journal of Basic Engineering, Trans. ASME 85, 528, 1963.
5. Jeffery, C., Creep Deformation of Metals, Polymers, Ceramics, and Composites, in ASM Handbook: Mechanical Testing and Evaluation, Vol. 8, ASM International, 2000.
6. Dieter, G. Mechanical Metallurgy, McGraw-Hill Book Company, New York, 1977.
7. Smoljan, B., Prediction of Mechanical Properties and Microstructure Distribution of Quenched and Tempered Steel Shaft, Journal of Materials Processing Technology, Vol. 175, 2006, pp.393-397.
8. Smoljan, B., Butković, M., Simulation of Mechanical Properties of Hardened Steel, Proceedings - MicroCAD'98, Miskolc, Hungary, 1998, pp.3-9.
9. Smoljan, B., Smokvina Hanza, S., Iljkić, D., Totten, G.E., Felde I., Computer Simulation of Mechanical Properties of Steel Dies, Proceedings - ICHT & SETD 2008, Bled, Slovenia, 2008.
10. Smoljan, B., Rubeša, D., Tomašić, N., Smokvina Hanza, S.,Iljkić, D., An Analysis of Application of Modified Jominy-test in Simulation of Cold Work Tool Steels Quenching, Int. J. Microstructure and Materials Properties, 2 (1) (2007), 24-34.

ANALIZA OŠTEĆENJA KLIZNOG LEŽAJA AGREGATA VODNE TURBINE SNAGE 1100 kW HE OZALJ 2

Branko Staniša
Sveučilište u Rijeci, Tehnički fakultet, Vukovarska 58, 51000 Rijeka
i Veleučilište u Karlovcu, Ivana Meštrovića 10, 47000 Karlovac
Lidija Ćurković
Sveučilište u Zagrebu, Fakultet strojarstva i brodogradnje, Ivana Lučića 5, 10000 Zagreb
Vladimir Rede
HEP-Proizvodnja, Pogon HE Ozalj, Nikole Tesle 2, 47280 Ozalj

Izvorni znanstveni rad / Original scientific paper

Sažetak: Hidroelektrana (HE) Ozalj 2 puštena je u pogon 1952. godine. Sastoji se od dvije Kaplanove vodne turbine D i E snage po 1100 kW. Na agregatu vodne turbine E nakon izvršenog remonta u 2007. godini došlo je do oštećenja kliznog ležaja. Klizni sloj bijele kovine ležaja bio je potpuno uništen. Zbog oštećenja kliznog ležaja morao se zaustaviti rad agregata vodne turbine. Oštećeni klizni ležaj je saniran prelijevanjem i strojnom obradom bijele kovine. U ovom radu dan je prikaz i analiza oštećenja kliznog ležaja agregata vodne turbine E u HE Ozalj 2. Istraživan je i analiziran mogući uzrok oštećenja kliznog ležaja.

Ključne riječi: vodna turbina, klizni ležaj, bijela kovina, oštećenje.

ANALYSIS OF THE HPP OZALJ 2 PLAIN BEARING DAMAGE OF THE 1100 kW WATER TURBINE GENERATING SET

Abstract: Ozalj 2 hydro power plant (HPP) was put in operation in 1952. It consists of two Caplan turbines, D and E, having the power of 1100 kW each. After the overhaul carried out in 2007, the plain bearing of the turbine E generating set was damaged. The sliding layer of the bearing white metal was extremely worn out. Due to the damaged plain bearing, the operation of the turbine generating set had to be stopped. The damaged plain bearing was repaired by a new coating of white metal and subsequent machining. This paper gives a description and an analysis of the damage on the HPP Ozalj 2 plain bearing of the turbine E generating set. A possible cause of the plain bearing damage was investigated and analyzed.

Key words: water turbine, plain bearing, white metal, damage

1. UVOD

U HE Ozalj 2 izvršen je redoviti remont agregata E Kaplanove vodne turbine u 2007. godini. Tijekom remonta agregata izvršena je vizualna kontrola, dimenzionalna kontrola i ispitivanje metodama bez razaranja materijala svih vitalnih dijelova [1]. Ispitivanjem metodama bez razaranja materijala pored ostalog otkrivene su mrežaste pukotine na kliznoj površini donjeg vodećeg kliznog ležaja vratila generatora. Zbog nedozvoljenih mrežastih pukotina na kliznoj površini bijele kovine kliznog ležaja izvršena je sanacija oštećenja. Sanacijom je preljevena i strojno obrađena bijela kovina kliznog ležaja. Sanirani ležaj je zadovoljio vizualnu i dimenzionalnu kontrolu, kao i kontrolu penetrantom i ultrazvukom, te je ugrađen u agregat.

Nakon izvršenih svih planiranih aktivnosti remonta agregata E vodne turbine, agregat je pušten u pokusni pogon. U pokusnom pogonu u trajanju od tri dana agregat je zadovoljio sva planirana ispitivanja o uspješnosti izvršenog remonta. Nakon 296 sati normalnog rada agregata E vodne turbine od završenog remonta u 2007. godini, došlo je do oštećenja donjeg vodećeg kliznog ležaja generatora. Zbog oštećenja kliznog ležaja morao se obustaviti daljnji pogon agregata E vodne turbine u HE Ozalj 2.

U ovom radu dani su osnovni tehnički podaci i opis agregata E Kaplanove vodne turbine u HE Ozalj 2. Dan je prikaz i analiza oštećenja donjeg vodećeg ležaja generatora. Prikazani su rezultati istraživanja i analize mogućeg uzroka oštećenja kliznog ležaja.

2. OSNOVNI TEHNIČKI PODACI I OPIS RADA AGREGATA E

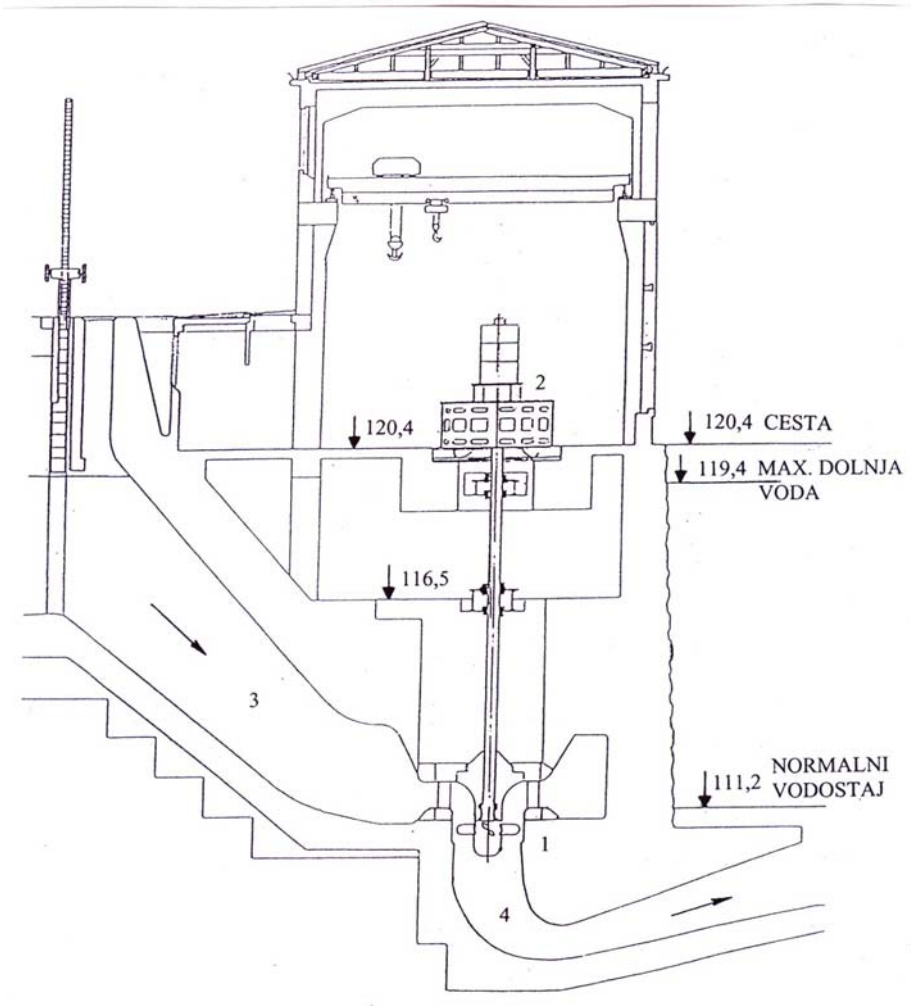
HE Ozalj 2 sastoji se od dva jednaka agregata D i E s Kaplanovim vodnim turbinana i trofaznim sinkronim generatorima za proizvodnju električne energije. Osnovni tehnički podaci agregata E su [2]:

Vodna turbina – tip: Kaplan
- nazivna snaga: 1100 kW
- instalirani protok : 17 m^3/s
- neto pad: 9,2 m
- brzina vrtnje: 300 min^{-1}

Generator – tip: S 240/54-20
- nazivna snaga: 1800 kVA
- nazivni napon: 6,3 kV
- nazivna struja: 165 A
- brzina vrtnje: 300 min^{-1}
- faktor snage cos φ: 0,7
- frekvencija: 50 Hz

Na slici 1. prikazan je uzdužni presjek kroz strojarnicu HE Ozalj 2. Iz slike je vidljiv agregat E s vodnom turbinom i generatorom vertikalne izvedbe, kao i dovod i odvod vode iz turbine. Generator se nalazi u strojarnici iznad vodne turbine. Vodna turbina i generator su spojeni pomoću međuvratila i krutih spojki što ih čini jedinstvenim agregatom. Generator je uležišten na dva klizna ležaja. Prvi ležaj je kombinirani aksijalno radijalni, tj. nosivi i vodeći klizni ležaj, a drugi je radijalni vodeći klizni ležaj. Rotor vodne turbine je uležišten na dva radijalna vodeća ležaja. Kompletan rotor generatora i turbine su ovješeni na aksijalni klizni ležaj generatora. U stator vodne turbine ugrađene su statorske zakretne lopatice, a u rotor su ugrađene četiri zakretne rotorske lopatice. Pomoću zakretnih statorskih i rotorskih lopatica može se protočni dio vodne turbine prilagoditi različitim protocima vode.

Voda ulazi u turbinu kroz dovodni tunel. U statorskim lopaticama turbine se tlačna energija vode pretvara u kinetičku energiju, a u rotorskim lopaticama se kinetička energija



Slika 1. Uzdužni presjek strojarnice s agregatom E Kaplanove vodne turbine u HE Ozalj 2: 1-vodna turbina, 2-generator, 3-ulazni kanal, 4-izlazni kanal

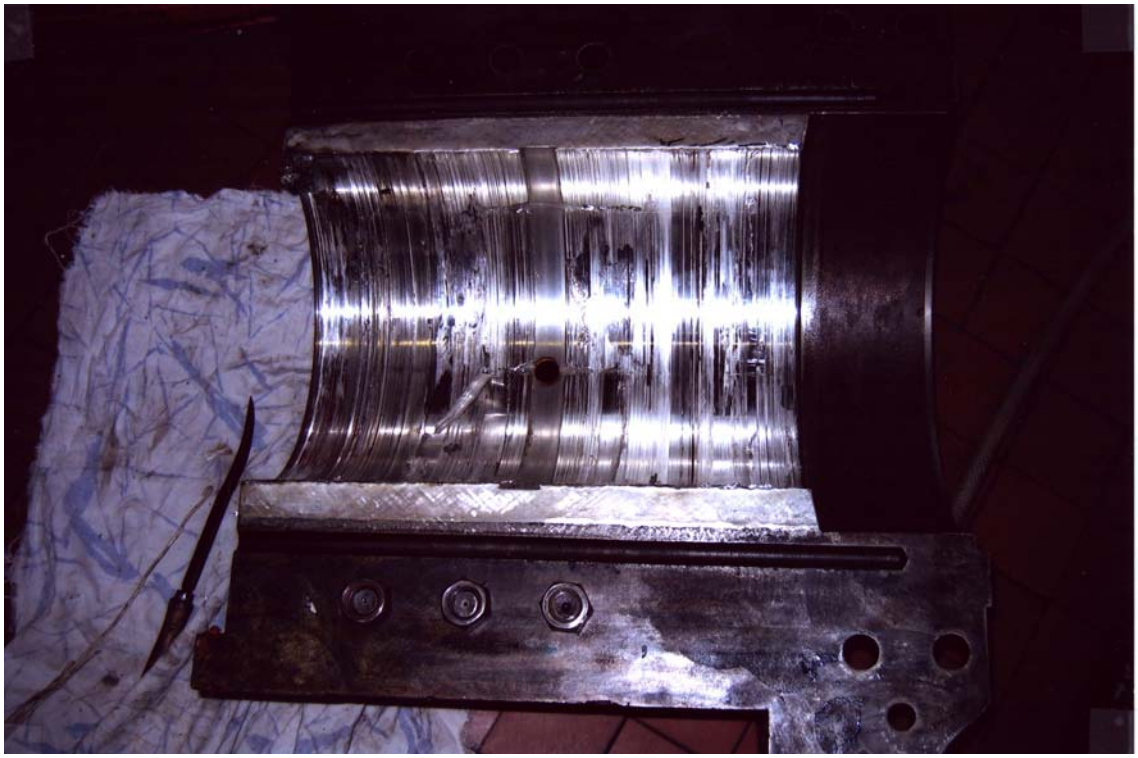
pretvara u mehanički rad u obliku vrtnje rotora koji pogoni generator. Nakon toga voda odlazi kroz izlazni difuzor i u donje korito rijeke Kupe.

3. PRIKAZ I OPIS OŠTEĆENJA KLIZNOG LEŽAJA AGREGATA E

U 2007. godini izvršen je redoviti planirani remont agregata E Kaplanove vodne turbine u HE Ozalj 2 [3]. Tijekom remonta agregata metodama bez razaranja materijala otkriveno je oštećenje donjeg vodećeg radijalnog kliznog ležaja generatora. Oštećenje je bilo u obliku nedozvoljenih mrežastih pukotina na kliznom sloju bijele kovine ležaja. Sanacija oštećenja ležaja izvršena je prelijevanjem kliznog sloja bijele kovine i strojnom obradom. Nakon sanacije ležaja izvršene su njegove uobičajene kontrole i ispitivanja ležaja metodama bez razaranja materijala. Izvršena je vizualna kontrola, dimenzionalna kontrola, ispitivanje penetrirajućim bojama na površinske pukotine kliznog sloja bijele kovine, kao i na rubno prianjanje sloja bijele kovine na osnovni materijal ležaja i ispitivanje ultrazvukom na prianjanje sloja bijele kovine na osnovni materijal ležaja [4]. Klizni ležaj je zadovoljio sva ispitivanja i ugrađen je ponovno u agregat.

Nakon završenog remonta agregat E je pušten u pokusni pogon. U pokusnom pogonu agregat je zadovoljo sva planirana ispitivanja, što je pokazalo da je remont uspješno izvršen. Nakon uspješnog pokusnog pogona agregata je pušten u normalni pogon.

Od završenog remonta agregata je normalno radio 296 sati, kada se pojavilo povišenje temperature od 70 ^{o}C saniranog donjeg vodećeg kliznog ležaja generatora. U normalnom pogonu temperatura mu je bila 32 ^{o}C. Zbog povišene temperature i težnje daljnjem povišenju agregat je isključen iz pogona. Pregledom ležaja nije se moglo utvrditi i otkloniti uzrok povišenja temperature ležaja, te je odlučeno da se isti demontira. Nakon demontaže ležaja vizualnim pregledom utvrđeno je jako oštećenje kliznog sloja bijele kovine. Prikaz oštećenog donjeg vodećeg kliznog ležaja generatora dan je na slici 2 i 3. Na danoj slici 3 moguće je vidjeti



Slika 2. Prikaz oštećenja donjeg vodećeg kliznog ležaja generatora agregata E

jako oštećenje kliznog sloja bijele kovine u obliku odnošenja i ljuštenja sloja bijele kovine. Vidljivo je da je klizni sloj bijele kovine ležaja oštećen je po cijeloj površini u obliku listića. Cijela klizna površina ležaja je potpuno uništena. Također je utvrđeno oštećenje rukavca ležaja u obliku riseva. Na slici 3. prikazan je detalj oštećenja bijele kovine ležaja. Iz dane slike je vidljivo oštećenje u obliku ljuštenja i odnošenja kliznog sloja bijele kovine ležaja. Na oštećenoj bijeloj kovini ležaja nije utvrđeno njeno pregrijavanje.

Pregledom oštećenog kliznog ležaja i kompletnog agregata E, kao i njegovog rada do oštećenja nije se mogao utvrditi uzrok oštećenja. Utvrđivanje uzroka oštećenja je pored ostalog važno, da ne bi zbog istog uzroka došlo do ponovnog oštećenja. Zbog toga se je pristupilo iztraživanju mogućeg uzroka oštećenja kliznog ležaja.

4. ISTRAŽIVANJE UZROKA OŠTEĆENJA KLIZNOG LEŽAJA

Za istraživanje mogućeg uzroka oštećenja detaljno je pregledan i analiziran oštećeni klizni ležaj. Pregledan je i kompletan ležajni blok sa sustavom za podmazivanje ležaja.

Također je pregledan kompletan agregat E i iz pogonskog dnevnika analiziran njegov rad od remonta do oštećenja kliznog ležaja. Iz svih tih pregleda i analiza nije se mogao utvrditi uzrok



Slika 3. Prikaz detalja oštećenja kliznog sloja bijele kovine ležaja

oštećenja ležaja. Uzrok oštećenja ležaja bi mogao biti neadekvatna bijela kovina kliznog sloja. Za provjeru da li ugrađena bijela kovina u ležaj odgovara propisanoj iz certifikata, dani su uzorci oštećene bijele kovine kliznog ležaja na kemijsku analizu sastava. U Laboratoriju za analizu metala Fakulteta strojarstva i brodogradnje u Zagrebu napravljena je kvantitativna kemijska analiza dostavljenih uzoraka bijele kovine:

1 - dubinska (strugotina)
2 - površinska (pločica)

Kemijska analiza uzoraka bijele kovine obavljena je spektrometrijskom metodom na uređaju ATOMSKI APSORPCIJSKI SPEKTROFOTOMETAR (AAS), TIP AA-6800, proizvođač Shimadzu. Kontrolne metode: gravimetrijski (Sn) i volumetrijski (Sb). Rezultati kvantitativne kemijske analize ispitivanih uzoraka 1 i 2 bijele kovine prikazani su u tablici 1.

Tablica 1. Rezultati kemijske analize uzorka bijele kovine kliznog ležaja

Oznaka uzorka	%										
	Sb	Cu	As	Bi	Ni	Pb	Cd	Fe	Al	Zn	Sn
1	8,25	1,30	<0,01	<0,01	0,0039	0,061	0,020	0,014	<0,003	<0,001	ostatak
2	8,92	0,67	<0,01	<0,01	0,0032	0,033	0,014	0,012	<0,003	<0,001	ostatak
3	7,20	3,20	0,005	0,001	0,001	0,023	0,001	0,002	0,0002	0,0026	89,6

U tablici 1. pod brojem 3 je radi usporedbe također dan sastav bijele kovine propisan od Nove tvornice kliznih ležajeva Karlovac, koja je istu bijelu kovinu ugradila u klizni ležaj. Usporedbom kemijskog sastava stvarno ugrađene bijele kovine u klizni ležaj dobivenog kemijskom analizom uzorka 1 i 2, sa propisanim sastavom od Nove tvornice kliznih ležaja može se utvrditi da je sastav ugrađene bijele kovine i propisane približno isti. Jedino je nešto veće odstupanje u sastavu bakra. Kemijskom analizom dobiveni sastav bakra iznosi uzorak 1 (Cu = 1,30 %) i uzorak 2 (Cu = 0,67 %), a propisani je (Cu = 3,2 %). Međutim, smatra se da ova razlika u sastavu bakra u stvarno ugrađenoj bijeloj kovini i propisanoj nije mogla biti uzrokom njenog oštećenja.

Obično kada je složeno utvrditi uzrok oštećenja tada se od mogućih uzroka metodom eliminacije utvrdi najvjerojatniji mogući uzrok. U većini slučajeva mogući uzroci oštećenja kliznog ležaja su:

- neadekvatna zračnost ležaja i rukavca,
- neadekvatno centriranje ležaja i vratila,
- nedostatak ulja za podmazivanje ležaja,
- neadekvatna temperatura ulja,
- mehaničke nečistoće, tj. upad stranog tijela,
- neadekvatno prianjanje bijele kovine na osnovni materijal ležaja,
- neadekvatni kemijski sastav bijele kovine.

Uvidom u mjerne protokole dimenzionalne kontrole i centriranja utvrđeno je da su u propisanim granicama. Iz pogonskog dnevnika utvrđeno je da je temperatura ulja za podmazivanje ležaja bila u propisanim granicama. Pregledom oštećenog ležaja nije utvrđen upad stranog tijela. Uvidom u mjerne protokole ispitivanja ležaja penetrantima i ultrazvukom utvrđeno je zadovoljavajuće prianjanje bijele kovine na osnovni materijal ležaja, kao i rubno nalijeganje. Iz rezultata ispitivanja kemijskog sastava oštećene bijele kovine proizlazi da on približno odgovara propisanom iz certifikata.

Iz eliminacije pojedinih navedenih mogućih uzroka oštećenja bijele kovine kliznog ležaja može se pretpostaviti kao mogući uzrok oštećenja nedostatak ulja za podmazivanje. Ulje je dolazilo u ležaj ali vjerojatno ne u dovoljnoj količini pa je došlo do oštećenja bijele kovine u obliku ljuštenja listića. Da je ležaj ostao bez ulja zbog povišene temperature bijela kovina bi se lokalno omekšala i bili bi na njoj tragovi povišene temperature. Nepostojanje uobičajenih tragova povišene temperature na oštećenoj bijeloj kovini može se objasniti time što je u ležaj ulje dolazilo ali ne u dovoljnoj količini.

Sanacija oštećenog kliznog ležaja izvršena je prelijevanjem oštećene bijele kovine i strojnom obradom. Nakon sanacije ležaj je zadovoljio sve propisane kontrole i ispitivanja. Oštećenja rukavca kliznog ležaja u obliku malih riseva i nanosa bijele kovine su sanirana. Klizni ležaj je ponovno ugrađen u agregat E, koji je uspješno pušten u pogon i ostao u trajnom pogonu.

5. ZAKLJUČAK

Na agregatu E Kaplanove vodne turbine u HE Ozalj 2, nakon 296 sati normalnog rada od planiranog redovitog remonta došlo je do oštećenja donjeg vodećeg kliznog ležaja generatora. Zbog oštećenja ležaja morao se obustaviti rad agregata E. Do oštećenja je došlo po cijeloj kliznoj površini bijele kovine ležaja u obliku ljuštenja listića.

Uobičajenim pregledima i ispitivanjima nije se mogao utvrditi uzrok oštećenja kliznog ležaja. Metodom eliminacije mogućih uzroka pretpostavio se kao najvjerojatniji mogući uzrok oštećenja, premala količina ulja.

Oštećeni klizni ležaj je saniran prelijevanjem bijele kovine i strojnom obradom. Agregat E je sa saniranim kliznim ležajem uspješno pušten u trajni pogon.

6. LITERATURA

[1] V. Krstelj, "Ultrazvučna kontrola: odabrana poglavlja", Sveučilište u Zagrebu Fakultet strojarstva i brodogradnje, Zagreb, 2003.

[2] Tehnička dokumentacija agregata E vodne turbine HE Ozalj 2.

[3] B. Staniša, T. Lucijanić, V. Rede "Analiza aktivnosti remonta vodne turbine HE Ozalj 2 u 2007. godini", 14. međunarodno savjetovanje HDO ODRŽAVANJE 2008, Šibenik 03. - 05.06.2008.

[4] B. Staniša, D. Brnadić, "Bezrazorna ispitivanja ležajeva u održavanju toplinskih turbina", 9. međunarodno savjetovanje HDO ODRŽAVANJE 2003, Opatija 26. - 28. 05. 2003., Zbornik radova, 217-224.

University of West Bohemia in Pilsen



Comparison of mechanical properties and behaviour systems thin film – substrate prepared by different technology of deposition

Štěpánek Ivo, Macháčková Kateřina, Jana Palubjaková, Department of Materials Science and Metallurgy, University of West Bohemia, Univerzitní 22, Pilsen, Czech Republic

Prethodno priopćenje / Preliminary

Abstract

The paper is devoted to evaluation comparison of mechanical properties and behaviour systems thin film – substrate with thin films prepared by different technology process of deposition. The basic material was the same for all deposition method HSS (with Mo) before deposition polished and HSS (with Mo and Co) for analysis influences of basic material on resulted behaviour of systems thin film - substrate. Thin films deposited on substrate was TiN from each technology process. Selected deposition process was given by firms offer deposition – PVD deposition - arc evaporation, evaporation by electron beem and magnetron sputtering. The main attention was on evaluation of mechanical properties and behaviour by indentation tests static and scratch. Thickness and abrasion resistivity of thin films were evaluated by calotest and thickness and its homogeneity by X-ray fluorescent method. Nanohardness and elastic plastic behaviour were evaluated by nanoindentation method. Adhesive and cohesive properties and behaviour and resistivity to indentation stress were evaluated by scratch indentation test.

Introduction

In this time very much different technology process for deposition thin films are offered and very much different kind of thin films with different composition chemical and structural is offered too. Each of technology process has some advantages and disadvantadges too. The concrete thin films has influenced by deposition process – type of deposition process and optimalisation deposition process parameters too. Deposition process is influence by wide range different macro and micro parameters. Some of this parameters is possible control and some of this parameters is not possible to control, but influence properties and behaviour of thin films too. The basic material is one of the most important of deposition parameters – its properties and behaviour – structure composition, chemical composition, mechanical and chemical resistivity too and the other. Beter prediction of behaviour in real stress conditions is possible to give by evaluation not only basic properties but by analysis behaviour during measurement method namely by indentation measurement during indentation process. For the best optimalisation process is very important optimalisation process of deposition on concrete basic material to real stress in practice [1] and optimalisation of analysis method for evaluation properties and behaviour of systems thin film – substrate [2].

Scratch indentation test

At the first the samples was evaluated by scratch indentation test. There was tested systems thin film – substrate with thin films TiN on substrate from HSS with Mo and Co and Mo. The measurements was realised in the mod increased acted normal force during measurement from 0 to 80 N. The indentor was standard Rockwell diamond indentor with radius of curve of tip 0.2 mm. The results are morphology of surface after scratch test (Fig. 1), dependence of signal acoustic emission on normal force (Fig. 2) and rate of normal force and friction force on normal force (Fig. 3).

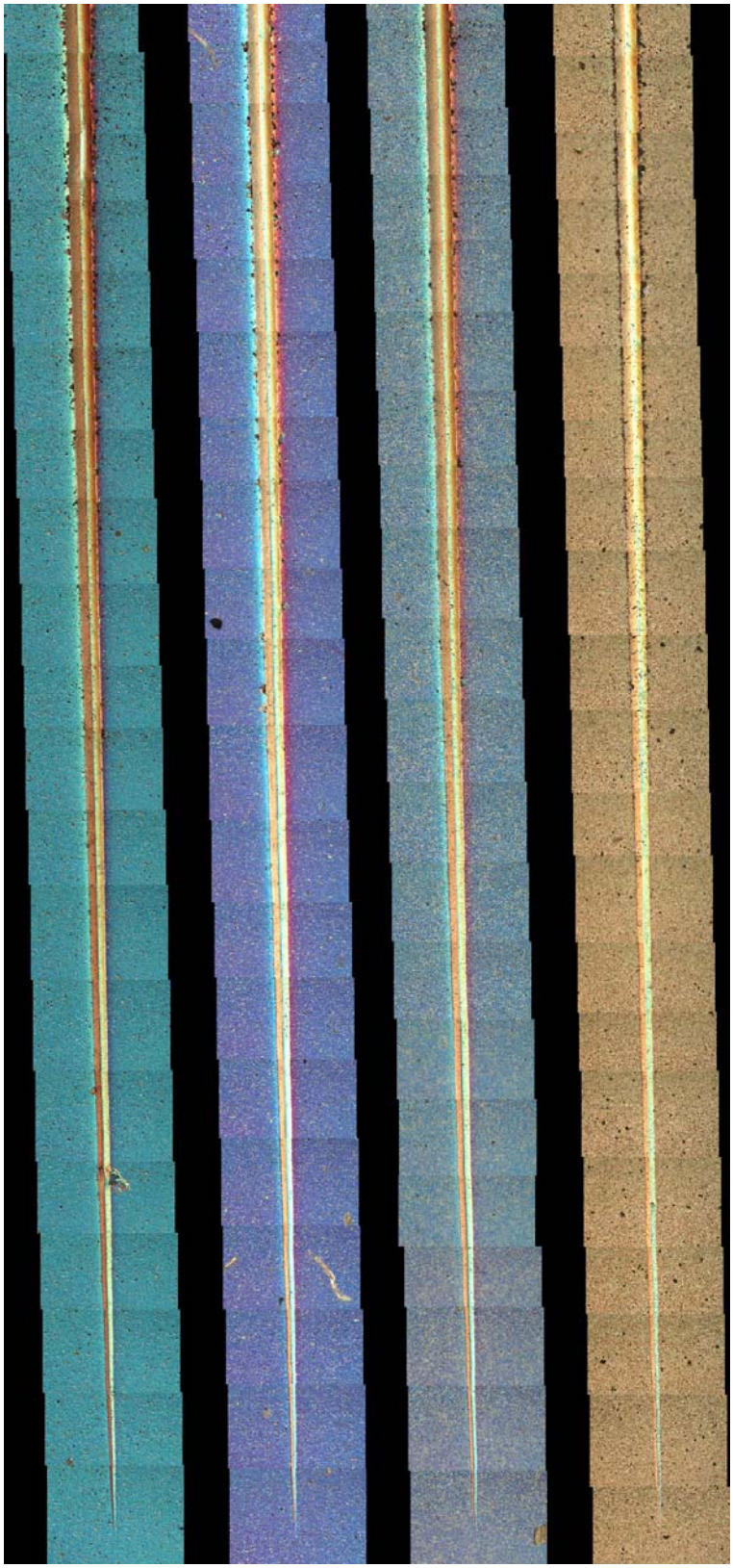


Fig.1: Morphology of surface of systems thin film – substrate after scratch test (1. – HSS without Co – thin film from arc evaporation, 2. HSS with Co – thin film from arc evaporation, 3. HSS without Co – electron beem evaporation, 4. HSS without Co – magnetron sputtering).

Morfology of scratches created during scratch test show, what the most fractured system of materials is system with thin films created by magnetron sputtering method. The highest resistance show the systém with thin film prepared by electron beem evaporation method. High resistance has systems with thin films prepared by arc evaporation method too.

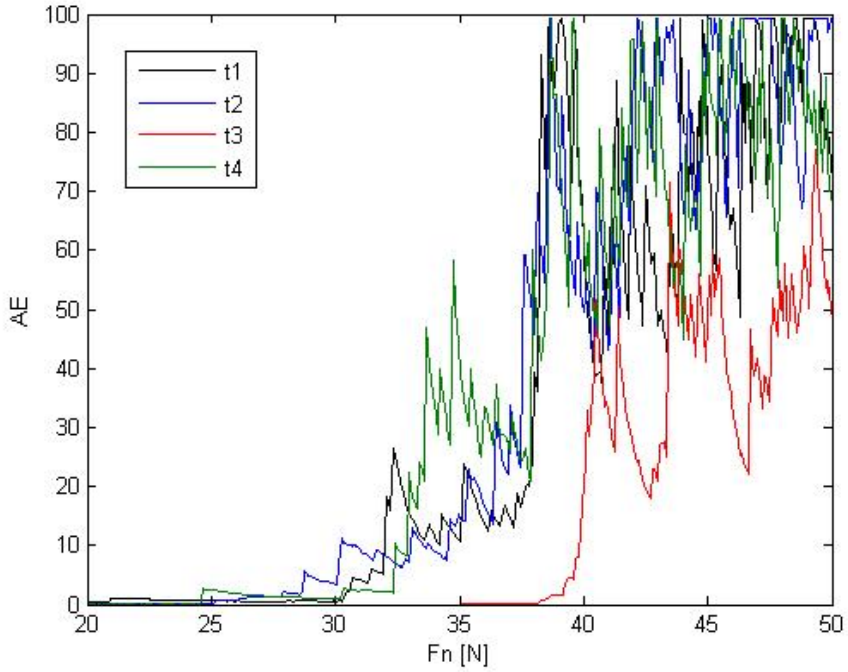


Fig. 2: Dependence of signal acoustic emission on value of normal force – labelling is the same as in Fig. 1

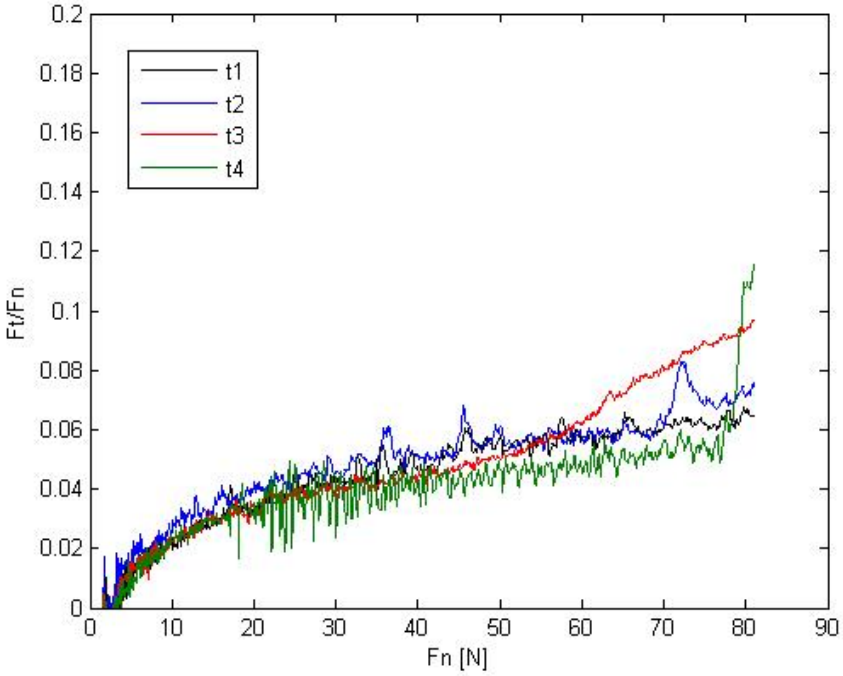


Fig. 3: Dependence of coaficient of friction on value of normal force

The acoustic emission signal show differences between fracturing all systems thin film - substrate during scratch indentation test. First signal of acoustic emission is on system with thin films prepared by magnetron sputtering - brittle failure. The best system from signal acoustic emission is TiN deposited by elektron beem evaporation and then by arc evaporation.

Coeficient of friction in dependence on normal force show, what the lowes value of coeficient of friction is on system with thin film TiN deposited by magnetron sputtering, but here is possible to view big fluctuation, which is given by brittle failuring during scratch indentation. In the second the lowest value of coeficient of friction is on system with thin film deposited by elektron beem evaporation process.

Nanoindentation measurement

The systems above mentioned was evaluated by nanoindentation too. Measurement was realised by maximal normal load 200 g (Fig. 4), 25 g (Fig. 5) and 2g (Fig. 6) for evaluation modification of surface of substrate under thin films by deposition process and hardening of surface of substrate by thin films (200 g), evaluation properties and behaviour on interface between thin films and substrate (25 g), evaluation properties and behaviour of thin films (2 g).

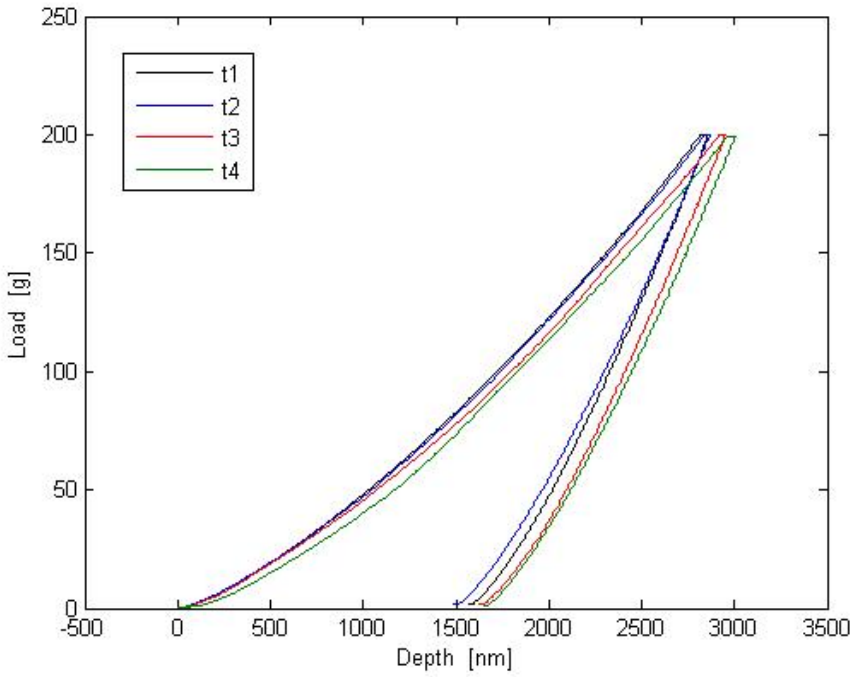


Fig. 4: Indentation curves with maximal load 200 g.

The indentation curves measured by mode 2 – loading, time delay 10 s, unloading with constant rate of loading show the highest hardening of surface is on systems thin films – substrate with thin films deposited by arc evaporation.

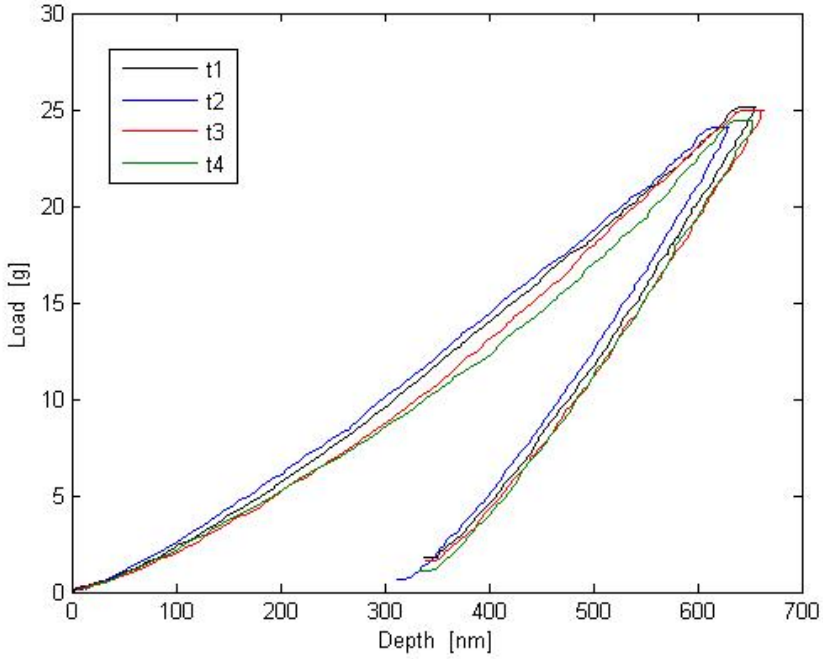


Fig. 5: Indentation curves with maximal load 25 g.

Indentation curves on Fig 5 measured by 25 g maximal load show the highest hardening of surface on systems with thin film from arc evaporation too. From this measurement is possible to view, what thin films has higher elasticity then substrate on all systems thin film - substrate.

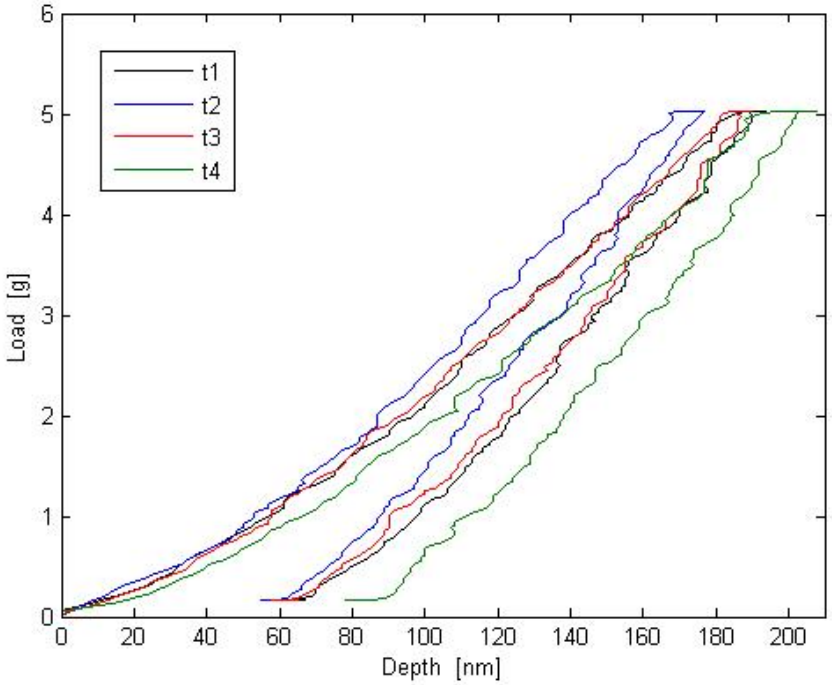


Fig. 6: Indentation curves with maximal load 2 g.

Indentation curves measured by maximal load 2 g (Fig. 6) give evaluation namely properties and behaviour thin films. The highest hardness has thin films deposited by arc evaporation. Similar hardness has thin film from electron beem evaporation. The elasticity of thin films is higher then substrate.

X-ray fluorescent method

The x-ray fluorescent method was used for evaluation thickness of thin films from different technology process of deposition. This method has advantages by nondestructive evaluation of thickness and possibility to evaluate thickness on real surfaces and real geometry. The other advantages is in possibility evaluate thickness in very small area of surface. The measurement by x-ray fluorescent method was used for evaluation profile of thickness across all samples. The samples has diameter 30 mm and measurement was realised from one edge across the centre to the second edge of samples.

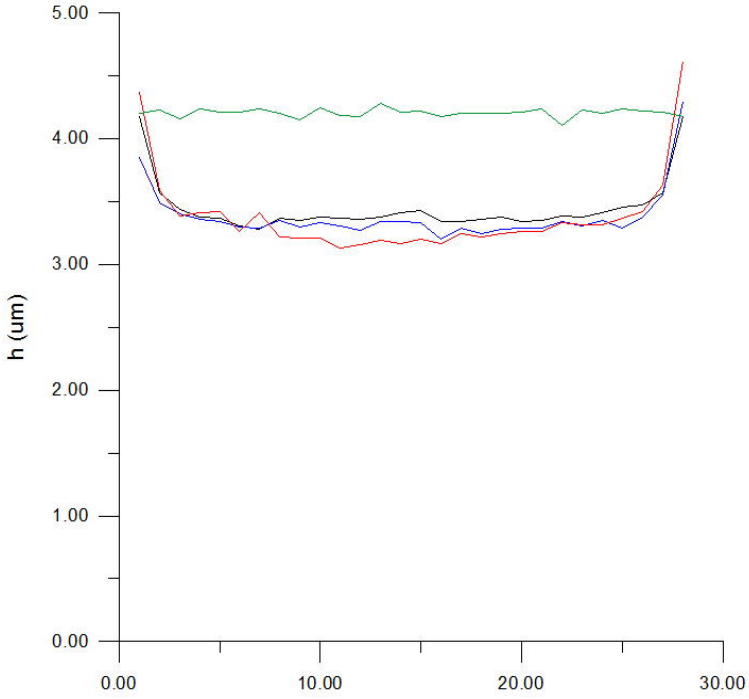


Fig. 7: Profile of thickness across surface of systems thin film - substrate

The results of measurement of profile thickness acros samples are in Fig. 7. From this figure is possible view what thickness is higher on the edges of samples. This is very important for different application. The homogeneity of thickness is only from deposition method magnetron sputtering.

Conclusion

There was evaluated different systems of thin film – substrate with the same substrate from HSS and the same kind of thin films but prepared by different technology process of deposition - PVD - arc evaporation, elektron beem evaporation and magnetron sputtering. The best resistence to scratch indentation test has system with thin films

prepared by elektron beem evaporation method deposition and arc evaporation. The lowest resistence has systems with thin films deposited by magnetron sputtering method of deposition. The highest hardening surface of systems is on systems with thin films prepared by arc evaporation and then by elektron beem evaporation. Very interesting results is from analysis profile of thickness across samples. The highest homogeneity of thickness across surface of samples has thin films prepared by magnetron sputtering and the lowest homogeneity of thickness has systems from electron beem evaporation method of deposition.

The paper is presented in the range of solution project n. FT-TA4/082.

Literature

1. I.Stepanek, Correlation between deposition parameters and method for evaluation properties and behaviour system of thin film - substrate, proceedings of conference Matrib 2000 Vela Luka – Croatia 2000
2. I.Stepanek, Evaluation of mechanical behaviour very different kind of material and thickness of films, proceedings of conference Matrib 2002, Croatia – Vela Luka 2002

University of West Bohemia in Pilsen



Possibility of evaluation of mechanical properties and behaviour of systems thin film – glass substrate by indentation tests

Štěpánek Ivo, Macháčková Kateřina, Department of Materials Science and Metallurgy, University of West Bohemia, Univerzitní 22, Pilsen, Czech Republic

Prethodno priopćenje / Preliminary

Abstract

The paper is devoted to evaluation properties and behaviour special system thin film – substrate prepared by sol gel deposition method. There are optimalised analytic method for evaluation of specific system, where substrate is very brittle, thin films are transparent and without color and thickness is very small. This paper show possibility of utilization of method for evaluation properties and behaviour system thin film – glass substrate. Static and scratch indentation was used for evaluation of mechanical properties and behaviour, adhesive cohesive behaviour, resistivity to indentation stress and elastic plastic behaviour. Thickness is evaluated by calotest measurement and by x-ray fluorescent method too. Calotest give possibility to evaluate resistivity to abrasive stress too.

Introduction

Thin films has very wide range of application from the point of view unique properties and behaviour of materials as thin films. Thin films has specific mechanical properties and behaviour, optical properties, electromagnetic properties, chemical properties and the other. Not only thin films dirrected to the application in environment with mechanical stress is important to evaluate from point of view mechanical properties and behaviour [1]. It is important tested all thin films for evaluation mechanical properties – adhesion, hardness, elastic and plastic behaviour and so on. It is very difficult evaluate adhesive properties of thin films from point of view different resistivity, different type of thin films – with bigger thickness, with very small thickness, non transparent or transparent, contrast between thin films and substrate. It is very difficult evaluate some properties more precisely. The most important are resistivity to some kind of stresses – mechanical stress, chemical stress and so on [2].

Scratch indentation test

First of all the scratch indentation was realised on systems thin film – glass substrate. At the first was setup standard parameters for measurement. Normal force was increased with constant rate of increasing of value from 0 to 30 N. Measurement was provided by standard diamond Rockwell indentor with curve of indentor tip with radius 0.2 mm. Morphology of scratches, acoustic emission signal and coeficient of friction was evaluated after measurement. Fig. 1 and 2 show the results of morphology, on fig. 3 dependence of acoustic emission signal on normal force is presented. The coeficient of friction give not significant diferences.

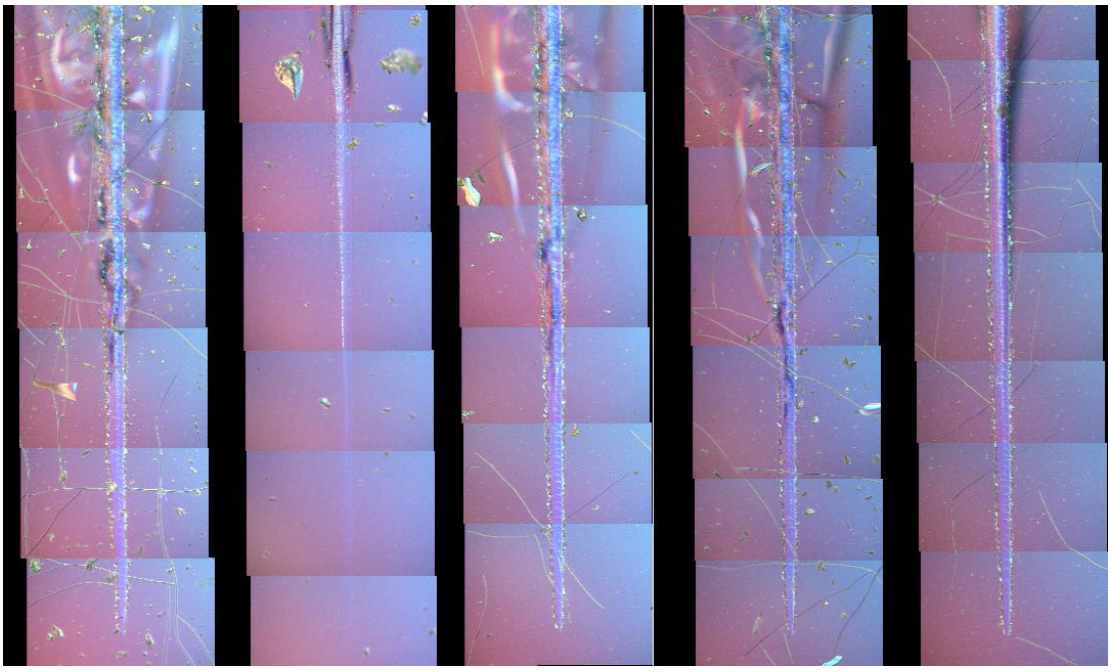


Fig. 1: Morphology of surface of systems thin films – substrate after scratch test – normal force 0 – 30 N and diamond Rockwell indentor 0.2 mm.

Fracturing around and in scratches on fig. 1 are very large. Substrate has brittle fracture under thin films and by this degradate all system thin film – glass substrate. The second system is the best from this evaluation. The fracturing of substrate is very large. We prepared refinement of measurement by changing parameters of scratch measurement – normal force between 0 to 25 N. We change rate of samples under indentor and we change geometry of indentor curve of tip of indentor from 0.2 mm on 0.5 mm of diameter.

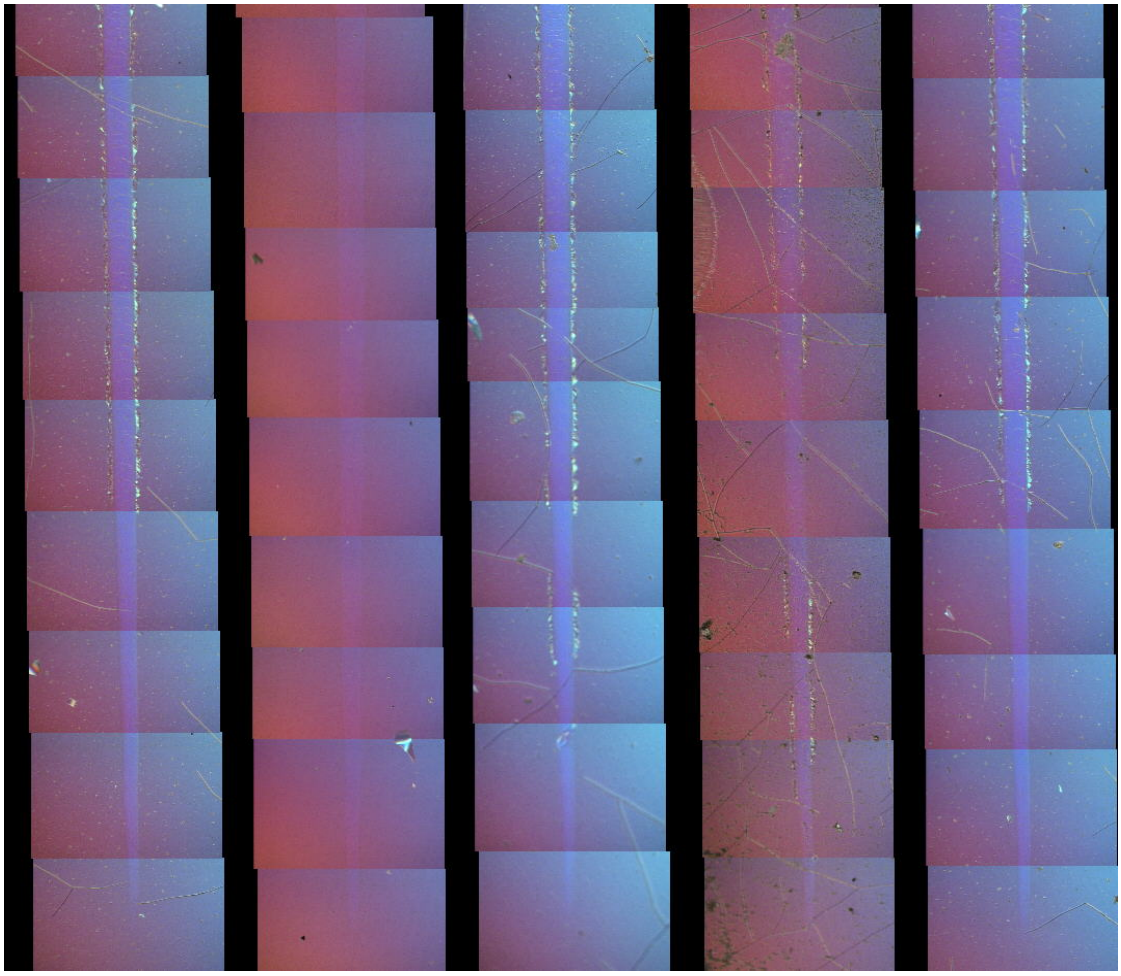


Fig. 2: Morphology of surface of systems thin films – substrate after scratch test – normal force 0 – 25 N and diamond Rockwell indentor 0.5 mm.

Fig. 2 show better differences between all systems thin film – glass substrate and we can analyse as the best system the second, the first and fifth. There is namely cohesive failures of thin films.

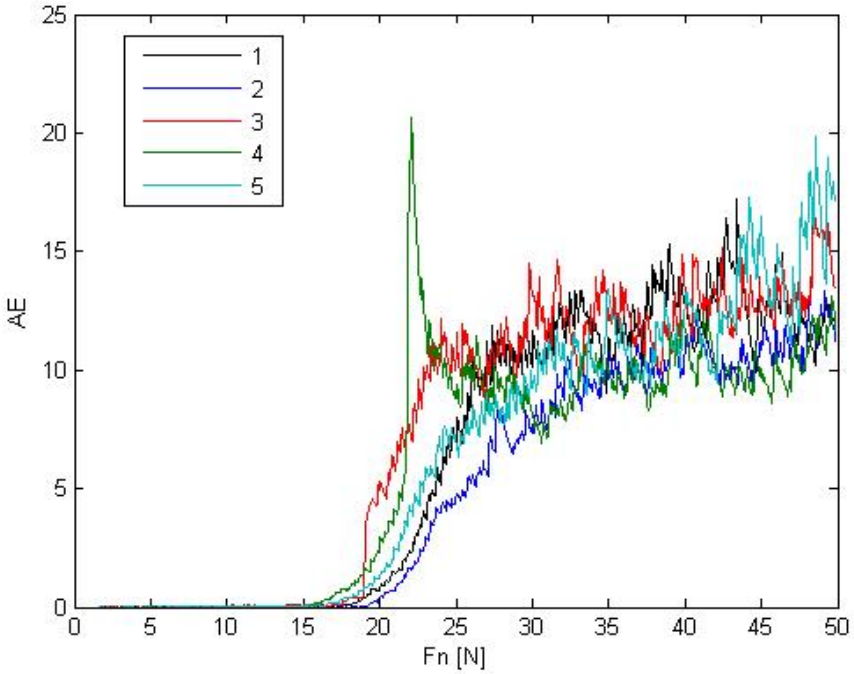


Fig. 3: Acoustic emission signal – dependence on normal force

Acoustic emission signal give results similar. The best systems are the 2 nd. Acoustic emission signal on surface of glass is very big, but by thin films this signal decrease because thin films hardening surface of all systems of materials.

Nanoindentation

Nanoindentation measurement was realised by setting mode 2 – indentation curve - loading, time delay 10 s and unloading. Measurement was provided by two different maximal load 25 g (Fig. 4) and 5 g (Fig. 5). Maximal load 25 g is for analysis modification of surface of glass by deposition process and 5 g is for evaluation differences between thin films on all systems thin film – glass substrate, because substrate is the same but thin films are different.

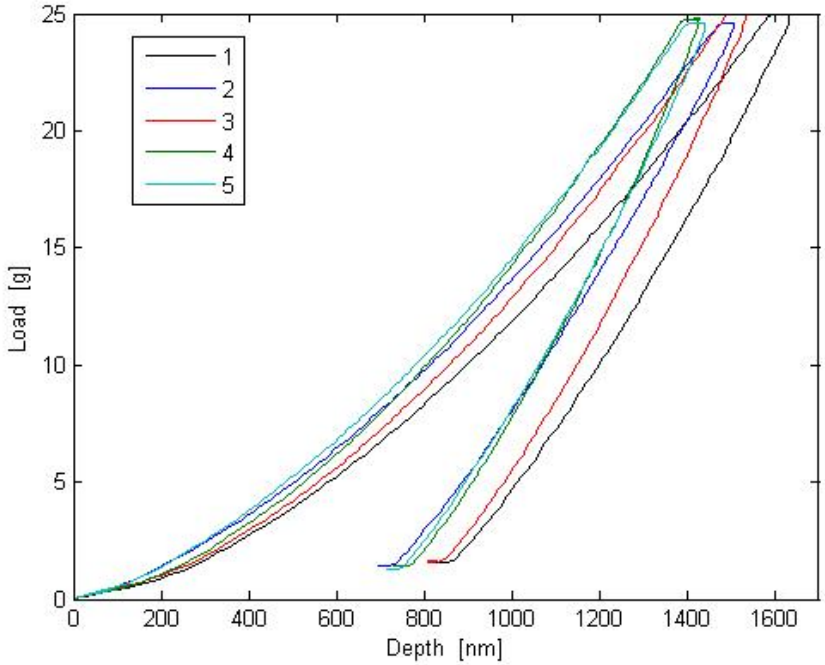


Fig. 4: Indentation curves from measurement by maximal load 25 g.

Indentation curves with maximal load 25 g (Fig. 4) show the highest hardening of surface on systems 4 th and 5 th. The curves on systems 1 st show the lowest hardening of surface. Optimal hardness and toughness is on 2 nd system thin film – glass substrate.

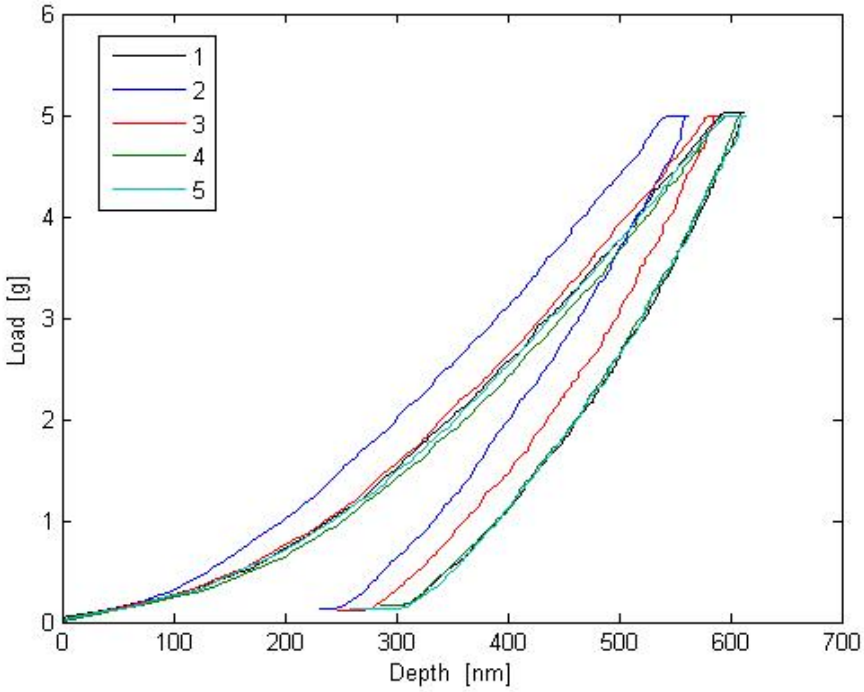


Fig. 5: Indentation curves from measurement by maximal load 5 g.

Measurement on Fig. 5 represent results from indentation by maximal load 5 g. The highest hardness is on 2 nd systems. The other systems are similar. The elasticity of thin films is higher then only surface of glass before deposition.

Thickness and abrasion resistivity

The thickness we try to evaluate by calotest and by x-ray fluorescent method. Calotest was realised by ball with diameter 25 mm and diamond paste. The thickness is very small and abrasion resistivity of thin films is very small too. It is very difficult evaluate thickness. The results show Fig. 6.

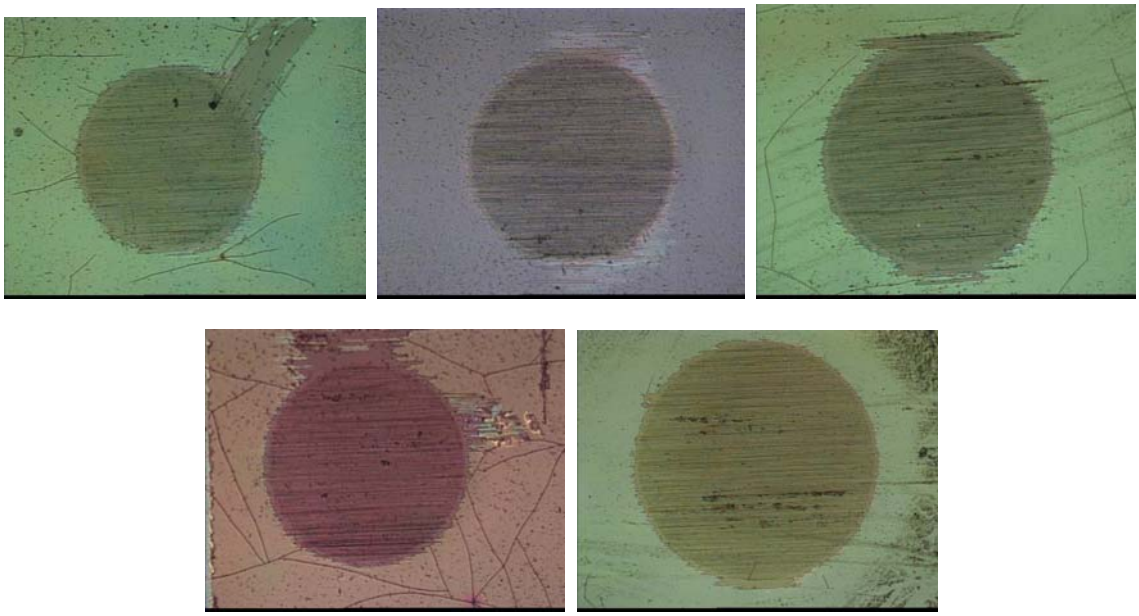


Fig. 6: Resulted morphology after calotest measurement

Thickness from this evaluation is 1 st 420 nm, 2 nd 400 nm, 3 rd 720 nm, 4 th 320 and 5 th 550 nm. The thickness is not precisely evaluated but the differences correspond with measerement by indentation method.

Measurement by x-ray fluorescent method is not possible to use because thickness is very small and glass has not charasteristic maximum in x-ray spectrum. The Fig. 7 show all spectrums and here is not possible evaluate differences. The Fig. 8 give result with measurement surface of glass substrate - brown thick line and here is not possible analyse differences between substrate and thin films.

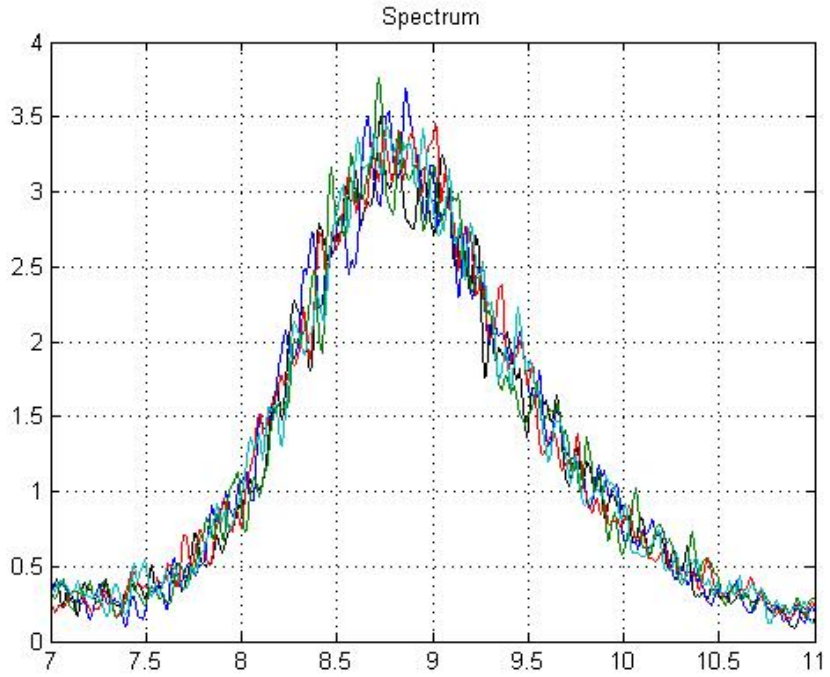


Fig. 7: X-ray fluorescent spectrums on all systems thin film – glass substrate

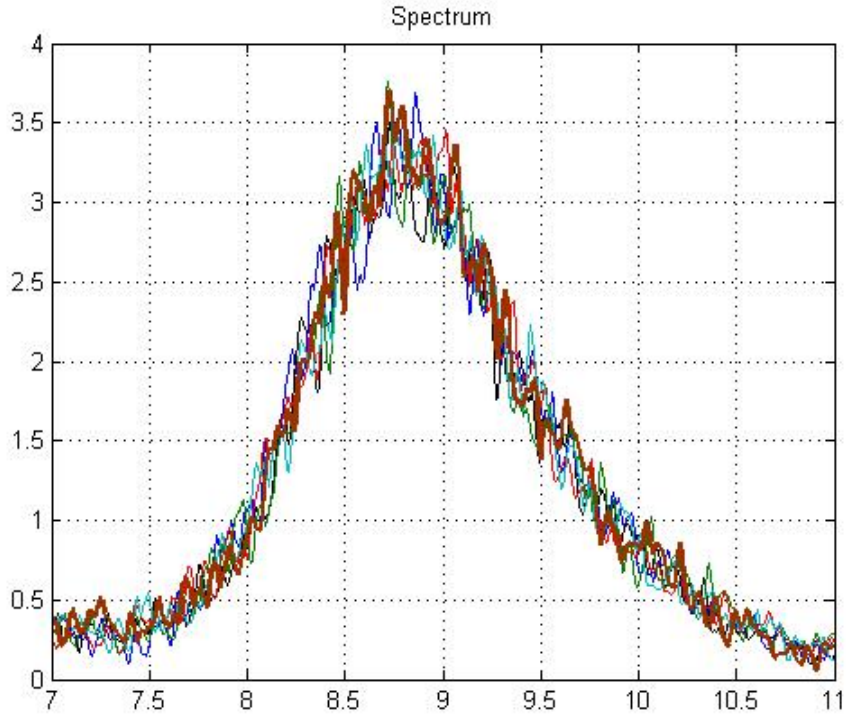


Fig. 8: X-ray fluorescent spectrums on all systems thin film – glass substrate with spectrum for surface of substrate before deposition – grown thick line.

Conclusion

The paper is dirrected for evaluation mechanical properties and behaviour of systems thin films – glass substrate. On the start the results give information what is not possible to evaluate these specific systems by our method for analysis. The problem is in very small thickness, small resistivity thin films, small resistivity surface of glass substrate – brittle fracturing, transparency of thin films and here are not differences in color in contrast with glass. The first results show what it is very important refinement of measurement by changing parameters of measurement – changing rate of samples under indentor, maximal load is important decrease and geometry of diamond Rockwell indentor was changed. There was evaluated adhesive cohesive behaviour, hardness and elastic plastic deformation by indentation and thickness by calotest and x-ray fluorescent method. The result give us differences. The highest resistivity is on systems 2 nd, then on systems 1 st and 5 th and the lowest resistivity is on systems 3 rd and 4 th. Thickness the highest on systems 3 rd and here is problem with resistivity. Optimal thickness is about 400 nm.

The paper is presented in the range of solution project GA CR n. 106/07/1149.

Literature

1. Štěpánek I., Michálek J., Němec R., Tengler M. – Evaluation of very thin films created by depositon process and degradation process by nanoindentaion tests, proceedings of conference Matrib 2004, Croatia 2004
2. Reindl R., Koutsky J., Stepanek I. - Step by step evaluation of combination stress of the thin film – substrate system, proceedings of conference AMME 2002, Poland 2002

STRUCTURE AND PROPERTIES OF MOLLUSC SHELLS

STRUKTURA I SVOJSTVA OKLOPA ŠKOLJAKA

Jelena Šubarić, Tomislav Filetin

Faculty of Mechanical Engineering and Naval Architecture, University of Zagreb,
I. Lučića 5, Zagreb, Croatia

Pregledni članak / Subject review

Abstract:
Biological materials are complex composites that are hierarchically structured and multifunctional. Their mechanical properties are surpassingly better than those of synthetic materials with similar phase compositions. Thus, biological materials are inspiring materials scientists in the design of novel materials. In this article we are discussing the structure and properties of abalone shell. Abalone shell is a biological hard tissue composed of inorganic and organic components. It possesses a segmented layered structure, which provides an excellent combination of strength, toughness and thermal insulating properties. Biomimetics (bionics) is studying this kind of systems in biology with the intent of reproducing the similar artificial. Some of the processes and techniques used for creating those biological structures have been described and also some examples of application are given.

Keywords: biomimetics, composites, strength, toughness

Sažetak:
Biološki materijali su složeni kompoziti hijerarhijske strukture s više funkcija. Njihova mehanička svojstva su neusporedivo bolja od svojstava umjetnih materijala sa sličnim komponentama. Zbog toga biološki materijali potiču znanstvenike na stvaranje novih materijala. Ovaj članak opisuje strukturu i svojstva oklopa školjke Petrovo uho. Oklop školjke je tvrdo biološko tkivo sačinjeno od anorganske i organske komponente. Posjeduje segmentiranu laminatnu strukturu koja daje odličnu kombinaciju čvrstoće, žilavosti i toplinsko-izolacijskih svojstava. Biomimetika (bionika) proučava takve biološke sustave s namjerom njihovog kreiranja ili reproduciranja sličnih umjetnih. Opisani su neki materijali i tehnološki postupci koji se koriste za oponašanje svojstava bioloških struktura, a navedeni su i primjeri njihove primjene.

Ključne riječi: biomimetika, kompoziti, čvrstoća, žilavost

1. INTRODUCTION

Biological materials and their skilled use have played a key role in the development of mankind and technology. From a mechanical point of view, there is nothing very special about the individual components of these materials. What distinguishes them is their structural hierarchy, which provides them with the potential of structural optimization at each of the structural levels and leads to a striking mechanical efficiency. Biological hard tissues are composites of minerals and organic macromolecules (proteins, polysaccharides, lipids) [1]. Their mechanical properties are often superior to human-made materials with similar phase compositions. They are made of simple and common materials (carbonates, oxides, sulphides), but have multifunctional properties. Over the lifetime of organism these materials are also monitored and self-repaired leading to durability that is much longer than it is possible in synthetic systems.

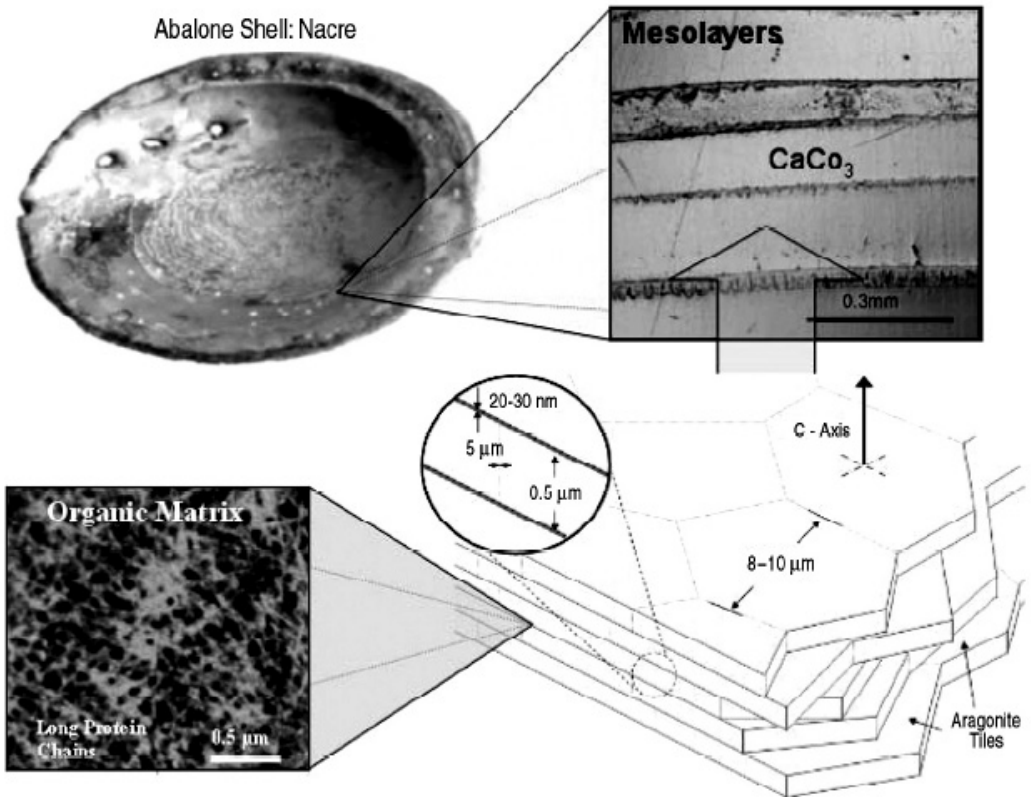


Figure 1. The hierarchy of the abalone shell [2]

Because of all those positive aspects of biological materials, over the last 50 years science called biomimetics has been developed. One major application of biomimetics is the field of biomaterials, which involves mimicking or synthesizing natural materials, and applying this to practical design. There are many examples of materials in nature that exhibit unique useful properties. One of the major advantages of biomaterials is that they are normally biodegradable. In biological systems the design of the material and structure are closely connected, whereas in synthetic materials there is a disciplinary separation between materials engineers and mechanical engineers. Biological materials are still of great importance today, even for high-tech applications, since they have properties which cannot easily be emulated by man-made materials.

2. STRUCTURE AND PROPERTIES OF MOLLUSC SHELLS

A typical mollusc shell has an outer organic layer (mainly protein), which acts as a basic for calcified parts of the shell to be laid down. The mineral is the calcium carbonate, usually in a form of aragonite, occasionally of calcite or amorphous. Mineral phase corresponds to approximately 95% of the total volume and thus provides the strength, whereas the organic component contributes to the ductility. There are five structural types of bivalve's shells: prism, nacre, crossed-lamellar, foliated and homogeneous [3]. Nacre is in general considerably stronger in tension, compression and bending than the other types [3]. These types of structure are arranged in two basic layers of the shell. There are different arrangements, depending on the type of the shell. An external layer of abalone shell is composed of large prismatic aragonite crystals of fairly high hardness. Its function is to stop any impact from the outside environment. An inside nacreous layer is designed to absorb the kinetic energy from the impact through ductility and enhanced toughness [4].
Nacre is composed of hexagonally shaped aragonitic (orthorhombic; $CaCO_3$) plates, 300±100 nm thick, surrounded by thin 10±5 nm film organic matrix that is successively stacked to form a layered nanocomposite. The plates form a brick-mortar structure, shown in figure 2.

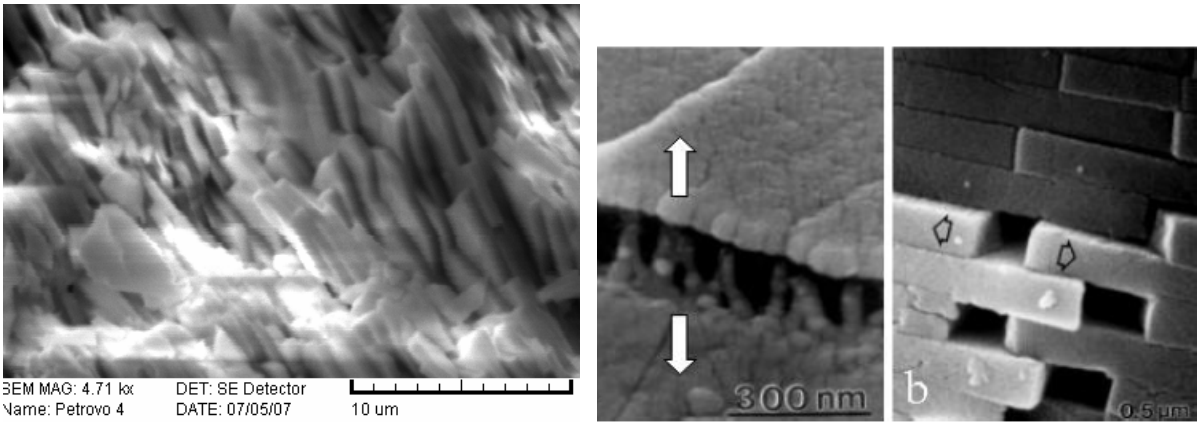


Figure 2. SEM images of nacre in abalone shell (left [5]) and deformation behaviour under static loading, representing normal and shear resolved stresses [1]

Bivalve shells present some problems in mechanical testing. Testing is confined to fairly large shells because of the radius of the curvature and anisotropic behaviour. Obtaining the uniform specimen can be unsuitable, because many are difficult to machine without inducing stress concentrations. And finally specimens are dry, not containing the original humidity and elasticity of proteins, which has a large effect on the strength of the specimens [3].
Some mechanical properties are given in the table 1.
In the case of impact, normal to the shell, nacreous layer experiences tension parallel to the plates. Plates begin sliding over each other and the hardening effect occurs. As the plates contain certain asperities, during the sliding, the climbing of opposite asperities is causing a transverse compressive stress responsible for the hardening. The organic matrix bridges between the plates are keeping the plates together and preventing uncontrolled crack growth.

Table 1. Mechanical properties of abalone shell

Mechanical property		**Value**	**Ref.**
Fracture toughness	K_{IC}	10±4 MPa $m^{1/2}$	[1]
Specific strength	R_f	200±40 MPa/(g/cm^3)	[1]
Modulus of elasticity (dry sample)	E_s	90 GPa	[4]
Modulus of elasticity (wet sample)	E_m	50 GPa	[4]
Microhardness	$HV_{0,2}$	200	[5]

There is a lack of data about thermal properties of this materials and structures. From the living environment of shells follows that those properties could be the indicators for possible heat insulating behaviour of similar synthetic materials in different technical usages.
Literature [9] offers the thermal properties data only for $CaCO_3$ (Table 2), which indicates approximate data for abalone shell.
Thermal diffusivity and thermal conductivity are similar like porcelain or same type of ceramics. Presumption is that the real shell has at least same good thermal insulating characteristics, but for this argumentation the additional investigations are necessary.

Table 2. Thermal properties of $CaCO_3$ [9]

Property	**Unit**	**Value**
Thermal diffusivity	m^2s^{-1}	$1{,}68x10^{-6}$
Thermal conductivity	W/mK	3,85
Thermal effusivity	$Jm^{-3}K^{-1}$	$2{,}97x10^3$

3. TECHNOLOGIES FOR FORMING OF SIMILAR SYNTHETIC MATERIAL STRUCTURES

The use of microscope and the other new devices for investigating and testing nanostructures and nanoproperties enabled us to discover some of the advantages of biological materials. Afterwards, the new technologies are in developing phase in order to artificially creating structures and materials similar as natural. They need to be efficient and cost-effective, so that these new materials would be competitive. Some of these possible technologies are discussed here.

3.1 Forming of multilayer thin coatings by means of PVD (Physical Vapour Deposition) process

Much interest has been placed on multilayer thin coatings, consisting the combination of brittle and soft layers of different materials, mimicking those found in the seashells. Significant advances in PVD, mainly Pulsed Filtered Cathodic Arc, have allowed accurate control of thin film properties enabling specifically tailored coatings to be engineered. Multilayer such as Al/W and Al/AlN are being made by this method. Al is relatively soft material and W and AlN are relatively hard, which mimics the abalone shell [6].

3.2 Forming of laminate by pressing the thin foils

This process is very simple and cost-effective. Its novelty lies in the fact that it is performed in open air and produces a full dance laminate composite. Thin foils, e.g. titanium and aluminium, are being pressed under high temperature and pressure in the hydraulic press. Processing temperatures are below 700 ºC and pressure is under 4 $MPam^2$, which makes very modest processing conditions [7]. This laminates are called MIL (metallic-intermetallic laminate) composites. Process is highly flexible since metal/alloy foils other than titanium can be used individually, or in combination. MIL composites using iron-based, nickel-based and cobalt-based alloys as the starting metal layer have been successfully produced using the described technique [7]. Also the use of initially ductile metallic foils enables the layer to be formed into complex shape. This opens the door for forming non-planar structures, such as rods, tubes, shafts, cones and complex tree-dimensional structures. The unique properties of MIL composites arise from the combination of high hardness and stiffness of the intermetallic phase, alternatively layered with high strength, toughness and ductility of metal alloys. MIL composites can also be formed with cavities that are afterwards filled (depending on application). They possess very good antiballistic properties, absorption of energy and damping of vibrations [7]. The most common are Ti-Al_3Ti MIL composites that imitate nacre in a seashell. Instead of Ti, alloys of Fe, Co and Ni could be used.

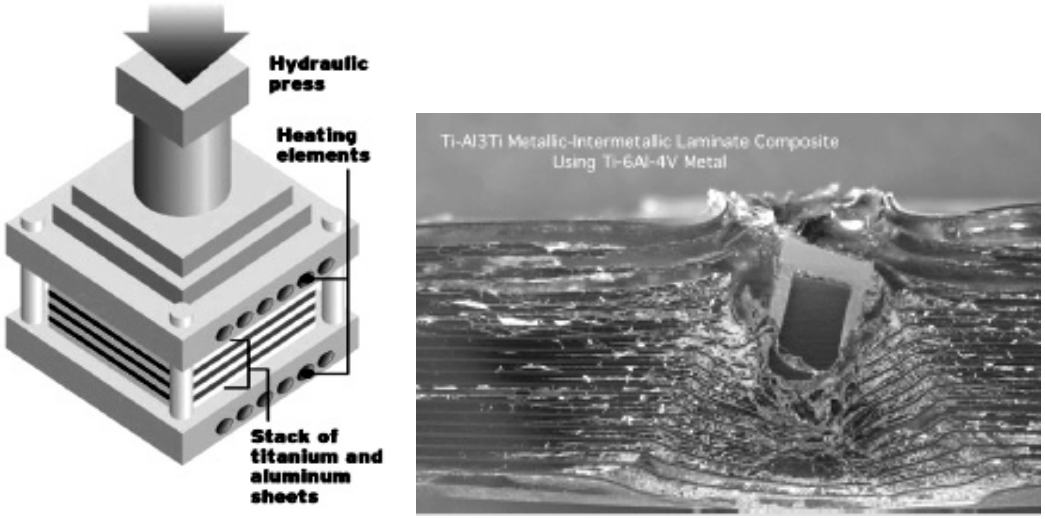


Figure 3. Platen press for fabrication of planar MIL composites (left) and a cross section of the impact location from the ballistic test on a Ti-Al_3Ti MIL composite [7]

3.3 Layered structures created by rapid prototyping

Rapid prototyping is a new method that enables creating materials layer by layer according to 3D CAD model. Also, it is possible to create composites of various materials such as metal, ceramics, glass, polymers and etc. Laminate composites like glass/epoxy resin and graphyte/silicium carbide, which imitate the structure of nacre in seashells have better ductility and hardness than pure glass [8].

CONCLUSION

Nature provides us with many different material structures whose properties and behaviour are very attractive for technical applications. Based on the testing of properties and characteristics of such structures, similar artificial materials are trying to be created by already known or by new processes. Those materials are in general nanostructured cellular or layered. The up growth of nanotechnology is accelerated the processes of creation of biomimetic materials. It has been proven that the properties of seashells can be the basis for development of materials with antiballistic laminated structures or with excellent thermal insulation properties. The future work goal is to analyse artificial materials and laminated structures with the corresponding combination of mechanical and thermal properties, like those found in seashells.

REFERENCES

[1] Sarikaya M., Fong H., Sopp J.M., Katti K.S., Mayer G.: Biomimetics: Nanomechanical Design of Materials through Biology; 2002, 15th ASCE Engineering Mechanics Conference, Columbia University, New York.

[2] Meyers M.A., Lin A.Y.M., Seki Y., Chen P., Kad B.K., Bodde S.: Structural Biological Composites: An Overview, JOM, 2006.

[3] Currey J.D.: Mechanical Properties of Mollusc Shell; Symposia of the Society for Experimental Biology, number XXXIV; Cambridge University Press, 1980.

[4] Barthelat F., Espinosa H.: Tensile Testing of Abalone Nacre Miniature Specimens Using Microscopy and Speckle Correlation; 2002 Annual meeting of the Society of Experimental Mechanics, June 10-12, Milwaukee, Wisconsin, 2002.

[5] Šubarić J.: Properties of biomimetic shell materials (Baccalareus work in Croatian), Faculty of Mechanical Engineering and Naval Architecture University of Zagreb, Zagreb, 2007.

[6] Burgman F.A.*, Xaio X.L.*, McCulloch D.G.*, McKenzie D.R**, Bilek M.M.M.**, Gan B.K.** and Ryves L.**: Relationship between microstructure, stress and hardness in multilayer coatings, *School of Applied Science, Melbourne, Australia and **School of Physics, Sydney, Australia, 2005.

[7] Vecchio K.S.: Synthetic Multifunctional Metallic-Intermetallic Laminate Composites, JOM, 2005 (3), 57.

[8] Calvert P., Cesarano J., Chandra H., Denhim H., Kasichainula S. and Vaidyanathan R.: Toughness in Synthetic and Biological Multilayered Systems; Phil. Trans. R. Soc. Lond. A 360, 199-209, (2002).

[9] Ramachandran, E., Raji, P., Ramachandran, K., Natarajan, S.: Photoacoustic study of the thermal properties of calcium carbonate - the major constituent of pancreatic culculi, Cryst. Res. Technol. 41, No1, 64-67, (2006).

STRUKTURE ŠTAPOVIMA PROSTORNO OJAČANIH KOMPOZITA

CYLINDRICAL-BARS SPACE-REINFORCED COMPOSITE STRUCTURES

Jadran Šundrica, Sveučilište u Dubrovniku, Ćira Carića 4, 20000 Dubrovnik, Hrvatska
Tomislav Filetin, Fakultet strojarstva i brodogradnje, Ivana lučića 4, HR - 10000 Zagreb

Izvorni znanstveni rad / Original scientific paper

Sažetak
Prikazano je oblikovanje modela ojačanja počevši od ortogonalno i neortogonalno ojačanih u dva pravca preko ravninski ojačanih u tri pravca do jednostavnih ojačanih u tri, četiri i šest pravaca i složenih ujednačenih i neujednačenih ojačanih u sedam, devet, deset i trinaest pravaca. Opisana je izrada i sheme slaganja struktura potrebnih za proizvodnju ortogonalno ravninski ojačanog laminata te postupak proračuna stupnja popunjenosti prostora takvih struktura. Tablično su prikazani izračunati stupnjevi popunjenosti prostora svih jednostavnih prostorno ojačanih struktura kao i geometrijski parametri neophodni za njihovu izradu. Prikazani su razrađeni modeli jednostavnih prostorno ojačanih struktura u tri, četiri i šest pravaca, izrađeni na računalu.

Ključne riječi: prostorno/ravninski ojačani kompoziti, modeli struktura

Abstract
This paper presents a methods of constructing models ranging from orthogonal and non-orthogonal reinforced structures in two directions, the plane reinforced ones in three directions, simple models reinforced in three, four, and six directions, and the complex balanced and non-balanced reinforced ones in seven, nine, ten and thirteen directions. Descriptions have been provided of design and layout scheme of structures required for the production of orthogonally plane-reinforced laminates and the calculation procedure of the space filling ratios of such a structure. Tables are given showing the space filling ratios of all the simple space-reinforced structures as well as the geometrical parameters necessary for their production. The paper gives a separate presentation of computer models of simple space-reinforced structures required for the production of composites reinforced in three, four, and six directions

Key words: space/plane-reinforced composites, models of structure models

1. Uvod

Proučavanje struktura prostornog ojačavanja povezana su s proizvodnjom naprednih kompozitnih materijala primjenjivih za najteže radne uvjete. Ovaj se rad bavi koncipiranjem modela struktura prostorno ojačanih struktura kompozita. Pristup se temelji na sustavnoj analizi od jednostavnijih prema složenijim modelima uz naglašenu težnju prema otkrivanju općih karakteristika modela ojačavanja.

S obzirom na tip strukture ojačavanja kompoziti se mogu podijeliti na laminate i prostorno ojačane tvorevine [1]. Najjednostavniji laminati nastaju popunjavanjem matrica paralelno postavljenim vlaknima. Opisi teorijskih shema popunjavanja i stupnja popunjenosti takvih materijala ojačanih u jednom pravcu paralelnim vlaknima jednakog promjera i vlaknima različitih promjera dani su u [2]. Prikazana opća shema popunjavanja matrice te izdvojene tri karakteristične sheme slaganja ojačala: kvadratna, heksagonalna i rombska kao njeni posebni slučajevi.

U cilju omogućavanja proračuna parametara potrebnih za izradu kompozita potrebno je poznavati maksimalni faktor popunjenosti prostora i njegovu ovisnost o razmaku među ojačalima. Faktor popunjenosti prostora je polazna osnova i za predviđanje mehaničkih svojstava kompozita što je temeljem objavljenih teorija sustavno prikazano u [3]. Teorijska razmatranja struktura laminata ojačanih u više pravaca su obuhvatila dvije strukture ojačane u ravnini u dva pravca i jednu strukturu ojačanu u ravnini u tri pravca jer se one mogu dobiti iz osnovnih struktura prostornog ojačavanja. Složenije strukture laminata ojačane u ravnini u više od tri pravaca se mogu analizirati kao kombinacije nastale rotacijom i ponavljanjem jednostavnijih struktura.

Složene strukture prostornog ojačavanja mogu se razmatrati kao rezultat kombiniranja jednostavnih struktura, a isto tako je moguće promatrati jednostavne strukture prostornog ojačavanja kao posebne slučajeve jedne opće strukture ojačane u trinaest pravaca (13D) [4].

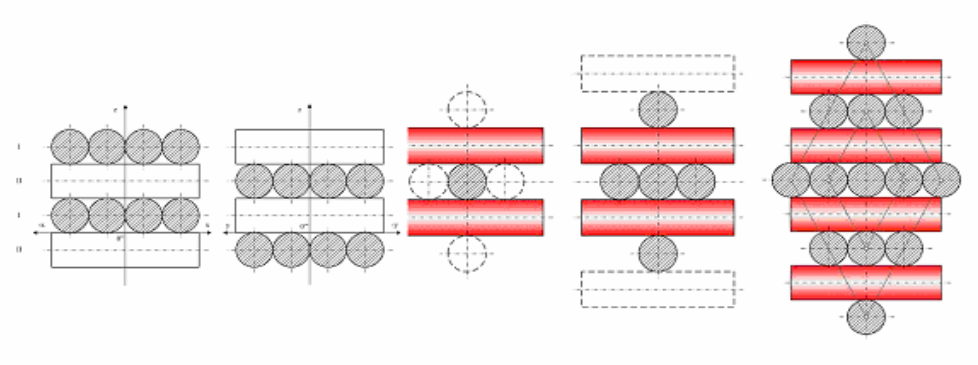
2. Sheme slaganja i proračun ortogonalnog laminata

2.1. Opis i sheme slaganja ortogonalnog (u dva pravca) ojačanog laminata

Kod laminata s više pravaca ojačavanja vlakna su postavljena u međusobno paralelnim ravninama s otklonom pravca pružanja. Ojačavanje u dva pravca postavljena u međusobno paralelnim ravninama upućuje na pravokutni raspored vlakana.

Gradnja strukture ojačavanja za laminat ojačan u dva okomita pravca (1:1) polazi od točke ishodišta koordinatnog sustava (0, 0, 0). Prvi snop ojačala (I) postavlja se u smjeru osi y, u ravnini xy. Maksimalna gustoća postiže se postavljanjem ojačala jednog do drugog bez razmaka između njih. Drugi snop ojačala (II) postavlja se ispod (II_d) i iznad (II_g) prvog snopa, u smjeru osi x, u ravninama paralelnima s ravninom xy. Orijentacija vlakana je za 90° zakrenuta u odnosu na osnovni snop. Na slici 1a prikazan je četveroslojni model ortogonalnog ravninskog ojačavanja dobiven ponavljanjem postavljanja prvog sloja (I_g) iznad prethodno postavljenog drugog (II_g) sloja.

Alternativni način izrade ravninski ortogonalno ojačanog laminata započinje postavljanjem osnovnog snopa i sljedeća dva snopa okomita u ravninama paralelnim s ravninom osnovnog snopa (prikazana crvenom bojom na slici 1b lijevo. Iduća četiri snopa ojačavanja postavljaju se u pravcima paralelnima s pravcem osnovnog snopa i to dva do njega, a po jedan ispod i iznad ojačala drugog snopa (prikazano crtkano na slici 1b lijevo, a puno na slici 1b-sredina). Korištenjem ove metodologije slaganja nastavlja se postavljanje novih snopova i povećavanje broja ravnina ojačavanja (slika 1b-desno).



a) *b)*

Slika 1. Shematski prikazi dobivanja laminata ojačanog u dva pravca
a) ortogonalne projekcije; b) opis i sheme slaganja

Pravokutna shema slaganja vidljiva na slici 1a se može smatrati jednim oblikom općenite rombske sheme slaganja, kako je to prikazano na slici 1b-desno.

2.2. Proračun stupanja popunjenosti f ortogonalnog ravninski ojačanog laminata

Stupanj popunjenosti f se određuje dijeljenjem površine ojačala P_o s ukupnom površinom P_u prema jednadžbi (1).

$$f = \frac{P_o}{P_u} \tag{1}$$

Za proračun laminata ravninski ojačanog u dva međusobno okomita pravca uzet će se sva četiri najgušće postavljena sloja prikazana na slici 1a. Razmak među vlaknima istog snopa je $d = 2r$, dok je udaljenost između vlakana susjednih, jednako orijentiranih snopova $2d$.

Razmak među vlaknima određuje stupanj popunjenosti u ravnini okomitoj na os postavljanja štapova.

Za ojačala kružnog presjeka površina P_o je jednaka: $P_o = 2r^2\pi$ (2)

Ukupna površina P_u je: $P_u = 16r^2$ (3)

Za stupanj popunjenosti prostora koristi se i pojam faktor popunjenosti (*f*). Za laminat ojačan u dva pravca, faktor popunjenosti za pojedinu os je jednak i iznosi:

$$f_i = \frac{P_o}{P_u} = \frac{2r^2\pi}{16r^2} = \frac{\pi}{8} = 0{,}3927 \tag{4}$$

Ukupni faktor popunjenosti se dobije kao suma faktora popunjenosti za dvije osi, odnosno:

$$f = \sum_{i=1}^{2} f_i = 2 \cdot \frac{\pi}{8} = 0{,}785398 \tag{5}$$

Povećanje faktora popunjenosti moguće je postići korištenjem ojačala kvadratnog presjeka. Faktor popunjenosti se za ojačala jednog snopa proračunava iz omjera površina sljedećim izrazom:

$$f_i = \frac{P_o}{P_u} = \frac{8}{16} = 0{,}5 \tag{6}$$

Ukupni faktor popunjenosti se dobije kao suma faktora popunjenosti za dvije osi i iznosi:

$$f = \sum_{i=1}^{2} f_i = 2 \cdot \frac{1}{2} = 1 \tag{7}$$

Ako presjek ojačala nije najveći mogući, između ojačala će postojati razmak *h* koji smanjuje faktor popunjenosti prostora. U tom slučaju faktor popunjenosti f_h računa se izrazom (8).

$$f_h = f \left(\frac{1}{1 + \frac{h}{d}} \right)^2 \tag{8}$$

gdje je *d* promjer ojačala.

3. Modeli struktura ravninski ojačanih laminata

3.1. Modeli struktura ortogonalnog laminata ojačanog u dva pravca

Ortogonalni ravninski ojačan laminat proračunat i opisan u prethodnoj točki ima pravokutni raspored oznake (1:1).

Model ortogonalno ravninski ojačanog laminata, izrađen računalom, maksimalne gustoće je prikazan na slici 2a, a računalni model ortogonalno ravninski ojačanog laminata s djelomično uklonjenim ojačalima koji predstavlja temelj za slaganje modela prostornog ojačavanja u tri pravca (3D) prikazan je na slici 3a.

3.2. Modeli struktura neortogonalnog laminata ojačanog u dva pravca

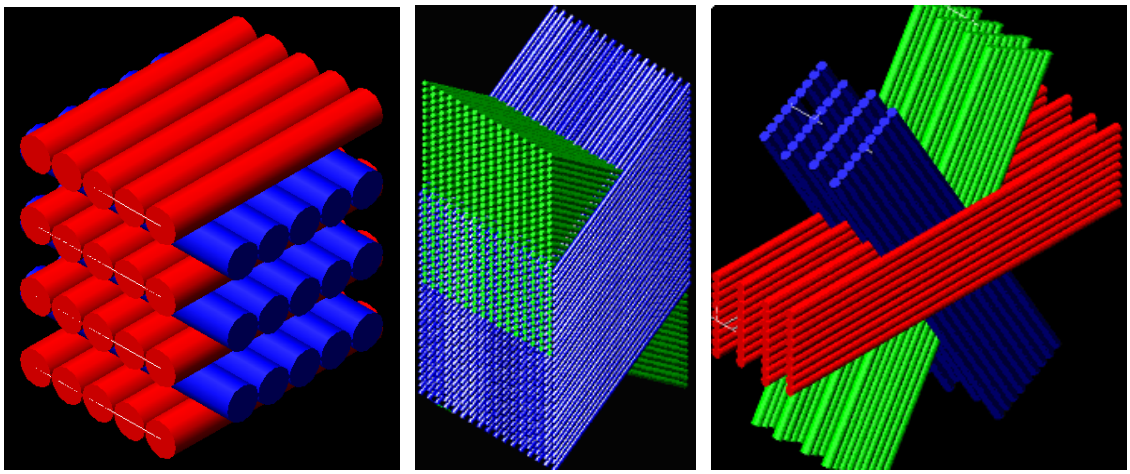
Uz ortogonalni ravninski ojačan laminat (slika 2a i 3a), moguće je snopove ojačala postaviti u dva neortogonalna pravca.

Na slici 2b prikazan je model ravninskih neortogonalnih ojačala, izrađen računalom, maksimalne gustoće postavljenih u dva pravca koji se sijeku pod kutom od 70º30'. Na slici 3b, prikazan je isti model ojačavanja kojem je uklonjen dio ojačala tako da tvori osnovu za slaganje prostornog modela ojačavanja u četiri pravca (4D).

3.3. Model struktura laminata ojačanog u tri pravca

Ravninski ojačani laminat je moguće složiti s ojačalima postavljenim u više od dva pravca. Najjednostavniji u ovoj grupi je laminat ojačan u tri pravca zvjezdastog rasporeda (1:1:1).

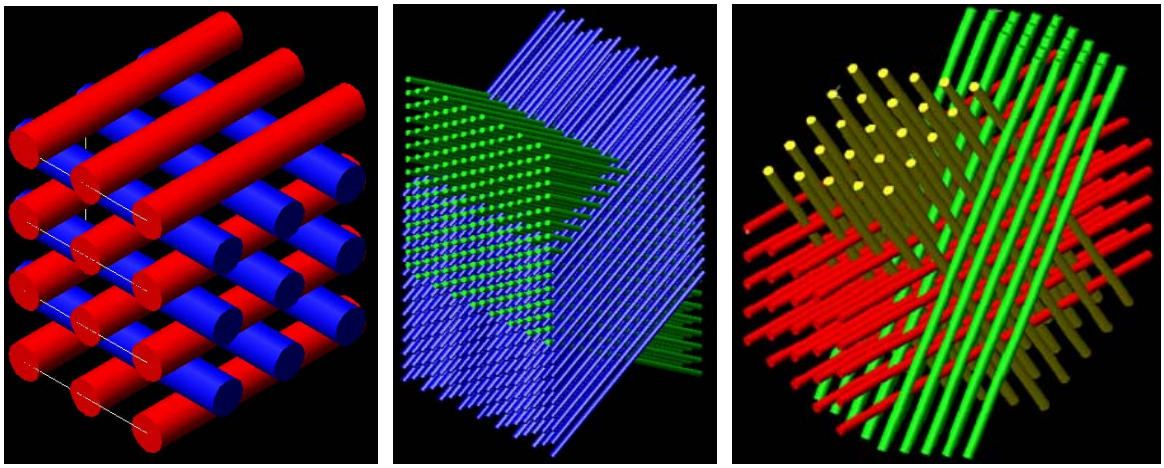
Na slici 2c prikazan je model ravninskih neortogonalnih ojačala maksimalne gustoće postavljenih u tri pravca koji se međusobno sijeku pod kutom od 60º. Na slici 3c, prikazan je isti model ojačavanja kojem su ojačala razmaknuta tako da tvore osnovu za izradu modela prostornog ojačavanja u šest pravaca (6D).



a) *b)* *c)*

Slika 2. Modeli ravninskih laminata, izrađeni računalom, maksimalne gustoće ojačanih: a) u dva okomita pravca; b) u dva neokomita pravca; c) u tri pravca

Maksimalna popunjenosti prostora za sve modele ravninskih laminata prikazanih na slici 2 je jednaka i proračunava se postupkom opisanim u točki 2. Popunjenost prostora u slučajevima postavljanja ojačala s razmakom prikazanih na slici 3 proračunava izrazom (8).



a) *b)* *c)*

Slika 3. Modeli ravninskih laminata, izrađeni računalom, s djelomično uklonjenim ojačalim (koji predstavljaju temelj za izradu modela jednostavnih prostornih ojačavanja) postavljenim: a) u dva okomita pravca; b) u dva neokomita pravca; c) u tri pravca

4. Strukture jednostavnih prostorno ojačanih kompozita

4.1. Geometrijski parametri jednostavnih prostorno ojačanih struktura

Za postavljanje ojačala i izgradnju prostorno ojačanih struktura potrebno je poznavati sheme slaganja i razmake između ojačala. Za svaku od jednostavnih struktura ojačavanja u tablici 1 navedena je shema postavljanja i teorijski najveći stupanj popunjenosti prostora za najčešće korištena ojačala kružnog presjeka izračunat po metodologiji opisanoj u točci 2. Osim toga u tablici 1 dani su i kutovi između prvog pravca i ostalih pravaca ojačavanja.

Tablica 1. Geometrijski parametri jednostavnih prostorno ojačanih struktura izrađenih iz ojačala kružnog presjeka

GEOMETRIJSKI PARAMETRI	BROJ PRAVACA OJAČAVANJA		
	Tri (3D)	Četiri (4D)	Šest (6D)
Shema rasporeda ojačala u svakom pravcu	Kvadratna	Heksagonalna	Rombska
Kutovi između osnovnog pravca ojačanja i drugih	2 x 90°	3 x 70,53°	1 x 90° 4 x 60°
Teorijski najveći udio površine štapova u jednom pravcu ojačavanja	$\frac{\pi}{16} = 0{,}196$	$\frac{\pi\sqrt{3}}{32} = 0{,}170$	$\frac{\pi\sqrt{2}}{54} = 0{,}082$
Teorijski najveći stupanj popunjenosti prostora	$\frac{3\pi}{16} = 0{,}5890$	$\frac{\pi\sqrt{3}}{8} = 0{,}6802$	$\frac{\pi\sqrt{2}}{9} = 0{,}4937$

Kod prostornog ojačavanja u tri pravca se očekuje najveća anizotropnost uz srednji stupanj popunjenosti prostora. Zatvorena poroznost posebno izražena kod ojačala kvadratnog presjeka u slučajevima maksimalnog udjela ojačala je prikriveni nedostatak ove strukture.

Iz tablice se vidi da se najveći stupanj popunjenosti postiže kod prostornog ojačavanja u četiri pravca (4D), uz relativno manju anizotropnost u odnosu na prostorno ojačavanje u tri pravca. Dodatna pogodnost ove strukture je tehnološki povoljna otvorena poroznost.

Ukoliko je zahtjev za izotropnost svojstava dominantan onda je prostorno ojačavanje u šest pravaca (6D) usprkos najmanjem stupnju popunjenosti prostora pravi izbor.

4.2. Struktura kompozita ojačanog u tri pravca

Model ortogonalno ravninski ojačanog laminata prikazan na slici 3a predstavlja temelj za slaganje modela prostornog ojačavanja u tri pravca (3D). Isti se dobiva postavljanjem trećeg snopa ojačala (prikazanog žutom bojom na slici 4a) okomito na ravninu slaganja prethodnih ojačala u otvore nastale odgovarajućim razmicanjem ojačala u prva dva pravca. Struktura kompozita ojačanog u tri pravca se može ostvariti i prema shemi naznačenoj u tablici 1 postavljanjem prvog snopa ojačala okomito na ravninu xy te alternativnim postavljanjem redova snopova ojačala u pravcu osi x i y. Na oba načina se dobiva ista struktura prikazana na slici 4a. Prilikom izrade stvarnih struktura prostornih ojačavanja potonji način se pokazao učinkovitiji.

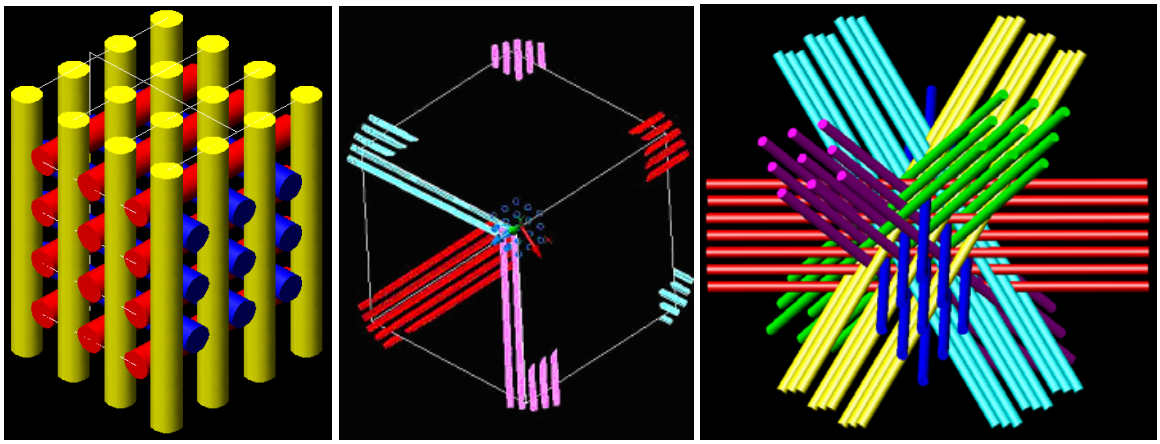
4.3. Struktura kompozita ojačanog u četiri pravca

Model prostornog ojačavanja u četiri pravca (4D) dobiva se alternativnim postavljanjem dva istovjetna za 90º zakrenuta modela ravninskih neotrogonalnih ojačala u dva pravca koji se sijeku pod kutom od 70º30' prikazana na slici 3b. Struktura kompozita ojačanog u četiri pravca se može ostvariti i prema shemi naznačenoj u tablici 1 postavljanjem prvog snopa ojačala okomito na ravninu xy te alternativnim postavljanjem triju redova snopova ojačala u pravcima zakrenutim za 120º i nagnutim pod kutom od 70º30'. Prilikom izrade stvarnih struktura prostornih ojačavanja primijenjen je treći način najbliži teorijskom obliku, a koji se pokazao najučinkovitiji. Prema njemu se ojačala alternativno postavljaju u smjerovima četiriju prostornih dijagonala kocke prema heksagonalnoj shemi (slika 4b).

4.4. Struktura kompozita ojačanog u šest pravaca

Popunjavajući model ojačavanja laminata u tri pravca s razmaknutim ojačalima prikazan na slici 3c s još tri snopa ojačala u pravcima zakrenutim za 120º i odgovarajućim

nagibom dobiva se struktura za izradu kompozita ojačanog u šest pravaca (6D) prikazana na slici 4c.



a) *b)* *c))*

Slika 4. Modeli struktura za proizvodnju jednostavnih prostorno ojačanih kompozita, izrađeni računalom; a) u tri pravca (3D); b) u četiri pravca (4D); c) u šest pravaca (6D)

Prilikom izrade stvarnih struktura prostornih ojačavanja primijenjen je drugi način bliži teorijskom koji se pokazao učinkovitiji. Prema njemu se dva snopa ojačala alternativno postavljaju vodoravno u okomitim pravcima prema rombskoj shemi a potom se ostala četiri snopa postavljaju prema istoj shemi u pravcima zakrenutim za 90º s nagibom od 45 º.

5. Strukture složenih prostorno ojačanih kompozita

5.1. Podjela složenih struktura prostorno ojačanih kompozita

Složeni prostorno ojačani kompoziti obuhvaćaju skupinu ujednačenih i neujednačenih kompozita. Najjednostavniji složeni prostorno ojačani kompozit je neujednačeni kompozit ojačan u pet pravaca (5D), a najsloženiji je ujednačeni kompozit ojačan u trinaest pravaca (13D).

Podjela i načini dobivanja složenih prostorno ojačanih kompozita dati su u tablici 2.

Tablica 2. Podjela i dobivanje složenih prostorno ojačanih kompozita iz jednostavnih

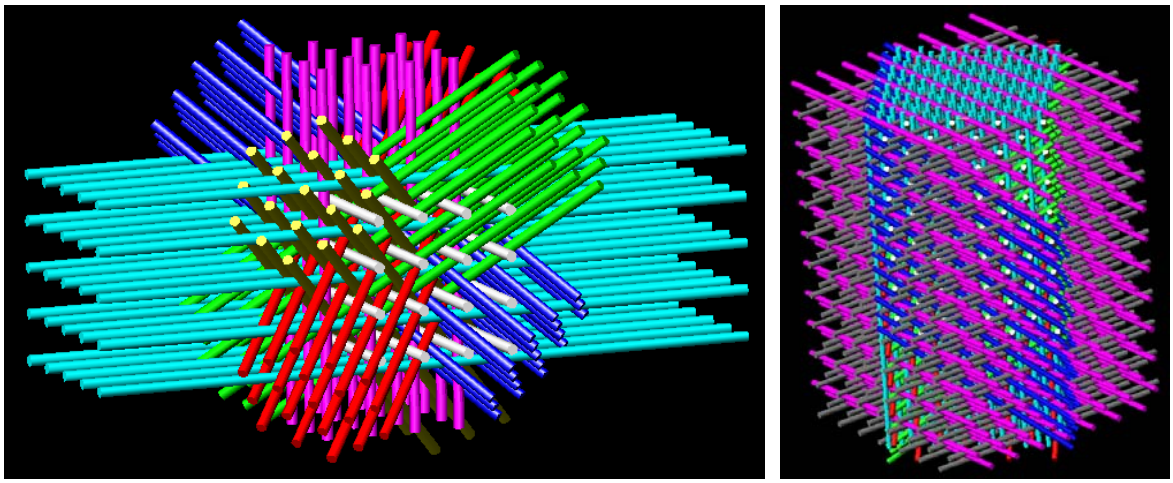
Struktura	Ujednačeni	Neujedna.	1D	3D	4D	6D	Kvadratna	Heks.	Rombska
5D	✗	✓	✓	✗	✓	✗	1	4	✗
7D	✓	✗	✗	✓	✓	✗	3	4	✗
9D	✓	✗	✗	✓	✗	✓	3	✗	6
10D	✓	✗	✗	✗	✓	✓	✗	4	6
11D	✗	✓	✓	✗	✓	✓	1	4	6
12D	✗	✓	✓✓	✗	✓	✓	2	4	6
13D	✓	✗	✗	✓	✓	✓	3	4	6

Bez obzira na broj pravaca ojačavanja, složeni kompoziti su sastavljeni od dva ili više laminata i/ili jednostavnih prostorno ojačanih kompozita. Uz postizanje približno jednake čvrstoće u više pravaca (kvazi izotropnost), složeni prostorno ojačani kompoziti pružaju i mogućnosti slaganja, koje dodatno povećavaju mehanička svojstva u željenom pravcu.

5.2. Strukture kompozita ojačanog u sedam pravaca (7D)

Svojstva kompozita ojačanih u sedam pravaca (7D) predstavljaju kombinaciju svojstava kompozita ojačanih u tri i četiri pravca.

Na slici 5a prikazan je model ujednačenog ojačavanja kompozitnog materijala u sedam pravaca (7D). Ojačavanje u sedam pravaca ima i svoju neujednačenu varijantu, prikazanu na slici 5b.



a) *b)*

Slika 5. Modeli ojačavanja kompozita u sedam pravaca (7D)izrađeni računalom; a) ujednačeni; b) neujednačeni

Strukture ojačavanja u sedam pravaca prikazane na slici 5 mogu se razmatrati kao popunjene inačice neujednačene strukture ojačane u pet pravaca (5D). Prvi stvarni model strukture ojačane u sedam pravaca (7D) je izrađen upravo potpunim popunjavanjem strukture ojačane u pet pravaca (5D) nastale postavljanjem ojačala u pravcima prostornih dijagonala kocke oko ojačala u pravcu osi z.

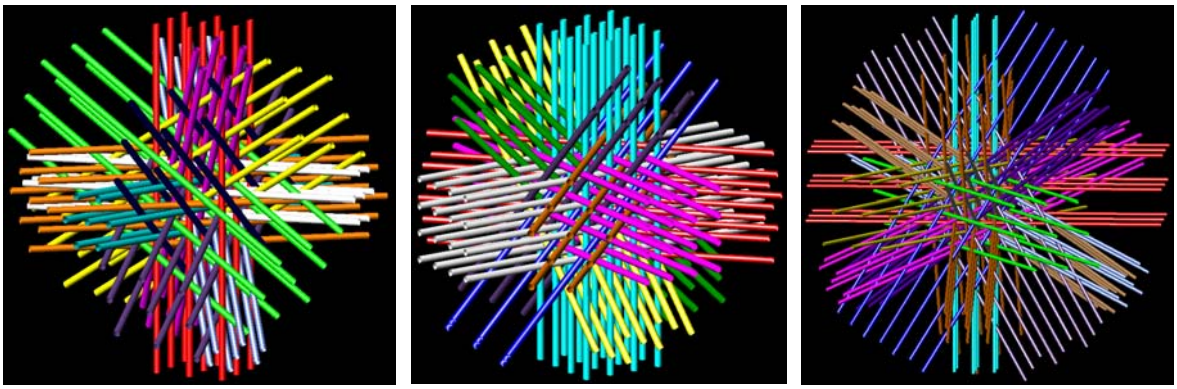
5.3. Strukture kompozita ojačanih u devet, deset i trinaest pravca

Svojstva ovih kompozita predstavljaju kombinaciju svojstava kompozita ojačanih u tri, četiri i šest pravaca. Složenost, ponajprije zbog broja pravaca ojačavanja iziskuje više materijala. Međutim potrošnju materijala kod ovakvih načina ojačavanja neekonomičnom čini višak materijala, tj. utrošeni materijal koji će obradom biti odbačen. Upravo je to najznačajniji nedostatak pri izradi, pa će se primjena ovakvih načina ojačavanja odnosi na visokoopterećene konstrukcije kod kojih ne postoji alternativa, a ekonomičnost ne predstavlja glavno ograničenje.

Struktura modela ojačavanja u devet pravaca (9D) je prikazana na slici 6a. Uočljive su tri kvadratne i šest heksagonalnih shema slaganja. Svojstva ovog kompozita predstavljaju kombinaciju svojstava kompozita ojačanih u tri i šest pravaca.

Struktura modela ojačavanja u deset pravaca (10D) je prikazana na slici 6b. Svojstva ovog kompozita predstavljaju kombinaciju svojstava kompozita ojačanih u četiri i šest pravaca.

Na slici 6c je prikazan model prostornog ojačavanja u trinaest pravaca (13D) nastao kombiniranjem svih modela jednostavnih prostorno ojačanih struktura. Dobivena struktura ima najujednačenija svojstva od svih ujednačenih prostorno ojačanih struktura.



a) *b)* *c))*

Slika 6. Modeli ojačavanja složenih ujednačenog kompozita, izrađeni računalom; a) devet pravaca; b) deset pravaca (10D); c) trinaest pravaca (13D)

Ujednačena struktura ojačavanja u trinaest pravaca (13D) se može smatrati univerzalnom jer je obuhvatila sve jednostavne prostorno ojačane strukture. Teorijski ona se može promatrati kao osnova za dobivanje svih prostorno ojačanih struktura kao i laminata smanjivanjem broja pravaca ojačavanja.

6. Zaključci

Razvoj proizvodnje prostorno ojačanih kompozita i laminata počinje modeliranjem jednostavnih struktura ravninski ojačanih u dva i tri pravca na koje je moguće nadograditi složenije modele prostorno ojačanih ujednačenih i neujednačenih struktura.

Pokazano je da su jednostavni opisi izrade i sheme slaganja struktura potrebnih za proizvodnju ortogonalno ravninski ojačanog laminata te postupak proračuna stupnja popunjenosti prostora takve strukture općenito primjenjivi za sve jednostavne prostorno ojačane strukture.

Uz geometrijske parametre neophodne za izradu, prikazani su izvorni modeli jednostavnih prostorno ojačanih struktura razvijeni računalom. Konstatirana je najveća anizotropnost prostornog ojačavanja u tri pravca uz srednji stupanj popunjenosti prostora i zatvorena poroznost posebno izražena kod ojačala kvadratnog presjeka. Kod prostornog ojačavanja u četiri pravca (4D) ostvaruje se najveći stupanj popunjenosti prostora, postiže se manja anizotropnost i tehnološki povoljna otvorena poroznost u odnosu na prostorno ojačavanje u tri pravca. Prostorno ojačavanje u šest pravaca (6D), usprkos najmanjem stupnju popunjenosti prostora, najpovoljnije je glede izotropnosti svojstava.

Posebno su prikazani modeli izrađeni na računalu svih složenih ujednačenih struktura potrebnih za proizvodnju odgovarajućih složeno prostorno ojačanih kompozita.

Literatura

[1] Tarnopol'skii, Yu. M., I.G. Zhigun, V.A. Polyakov, *Spatially Reinforced Composites,* Tehnomic Publishing Co. Inc, Lancaster, USA, 1992.

[2] Šundrica, J., Jurjević, N., Prčan, M., *Filling of a matrix with parallel aligned fibres,* International Conference Materials - Energy – Design MED06, The book of papers, Dublin Institute of Technology, Dublin, 2006. (147-154)

[3] Smojver, I., *Mehanika kompozitnih materijala,* Fakultet strojarstva i brodogradnje Sveučilišta u Zagrebu – Podloge za predavanja, Zagreb, 2007.

[4] Šundrica, J., *Modeli prostorno ojačanih struktura kompozita,* Doktorski rad, Fakultet strojarstva i brodogradnje Sveučilišta u Zagrebu, Zagreb, 2008.

INTEGRACIJSKI TRENDOVI RAZVOJA TISKARSKIH SUSTAVA

INTEGRATION TRENDS IN DEVELOPMENT OF PRINTING SYSTEMS

Ante Tabak*, Nikola Mrvac, Kristijan Golubović**, Antun Koren****
*Razina3, Dankovečka 1a, Zagreb, **Grafički fakultet Zagreb, Getaldićeva 2, Zagreb, Crotia

Stručni članak / Professional paper

Abstract: Classic graphic production is a series of unconnected processes. Every process has, as output, a product which serves as input for the next process. Information needed for the next stage is transferred as written data, in form of internal communication. Probability for a mistake is great, the data regarding non-standard jobs can be incomplete, or especially by increased production, replaced by wrong data. Considering very different nature of single processes, there are just a few firms equipped for whole production. It is common that some of the processes are made outside the firm – prepress, film making or binding. Such discontinued production is slow, with lot of waste and often does not satisfy the customer. With introduction of digital systems – first in prepress and then in production itself – the process is speeding up, but also results in multitude of different standards which are partially or completely incompatible.

Key words: Graphic Production, Printing Systems, Integration Trends

Sažetak: Klasična grafička proizvodnja – niz je međusobno nepovezanih procesa. Svaka faza kao izlaz ima neki proizvod koji je sirovina za drugu fazu. Potrebni podatci za slijedeću fazu prenose se putem pisanih podataka, u obliku interne komunikacije. Mogućnost pogreške je velika, kod nestandardnih poslova podaci mogu biti manjkavi ili, naročito pri velikom opsegu posla zamijenjeni krivima. Zbog izrazito različite prirode pojedinačnih faza, malo firmi ima kompletnu opremu za cijelu proizvodnju. Često se neka faza obavlja kao vanjska usluga – prijelom, izrada filmova ili uvez. Takva diskontinuirana proizvodnja je spora, uz mnogo škarta i često ne zadovoljava naručioca.

Uvođenjem digitalnih sustava – prvo u pripremnom dijelu proizvodnje, a zatim i u samu proizvodnju - proces se ubrzava, ali i rezultira mnoštvom različitih standarda, međusobno potpuno ili djelomično nekompatibilnih.

Ključne riječi: grafička proizvodnja, tiskarski sustavi, integracijski trendovi

1. UVOD

Prijelaz konvencionalnih sustava izrade tiskovnih formi na CTP sustave rezultirao je nestankom niza nekonvencionalnih zanimanja. Sukladno tome donio je i nove podjele rada kod proizvodnje tiskovnih predložaka [1, 7, 12, 13].
Suvremena tehnologija omogućuje svima prijelom i oblikovanje. Pri tome se koriste raznim programima i formatima datoteka. Kod preuzimanja tih datoteka za izradu otiska suočavamo se često s istim problemima. Nove tehnologije zahtijevaju nova znanja. Nastaju nova zanimanja[2, 14].
Većina tiskara je opremljena CTF (Computer to Film) ili CTP (Computer to Plate) uređajima što omogućuje dostavu digitalnih tiskovnih predložaka. Film kao univerzalni medij za izmjenu između firmi koje sudjeluju u tiskovnoj proizvodnji je zaostao. U tom smislu struka je pronašla adekvatnu zamjenu za film i to u digitalnom obliku. Također povećani ritam rada i vremenski pritisak obavezuju firme na što veću automatizaciju radnog tijeka, što je također moguće samo s digitalnim podacima.
PDF (Portable Document Format) kao format datoteke u tom slučaju nudi niz pogodnosti. Može se napraviti iz svih programa. Nije ovisan o obliku tiskovne forme i može skupiti sve podatke koje su potrebni za osvjetljavanje [3, 4].
Osim tiskara koje zahtijevaju sve više PDF kao format datoteke, PDF zahtijevaju i klijenti koji su prepoznali prednosti PDF formata [9] te se u tom smislu on nameće kao nužnost. PDF može poslužiti kao priprema za bilo koju tehniku tiska. U tom smislu se najviše i najbrže nametnuo kod digitalnog tiska, sukladno rokovima i manjoj mogućnosti pogrešaka.
U skladu s navedenim određeni su i ciljevi ovog rada, koji su usmjereni kako bi se opisali očigledni integracijski procesi u tiskarskoj industriji. Ciljevi rada su da se kroz provedbu eksperimenta prikažu prednosti i eventualni nedostaci očiglednih navedenih trendova.

2. DIGITALNI TIJEK RADA (WORKFLOW)

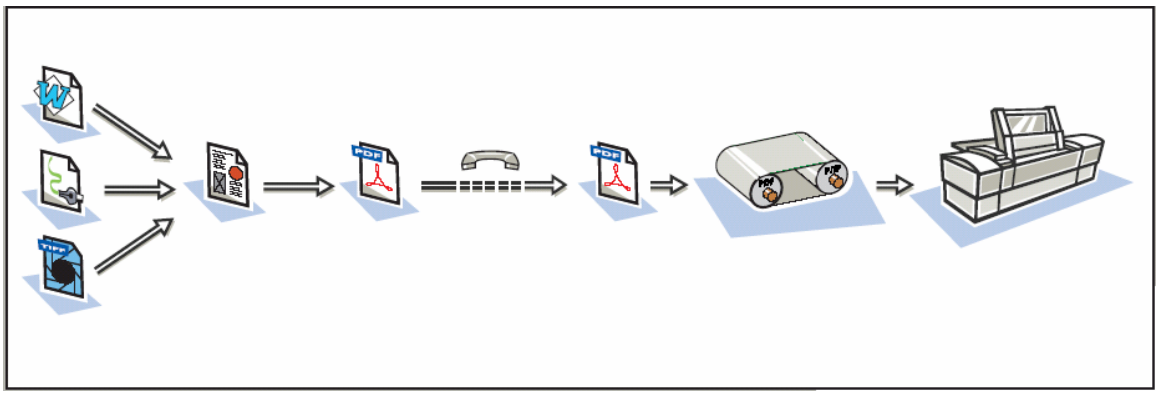
Korištenjem digitalnog tijeka procesa smanjuje se broj koraka u proizvodnji [7]., a time i troškovi proizvodnje [9]. Prednost je i u tome što se povećava kvaliteta, a smanjuje vrijeme izrade i postotak otpada.
Workflow leži u srcu pojedinog posla. On nije alat već se prilagođava zahtjevima i poslovima određene organizacije ovisno o načinu i vrsti posla koju obavlja [5].
Važno je da se uspostavi standardizirani tijek rada s operativnim procedurama koje se mogu primijeniti bez obzira na tip i vrstu posla koji se zaprimi [11].
Karakteristike:
- ušteda vremena – (vrijeme izrade ploča i filmova je znatno ubrzano)
- ušteda materijala – korištenjem CTP tehnologije nema potrebe za izradom filmova, a smanjuje se i otpad papira potreban za pripremu tiskarskih strojeva
- povećanje kvalitete
- kontrola kvalitete
- digitalna izrada probnog otiska – što točnije simuliranje otiska
- dozvoljene su promjene u zadnji tren
- arhiviranje podataka – ušteda na prostoru
- backup – sprječava gubitak podataka koji bi imali velike negativne posljedice u vremenu i troškovima

Dijelovi grafičkog proizvoda (stranice) izrađuju u raznoraznim grafičkim odnosno tekstualnim programima. Nakon toga se izrađuje PDF dokument. Taj postupak se izvodi na više načina:

- neki programi imaju direktnu funkciju za eksportiranje PDF-a (Adobe Library)
- korištenje Acrobat Distiller-a za konvertiranje PostScript datoteka u PDF dokumente ako program ima funkciju spremanja u PostScript

Izrađivač PDF dokumenta vizualno ga kontrolira i potom šalje tiskari.
U tiskari se PDF stranice pripremaju za osvjetljavanje filma ili za snimanje tiskovne forme. Nakon kontrole kompatibilnosti PDF-a za RIP i tisak stranice se slažu u tiskovne forme.

Ti poslovi se mogu ručno odraditi s pojedinim programima ili se koristi moderan PDF-radni tijek (workflow) za automatiziranje proizvodnje, kao što je PRINERGY od Heidelberga i Creo (LINK) [6].



Slika 1 - Prikaz jednostavnog radnog tijeka.

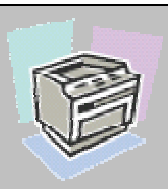
Radni tijek PDF—a počinje kod izrade stranica. Kompaktni PDF dokumenti se potom šalju tiskari, gdje se dodatno obrađuju za tiskanje [8]. Velika prednost radnog tijeka PDF-a je da se vrijeme proizvodnje može optimalno predvidjeti.

3. IZRADA PDF DOKUMENTA

PDF dokumenti se mogu izraditi na razne načine, međutim nisu svi načini prikladni za izradu tzv. «Highend-PDF» [14]. Pod tim pojmom se podrazumijeva PDF dokument koji se može ispisati visokom rezolucijom.
Jedan od najsigurnijih načina izrade PDF-a je konvertiranje PostScript-dokumenata pomoću programa «Acrobat Distiller», gdje se veličina i kvaliteta dokumenta mogu optimalno podesiti [15]. Točnim postavkama u Distiller-u moramo dati veliku pozornost jer Distiller nije samo namijenjen za izradu Highend-PDF dokumenata, nego i za izradu PDF dokumenata namijenjenih za Internet. U skoroj budućnosti će većina svih DTP-programa imati opciju direktnog eksportiranja PDF-a. Naime firma Adobe nudi softverskim kompanijama svoju «PDF Library», koja svim proizvođačima softvera dozvoljava direktnu izradu PDF-datoteka.

Preduvjet za uspješnu upotrebu PDF-a u digitalnom radnom tijeku je pravilna izrada PDF dokumenta. Ako se napravi bilo kakva pogreška, već je prekasno za intervenciju. Zbog toga pravilnoj izradi PDF-a moramo pokloniti posebnu pažnju.
Izrada PDF-a može biti podešena pomoću mnogih parametara. Razne postavke su potrebne jer se pomoću Distiller-a izrađuju PDF-dokumenti za razne potrebe. Kod izrade PDF dokumenta koji je namijenjen za Internet ili za CD-ROM imamo karakteristike koje su važnije nego kod dokumenata koji se kasnije moraju osvjetljavati i otisnuti [10].

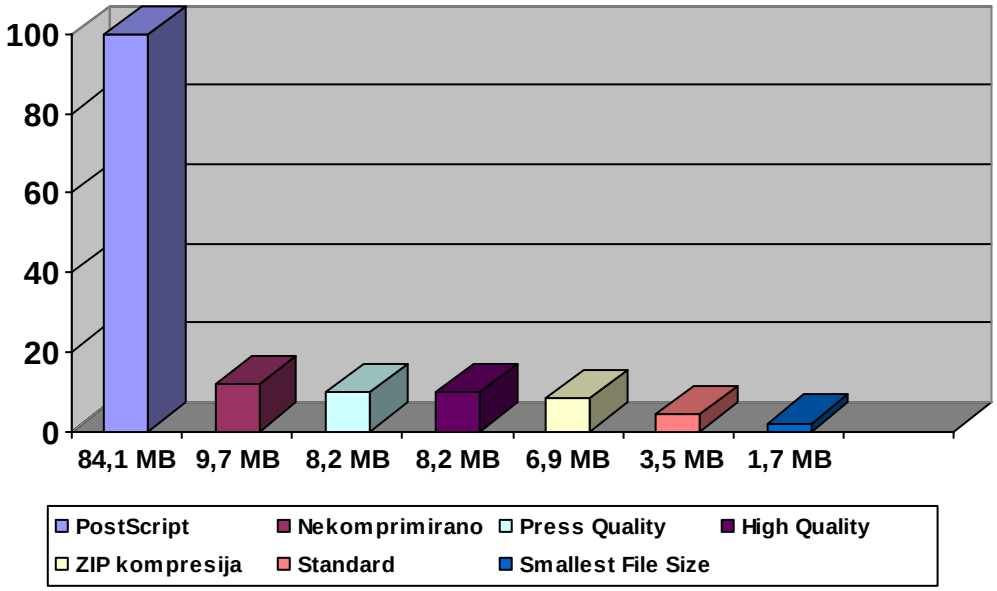
Tablica 1 - Izrada PDF dokumenta ovisno o načinu upotrebe

Karakteristike			
	MONITOR	PRINTER	OSVJETLJIVAČ
Rezolucija slike	72 dpi	150 dpi	300 dpi
Kompresija	Niska kvaliteta	Srednja kvaliteta	Visoka kvaliteta
Spektar boja	sRGB	RGB ili CMYK	CMYK
Uključivanje fontova	Ne	Potpuna	Potpuna
Optimirano za internet	Da	Ne	Ne

4. EKSPERIMENTALNI DIO

4.1. Statistički prikaz posljedica pojedinih načina kompresije u «Distiller»-u

Kod digitalne proizvodnje količina podataka igra veliku ulogu. Tiskarski arak s nekoliko slika brzo dostiže veličinu od nekoliko gigabajta. Pomoću PDF-a uspijevamo maksimalno reducirati veličinu datoteke, jer u PDF dokumentu se svaki tip podatka može individualno komprimirati. Kod kompresije višetonskih slika vide se najbolji rezultati. PDF koristi JPEG-kompresiju za reduciranje veličine podataka kod višetonskih slika. Kod nje se može birati između raznih načina kompresije. Uglavnom se preporučuje izbor «visoke kvalitete» (High Quality).
Iz grafikona se mogu vidjeti posljedice pojedinih načina kompresije. Kod preporučene postavke su nam od izvornih 84,1 MB ostala samo još 8,2 MB, ali još je uvijek dovoljno informacija za osvjetljavanje. Vizualno se ne može primijetiti razlika. Smanjena veličina datoteke enormno pojednostavljuje spremanje (arhiviranje) i prenošenje podataka. Ispis stranica također se pomoću kompresije vidno ubrzava, jer je dekomprimiranje u RIP-u inače brže nego prenošenje nekomprimiranih podataka preko kompjuterske mreže.



Slika 2 - Statistički prikaz posljedica pojedinih načina kompresije u «Distiller»-u

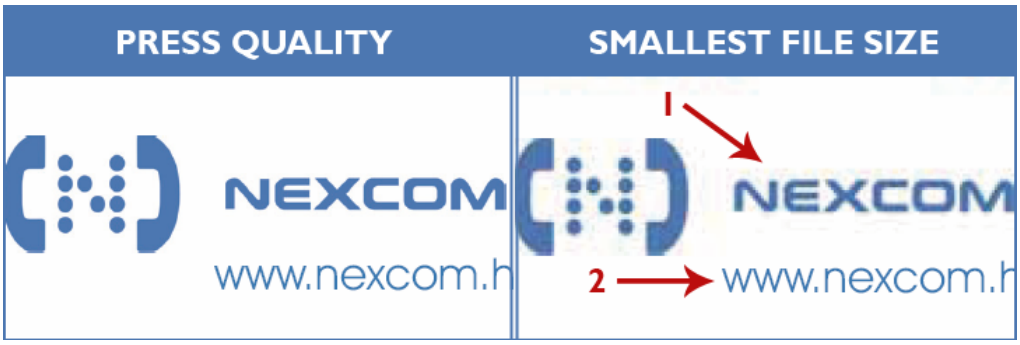
Tablica 2 - **Podaci o eksperimentu:**

Korištena verzija programa:	Acrobat Distiller 6.0
Korištene postavke:	Standardni postavke (joboptions) koje nudi Distiller 6.0: *High Quality, Press Quality, Standard, Smallest File Size*
	«Nekomprimirano» - isključene postavke za komprimiranje slika.
	«Zip kompresija» - umjesto «JPEG»-metodom koristimo kompresiju slike «ZIP»-metodom
Kompatibilnost:	Acrobat 5.0 (PDF 1.4)

4.2 Vizualna usporedba otisaka pojedinih PDF dokumenata stvorenih standardnim načinima kompresije u «Distiller»-u

Postavke «Distiller»-a mogu se spremiti u datoteci koja se naziva «joboptions»-datoteka. Postoje standardne «joboptions» - datoteke koje su instalacijom «Acrobat Distiller-a» automatski uvrštene u program.
U eksperimentu su se za izradu PDF-a iz PostScript datoteke koristile između ostalog takve datoteke koje su kod otiskivanja izrađenih PDF-dokumenata iznimno utjecali na rezultat.
Naime, sveukupno nakon otiskivanja svih PDF-dokumenata moramo konstatirati da razlike između otisaka komprimiranih PDF dokumenata s postavkama *«High Quality», «Press Quality», «nekomprimirano»* i *«Zip kompresija»* gotovo nema. Također uspoređujući te otiske s otiskom izvorne PostScript datoteke ne vidimo razlike u kvaliteti. Očigledno se ovdje potvrđuju glavne karakteristike PDF formata koji nudi skoro istu kvalitetu otiska kao izvorna PostScript datoteka uz nekoliko puta manju veličinu datoteke. Nasuprot tome moramo napomenuti da se kvaliteta ne gubi uglavnom kod gore navedenih postavki, koje su preporučene za kvalitetno osvjetljavanje.

Naime, kad pogledamo otiske PDF dokumenata izrađenim s postavkama «Standard» i «Smallest File Size» onda brzo uočavamo gubitke u kvaliteti.
U usporedbi s ostalim otiscima primjećuju se nejasnoće i to uglavnom kod slika. Primjeri usporedbe otisaka PDF dokumenata izrađenih s postavkama «Press Quality» i «Smallest File Size» se mogu vidjeti na slici 2.



Slika 3 - Uzorak 1. Logotip (desno) je nejasan jer je maksimalno komprimiran. Tekst se komprimira ZIP-metodom, nema gubitka kvalitete.



Slika 4 – Uzorak 2 - ne vidi se promjena u boji, ali se vide nejasnoće u pozadinskoj slici. Tekstovi koji ne pripadaju slici ostaju nepromijenjeni.



Slika 4- Uzorak 3. Detaljni prikaz kompresije teksta. Nema gubitka kvalitete jer se za tekst i vektorske grafike koristi ZIP-metoda

Prikazivanjem ovih usporedbi otisaka vidimo da načini kompresije ne djeluju na sve objekte jednako. Slike se komprimiraju i razlika je uočljiva, ali kod tekstova koji nisu dio slike i vektorskih grafika razlike su gotovo nikakve. Kao što je već rečeno u poglavlju 4.3.2.2.1 ovdje se susrećemo s činjenicom da se tekstovi i vektorske grafike uvijek komprimiraju s ZIP-metodom kod koje nema gubitka podataka, tj. kvalitete.

5. DISKUSIJA I ZAKLJUČCI

Statističkom i vizualnom analizom kompresije PostScript datoteka možemo potvrditi učinkovitost PDF formata u tiskarskoj industriji. Najjača karika PDF-a i što potvrđuju i rezultati eksperimenta je očuvanje kvalitete pri drastičnom smanjenju veličine datoteke.
Što se tiče tiskarske industrije, gdje kvaliteta otiska igra najveću ulogu, ostaje pravilo izrađivanja tzv. «Highend-PDF»-a koji se mogu koristiti na osvjetljivaču visoke rezolucije. S druge strane PDF dokumenti koji imaju vidljivi gubitak kvalitete u odnosu na PostScript datoteku nisu nepotrebni. Naime, postoje mediji gdje su brzina učitavanja dokumenta i kvaliteta prijenosa informacije važniji negoli kvaliteta slikovnih informacija. To su Internet, CD-ROM i slični mediji [16]. Ta činjenica da za svaku namjenu možemo izraditi odgovarajući PDF-dokument pokazuje svestranost PDF-formata koja upravo osvaja sve više korisnika razmjene slikovnih i tekstovnih informacija.
PDF tehnologija ukupno gledajući ima veliki utjecaj na grafičku struku. PDF je digitalna zamjena za film kao medij koji se razmjenjuje i arhivira. PDF poboljšava i pojednostavljuje suradnju između partnera u tiskarskoj proizvodnji. Također s PDF-om se potiču standardizacija i automatizacija u proizvodnji.

Za tradicionalne djelatnike tiskarske pripreme PDF predstavlja idealnu odskočnu dasku za nove medije kao CD-ROM i Internet i tako nudi tim poduzećima nove mogućnosti.
Prelazak na PDF se doima bržim nego nekadašnji prijelaz na PostScript. To ima više razloga, koji zbog opsega ovog rada neće biti ovdje analizirani. Danas se proizvođači i korisnici slažu u činjenici da PDF predstavlja pravi put.

6. LITERATURA

1. «Basic JDF Tutorial» http://www.cip4.org/, 2.12.2007.
2. «CIP4-Vernetzung» http://www.kommtech.uni-wuppertal.de/CIP4-Vernetzung.1056.0.html, 2.12.2007.
3. «Job-Definition-Format (JDF) im Überblick» http://www.kommtech.uni-wuppertal.de/JDF___JMF__CIP4.1058.0.html, 2.12.2007.
4. «Perfektion mit PDF/JDF-Workflow» "http://www.drucken.de/fileadmin/download/Artikel/schotte_printready.pdf
5. Adobe Acrobat & PDF Basics, 1999. http://www.pdfzone.com
6. Baumgartner S., (2005), Using JDF in Small and Medium Sized Printing Plants, www.cip4.org/document_archive/documents/2005_sbDA_UseOfJDF.pdf, 20.05.2007.
7. Boyd A., (2005), Organizations Shift Focus To Information Managment: The Role Of Documents In Highly Effective Business Processes, available from: http://www.edsf.org/img/Organization_Shift_Focus.pdf, 01.05.2007.
8. Imaging Technologie: PDF und die Bilder http://www.digit.de/know_how/qtvr/know_how_PDF_und_Bilder.htm#Anchor-Distiller-Einstellungen-33869, 30.11.2007.
9. Keif M., (2007), Estimating and Job Costing Digital Printed Matter, http://www.edsf.org/pdfs/EDSF2007_TrendsSurvey.pdf 10.06.2007.
10. Kipphan H., (2001), Handbook of Print Media, Technologies and Production Methods, Springer, Hedelberg
11. Lee B., (2005), The Global Impact of JDF on the Graphic Communications Industry, http://www.edsf.org/images/Global_impact_JDF.pdf, 10.06.2007.
12. Lindstrom P., (2006), Developments in Prepres Technology, Pira International Ltd. Surrey
13. Piontek D., (2006), Developments in Postpress Technology, Pira International Ltd. Surrey, UK 2006.
14. Stephan Jaeggi, «PDF Workflow / Basics «, Heidelberger Druckmaschinen AG, 1999.
15. Thomas Müller, «PDF Workflow» www.heidelberg.com, 30.11. 2007
16. Watson J., Ranganathan C.,Document communications, Industry Trends, Survey Results, http://www.edsf.org/pdfs/EDSF2007_TrendsSurvey.pdf), 10.06.2007.

PLUTAJUĆA PLATFORMA ZA PRIKUPLJANJE OTPADA NA AKUMULACIONIM JEZERIMA

Autori:
Dr.Sc.Dragi Tiro, docent,
Univerzitet „Dž. Bijedić“,
Mašinski fakultet Mostar,

Dr.Sc.Jusuf Kevelj, van.profesor,
Univerzitet „Dž. Bijedić“,
BiH Mašinski fakultet Mostar, BiH

Dr.Sc.Senad Rahimić, docent,
Univerzitet „Dž. Bijedić“,
Mašinski fakultet Mostar

Stručni članak / Professional paper

Abstract
There is a problem of a floating waste appearance in the artificial lakes of company “Hidroelektrane na Neretvi”. The exceeds waste volume appears by reason of the rainfall, permanent variation of the water’s level at the lakes and the river Neretva as well as the human indolence. The company “Hidroelektrane na Neretvi” attempts to solve this problem. *The Faculty of Mechanical Engineering at University “Dž. Bijedić” in Mostar* has been engaged at the designing of floating platform for the waste collecting. The system of waste collecting is described in this paper as well as the floating platform project and the settlement of problem.

Key word: a system of waste collecting, a floating platform, an artificial lake

Sažetak:
Na vještačkim akumulacionim jezerima Hidroelektrana na Neretvi izražen je problem pojave velike količine plutajućeg otpada, koji nastaje uslijed velikih kiša (oborinskih voda), stalnih promjena nivoa vode u jezerima i rijeci Neretvi, te uslijed ljudskog nemara. Firma Hidroelektrane na Neretvi nastoji riješiti ovaj problem, a Mašinski fakultet u Mostaru je angažiran na projektiranju plutajuće platforme za prikupljanje otpada. U radu je objašnjen sistem prikupljanja otpada, projekat plutajuće platforme i rješenje ovog problema.

Ključne riječi: sistem prikupljanja otpada, plutajuća paltforma, umjetno jezero

1. Uvod

Plutajući otpad nastaje uslijed velikih kiša (oborinskih voda), stalnih promjena nivoa vode u jezerima i rijeci Neretvi, te uslijed ljudskog nemara. Zbog kretanja vode i dejstva vjetra taj otpad se uglavnom gomila uz samu branu, što stvara stanovite probleme pri proizvodnji električne energije, a dolazi i do zagađenja čovjekove okoline. Otpad ne zagađuje samo vodu, jer prilikom spuštanja nivoa vode u vještačkim jezerima on ostaje i na obali.

2. Sistem prikupljanja otpada

Da bi riješila ovaj problem firma Hidroelektrane na Neretvi je razvila sistem za prikupljanje plutajućeg otpada na akumulacionim jezerima, koji se satoji od:

- sakupljanja otpadaka po površini jezera pomoću broda za sakupljanje, koji je opskrbljen bagerskom kašikom sa otvorima za cijeđenje vode;
- utovara otpadaka u kontejner, koji se nalazi na plutajućoj platformi;
- podizanja napunjenog kontejnera dizalicom i njegovog postavljanja na specijalizovani kamion za odvoz kontejnera sa smećem;
- odvoza opadaka na deponiju;
- spuštanja praznog kontejnera pomoću dizalice na plutajuću platformu.

Plutajuća platforma, dakle, služi za nošenje kontejnera za otpadke. Također, platforma mora omogućiti radniku – opslužiocu da sa broda pređe na platformu, kako bi prilikom postavljanja praznog kontejnera centrirao isti na predviđeno mjesto na platformi, otkačio prazan kontejner od dizalice i zakačio pun kontejner za dizalicu. Čišćenje platforme se vrši po povoljnim meteorološkim uslovima. Mašinski fakultet u Mostaru je angažiran na projektiranju plutajuće platforme za prikupljanje otpada.

Dimenzije kontejnera za prikupljanje otpada su: dužina: 2300mm, širina 1400mm - gornji dio, 1300mm – osnovica, visina: 900mm, težina: cca 300kg.

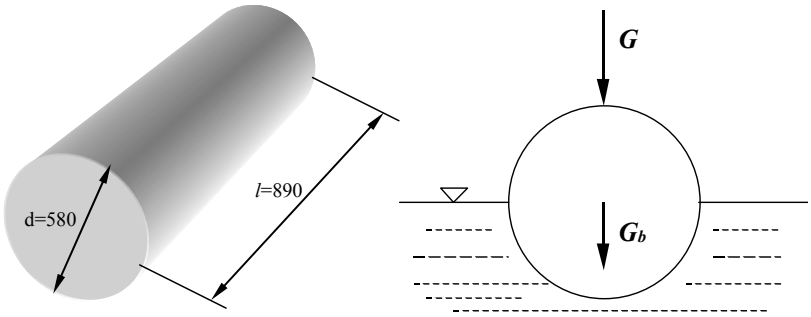
3. Plutajuća platforma

Plutajuća platforma je čelična konstrukcija sa drvenim podom, koja se sistemom obuhvatnih nosača oslanja na plovke (slika 2). Plovci su zapremine 208 litara (dm^3), dimenzija Φ0,58m x 0,89m. Platforma mora imati zaštitnu ogradu po obodu, radi zaštite opslužioca. Proračunom je potrebno dobiti broj plovaka, nosivost platforme i njenu stabilnost.

3.1. Proračun plutajuće platforme

U okviru projekta izvršen je detaljan proračun platforme, a u ovom radu dati su najvažniji rezultati za sistem prikupljanja plutajućeg otpada.

3.1.1. Proračun nosivosti plovaka i platforme



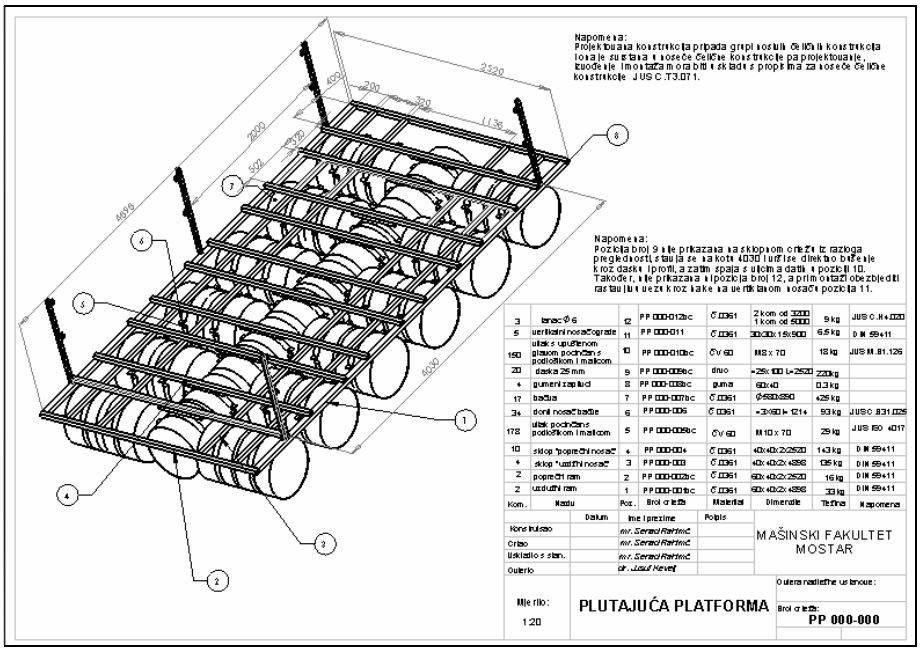
Slika 1. Dimenzije i opterećenje plovka

Osnovne veličine (sa slike 1.): G – opterećenje plovka, G_b- težina plovka

Jednačina ravnoteže:

$$G+G_b=V\cdot\gamma_v \qquad (1)$$

gdje je: V – istisnuta zapremina vode (uronjena zapremina plovka), a γ_v – specifična težina vode. Ako se plovak uroni do pola pod težinom G iz (1) se dobije da je G=908,14N što je približno masi od 93 kg. Ako se plovak uroni cijeli pod težinom G dobija se maksimalna nosivost G=2061,52N ≈ 210 kg.



Slika 2. Sklopni crtež plutajuće platforme (podne daske nisu prikazane radi bolje vidljivosti ostalih dijelova)

Ako se usvoji pontonska platforma sa 17 plovka uronjenih do pola, tada je nosivost (bez težine plovka): 17 ⋅ 93=1581 kg, a maksimalna nosivost (bez težine plovka): 17 ⋅ 210=3570 kg. Težina platforme prema sklopnom crtežu u konstruktivnoj dokumentaciji (slika 2.) je 702,8kg, pa je maksimalna nosivost platforme 3570-702,8=2867,2kg. Sa koeficijentom sigurnosti ν=1,4 maksimalna dozvoljena nosivost plutajuće platforme iznosi 2000kg.

Ukupna maksimalna težina tereta, pontonske platforme i plovka bi bila 3570+17⋅25=3995kg.

3.1.2. Proračun stabilnosti platforme

Uslov stabilnosti:

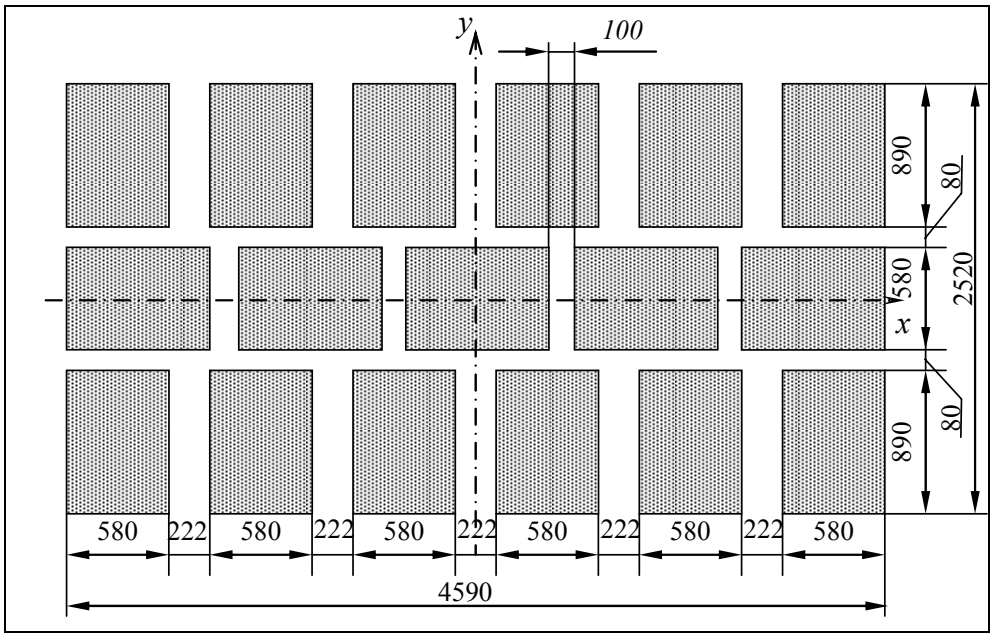
$$\boldsymbol{r > \delta,} \tag{2}$$

gdje je r – metacentrični polumjer, δ – rastojanje između težišta sistema C i centra potiska D.

- Metacentrični polumjer:

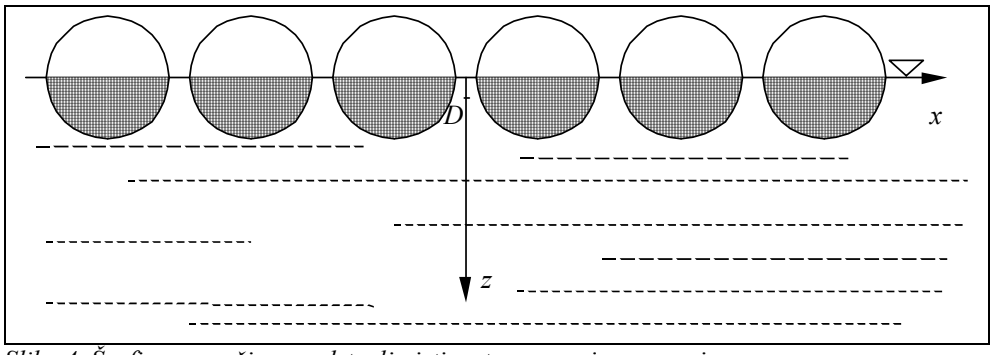
$$r = \frac{I}{V}, \tag{3}$$

gdje je I – moment inercije površine plivanja, V – istisnuta zapremina.



Slika 3. Raspored površina plivanja plovaka.

Moment inercije površine plivanja – *I* – u slučaju više plovaka određuje se za osu koja je presjek ravni simetrije platforme i ravni plivanja. To su ose *x* i *y* na slici 3.
Po *Štajnerovoj* teoremi moment inercije je jednak zbiru sopstvenog i položajnog momenta, tako da se dobija: $I_x=4,596m^4$; $I_y=17,0241m^4$.



Slika 4. Šrafirna površina predstavlja istisnutu zapreminu u ravni x-z.

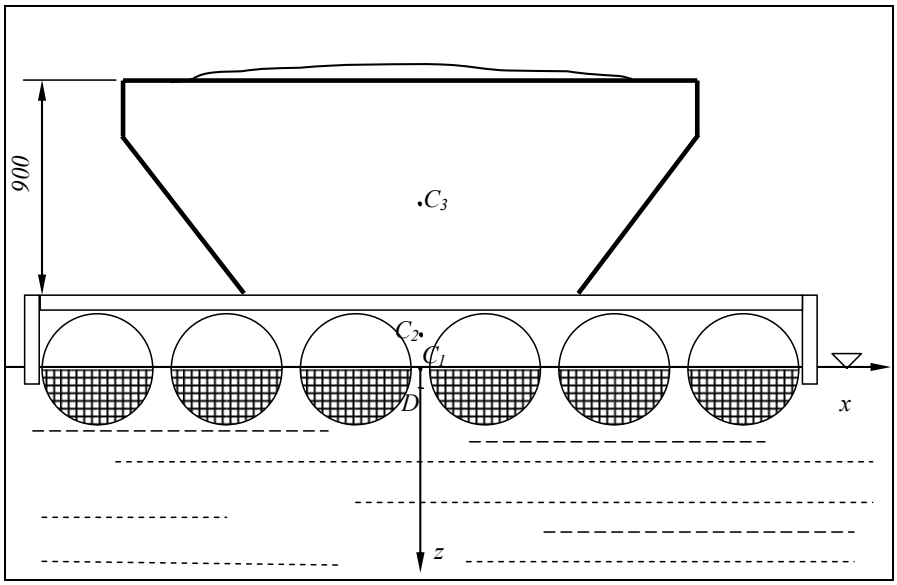
Metacentrični polumjer: $r_x = \frac{I_x}{V} = \frac{4,596m^4}{1,999m^3} = 2,299m$; $r_y = \frac{I_y}{V} = \frac{17,0241m^4}{1,999m^3} = 8,516m$

- Rastojanje δ između težišta sistema C i centra potiska D:
Centar potiska D je u težištu istisnute zapremine. Koordinate centra potiska su: $x_D=0$; $y_D=0$, a koordinata $z_D=0,12308m$ (slika 4).
Težište sistema C se dobija preko težišta plovka C_1, platforme C_2 i kontejnera C_3.
Koordinate težišta su $x_C=0$; $y_C=0$; a koordinata z_c se određuje iz momentne jednačine:

$$G_1 \cdot z_1 + G_2 \cdot z_2 + G_3 \cdot z_3 = (G_1 + G_2 + G_3) \cdot z_C$$

$$z_C = \frac{G_1 \cdot z_1 + G_2 \cdot z_2 + G_3 \cdot z_3}{G_1 + G_2 + G_3}$$

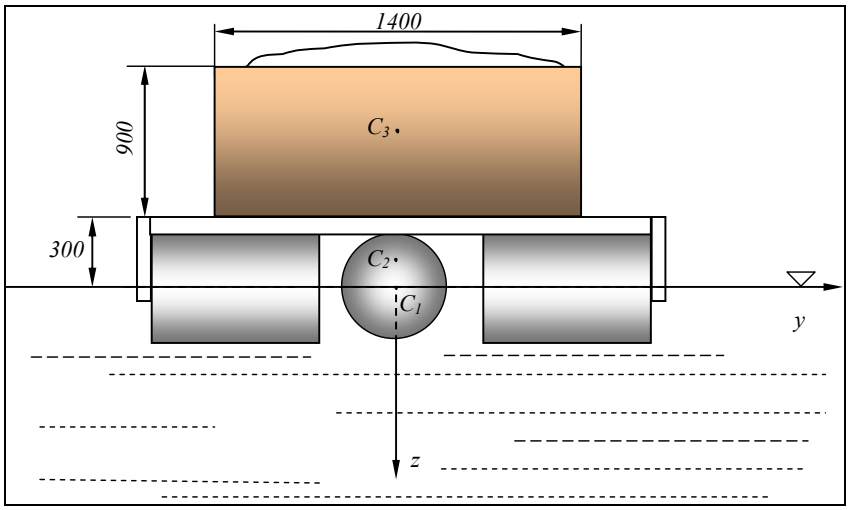
$$z_C = \frac{4169,25N \cdot 0m + 6894N \cdot 0,25m + 9810N \cdot 0,4m}{4169,25N + 6566N + 9810N} = 0,275m$$



Slika 5. Položaji težišta u ravni x-z.

Rastojanje δ: $\delta = z_C + z_D = 0{,}275m + 0{,}12308m = 0{,}398m$

Pošto su metacentrični polumjeri: $r_x = 2{,}299m$ i $r_y = 8{,}516m$, obadva su veća od $\delta = 0{,}398m$, pa je uslov stabilnosti $r > \delta$ zadovoljen.



Slika 6. Položaji težišta u ravni y-z.


Slika 7. Sakupljanje plutajućeg otpada kod brane hidroelektrane Grabovica.

4. Zaključak

Firma Hidroelektrane na Neretvi je nabavila motorni čamac sa bagerskom **žlicom** sa otvorima za cijeđenje vode za sakupljanje otpada sa površine. Plutajuća platforma je izrađena i cjelokupni sistem za prikupljanje otpada je stupio u rad. Dosadašnja iskustva su vrlo pozitivna i problem plutajućeg otpada je riješen, međutim, u narednom periodu biti će izrađene plutajuće platforme za svako **umjetno** jezero na Neretvi, kako se ne bi postojeća platforma dizalicom i vozilom transportirala sa jezera na jezero.

Sistem prikupljanja plutajućeg otpada će se nastojati poboljšati, ako je to moguće. U tom smislu, Mašinski fakultet Mostar će i putem savjetovanja, razmjenom mišljenja i iskustava nastojati pridonjeti tom poboljšanju.

MICROCALORIMETRIC STUDY ON CALCIUM ALUMINATE CEMENT HYDRATION

Neven Ukrainczyk[1], Juraj Šipušić[1], Pero Dabić[2], Tomislav Matusinović[1]
[1] Faculty of Chemical Engineering and Technology, University of Zagreb, Marulićev trg 20, Zagreb, Croatia
[2] Faculty of Chemistry and Technology, University of Split, Teslina 10/V, Split, Croatia

Corresponding author: N. Ukrainczyk: **nukrainc@fkit.hr**

Izvorni znanstveni rad / Original scientific paper

Abstract

Calcium aluminate cement (CAC) is very versatile special cement used for specific applications. During the hydration of CAC a large quantity of heat is liberated within one day that causes a considerable increase of temperature in material.

This paper examines the hydration of three samples (A, B and aged B) of commercial CAC ISTRA 40 (producer: Istra Cement, Pula, Croatia). The rate of heat generation of cement pastes due to the hydration reactions was measured at several temperatures with differential micro-calorimeter. In the experiments water to cement ratio was also varied and in one sample quartz sand was added.

When CAC and water first come in contact far less heat is liberated, than for Portland cement. Higher water to cement ratio increases the heat evolved at later ages due to higher quantity of water available for hydration. Cement mortar prepared with milled quartz sand showed 1.2 h shorter setting time than corresponding neat CAC paste. This could be explained by more germination sites available for the nuclei to start the hydration precipitation. Except for the change in the setting time there are no other significant differences in the kinetics of hydration when compared to original cement sample. Due to a water and CO_2 uptake from the environment the aged sample has a greater weight loss on ignition, shorter setting time, lower hydration rate and lower heat of hydration evolved in comparison to original sample. Contrary to previous reports in literature acceleration of CAH_{10} formation was observed in 5 to 10 ^{o}C temperature range. Heat generation data obtained could not be satisfactory fitted by the Avrami-Erofe'ev nucleation and growth kinetic model.

Keywords: calcium aluminate cement, calorimetry, heat of hydration, kinetics.

1 Introduction

Due mainly to their higher cost, calcium aluminate cement (CAC) do not compete directly with Portland cements. Despite the well documented construction failures in the 1970's, if CAC is used correctly as recommended (w/c < 0.4, adequate curing), it is a good constructional material to be advantageously employed with high performance in specific applications (resistance to chemical attack, high early strength, refractory, resistance to abrasion, low ambient temperature) [1,2]. Although the hydration of CAC represents a process of commercial and industrial importance, the physical and chemical processes involved during hydration are not yet well understood [1-5]. Hydraulic hardening of CAC is primarily due to the hydration of $CaAl_2O_4$, but other compounds may also participate in the hardening process especially in long term strength development. The hydration of CAC is temperature dependent, yielding CAH_{10} (cement notation: C[CaO], A[Al_2O_3], H[H_2O]) as main products at temperatures less than 20 °C, C_2AH_8 and AH_3 at about 30 °C and C_3AH_6 and AH_3 at temperatures greater than 55 °C. CAH_{10} and C_2AH_8 are known to be metastable at ambient temperature and convert to the more stable C_3AH_6 and AH_3 with consequent material porosity increase and loss of strength. The conversion is accelerated by temperature and moisture availability for the dissolution and re-precipitation processes to take place [2]. During the hydration of CAC a large quantity of heat is liberated in a short period (first 24 h) that can cause a considerable increase in material temperature. It is important to ensure adequate curing during the initial hardening stage. This may be achieved by spraying with cold water during the 24 hour period after placing or by the use of a curing membrane, or wet sacking to prevent excessive heating and water loss.

By means of the heat released, it is possible to determine the degree of hydration relative to hydration duration according to the equation:

$$\alpha(t) = \frac{Q(t)}{Q_{\max}} \tag{3}$$

where $Q(t)$ is heat released by time t, and $Q_{\max}$ represents the total heat a sample can release. The rate of heat generation, q can thus be expressed proportional to the rate of reaction:

$$q(t) = Q_{\max} \frac{d\alpha(t)}{dt} \tag{4}$$

The data of pure Portland cement minerals usually fit [6] the Avrami-Erofe'ev nucleation and growth kinetic model:

$$\frac{d\alpha}{dt} = nKt^{n-1} \exp(-Kt)^n \tag{5}$$

where K is a rate parameter and n is a power law index. However, the hydration rate is controlled by dissolution process, mass transfer, nucleation and growth of crystals and rate of reaction between water and cement at its boundary.

This paper presents results of calorimetric study on calcium aluminate cement hydration for the sake of elaboration of the hydration model which would predict the hydration rate, $d\alpha/dt$ relative to the hydration degree, α and temperature, T. In cement application, the model will enable a real simulation of temperature distribution in material and better planning of curing during early age of hydration to obtain better durability and functionality.

2 Experimental

The CAC used was taken from a regular production of Istra Cement International, Pula, Croatia. The cement has the following nominal oxide mass fraction composition: CaO 37-40%, Al_2O_3 39-42%, Fe_2O_3 14-17%, SiO_2 2-5%, MgO<1.2% and SO_3<0.4%. Residue on sieve at 90 μm 4%, fineness (Blaine) 3350 cm^2/g, bulk density 1.15 g/cm^3, specific gravity 3.20 g/cm^3. The main compounds are monocalcium aluminate, CA and ferrite phase (C_4AF-C_6AF_2), with mayenite, $C_{12}A_7$,

gehlenite, C_2AS and β-C_2S as minor compounds [2]. The samples A and B were used as received while the third sample aB is cement B aged for one year. About 20 g of sample B is sealed for one year in a little PE bag at laboratory conditions (20 °C and ~55 % r.h.). For preparing cement mortar, quartz sand (99 % SiO_2, size 1 mm) milled for 1 h in planetary mill (Fritsch, Pulverisette 5, *α*-Alumina pot and grinding balls) was used.

The rate of heat generation of the prepared CAC samples has been determined by the differential isoperibolic-conduction microcalorimeter developed at the Technical University of Budapest. It is capable of giving information on heat evolution from the instant the water was injected in cement sample holder. As hydration heat evolves the small temperature difference across a thermopile (consisting of 18 thermocouples) between the sample cell and reference cell produces a voltage that is logged at regular time intervals (10 s) by a microvoltmeter (Data logger Almemo-2390-8, with DC Millivolt Connectors, resolution 1μV). The calorimeter operates under isoperibolic conditions with small temperature difference. The rate of heat generation at time *t*, is calculated applying Tian's equation [7,8]:

$$\frac{dQ}{dt} = \frac{c_p}{m\,g}\left(\frac{dU}{dt} + \beta U\right) \tag{2}$$

where *U* is the voltage difference (referenced to baseline), c_p is effective heat capacity of calorimeter (J/°C), *g* is voltage to temperature conversion constant (μV/°C), *β* is calorimeter cooling constant (s^{-1}), and *m* is cement mass. Small samples, 4g of cement, is used to avoid undesirable temperature rise in the cell. More detailed operation and calibration of the calorimeter is described elsewhere [7]. The cement and appropriate amount of water was left to reach thermal equilibrium (overnight) in an ultrathermostat before the water was injected into the cement sample holder to start the hydration. Results are presented as an average of two measured curves. Uncertainty of the microcalorimetric measurement of heat evolved (Q/Jg^{-1}, with 95% confidence) is evaluated to be ± 3%.

The composition of cement and hydrates formed was investigated by X-ray diffraction (XRD). The cement samples were investigated by loss on ignition determined by firing at 950 °C in laboratory furnace.

First serial of experimental work was done on as received samples A and B for cement pastes and mortars mix proportions given in Table 1. Temperature, *T*, water to cement ratio, *w/c*, and sand-cement ratio, *s/c* was varied. High *w/c* ratios were used in order to assure good wetting of the cement. Second serial was conducted on aged sample, Table 2.

3 Results and discusion

XRD on samples hydrated at appropriate temperature for 30 h confirmed the hydrate compositions expected from the literature. At 5 °C only CAH_{10} was observed, while at 20 °C a small quantity of C_2AH_8 and AH_3 could be detected. At 30 °C C_2AH_8 and AH_3 are main products with appearance of C_3AH_6 but no CAH_{10} was observed.

Results of investigations of CAC sample A and B hydration by microcalorimeter are given in Figures 1-3 and Table 3. In Figures 1 and 3a only rate of heat generation ($q=dQ/dt$, $J\,h^{-1}g^{-1}$) is presented while in others heat evolution obtained by integration of (1), *Q*, Jg^{-1} is also added.

Times of initial and final set were established from the microcalorimetry results. Initial set is acquired from the intersection of two straight lines [6,9]: one fitted through the induction period of the curve and the other fitted through the inflection point of the rising slope of main peak ($tg\alpha_{i.p.}$). The final set can be approximated at the point of maximal heat generation $t_{q\max}$. Unlike calorimetry, the Vicat initial setting time is significantly affected by *w/c* due to the consistency of the paste being tested [6]. In a more fluid paste longer time is needed to reach the required resistance to penetration.

Table 1. First serial of cement pastes and mortars mix proportions.

Label	Sample	*w/c*	*s/c*	*T*/°C
A20C0.4	A	0.4	-	20
A20C0.5	A	0.5	-	20
A20C1.0	A	1.0	-	20
A20C0.5S	A	0.5	1,0	20
B20C0.4	B	0.4	-	20
B20C0.5	B	0.5	-	20
B5C0.4	B	0.4	-	5
B5C0.5	B	0.5	-	5
B10C0.4	B	0.4	-	10
B10C0.5	B	0.5	-	10
B10C1.0	B	1.0	-	10
B30C0.4	B	0.4	-	30
B30C0.5	B	0.5	-	30

Table 2. Second serial of cement pastes mix proportions for the study of aged cement sample.

Label	Sample	*w/c*	*T*/°C
aB14C0.4	aB	0.4	14
aB14C0.5	aB	0.5	14
aB20C0.5	aB	0.5	20

Far less heat is liberated when cement and water first come in contact than for Portland cement. This heat is attributed mainly to the cement wetting and dissolution processes occurring during the first minutes of hydration. During the induction period a small rate of heat generation is observed (~1 J(h g)$^{-1}$), whose length is determined by temperature, water content and cement composition. Induction period is followed by the onset of the accelerated stage of reaction due to massive precipitation of hydrates. The maximum of heat generation amounts up to 55 J(h g)$^{-1}$ and is reached in only few hours after the onset of the accelerated stage. In comparison to PC that is up to six time greater rate of maximal heat generation.

Influence of the water to cement ratio, *w*/*c* on CAC hydration at 20 °C is shown in Figure 1a. Samples prepared at higher *w*/*c* show greater rate of heat generation at later ages. From the comparison of the *w/c* impact in Figure 1a it can be concluded that the limiting reactant is water. Due to water consumption, hydration reaction is slowing down. This principal influence of *w/c* is also visible immediately before the maximum of the main peak with higher values of q_{max} for higher *w/c*. We argue that this can be the case only if the reaction i.e. interaction on cement boundary is the main rate limiting mechanism.

In Figure 1b a comparison of mortar (A20C0.5s) and paste hydration (A20C0.5) is presented by translating paste hydration to overlap the onset of the main peak. Cement sets faster (Table 3, Δt_v = 1.2 h) in the form of the sand-cement mortar than neat paste. The massive hydrate precipitation begins after nuclei germination from the saturated solution. The reason for slower activity in the neat paste could be explained by the lack of germination sites for the nuclei to start the hydration precipitation. After the onset of the main peak the hydration rate is faster for the sand-cement mortar due to more germination sites. A little time past the maximal rate, with higher value for mortar, the hydration continues slower in comparison to neat paste.

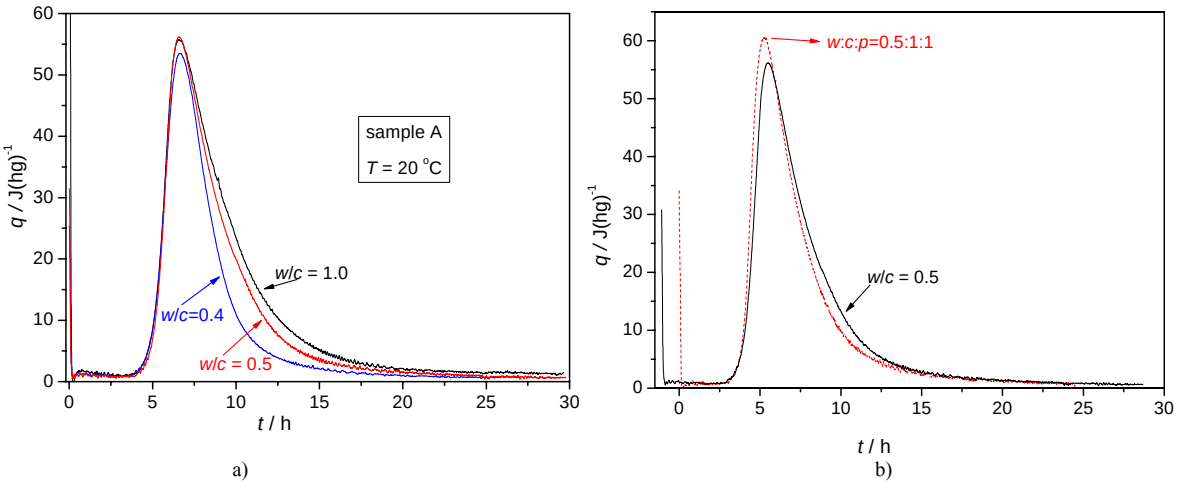


Figure 1. Heat generation during hydration at 20 °C: a) influence of *w/c*, and b) comparison of mortar (A20C0.5s) and paste hydration (A20C0.5 – translated hydration start).

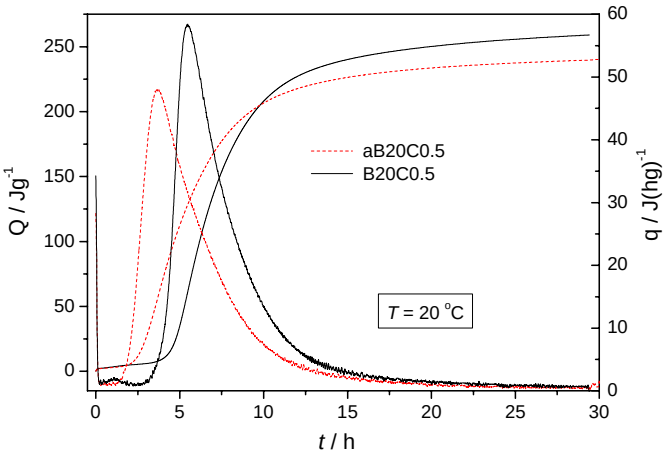


Figure 2. Comparison of sample B and sample aB (one year sealed in a little PE bag at 20 °C and 55% r.h) hydration.

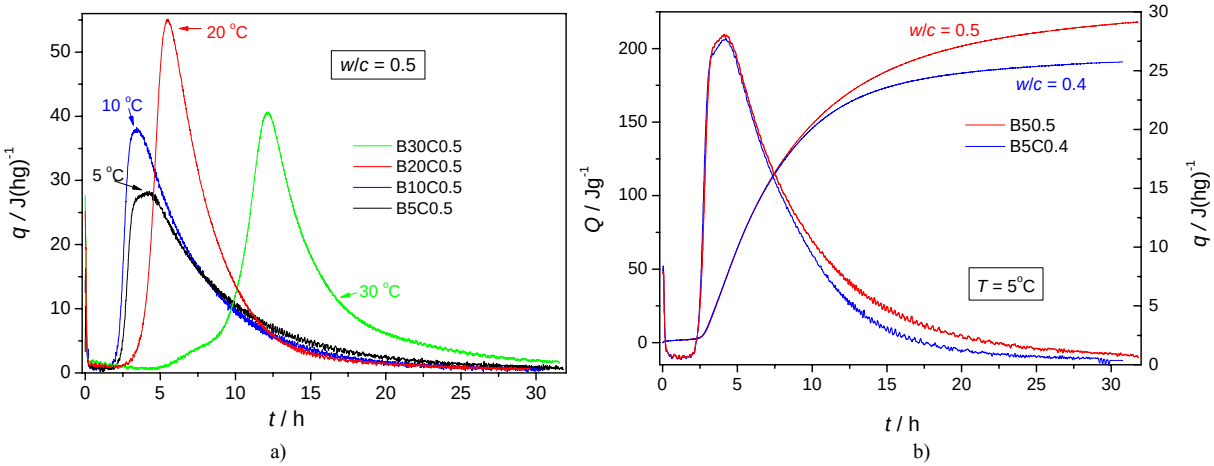


Figure 3. Heat generation during hydration: a) Influence of temperature on hydration, and b) influence of *w/c* on hydration at 5 °C.

Table 3. Results of the investigations by microcalorimeter: hydration heat evolved after 24.5 h ($Q_{t=24.5h}$), maximal rising slope at inflection point of main peak ($tg\alpha_{i.p.}$), main peak maximal heat generation (q_{max}) at time $t_{q\max}$, and initial setting time (t_{set}).

Label	$Q_{t=24.5\,h}$ / Jg^{-1}	$tg\alpha_{i.p.}$/ $Jh^{-2}g^{-1}$	q_{max} / mWg^{-1}	$t_{q\max}$ / h	t_{set} / h
A20C0.4	204.3	41.5	14.9	6.6	5.0
A20C0.5	250.0	48.5	15.6	6.5	5.1
A20C1.0	287.6	51.3	15.7	6.5	5.1
A20C0.5S	243.5	62.7	16.9	5.2	3.9
B20C0.4	207.7	45.0	15.1	5.5	3.9
B20C0.5	253.3	46.8	15.3	5.5	4.0
B5C0.4	187.5	42.2	7.7	4.2	2.4
B5C0.5	210.2	40.9	7.8	4.2	2.5
B10C0.4	196.5	49.7	10.6	3.6	2.3
B10C0.5	225.2	50.3	10.5	3.4	2.2
B10C1.0	253.4	32.3	9.3	3.4	1.7
B30C0.4	216.1	26.6	13.1	12.2	9.6
B30C0.5	243.3	19.3	11.3	11.6	9.7
aB14C0.4	190.8	27.6	10.1	3.5	1.6
aB14C0.5	236.1	26.0	10.4	3.6	1.6
aB20C0.5	237.2	35.4	13.3	3.6	2.0

The difference in heat evolved of 2.8 %, Table 3, points out that practically the same hydration degree is achieved after 1 day. The smaller value for mortar could be explained by the wetting of sand. Slope at the inflection point of main peak is 29 % higher for the hydration with sand addition, Table 3 and Figure 1a. Comparison of hydration A and B samples (not depicted in this paper) resulted in difference of heat evolved by 1.8 % and 1.9 % for *w/c* of 0.4 and 0.5, respectively. Considering the measurement uncertainty of measured evolved heat (± 3%) and by comparison of curve shape by translation, it can be concluded that except for the change in the setting time (Δt_v = 1.1 h) there are no other significant differences in the kinetics of hydration of samples A and B, Table 3.

Loss on ignition measurement on samples A, B and aB has indicated 0.90, 0.88 and 3.14 % mass reduction, respectively. The aged sample shows greater mass loss due to a water and CO_2 uptake from the environment. It should be noted that only ~ 20 g of sample was aged, and the uptake for larger samples (25 kg in original bag) is expected to be pronounced only on sample periphery.

Results of the investigation of the age impact onto hydration are shown in Figure 2 and Table 3. The aged sample in comparison to original sample B show the quicker setting time, lower hydration rate, the flatter and longer main peak in the heat generation and lower heat evolved.

The influence of temperature on the rate of hydration is presented in Figure 3a. Increasing temperature from 5 to 10 °C increases the rate of formation of CAH_{10} but above 20 °C the low level of supersaturation, sluggish nucleation of CAH_{10} and the massive gel formation retards the setting time and hydration rate. The maximal rate of heat evolution occurs at 20 °C. The flatter and longer main peak in the heat generation at 30 °C than at 20 °C supports the notion of slow growth and crystalisation of C_2AH_8 up to this temperature [9] with the formation of both CAH_{10} and C_2AH_8 in proportions that vary over the temperature range. Contrary to Bushnell and Banfill [6,9], who

reported retardation of CAH_{10} formation with increased temperature in the range 5 – 15 ^{o}C, Figure 3 shows clearly acceleration of CAH_{10} formation. Banfill concluded, by applying Avrami-Erofe'ev equation that the maximum rate of heat evolution and the time at which it occurs are reliable kinetic parameters to quantify the hydration rate. In this study heat generation data obtained could not be satisfactory fitted by the Avrami-Erofe'ev nucleation and growth equation. The appropriateness of using Avrami-Erofe'ev analysis for describing whole hydration process is disputable, because the rate of reaction is not solely governed by the nucleation and growth mechanism.

Figure 3b shows the influence of *w/c* on CAC hydration at 5 ^{o}C. With decreasing temperature (20-5 ^{o}C), compare Figures 1a and 3 b, the retardation of hydration rate due to self-desiccation is occurring latter referring to the main maximum.

4 Conclusions

Determining the heat of hydration of cement material will enable, in practice, the realistic simulation of temperature distribution in material and easier planning of curing in the early stage of hydration with the purpose of achieving better durability and functionality of placed material.

Far less heat is liberated when cement and water first come in contact than for PC. Higher *w/c* increases the heat evolved due to higher degree of hydration. Cement sets faster (1.2 h) in the form of the sand-cement mortar than neat pastes. This could be explained by the lack of germination sites for the nuclei to start the hydration precipitation.

Except for the change in the setting time (Δt_v = 1.1 h) there are no other significant differences in the kinetics of hydration of used original cement sample. Due to a water and CO_2 uptake from the environment the aged sample has a quicker setting time, lower hydration rate and lower heat evolved in comparison to original sample.

Contrary to previous reports in literature acceleration of CAH_{10} formation was observed for 5-10 ^{o}C. Obtained heat generation data could not be satisfactory fitted by the Avrami-Erofe'ev nucleation and growth kinetic model due to its non-appropriateness for describing the hydration process in the whole stage.

5 Acknowledgement

The authors acknowledge financial support from the Croatian Ministry of Science Education and Sports under project's no. 125-1252970-2983 "Development of hydration process model" and project's no. 011-1252970-2254 "Cement composites and stabilization of harmful wastes".

6 References

1. R.J. Mangabhai, Ed., Calcium Aluminate Cements, Chapman and Hall, London, 1990.
2. R.J. Mangabhai, F.P. Glasser, Calcium Aluminate Cements 2001, Edinburgh, UK, 2001.
3. N. Ukrainczyk, T. Matusinović, S. Kurajica, B. Zimmermann, J. Šipušić, Dehydration of a layered double hydroxide-C_2AH_8, Thermochimica Acta 464 (2007) 7–15.
4. T. Matusinović, N. Vrbos, J. Šipušić, Rapid setting and hardening calcium aluminate cement materials, Zement-Kalk-Gips International 5 (2005) 72-79.
5. T. Matusinović, N. Vrbos, D. Curlin, Lithium salts in rapid setting high-alumina cement materials, Ind. Eng. Chem. Res. 33 (1994) 2795– 2800.
6. P. F. G. Banfill, Superplasticizers for Ciment Fondu. Part2: Effect of temperature on the hydration reaction, Advances in Cement Research, 7 (1995) 151-157.
7. R. Krstulović, P. Krolo, T. Ferić, Microcalorimetry in the cement hydration process, Periodica Polytehnica 33(1982) 315-321.
8. E. Calvet, H. Prat, Recent Progress in Microcalorimetry, Ed. H.A. Skinner, Oxford, 1963.
9. S.M. Bushnell-Watson, and J.H. Sharp, The effect of temperature on the setting behaviour of refractory calcium aluminate cement, Cem. Concr. Res. 16 (1986) 875-884.

UTJECAJ TEMPERATURE IZOTERMIČKOG POBOLJŠANJA NA SVOJSTVA NODULARNOG LIJEVA
INFLUENCE OF AUSTEMPERING TEMPERATURE ON MECHANICAL PROPERTIES OF ADI

Z.Veljačić*, Z.Schauperl**

Brodosplit – brodogradilište d.o.o
Put Supavla 21, HR - 21000 Split
Fakultet strojarstva i brodogradnje
Ivana Lučića 5, Zagreb

Stručni članak / Professional paper

Sažetak:
U radu je ispitivan utjecaj različite temperature izotermičkog poboljšavanja na mehanička svojstva nodularnog lijeva kvalitete NL 60. Temperature izotermičkog poboljšavanja su bile 240°C i 380°C. Nakon provedene toplinske obrade ispitana su i uspoređena osnovna mehanička svojstva uzoraka i njihova mikrostruktura.

Ključne riječi: nodularni lijev, mehanička svojstva, mikrostruktura

Abstract:
In this paper influence of two different austempering temperatures on mechanical properties of ADI material is described. Specimens were made of ductile iron NL60 quality, and austempering temepratures were 240°C and 380°C. After heat treatment hardness and ductility of specimens were tested and compared. The microstructures of specimens before and after heat treatment are presented.

Key words: ADI, mechanical properties, microstructure.

1. UVOD

Nodularni ili žilavi lijev svoju primjenu u industriji nalazi od sredine 20. stoljeća. Za jače opterećene strojne dijelove koristi se nodularni lijev obrađen posebnom vrstom toplinske obrade, izotermičkim poboljšavanjem (austempering proces).
Perlitni žilavi lijev prije izotermičkog poboljšavanja ima mikrostrukturu čija se matrica sastoji od perlita u kojoj su raspoređene kuglice (nodule) grafita. Nakon izotermičkog poboljšavanja, matrica materijala sastoji se od bainita i zaostalog austenita. Količina zaostalog austenita iznosi između 20 i 40% [1,2]. Austenit u matrici materijala koja se pretežno sastoji od bainita doprinosi visokoj žilavosti i duktilnosti izotermički poboljašanog žilavog lijeva. On se može pretvoriti u martenzit hladnom deformacijom što otvara mogućnost da se nakon izotermičkog poboljšavanja površina predmeta dodatno očvrsne (npr. sačmarenjem).
Kombiniranjem kvalitete polaznog materijala i parametara izotermičke pretvorbe mogu se postići izuzetno dobra mehanička svojstva nodularnog lijeva (vlačna čvrstoća do 1400MPa i tvrdoća preko 40HRC) uz odgovarajuće uštede u proizvodnim troškovima, odnosno povećanju produktivnosti.

Osim o kvaliteti polaznog materijala, svojstva nodularnog lijeva nakon izotermičkog poboljšavanja ovise o parametrima postupka toplinske obrade [2] i to o:

- temperaturi austenitizacije;

- vremenu držanja na temperaturi austenitizacije;
- brzini ohlađivanja sa temperature austenitizacije na temperaturu izotermičke pretvorbe;
- temperaturi izotermičke pretvorbe;
- vremenu držanja na temperaturi izotermičke pretvorbe.

U nastavku rada ispitani su utjecaji dvije različite temperature izotermičke pretvorbe na osnovna mehanička svojstva izotermički poboljšanog nodularnog lijeva kvalitete NL 60.

2. IZRADA UZORAKA

Uzorci za ispitivanje izrađeni su iz nodularnog lijeva NL 60 proizvedenog u „Brodosplit“ brodogradilištu. Izlivena su tri različita oblika odljevaka različitih oblika i dimenzija, slika 1, sa namjerom daljnjih znatno širih istraživanja, kod kojih je izotermičko poboljšavanje jedna od faza.



Slika 1. Odljevci NL 60.

Kemijski sastav odljevaka prikazan je u tablici 1.

Tablica 1. Kemijski sastav odljevaka.

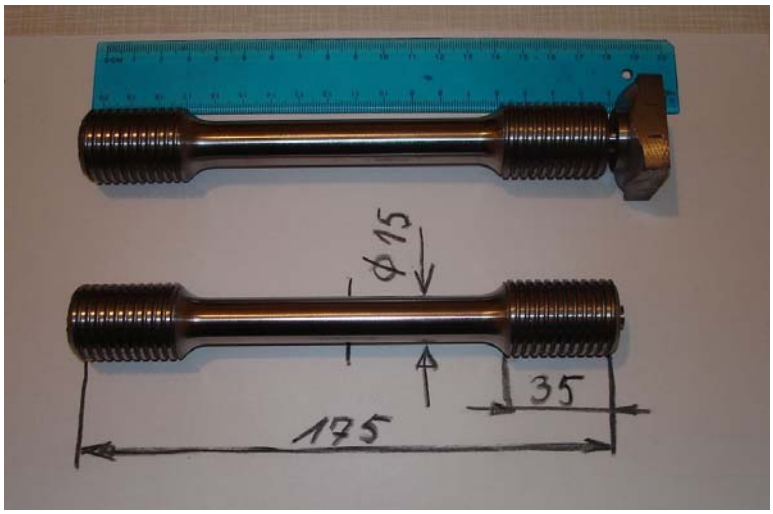
C	**Si**	**Mn**	**P**	**S**	**Cu**	**Mg**
3.57 %	2.49 %	0.113 %	0.029 %	0.007 %	0.4 %	0.057 %

Homogenost odljevaka pločastog oblika rendgenski je ispitana te je ustanovljeno da su odljevci bez značajnih grešaka.

3. KARAKTERIZACIJA NODULARNOG LIJEVA PRIJE TOPLINSKE OBRADBE

Nakon izrade odljevaka provedeno je ispitivanje mehaničkih svojstava proizvedenog materijala. Proveden je statički vlačni pokus, te ispitana tvrdoća i žilavost materijala. Epruvete izrađene za statički vlačni pokus su standardnih dimenzija i prikazane su na slici 3.

.



Slika 3. Epruvete za ispitivanje mehaničkih svojstava

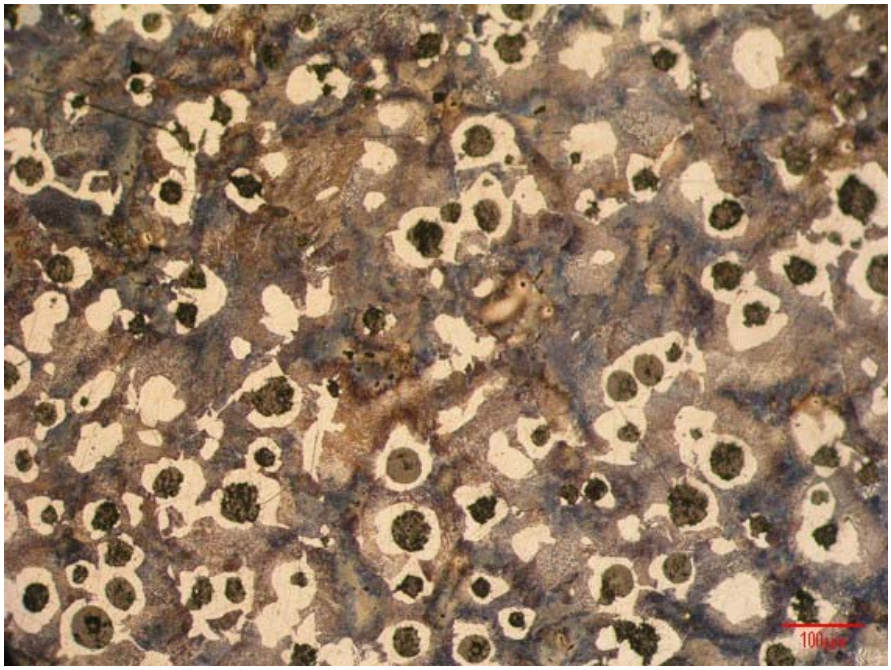
Srednje vrijednosti dobivenih rezultata statičkog vlačnog pokusa su:

R_m – 638 MPa
$R_{p0,2}$ – 452 MPa
A5 – 11,3%

Tvrdoća je izmjerena po metodi Brinell i srednja vrijednost tvrdoće iznosi 190HB.

Ispitana je i žilavost materijala standardnim postupkom pomoću Charpy-evog bata. Rezultati ispitivanja udarne radnje loma kod svih epruveta su bili ujednačeni i srednja vrijednost je 2 J.

Analizirana je i mikrostruktura izlivenog materijala. Uzorci su pripremljeni uobičajenim postupkom za tu vrstu materijala: izrezani, brušeni, polirani te nagriženi u nitalu. Mikrostruktura u nagriženom stanju je prikazana na slici 4.

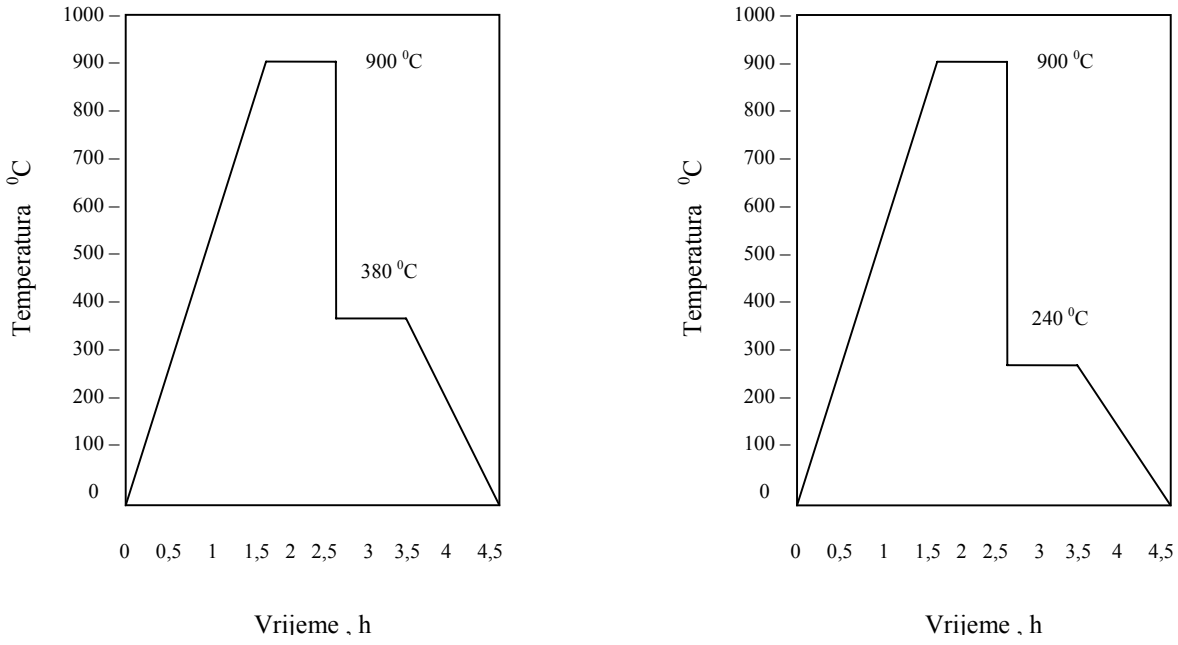


Slika 4. Mikrostruktura odljevka prije toplinske obrade.

Analizom mikrostrukture vidljive su nodule grafita, te perlitna matrica s feritnim područjima oko nodula grafita.

4. IZOTERMIČKO POBOLJŠAVANJE NL 60

Iz odljevaka strojnom obradom su izrađeni uzorci i podijeljeni u dvije skupine za daljnja ispitivanja. Toplinska obrada tih uzoraka se sastojala od grijanja na temperaturu austenitizacije 900°C, a vrijeme držanja uzoraka na toj temperaturi je bio jedan sat. Potom je jedna skupina uzoraka naglo ohlađena i držana jedan sat u tekućoj soli na 380°C, a druga na 240°C. Nakon toga je uslijedilo postupno hlađenje do sobne temperature.
Postupak je dijagramski prikazan na slici 5.



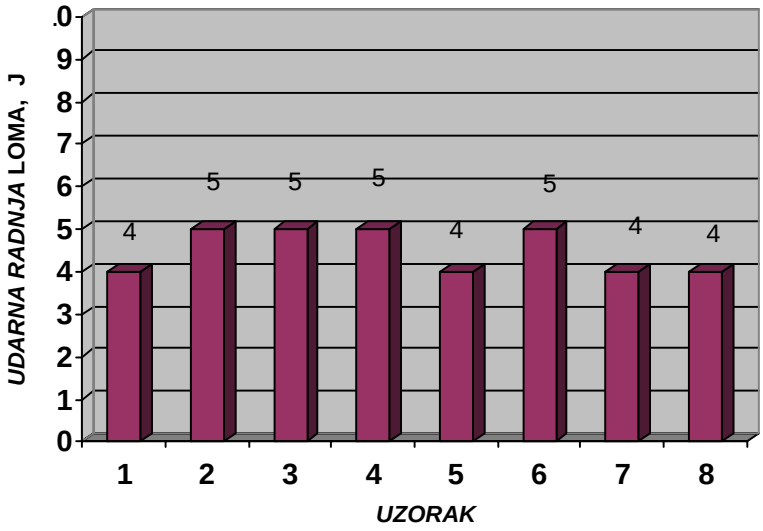
Slika 5. Dijagrami izotermičke pretvorbe

5. KARAKTERIZACIJA NODULARNOG LIJEVA NAKON TOPLINSKE OBRADBE

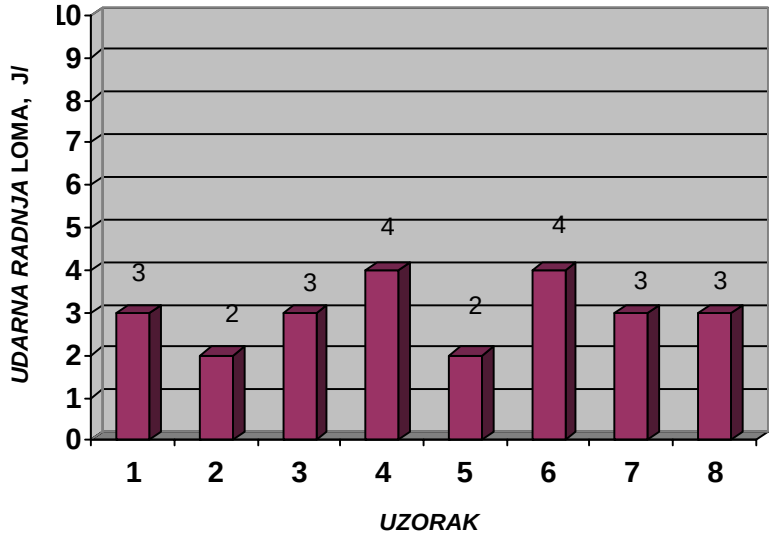
Kako bi se odredio utjecaj temperature izotermičke pretvorbe na mehanička svojstva nodularnog lijeva, nakon toplinske obrade ponovo je ispitana tvrdoća i žilavost tog materijala. U tablici 2 prikazane su dobivene vrijednosti tvrdoće po Brinellu.

Temp. izoter. pretvorbe	***HB***								
	1	***2***	***3***	***4***	***5***	***6***	***7***	***8***	$\overline{X}$
900/240ºC	444	452	444	452	454	446	454	446	**449**
900/380ºC	276	285	275	285	285	283	285	285	**282**

Prilikom ispitivanja udarne radnje loma izotermički poboljšani uzorci pokazali su određeno rasipanje rezultata za razliku od toplinski neobrađenih uzoraka, slike 6 i 7.



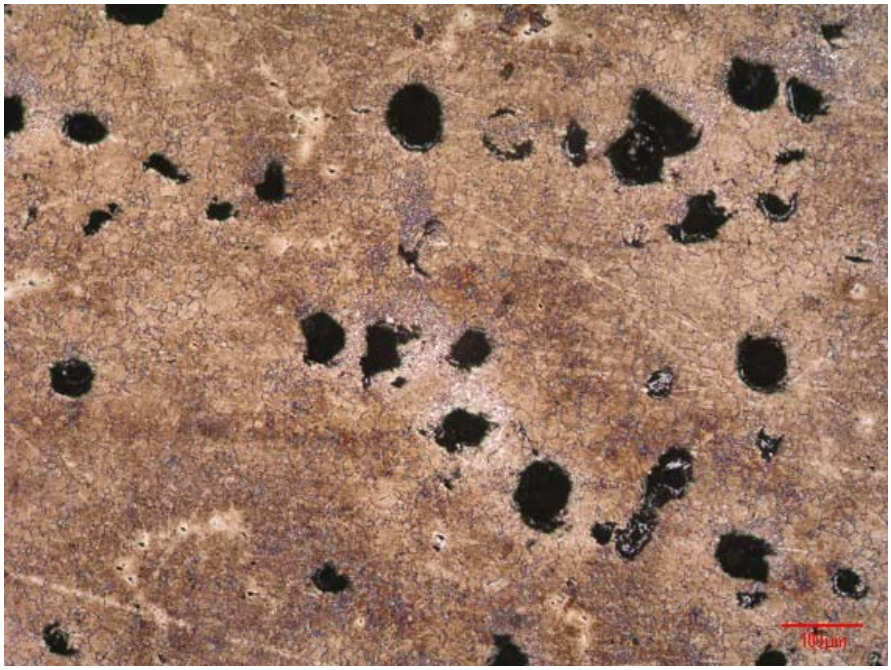
Slika 6. Grafički prikaz rezultata udarne radnje loma za uzorke izotermički poboljšane pri 240 ^{0}C



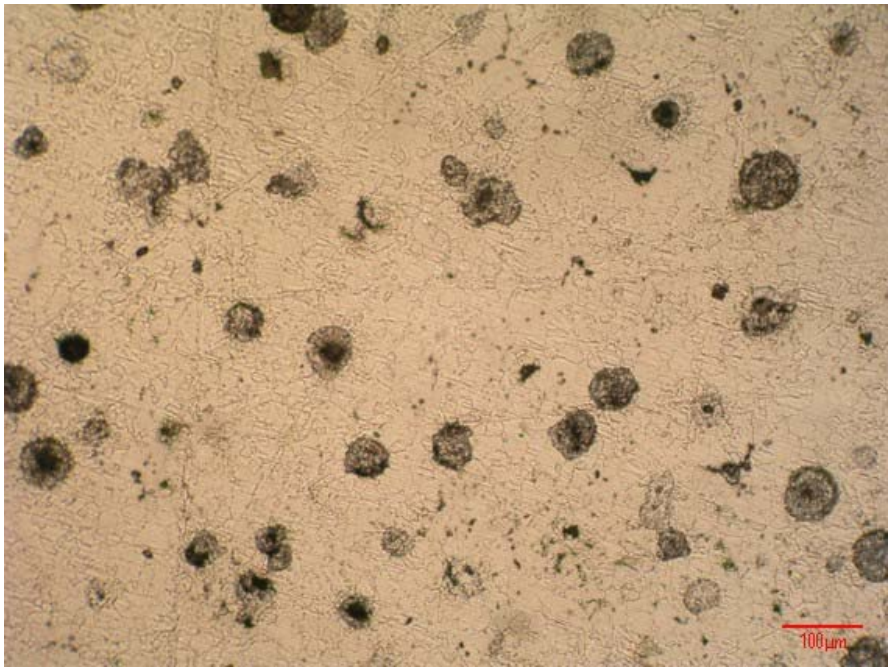
Slika 7. Grafički prikaz rezultata udarne radnje loma za uzorke izotermički poboljšane pri 380 ^{0}C

Kao što je vidljivo na dijagramima rasipanje je veće kod uzoraka izotermički poboljšanih pri 380°C.

Analizirana je i mikrostruktura toplinski obrađenih uzoraka. Uzorci su pripremljeni uobičajenim postupkom za tu vrstu materijala: izrezani, brušeni, polirani te nagriženi u nitalu. Mikrostruktura u nagriženom stanju je prikazana na slikama 8 i 9.



Slika 8. Mikrostruktura materijala uzorka izotermički poboljšanog pri 240 ^{0}C.



Slika 9. Mikrostruktura materijala uzorka izotermički poboljšanog pri 380 ^{0}C.

6. ZAKLJUČAK

Na temelju provedenih ispitivanja može se zaključiti slijedeće:

- Izotermičkim poboljšavanjem promijenjena je struktura nodularnog lijeva, a time su promijenjena i mehanička svojstva materijala. Analizom mikrostrukture vidljiva je uredna struktura u toplinski neobrađenim uzorcima. Struktura tih uzoraka se sastoji od grafitnih nodula sa perlitno-feritnom strukturom. U toplinski obrađenim uzorcima vidljiva je transformirana mikrostruktura, također homogena.
- Utvrđeno je da se toplinskom obradbom povećala tvrdoća i žilavost uzoraka u odnosu na toplinski neobrađene. Tvrdoća uzoraka izotermički poboljšanih na 240ºC je značajno viša od uzoraka poboljšanih na 380ºC. Osim tvrdoće i žilavost uzoraka poboljšanih na 240ºC je veća i nije prisutno rasipanje vrijednosti kao kod drugih uzoraka.
- Dobiveni rezultati ukazuju da izotermička pretvorba nodularnog lijeva NL60 pri nižim temperaturama stvara više bainita (tvrde faze), a manje zaostalog austenita (meke faze) što za posljedicu ima značajno bolja mehanička svojstva.

7. LITERATURA

1. E. Dorazil, The mechanical properties of austempered ductile iron, Foundry 160, 1986, 36-45

2. Ljevarstvo – Glasilo saveza ljevača Hrvatske, Izotermički poboljšani žilavi lijev i njegova primjena na visokoopterećene elemente, Rijeka , Prosinac 1985., 51-68

OZNAČIVANJE ŽELJEZNIH LJEVOVA PO EUROPSKIM STANDARDIMA

DESIGNATION OF CAST IRONS BY EUROPEAN STANDARDS

Ivan Vitez, Dragomir Krumes
Strojarski fakultet Slavonski Brod, Sveučilišta J.J. Strossmayera u Osijeku,
Trg I.B. Mažuranić 2, HR-3500 Slavonski Brod
Borut Kosec
NFT University of Ljubljana, Slovenija
Dražen Dolovčak, dipl.ing. strojarstva
Đuro Đaković Specijalna vozila d.d., HR-3500 Slavonski Brod

Pregledni članak / Subject review

Sažetak: U radu je obrađeno označivanje željeznih ljevova po europskim standardima koje je uvedeno kao standard DIN EN 1560 od 1997. Europski sustav označivanja sastoji se iz šest pozicija koje su kombinacija slovnih oznaka i brojčanih podataka na temelju svojstava materijala. U tablicama su dani opći podaci te pregledno nove i stare oznake sa svojstvima za čelične, sive i nodularne ljevove, kao i za temper ljevove.

Ključne riječi: željezni ljevovi, označivanje, europski standardi, primjeri

Abstract: This paper gives an overview of the designation systems for cast irons by european standards which was introduced through standard DIN EN 1560 from 1997. European designation system for cast irons consist of on six positions which are combinations of letter symbols and numbers on the basis of materials properties. In the tables are given information in general and clearly laid-out new and old designations with properties for cast steel, for grey cast irons, for spheroidal graphite cast irons and for malleable cast irons.

Key words: cast irons, designation, european standards, examples

1. UVOD

U radovima prvog autora i suradnika [1, 2, 3] predstavljeno je označivanje čelika po europskim standardima uz kratke komentare iz četiri najvažnija standarda i to:
1. EN 10020 : 2000 – Definicije i razredba vrste čelika,
2. EN 10027–1 : 1991 – 1. dio – Nazivi čelika, glavne oznake,
3. EN 10027–2 : 1991 – 2. dio – Brojevi čelika i
4. CR 10260 : 1998 – Dodatne oznake (uz EN 10027 – 1).

Radi kompletiranja materije o označivanju legura željeza prema europskim standardima u ovom radu je predstavljeno označivanje željeznih ljevova prema svojstvima i to za čelične, sive i nodularne, kao i za temper ljevove. Europski sustav označivanja željeznih ljevova uveden je 1997. godine u standardu: DIN EN 1560 "Ljevarstvo – sustav označivanja za željezne ljevove – oznake materijala i brojevi materijala [3, 4].

2. OZNAČIVANJE ŽELJEZNIH LJEVOVA SLOVNIM OZNAKAMA

Oznaka materijala se sastoji iz najviše šest pozicija (mjesta), koje su kombinacija slovnih oznaka i brojčanih podataka na temelju svojstava materijala. Neke od tih pozicija moraju obvezno biti ispunjene. Pojedine pozicije u oznaci se odvajaju crticama – **primjer 1: EN – GJS – 400 – 15 – LT – U**.
Objašnjenje europskog sustava označivanja željeznih ljevova i danog primjera oznaka materijala pokazano je pregledno u tablici 1 [3, 4].

Tablica 1. Europski sustav označivanja željeznih ljevova slovnim oznakama

Pozicija (mjesto)	Oznaka materijala	Primjer 1
1	**EN** za europski standard (može se izostaviti ako je u crtežu dan broj standarda – EN 1563 –); smije se koristiti samo za standardne materijale	EN
2	**G** za odljevak (iz njemačkog "Gussstück") **J** za željezo (iz engleskog "Iron", može se zamijeniti sa brojem "1"	GJ
3 *	Vrste grafita: L = listićav, lamelarni (engl. "lamellar") S = kuglast, nodularni (engl. "spheroidal") M = čvorast, temper (engl. "malleable")	S
4 **	Mikro – odnosno makrostruktura (opcionalno): B = crna temperna (engl. "black") W = bijela temperna (engl. "white")	- - -
5	Klasifikacija prema mehaničkim svojstvima (vlačna čvrstoća R_m u MPa i istezljivost A u % ili alternativno kroz tvrdoću) ili klasifikacija prema kemijskom sastavu (simbol elementa + zaokruženi sadržaj u %)	400 – 15 - - -
6	Dopunski zahtjev: LT = zajamčeni udarni rad loma na sniženoj temperaturi RT = zajamčeni udarni rad loma na sobnoj temperaturi	LT
Još 6	Način proizvodnje uzoraka za ispitivanje: S = posebno lijevan (engl. "separately cast") U = lijevan s odljevkom (engl. "cast – on) C = izrezan iz odljevka (engl. "casting")	U

* **Vrsta grafita** može biti označena još i slijedećim slovima:
V–vermikularan, N–bez grafita (tvrda ledeburitna mikrostruktura), Y–posebna mikrostruktura definirana u odgovarajućem standardu.

** Mikro– odnosno makrostruktura može biti i:
A–austenitna, F–feritna, P–perlitna, M–martenzitna, L–ledeburitna, Q–gašena, T–gašena i popuštena (poboljšana).

Kada se ljevovi razvrstavaju prema kemijskom sastavu, tada je prvi znak na petom mjestu X. Ako se ne naznačuje maseni udio ugljika, slijede simboli najznačajnijih legirnih elemenata slijedom opadanja udjela tih elemenata. Maseni udjeli elemenata naznačuju se u postotcima zaokruženim za cijeli broj. Brojevi se međusobno odvajaju crticama. To je slučaj kod austenitnih odljevaka i odljevaka otpornih na trošenje [5].

Primjer 1 – oznaka za nodularni lijev s vlačnom čvrstoćom od 400 MPa i minimalnom istezljivošću od 15% sa zajamčenim udarnim radom loma na sniženoj temperaturi od uzorka lijevanog sa odljevkom (dan u tablici 1).

Primjer 2 – oznaka za austenitni odljevak s kuglastim grafitom i približnog kemijskog sastava: ≤3% C, **15**% Ni, **6**% Cu i **2**% Cr uz ≈2% Si, ≈1% Mn i ≤0,25% P ima slijedeću oznaku:
EN – GJSA – XNiCuCr15 – 6 – 2.

Kada se zahtijeva naznačivanje masenog udjela ugljika, on se treba označiti njegovim postotkom puta 100 iza znaka X. Kada se željezni ljevovi trebaju klasificirati prema dodatnim dopunskim zahtjevima, tada simbol treba biti odvojen crticom od 5 mjesta:
D – primarno odljeveno stanje, **H** – toplinski obrađen odljevak, **W** – zavarljivost za zavareno mjesto, **Z** – dodatni zahtjevi specificirani u narudžbi.
Označivanje željeznih ljevova slovnim oznakama prema europskom sustavu dobro je razumljivo i jednoznačno s dosadašnjim oznakama po DIN-u.
Slično je također i označivanje po međunarodnom ISO-sustavu. Ipak su novi sustavi označivanja nešto kompliciraniji od starih sustava, te bi osobito kod malih dijelova bio poželjan po mogućnosti kraći sustav označivanja.
Oznaka iz navedenog primjera 1 (tablica 1) za nodularni lijev s R_m = min. 400 MPa, A_5 = min. 15% i zajamčenim udarnim radom loma na sniženoj temperaturi od ispitnog uzorka lijevanog s odljevkom, izgleda po ISO-sustavu ovako:
$\underbrace{\text{ISO1083}}_{1}/\underbrace{\text{JS}}_{2}-\underbrace{400-15}_{3}/\underbrace{\text{LT}-\text{U}}_{4}$, tj. manji je broj pozicija i nema slova "G" (pozicije 1, 2, 3, a pozicija 4 je umjesto 6 po EN).

Primjer 3 – oznaka za sivi lijev s lamelarnim grafitom, posebno lijevani uzorak:
EN – GJL – 200C s R_m = min. 200 MPa, standardni materijal,

Primjer 4 – oznaka za crni temper lijev, uzorak izrezan iz odljevka:
EN – GJMB – 550 – 4C s R_m = min. 550 MPa, A_5 = min. 4%, standardni materijal.

3. OZNAČIVANJE ŽELJEZNIH LJEVOVA BROJEVIMA MATERIJALA

Za označivanje željeznih ljevova brojevima materijala koristi se devet mjesta (tablica 2) [3, 5, 6].

Tablica 2. Označivanje željeznih ljevova brojevima materijala

Pozicija (mjesto)	1	2	3	4	5	6	7	8	9
Oznaka	E	N	-	V	V	n	n	n	n

V – veliko slovo, n – arapski brojevi ovisno o mjestu

Mjesto 1 do 3: EN – kod brojčanog označivanja materijala (npr. EN – JL1020) potrebno je navesti broj dotične norme pri čemu se oznaka ubacuje između EN i crtice:

npr. EN 1561–JL1020, gdje znače: EN – standardni materijal; DIN EN 1561 broj norme; JL sivi lijev s listićavim grafitom; 1020 : 1–vlačna čvrstoća; 02–broj materijala u skupini; 0 – nema posebnih uvjeta.

Mjesto 4: J

Mjesto 5: Oznaka za oblik grafita ili vrstu mikrostrukture: L–listićav; S–kuglast; M–čvorast (temper); V–vermikularan; N–bez grafita – tvrda ledeburitna mikrostruktura; Y–posebna mikrostruktura definirana u odgovarajućem standardu.

Mjesto 6: Oznaka za jedno od osnovnih svojstava lijeva: 0–rezervirano; 1–vlačna čvrstoća; 2–tvrdoća; 3–kemijski sastav; 4 do 9 rezervirano.

Mjesto 7 i 8: Dvoznamenkasta oznaka od 00 do 99 reprezentira pojedinu vrstu materijala.

Mjesto 9: Oznaka za posebne uvjete za dotični materijal.
0–nema posebnih uvjeta; 1–posebno lijevan ispitni uzorak; 2–ispitni uzorak lijevan zajedno s odljevkom; 3–ispitni uzorak izrezan od odljevka; 4–udarni rad loma pri sobnoj temperaturi; 5–udarni rad loma pri sniženoj temperaturi; 6–specificirana zavarljivost; 7–odljevak; 8–toplinski obrađen odljevak; 9–dodatni zahtjevi navedeni u narudžbi ili kombinacija pojedinačnih zahtjeva.

4. USPOREDBA STANDARDA

U tablici 3 dana je usporedba standarda za željezne ljevove (novih i starih).

Tablica 3. Usporedba novih i starih standarda za željezne ljevove [3, 4]

Grupa materijala	Oznaka i broj standarda			
	EN (europska)	ISO (međunarodna)	stara DIN	stara HRN
Sivi lijev s lamelarnim grafitom	DIN EN1561: 1997	ISO 185:1988 (u reviziji)	DIN 1691 (povučen)	HRN C.J2.020: 1987
Temper lijev	DIN EN 1562: 1997	ISO 5922:1981 (u reviziji)	DIN 1692 (povučen)	HRN C.J2.021: 1987
Nodularni lijev (kuglasti grafit)	DIN EN 1563: 1997	ISO 1083:1987 (u reviziji)	DIN 1693 (povučen)	HRN C.J2.022: 1987
Bainitni lijev s kuglastim grafitom	DIN EN 1564: 1997	ISO/CD 17804 (prednacrt)	nije bio	nije bio
SiMo-lijev s kuglastim ili vermikularnim grafitom	nije bio	nije bio	nije bio	nije bio
Lijev s vermikularnim grafitom	nije bio	ISO/WD 16112 (prednacrt)	VDG-List W50 ASTM A842-85 (USA)	nije bio
Austenitni željezni lijev	DIN EN 13835: 2003	ISO 2892:1973 (u reviziji)	DIN 1694 (povučen)	nije bio
Željezni lijev otporan na trošenje	DIN EN 12513: 2000	ISO/CD 21988 (prednacrt)	DIN 1695 (povučen)	nije bio
Sirovo željezo	DIN EN 10001: 1991	ISO 9147:1987	nije bio	HRN C.J2.010: 1982 (sivo ljevaoničko)
SUSTAV OZNAČIVANJA	DIN EN 1560: 1997	ISO/TR 15931 (prednacrt)	DIN 17007-3 (povučen)	prema starim standardima

5. TABLICE S OZNAKAMA I SVOJSTVIMA ŽELJEZNIH LJEVOVA

U tablicama 4 do 7 dane su usporedbe nove i stare oznake za čelične, sive i nodularne ljevove, te za temper ljevove.

Tablica 4. Klasifikacija i zajamčena svojstva nelegiranog čeličnog lijeva [5]

Oznaka lijeva prema			R_m, MPa	$R_{p0,2}$, MPa	A_5 min, %	Z min, %	KU min, J	R_e / R_m	% C	Kritična debljina stjenke, mm
EN	stara									
	HRN	DIN								
GS185N GS185KRN	ČL0300 ČL0301	GS-38 GS-38.3	370	185	25	35	- 35	0,5	<0,25	13,5
GS225N GS225JRN	ČL0400 ČL0401	GS-45 GS-45.3	440	225	22	30	- 28	0,5	≈0,25	18,5
GS255N GS255JRN	ČL0500 ČL0501	GS-52 GS-52.3	510	255	18	25	- 21	0,5	≈0,30	27
GS295N GS295JRN	ČL0600 ČL0601	GS-60 GS-60.3	590	295	15	-	- 14	0,5	≈0,40	39
GS345J0N GS345J2N	ČL0602 ČL0603	GS-62 GS-62.3	610	345	15	-	- 14	0,55	≈0,40	
GS410N	ČL0700	GS-70	690	410	12	-	-	0,6	≈0,50	

Tablica 5. Klasifikacija i čvrstoćna svojstva standardiziranih vrsta sivog lijeva [5]

Oznaka lijeva prema			R_m, MPa za ispitni uzorak ϕ 30 mm	R_{ms}, min MPa	Raspon oslonaca pri savijanju L, mm
EN	stara				
	HRN	DIN			
EN-GJL100S	SL 100	GG-10	100…150	-	400, d = 20 mm
EN-GJL150S	SL 150	GG-15	150…200	310	400, d = 20 mm
EN-GJL200S	SL 200	GG-20	200…250	380	400, d = 20 mm
EN-GJL250S	SL 250	GG-25	250…290	450	400, d = 20 mm
EN-GJL290S	SL 300	GG-30	290…340	470	400, d = 20 mm
EN-GJL340S	SL 350	GG-35	340…390	530	600, d = 30 mm
EN-GJL390S	SL 400	GG-40	> 390	590	600, d = 30 mm

R_m - vlačna čvrstoća; R_{ms} - savojna čvrstoća u MPa

Tablica 6. Oznake i zajamčena svojstva standardiziranih vrsta nodularnog lijeva [7]

Oznake po EN		Stare oznake		Vlačna čvrstoća MPa	Granica razvlačenja MPa	Istezanje A_5, min. %	Tvrdoća HB
kombinirane	brojčane	HRN	DIN				
EN-GJS-350-22 LT	EN-JS 1015			350	220	22	150-170
EN-GJS-350-22 RT	EN-JS 1014	NL 370-17	GGG-35.3	350	220	22	
EN-GJS-350-22	EN-JS 1010			350	220	22	
EN-GJS-400-18 LT	EN-JS 1025			400	240	18	160-170
EN-GJS-400-18 RT	EN-JS 1024	NL 400-12	GGG-40.3	400	250	18	
EN-GJS-400-18	EN-JS 1015		GGG-40	400	250	19	160-190
EN-GJS-400-15	EN-JS 1030			400	250	15	
EN-GJS-450-10	EN-JS 1040			400	310	10	
EN-GJS-500-7	EN-JS 1050	NL 500-7	GGG-50	500	320	7	190-210
EN-GJS-600-3	EN-JS 1060	NL 600-3	GGG-60	600	370	3	210-230
EN-GJS-700-2	EN-JS 1070	NL 700-2	GGG-70	700	420	2	230-240
EN-GJS-800-2	EN-JS 1080	NL 800-2	GGG-80	800	480	2	240-260
EN-GJS-900-2	EN-JS 1090		GGG-90	900	600	2	260-280

Tablica 7. Standardizirane vrste crnog i bijelog temper lijeva i propisana mehanička svojstva [3, 5]

Oznaka lijeva prema			R_{m*}, min MPa	$R_{p0,2}$* min, MPa	A_5*, min %	HB	Mikrostruktura
EN	stara						
	HRN	DIN					
EN-GJMB-300-6S	CTEL 30-06	GTS-30	300	-	6	< 170	ferit + grafit
EN-GJMB-350-10S	CTEL 35-10	GTS-35	350	200	12	< 150	ferit + grafit
EN-GJMB-450-6S	CTEL 45-06	GTS-45	450	300	7	160…200	perlit + ferit + grafit
EN-GJMB-550-4S	CTEL 55-04	GTS-55	550	360	5	180…250	perlit + (ferit) + grafit
EN-GJMB-650-2S	CTEL 65-02	GTS-65	650	430	3	210…250	perlit + grafit
EN-GJMB-700-2S	CTEL 70-02	GTS-70	700	550	2	240…270	perlit + grafit
EN-GJMW-350-4S	BTEL 35-04	GTW-35	340…360*	-	3…6*	220	zrnati perlit + grafit
EN-GJMW-380-12S	BTEL 38-12	GTW-S38	320…400	170…210	8…15	200	
EN-GJMW-400-5S	BTEL 40-05	GTW-40	360…420	200…230	3…10	220	
EN-GJMW-450-7S	BTEL 45-07	GTW-45	400…480	230…280	5…12	200	

* Vrijednosti R_m, $R_{p0,2}$ i A_5 ovise o dimenzijama ispitnog uzorka. Istezljivost je to viša što je tanja stjenka.
- GJMB – crni temper ljevovi
- GJMW – bijeli temper ljevovi

6. ZAKLJUČAK

Preuzimanjem sustava označivanja željeznih ljevova prema europskim standardima zemlje u tranziciji prave važan iskorak prema europskim integracijama. Ovaj sustav trebaju što prije usvojiti i primjenjivati u uporabi kako stručnjaci u raznim industrijskim grupacijama, tako i nastavnici na svim stupnjevima tehničke stručne izobrazbe kadrova. U prijelaznom periodu treba pored novih oznaka po EN, koristiti i stare oznake ljevova po HRN i DIN-u.

LITERATURA

[1] Vitez I., Kladarić I., Sebastijanović S.: Prilog označivanju čelika po europskim standardima, 5th International scientific Conference RIM 2005 – SCIENTIFIC BOOK, 111-116, Bihać, Bosna i Hercegovina, 14-17.09.2005.

[2] Vitez I., Kladarić I., Marković R.: Europske norme za nove sustave označivanja čelika, Tehnički vjesnik 10 (2003) (1), 49-61.

[3] Vitez I., Kladarić I., Marušić, V.: Osnovi proizvodnje i označivanja metala, Strojarski fakultet, Slavonski Brod, 2008.

[4] *** Gießereitechnische Normung, Gusseisen- und Stahlgusswerkstoffe, Stand: 16.06.2002., VDG-Fachgruppe 5 Normung, Verein Deutscher Giessereifachleute e.V.

[5] Filetin T., Kovačiček F., Indof J.: Svojstva i primjena materijala, FSB-Zagreb, 2002.

[6] Zupančič D.: Označevanje materialov, Strojniški vestnik, 46, 2000, 1, 53-56.

[7] Vitez I., Novoselović D.: Prilog kontroli kvalitete nodularnog lijeva, Ljevarstvo 48 (2006) 1, 9-13.

UTJECAJ OMJERA POČETNIH KONCENTRACIJA OLOVA I CINKA U BINARNIM VODENIM OTOPINAMA NA NJIHOVO UKLANJANJE NA PRIRODNOM ZEOLITU

THE EFFECT OF INITIAL CONCENTRATION RATIO OF LEAD AND ZINC IN A BINARY METAL ION SOLUTION FOR THEIR REMOVAL ON NATURAL ZEOLITE

N. Vukojević Medvidović, J. Perić, M. Trgo, I. Nuić
Sveučilište u Splitu, Kemijsko-tehnološki fakultet u Splitu, Teslina 10/V, 21000 Split, Croatia

Izvorni znanstveni rad / Original scientific paper

Abstract:
The removal of lead and zinc ions from a binary aqueous solution using a fixed bed of natural zeolite - clinoptilolite has been examined. Experiments were carried out in a glass laboratory column at isothermal conditions. The total initial concentration of binary metal ion solution was kept constant, while the concentration ratios for lead and zinc were Pb / Zn = 0.68, 1.08 and 2.04. The results are shown by breakthrough curves. Based on their shape, it has been assumed that ions of both metals bind simultaneously until the breakthrough point. As the process progresses, the lead ions bind in greater quantities than the zinc ions, which can be attributed to the displacement of bound zinc. This is confirmed by the regeneration curve, where the quantity of eluted lead is significantly higher than that of zinc. The parameters of breakthrough curves and regeneration curves (q_B, q_E, n_S, n_B, n_R) have been calculated by graphical integrations.

Keywords: binary solution, lead, zinc, natural zeolite, column method

Sažetak:
Ispitano je uklanjanje olova i cinka iz binarnih vodenih otopina na prirodnom zeolitu - klinoptilolitu postupkom u koloni. Eksperimenti su provedeni u laboratorijskoj staklenoj koloni pri izotermnim uvjetima. Ukupna početna koncentracija binarne vodene otopine održavana je približno konstantnom, dok su odnosi koncentracija olova i cinka u otopini mijenjani od Pb / Zn = 0.68, 1.08 i 2.04. Rezultati su prikazani krivuljama proboja. Na temelju njihovog oblika pretpostavljeno je da se do točke proboja oba metalna iona vezuju istovremeno. Kako proces napreduje, olovo se vezuje u većoj količini, pri čemu vjerojatno istiskuje već vezane ione cinka na zeolitu. Ovo je potvrđeno krivuljama regeneracije iz kojih je izračunata veća količina eluiranog olova u odnosu na cink. Karakteristični parametri krivulja proboja i regeneracije (q_B, q_E, n_S, n_B, n_R) izračunati su grafičkom integracijom.

Ključne riječi: binarna otopina, olovo, cink, prirodni zeolit, postupak u koloni

1. UVOD

Otpadne vode iz mnogih industrija poput metalurgije, industrije prerade i površinske zaštite metala, kemijske industrije, industrije papira, boja, lakova, tekstilne industrije, rafinerije, petrokemije itd. su onečišćene teškim metalima. Vrijednosti dopuštenih koncentracija teških metala u otpadnim vodama koje se mogu ispustiti u kanalizaciju ili prirodne prijamnike su vrlo niske, pa je za njihovo uklanjanje potrebno koristiti vrlo skupe sofisticirane tehnike. Nadalje, većina industrijskih otpadnih voda obično sadrži više teških metala u smjesi, te je nužno ispitati i razviti nove metode njihova uklanjanja. Istraživanja su usmjerena na istovremeno uklanjanje dvaju ili više metalnih iona na različitim adsorbensima. Rezultati novijih istraživanja pokazuju da se uklanjanje više teških metala može uspješno provesti korištenjem prirodnih zeolita [1-6]. U ovom je radu ispitan utjecaj omjera početnih koncentracija olova i cinka u binarnim vodenim otopinama na njihovo uklanjanje na prirodnom zeolitu klinoptilolitu.

2. EKSPERIMENT

Uzorak prirodnog zeolita porijeklom je iz depozita Vranjska Banja (Srbija), s udjelom zeolitne mineralne komponente - klinoptillolita > 80 %. Uzorak je analiziran, samljeven i prosijan na veličinu čestica 0.6-0.8 mm, te sušen pri 60 ^{o}C, te analiziran na kemijski i mineraloški sastav [7-9].

Binarne vodene otopine olova i cinka iste ukupne početne koncentracije, a različitog omjera koncentracija Pb / Zn = 0.68, 1.08 i 2.04 pripravljene su otapanjem $Pb(NO_3)_2$ i $Zn(NO_3)_2$ u redestiliranoj vodi. Točne početne koncentracije olova i cinka u otopini određene su kompleksometrijski, korištenjem visokoselektivnih indikatora [10].

Eksperimenti su provedeni u staklenoj koloni unutarnjeg promjera 12 mm i visine 500 mm, ispunjenoj s uzorkom zeolita do visine od 40 mm, a što odgovara volumenu sloja zolita od 4.52 cm^3, odnosno masi od 2.9 g. Binarna vodena otopina propuštana je kroz sloj zeolita od vrha prema dnu u koloni (tzv. down flow mode), uz protok od 1 ml/min.

Nakon svakog radnog ciklusa proveden je ciklus regeneracije s otopinom $NaNO_3$ koncentracije 176.5 mmol/l i protoka od 1 ml/min. U odabranim vremenskim intervalima na izlazu iz kolone tijekom radnog ciklusa i ciklusa regeneracije sakupljani su uzorci efluenta, u kojima je određena koncentracija olova i cinka. U tablici 1. su prikazani eksperimentalni uvjeti provedbe radnog ciklusa.

Tablica 1. Eksperimentalni uvjeti radnog ciklusa.

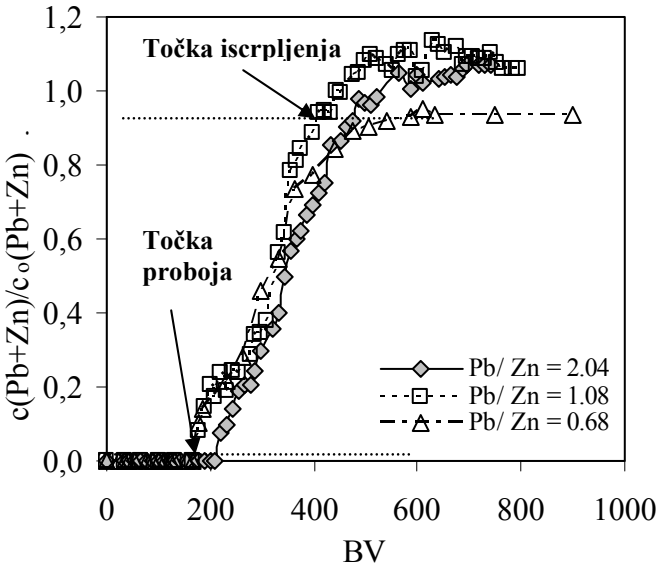
Oznaka ciklusa	c_o(Pb+Zn), mmol/l	c_o(Pb), mmol/l	c_o(Zn), mmol/l
Pb / Zn = 2.04	1.085	0.728	0.357
Pb / Zn = 1.08	1.115	0.578	0.537
Pb / Zn = 0.68	1.136	0.461	0.675

3. REZULTATI I RASPRAVA

Tijek radnog ciklusa i ciklusa regeneracije praćen je određivanjem ukupne i pojedinačnih koncentracija olova i cinka u efluentu. Eksperimentalni rezultati tijekom radnog ciklusa grafički su prikazani krivuljama proboja tj. kao ovisnosti ukupne i pojedinačnih

koncentracija metalnih iona u efluentu (c/c_o) o vremenu ili BV-u otopine koja je prošla kroz sloj. Vrijednost BV izračunata je kao omjer volumena otopine protekle u određenom vremenu i volumena sloja zeolita u koloni.

Na slici 1. prikazane su krivulje proboja za binarne otopine različitih omjera koncentracija olova i cinka.



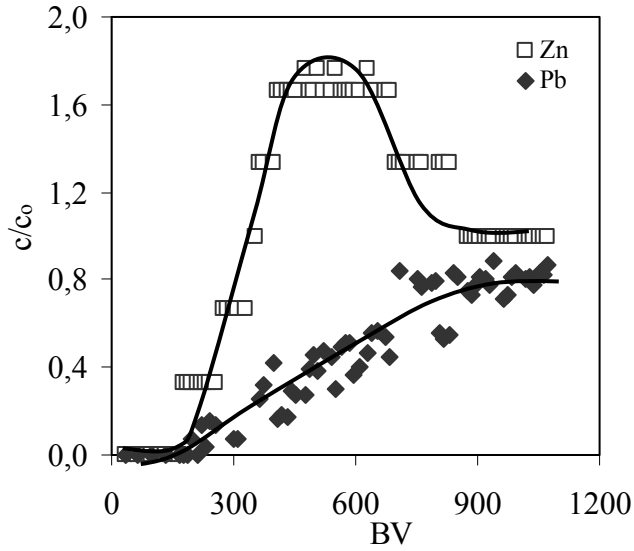
Slika 1. Krivulje proboja za binarne otopine različitih omjera koncentracija olova i cinka.

Točke proboja za sve tri krivulje su vrlo bliske, nakon čega vrijednosti c/c_o rastu do točke iscrpljenja. Pri tome kod omjera Pb/Zn = 0.68, vrijednosti c/c_o kontinuirano rastu do $c/c_o \approx 1$, dok za omjere Pb/Zn = 1.08 i 2.04, vrijednosti c/co > 1. To je neočekivano, jer znači da ukupna koncentracija određena u efluentu je veća od ukupne koncentracije ulazne otopine.

Iz tog razloga su analizirane krivulja proboja pojedinačnih iona olova i cinka za omjer Pb/Zn = 1.08, a što je prikazano na slici 2.

Krivulja proboja za cink ima oštar nagib i postiže maksimalnu vrijednost $c/c_o = 1.766$, nakon čega ova vrijednost pada i postaje konstantna kod $c/c_o = 1$. Krivulja proboja olova je znatno položenija, tj. ima manji nagib nego krivulja za cink. Vrijednosti c/c_o za olovo kontinuirano rastu do ujednačene vrijednosti od $c/c_o \approx 0.8$.

Ovakav oblik krivulja proboja može se objasniti vezivanjem obaju metalnih iona na zeolitu do točke proboja, nakon čega se olovo vjerojatno vezuje u znatno većoj količini u odnosu na cink. Kako proces vezivanja olova napreduje, on zbog svojeg većeg afiniteta izmjene istiskuje cink iz zeolita, te koncentracija cinka u efluentu raste. Zato je koncentracija cinka u efluentu i do 70 % veća od koncentracije u ulaznoj otopini. Kako je izmjena iona cinka s ionima olova na zeolitu spora, krivulja proboja za olovo je znatno položenija, a točka iscrpljenja za olovo, kako se vidi na slici 2, postiže se tek kod vrijednosti BV > 800. Ovaj efekt međusobnog istiskivanja metalnih iona kod njihova uklanjanja iz binarnih vodenih otopina posljedica je različite selektivnosti zeolita prema metalnim ionima, kao i različitog afiniteta izmjene metalnih iona na zeolitu.



Slika 2. Pojedinačne krivulje proboja pri omjeru koncentracija Pb/Zn = 1.08.

Kapaciteti q_B i q_E izračunati su prema metodi koju je predložio Michaels [1, 11]. Prema ovoj metodi, kapacitet u točki proboja q_B određuje količinu metalnih iona vezanih na zeolitu do točke proboja u mmol/g, a kapacitet u točki zasićenja q_E predstavlja količinu metalnih iona koja se vezala na zeolitu do točke zasićenja u mmol/g. Grafičkom integracijom površine iznad krivulje proboja prema jednadžbama (1) i (2) izračunati su kapaciteti q_B i q_E, a vrijednosti su date u tablici 1.

$$q_B = \frac{\int_0^{V_B} (c_o - c)dV}{\rho \cdot H \cdot A} = \frac{c_o \cdot V_B}{m} \qquad (1)$$

$$q_E = \frac{\int_0^{V_E} (c_o - c)dV}{\rho \cdot H \cdot A} = \frac{\int_0^{V_E} (c_o - c)dV}{m} \qquad (2)$$

gdje je:

c_o - koncentracija Pb i/ili Zn u influentu, mmol/l; c - koncentracija Pb i/ili Zn u vremenu t, mmol/l; V_B - volumen efluenta do točke proboja, l; V_E - volumen efluenta u točki zasićenja, l; m - masa zeolita u koloni, g; ρ - gustoća sloja zolita, g/m^3; H - visina sloja zeolita u koloni, m; A - površina poprečnog presjeka kolone, m^2.

Kako procjena vrijednosti volumena u točki proboja V_B i točki zasićenja V_E iz krivulje proboja može biti nepouzdana, ta se poteškoća prevladava općenitim pravilom da V_B predstavlja volumen efluenta u kojem koncentracija metalnog iona postiže vrijednost 5 % od koncentracije u influentu, a V_E volumen u kojem koncentracija metalnog iona postiže vrijednost 95 % od koncentracije u influentu.

Iz tablice 1. uočava se da vrijednosti ukupnog kapaciteta olova i cinka q_B i q_E neznatno rastu s porastom udjela olova u influentu. Međutim, vrijednosti kapaciteta za olovo i cink u točki proboja su različite, i ovise o omjeru koncentracija olova i cinka u influentu. Kako

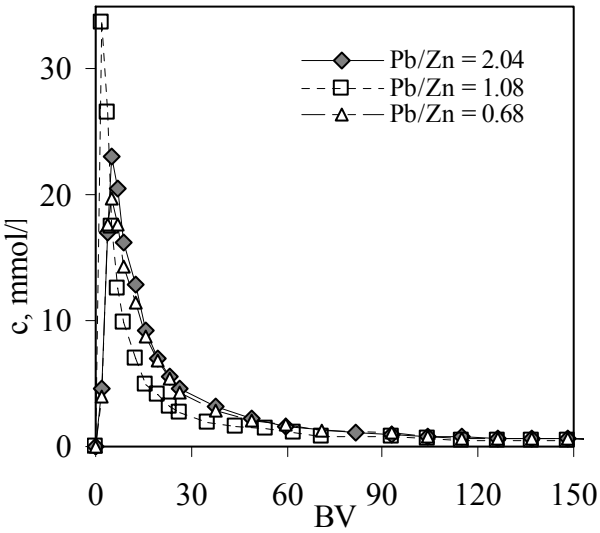
proces napreduje, to vrijednost kapaciteta u točki zasićenja (q_E) za olovo raste u odnosu na cink, što potvrđuje našu pretpostavku da olovo istiskuje cink tijekom radnog ciklusa.

Tablica 1. Kapaciteti q_B i q_E izračunati iz ukupne i pojedinačnih krivulja proboja olova i cinka u efluentu.

Oznaka ciklusa		V_B, BV	V_E, BV	q_B, mmol/g	q_E, mmol/g
Pb / Zn = 2.04	Pb+Zn	221	486	0.373*	0.588*
	Pb			0.232	0.469
	Zn			0.114	0.091
Pb / Zn = 1.08	Pb+Zn	177	420	0.315*	0.544*
	Pb			0.139	0.318
	Zn			0.146	0.196
Pb / Zn = 0.68	Pb+Zn	176	441	0.291	0.533
	Pb			0.127	-
	Zn			0.186	-

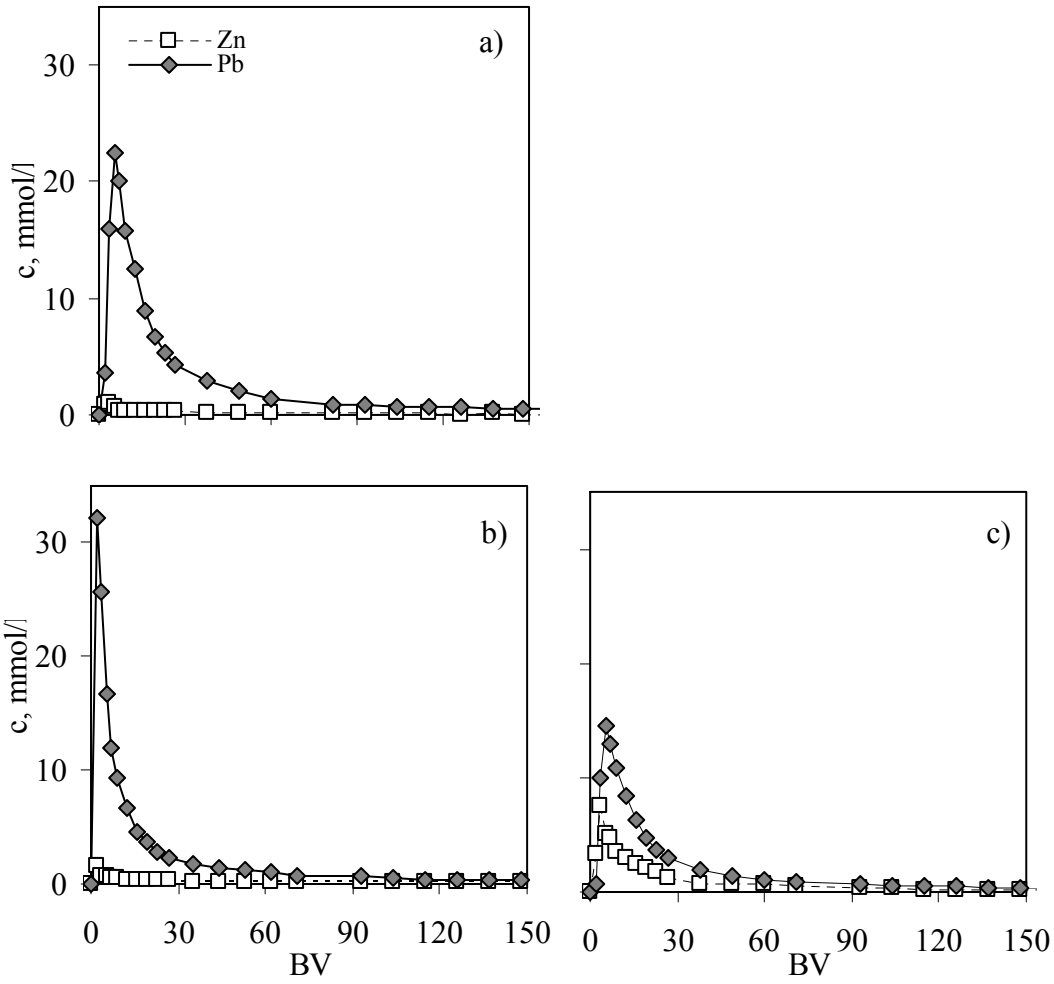
* *Mala odstupanja q(Pb+Zn) = q(Pb) + q (Zn) su posljedica grafičke integracije.*

Nakon radnog ciklusa proveden je ciklus regeneracije kojim se vezani ioni cinka i olova eluiraju iz kolone, a zeolit se obnavlja za sljedeći radni ciklus. Rezultati određivanja koncentracija cinka i olova u efluentu tijekom ciklusa regeneracije su prikazani krivuljama regeneracije na slici 3.



Slika 3. Krivulje regeneracije za binarne otopine različitih omjera koncentracija olova i cinka.

Sve krivulje regeneracije prvo pokazuju nagli porast ukupne koncentracije, nakon čega ta vrijednost pada do približno konstantne vrijednosti od ≈ 0.5 mmol/l. Za potpunu regeneraciju sloja zeolita utrošeno je 90-100 BV otopine za regeneraciju u sva tri slučaja. Krivulje regeneracije dobivene preko praćenja koncentracija u efluentu za svaki pojedini metalni ion prikazane su na slici 4. Uočava se da su krivulje regeneracije za olovo znatno izraženije u odnosu na krivulje regeneracije za cink, što ukazuje da je na zeolitu najvećim dijelom bilo vezano olovo.



Slika 4. Krivulje regeneracije za binarne otopine različitih omjera koncentracija olova i cinka: a) Pb / Zn = 2.04; b) Pb / Zn = 1.08; c) Pb / Zn = 0.68.

Količine eluiranih metalnih iona iz sloja zeolita tijekom ciklusa regeneracije n_R izračunate su grafičkom integracijom površina ispod krivulja regeneracije za cink i olovo na slici 4., a prema jednadžbi (3) [12]:

$$n_R = \int_0^{V_R} c \, dV \tag{3}$$

gdje je:

c - koncentracija Pb i/ili Zn u efluentu u vremenu t, mmol/l

n_R - ukupna količinu Pb i/ili Zn koja se procesom regeneracije uklonila iz zeolita, mmol

V_R - volumen efluenta u točki kada se proces regeneracije prekida, l.

Količine eluiranih metalnih iona iz sloja zeolita tijekom ciklusa regeneracije n_R uspoređene su sa količinama metalnih iona unešenih u kolonu s otopinom n_S, i količinama metalnih iona vezanih na sloju do točke proboja, n_B, a grafički su prikazane na slici 5. Vrijednosti n_S i n_B su izračunate prema jednadžbama (4) i (5) [12]:

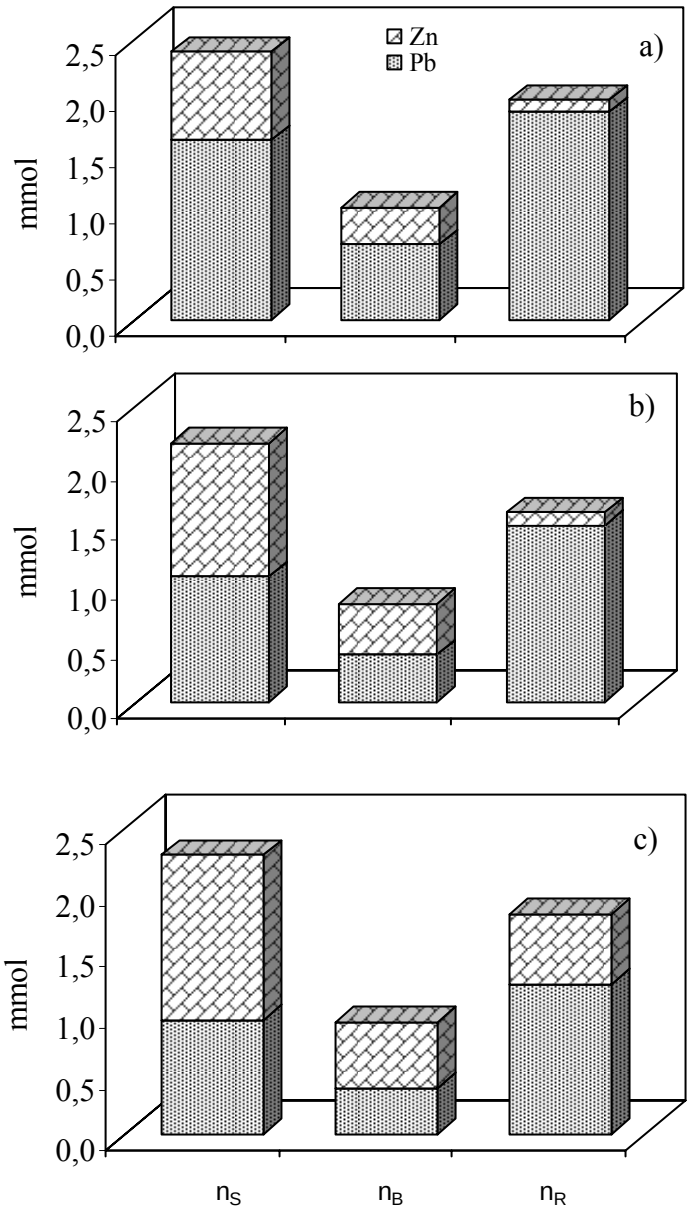
$$n_B = q_B \cdot m \tag{4}$$

$$n_S = c_o \cdot Q \cdot t_E \tag{5}$$

gdje je:

n_B - ukupna količina Pb i/ili Zn vezanih na zeolitu do točke proboja, mmol
n_S - ukupna količina Pb i/ili Zn unešena s otopinom u kolonu, mmol
Q - protok otopine, l/h
t_E - vrijeme do točke zasićenja, h.

Usporedba n_S, n_B i n_R pri uklanjanju olova i cinka na zeolitu iz binarnih vodenih otopina različitih omjera pojedinačnih početnih koncentracija prikazana je na slici 5.



Slika 5. Usporedba n_S, n_B i n_R za binarne otopine različitih omjera koncentracija olova i cinka: a) Pb / Zn = 2.04; b) Pb / Zn = 1.08; c) Pb / Zn = 0.68.

Uočava se da su količine eluiranog cinka n_R znatno manje od količine eluiranog olova što ukazuje da je na zeolitu najvećim dijelom bilo vezano olovo, a čime se potvrđuje pretpostavljeni efekt istiskivanja cinka tijekom radnog ciklusa.

Zahvala

Prikazani rezultati proizašli su iz znanstvenog projekta "Prirodni zeoliti u zaštiti voda" kojeg financijski podupire Ministarstvo znanosti, obrazovanja i športa Republike Hrvatske, te im se ovim putem zahvaljujemo.

Literatura:

[1] L. D. Benefield, J. F. Judkins, B. L. Weand, Process chemistry for water and wastewater treatment, New Jersey: Prentice-Hall, Inc (1982) 307-399.
[2] A. Groffman, S. Peterson, D. Brookins, Removing lead from wastewater using zeolites, Water Environ. Technol. 4 (1992) 54-59.
[3] M. Pansini, Natural zeolites as cation exchangers for environmental protection, Mineral. Deposita 31 (1996) 563-575.
[4] J. Perić, M. Trgo, N. Vukojević Medvidović, Removal of zinc, copper and lead by natural zeolites - a comparison of adsorption isotherms, Water Res. 38 (2004) 1893-1899.
[5] S. Ahmed, S. Chughtai and M. A. Keane, The removal of cadmium and lead from aqueous solution by ion exchange with Na-Y zeolite, Sep. Purif. Technol. 13 (1998) 57-64.
[6] M. A. Keane, Role of the alkali metal co-cation in the ion exchange of Y zeolites III. Equilibrium properties of the Ni/Cu/Na-Y and Ni/Cu/K-Y zeolite systems, Microporous Mater. 4 (1995) 359-368.
[7] I. Voinovitch, J. Debrad-Guedon, J. Louvrier, The Analysis of Silicates, Israel Program for Scientific Translations, Jerusalem (1966) 127-129.
[8] Databases JCPDS, International Center for Diffraction Data, Philips Analytical (1993).
[9] M. M. J. Treacy, J. B. Higgins, Collection of Simulated XRD Power Patterns for Zeolites, 4th revised ed., Elsevier /Structure Commission of the International Zeolite association, The Netherlands (2001) 182-185, 368.
[10] Complexometric Assay Methods with Triplex, E. Merck (ed.) Darmstadt (1982) 76-77.
[11] N. Vukojević Medvidović, J. Perić, M. Trgo, Column performance in lead removal from aqueous solution by fixed bed of natural zeolites-clinoptilolite, Sep. Purif. Technol. 49 (2006) 237-244.
[12] N. Vukojević Medvidović, J. Perić, M. Trgo, M.N. Mužek, Removal of lead ions by fixed bed of clinoptilolite – The effect of flow rate, Microporous Mesoporous Mat. 105 (2007) 298-304.

PONAŠANJE PORTLAND CEMENTNOG MORTA S DODATKOM LETEĆEG PEPELA U OKOLIŠU SULFATA

BEHAVIOUR OF FLY ASH – BASED MORTARS IN SULPHATE ENVIRONMENTAL

Jelica Zelić, Jelena Ninčević, Dražan Jozić & Draga Krpan-Lisica
Sveučilište u Splitu, Kemijsko-tehnološki fakultet, teslina 1o/5, 21 000 Split, Hrvatska
E-mail: zelic@ktf-split.hr

Izvorni znanstveni rad / Original scientific paper

Sažetak: U radu je ispitivan utjecaj letećeg pepela iz termoelektrane ložene ugljenom (TE Plomin 2, Plomin, Hrvatska) na otpornost cementnog morta izloženog 280 dana djelovanju agresivnog okoliša 5 % otopine Na_2SO_4. Ispitivanja su provedena mjerenjem promjena tlačne čvrstoće i mase uzoraka morta, te određivanjem sadržaja slobodnog $Ca(OH)_2$ i ukupno kemijski vezane vode u ovisnosti o dodatku letećeg pepela (5-40 mas. %). Prisutnost nastalih faza tijekom sulfatne korozije određena je toplinskom analizom (TG/DTG-DTA) i difrakcijom rendgenskih zraka na polikristalnim uzorcima cementnog morta. Mortovi koji sadrže više od 20 mas. % letećeg pepela pokazuju bolju sulfatnu otpornost u odnosu na mort bez dodatka letećeg pepela. Zbog manjeg sadržaja $Ca(OH)_2$ spriječeno je izluživanje vapna pa tako i nastajanje gipsa i velike količine etringita, kao produkata sulfatne korozije, što je i potvrđeno rendgenskom difrakcijskom analizom.

Ključne riječi: leteći pepeo, portland cement, sulfatna korozija, tlačna čvrstoća, mort, slobodni $Ca(OH)_2$

Abstract: In this paper, the effect of fly ash from the Plomin 2 Thermal Power Plant (Plomin, Croatia) on corrosion resistance of cement mortars exposed to sulphate attack (5 % solution of Na_2SO_4) within 280 days period has been studied. Compressive strength and mass changes, the free $Ca(OH)_2$ and total chemical bound water content of mortars as a function of fly ash content (5-40 mass %) have been investigated. The phases formed during the corrosion process have been estimated by thermal analysis (TG/DTG-DTA) and X-ray powder diffraction. The addition of fly ash results in less the $Ca(OH)_2$ content and consequently less gypsum and ettringite formed during the sulphate immersion of mortars. Mortars containing more than 20 mass % of fly ash are characterised by a better sulphate resistance than a mortar without fly ash addition, due to the absence of gypsum and the presence of small quntities of ettringite, detected by XRD analysis.

Key words: Fly ash, Portland cement,sulphate corrosion, compressive strength, mortar, free $Ca(OH)_2$

UVOD

Korozija cementnog kamena (morta/betona) je posljedica djelovanja kemijski agresivne sredine na komponente cementnog kamena, pri čemu nastaju produkti koji narušavaju njegovu strukturu i svojstva. Najveći dio prirodnih agresivnih voda s kojima beton dolazi u dodir tijekom njegove eksploatacije u prirodnom okolišu su sulfatne vode. Korozija betona uzrokovana otopinom Na_2SO_4 dovodi do konverzije produkata hidratacije cementa u etringit, gips i druge produkte korozije te do destibilizacije C-S-H gela[1]. Reakcije korozije pod utjecajem Na_2SO_4 mogu se prikazati jednadžbama (1) – (3):

$$Ca(OH)_2 + Na_2SO_4 \cdot 10\ H_2O \rightarrow CaSO_4 \cdot 2H_2O + 2NaOH + 8H_2O \quad (1)$$

$$3CaO \cdot Al_2O_3 \cdot 12H_2O + 3(CaSO_4 \cdot 2H_2O) + 14H_2O \rightarrow 3CaO \cdot Al_2O_3 \cdot 3CaSO_4 \cdot 32H_2O \quad (2)$$

$$2(3CaO \cdot Al_2O_3 \cdot 12H_2O) + 3(NaSO_4 \cdot 10H_2O) \rightarrow$$
$$\rightarrow 3CaO \cdot Al_2O_3 \cdot 3CaSO_4 \cdot 32H_2O + 2Al(OH)_3 + 6(NaOH) + 17\ H_2O \quad (3)$$

Razvojem tehnologije betona i postavljanjem sve većih zahtjeva za njegovom kakvoćom (čvrstoća, trajnost i otpornost prema korozijskim agensima), cementu se kao osnovnoj reaktivnoj komponenti betona dodaju pucolanski dodaci, kao što su filtarska SiO_2 prašina iz proizvodnje ferosilicija ("silica fume"), granulirana troska visoke peći i leteći pepeo iz termoelektrana loženim ugljenom.

Utjecaj letećeg pepela na hidrataciju portland cementa ovisi o sadržaju i vrsti letećeg pepela, odnosno o njegovoj reaktivnosti. S obzirom na sadržaj CaO, prema američkoj normnoj specifikaciji ASTM C 618, leteći pepeli se mogu svrstati u dvije glavne skupine: (i) leteći pepeli klase "F", s niskim sadržajem CaO (do 5 mas. %) i , (ii) leteći pepeli klase "C", s visokim sadržajem CaO (15 - 40 mas. %)[2].

Zbog svojih karakterističnih svojstava, leteći pepeo (LP) predstavlja pucolanski dodatak koji zapunjuje pore nastalog cementnog kompozita, te pucolanskom reakcijom reagira s $Ca(OH)_2$, nastalim tijekom hidratacije portland cementa, stvarajući na taj način čvršći i stabilniji kompozit. Rane čvrstoće betona s dodatkom letećeg pepela obično su niže, a poslije mogu biti i više od čvrstoća referentnog betona ili specificirane čvrstoće[3]. Kao posljedica prijelaza većih pora u manje, u kasnijim vremenima hidratacije, povećava se i diskontinuitet pornog sustava što vodi boljoj nepropusnosti cementnog kompozita s dodatkom LP. Prisutnost letećih pepela može utjecati na poboljšanje sulfatne otpornosti cementnog kompozita. Zamjenom dijela portland cementa s dijelom letećeg pepela smanjuje se udio slobodnog $Ca(OH)_2$ i udio minerala C_3A, važnih komponenata za proces sulfatne korozije. U pasti portland cementa s dodatkom letećeg pepela nastaju AFm faze umjesto AFt faza koje uzrokuju znatno veće bubrenje[3].

Svrha ovog rada je ispitivanje utjecaja letećeg pepela iz domaće TE Plomin 2 na ponašanje cementnog morta izloženog djelovanju Na_2SO_4. Razvoj i tijek korozije praćen je određivanjem promjena mehaničkih osobina i strukturnih promjena u uzorcima cementnog morta tijekom njihovog 280-dnevnog boravka u 5 % otopini natrijevog sulfata.

EKSPERIMENTALNI DIO

Materijali i uvjeti rada

Leteći pepeo. Dobiven je iz filtarskog postrojenja termoelektrane ložene ugljenom, TE Plomin 2, Plomin, Hrvatska. Sadrži visoki udjel (SiO_2+Fe_2O_3+Al_2O_3) od 79,37 mas. % i niski udjel CaO (2,81 mas. %). Specifična površina (Blaine) je 312,9 m^2/kg, a gustoća je 1,839 kg/m^3. Sastoji se uglavnom od amorfne, strukturno neuređene alumosilikatne faze,

a glavne kristalne faze su: kvarc, mulit i hematit[4,5]. Ova svojstva, prema ASTM C 618 i HRN EN 450, svrstavaju ga u mineralni dodatak "klase F" za primjenu u portland cementu / betonu[2,6].

Portland cement. Korišten je industrijski portland cement, oznake CEM I 42,5R (Dalmacijacement-CEMEX, Kaštel Sućurac, Hrvatska). Mineraloška analiza (Bogue) cementa je, u mas. %: C_3S = 56,38; C_2S = 18,04; C_3A = 9,30; C_4AF = 8,29. Specifična površina (Blaine) cementa je 332,90 m^2/kg, a gustoća je 2,564 kg/m^3.

Otopina Na_2SO_4. Pripravljena je 5 % otopina Na_2SO_4 otapanjem 1043,72 g $Na_2SO_4 \cdot 10H_2O$ u 9,205 dm^3 destilirane vode pri 20 ± 1 °C .

Cementni mort. Cementni mort je pripravljen prema hrvatskoj normi HRN EN 196-1[7] . Kao agregat korišten je standardni kvarcni pijesak. Omjer agregat/vezivo u svim mješavinama je bio stalan i iznosio je 3:1. Količina potrebne vode za pripravu mortova bila je promjenjiva, pa su uzorci morta izrađeni tako da imaju istu konzistenciju mjerenjem prostiranja morta na potresnom stolu u granicama od 156 – 165 mm. Mortovi s dodatkom letećeg pepela (LP) su pripravljeni zamjenom cementa s 5, 15, 20, 25, 30 i 40 mas. % LP. Oznaka mortova je kako slijedi: PB5, PB15, PB20, PB25, PB30 i PB40. Uzorak bez dodatka LP označen je kao PB0. Pripravljeni mortovi, dimenzija 40x40x160 mm, njegovani su 24 sata u klima komori (20 °C i RH = 95 %), a zatim u vodovodnoj vodi do starosti od 28 dana. Poslije 28 dana, prizmice su istovremeno uronjene u 5 % otopinu Na_2SO_4 i vodovodnu vodu na period od 280 dana. Uzorci morta uronjeni u vodovodnu vodu predstavljaju kontrolne (referentne) uzorake. U tablici 1 dat je sastav mješavine i oznaka uzoraka morta.

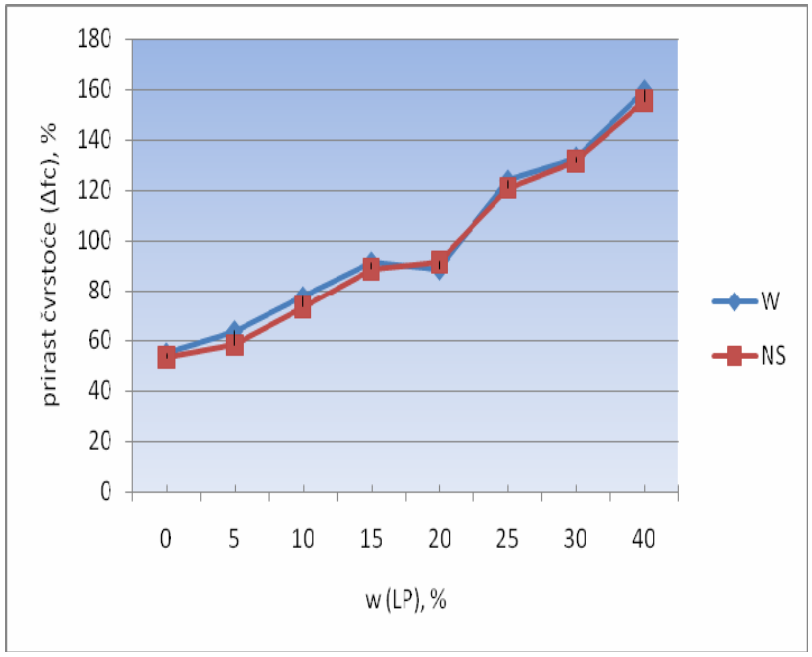
Tablica 1. Sastav i oznake uzoraka cementnog morta

Materijali	Oznake uzoraka						
	PB0	PB5	PB15	PB20	PB25	PB30	PB40
Standardni pijesak /g	2700	2700	2700	2700	2700	2700	2700
Cement /g, (c)	900	855	765	720	675	630	540
Leteći pepeo /g, (LP)	0	45	135	180	225	270	360
$V(H_2O)$ / cm^3, (v)	450	446	438	432	430	428	428
v / c	0,50	0,521	0,57	0,60	0,637	0,679	0,79
Konzistencija / mm	165	164	164	159	163	157	156
v / (LP+c)	0,50	0,495	0,486	0,48	0,477	0,475	0,475

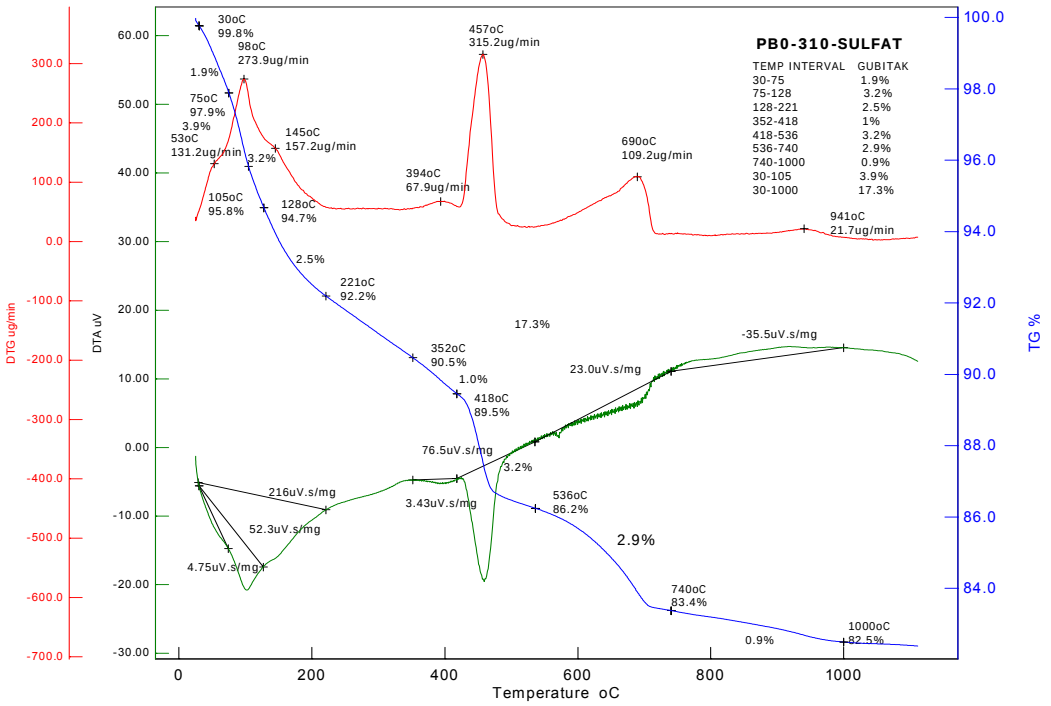
Razvoj i tijek korozije. Uzorcima cementnog morta bez i s dodatkom LP razvoj i tijek korozije praćen je određivanjem promjena tlačne čvrstoće (HRN EN 196-1) i mase uzorka (digitalna vaga, Tehnica, Exacta 1200 EB) te određivanjem sadržaja slobodnog $Ca(OH)_2$ i ukupno kemijski vezane vode za C-S-H faze primjenom toplinske analize (TG/DTG-DTA sustav Pyris Diamond, Perkin Elmer) u struji dušika (200 cm^3/min) i uz brzinu zagrijavanja od 20 ^oC/min . Difrakcijske slike polikristalnih uzoraka snimljene su pomoću uređaja PANalytica X`Pert Pro s izvorom Cu-Kα-zračenja (radni napon od 45 kV i struja jakosti 40 mA) i vertikalnim goniometrom X`Celerator, u kutnom području od $4^o \leq 2Theta \leq 60^o$. Kvalitativna i kvantitativna analiza izvedena je korištenjem ICDD (International Center for Diffraction Data) baze podataka.

REZULTATI I RASPRAVA

Na slici 1 su prikazani rezultati ispitivanja prirasta tlačne čvrstoće (Δfc, %) uzoraka morta (PB0 - PB40) poslije 280 dana izlaganja u vodovodnoj vodi (W) i u otopini Na_2SO_4 (NS). Iz slike je vidljivo da svi uzorci cementnog morta (PB0 – PB40) pokazuju isti trend povećanja tlačne čvrstoće bez obzira na uvjete njegovanja, tj. u vodovodnoj vodi i/ili u agresivnoj otopini Na_2SO_4. Veći prirast tlačne čvrstoće, vidljiv za uzorke morta s dodatkom letećeg pepela iznad 20 mas. %, potvrđuje dvostruki učinak finih čestica LP, koje, osim što pucolanskom reakcijom s hidratacijom nastalim $Ca(OH)_2$ stvaraju nove C-S-H faze, imaju i ulogu punila koji zapunjuje pore nastalog kompozita, smanjuje poroznost i na taj način poboljšava njegova svojstva stvarajući čvršći i stabilniji cementni kompozit[8].

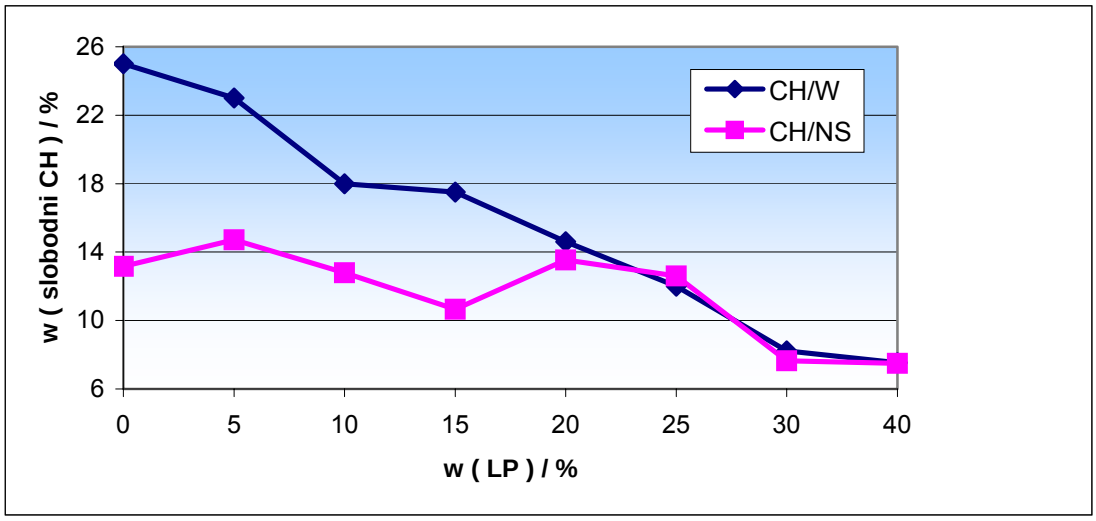


Slika 1. Grafički prikaz prirasta čvrstoće uzoraka morta ovisno o udjelu LP-a (W - vodovodna voda, NS - otopina Na_2SO_4).



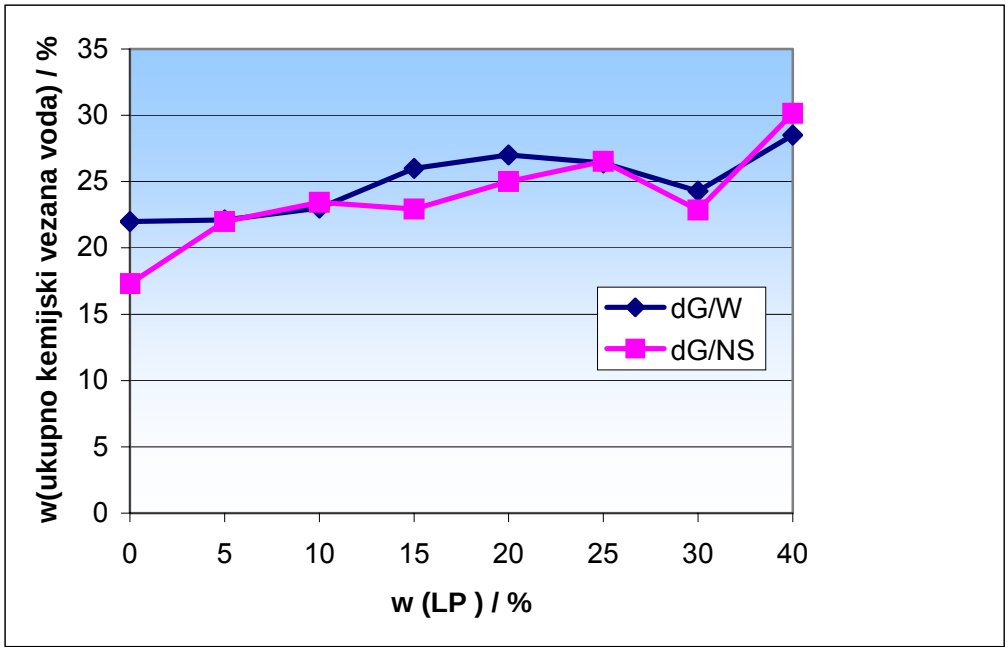
Slika 2. TG/DTG-DTA krivulje za uzorak PB0 poslije 280 dana boravka u 5 % otopini Na_2SO_4 .

Napredovanje procesa korozije u uzorcima morta bez i s dodatkom letećeg pepela (0 – 40 mas. %) praćeno je određivanjem promjene slobodnog $Ca(OH)_2$ – portlandita (CH) pomoću toplinske analize TG/DTG-DTA (slika 2). Sadržaj CH određen je iz gubitka mase u temperaturnom području od 420 – 560 ^oC, a sadržaj ukupno kemijski vezane vode za C-S-H faze iz gubitka mase u temperaturnom području od 30 – 1000 ^oC na TG/DTG krivuljama. Dobivene vrijednosti su preračunate na 100 % masu cementa[8].



Slika 3. Sadržaj slobodnog, nevezanog CH u uzorcima morta ovisno o udjelu LP-a (CH/W - vodovodna voda, CH/NS - otopina Na_2SO_4).

Ponašanje uzoraka morta, izloženih otopini sulfata, ocijenjeno je usporedbom ponašanja uzoraka morta koji su istovremeno njegovani u vodovodnoj vodi. Sadržaj slobodnog CH u uzorcima morta izloženih otopini Na_2SO_4 u ovisnosti o masenom udjelu letećeg pepela prikazan je na slici 3. U istom dijagramu ucrtan je i sadržaj slobodnog CH u uzorcima morta istovremeno njegovanim u vodovodnoj vodi. Na taj način je utvrđeno da uzorci morta s dodatkom LP-a iznad 20 mas. % pokazuju veću otpornost prema izluživanju CH tijekom sulfatne korozije, jer se krivulja promjene sadržaja slobodnog CH u ovisnosti o dodatku LP-a za uzorke njegovane u vodovodnoj vodi (CH/W) podudara s krivuljom promjene sadržaja CH za uzorake morta koji su izloženi djelovanju otopine Na_2SO_4 (CH/NS).



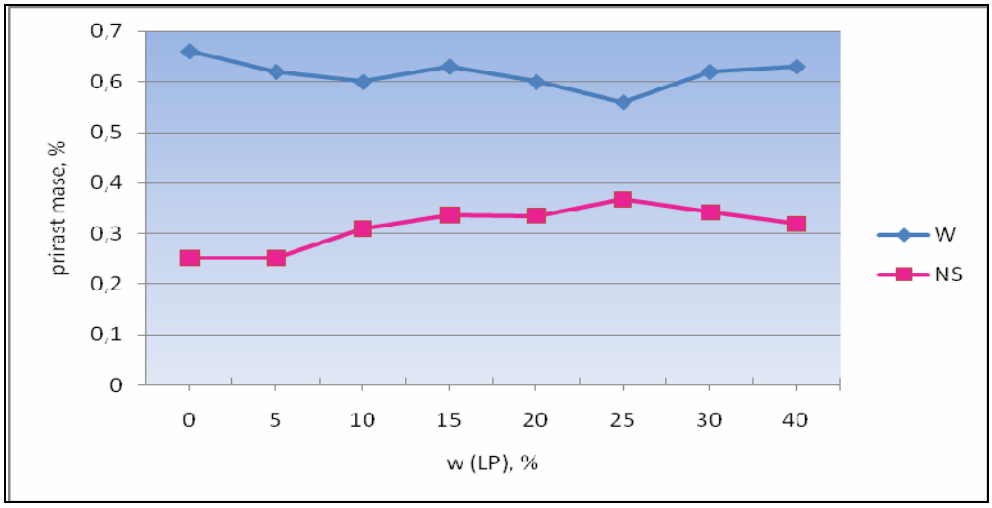
Slika 4. Sadržaj slobodnog, nevezanog CH u uzorcima morta ovisno o udjelu LP-a (dG/W- vodovodna voda, dG/NS - otopina Na_2SO_4).

Na slici 4 prikazana je promjena sadržaja ukupno kemijski vezane vode za C-S-H faze u uzorcima morta poslije 280 dana boravka u otopini Na_2SO_4 ovisno o dodatku LP-a. Uz ovu krivulju u dijagramu je ucrtana i krivulja promjene sadržaja ukupno kemijski vezane vode za uzorke morta istovremeno tretirane u vodovodnoj vodi. Uočava se da se krivulja promjene ukupno kemijski vezane vode u uzorcima morta (PB5 –PB40) njegovanim u vodovodnoj vodi (dG/W) gotovo podudara s krivuljom promjene ukupno kemijski vezane vode u uzorcima morta izloženim sulfatnoj koroziji (dG/NS), što ukazuje da nema razaranja C-S-H gela pod utjecajem sulfatne korozije.

Na slici 5 prikazana je promjena mase uzoraka cementnog morta ovisno o uvjetima njegovanja (vodovodna voda i/ili otopina Na_2SO_4). Vidljivo je da svi uzorci morta, bez obzira na uvjete njegovanja, pokazuju prirast mase. Veći prirast mase (oko 0,66 %) pokazuju uzorci morta tijekom hidratacije u vodovodnoj vodi (W), dok je prirast mase

mortova u otopini Na_2SO_4 (NS) niži (0,33 %). U otopini Na_2SO_4 veći prirast mase pokazuju uzorci morta s dodatkom LP-a iznad 10 mas. % (PB10 - PB40) u odnosu na uzorke morta bez i s 5 mas. % dodatka LP-a (PB0 i PB5), što je u suglasju s rezultatima prirasta tlačnih čvrstoća ovih mortova. To ukazuje da paralelno s procesom hidratacije teče i pucolanska reakcija, a posljedično tome, sadržaj slobodnog vapna je manji, spriječeno je veće izluživanje CH pa tako i nastajanje velike količine gipsa i etringita tijekom sulfatne korozije.

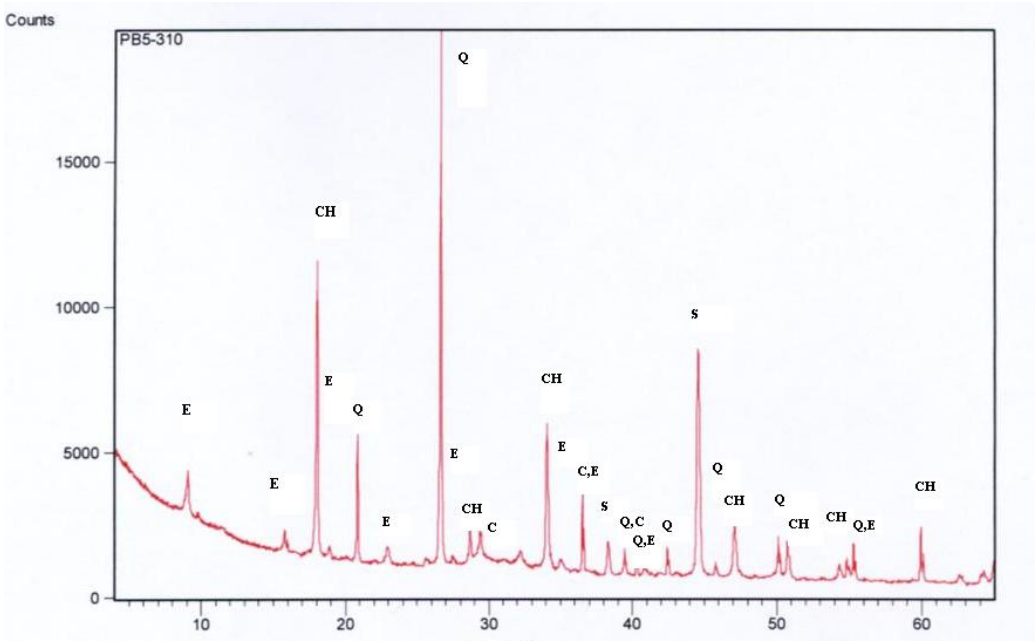
Promjena mase uzoraka morta može se uzeti kao pokazatelj fizičko-kemijskih procesa koji se događaju tijekom sulfatne korozije. Općenito, gubitak mase uzoraka cementnog kompozita ukazuje na izluživanje CH i razaranje C-S-H faze mnogo prije nego što su oštećenja uzorka vidljiva[10].



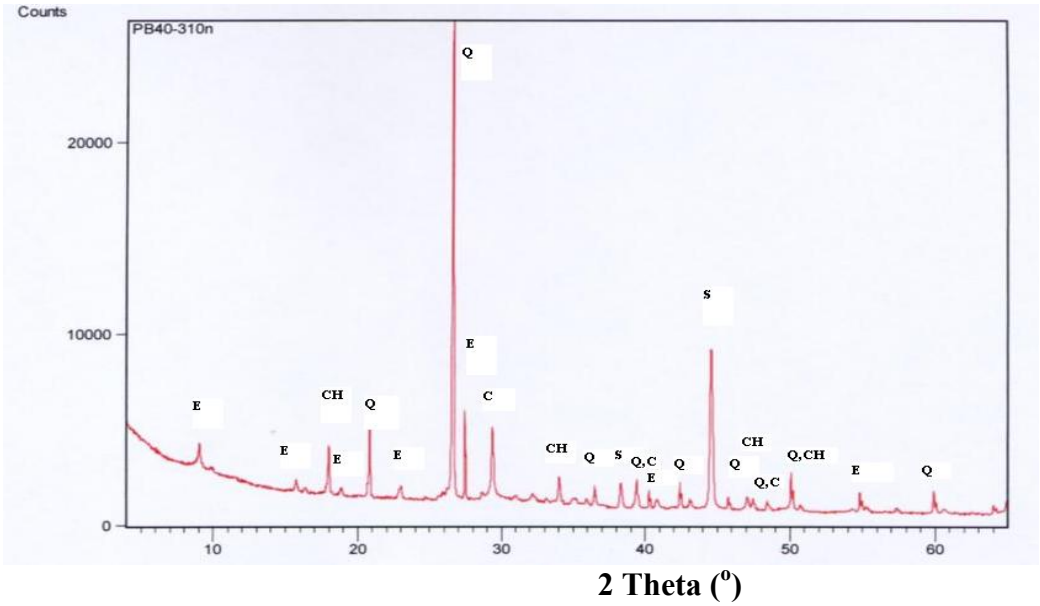
Slika 5. Prirast mase uzorka morta (PB0 - PB40) ovisno o udjelu LP-a (W -vodovodna voda , NS - otopina Na_2SO_4).

Rendgenskoj difrakcijskoj analizi podvrgnuti su uzorci morta s udjelom letećeg pepela s 5 i 40 mas. % poslije 280 dana izlaganja utjecaju otopine Na_2SO_4 . Na slikama od 6 i 7 su prikazani difraktrogrami uzoraka PB5 i PB40 u području 2Θ od 4 – 60 ^{o} i označene su uočene faze: etringit (E), kalcit (CC), kvarc (Q), koji se koristio kao agregat u pripremi cementnog morta, i kalcijev hidroksid (CH). Difrakcijski maksimum ($2\Theta = 44,5\ ^{o}$) pripada nosaču uzorka i nosi oznaku S. Iz slika je vidljivo da uzorci PB5 i PB40 sadrže etringit, nastao kao produkt sulfatne korozije. Prisutnost gipsa nije uočena, pa je za pretpostaviti da je gips tijekom 280 - dnevne korozije potpuno prešao u etringit. Na slici 7 se uočava smanjenje intenziteta difrakcijskih maksimuma etringita i CH u uzorku PB40 u odnosu na intenzitete istih faza u uzorku PB5 (slika 6), što potvrđuje da povećani dodatak letećeg pepela poboljšava otpornost cementnog morta. Ovo se može objasniti dvostrukom ulogom letećeg pepela, koji; (i) u ranoj fazi hidratacije djeluje kao nukleacijsko mjesto gdje se talože hidratacijski produkti, što potiče hidrataciju cementa i osigurava veću količinu CH raspoložljivog za pucolansku reakciju, i (ii) u kasnijoj fazi hidratacije, amorfni alumosilikati iz LP pucolanskom reakcijom kemijski reagiraju s hidratacijom nastalim CH tvoreći nove C–S–H faze koje dodatno ugušćuju razvijenu mikrostrukturu cementnog kompozita[5]. Zbog pucolanske reakcije, sadržaj slobodnog CH u ovim uzorcima cementnog

morta je manji zbog čega je spriječeno veće izlučivanje CH, pa tako nastajanje gipsa i velike količine etringita, kao produkata sulfatne korozije



Slika 6. Difrakcijska slika polikristalnog uzorka morta PB5 poslije 280 dana izlaganja utjecaju otopine Na_2SO_4 .



Slika 7. Difrakcijska slika polikristalnog uzorka morta PB40 poslije 280 dana izlaganja utjecaju otopine Na_2SO_4 .

gdje je:
E-etringit, CH-kalcijev hidroksid (portlandit), CC-kalcit, Q-kvarc, S-nosač uzorka.

ZAKLJUČCI

1. Rezultati ispitivanja otpornosti uzoraka cementnog morta, poslije 280 dana boravka u agresivnoj otopini sulfata ($w(Na_2SO_4)$ = 5 %), ukazuju da su uzorci sa zamjenskim dodatkom letećeg pepela iznad 20 mas. % otporniji prema korozijskom djelovanju sulfata, jer ovi uzorci pokazuju:
   - isti trend povećanja tlačne čvrstoće bez obzira na uvjete njegovanja morta, tj. u vodovodnoj vodi i/ili u agresivnoj otopini Na_2SO_4,
   - nije uočeno izluživanje CH niti razaranje C–S–H gela tijekom sulfatne korozije, jer se krivulje promjene sadržaja slobodnog CH i ukupno kemijski vezane vode za uzorke istovremeno izložene utjecaju otopine sulfata i njegovane u vodovodnoj vodi podudaraju,
   - manji sadržaj slobodnog CH spriječava izluživanje CH; zbog povećanog udjela letećeg pepela (efekt razrijeđenja) i pucolanske reakcije sadržaj CH raspoložljiv za reakciju sa sulfatnim ionima je snižen, pa tako i nastajanje gipsa i velike količine etringita, kao produkata sulfatne korozije, što je potvrđeno i rendgenskom difrakcijskom analizom.

2. Uzorci cementnog morta s dodatkom letećeg pepela iznad 10 mas. %, poslije 280-dnevnog izlaganja u otopini Na_2SO_4, pokazuju veći prirast mase od uzoraka bez i s 5 mas. % letećeg pepela, jer se uz povećani dodatak LP-a pucolanskom reakcijom stvara veća količina C-S-H faze, a sadržaj slobodnog vapna je manji pa je spriječeno veće izluživanje CH i razaranje C-S-H faze.

LITERATURA

1. M. Santhanam, M. D. Cohen, J. Olek: *Cement and Concrete Research*, 33 (2003) 341-346.
2. ASTM C 618-1994: Standard specification for coal fly ash and raw or calcined natural pozzolan for use as a mineral admixture in portland cement concrete. *Annual book of ASTM Standards*, Philadelphia, 1994.
3. A. Đureković: *Cement, cementni kompoziti i dodaci za beton*, Zagreb: Institut građevinarstva Hrvatske, Školska knjiga, 1996.
4. D. Jozić, J. Zelić: *Ceramics-Silikaty*, 2 (2006) 98 - 105.
5. D. Jozić: *Doktorska disertacija*, Sveučilište u Splitu, Kemijsko-tehnološki fakultet, Split, 2007.
6. HRN EN 450-2000: Leteći pepeo kao dodatak betonu. Definicije, zahtjevi i nadzor nad kakvoćom.
7. HRN EN 196 – 1- 2005: Metode ispitivanja cementa – 1. dio: Određivanje čvrstoće.
8. J. Zelić: *Doktorska disertacija*, Sveučilište u Splitu, Tehnološki fakultet, Split, 1997.
9. J. Ninčević: *Diplomski rad*, Sveučilište u Splitu, Kemijsko-tehnološki fakultet, Split, 2008.
10. C. D. Lawrence: *Cement and Concrete Research*, 22 (1992) 1047-1058.

POZVANO PREDAVANJE

ENERGY ABSORBING STRUCTURES FOR THE ROADSIDE SAFETY EQUIPMENT

Dr.sc. Dražen Živković, (FESB)
Dr.sc. Dražen Bajić (FESB)

Izvorni znanstveni rad / Original scientific paper

ABSTRACT

While the majority of automobile crashes involve vehicle-to-vehicle impacts, a number of traffic incidents involve vehicles impacting roadside structures. Leading EU countries had recognized the need for the passive safety improvement of the roadside structures, as an important step to achieve reduction of serious occupant injuries. Existing roadside structures are designed to maximize performance and minimize cost. However, there are still many fatalities and serious injuries on the road networks.

The properties improvement of existing roadside equipment and development of new structures, as well as the testing methods, has to be a matter of permanent interest for everyone who deals with road traffic problems. Devastating injury statistic of traffic road accidents with car – roadside structure collision, demands permanent research of better roadside equipment. According to the data of Croatian Ministry of Home Affairs for Split-Dalmatian County, in the period from 2002 to 2003 year, there were 6 fatalities and 28 persons who were seriously injured.

The automotive industry makes the great effort to meet more and more rigid norms for the occupant passive safety. These efforts will be fully expressed only with parallel development of roadside infrastructure. The elements of roadside infrastructure have to be designed in manner to absorb as much as possible the kinetic crash energy with predictable elements deformation. These crash conditions will insure more favorable decelerations during the crash, and that means less injury for the car occupants.

The aim of this article is to point out that in the Croatia there is also a permanent need for research in the field of roadside equipment, all with main purpose for improvement of the traffic passive safety.

This article contains some pictures that may cause uncomfortable feelings to someone. The authors apologize themselves.

KEYWORDS: roadside structures, crash energy absorbing material, passive safety

1. INTRODUCTION

The improvement of the road traffic safety is an important task for anyone who deals with automotive and road transport industry. In the last few decades a great efforts have been made in automotive industry on the improvement of vehicles safety devices as are: bumper systems, airbags, crash energy zones, etc.) In the same time less attention has been paid to new developments in the roadside equipment. Existing roadside equipment (as: fencing, lighting columns, support structures of vertical signs, W-beam guardrail systems, etc.) are designed according the principle of acceptable performance with minimum production cost. The analysis of traffic accident consequences, where the vehicle crashes in some of the roadside equipment, leads to conclusion that most of existing roadside equipment is "dangerous" structures.

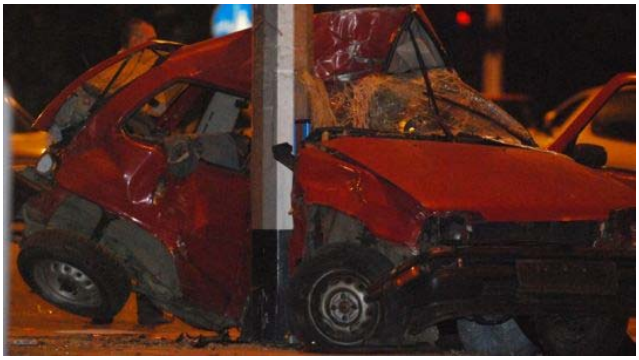


Figure 1. A passenger car impact with lighting column

The impacts with lighting columns and vertical signs supports cause serious injuries, very often with fatality (as it was on *fig.1*). The similar thing is with guide rails that are currently installed along the roads. Steel guide lines systems are relative safe for passenger cars, but most of these systems are not capable of containing the heavier trucks and modern road vehicles as SUV. On the other side the concrete barriers, capable of containing the heavier trucks, are less safe for smaller cars, causing serious injuries to the car occupants.
Similarly the great safety traffic problem is tree-lined streets. Along these mainly city streets the lines of trees are planted, often less than *1 m* far from the roadway edges. No matter how much, these lines of trees make more comfortable felling in the city environment, in the same time they are "dangerous" structures alike lighting columns.



Figure 2. The marked tree in the line of trees

This demand for more safe roadside equipment was also recognized and pointed out by the European Commission, who announced its decision to take concrete action on road infrastructure safety in its "White Paper on European Transport Policy for 2010[1] and in its Communication on a European Road Safety Action Programme of 2 June 2003 [1].

In order to provide for expert input at an early stage and with regard to transparency policy, the Commission established a ***Working group on infrastructure safety*** *in 2002. 11 Member States participated in this Group[2] and give detailed advice on practices in their countries on road infrastructure safety procedures. The result of this working group reveals a widespread deficit of feedback concerning the effectiveness of the management systems, which makes any improvement on a "best practice" basis improbable*.

In addition, the FIA, representing more than 100 million motorists worldwide and more than 40 million citizens in the EU, called on the European Commission for "legislation to lead to a rapid improvement of road infrastructure", stressing that "guidelines alone will not be enough to halve road deaths by 2010". This very clear statement from major road organizations shows that there is a growing impatience from the road user community at the lack of progress concerning safety of roads [1].

2. THE STATE OF THE SAFETY ROADSIDE EQUPIMENT IN CROATIA

According to the purpose the structures of roadside equipment may be classified in two main groups [2]:

- protecting equipment (as: barriers, guide rails, etc),
- support equipment (as: sign support columns, light columns, etc.).

2.1. PROTECTING EQUIPMENT

In this group belong: protecting fence, guide rails, median concrete barriers, working zone barriers etc. Their main purpose is to separate the opposite traffic lines, and to separate the roadway from the environment. They are designed in lot of various types, but their common property is strong and mostly rigid construction.

The protecting fences are usually made from various steel profiles, and it may be said that they are less dangerous than other protecting structures.

The guide rails are designed in lot of various types. But mostly they are constructed from steel I-profile vertical support and steel W-profile longitudinal bumper. In traffic accidents with passenger cars they are capable to keep the car on the roadway, but their rigid construction is very dangerous for the car occupants. The existing guide rails in Croatia have very weak kinetic energy absorbing characteristic. The analysis of the accidents allow to say that impact speed more than *50 km/h* may cause very serious injuries and even occupant deadly end. The consequences of these accidents are also in function of impact angle. The second problem, and not less important, is that existing bumpers are not capable to contain heavier vehicles.

[1] Commission White Paper of 12 September 2001: "European transport policy for 2010; time to decide" COM (2001) 370
[2] Austria, Belgium, Denmark, Germany, Finland, Greece, Italy, Norway, Portugal, Sweden and the UK



Figure 3. The protecting fences

The concrete barriers are made from steel reinforced concrete. They are usually used on the road connections to main road or highway. These fences are capable to contain heavy trucks and busses, but they are very harmful for passenger cars.



Figure 4. The concrete barrier

2.2. SUPPORT EQUIPMENT

The elements from this group are designed as columns and consoles. The most significant, and the most numerous elements of roadside equipment are various types of columns, which support traffic signs and road lightening. These structures may be classified as most dangerous elements of roadside equipment. They are designed to withstand the strong winds, so they are usually made from steel tubes strongly anchored to concrete base. These are rigid structures with week plastic properties. The diameters of steel tubes vary upon the purpose, but in the collisions with passenger cars all of them act as “knife” that easily entered into car body. Unfortunately the most of mentioned collisions causes very serious injuries and fatalities. Beside this low energy absorbing property, these steel tubes are usually placed very near to roadway edges, without any protecting fence in front of them. As the new urban streets, wide and strait, enable higher driving speeds, any collision of passenger car with existing anchored steel tube will possibly result with fatality.

Although the tree lines on the urban roads are not classified as roadside infrastructure equipment, but they act very similarly as steel tubes. So it is also important to protect the traffic participators from the direct dangerous collisions with trees from line of trees.



Figure5. The lighting column



Figure 6. The tree-lined street

3. DEVELOPMENT TRENDS OF ROADSIDE EQUIPMENT

As the authors know in Croatia there are no organizations that systematically work on development of new and reconstruction of existing roadside equipment. The Croatian norms that deal with design of roadside equipment are not mainly coordinated with new European norms. So in this part of the article new European trends and some of new roadside equipment designs will be presented.

3.1. VERTICAL SUPPORT STRUCTURES

The vertical support structures have to be tested according to EN 12767 (*"Passive safety of support structures for road equipment – Requirements and test methods"*). The products are classified into performance types based on three factors [3]:

a. Speed class (impact speeds used in the test),

b. Effect of the impact upon the speed,
   HE (high energy absorbing) – slows the vehicle considerably
   LE (low energy absorbing) – slows the vehicle to some extend
   NE (non-energy absorbing) – slows the vehicle slightly or not at all

c. Level of occupant risk (occupant safety level).
   level 1 – the highest risk, level 2 – medium risk, level 3 – lowest risk
   level 4 – non harmful, light support structures

Table 1. Energy absorption categories

Impact speed *(km/h)*	50	70	100
Energy absorption	**Exit speed** *(km/h)*		
HE	v =0	0< v = 5	0< v = 50
LE	0< v = 5	5< v = 30	50< v = 70
NE	5< v = 50	30< v = 70	70< v = 100

This norm is not a product norm, the normal product norms such as EN40 for lighting columns and EN12899-1 for fixed vertical road traffic signs, must apply. It is a voluntary

additional standard giving the means to classify items of road equipment in terms of the potential severity of injury to the occupants of vehicles in collision with those items [4].

This norm enables traffic expert to determine the level of energy absorption of the road structure and the passive safety described by the Accident Severity Index (ASI) and Theoretical Head Impact Velocity (THIV). The ASI gives an indication of the accelerations that are acting on the vehicle occupants during the crash, while the THIV is theoretical velocity at which the head of the driver hints an interior part, e.g. the steering wheel or the dashboard. The lower the values for both indicators, the structure is safer. [5]

According to EN 12767 several new designed support vertical columns were tested. Two of those new designed will be presented in this article.

The first one is the lighting column made from polymer composite and manufactured at *Swedamast, Leeuwarden (Netherlands).* This light lighting column was developed under the European research project ***Ecosafe***. The overall objective of Ecosafe is to improve roadside safety systems by the versatile use of fiber reinforced polymer composite materials in these systems [5].



Figure 7. The polymer prototype composite column test (Ecosafe)

Test results lead to conclusion that the ASI and THIV are very low, which indicates that the column has a very good passive safety performance. The measured ASI, THIV and energy absorption categorize this column according EN 12767 as being "*100, LE, 3" (100 km/h speed class, Low Energy absorbing, safety level 3).* The ASI and THIV values give information on the primary contact – impact, where splitting of the composite enabled the column to absorb impact energy at reduced decelerations. But, the secondary impact proved to be critical during this crash test. The column folded and rotated around the front of the car, causing the upper part of the column to hit the roof of the car at a high downward velocity.

The second one is lattice mast designed and manufactured by *Juralco As, (Norway).* It is made from aluminum alloy, according to EN 12767. The foundation is made from reinforced concrete with bolts. During the impact the structure bends or brakes depending on impact speed. All *Juralco* lattice masts ensure impact safety classified by *100,NE, 2-3.* The figure 8

shows the concurrent test for passenger car impact to the steel post and aluminum alloy lattice vertical sign support [3].




The passenger car impacts the steel post




The passenger car impacts the aluminum lattice vertical sign support

Figure 8. The concurrent test for passenger car impact (Juralco)

The test results show that the car, which impact the lattice support, was less damaged than the car that impact the steel post. The lattice vertical supports can be designed enough rigid to withstand the wind and other natural loads, while in the same time are very safe for the occupants in the passenger cars.

3.2. THE GUIDE RAIL SYSTEMS

The most important requirement is that the vehicles must be contained and not allowed to break through the barrier. Containment of vehicles means deceleration of the vehicle until its lateral velocity (perpendicular to the direction of travel) is decreased to zero. To make this deceleration possible, the safety barrier has to absorb and/or dissipate the kinetic energy of the vehicle. To comply with all necessary requirements, a two-step energy absorbing guide rail system was developed within the framework of Ecosafe project [5]. The system is named "*Tilting Bird"*. The figure 9 shows the main elements of this tilting guide rail system.

This system was full-scale crash tested by the TNO Automotive at the test center of RDW[3], and all according to EN 1317.

[3] "Rijksdienst voor het Wegverkeer», Lelystand, Netherlands

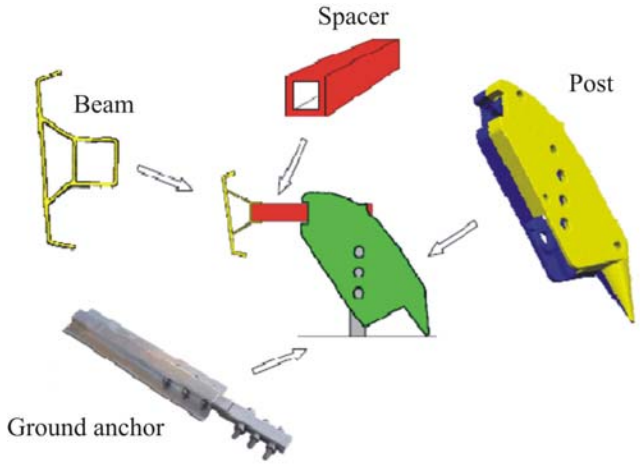


Figure 9. The "Tilting Bird" guide rail system (Ecosafe) [5]

The first step works for both the car and bus impact and absorbs energy at a relatively low force level. This ensures that the decelerations in this first step are not too severe. This first step is sufficient to contain the passenger car, but this does not absorb enough energy to contain the bus. Therefore a second step is activated, where the force level increases and absorbed energy per traveled distance as well.

This design uses a longitudinal beam – quite similar to the rails in most of current steel systems – with an energy absorbing element behind the beam (spacer). During activation of second step, the post rotates (tilts) backward, thereby crushing an energy absorber that is placed at the back of the post. As the system tilting backward, the front part with beam increases in height, which prevents the vehicle from rolling over the safety barrier system [5].

The test results showed that safety guide rail is enough safe for passenger cars, although the full-scale test with the bus showed that design of the beam has to be reviewed. The actual design is not able to properly transfer the load from the vehicle to the post.

3.3. THE IDEAS FORM FESB - DEPARTMENT FOR MECHANICAL TECNNOLOGY[4]

In last four years within the preparation of project proposal ("The development and usage of impact energy absorbing materials"[5]) a few research works were done. Some of the ideas from this research will be presented in this article.

3.3.1. The energy absorbing cushion

The protecting energy absorbing cushion is designed to protect the car occupants from existing columns and trees. It has two important tasks: to increase the impact zone and to absorb the part of the car kinetic energy. The figure 10 illustrates the performance of this cushion.

[4] University of Split, Faculty for Electrical Engineering, Mechanical Engineering and Naval Architecture, CROATIA

[5] The project proposed to Croatian Ministry of Science, Education and Sports, developed by Material Program of the Mechanical Technology Department, FESB, Split

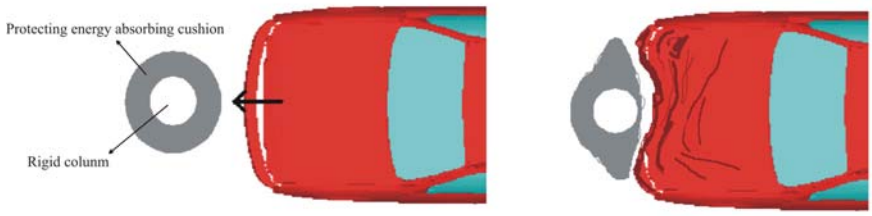


Figure 10. The energy absorbing cushion

The energy absorbing cushion is to be made from composite metal foams (based on aluminum alloys). Some aluminum alloy foams have the possibility of absorbing kinetic impact energy of *1,5 MJ/m*^{3} with *55%* plastic deformation [6]. The calculation of cushion plastic deformation of *0,055 m*^{3} shows that the absorbed energy will be about *82,5 kJ*. Assuming the passenger car with average mass of *1300 kg*, the car will spend about *40 km/h* of its speed on plastic deformation of protecting cushion. This is only the part of car speed that will be absorbed by the plastic deformation of cushion, and the other part will be absorbed from the car body. Some calculations lead to conclusion that the car occupants will not suffer serious injuries at the impact speed of *60 km/h* (the usual speed in the urban environment). For more realistic results it is necessary to obtain the full-scale tests.

3.3.2. The energy absorbing column

The energy absorbing column consists of AA 5083 tube filled with aluminum alloy metal foam. The tube has standard dimensions. The outer diameter is *256 mm* and inner diameter is *250 mm.* At distance *300 mm* from the bottom, the tube is perforated in the length of *500 mm.* This perforated part of the pipe is placed on the height of usual impact zone for small cars (fig.11.). The main column features are: predictable tube deformation (fig. 12.) and good enough impact energy absorption. The full column height is 3 m.

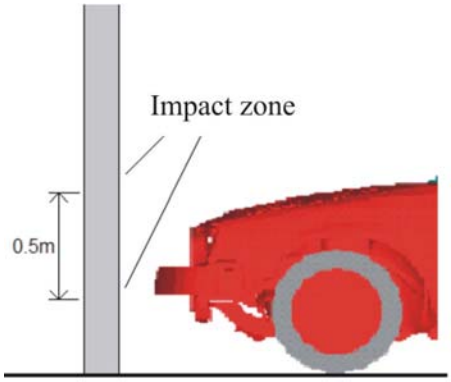


Figure 11. The column impact zone

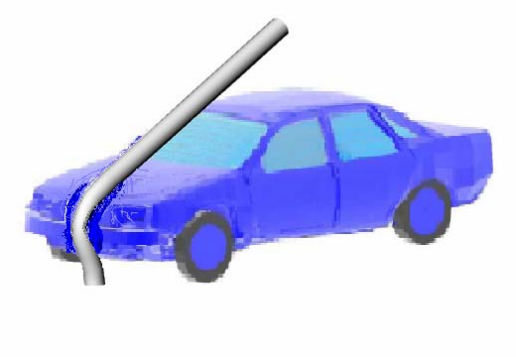
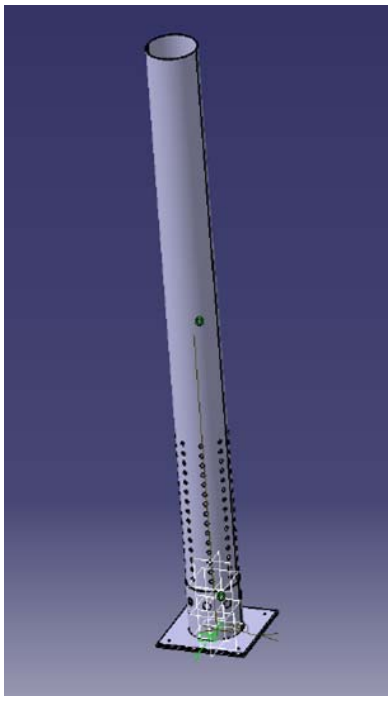


Figure 12. Predictable tube deformation



The main tube is fixed with screws to outer base tube, which is welded to the base plate. The base of the column can be made from AA 5083 or steel. If it is made from steel special attention has to be paid on possible corrosion process.

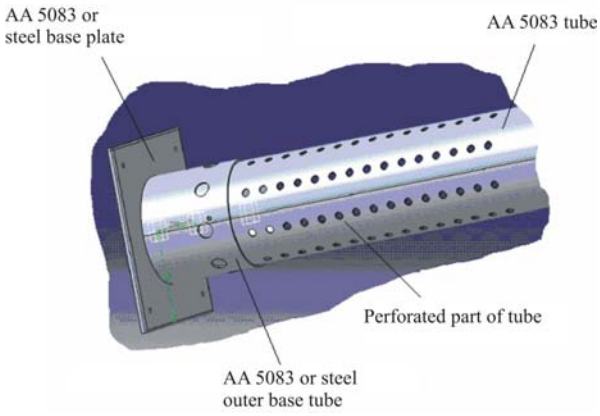


Figure 13. The energy absorbing column [2]

According to the literature [7], the stress distribution during the small car impact into a column is illustrated on the figure 12.

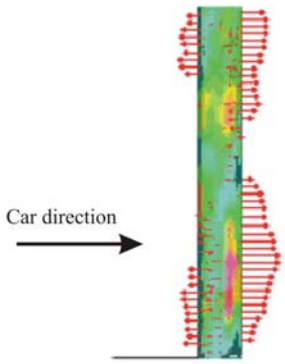


Figure 12. Stress distribution during impact "car-column"

Assuming the aluminum tube mechanical properties and also energy absorbing property of aluminum metal foams, the calculation results show that this structure is capable to absorb impact kinetic energy in the range from *15* to *22 kJ*. These theoretical values depend on tube properties and also the properties of used metal foam. Only the full-scale tests can validate this theoretical research.

4. CONCLUSION

It is safe to say that, in spite of intensive development of the car passive safety systems (as crash predictable computer program), it is impossible to avoid the driver mistakes that cause the traffic accidents. It also may be said that development and usage of new passive safety car equipment is not enough to decrease the serious consequences of the traffic accidents, in which the vehicles impact the roadside structures. According to the literature [8] in some EU countries one fourth of all traffic accidents depends on the crashes "car to roadside structures". All the traffic accidents analysis leads to the conclusion that it is very important to research and improve existing roadside equipment, and also to develop new design with new materials structure. The design has to be developed in the direction of predictable structure deformation, and the constructive material must have good kinetic energy absorbing property. These materials are mainly aluminum alloys, which are, form the ecological point of view, more acceptable than existing steel.

This conclusion is not suggested that existing roadside equipment should normally be replaced solely to obtain the passive safety benefits. The road lighting and traffic sign infrastructure that is passed its design life and in proof condition, and also will have to be replaced in the near future, can be replaced with new equipment designed towards the EN12767. The benefits in injury accident reduction can be obtained for only the marginal extra cost of passive safety equipment against existing standard equipment. This should be the way forward.

LITERATURE

[1] STAFF WORKING DOCUMENT OF THE SERVICES, Annex to the Proposal for a Directive of the European Parliament and of the Council on road infrastructure safety management, Executive Summary of the Impact Assessment, http://ec.europa.eu/transport/roadsafety_library/infrastructure/summary_impact_assessment_en.pdf

[2] BLAJIĆ, M., "Materijali koji upijaju energiju i njihova primjena u cestovnoj infrastrukturi", Diplomski rad, FESB, Split, 2005.

[3] EINNAR ENGINEERING NEWS No 12B, Finish Road Administration, Technical Services, "Vertical sign support with passive safety", Finland, 2005 http://www.tehallinto.fi/finnar

[4] SIMPSON, D. "EN 12767 – a new tool in accident reduction", Traffic engineering & control, vol.41, No 7, Hemming, London, 2000.

[5] GAN, MD., ANTONELLI, V., "Composite and roadside safety – Development of a composite lighting column and guardrail system", 14th International Conference on composite materials, Dearborn, Michigan, USA, 2003

[6] FILETIN, T., KRAMER, I., MARIĆ, G., Metalne pjene, Hrvatsko društvo za material i tribologiju, ISBN 953-7040-03-8, Zagreb, 2003.

[7] RIVAS, C.B., “Development of energy Absorbing Roadside Structures, Master degree of Science, Chalmers University of Technology, Goteborg, Sweden, 2002.

[8] WARD, D., ROMPE, K., “Third European Road Safety Action Programme”, http://ec.europa.eu/dgs/energy_transport/forum/works/doc/2004_05_11_road_safety_en.pdf

MIKROSTRUKTURA I SVOJSTVA ODLJEVKA KLIPA OD Al LEGURE

Dr.sc. Dražen Živković, dipl.ing
Tonći Ursić, dipl.ing.
Branimir Lela, dipl.ing.

Izvorni znanstveni rad / Original scientific paper

SAŽETAK

S obzirom na funkciju koju obavlja, klip pripada glavnim dijelovima motora s unutrašnjim izgaranjem. Za izradu klipova najčešće se koriste legure aluminija sa silicijem, ali koriste se i drugi materijali kao što su: sivi lijev, keramike, kompoziti itd. Klipovi iz aluminijevih legura uglavnom se izrađuju lijevanjem (gravitacijsko, tlačno). Za potrebe ovog rada odliven je klip iz Al legure AlSi12CuNiMg, na kojem je za vrijeme procesa hlađenja izvršeno mjerenje brzina hlađenja na tri različita mjesta. S tih mjesta uzeti su uzorci za metalografska i mehanička ispitivanja. Nakon analize rezultata, na istim uzorcima provedena je toplinska obrada sa svrhom ujednačavanja strukture. Dobiveni rezultati ukazali su na postojanje strukturnih razlika, kao i razlika u tvrdoći. Međutim, naknadnom toplinskom obradom uzoraka postiglo se ujednačavanje strukture uz neznatne razlike tvrdoće.

KLJUČNE RIJEČI

Klip, Al-Si legure, lijevanje, brzine hlađenja, mikrostruktura

MICROSTRUCTURE AND PROPERTIES OF ALUMINUM ALLOY CAST PISTON

ABSTRACT

The piston is one of the main parts of an internal-combustion engine. As the material for piston design Al-Si alloys are mostly used, although the materials like gray iron, ceramics, composites etc. are also used. The aluminum alloy pistons are usually made by gravity or pressure casting technology. For this work the piston from aluminum alloy AlSi12CuNiMg was cast. The cooling rate was measured on three various position of the piston. The specimens were taken out from each position and metallographic research was conducted. Also the hardness testing was done. The specimens were subjected to heat treatment with purpose of microstructure homogenization. The obtained results have shown the microstructure differences, as also the hardness differences. The additional heat treatment had homogenized the microstructure with the marginal hardness decrease.

KEY WORDS

Piston, Al-Si alloys, casting, cooling rate, microstructure

1. UVOD

Klip je najopterećeniji dio motora. Za njegovo dobro ponašanje u pogonu treba pravilno odrediti oblik, dimenzije i materijal. Zbog toga se već desetljećima konstrukcijom i proizvodnjom klipova bave uglavnom specijalizirani proizvođači, koji nastupaju kao partneri proizvođača motora. Klip je jedan od glavnih razloga koji ograničavaju povećanje brzine vrtnje klipnih motora.

Sile na klipu, zahtjev za što manjom masom, visoke radne temperature klipa, naprezanja koja kod tih povišenih temperatura često idu do same granice izdržljivosti materijala, a sve to zahtijeva vrlo pažljivo dimenzioniranje samoga klipa, osovinice i ležaja osovinice. Klip je dakle, jedan od najosjetljivijih dijelova u motoru, a njegova konstrukcija je uvijek kompromisno rješenje ovih, međusobno suprotnih zahtjeva. Usprkos prethodnih, danas već vrlo usavršenih metoda proračuna, konačnu riječ ima ispitivanje probnih uzoraka.

Glavni zahtjevi koji se postavljaju za klip su što manja masa (smanjenje inercijskih sila) i što bolja toplinska vodljivost (učinkovito hlađenje). Navedenim zahtjevima najbolje odgovaraju Al-legure na bazi silicija [1].

Eutektička legura aluminija s *12%* Si uvedena je već 1926. godine u proizvodnju automobilskih motora kao standardni materijal za klipove, te do danas joj nije pronađena bolja zamjena. Aluminijeva legure za klipove sadrže kao dodatke od *11* do *13%* Si, te približno po *1 %* Cu, Ni i Mg. Povećanjem udjela Si dobivene su nadeutektičke legure s približno *18 %* do *24 %* Si, kod kojih je toplinsko širenje manje, a otpornost na trošenje veća, ali na štetu čvrstoće. Legure aluminija s bakrom, koje su se nekad upotrebljavale zbog veće čvrstoće kod povišenih temperatura, danas se rijetko primjenjuju [1].

Silicij se kao legirajući element dodaje aluminiju uglavnom radi snižavanja temperature tališta bez pojave krhkih lomova legure. Silicij je kao nečistoća prisutan u gotovo svim aluminijskim materijalima. U tehničkim legurama aluminija, silicija se može naći i u količini do *23%*.

Kod aluminijevih legura sa silicijem namijenjenih za lijevanje razlikujemo 3 karakteristična područja. To su: podeutektičko područje pri koncentraciji silicija od *5,5* do *10,5%*, eutektičko područje u koncentracijama silicija od *10,5* do *13,5%*, te nadeutektičko područje pri legiranju aluminija sa silicijem u količini većoj od *16 %*.

Ovisno o koncentraciji silicija u leguri aluminija, na kraju procesa skrućivanja i hlađenja, dobit će se bitno različita mikrostruktura legure. Kod podeutektičkih legura, legure se uglavnom sastoji od primarne Al faze, a ostatak silicija s aluminijem tvori eutektikum. Legure eutektičke koncentracije imaju najnižu temperaturu tališta (ispod *600°C*) [2].

Kod nadeutektičkih legura najprije dolazi do skrućivanja silicija u obliku vrlo tvrdih i krhkih kristala koji kasnije ostaju zarobljeni unutar relativno mekane matrice (primarna faza i eutektikum). Zbog toga su legure nadeutektičke koncentracije relativno otporne na trošenje i imaju niži koeficijent toplinskog rastezanja. Svoju osnovnu primjenu našli su u izradi klipova i blokova za motore s unutarnjim izgaranjem.

Nedostaci nadeutektičkih legura aluminija i silicija očituju se u: visokoj temperaturi tališta (iznad *700 – 760* ^{O}C), dugim periodom skrućivanja, sklonosti ka nastajanju poroziteta unutar materijala, oslabljenim mehaničkim svojstvima te problematičnom obradom odvajanjem čestica zbog tvrdih kristala silicija raspoređenih u mekanoj matrici.

Aluminijske legure eutektičke i podeutektičke koncentracije najčešće se koriste za izradu klipova, blokova i glava motora. Dobra livljivost, niska temperatura tališta, dobra mehanička svojstva, te relativno visoka čvrstoća i dinamička izdržljivost, razlog su zašto su ove legure našle veliku primjenu pri lijevanju odljevaka tankih stijenki [2].

Gustoća silicija je *2.3 g/cm*^{3} , a aluminija *2.7 g/cm*^{3} . Silicij je dakle jedan od elemenata koji se mogu dodavati aluminiju bez gubitaka prednosti niske mase aluminija. Relativno nizak koeficijent temperaturne dilatacije, velika otpornost na trošenje, visoka čvrstoća, vrlo dobra livljivost su karakteristike zbog kojih se Al-Si legure koriste za velik broj dijelova u auto i aeroindustriji. Primjenjuju se u širokom rasponu dijelova od klipova, cilindara, blokova i raznih cijevi. Silicijeva faza u Al-Si legurama ponekad je grubozrnata što vodi slabijim mehaničkim svojstvima. Bržim skrućivanjem može se bitno modificirati morfologija silicijeve faze. Ove legure su dendritne građe, čijem nastanku pogoduje sporije hlađenje, dok brže hlađenje pogoduje zrnastoj građi. Udio površine primarnih silicijevih kristala nije velik i ovisno o udjelu silicija kreće se do najviše *8%*. Intermetalni uključci Cu i Mg su fino i homogeno raspršeni u matrici aluminija. Ove legure se koriste kao legure za kovanje i lijevanje [3].

2. EKSPERIMENTALNI RAD

Za potrebe ovog rada odliven je klip za brodski motor Yanmar tip PMX 8. Klip je odliven u kokili, na kojoj su na tri mjesta bila smještena ticala termometara za praćenje promijene temperature. Jezgra je izrađena od šamotne pješčane mješavine. Kao legura za lijevanje korišteni su stari klipovi diesel motora automobilske marke Mercedes [4].

2.1. MATERIJAL

Kemijski sastav Al-Si legure dat je u tablici 1.

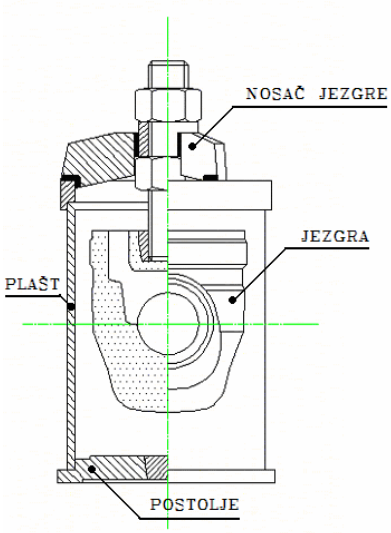
Tablica 1. Kemijski sastav legure klipa

Kemijski sastav legure klipa (%)										
Al	Si	Cu	Ni	Mg	Fe	Pb	Zn	Mw	Sw	Ti
84,448	11,368	1,182	1,156	1,002	0,685	0,208	0,037	0,036	0,024	0,017

Prema kemijskom sastavu dobivena legura odgovara standardnoj leguri oznake *AlSi12CuNiMg.*

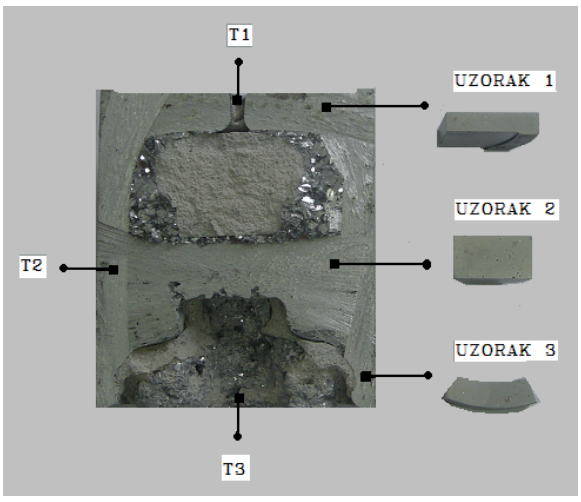
2.2. IZRADA I PRIPREMA KOKILE ZA LIJEVANJE

Kokila je izrađena iz čelika [4]. Kokila se sastoji od četiri dijela: postolja, plašta, nosača jezgre i jezgre (sl. 1).



Slika 1. Kokila za lijevanje klipa

Na postolje se postavlja plašt. Plašt je izrađen od čelične cijevi vanjskog promjera *100 mm* i unutarnjeg *92 mm*. Unutarnji dio postolja formira čelo klipa pri čemu je dio bliže plaštu malo upušten. Unutarnji promjer plašta je nešto veći od promjera gotovog klipa zbog dodatka za strojnu obradu, te on formira vanjsku stjenku klipa. Visina plašta je također nešto veća od visine klipa. Nosač jezgre je najsloženiji dio kokile, sastoji se od prstena koji se postavlja na gornjem rubu plašta. Na njemu su zavarena tri nosača, a koja su opet zavarena za dio kroz koji prolazi vijak za pozicioniranje jezgre. Vijak je *M20*, te je s dvije matice pritegnut za nosač.
U postolju i na plaštu su napravljeni provrti za čahure koje služe za postavljanje termometara. Bakrene čahure služe kako bi zaštitile termoparove od njihovog direktnog kontakta s talinom. Na plaštu se nalaze dva provrta, jedan pri vrhu plašta gdje će biti dno klipa, a drugi u području gdje će biti osovinica klipa. Provrt na postolju smješten je u samom središtu i nalazit će se u području čelu klipa. Položaj ticala termometara (T1, T2 i T3) prikazan je na slici uzdužnog presjeka odljevka klipa (sl. 2).



Slika 2. Uzdužni presjek odljevka klipa [4]

Prilikom lijevanja u kokilu, ista treba biti zagrijana blizu temperature tališta aluminijeve legure, kako bi se spriječile posljedice naglog skrućivanja kao što su: nedolivena mjesta, neravne i nepravilne površine. Kokila je zagrijana plinskim plamenikom na temperaturu od oko $580^{o}C$ (sl. 3).



Slika 3. Zagrijavanje kokile na radnu temperaturu

2.3. LIJEVANJE I SKRUĆIVANJE ODLJEVKA

Kad se kokila zagrijala na dovoljnu temperaturu u čahure su postavljena ticala termometra. Nakon što je lonac s talinom izvađen iz peći, te s površine taline uklonjene nečistoće, slijedilo je lijevanje u zagrijanu kokilu. Lijevanje je provedeno tako da sva talina koju izlijevamo otječe kroz razvodni sustav, omogućujući istovremeno nesmetan prolazak zrak i plinova iz kalupa (sl. 4). Pri naglom lijevanju mogli bi ostati zarobljeni zrak i plinovi, te prouzročiti greške na odljevku.



Slika 4. Lijevanje taline u kokilu

2.4. IZRADA I PRIPREMA UZORAKA

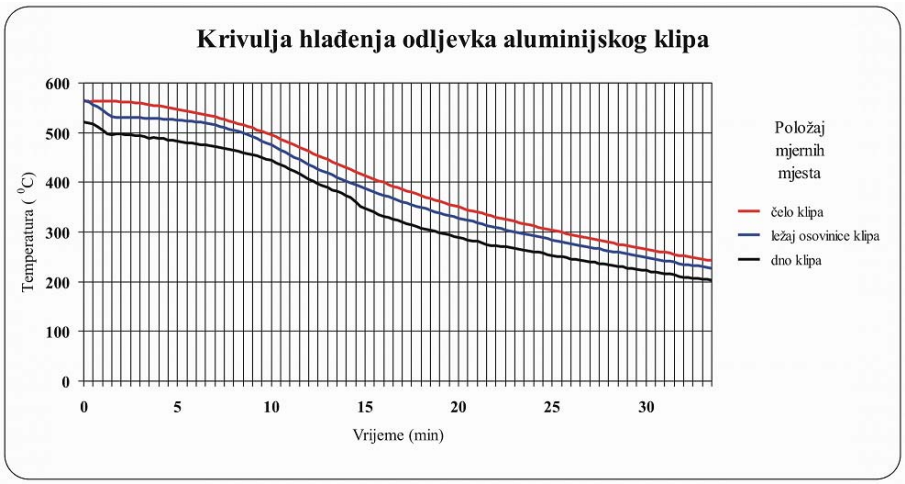
Kako se brzina hlađenja mjerila na tri mjesta: čelu, području ležaja osovinice klipa i dnu klipa, tako su i uzorci za ispitivanja uzeti s tih pozicija (sl. 2). Mjerenje brzine hlađenja trajalo je do temperature od $200\ ^{o}C$, jer je proces hlađenja do sobne temperature proveden ubrzano (hlađenjem vodom).

Uzorci su izrađeni tako što je klip prepiljen na dvije polovice. Iz jedne polovice izrezani su uzorci s tri pozicije. Nakon toga neravni uzorci poravnati su na stroju za brušenje uz hlađenje emulzijom. Uzorci su zatim fino ručno brušeni dok nismo dobili zadovoljavajući sjaj površine. Konačna priprema površine uzoraka provedena je poliranjem. Polirane površine su travljene razrijeđenom 5% fluorovodičnom kiselinom.

Za potrebe toplinske obrade izrađena su još po dva uzorka za svaku poziciju. Toplinska obrada je provedena zagrijavanjem uzoraka na temperature od *250 ^{o}C* i *500 ^{o}C*. Uzorci su ponovno brušeni, polirani i travljeni fluorovodičnom kiselinom.

3. ISPITIVANJE I ANALIZA REZULTATA

Rezultati mjerenja brzine hlađenja aluminijskog klipa dati su u dijagramu na slici 5.



Slika 5. Krivulje hlađenja aluminijskog klipa [4]

Hlađenje odljevka provedeno je na zraku do temperature od *200 ^{o}C*, dok je sobna temperatura postignuta ubrzanim hlađenjem u vodi. Iz dijagrama krivulja hlađenja uočava se da ne postoji razlika u temperaturnom gradijentu između tri mjerna mjesta na odljevku klipa. To znači da su brzine hlađenja bile ujednačene, što je posljedica dobre toplinske vodljivosti, kako materijala odljevka tako i materijala kokile.

Tvrdoća je ispitana na Vickers uređaju pri opterećenju od oko *100 N*. Za svaki od tri uzorka, za sva tri stanja obrade, izvršeno je po pet mjerenja, a rezultati mjerenja su svedeni na srednju vrijednost. Podaci o tvrdoći dati su u tablici 2.

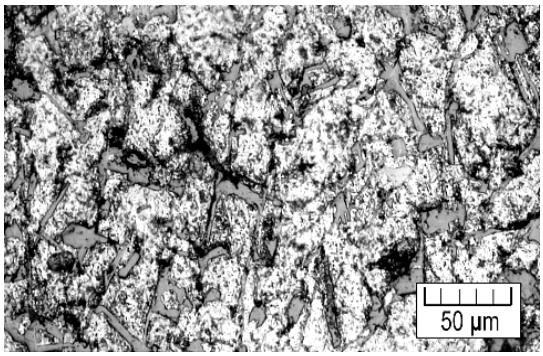
Tablica 2. Rezultati ispitivanja tvrdoće

OBRADA	**Tvrdoća (HV)**		
	ČELO KLIPA	OSOVINICA KLIPA	DNO KLIPA
Izvorno stanje	110	92	90
250°C	90	80	80
500°C	47	43	41

Prikazani rezultati, kod izvornog stanja, ukazuju na ujednačenost tvrdoće u područjima ležaja osovinice klipa i dna klipa, dok je tvrdoća za oko 20% veća na čelu klipa. Veća vrijednost tvrdoće u području čela klipa može se objasniti povećanim sadržajem silicijevih faza, a koja je posljedica segregacije silicija u loncu s talinom. Razlike u količini silicijevih faza nastale su tako što je dio silicija u talini, kao lakša komponenta, isplivao prema površini i tu je došlo do povećanja njegove koncentracije. Pri lijevanju talina s vrha ljevačkog lonca popunjavala je dno kalupa, odnosno područje čela klipa, dok je talina s dna lonca popunjavala volumen u gornjem dijelu kalupa (dno klipa) [4].

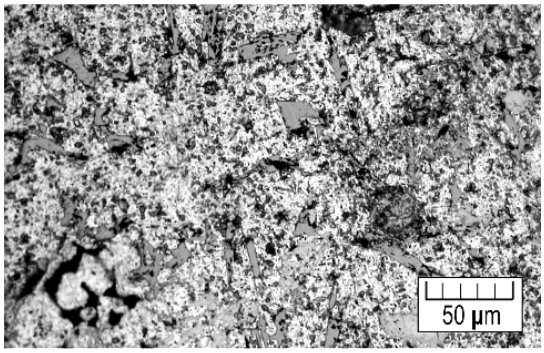
Nakon grijanja uzoraka na temperaturu od oko *250 ^{o}C,* te umjerenog hlađenja na zraku došlo je do homogenizacije strukture i neznatnog pada tvrdoće, a što je posljedica povećanja zrna u odnosu na izvorno stanje. Zagrijavanje na ekstremnu temperaturu od *500 ^{o}C* dovelo je do velikog povećanja α (Al) zrna, kao i do pojave iznojavanja silicijevih faza. Ta pojava rezultirala je smanjenim postotkom silicija u materijalu odljevka.

Analiza mikrostrukture provedena je pomoću svjetlosnog optičkog mikroskopa *Opton* tip *Axioskop*. Povećanje je iznosilo *250* puta. Prepoznavanje i tumačenje faza na metalografskim slikama provedeno je pomoću metalografskog atlasa *Metals Handbook, vol.7 – Atlas of microstructures of industrail alloys.*



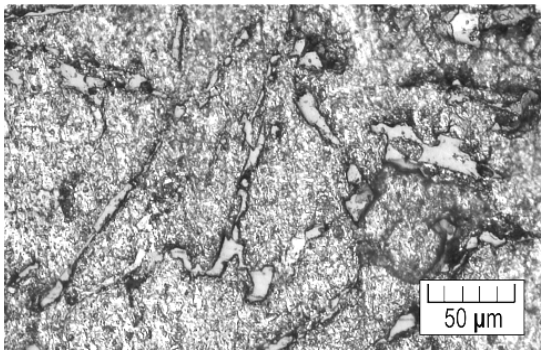
Slika 6. Čelo klipa; Al legura AlSi12CuNiMg;

Na slici 6 uočava se: dendritna mreža eutektičkog silicija (srednje siva boja), kristali intermetalnih spojeva Mg_2Si (svjetlija crna boja), Cu_3NiAl_6 (svjetlo siva boja), $NiAl_2$ (tamno siva boja), kristali Si (crna boja) i zrna α(Al) (svjetla površina) [5].



Slika 7.Ležaj osovinice klipa; Al legura AlSi12CuNiMg

Slično kao na slici 6, uz nešto manje crnih područja što ukazuje na manji udio silicija. Vide se i razlike u građi i rasporedu zrna.



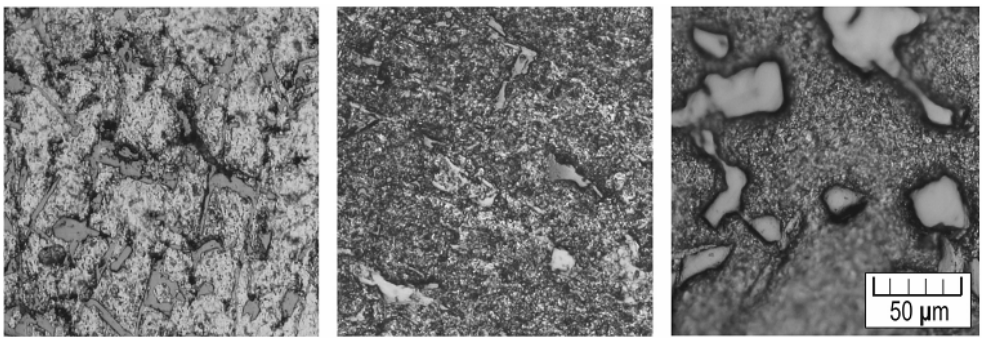
Slika 8. Dno klipa; Al legura AlSi12CuNiMg

Također slično kao i na dvije prethodne slike, manje je crnih područja nego na prvoj, te također su vidljive razlike u građi i rasporedu zrna. Uočavaju se nešto veća područja zrna α(Al).

Na metalografskim slikama ne uočavaju se značajnije razlike u veličini zrna, a što je posljedica ujednačene brzine hlađenja u svim presjecima odljevka. Ipak postoje određene razlike u tipu i vrsti kristalnih zrna, pa je u svrhu ujednačavanja strukture provedena toplinska obrada. Kao što je ranije istaknuto spomenute razlike imaju utjecaja na mehanička svojstva.

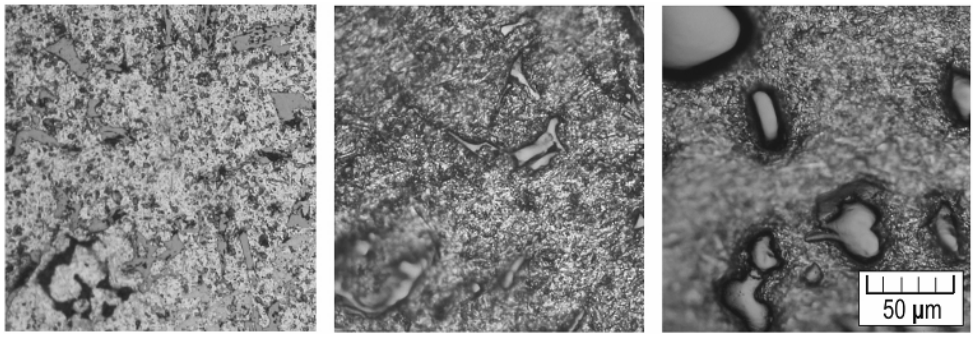
Toplinsku obradu ćemo provesti na dvije temperature od *250°C* i *500°C*. Prva toplinska obrada smatra se grijanjem, a druga toplinska obrada žarenjem.

Na slikama je vidljivo da se struktura ujednačila kod temperature od *250 ^{o}C*, dok se kod temperature od *500 ^{o}C* primjećuje porast zrna α(Al) (sl. 9, 10, 11). Na ovoj temperaturi pojavilo se i iznojavanje materijala, jer je tom temperaturom dosegnuto talište jedne od faza, koja je onda izbila na površinu (sl. 12).



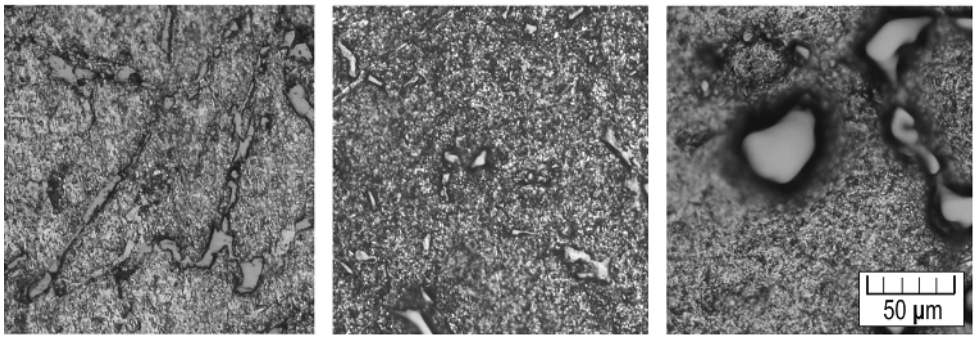
izvorna struktura *grijano na 250°C* *žareno na 500°C.*

Slika 9. Čelo klipa



izvorna struktura *grijano na 250°C,* *žareno na 500°C.*

Slika 10. Ležaj osovinice klipa



izvorna struktura, *grijano na 250°C,* *žareno na 500°C.*

Slika 11. Dno klipa



Slika 12. Iznojavanje materijala

4. ZAKLJUČAK

Cilj ovog rada bio je utvrđivanje postojanja razlike u brzinama hlađenja na tri različita mjesta odljevka, kao i ispitivanje njihovog utjecaja na strukturu i svojstva odljevka klipa.
Iz dijagrama brzina hlađenja vide se razlike u temperaturama na pojedinim mjestima, ali se ne uočavaju znatnije razlike u samim gradijentima brzina hlađenja. Na metalografskim slikama uzoraka ne primjećuju se razlike u veličini zrna što je i logično jer su razlike u brzinama hlađenja neznatne. Kako su neke razlike ipak vidljive, kao što su crna područja koja predstavljaju silicijevu fazu i faze silicijevih spojeva, zaključeno je da su ona uvjetovala razlike u tvrdoći jer je silicij izrazito tvrd. Razlike u količini silicijevih faza nastale su tako što je dio silicija u talini, kao lakša komponenta, isplivao prema površini i tu je došlo do povećanja njegove koncentracije. Pri lijevanju je talina s vrha lijevačkog lonca popunjavala dno kalupa odnosno područje čela klipa, a ona s dna lonca je završila u višim dijelovima

kalupa odnosno u području dna klipa. Rezultat svega ovoga je razlika u strukturi i tvrdoći, odnosno mehaničkim svojstvima. Kako klip treba u svim područjima imati jednaka svojstva jer bi inače moglo nastupiti i nejednoliko trošenje, provedena je toplinska obrada grijanjem i žarenjem na temperaturi od *250°C*, odnosno *500°C*. Rezultat toplinske obrade na *250°C* bila je homogena struktura svih uzoraka s nešto nižom tvrdoćom. Na temperaturi od *500°C* došlo je do povećanja područja α(Al) kristala koja su postala izrazito velika, a što je rezultiralo velikim padom tvrdoće.

LITERATURA

[1] T.Aikawa: ALUMINIUM ALLOY FOR INTERNAL COMBUSTION PISTON; (12.7.1999), http://www.freepatentsonline.com/5996471.html

[2] Keys to metal: ALUMINIUM-SILICON ALLOYS; http://www.key-to-nonferrous.com/default.aspx

[3] MATERIALS; http://www.omegapistons.com/index.php

[4] T.Ursić: UTJECAJ BRZINE HLAĐENJA NA STRUKTURU I SVOJSTVA ODLJEVKA KLIPA OD Al LEGURE; Diplomski rad, 2007, Fakultet elektrotehnike, strojarstva i brodogradnje, Split,

[5] Aluminium-Silicon Casting Alloys: Atlas of Microfractographs; http://www.asminternational.org/bookstore